Current Clinical Neurology
Series Editor: Daniel Tarsy

Fatta B. Nahab
Noriaki Hattori *Editors*

Neuroimaging of Movement Disorders

Humana Press

Current Clinical Neurology

For further volumes:
http://www.springer.com/series/7630

Fatta B. Nahab • Noriaki Hattori
Editors

Neuroimaging of Movement Disorders

Humana Press

Editors
Fatta B. Nahab
Department of Neuroscience
University of California at San Diego
La Jolla, California
USA

Noriaki Hattori
Neurorehabilitation Research Institute
Morinomiya Hospital
Osaka
Japan

ISBN 978-1-62703-470-8 ISBN 978-1-62703-471-5 (eBook)
DOI 10.1007/978-1-62703-471-5
Springer New York Heidelberg Dordrecht London

Library of Congress Control Number: 2013939745

Printed on acid-free paper

Humana Press is a brand of Springer
Springer is part of Springer Science+Business Media (www.springer.com)

. . . to the beautiful moon and the glorious earth

. . . to the patients who suffer from movement disorders, their caregivers, and our families and loved ones

Preface

One of the last frontiers of science remains the human brain. Despite the vast energy spent understanding this amazing machine, we still know so little. One of the revolutions sweeping neuroscience has been the use of various technologies to peer into the brain noninvasively to discover its inner workings. With ever improving machinery, data collection techniques, and analysis methods, researchers are now being presented with an exponentially increasing amount of data that they must wade through and interpret in the context of existing knowledge.

In the field of neurological movement disorders, this information explosion has been no different, though the causes and pathology of most disorders remain unknown. The use of neuroimaging has been important to unlocking the causes of abnormal motor control, though by comparison to other areas of neuroscience remains at a relatively early stage. Challenges to the use of neuroimaging in this field are further compounded by the very fact that this patient population has abnormal movements that may limit the ability to collect high-quality data. In addition, the field of neuroimaging possesses the double-edged sword of producing both true believers and skeptics at once by generating beautiful results that are all too frequently oversimplified and overinterpreted. These are just some of the challenges that need to be addressed in order to advance our understanding.

This book is not the first to cover the topic of Neuroimaging in Movement Disorders, and will certainly not be the last. Our goal was to bring together an impressive group of leaders in their respective fields from across the globe to discuss current knowledge. Furthermore, authors were encouraged to discuss controversies such as conflicting findings and methodological limitations in order to provide the reader with a comprehensive yet pragmatic understanding of the state of science. Lastly, these experts were asked to provide their insights about where future research is moving or should be directed.

The topics of the book chapters provide both comprehensive reviews of various neuroimaging methods and also more in-depth summaries of the contributions made by neuroimaging in individual movement disorders. Although many of the neuroimaging methods that are discussed have not been routinely used in clinical practice, the authors have done an excellent job of providing the reader with adequate

detail to understand the requirements for using these methods and in some cases even the starting knowledge to begin local implementation.

We are grateful to each contributor for the time and effort invested on this project. Without their devotion to sharing knowledge, the advancement of our common understanding would not be possible. It is also important to recognize the immense contributions made by patients and families to further our shared goal of curing these neurological disorders.

Fatta B. Nahab MD
Noriaki Hattori MD, PhD

Contents

Abbreviations

1H-MRSI	Proton Magnetic Resonance Spectroscopic Imaging
AADC	Aromatic Amino Acid Decarboxylase
ACC	Anterior Cingulate Cortex
AD	Alzheimer's disease
ADC	Apparent Diffusion Coefficient
ADHD	Attention Deficit Hyperactivity Disorder
AHCD	acquired hepatocerebral degeneration
Ala	Alanine
ANOVA	Analysis of Variance
AOPTD	Adult Onset Primary Torsion Dystonia
aPS	Atypical Parkinsonian Syndrome
ASL	Arterial Spin Labeling
AT	Ataxia Telangiectasia
BCI	Brain-Computer Interface
BLS	Blepharospasm
BOLD	Blood Oxygenation Level Dependent
BSPDC	Bilateral Striato-Pallido-Dentate Calcinosis
CBD	Corticobasal Degeneration
CBF	Cerebral Blood Flow
CBS	Corticobasal Syndrome or Corticobasal Degeneration
CBV	Cerebral Blood Volume
CD	Cervical Dystonia
ChAc	Chorea-acanthocytosis
Cho	Choline
cMRI	Conventional Magnetic Resonance Imaging
CNS	Central Nervous System
Cre	Creatine
CSF	Cerebrospinal Fluid
CT	Computed Tomography
CVD	Cerebral Vascular Disease
DAT	Dopamine Transporter
DAVF	dural arteriovenous fistula

DBS	Deep Brain Stimulation
DCM	Dynamic Causal Modeling
DDS	Dopamine Dysregulation Syndrome
DeoxyHb	Deoxygenated Hemoglobin
DKI	Diffusion Kurtosis Imaging
DLB	Dementia with Lewy Bodies
DLPFC	Dorsolateral Prefrontal Cortex
DMN	Default Mode Network
DTI	Diffusion Tensor Imaging
DOPA	Dihydroxyphenylalanine
DWI	Diffusion Weighted Imaging
EEG	Electroencephalography
EPI	Echo Planar Imaging
ET	Essential Tremor
FA	Fractional Anisotropy
FDG	^{18}F-deoxyglucose
FID	Free Induction Delay
FLAIR	Fluid-Attenuated Inversion Recovery
fMRI	Functional Magnetic Resonance Imaging
FOG	Freezing of Gait
FRDA	Friedreich's Ataxia
FSE	Fast Spin Echo
FXTAS	Fragile-X-associated Tremor/Ataxia Syndrome
GBA	Glucocerebrosidase
GLM	General Linear Model
Glx	Glutamate/Glutamine/GABA
GM	Gray matter
GMM	Gaussian mixed model analysis
$GP_{i/e}$	Globus Pallidus (interna/externa)
gPS	Monogenetic Parkinsonian Syndromes
GRE	Gradient Recalled Echo
HD	Huntington's disease
IBGC	Idiopathic Basal Ganglia Calcification
ICD	Impulse Control Disorders
iPD	Idiopathic Parkinson disease
Lac	Lactate
LC	Locus Ceruleus
LN	Lenticular Nucleus
LN^+	Lenticular Nucleus Hyperechogenicity
M1	Primary Motor Cortex
MCP	Middle Cerebellar Peduncle
MD	Mean Diffusivity
MEG	Magnetoencephalography
mI	Myoinositol
MR	Magnetic Resonance

MRPI	Magnetic Resonance Parkinsonism Index
MRS	Magnetic Resonance Spectroscopy
MS	Multiple Sclerosis
MSA	Multisystem Atrophy
MSA-C	MSA with predominant cerebellar findings
MSA-P	MSA with predominant parkinsonism
MTC	Magnetization Transfer Contrast
NBIA	Neurodegeneration with Brain Iron Accumulation
NAA	N-acetylaspartate
NIRS	Near Infrared Spectroscopy
NMR	Nuclear Magnetic Resonance
NPH	Normal pressure hydrocephalus
OCD	Obsessive Compulsive Disorder
OxyHb	Oxygenated Hemoglobin
PCA	Principal Component Analysis
PDD	Parkinson Disease with Dementia
PET	Positron Emission Tomography
PKAN	Panthothenate Kinase-associated Neurodegeneration
PMC	Premotor Cortex
PMd	Dorsal Premotor Cortex
PPI	Psychophysiological Interaction
PSP	Progressive Supranuclear Palsy
rCMA	Rostral Cingulate Motor Area
RD	Radial Diffusivity
ReHo	Regional Homogeneity
RF	Radio Frequency
RN	Red Nucleus
ROI	Region of Interest
RS-fMRI	Resting State Functional Magnetic Resonance Imaging
SCA	Spinocerebellar Ataxia
SCP	Superior Cerebellar Peduncle
SD	Spasmodic Dysphonia
SEM	Structural Equation Modeling
SMA	Supplementary Motor Area
SN	Substantia nigra
SNc	Substantia Nigra pars Compacta
SN^+	Substanita nigra hyperechogenicity
SNR	Signal to Noise Ratio
SPECT	Single Photon Emission Computed Tomography
SPM	Statistical Parametric Mapping
SVM	Support Vector Machine
SWEDD	Scans Without Evidence of Dopaminergic Deficit
T	Tesla
T1WI	T1-weighted imaging
TBSS	Tract-based Spatial Statistics

TCS	Transcranial Sonography
TE	Echo Time
THI	Tissue Harmonic Imaging
TI	Inversion Time
TR	Repetition Time
Trace(D)	Trace of the Diffusion Tensor
TS	*Gilles de la Tourette* syndrome
UPDRS	Unified Parkinson Disease Rating Scale
VBM	Voxel-based Morphometry
VBR	Voxel-based Relaxometry
VCDR	voxels for all connectivity-defined sub-regions
Vim	Ventralis intermedius nucleus [thalamus]
VMAT	Vesicular Monoamine Transporter
Vop	Ventralis oralis posterior nucleus [thalamus]
vPD	Vascular Parkinsonism
WD	Wilson's Disease
WM	White matter
WMC	White matter changes

Contributors

Ettore A. Accolla LREN, Département des Neurosciences Cliniques, Centre Hospitalier Universitaire Vaudois (CHUV), Université de Lausanne, Rue du Bugnon 46, 1011 Lausanne, VD, Switzerland

Campus Virchow Klinikum, Charité University Medicine Berlin, Berlin, Germany
e-mail: ettoreaccolla@gmail.com

Stefanie Behnke Department of Neurology, Saarland University Hospital, Kirrberger St, 66421 Homburg Saar, Germany
e-mail: s.behnke3@gmx.de

Daniela Berg Department of Neurodegeneration, Hertie Institute for Clinical Brain Research, Hoppe-Seyler-Str. 3, 72076 Tübingen, Germany
e-mail: daniela.berg@uni-tuebingen.de

Kevin M. Biglan Department of Neurology, University of Rochester, 1325 Mt. Hope Avenue, Suite 160, Rochester, NY 14620, USA
e-mail: kevin_biglan@urmc.rochester.edu

Norbert Brüggemann Department of Neurology, University of Lübeck, Ratzeburger Allee 160, 23552 Lübeck, Germany
e-mail: norbert.brueggemann@neuro.uni-luebeck.de

Fernando Cendes Department of Neurology, State University of Campinas-UNICAMP, Rua Vital Brasil, 251, Cidade Universitária Zeferino Vaz, Campinas, São Paulo 13083-888, Brazil
e-mail: fcendes@unicamp.br

Anelyssa D'Abreu Department of Neurology, State University of Campinas-UNICAMP, Rua Vital Brasil, 251, Cidade Universitária Zeferino Vaz, Campinas, São Paulo 13083-888, Brazil
e-mail: anelyssa@gmail.com

Bogdan Draganski LREN, Département des Neurosciences Cliniques, Centre Hospitalier Universitaire Vaudois (CHUV), Université de Lausanne, Rue du Bugnon 46, 1011 Lausanne, VD, Switzerland

Mark Hallett Human Motor Control Section, National Institute of Neurological Disorders and Stroke, National Institutes of Health, Building 10, Room 7D37, 10 Center Drive, Bethesda, MD 20892-1428, USA
e-mail: hallettm@ninds.nih.gov

Takashi Hanakawa Department of Molecular Imaging, Integrative Brain Imaging Center, National Center of Neurology and Psychiatry, 4-1-1 Ogawahigashi, Kodaira 187-8511, Japan
e-mail: hanakawa@ncnp.go.jp

Noriaki Hattori Neurorehabilitation Research Institute, Morinomiya Hospital, 2-1-88, Morinomiya, Joto-ku, Osaka 536-0025, Japan
e-mail: hattori@omichikai.or.jp

Silvina G. Horovitz Human Motor Control Section, Medical Neurology Branch, National Institute of Neurological Disorders and Stroke, National Institute of Health, Building 10, Room 7D37, 10 Center Drive, Bethesda, MD 20892-1428, USA
e-mail: silvina.horovitz@nih.gov

Kazumi Iseki Department of Behavioral Neurology and Cognitive Neuroscience, Tohoku University Graduate School of Medicine, 2-1, Seiryo-machi, Aoba-ku, Sendai, Miyagi 980-8575, Japan
e-mail: kazumi.iseki@gmail.com

Kohsuke Kudo Division of Ultrahigh Field MRI, Institute for Biomedical Sciences, Iwate Medical University 19-1 Uchimaru, Morioka 020-8505, Japan
e-mail: kokudo@iwate-med.ac.jp

Corneliu C. Luca Department of Neurology, Miller School of Medicine, University of Miami, 1150 NW 14th Street, PAC Suite 401, Miami, FL 33136, USA
e-mail: cluca@med.miami.edu

Joseph C. Masdeu Section on Integrative Neuroimaging National Institutes of Health (NIH/NIMH-CBDB), Intramural Research Program 9000 Rockville Pike Building 10, Room 3C111 Bethesda, MD 20892-1365
e-mail: masdeu@nih.gov

Andrew McGarry Department of Neurology, Movement Disorders Division, Cooper University Hospital at Rowan University, 3 Cooper Plaza, Suite 320, Camden, NJ 08103, USA
e-mail: McGarry-Andrew@cooperhealth.edu

Masahito Mihara Department of Neurology, Graduate School of Medicine, Osaka University, 2-2, D-4 Yamadaoka, Suita, Osaka 565-0871, Japan
e-mail: mihara@neurol.med.osaka-u.ac.jp

Ichiro Miyai Morinomiya Hospital, 2-1-88, Morinomiya, Joto-ku, Osaka 536-0025, Japan
e-mail: miyai@omichikai.or.jp

Christoph Mueller Department of Neurology, Innsbruck Medical University, Anichstrasse 35, Innsbruck, Austria
e-mail: christoph.mueller@i-med.ac.at

Fatta B. Nahab Department of Neuroscience, University of California, San Diego, 8950 Villa La Jolla Drive, Suite C112, La Jolla, CA 92037, USA
e-mail: fnahab@ucsd.edu

Pradip M. Pattany Department of Radiology, Miller School of Medicine, University of Miami, Miami, Florida, USA
e-mail: ppattany@med.miami.edu

Nicola Pavese Centre for Neuroscience, Hammersmith Hospital Campus, Imperial College London, DuCane Road, London W12 ONN, UK
e-mail: nicola.pavese@imperial.ac.uk

Werner Poewe Department of Neurology, Innsbruck Medical University, Anichstrasse 35 Innsbruck, 6020 Austria
e-mail: werner.poewe@i-med.ac.at

Makoto Sasaki Division of Ultrahigh Field MRI, Institute for Biomedical Sciences, Iwate Medical University, 19-1 Uchimaru, Morioka, Iwate 020-8505, Japan
e-mail: masasaki@iwate-med.ac.jp

Klaus Seppi Department of Neurology, Medical University Innsbruck, Anichstrasse 35 Innsbruck, A-6020 Austria
e-mail: klaus.seppi@i-med.ac.at

C. L. Stanton Department of Radiology, Miller School of Medicine, University of Miami, Miami, FL, USA
e-mail: Cstanton@med.miami.edu

Yen F. Tai Department of Neurology, Imperial College Healthcare NHS Trust, Fulham Palace Road, London W6 8RF, UK
e-mail: yen.tai@imperial.ac.uk

J. C. Masdeu New York Medical College, Valhalla, NY, USA
e-mail: masdeu@nymc.edu

Yau-Yau Wai Medical Imaging and Radiological Sciences, Chang Gung University, 259 Wen-Hua 1st Road, Taoyuan County, Taiwan
e-mail: yauwaiwu@ms4.hinet.net

Jiun-Jie Wang Medical Imaging and Radiological Sciences, Chang Gung University, 259 Wen-Hua 1st Road, Taoyuan County, Taiwan
e-mail: jwang@mail.cgu.edu.tw

Tao Wu Department of Neurobiology, Xuanwu Hospital, 45 Changchun Street, Bejing 100053, China
e-mail: wutao69@gmail.com

Fumio Yamashita Division of Ultrahigh Field MRI, Institute for Biomedical Sciences, Iwate Medical University 19-1 Uchimaru, Morioka 020-8505, Japan
e-mail: fyamashi@iwate-med.ac.jp

Chapter 1
Introduction to Neuroimaging

Christian LoRe Stanton and Pradip M. Pattany

A Brief History of Neuroimaging

It has been said that modern scientists stand on the shoulders of giants, but perhaps more appropriately in modern neuroscience it can be said that we see through the lenses of the visionaries before us. Aside from relatively primitive neurosurgical techniques and the fortunately isolated instances of vivisection [1, 2], neuroscientists throughout the vast majority of the previous millennia were only able to hypothesize and essentially "imagine" the anatomic and physiologic state of a living human brain. It was not until the twentieth century that visualizing the central nervous system (CNS) in vivo would be a feat widely attainable by neuroscientists, finally leaving the realm of imagination and entering the realm of imaging.

The earliest forms of neuroimaging involved adaptations of conventional radiologic techniques derived from the discoveries of Roentgen and his cohorts at the turn of the twentieth century [3]. By the early 1920s, the American Neurosurgeon Walter Dandy had developed two techniques using air as a contrast agent which, for the first time, allowed radiographic visualization of lesions restricted to the CNS by differentiating the ventricular system from the brain [4, 5]. Although their utility is significantly limited by modern standards, the techniques developed by Dandy were indispensable to neuroimaging throughout much of the twentieth century. Toward the end of the 1920s, Portuguese Neurologist Antonio Moniz developed the first cerebral angiograms [6], a modality whose value is still readily apparent in modern neuroimaging. It was not until the 1970s that computed tomography (CT) appeared as a useful modality, quickly becoming established as a vital neuroimaging tool. Despite its steady development and undeniable utility, CT still abides by conventional

C. L. Stanton (✉) · P. M. Pattany
Department of Radiology, Miller School of Medicine,
University of Miami, Miami, FL, USA
e-mail: Cstanton@med.miami.edu

P. M. Pattany
e-mail: ppattany@med.miami.edu

F. B. Nahab, N. Hattori (eds.), *Neuroimaging of Movement Disorders,*
Current Clinical Neurology 44, DOI 10.1007/978-1-62703-471-5_1,

radiologic principles and has the drawback of potentially high levels of ionizing radiation exposure [7]. Furthermore, a relative deficiency in depicting soft tissue detail has always limited its scope in the evaluation of CNS pathology, as such a detailed discussion of CT is outside the intended scope of this chapter [8].

Although the middle of the twentieth century may seem to be characterized by a paucity of progress in neuroimaging, the foundations for its most revolutionary milestone were in fact being laid with the development of nuclear magnetic resonance (NMR). These developments would culminate in a particularly fascinating era in neuroimaging: the emergence of widespread use of structural magnetic resonance imaging (MRI) in the 1980s [9]. In the early 1990s, the first functional MRI was performed, paving the way for its modern form as a prevailing modality beside other functional neuroimaging techniques with earlier origins such as single-photon emission computed tomography (SPECT) and positron emission tomography (PET) [10]. Since its inception, MRI has provided some of the most important advances in medicine and its implementation as an adaptable clinical and investigational tool has become indispensable in modern neuroscience—warranting the special attention it receives in this chapter.

The composite works of a multitude of brilliant twentieth century scientists are too vast and important to implicate any individual, but a summary of MRI's collaborative development is a testament to its far-reaching significance. The early discoveries of NMR physics can be partially attributed to the hastened advancement of technologies during World War II [11]. Numerous discoveries expanded the science in the decades following the war to include applications in chemistry and biochemistry, including the analysis of the molecular structures of compounds within a test tube via NMR spectroscopy. Following revolutionary discoveries in the 1970s, it was realized that the scope of NMR could be broadened to include applications to imaging and medicine [9]. While maintaining the core principles and the use of strong magnets and radiowaves, the human body could now essentially substitute for the test tube and allow for investigation of the constituent tissues within.

The potential utility of NMR to human neuroscience would be heralded by the first human head MRI image obtained in 1978 (Fig. 1.1). Although seemingly quite primitive, it was revolutionary for its time and alongside the earlier neuroimaging techniques is a reminder of how far we have come in a relatively short period. As we, the collective neuroimagers (i.e., the technologists, physicists, scientists, and physicians), observe the images on our monitors today it is worth remembering that we are the beneficiaries of the ingenuity and efforts of countless visionaries before us.

MRI Principles

The science behind MRI is far from intuitive and the detailed physics are outside the purview of this chapter. However, a solid foundation is important for understanding the various MRI neuroimaging methods. To that end, the core concepts and terminology are reviewed here.

Fig. 1.1 First ever human head image using MRI at 0.1 T from EMI Central Research Laboratories. For this image CT-type "back projection" was used. (Courtesy of Ian Young and first published in an article from the November, 1978 issue of *New Scientist* magazine)

The Proton

At its core, MRI involves the interaction of several sources of electromagnetism, which include those inherent to the machine as well as those intrinsic to the organism being studied. Extending NMR principles we could gather information from the nuclei of a multitude of molecules within a given sample, provided that they have an odd number of protons, have a spin, and are mobile enough to change direction. However, in clinical MRI, there is a focus on the hydrogen nuclei. This is primarily due to its abundance in the body, mostly in the form of water, but also in various other forms such as fat. Each hydrogen atom's nucleus is comprised of a single proton. The positively charged proton is naturally spinning on its axis which, by the rules of electromagnetism, results in the creation of tiny magnetic fields. In essence, each proton acts as a tiny bar magnet with a specific strength and directionality (i.e., they are vectors). However, with their random orientations and movements there is usually no net magnetic effect. It is the composite magnetic activity of numerous protons with which we are interested and the smallest volume of tissue (or voxel) that is measured to eventually produce the final MR image, comprising the net effect of trillions of protons within a single cubic millimeter (1 mm^3).

The Static External Magnetic Field (B_0)

The most powerful source of electromagnetism arising from the MRI is the static magnetic field to which the subject is exposed in the center of the machine, which in short-hand is called B_0 ("B-nought"). As with the proton magnetic fields, B_0 is a vector and the strength of this field is inherent for a given machine as measured in

Tesla (T), with most clinical machines currently at the 1.5 T strength. The so-called "high-field" MRI is also becoming widespread at levels of 3 T and greater, which has some important implications that will be addressed later. Although B_0 is a static field in the sense that it persists throughout the entirety of the acquisition process, it is important to note that it is not completely uniform and there are tiny variations in the magnetic field (i.e., it has inhomogeneities). This latter property has multiple implications, as it affects the quality of the final images and it also underlies the concepts of T2 and T2* ("T2-star").

As the subject is exposed to B_0, their protons are influenced in two main ways. First, the previously randomly oriented tiny magnetic vectors of the protons become aligned in the same plane as B_0 and obtain a net directionality along that axis. This novel orientation of the protons net vector is known as longitudinal magnetization. The second outcome is that the protons gain a type of motion known as "precession", in which each proton moves gyroscopically (i.e., similar to a wobbling top). The precession (or "resonant") frequency for the protons is characteristic for a given B_0, increasing with higher field strengths. We can temporarily alter B_0 by several means and it is the resultant variable frequency of the protons, which fundamentally makes MRI possible. The above conditions of longitudinal magnetization and precession can be considered an equilibrium state from which other parts of the MRI acquisition process can be understood.

The Radiofrequency (RF) Pulse

A second source of electromagnetism, known as the radiofrequency (RF) pulse, is then administered from an RF coil at a specific frequency (i.e., resonant frequency). There are usually multiple RF pulses administered during an acquisition process which can vary in their angles with respect to B_0 (e.g., 90°, 180°, etc.) and the predetermined interval of their occurrence, the variable effects of which will become clearer when we touch upon specific sequence protocols. The initial pulse is usually known as an "excitation pulse" and we can first consider the outcome of this. Upon receiving the appropriate frequency of RF pulse, the given groups of protons absorb energy and are excited into two important reactions that occur simultaneously. First of all, the protons' magnetic field vector rotates away from the equilibrium plane of B_0, such that there is no longer a net longitudinal magnetization. Secondly, the movements of the protons are harmonized, such that their precession frequencies are now in-sync ("in-phase") with each other or have "phase-coherence" and the protons now have a net transverse magnetization. In the presence of B_0, it is actually the dynamic state of this net transverse magnetization that produces a radiowave and induces a current in a RF coil (usually different from the one that transmitted the RF pulse) that eventually leads to an MR signal from the tissues of interest.

*T1, T2, and T2**

Soon after administration of the RF excitation pulse, the protons begin giving off absorbed energy to their local molecular environment (known as their "lattice") and their vectors eventually return to the plane of B_0, reestablishing longitudinal magnetization. When plotted over time, you can see that this relaxation process occurs exponentially and the measured time constant of this up-sloping curve is called T1, which is characteristic for given tissues and will therefore vary between voxels. This process is known equivalently as longitudinal, T1 or spin-lattice relaxation.

Occurring simultaneously is a process involving loss of phase-coherence of the precessing protons that, in distinction from above, involves an exchange of energy between protons (instead of the environment). As mentioned, B_0 has slight field strength inhomogeneities and the local magnetic environment experienced by each group of protons is also inherently inhomogeneous. Together these processes contribute to reestablishing the protons variable precession frequencies, i.e., they undergo "dephasing" and a net reduction of transverse magnetization a process known as free induction decay (FID). The process of energy exchange between protons is known equivalently as "spin-spin" or T2 relaxation. This component can be isolated by temporarily eliminating B_0 inhomogeneities, which is one of the other functions of RF pulses in spin-echo (SE)-based techniques. The resultant relaxation effects are plotted over time and the time constant of the exponentially decaying curve is called T2, which again is characteristic for given tissues and will vary between voxels.

The composite process of FID, encompassing the contributions of both spin-spin and B_0 inhomogeneities is described by the time constant T2*. T2* relaxation can result in rapid dephasing of the transverse magnetization which decreases the strength of the echo signal and can lead to clinically useless images. It is for this reason that it is often desirable to suppress T2* effects. However, at other times it is desirable to accentuate T2* effects, leading to greater conspicuity of certain tissues among other uses to be detailed later.

By convention, tissues with shorter T1 relaxation time constants appear as higher signal intensity (e.g., fat and white matter), while those with longer ones have lower signal intensity. Conversely, longer T2 relaxation time constants appear as higher signal intensity (e.g., cerebrospinal fluid (CSF)) while shorter ones have lower signal intensity. Further details of what determines the particular T1 and T2 of the different tissues (both normal and pathologic) can be found in any comprehensive MRI text, with characteristic tissue signals summarized in Table 1.1. The most important point to remember is that the variability of the time constants between different tissues determines their signal intensities and the differences in signal intensities between the voxels in a sample of interest; therefore, represent the contrast in our final images. In general terms, it is established that T1 effects give better anatomic information, while T2 effects can be more useful for evaluation of pathology—with much overlap in practice.

Virtually in all MRI images, the independent effects of T1 and T2 are each contributing to various degrees, but the greatest contrast in our images is obtained by

Table 1.1 Differentiation of tissue type based upon MRI weighting and signal intensities

Weighting	Signal intensity	Tissue examples
T1	Dark	Air
		Fast-flowing blood
		Mineral rich tissue (e.g., cortical bone)
	Low	High free-water content (e.g., edema, CSF)
	Intermediate	Proteinaceous tissue
	Bright	Fat
		Blood products (intracellular metHb)
		Slow-flowing blood
T2	Dark	Air
		Fast-flowing blood
		Mineral-rich tissue (e.g., cortical bone)
	Low	Bone islands
	Intermediate	Fat
	Bright	High free-water content (e.g., edema, CSF)
		Proteinaceous tissue
		Blood products (oxyHb, extracellular metHb)

CSF cerebrospinal fluid, *metHb* methemoglobin, *oxyHb* oxygenated hemoglobin

maximizing the difference between the time constants of the various tissues. It is the responsibility of neuroimagers to maximize the clinical utility of the images, which includes independently promoting T1 or T2 weighting and dividing these into different imaging series to interpret their effects separately. In order to increase the contributions by either T1 or T2 effects, we "weight" the images by selecting parameters that will give us the greatest differences in signal intensity between tissues of interest (i.e., contrast). For a given sequence, we can choose how long after the excitation pulse we want the MR to initialize the "readout" of the echo signals, a parameter known as echo time (TE) as well as the time between subsequent excitation pulses, a parameter known as repetition time (TR). Essentially, a short TR setting (400–800 ms) in conjunction with a short TE setting (5–30 ms) will yield tissue contrast that emphasizes differences in T1 signal, while a long TR will minimize the differences in T1 signal. An appropriately long TE setting (60–120 ms) will emphasize tissue differences in T2 signal; however, the TE must not be too long, because the progressively weakening T2 signal will eventually result in poor image quality. As you will see, we can also affect the resultant images by adjusting other parameters in the various sequence protocols.

Gradients, K-Space, and the Fourier Transformation

Gradients are an additional source of electromagnetism administered from other coils in the MRI and can be utilized in a variety of ways via the same basic effect: temporarily altering B_0 in a predictable manner. One important use of gradients is in their pulsatile application along the different axes of B_0 contributing to slice selection,

frequency encoding, and phase encoding of the protons. An abstract concept called *k*-space is essentially a 2D matrix representing the raw frequency-encoded and phase-encoded data derived from the steps above. In some basic sequence protocols, *k*-space is filled row-by-row, requiring multiple repetitions of the acquisition steps to populate the entire matrix. The end result of a complicated interaction between the RF pulses and gradients will be a spatially encoded MR signal in this form.

Even though each voxel is uniquely encoded by the steps above, it is actually a single-summed signal (i.e., the "bulk magnetization"), which is detected in MRI. In order to convert this raw data into useful images, it is necessary to disentangle the signal; this is done by breaking it down into its component frequencies, an automated process that is dictated by the mathematical algorithm known as the Fourier Transformation. With the culmination of the above steps, we have established our final images that have been imparted with spatial information and signal intensities that contrast the tissues of interest in our subject.

Conventional MRI Sequence Protocols

Since the early days of conventional MRI, a multitude of pulse sequence protocols (or "protocols" as they will be referred to) have been developed. Although the same basic principles are utilized, each of the protocols differs in the details of acquisition as well as in the final product and therefore their specific utility in neuroimaging. Some protocols allow for faster acquisition times, improved image quality, or even accentuation of various tissue contrasts. There is usually a compromise with the various MRI protocols and creating a balance of the best possible signal, contrast, and spatial resolution in the shortest possible time is a basic goal of the neuroimager. Fortunately, many of these can be acquired and interpreted in combination for a given patient, contributing to MRIs flexibility in clinical applications. Although there are hundreds of different protocols with a variety of acronyms, we will focus on some of the core protocols in generic categories.

Spin-Echo (SE)

Spin-Echo (SE) was the most commonly used protocol during the infancy of MRI and it continues to have specific utility. The defining acquisition characteristic for SE protocols come from the application of an initial 90° RF excitation pulse followed by a 180° RF "refocusing pulse", with a couple of relevant consequences. First of all, this creates a focused SE signal measured at time TE, which leads to the population of a single line of the *k*-space matrix during each TR cycle (i.e., between excitation pulses). Also, as previously alluded to, the RF refocusing pulse neutralizes contributions from T2* effects, which allows for a "true T2" signal.

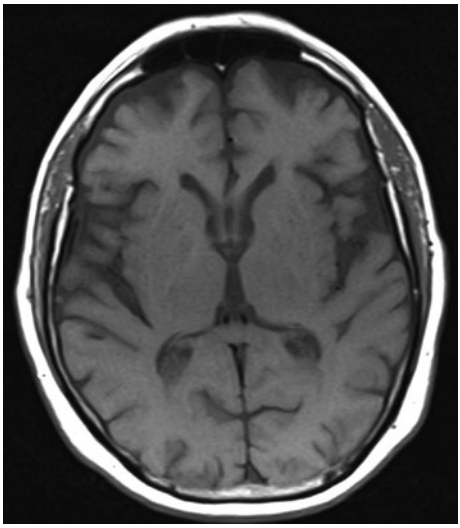

Fig. 1.2 T1 SE axial image obtained at 1.5 T, TR = 570 ms, TE = 17 ms

Adjustments of the TR and TE are the parameters utilized in SE to T1 or T2 weight the resultant images. Because each TR in basic SE sequences results in population of only a single line of *k*-space, the TR cycle must be repeated numerous times and is the most time-consuming parameter. Therefore, TR is set to as short as possible which, along with a short TE, results in T1 weighting. Thus, the greatest clinical utility of basic SE protocols reside in the creation of T1-weighted images, while acquisition of T2-weighted images can be time prohibitive and other protocols have been developed to allow for this (Fig. 1.2).

Fast Spin-Echo (FSE)

The utility of Fast Spin-Echo (FSE) protocols comes mainly from their improved acquisition efficiency. This is accomplished by various alterations to the basic SE protocol with respect to the RF pulses and spatial encoding steps. These alterations usually include a rapidly repeating refocusing pulse, which yields a series of SE signals (or an "echo train") that are subjected to different encoding gradients, allowing for population of multiple lines of *k*-space during each single TR. Therefore, in FSE there are additional parameters under our control, including the number of SEs to be produced during a given TR known as the "echo train length" (ETL), which directly contributes to the rapidity of acquisition. The SE signals in FSE are also each recorded at different TEs; so, this adjustable parameter is actually known as "effective TE."

Building upon their slower predecessor, FSE protocols have become ubiquitous in modern neuroimaging. In addition to the reduced acquisition time, FSE protocols can also improve image quality. Signal contributions from T2* effects are further

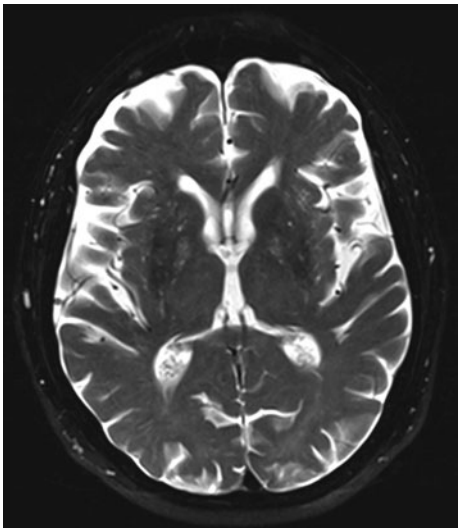

Fig. 1.3 T2 FSE axial image obtained at 1.5 T, TR = 5370 ms, TE = 111 ms

minimized by the repetitive refocusing pulses. However, these faster protocols also have their own disadvantages including potentially higher signal from certain tissues (e.g., fat and CSF), which can limit evaluation of parenchyma particularly at the skull base and periventricular regions. These limitations can be largely addressed by complementary methods as we will see shortly in Fig. 1.3.

Gradient Recalled Echo(GRE)

Another group of protocols known generically as gradient recalled echo (GRE) offer even faster acquisition times than the various SE techniques, but this is at the cost of potentially noisier images. This sequence differs from SE techniques by the potential use of partial flip angles (i.e., less than 90°) as well as the use of gradients (applied bidirectionally) to dephase and then rephase transverse magnetization and form a gradient-echo signal. So, the adjustable parameters in GRE include TR and TE as well as the choice of the particular partial flip angle. Partial flip angles result in less substantial tipping of the protons' magnetic vectors from the longitudinal plane and therefore faster recovery of full longitudinal magnetization allowing for shorter TRs. Without the use of the refocusing RF pulse, it is also possible to measure the echo signal sooner than in SE protocols (i.e., the TE can be shorter). However, this also yields preservation of T2* effects, which can result in signal loss and geometric distortion. These T2* (or "magnetic susceptibility") effects can especially limit evaluation in areas with different tissue types abutting one another, for example, at the interface of air and soft tissues at the paranasal sinuses. Conversely, GRE can exploit these T2* effects, for example, allowing easier detection of certain tissues such as blood. Therefore, the utility of GRE protocols in conventional MRI lies in the

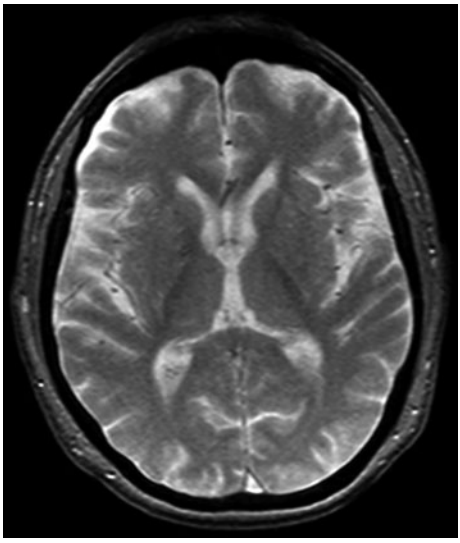

Fig. 1.4 GRE axial image obtained at 1.5 T, TR = 464 ms, TE = 10 ms, flip angle = 20

rapid acquisition of T1-weighted images and these "T2-like" images. As we will see, T2* effects are also important for some of the advanced MRI techniques (Fig. 1.4).

Echoplanar Imaging (EPI)

Another unique conventional MRI protocol is echoplanar imaging (EPI). This is a modified protocol that can utilize various RF excitation pulses (i.e., similar to GRE), but requires high-performance gradient coils to produce images very rapidly. The characteristic use of a continuously cycling gradient produces multiple echo signals with different phase-encoding and allows for prompt filling of multiple lines of *k*-space in a single TR cycle. The resultant speed of EPI minimizes motion artifact and there is also increased sensitivity to T2* effects. These characteristics allow for its use in some of the advanced MRI techniques, which rely on rapid physiologic processes that could not be readily demonstrated with slower protocols.

Inversion Recovery

Inversion recovery is one of several types of protocols that have been developed to allow suppression of signals coming from various tissues. These particular sequences take advantage of a concept known as "magnetization preparation." Essentially, they consist of first administering a 180° pulse to invert the longitudinal magnetization vector into the opposite direction. This "inversion recovery" pulse is administered at

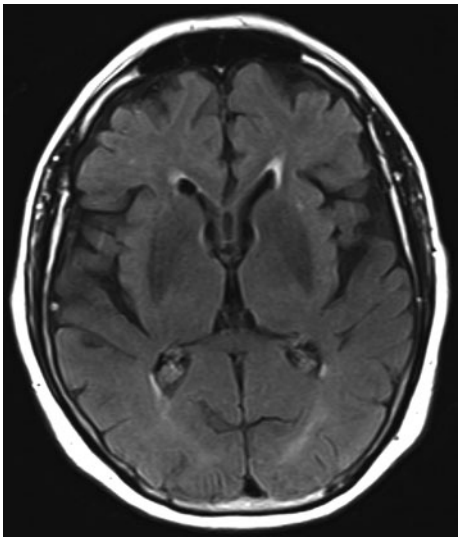

Fig. 1.5 FLAIR axial image obtained at 1.5 T, TI = 2500 ms, TR = 8000 ms, TE = 128 ms

defined intervals for specific tissue suppression based on that tissues characteristic time constants, a novel parameter known as inversion time (TI). An excitation pulse is still necessary to yield transverse magnetization and eventually create a measurable signal; so, these special pulses are then followed by a standard protocol to obtain the final images.

The main clinical utility of inversion recovery protocols in neuroimaging comes from improved contrast between tissues of interest without interference by signal from extraneous tissues, but another common use is as an aid to tissue characterization. It can be used with SE, FSE, or GRE protocols, for example, to suppress the normally high signal of fat. A specific subtype known as fluid-attenuated inversion recovery (FLAIR) is a FSE-based protocol that has become nearly ubiquitous in neuroimaging MR acquisitions. FLAIR uses a long TI (similar to the relaxation time of fluid) to null the normally high T2 signal arising from CSF. This leads to a T2-like image of the brain parenchyma allowing easy discrimination of high T2 signal related to edematous or inflammatory changes while eliminating any confusion from adjacent CSF signal. The clinical utility of FLAIR is therefore primarily in the improved evaluation of periventricular lesions and those near the cortical surfaces. Of course, these complementary protocols come with their own disadvantages including longer acquisition times, the potential for erroneous tissue suppression, as well as diminished signal strength (Fig. 1.5).

Advanced MRI and Functional Neuroimaging Techniques

While the MRI protocols above provide information derived from the activity of protons on a subatomic level, their basic applications primarily offer a structural perspective of the status of the brain in their final products. However, extension of

the same MR principles with various modifications to the acquisition processes have lead to a variety of advanced neuroimaging techniques. Along with other modalities such as those falling under the auspices of nuclear medicine known as emission tomography, these techniques can provide unique information at the cerebrovascular, metabolic, and biochemical levels. These techniques greatly expand clinical and investigational opportunities, including evaluation of pathology on temporal scales not possible with purely structural imaging. Inherent to these multidisciplinary applications is the need to grasp the relevant physiologic basis for understanding the specific types of information that these various techniques can provide. Accordingly, we will now focus upon several of the advanced MR-based techniques as well as the effects of high-field MRI, followed by an overview of emission tomography.

Diffusion-Weighted Imaging (DWI)

Diffusion-weighted imaging (DWI) has become an integral part of clinical neuroimaging. With an acquisition method that usually utilizes the rapid EPI protocol, DWI also requires the application of a pair of strong "diffusion" gradients. These motion-sensitizing diffusion gradients utilize signal dephasing to highlight the movements of water molecules. Movement of water is random and can be considered unrestricted in relatively homogeneous environments such as CSF and (to a lesser extent) normal gray matter. The protons whose movement is restricted will stay in the same general area and the dephasing effects of the first diffusion-encoding gradient will essentially be negated by the second diffusion-encoding gradient, while protons whose movement is unrestricted will not be in the same given area and will experience a different subsequent gradient strength resulting in signal loss. The areas corresponding to restricted movement will thus demonstrate higher signal intensity on the final DWI images.

It is important to note that there are some inherent T2 effects maintained in the final images. These T2 effects can result in misleading signal characteristics including high- or isointense signals on DWI, the so-called "T2-shine-through" and "T2 washout." For this reason, among others, it is necessary to correlate the DWI images with complementary image series that are obtained in conjunction. The best known of these additional series are the apparent diffusion coefficient (ADC) maps, which can be thought of as more accurately reflecting the diffusion characteristics of the tissue of interest. Accordingly, ADC maps can help distinguish signal on DWI images representing "true" diffusion (seen as lower signal intensity on ADC) from that attributable to the T2 effects.

The most evident clinical value of DWI has been as the basis for a revolution in stroke imaging. In ischemic brain parenchyma, the affected cells lack an energy supply and can no longer use their ATP-powered transport channels, which leads osmotically to an increase of intracellular water molecules (i.e., cytotoxic edema) with resultant restricted diffusion and high DWI signal in these areas during acute infarction. In addition to confirming true restricted diffusion, correlation with the complementary

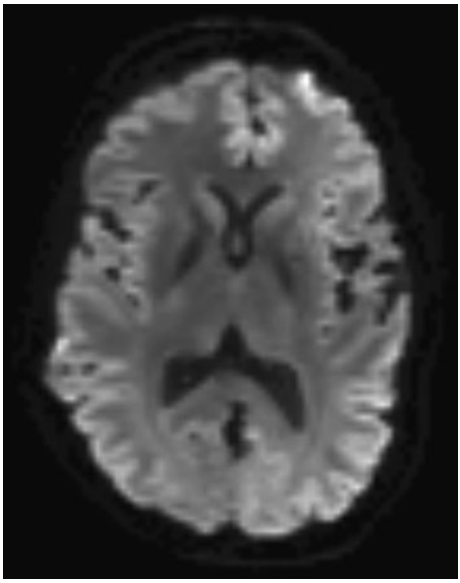

Fig. 1.6 DWI axial image obtained at 1.5 T, TR = 7300 ms, TE = 84 ms, and B-value = 1000

Fig. 1.7 ADC axial image obtained at 1.5 T, TR = 7300 ms, TE = 84, and B-value = 1000

ADC maps can also help determine the chronicity of strokes. There are several additional pathologic processes, with various reasons for restricted diffusion, whose diagnoses have been aided by the emergence of DWI. These include a number of diverse processes such as abscesses, Creutzfield-Jakob disease, and lymphoma just to name a few (Figs. 1.6 and 1.7).

Diffusion Tensor Imaging (DTI)

A fascinating iteration of DWI methodology known as diffusion tensor imaging (DTI) has permeated neuroimaging research in recent years and holds enormous promise for clinical applications. The utility of DTI lies in its ability to evaluate the course and integrity of white matter tracts in vivo, which may open up new horizons in neuroscience that have largely evaded sufficient scrutiny by earlier neuroimaging methods. As with DWI, the measurements of DTI are focused on water movement patterns. The bundles of white matter tracts coursing through the CNS primarily consist of axons and their surrounding myelin sheaths. These lipid sheaths are largely impermeable to water diffusion, resulting in the restriction of water movement to the longitudinal trajectories of the axons. The acquisition protocol builds upon DWI with the requisite inclusion of at least six measurements of diffusion-encompassing values of spatial direction. These measured values allow the creation of a mathematical ellipsoid or "tensor," from which postprocessing methods can reconstruct images that display information about white matter tracts in several forms. The most commonly used DTI map depicts "fractional anisotropy" (FA), which is a measure affected by multiple tissue factors, but which essentially represents the extent of diffusion directionality and potentially indicates the orientation and integrity of given areas of white matter tracts. Alternatively, DTI information can be displayed in a color-coded map demonstrating the relative orientation of white matter tracts within the brain parenchyma. DTI information can also be displayed in a 3D format known as "tractography," which uses the additional parameter of strategically placed "seed-points" to highlight tracts associated with regions of interest.

Current clinical use of DTI is limited, but includes preoperative evaluation of brain tumors to assess involvement of white matter tracts. The full potential of DTI has yet to be realized, but its current widespread investigational use suggests imminent expansion of its clinical applications to include areas such as demyelinating diseases, traumatic brain injury, and developmental disorders among others (Figs. 1.8 and 1.9).

Magnetic Resonance Spectroscopy (MRS)

Magnetic resonance spectroscopy (MRS) is a distinctive modality that has carved out a niche in neuroimaging by highlighting the particular molecular constituents in given samples of brain parenchyma. Although the MRS technique is closely related to NMR techniques used to analyze many different types of molecules in chemistry, its use in clinical neuroimaging again focuses primarily on hydrogen nuclei. In MRS, hydrogen nuclei are evaluated with respect to their presence in specific metabolites. The patterns of their distribution within these metabolites yield slightly different and predictable shifts in resonant frequency, and the relative proportion of these compounds can therefore be indirectly measured. The final image product of MRS includes a plot of the relative concentrations or "spectra" of these metabolites in values of parts per million (PPM). The particular metabolic spectra are associated

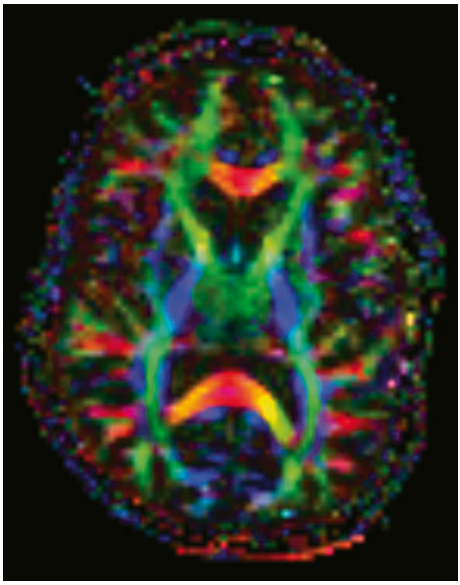

Fig. 1.8 DTI axial color-map image obtained at 3 T, by convention *red* indicates right–left, *blue* indicates superior–inferior, and *green* indicates anterior–posterior orientations

with pathophysiology of varying specificity, some of which can be disease defining (e.g., elevated NAA in Canavan disease) and others which can be suggestive (e.g., malignancy associated with elevated Cho, Lac, Lip, and decreased NAA, Cr). The most clinically relevant metabolites and some of their associations are summarized in Table 1.2.

MRS acquisition consists of obtaining structural MR images via a conventional protocol and selection of the voxel(s) of interest (VOI) along with the use of one of several methods for obtaining the spectra, including single-voxel spectroscopy (SVS)

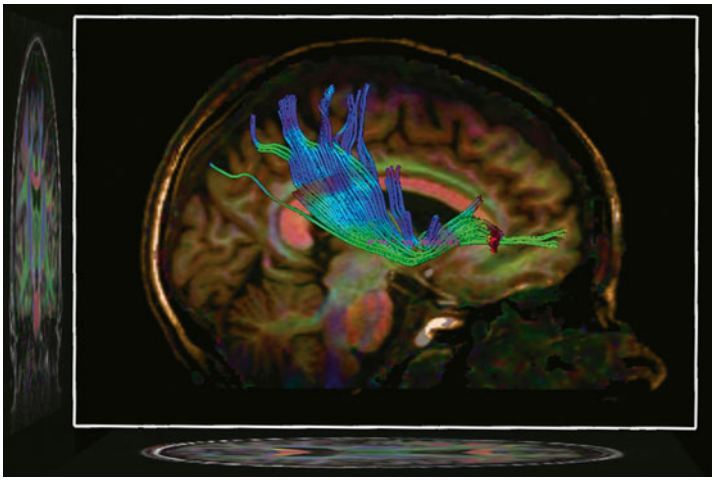

Fig. 1.9 Sagittal tractography image obtained at 3 T with "seed-point" placed near the basal ganglia

Table 1.2 Summary of MRS metabolite markers and clinical associations

Metabolite (symbol)	Physiologic significance	Common associations	
N-Acetyl-Aspartate (NAA)	Viable neuron marker	Elevated	Canavan disease
		Decreased	Many lesions
Choline (Cho)	Cell membrane metabolism marker	Elevated	Tumors, demyelination
Creatine (Cr)	Energy metabolism marker	Relatively constant	
Myoinositol (mI)	Glial cell marker	Elevated	Glioma, multiple sclerosis gliosis, Alzheimer disease
		Decreased	Herpes encephalitis
Glutamate–glutamine and GABA (Glx)	Intracellular neurotransmitter	Elevated	Hepatic encephalopathy, severe hypoxia
Free Lipids (Lip)	Lipid droplet formation (e.g., membrane breakdown or necrosis)	Elevated	Necrotic tumors
Lactate (Lac)	Anaerobic metabolism marker	Elevated	Ischemia, seizure, mitochondrial disorders
Alanine (Ala)	Anaerobic metabolism marker	Elevated	Meningioma, abscess

and multivoxel techniques, the latter of which is also known as magnetic resonance spectroscopic imaging (MRSI). SVS utilizes one of several special protocols to obtain the spectra (e.g., "PRESS" or "STEAM"), which are characterized by the use of slice-selective RF pulses and gradients to focus upon an echo signal from a single or a few VOI(s), each typically measuring 2 cm^3. MRSI differs technically by the use of extra phase-encoding gradients to sample more abundant *k*-space data and the use of a frequency-encoding gradient to obtain metabolite spectra, and it differs practically by allowing analysis of more VOIs usually measuring 8 cm^3 along with the ability to analyze spectra from multiple inner voxels measuring 1 cm^3. Aside from practical considerations such as availability and acquisition time, the choice of MRS method is also based upon the particular clinical or investigational question. The faster SVS method has seen more widespread clinical implementation partly because it can use a shorter TE (generally around 35 ms vs. 140 ms in MRSI), which leads to less signal loss and therefore higher signal to noise ratio (SNR). The particular TE setting also influences the ability to evaluate spectra of particular metabolites with some (e.g., Glx and mI) better depicted at a lower TE, which has historically limited the assessment of associated pathologies (e.g., hepatic encephalopathy) to the SVS methods. The MRSI method maintains the potential for better spatial resolution and a more widespread survey of brain parenchyma along with the ability for voxel repositioning in the postprocessing stages. Such attributes can be advantageous in certain settings, particularly if the goal is lesion localization, for example, discerning epileptogenic foci and determining regions of greatest metabolic activity in tumor imaging.

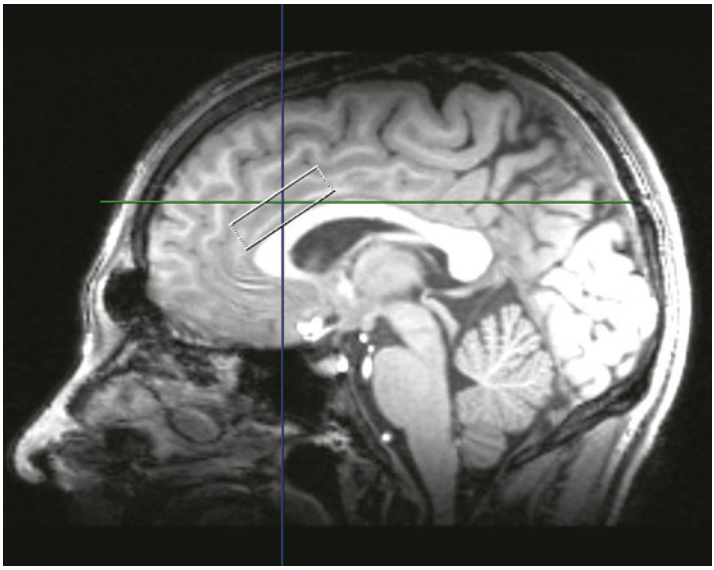

Fig. 1.10 MRS single-voxel sagittal image with voxel of interest (2.5 cm × 2.5 cm × 1.5 cm) placed in the anterior cingulate gyrus

Practical limitations to MRS such as acquisition time and preference for a very homogeneous B_0 have become less impactful with developments such as high-field MRI and special inhomogeneity-correcting "shim" gradient coils. The current clinical role of MRS remains primarily as a complement to conventional MRI, adding valuable information in diverse clinical settings, most extensively in tumor imaging. Investigational use of MRS has expanded its scope and has even led to the discovery of rare metabolic disorders in recent years (Figs. 1.10, 1.11, 1.12, and 1.13).

Functional MRI (fMRI)

Inherent to its application to dynamic neuroimaging, functional MRI (fMRI) has a number of unique considerations that distinguish it from the other MRI methods. Currently, the prevailing modality is known as blood oxygen level-dependent functional MRI (BOLD-fMRI), which takes advantage of regional changes in perfusion as a result of physiologic cerebrovascular autoregulation and the different oxygenation states of hemoglobin as the basis for MR contrast. The magnetic properties of hemoglobin vary such that oxygenated hemoglobin (HbO_2) causes increased local magnetic field inhomogeneities resulting in T2* lengthening (and higher signal intensity) relative to deoxyhemoglobin (Hb). After obtaining high-resolution structural images via a conventional protocol, BOLD-fMRI usually utilizes an EPI-based protocol for its acquisition speed and inherent sensitivity to T2* effects. With some

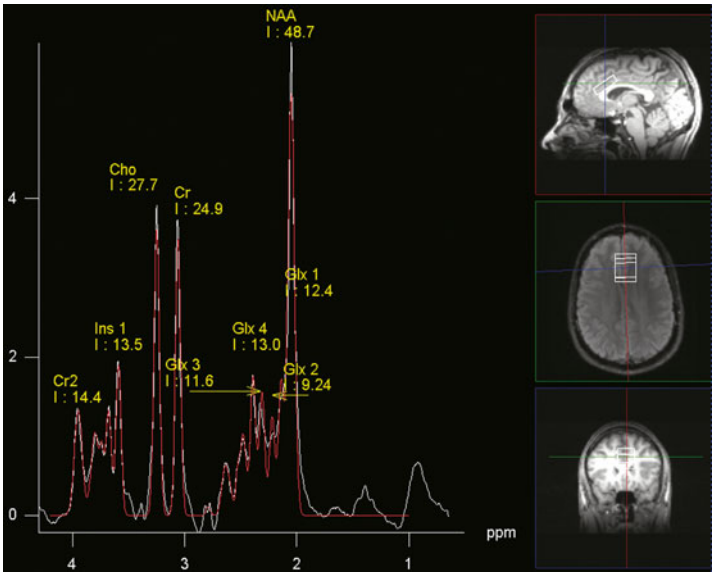

Fig. 1.11 Typical appearance of a nonpathologic spectra corresponding to the voxel of interest in Fig. 1.10

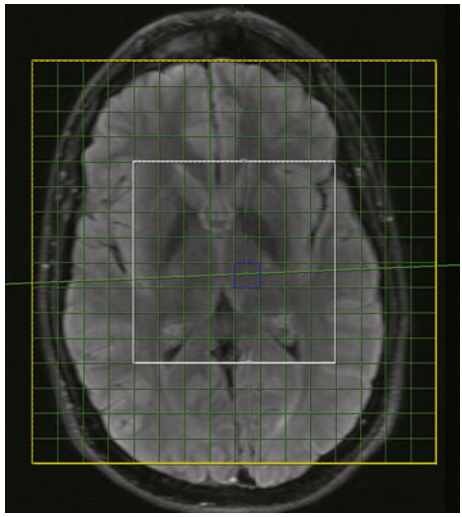

Fig. 1.12 MRS multivoxel image of a 49-year-old female obtained at 3 T, with an inner *white* grid encompassing the multivoxel region and the *blue* grid representing the voxel of interest (1 cm × 1 cm × 1.5 cm) selected in the thalamus

exceptions noted below, most fMRI acquisitions involve a particular event (i.e., task or stimulus), which results in elevated regional brain activity and extraction of the locally available oxygen from HbO_2. After an initial drop in HbO_2, the blood vessels exhibit compensatory vasodilation and increased blood flow, which soon yields an abundance of HbO_2 and the greater HbO_2 to Hb ratio amplifies local magnetic field

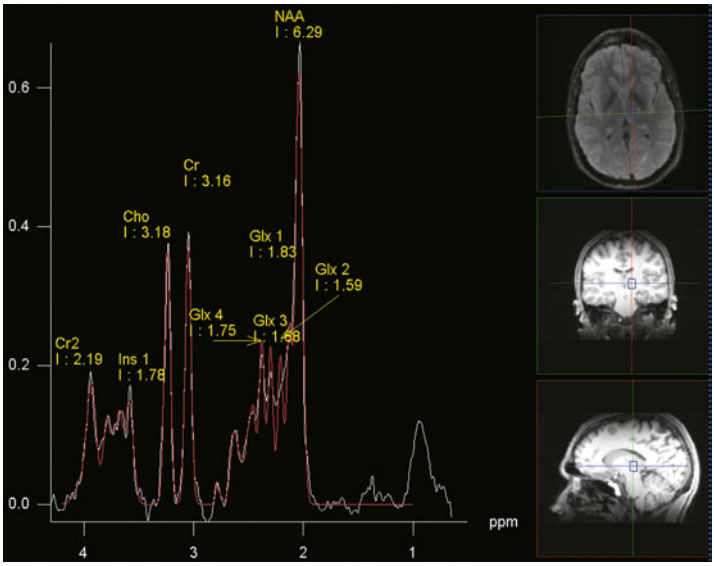

Fig. 1.13 Typical appearance of a nonpathologic spectra corresponding to the voxel of interest in Fig. 1.12

inhomogeneities (T2* effects). After being subjected to processing techniques and statistical analyses, it is this difference in T2* signal between the event and baseline states that allows for creation of meaningful maps of brain activity.

A critical element of both clinical and investigational fMRI acquisition is the choice of study design which will dictate the timing, order, and even presence (or absence) of various events involving the subject. The fMRI study designs usually fall into one of several categories including block design, event-related design, and mixed designs. Block design involves continuous signal acquisition while alternating blocks of events and (commonly) resting states and it is usually the preferred paradigm when simply detecting regions of sustained neural activity is sufficient. Event-related design involves interspersed signal acquisition after brief events and allows for characterization of transient variations in the BOLD response. Mixed designs combine elements of those above and allow for elucidation of brain regions involved in either transient or sustained activity. In other fMRI designs, specific events and subject participation are absent (i.e., no tasks or stimuli) and spontaneous BOLD activity is monitored and correlated with measurements from other modalities such as electroencephalography (EEG).

Compared with alternative functional modalities such as SPECT and PET, BOLD-fMRI boasts superior spatial and temporal resolution and does not require intravenous administration of exogenous substances or exposure to radiation. For these reasons along with the practical advantage of relatively easy integration into conventional MRI acquisitions, BOLD-fMRI has become the preeminent functional neuroimaging modality. Its investigational use is widespread in several facets of neurological, psychiatric, and psychological research and has resulted in the implication of the neural

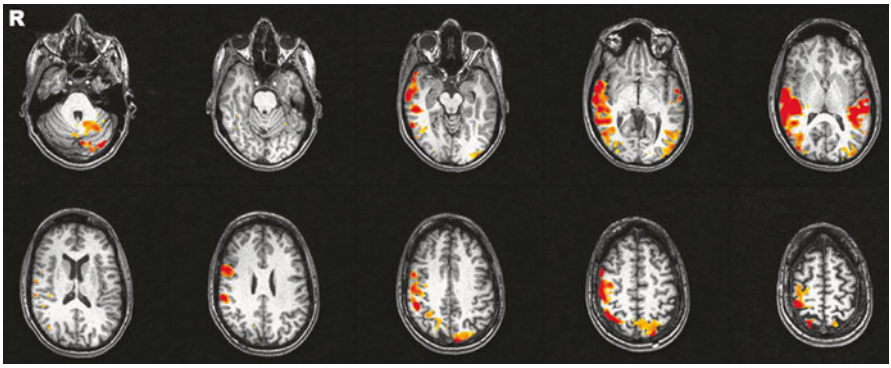

Fig. 1.14 3 T functional MRI involving auditory passive listening task demonstrating activation map of brain regions that are task-responsive overlaid on 3D T1 volume

substrates to numerous human processes. The clinical utility of BOLD-fMRI has been most consistently (and successfully) used for surgical planning, with the goal of mapping language, motor, and sometimes memory areas in attempts to preserve dominant areas of function during treatment.

As suggested by relatively sparse clinical applications, BOLD-fMRI does have a number of technical and practical limitations. In order to obtain useful images, it is necessary to minimize head movement for extensive periods of time and, in addition to excluding certain patient populations, this can limit motor function studies to simple tasks. The signal derived from the BOLD response is also relatively weak and the presence of multiple sources of noise (common to most MR acquisitions) results in a low contrast to noise ratio (CNR). It is for these reasons among others that processing methods and statistical analyses are necessary for creating the final BOLD-fMRI maps. These processing methods, both within an individual (e.g., realignment and slice timing correction) and between research subjects (e.g., normalization and smoothing), as well as the numerous statistical analyses can be cumbersome and underscore the challenging nature of BOLD-fMRI to the neuroimager. Even when the appropriate study design is chosen and the above elements are optimized, drawing causal relationships between events and brain activity can be flawed and findings must be interpreted carefully. Therefore, particularly in its investigational use, it may be best utilized as a group-level analytical tool to complement additional testing modalities. Despite these limitations, BOLD-fMRI will likely remain the dominant functional neuroimaging method for many applications. Technological developments in BOLD-fMRI have dwindled in recent years, but considerable efforts continue in refining acquisition guidelines and expanding its applications with prospects of improving clinical uses for such pathologies as Alzheimer disease, dyslexia, and schizophrenia, among others (Fig. 1.14).

High-Field MRI

Partially prompted by its value in advanced modalities, high-field MRI (i.e., 3 T and higher) has become commonplace not only in research, but increasingly within clinical neuroimaging also. The potential advantages with these higher magnetic fields include improved signal strength, which enables increased spatial (and spectral) resolution and decreased acquisition times. Some of the benefits of high-field MRI have already become clinically relevant, for example, the effective utilization of the previously described advanced techniques of DWI, MRS, and fMRI. However, some important considerations arise including the altered relaxation time constants of the various tissues within the body. T1 relaxation lengthens significantly in most tissues and the T1 contrast between tissues is actually diminished because the curves of their time constants (i.e., their signal intensities) converge. T2* effects are also enhanced at high-field strengths, with mixed consequences as previously specified. A potentially concerning safety issue associated with higher field strengths is a greater deposition of energy in the form of heat, a concept known as the specific absorption rate or SAR. As seems to always be the case in MRI, several adaptations have been developed to address such limitations and the use of high-field technology should continue to expand the potential applications of many of the MRI techniques.

Emission Tomography

In contrast to the MRI techniques addressed in detail thus far, SPECT and PET begin with the requisite administration of exogenous agents, namely radiopharmaceuticals. Radiopharmaceuticals are usually composed of a compound that interacts in a specific manner with the body and a radioactive label (i.e., isotope) that decays and emits radiation on the gamma-ray spectrum (either directly or indirectly). This radiation is detected by scintillation crystals and eventually yields the final imaging product in the form of 2D or 3D image data sets, with the number of radiation "counts" in each pixel or voxel essentially representing probability maps of the biologic distribution. The differences between SPECT and PET are primarily based upon the categories of radiopharmaceuticals used as well as in some components of the corresponding detection hardware. As in all neuroimaging, while cost and availability are always considerations the ultimate deciding factor for the use of SPECT or PET are the biological considerations underlying the clinical or investigational context.

SPECT uses a variety of radiopharmaceuticals that directly produce photons (i.e., discrete gamma-rays) that are emitted around the subject and must traverse collimators before being measured by a gamma-camera system. The collimators are usually composed of perforated lead constructs that impart spatial information by narrowing the direction of photon travel (i.e., the field of view). A number of modifications to collimator and gamma-camera design have been developed over the years, leading to improvements in detection sensitivity and spatial resolution. Compared with PET, SPECT advantages include being relatively inexpensive and widely available as well

as the use of radiopharmaceuticals with long half-lives allowing the possibility of transport from the production facility to distant centers.

Historically, the most commonly used radiopharmaceuticals in clinical SPECT neuroimaging have included several "brain-specific" lipophilic compounds that cross the blood–brain barrier and are generally converted to hydrophilic compounds that become trapped intracellularly for a period of time. The distribution of these compounds, including technetium exemetazine (Tc99m-HMPAO) and technetium bicisate (Tc99m-ECD), parallel cerebral blood flow. While they have similar clinical uses, these radiopharmaceuticals differ in a number of ways including radiolabeling procedure time, required dosage, peak activity (and time to imaging) as well as degree of first pass extraction and clearance rate. The end product of such SPECT neuroimaging is a depiction of perfusion with observational windows that can begin within seconds and last hours or even days, potentially allowing for repeat acquisitions as needed. Such depiction of perfusion patterns has found utility in a number of clinical settings. For example, it can be used to help localize epileptogenic foci in patients with normal structural MRI and nonlocalizing EEGs. Other applications include various dementias and neurodegenerative diseases as well as stroke and determination of brain death (the latter can also be done via static "planar" scintigraphic imaging). A variety of other radiopharmaceuticals can be used in clinical SPECT, including thallium-201, which can help differentiate radiation necrosis from recurrent tumor and toxoplasmosis from lymphoma. Investigational uses of SPECT have included evaluation of numerous neurologic and psychiatric disorders such as schizophrenia, attention deficit disorders, and both illicit and therapeutic drug effects.

PET is characterized by the use of radiopharmaceuticals with special isotopes that decay with the formation of positrons, which are subatomic particles that have the same mass but opposite charge of electrons. When these positrons encounter an electron they collide and undergo annihilation, which yields the production of two photons (i.e., gamma rays) of equal energy that are emitted in opposite directions. Instead of the physical collimators used in SPECT to provide spatial information, PET takes advantage of the annihilation by recording energy from the photon pairs in their opposing trajectories, known as coincidence detection. This "electronic collimation" yields greater detection sensitivity and spatial resolution compared with SPECT. Independent PET imaging is becoming scarce particularly in the clinical setting, as the hydrid modality of PET-CT is increasingly the norm. The contiguous acquisition with coregistration of both structural and functional data seen in PET-CT not only offers the obvious benefit of accurate anatomic correlation of the functional information, but also has other advantages such as more precise correction for an entity called attenuation, which can underestimate the number of counts particularly in anatomically deeper tissue.

The principal radiopharmaceutical ubiquitous in clinical PET is [^{18}F]-flourodeoxyglucose (FDG), whose behavior and distribution reflects the process of cellular glucose uptake mirroring cerebral metabolism. Gray matter typically exhibits avid FDG uptake, and the cerebellum is sometimes used as a reference standard in interpreting the degree and patterns of cerebral metabolism. The end

product of FDG-PET (and PET-CT) is the production of relatively sensitive depictions of metabolic patterns that reflect a variety of processes and can be used in a number of neuroimaging settings that overlap considerably with those in SPECT. Investigational use of PET has also increasingly included sophisticated analytical methods that involve monitoring radiopharmaceutical infusion rates and estimating compartmental distribution, allowing for depiction of quantitative data. While PET offers several advantages over SPECT, including the better spatial resolution and a more accurate depiction of cerebral metabolism, it is not without its limitations. The requisite positron-emitting isotopes undergo rapid radioactive decay, with half-lives of no longer than a few hours. While this property keeps the radiation dose to reasonably low levels, it also means that their production usually requires close proximity to a cyclotron (particle accelerator). Difficulties in interpretation have also limited FDG-PET in some settings, including CNS tumor imaging where the levels of uptake seen in many malignancies are often obscured by the background uptake in the normal gray matter. In both SPECT and PET, the use of radiopharmaceuticals also necessitates the maintenance of quality control standards and informed precautions to minimize potential toxicity and radiation exposure.

Emission tomography is partially being supplanted by fMRI for many applications in functional neuroimaging, though the viability of SPECT and PET will likely be maintained through the continued development of unique radiopharmaceuticals. While the properties of FDG remain useful in several settings, a number of other radiopharmaceuticals have been developed for PET, which reflects such processes as oxygen consumption, cerebral blood flow, and tumor-specific metabolism; but, these are mostly relegated to the investigational realm at present. Perhaps the most promising radiopharmaceuticals are the various classes of radiolabeled molecular probes capable of illuminating the status of various pathologic and endogenous entities, including those within neurotransmitter pathways. Several of these novel probes have been recently implemented in clinical settings, most notably those targeting amyloid plaque and dopamine transporters to help discriminate Alzheimer disease and Parkinson disease, respectively. Numerous other molecular probes are under investigational use, some of which will likely be clinically translated in the near future.

Conclusions and Future Outlook

Benefitting from the visionaries that preceded us, we are fortunate to have the ability to image what early neuroscientists could only imagine. Building upon the earlier groundbreaking work, the refinements and novel contributions made by modern scientists have taken neuroimaging to an incredible clinical frontier. While numerous imaging modalities have provided specific information, none has been more versatile than MRI. The modifiable nature of MRI is perhaps its greatest attribute, allowing unprecedented influence by neuroimagers and becoming firmly entrenched in both clinical and investigational realms. Molecular neuroimaging, with emission tomography at the forefront, is evolving and will undoubtedly uncover hidden secrets in

neuroscience while helping diagnose and guide treatments for an array of diseases. Hybrid technologies such as PET-MRI, currently only found in a few institutions, can provide a plethora of structural and functional information in a single configuration and may eventually find widespread implementation. Few could have predicted how far neuroimaging has come since the acquisition of the first human head MRI and even fewer still could have predicted exactly how far neuroimaging has come since its advent at the turn of the twentieth century. Assuming a similar rate of technological progress, predicting exactly what the future holds for neuroimaging is virtually impossible, but there is little doubt that it will be fascinating. Regardless, neuroimagers themselves must remain adaptable and open to interdisciplinary collaboration as paradigm-shifting technologies inevitably arise.

References

1. Fratti P, et al. Neuroanatomy and cadaver dissection in Italy: history, medicolegal issues and neurosurgical perspectives. J Neurosurg. 2006;105:789–96.
2. Moon K, Filis AK, Cohen AR. The birth and evolution of neuroscience through cadaveric dissection. Neurosurgery. 2010;67(3):799–809; discussion 809–10.
3. Leeds NE, Kieffer SA. Evolution of diagnostic neuroradiology from 1904 to 1999. Radiology. 2000;217:309–18.
4. Dandy WE. Ventriculography following the injection of air into the cerebral ventricles. AJR Am J Roentgenol. 1919;6:26–36.
5. Dandy WE. Roentgenography of the brain after the injection of air into the spinal canal. Ann Surg. 1919;70:397.
6. Moniz EL. L'Angiographiecerebrale. Paris: Masson & Cie; 1934; pp. 142–214.
7. Brenner DJ, Hall EJ, Phil D. Computed tomography—an increasing source of radiation exposure. N Engl J Med. 2007;357:2277–84.
8. Brant-Zawadzki M, et al. NMR demonstration of cerebral abnormalities: comparison with CT. AJR Am J Roentgenol. 1983;140:847–54.
9. Christie DA, Tansey EM, editors. Making the human body transparent: the impact of nuclear magnetic resonance and magnetic resonance imaging. London: Wellcome Institute for the History of Medicine. 1996; http://www. history. qmul.ac.uk/ research/modbiomed/Publications/ wit_vols/44824.pdf. Accessed 6 Jan 2012.
10. Abraham T, Feng J. Evolution of brain imaging instrumentation. Semin Nucl Med. 2011;41(3):202–19.
11. Gerstein M. Purcell's role in the discovery of NMR: contingency versus inevitability. Am J Phys. 1994;62(7):596–601.

Chapter 2
Morphometric Analyses in Movement Disorders

Bogdan Draganski and Ettore A. Accolla

Introduction to Magnetic Resonance Imaging (MRI) Techniques

With the aim of accurately characterizing the structural brain changes associated with neurological disorders, the spectrum of MRI techniques implemented in neuroimaging research is increasingly growing. Currently, MR data is acquired in high resolution, with optimal gray/white matter contrast and potential to provide information about white matter fiber tract orientation and integrity. Recent advances include semiquantitative and quantitative structural MR imaging, offering insight into specific brain tissue properties.

T1-Weighted Imaging

Current morphometry studies rely mostly on relative changes in brain volume and cortical thickness measured on T1-weighted images, making them dependent on MR scanner hardware, which impairs standardization for wide clinical use. T1-weighted images are widely used in brain morphometry, because they provide sufficient

E. A. Accolla (✉)
Campus Virchow Klinikum, Charité University Medicine Berlin, Berlin, Germany
e-mail: ettoreaccolla@gmail.com

Department of Neurology, Campus Virchow Klinikum, Charité – University Medicine Berlin, Augustenburger Platz 1, 13353 Berlin, Germany

B. Draganski
Max Planck Institute for Human Cognitive and Brain Sciences, Centre Hospitalier Universitaire Vaudois (CHUV), Leipzig, Germany
e-mail: bogdan.draganski@gmail.com

Mind Brain Institute, Charité and Humboldt University, Berlin, Germany

E. A. Accolla · B. Draganski
LREN, Département des Neurosciences Cliniques, Centre Hospitalier Universitaire Vaudois (CHUV), Université de Lausanne, Rue du Bugnon 46, 1011 Lausanne, VD, Switzerland

F. B. Nahab, N. Hattori (eds.), *Neuroimaging of Movement Disorders,*
Current Clinical Neurology 44, DOI 10.1007/978-1-62703-471-5_2,

contrast between gray and white matter in most cortical areas [1]. However, there is significant age-dependant contrast decrease in subcortical structures with high iron content (e.g., pallidum) that limits the reliability of automated tissue classification algorithms in these areas particularly relevant to movement disorders.

Diffusion-Weighted Imaging (DWI)

Diffusion-weighted imaging (DWI) is sensitive to Brownian motion of molecules, thus utilizing proton behavior in brain tissue water. The most wide-spread DWI-based technique—diffusion tensor imaging (DTI), describes the restricted brain tissue water diffusion properties in three ways: (1) by predominant diffusion directions, (2) by degree of anisotropy (fractional anisotropy—FA) , or (3) by magnitude of diffusion (mean diffusivity—MD) [2]. Tissue loss is commonly associated with MD increases due to enlarged extracellular spaces, while FA decreases are caused by reduction in cellular boundaries hindering diffusion. FA/MD estimates in gray matter are thought to represent variable densities of myelinated axons since the water diffusion in gray matter is almost negligible.

Relaxometry-Based Multiparameter Mapping

Relaxometry comprises advances in quantitative mapping of magnetization transfer, T1- and $T2^*$-relaxation based on well-defined biophysical models. Quantitative MRI reproducibly maps the physical properties of water that govern MR contrast. The major contrast parameters analyzed are longitudinal relaxation rate ($R1 = 1/T1$), magnetization transfer (MT) saturation, and effective transverse relaxation rate ($R2^* = 1/T2^*$), as these reflect water content, myelination, and iron concentration [3–5]. Beyond serving as surrogate parameters, they depend on microscopic tissue properties of brain tissue. The parameter maps exhibit considerable regional variability: the largest variation is usually due to differences between gray and white matter. In addition, a comparative study demonstrated advantages of using MT saturation maps for tissue classification in basal ganglia and thalamus due to superior gray/white matter contrast [5].

Computational Neuroanatomy Methods

Computational neuroanatomy comprises diverse (semi) automated volume-, surface-, and shape-based techniques developed to investigate brain structure in cross-sectional and longitudinal study designs. We provide short descriptions of the principle methods in order to help the reader with interpretation of occasional discrepancies reported in the literature.

Data Processing

Volume-Based Methods (Volumetry)

Manual and semiautomated region-of-interest (ROI) approaches dominated the field of volumetry until computational neuroanatomy offered feasible and unbiased ways for performing whole-brain analyses. Although widely accepted in the medical community, manual 2- or 3D ROI measurements are labor intensive, subject to interrater variability, and potentially insensitive to concomitant changes in other brain regions.

Voxel-based morphometry (VBM) in the framework of Statistical Parametric Mapping (SPM, http://www.fil.ion.ucl.ac.uk/spm) represents a fully automated approach for volume assessment within/between cohort(s). The name is derived from the smallest spatial unit in the MR data—voxel, introduced in order to represent the 3D extent of a 2D pixel. VBM includes an iterative algorithm combining voxel-by-voxel classification (i.e., segmentation) of MR data into different tissue classes—gray matter, white matter, cerebrospinal fluid, and nonbrain voxels (e.g., skull) with registration to a common anatomical space (i.e., "spatial normalisation"). A criterion for segmentation is the intensity of a particular tissue type constrained anatomically by a priori existing tissue-specific probability maps. Subsequently, tissue-specific segments are corrected (i.e., "modulated") for the linear and nonlinear effects of the spatial registration by using the Jacobian determinants in order to preserve the initial volumes. Following this step, the segments are low-pass filtered by convolution with an isotropic Gaussian kernel (i.e., smoothing) [6].

Surface-Based Methods

Following a segmentation step with computation of tissue class surfaces similar to the VBM, white matter surfaces can be expanded out to the gray matter/cerebrospinal fluid boundary using surface deformation algorithms. This procedure permits close matching of gray matter and white matter boundaries, such that cortical thickness can be calculated on the basis of the distance between surfaces. Image registration can be performed either in a canonical manner or using "inflated" spherical representations of the brain and surface-based coordinate systems. Subsequently, cortical thickness data are subject to spatial smoothing for statistical analysis [7].

Statistical Analyses

Imaging data is usually analyzed in the framework of Random Field Theory following the General Linear Model. The most frequently used mass-univariate models, based on least-square fitting of a General Linear Model at each voxel provide a generic

framework in which signal at each voxel is explained by a linear combination of a priori defined variables. The advantage of using mass-univariate methods is that they make spatially localized inferences that explain the disease or the clinical correlates of the particular disorder. Depending on the data representation (i.e., voxel-based or surface-based), the algorithms compute voxel- or vertex-based statistical parametric maps, which identify brain regions containing significant differences of gray matter volume or cortical thickness. Depending on the hypothesis and the questions to be addressed, one can use *t*-tests, one-, two-way independent analysis of variance (ANOVA), or multiple regression analysis. The statistical designs include a global variable (e.g., the total intracranial volume) as a covariate in order to control for global differences and focus on the regional differences in the gray or the white matter.

Recent developments in multivariate analysis of brain images allow for the classification of individual anatomical data based on prelearned characteristic patterns using support-vector machines (SVMs) [8].

SVMs are based on principles in the context of machine learning theory, where individual MR images are treated as points located in a high-dimensional space. SVM requires a measure of similarity between each pair of images. In principle, images of subjects within the same diagnostic group should be more similar to each other, than they would be to images of subjects from another group. Linear SVMs work by finding the optimal separating hyperplane that maximizes the margin between the groups. After training a SVM, there will be a number of points in the training data, which touch the hyperplanes defining the margin. The optimal separating hyperplane can be described as a simple function of these points (known as "support-vectors"). During training, the SVM assigns a specific weight to every scan reflecting the importance of that scan for group separation. Our group has further developed existing methods and applied supervised classification on data from patients with neurodegenerative diseases and healthy subjects [9].

The optimal implementation of classification methods relies on a careful study population selection, and on the minimization of variables of no interest both in patients' and control groups. Other methods are based on the Gaussian mixture model and principal component analysis (GMM/PCA). The GMM/PCA approach extracts subject groupings from the data. Therefore, this approach does not depend on a priori knowledge of subgroups, but uses a probabilistic classification method to find the probability that a particular subject belongs to one or another subgroup. Patterns are assumed to be similar within a subgroup, but vary between subgroups [10, 11].

Application of Morphometric Analyses to Movement Disorders

The clinical routine in movement disorders often requires visual inspection of MR images by a neuroradiology specialist. The differential diagnosis of primary versus secondary forms of disease or MR signal abnormalities due to metabolite

deposition are among the most frequent referral reasons, to name a few. Computational neuroanatomy offers an unbiased way for assessment of brain structure and tissue property; however, the current status of data processing and statistical analysis limits its feasibility as a tool for diagnostic work-up.

Idiopathic Parkinson Disease (iPD)

A diagnosis of idiopathic Parkinson disease (iPD) is primarily made based on clinical criteria. Structural MRI is mainly required for differentiation from secondary forms. Nevertheless, research in the field of computational anatomy aimed to shed light on basic pathophysiology mechanisms of iPD in order to allow for early diagnosis by investigation of the relationship between brain structure and clinical signs.

Despite controversial results regarding the pattern of changes, early volumetric studies in iPD found increased age-dependant atrophy in patients when compared with controls [12–14]. Current computational anatomy research focuses on three main areas: (1) the development of MR sequences allowing for optimal delineation of the boarders of substantia nigra (SN); (2) the investigation of the differential pattern of brain structure changes associated with either motor or nonmotor symptoms in iPD; and (3) the validation of computational anatomy as noninvasive diagnostic tool and predictive biomarker in early stages of disease [15].

Substantia Nigra Delineation and Connectivity

Considering the fact that loss of dopaminergic neurons is a hallmark of iPD, a considerable effort has been devoted to develop MR protocols allowing for optimal delineation and subsequent volumetric estimation of the SN. Volumetric ROI analysis based on quantitative T1 images and manual segmentation revealed significantly smaller SN volumes and a relative contrast reduction in iPD compared with controls [16]. The iron deposition in SN with increase in T2 signal motivates the usage of this technique for SN assessment resulting in particularly good correspondence to histology when applying T2*-imaging protocols [17–21]. Some encouraging results have also been obtained with fast spin-echo T1 sequences [22, 23], including measurements based on MT effects [16], which take advantage of the higher contrast offered by neuromelanin for segmenting SN from the surrounding tissue.

Recent studies investigating anatomical connectivity features of SN have demonstrated a lower connectivity probability between SN and putamen/thalamus in iPD using diffusion-based tractography. Even if not reaching statistical significance, the authors report FA reductions in the SN of iPD patients, corroborating previous findings [24]. Combining R2* and FA in the whole SN has thus far yielded the best results [25]. Unfortunately, these methods rely on a manual segmentation of the SN, which is by definition time consuming and operator dependent.

Differential Patterns of Brain Structure Changes

From a theoretical point of view, iPD patients should share a common pattern of neurodegeneration. Conversely, the existence of differential patterns of brain changes in the presence of common underlying pathophysiological mechanisms would point to a heterogeneous nature of iPD and will substantiate attempts of a novel nosological classification in clinical subtypes.

Despite the accumulating knowledge about basic principles of basal ganglia organization, the accurate characterization of the link between brain structure changes and specific symptoms has proved to be challenging. The structure–function relationship gains on relevance, particularly when trying to understand and improve recent advances in patient's treatment offered by deep brain stimulation (DBS). This could be exemplified by the good response of rigidity and tremor to DBS, contrasting the limited effect of stimulation on balance, gait impairment, and cognitive functions.

Morphometric studies have proved to be useful when addressing specific pathophysiological questions by providing robust results mainly depending on the appropriate selection of study populations and clinical evaluations. For example, the presence of gray matter loss in parieto-temporal association areas was demonstrated to be related to higher order discriminative sensory dysfunctions, thus providing novel and relevant insight on the origin of the movement slowing typical for Parkinson disease [26]. Along these lines, Kassubek et al. [27] showed a correlation between the amplitude of resting tremor and contralateral thalamic gray matter density leaning on a theoretical assumption that the disruption of cerebello-thalamo-cortical loops is linked to resting tremor in iPD. Similarly, frontal gray matter volume reduction is associated with freezing of gait and dysexecutive symptoms corroborating the idea of movement planning deficits in iPD [28, 29]. While the majority of VBM studies in iPD show robust results, there is some controversy, which underscores the difficulty of standardizing study populations.

Concerning correlation between brain structure changes and nonmotor signs in iPD, a recent study demonstrated association between white matter loss in the right frontal lobe and depressive symptoms in iPD patients [30]. Despite limited number of observations, VBM findings confirm similar findings in major depression [31] and AD, [32] to support the evidence for limbic system involvement in iPD. Depression and apathy are invalidating and highly prevalent symptoms in the iPD population, and are a direct part of the disease rather than of reactive origin, as proved by epidemiological studies [33].

Cognitive dysfunction develops in advanced disease stages of iPD. Disentangling the neural correlates of dementia in iPD has an impact not only for this disorder, but also for understanding normal cognition. According to a recent VBM study, there is bilateral gray matter loss in the frontal lobes extending posteriorly to the lateral, medial temporal lobes, and occipital cortex in iPD with dementia (PDD) [34]. Atrophy of hippocampus and para-hippocampal gyrus was observed in Alzheimer's Disease (AD), but not in PDD; thus, demonstrating a different

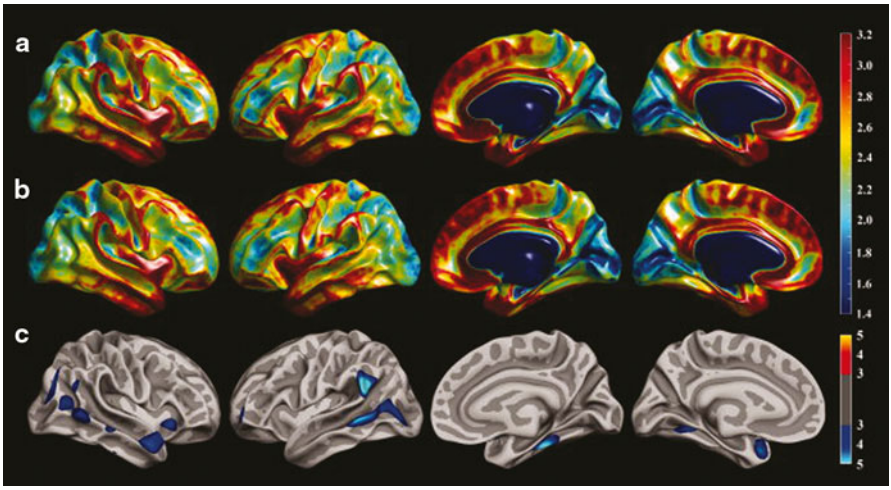

Fig. 2.1 Average cortical thickness and statistical results rendered on semiinflated white matter surface. The average regional cortical thickness of healthy controls (**a**) and patients with Parkinson's disease (PD) (**b**) are expressed as color scale. **c** The cortical areas where the thickness is thinner in patients with PD than that of controls are expressed as cold colors. The *upper* color scale bar shows cortical thickness (mm) and the *lower* color scale bar shows logarithmic scale of *P*-values (− log10P) [43]

pattern of neurodegeneration between the two syndromes. The presence of hippocampal involvement in PDD is still a matter of debate, and even most recent studies show controversial results [35, 36]. Studies making use of global brain structure metrics—the semiautomated assessment of white matter hyperintensities and total brain volume failed to show their significance as predictor of cognitive dysfunction in a large cohort of iPD [37, 38]. Looking for regional changes, VBM findings revealed increased regional volume loss in iPD patients with early dementia compared with those developing late dementia. The presented results are also interesting from a methodological point of view due to the fact that findings with and without adjustment for the interpolation effects of spatial normalization ("modulated" versus "unmodulated") in the same cohorts showed no correlation, thus confirming the need to interpret "unmodulated" results as by-products of registration errors [39].

Beyond this, whole-brain VBM and ROI studies have demonstrated right fusiform and superior temporal gyrus white matter involvement as well as limbic and striatal atrophy correlating with cognitive abilities in demented and nondemented iPD patients [40–42]. The cortical thickness analysis in nondemented iPD patients revealed a widespread pattern of cortical thinning following the distribution pattern of neocortical Lewy bodies (Fig. 2.1) [43]. The investigation of subcortical structures showed a reduction of caudate volume associated with a degeneration of the dorso-lateral-prefrontal-circuit [36].

Dementia with Lewy Bodies (DLB)

A promising future direction in computational anatomy is the intention to create reliable neuroimaging biomarkers for early differentiation between DLB and dementia/parkinsonism. Contrary to ROI analyses showing volumes and atrophy rates in DLB within the normal range, the whole-brain comparison between DLB and demented iPD patients revealed greater regional volume loss in temporal, parietal, and occipital lobes for DLB patients despite the similar degree of dementia [39]. Interestingly, the pattern of volume loss in DLB was different from the frontal and temporal regional atrophy present in AD patients. According to another VBM study, DLB patients had significantly reduced right-sided fronto-temporal gray matter volume compared with iPD patients [44]. DLB patients show a characteristic pattern of white matter involvement with FA reductions in posterior regions correlating with poor performance in visuo-spatial tasks [45].

The overall conclusion from comparative morphometry studies in iPD, including AD cases, confirms the notion based on clinical experience that DLB and iPD with dementia might represent subtypes of the same spectrum of disorder with distinct patterns of brain structure changes reflecting dysfunction in specific cognitive domains.

Establishing Brain Morphometry as a Noninvasive Diagnostic and Predictive Biomarker in Early Stages of Disease

Neuropathological studies confirm the notion that at the time of first clinical signs, the underlying neurodegenerative process has been progressing for at least 10 years [46]. This motivates the continuous interest to investigate iPD-specific brain atrophy patterns bearing the theoretical possibility of high diagnostic and predictive value. The development of sensitive biomarkers at a very early clinical stage or even before symptom onset could pave the way to measure the efficacy of putative disease-modifying treatments. The assumption here is that neuroimaging can capture correlates of specific neuronal loss in early iPD.

Considering the fact that olfactory impairment is one of the first clinical signs in iPD, VBM studies focused on correlation between the degree of olfactory impairment and brain structure. Early iPD patients showed a trend for positive correlation between olfaction scores and gray matter volume in the right piriform gyrus, while moderately advanced iPD patients showed a positive correlation between olfaction and right amygdala volume [47]. Along these lines, a ROI study using DTI and olfactory testing differentiated between early-stage iPD patients and controls based on reduced FA in the anterior olfactory region [48]. Whole-brain studies in early stages of IPD demonstrated FA and MD changes in the frontal lobe white matter indicating an early microstructural damage [49, 50]. Considering the early involvement of brainstem

structures in iPD, a ROI study showed significant volume reduction in the rostral medulla oblongata and the caudal pons [51].

A common limitation of previous studies aiming at preclinical diagnosis is the inclusion of patients even at the very early stages of motor dysfunction, which could pose a hurdle to start neuroprotective drug interventions.

Atypical Parkinsonisms

Progressive supranuclear palsy (PSP) and corticobasal syndrome (CBD) are neurodegenerative diseases pathologically classified as tauopathies. The differential diagnosis is based mainly on clinical criteria and lacks the required specificity and sensitivity. Multisystem atrophy, in its two clinical manifestations, with cerebellar (MSA-C) or parkinson-like (MSA-P) phenotype paralleled by prominent autonomic failure belongs neuropathologically to the family of synucleinopathies, but shares with PSP and CBD a more rapid progression to severe disability than iPD [52]. In early stages, the clinical manifestations of atypical parkinsonisms can mimic iPD and the differential diagnosis poses a challenge even to an experienced movement disorders specialist. Hence, numerous MR studies have attempted to find subtle morphometric differences allowing for earlier and more accurate diagnosis.

Progressive Supranuclear Palsy (PSP)

Although many studies reported successful differentiation of PSP from other forms of parkinsonism in the advanced stages of disease, there is still little evidence for an added diagnostic value of computational anatomy studies in the early phase. Volumetric and VBM studies confirm neuropathological findings with a prominent involvement of mesencephalic structures [53, 54]. The extent of cortical atrophy involves the medial frontal and lateral middle frontal gyri, the insular region comprising frontal opercula, SMA, and left mediotemporal areas [55]. The reported diagnostic accuracy distinguishing between iPD and PSP shows 84.3 % sensitivity and 79 % specificity using clinical criteria as a gold standard [56].

Corticobasal Degeneration (CBD)

Considering the substantial divergence between diagnosis based on clinical and neuropathology criteria, the existence of CBD as a clinico-pathological entity is still debated [57]. In clinically defined CBD cases, visual inspection of clinical scans can be enough to observe the typical asymmetric atrophy involving the frontal and parietal lobes. Accordingly, VBM studies in CBD showed a specific pattern of gray

matter volume reduction involving the bilateral premotor cortex, superior parietal lobules, and striatum [58]. Another piece of evidence supporting the notion about differential physiopathology of cognitive decline in atypical parkinsonism is brought by a combined pathology-VBM study showing that subcortical white matter volume reductions in PSP are the strongest predictor of cognitive impairment opposed to cortical gray matter changes in CBD [59]. Using an ROI approach, Rizzo et al. [60] computed apparent diffusion coefficient (ADC) maps from DWI data to differentiate between iPD, CBD, and PSP (Richardson syndrome phenotype). ADC changes in putamen differentiated between typical and atypical PD forms, but failed to distinguish between CBD and PSP. Interestingly, the calculated hemispheric symmetry ratio demonstrated 100 % sensitivity and specificity for accurate differentiation of CBD from PSP and iPD patients.

Multisystem Atrophy (MSA)

A number of brain structure changes in MSA—most notably putaminal atrophy—have been reported in the literature. Novel in the field of automated morphometry is the combination of VBM and voxel-based quantification (VBQ) analysis. This approach was employed to differentiate between MSA-C and MSA-P variants of MSA demonstrating more severe infratentorial volume loss in MSA-C with pronounced T2-relaxation reduction in cerebellum and brain stem [61]. Using VBM and a prospective design, Brenneis et al. [62] found widespread cortical and subcortical atrophy in MSA as opposed to normal findings in iPD. In addition, MSA patients showed a positive correlation between cortical volume loss and disease duration, and a negative correlation in the striatum. The author's supposition here was that early basal ganglia atrophy drives late onset cortical atrophy.

Diffusion parameters such as ADC raised hopes for deeper insight in the pathophysiology of atypical parkinsonism. In a recent study, ADC parameters in preselected ROIs differed between iPD, MSA, and PSP patients. In particular, ADC values in the pons, middle cerebellar peduncle, cerebellar white matter, and cerebellar dentate nucleus were higher in MSA than in PSP and controls; in PSP, they seemed to be higher in midbrain, globuspallidus, and caudate [63].

Most VBM studies are conducted at a group level and, although providing valuable information about the disease progression, are not suitable for studying the single-subject case. Manual scalar assessment of brain stem morphology characteristics have often been adopted with success, achieving differentiation of PSP from MSA with a sensitivity of 100 % and specificity of 90.5 % on the single-subject level, but suffer some operator-dependent limitations, or are extremely time consuming [64–66]. A recent study attempted to overcome these limitations by classifying quantitative structural whole-brain imaging data by employing a support vector machine approach [67]. This method proved to be quite promising, especially for differentiating PSP from iPD, with up to 96.8 % accuracy. In MSA versus iPD, an accuracy of 71.9 % was achieved; sensitivity, however, was low with 36.4 %. Interestingly, the

support vector machine could not differentiate between iPD and healthy subjects, which, according to authors' opinion, is in line with the sparse results of previous VBM studies in iPD patients without dementia. This study demonstrates the need to combine established and novel computational techniques in order to achieve unbiased and reproducible results. For infrequent conditions such as atypical parkinsonism, the aim is to extend the observations to larger cohorts by taking care to reduce hardware- and operator-dependent biases.

Dystonia

The precise pathophysiological mechanisms underlying the occurrence of primary torsion dystonias (PTD) remain elusive. By definition, the brain structure in idiopathic dystonia is normal on neuroradiology inspection. The involvement of basal ganglia initially suggested by lesion studies and theoretical models were confirmed by subsequent morphometric MR studies [68]. In recent years, computational anatomy findings confirmed the extent of structural changes to other brain areas, most notably sensorimotor cortex and cerebellum.

Evidence arising from lesional and neurophysiology studies in humans and animals implicate the putamen for its critical role in the pathogenesis of dystonia [69, 70]. A bilateral increase in putaminal gray matter was demonstrated in patients with blepharospasm (BLS) [71, 72], focal hand dystonia [71], cervical dystonia, spasmodic dysphonia, and musician's dystonia [73]. However, there are controversial results, particularly in BLS [74] and cervical dystonia [75, 76] reporting volume decreases (Table 2.1). A potential explanation was suggested by a recent study in musician's dystonia. Putamen gray matter volumes in professional pianists were increased in the presence of dystonia and correlated inversely with skilled piano playing performance even in healthy subjects. Immobilization of the affected hand in dystonic musicians was accompanied by gray matter putamen volume reduction promptly inversed after some weeks of practice [77]. Altogether, the published studies point mainly toward a volume increase rather than decrease, but the reason of such inconsistencies is hard to explain. We favor the idea of the occurrence of abnormal adaptive processes, with aberrant plasticity and variations in putamen volume in either direction, the underlying pathological and synaptic mechanisms not being sufficiently accessible to current neuroimaging techniques.

The involvement of brain structures other than putamen is backed by evidence for gray matter increase in the right internal globus pallidus [79], thalamus, caudate, superior temporal lobe, and left cerebellum [74]. Focal hand dystonia is associated with bilateral thalamic volume reductions [82, 83] and bilateral accumbens and internal globuspallidus increases [76]. Concerning DWI- derived parameters, studies in dystonic patients demonstrate FA reductions in corpus callosum, pallidum, and caudate [84]. According to Fabbrini et al. [85], there is decreased MD in the caudate, and putamen unilaterally paralleled by bilateral thalamic FA decrease in cervical dystonia. An increase of cerebellar gray matter volume has consistently been observed in focal

Table 2.1 Voxel-based morphometry (VBM) studies of primary dystonias are shown according to type of dystonia. (From [78])

Blepharospasm	16/16	Put (↑)		IPL (↓)		Etgen et al. [72]
Blepharospasm	11/14	Caud (↑) Put (↓)	Hem (↑)		Thal (↓)	Obermann et al. [74]
Cervical dystonia	10/10	GP (↑)	Floc (↑)	PM (↑) SMA (↓) DLPFC (↓) OCC (↓)		Draganski et al. [79]
Cervical dystonia	11/31					Egger et al. [76]
Cervical dystonia	9/14	Caud (↑) Put (↓)	Hem (↑)	STL (↑)	Thal (↑)	Obermann et al. [74]
Cervical dystonia	29/28	Put (↑) GP (↑)				Draganski et al. [80]
Cervical dystonia	19/28	Caud (↓) Put (↓)		PM (↓) SMC (↓)		Pantano et al. [75]
DYT1 dystonia	11/11	Put (↓)				Draganski et al. [80]
Focal hand dystonias	36/36			SMC (↑)		Garraux et al. [81]
Focal hand dystonias	11/31	GP (↑)				Egger et al. [76]
Generalized (idiopathic)	9/31	GP (↑)				Egger et al. [76]
Writer's cramp	30/30		Hem (↓)	SMC (↓)	Thal (↓)	Delmaire et al. [82]
Writer's cramp	14/14			PM (↑)		Granert et al. [77]

Arrows indicate increased (↑) or decreased (↓) regional volumes. Studies comparing multiple types of dystonia with a single control group are listed according to the type of dystonia rather than as a combined group

Caud caudate, *Cing* cingulate gyrus, *DLPFC* dorsolateral prefrontal cortex, *Floc* cerebellar flocculus, *GP* globus pallidus, *Hem* cerebellar hemisphere, *IPL* inferior parietal lobule, *PreF* prefrontal cortex, *NA* nucleus accumbens, *OFC* orbitofrontal cortex, *OCC* occipital cortex, *PM* primary motor cortex, *Put* putamen, *SMC* sensorimotor cortex, *STL* superior temporal lobe, *SMA* supplementary motor area

dystonia [74, 79, 82, 86], most likely reflecting compensatory mechanisms [86]. At the cortical level, findings are also more consistent and show volume increases in sensorimotor areas [76, 79, 82, 81]. On the opposite, the results of the single study demonstrating sensorimotor cortex volume reduction progressing toward the 5 years follow-up scan in the absence of cervical dystonia symptom progression could be interpreted as age-related effects.

In summary, the provided evidence for subtle structural changes in primary dystonias converges to regional volume increases and microstructural modifications in basal ganglia, sensorimotor cortex, and cerebellum. The prevalent interpretation links the presence of volume expansion with the notion of abnormal brain plasticity in dystonia. The inconsistencies among studies arise most probably not only from methodological differences, but also from the choice of studied populations based mainly on clinical phenotype rather than genetic characterization.

Considering the fact that generalized early-onset dystonias are associated with genetic abnormalities under the modulatory impact of variable dominance and penetrance, neuroimaging research started investigations looking for informative genotype–phenotype interactions [87, 88]. Albeit morphometric alterations in

patients brains could be an effect of brain plasticity secondary to the dystonic movements and postures and not their cause, findings from symptomatic carriers of particular genetic mutations suggest complex genotype–phenotype interactions. A voxel-based analysis of anatomical connectivity maps obtained with probabilistic diffusion tractography in manifesting and nonmanifesting DYT1 and DYT6 carriers, including correlation with cerebral blood flow PET measurements and assessment of motor behavior, showed reduced fiber integrity in the cerebellum-thalamus-cortex axis. Previous VBM study demonstrated morphometric correlates of an interaction between phenotype (i.e., presence of dystonic symptoms) and genotype (presence of a DYT1 gene mutation) with putamen volume changes in familial, sporadic non-DYT1 adult onset primary torsion dystonia (AOPTD), and DYT1 gene mutation carriers [80]. Further exploration in individual gene carriers supported the notion of phenotype penetrance determination by connectivity differences in the proximal cerebellar segment of the cerebellum-thalamus-cortex axis [89].

Correlation between brain structure and behavioral parameters capturing subclinical pathology in familial AOPTD supported the hypothesis that basal ganglia volume changes are neural correlates of specific dystonia endophenotypes. ROI analysis demonstrated putamen volume expansion in nonmanifesting family members of familial AOPTD with pathological temporal discrimination thresholds for visual and tactile stimuli [73]. Dissecting further the morphometric correlates of familial and sporadic AOPTD endophenotypes, the authors found volume changes in primary somatosensory cortex, putamen and caudate depending on spatial discrimination thresholds or familial background.

The conclusion from these studies is that subtle sensory abnormalities are related to brain structure changes, though the interaction between differential subclinical sensory pathology and putamen volume with possible genetic modulation remains to be elucidated. From a pathophysiological point of view, we favor the idea that a defective sensorimotor integration promotes aberrant plasticity, as measured in terms of morphometric changes, and is eventually responsible for the loss of the harmonic interplay of agonists and antagonists muscle groups, typical of dystonia.

Huntington's Disease (HD)

HD is a paradigmatic genetic neurodegenerative disease with dominant monoallelic transmission and full penetrance, and a highly predictable course within triplet expansion variability. The possibility of a presymptomatic diagnosis and the intense research for disease-modifying compounds create the need for a reliable marker of HD progression even before symptom onset. Progressive caudate atrophy in HD is a well-known pathological manifestation, which is easily detectable on conventional MRI images when the symptoms are established [90]. Disregarding methodological differences, morphometry studies also agree on the presence of progressive caudate tissue loss in HD correlating with CAG repeat length, cognitive and motor performance [91, 92].

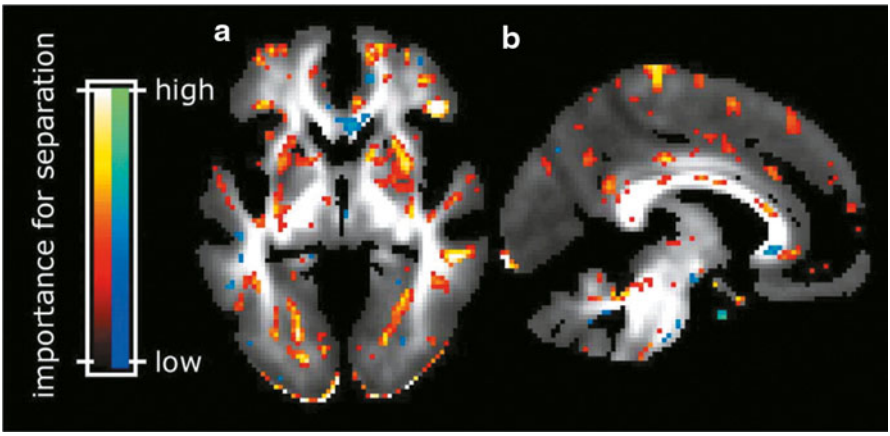

Fig. 2.2 Cortical thickness maps. Starting from the *left*, each group of six maps represent the comparison of cortical thickness between each prodromal HD group and the controls (*Dx* diagnosed). Left hemisphere is only shown. The *top row* shows (from *left* to *right*) *lateral* and *medial* views, the *second row* shows *dorsal* and *ventral* views, and the *last row* shows *anterior* and *posterior* views, respectively [101]

Novel aspects in computational anatomy studies of HD are the attempts to characterize spatial pattern and temporal dynamics of extrastriatal structure changes in different stages of disease progression. Specific atrophy patterns have been described by a prospective VBM study in frontal, middle temporal, insular, and cerebellar areas, which correlated with symptom severity and CAG repeat length [93]. Progression rate correlates both with CAG repeats length and with age of onset, although not always with both, indicating the possible existence of other epigenetic factors modulating the local neurodegeneration [94]. Recent cortical thickness analysis demonstrated high topographic anatomical sensitivity to both motor and cognitive dysfunctional aspects in a wide span of disease-progression phenotypes [95].

Analysis of DWI data in HD tested the hypothesis of preferential loss of connections along specific radiating directions. Parallel increases in FA/MD were associated with dispersion of the principal diffusion direction with emphasis on striatopallidal connections [96]. Taking advantage of improved corpus callosum segmentation, diffusion-weighted parameter analysis showed specific regional changes in white matter integrity correlating with cognitive performance in early HD patients, suggesting dysfunctional interhemispheric information transfer [97]. White matter morphometry proved to be of great value for accurate automated classification in presymptomatic HD mutation carriers [10, 98]. In the caudate, FA and MD were decreased in presymptomatic HD, but increased in definite HD, suggesting developmental alterations leading to a peculiar histological architecture, preceding the onset of neurodegeneration [99].

Gray matter reductions in hypothalamus have been shown to differentiate gene carriers from controls [100]. Cortical thinning in the posterior–superior cerebrum

has been found up to 15 years before the overt clinical onset (Fig. 2.2, [101]). Additional evidence of a smaller intracranial volume in prodromal HD [102] indicated total brain volume as an interesting group-level biomarker [98]. Relaxometry studies in HD demonstrated a lower peak height of the gray matter MT ratio in symptomatic mutation carriers [103]. Despite the limited number of studies utilizing relaxometry techniques, the field is open for more investigation considering recent evidence for a pivotal role of altered iron homeostasis early in disease course [104].

Essential Tremor (ET)

The precise etiology, clinical classification, and differentiation of essential tremor (ET) and tremor associated with dystonia are still subject of debate. Converging data indicate heterogeneity of the disorder, a pivotal role for genetic factors and possible association with risk for iPD.

Corresponding to the current status of debate, only a few morphometric studies of ET have been published. A cerebellar involvement is suggested by the clinical presentation, often associating the signs of kinetic tremor to an underlying ataxia [105], which are further confirmed by neuropathological data with loss of Purkinje cells [106]. Early VBM studies have demonstrated a very localized involvement of the cerebellum in patients with head tremor [107, 108].

The involvement of cerebellum has been further confirmed by diffusion-weighted studies showing MD increases and FA decreases in the inferior cerebellar peduncles [109]. The interhemismpheric asymmetry of the FA reductions was explained as an effect of handedness, responsible for a relatively higher myelination on the dominant side. This interpretation is hard to prove, and a subsequent study failed to reproduce the findings [110]. The analysis was extended to whole-brain analysis using tract-based spatial statistics (TBSS) that showed increase of MD in the right cerebral hemispheric WM, involving the internal capsule, external capsule, and frontoparietal lobar WM, bringing strong arguments for extracerebellar involvement [111].

Actually, a growing body of evidence suggests the presence of a more widespread white matter axonal damage in ET. From a clinical perspective, this is in line with the coexistence of mild cognitive impairment, olfactory dysfunction and personality changes, and gives further support to the idea of ET as a neurodegenerative disease [112]. More recent whole-brain VBM comparisons between ET and healthy controls demonstrated white matter changes in the midbrain, occipital lobes, and right frontal lobes in addition to the expected gray matter bilateral changes in the cerebellum [113, 114].

The exploration of brain structure in ET remains at the descriptive level with attempts for more thorough differentiation from other tremor entities. One of the challenges for the future research remains the whole brain assessment and tissue characterization of specific endophenotypes in genetically defined populations.

Gilles de la Tourette Syndrome (TS)

From a classical reductionist perspective, Gilles de la Tourette syndrome (TS) was considered a pediatric psychiatric disease further supported by the lack of evidence of associated brain abnormalities. Due to a high variability of clinical presentation and comorbidities as obsessive–compulsive disorder (OCD) and attention deficit-hyperactivity disorder (ADHD), structural imaging studies reported controversial anatomical findings. Nevertheless, most of structural changes corroborate the hypothesis of alterations in cortico-striato-thalamo-cortical circuits. Several network nodes involved in TS etiopathology were identified by studies using VBM, cortical thickness, and local diffusivity properties.

Computational anatomy studies suggest the existence of a "somatotopy" relating volumetric decrease with tics distribution [115–119]. Simple facial tics are associated with relative atrophy in the motor cortex limited to upper limb and face representation areas, while more diffuse cortical thinning including right orbitofrontal cortex was found in complex tics involving different body parts [119]. Dysfunction of orbitofrontal cortex could explain deficits in the flexible control of behavior [120]. Indeed, the predominant involvement of (left) inferior frontal gyrus has been observed in patients with TS and OCD and/or ADHD [121] confirming the importance of the frontal cortex in voluntary control [122].

The "limbic" structures of anterior cingulate cortex, hippocampus, and amygdala represent the fronto-striatal matrix linked directly to the ventral striatum where motivational and incentive behaviors are regulated [123]. ROI studies focusing on hippocampus described an association of regional atrophy with tics severity and the occurrence of OCD [119]. Considering the strong reciprocal connections between hippocampus and orbitofrontal cortex [124], the observed parallel structural changes suggest a disruption of specific networks involved in anticipation, evaluation, and learning. Similarly, the reports about anterior cingulate cortex thinning can be interpreted as related to the intensity of OCD symptoms [119]. This is in line with studies in OCD patients and supports the current view on anterior cingulate cortex (ACC, and ventral ACC in particular) in the regulation of emotional information and anxiety [125].

Basal ganglia volume decreases are the most consistent findings in ROI studies. Even during childhood, caudate volume loss appears to have a predictive value regarding the OCD and tic symptom severity in adolescence [126–128]. Further studies confirmed the presence of structural abnormalities in the ventral striatum [116, 117]. Beyond basal ganglia involvement, studies report alterations in thalamic microstructure with increased MD and axial diffusivity in TS patients [129, 130]. Altogether, the existing evidence supports an involvement of the basal ganglia restricted to the ventral regions considered functionally as part of the limbic system.

One of the most reproducible changes of anatomical regions in TS are somatosensory cortex alterations [115, 116, 118, 119]. Despite a certain agreement regarding the anatomical pattern, the directionality of changes in this region remains controversial [117, 119]. We favor the idea of occurrence of structural changes in cortical areas

resulting from increased processing demands and their integration into repetitive motor patterns [131]. Alternatively, somatosensory cortex modifications could arise as an adaptation to dysfunctional secondary somatosensory areas as the parietal operculum bilaterally, which showed consistent gray matter volume/cortical thickness decreases [119, 132, 133].

In summary, a multimodal imaging approach making use of different protocols can help gain in-depth knowledge in TS underlying pathophysiological processes. In addition, novel computational tools are the most likely technological advances to rely on through their capacity of modeling complex genetic and imaging information [134].

Conclusions and Future Directions

In the last decade, we have witnessed the steadily expanding field of morphometry. New methods and imaging techniques have provided converging evidence for abnormal structure–function relationships in the field of movement disorders. However, the usefulness of computational neuroanatomy in the clinical routine is questioned due to the plenitude of controversial findings in the published literature. Promising results based on automated classification of the individual patient's structural MRI data and technical developments offering quantitative parameter mapping based on defined biophysical models appear to overcome this natural scepticism and are redefining the value of computational neuroanatomy in the clinical diagnostic work-up agenda.

References

1. Ashburner J, Csernansky JG, Davatzikos C, Fox NC, Frisoni GB, Thompson PM. Computer-assisted imaging to assess brain structure in healthy and diseased brains. Lancet Neurol. 2003;2(2):79–88.
2. Basser PJ, Pierpaoli C. Microstructural and physiological features of tissues elucidated by quantitative-diffusion-tensor MRI. J Magn Reson B. 1996;111(3):209–19.
3. Helms G, Dathe H, Kallenberg K, Dechent P. High-resolution maps of magnetization transfer with inherent correction for RF inhomogeneity and T1 relaxation obtained from 3D FLASH MRI. Magn Reson Med. 2008;60(6):1396–407.
4. Helms G, Finsterbusch J, Weiskopf N, Dechent P. Rapid radiofrequency field mapping in vivo using single-shot STEAM MRI. Magn Reson Med. 2008;60(3):739–43.
5. Helms G, Draganski B, Frackowiak R, Ashburner J, Weiskopf N. Improved segmentation of deep brain grey matter structures using magnetization transfer (MT) parameter maps. Neuroimage. 2009;47(1):194–8.
6. Ashburner J. Computational anatomy with the SPM software. Magn Reson Imaging. 2009;27(8):1163–74.
7. Dale AM, Fischl B, Sereno MI. Cortical surface-based analysis. I. Segmentation and surface reconstruction. Neuroimage. 1999;9(2):179–94.

8. Klöppel S, Draganski B, Golding CV, et al. White matter connections reflect changes in voluntary-guided saccades in pre-symptomatic Huntington's disease. Brain. 2008;131(Pt 1): 196–204.
9. Klöppel S, Chu C, Tan GC, et al. Automatic detection of preclinical neurodegeneration: presymptomatic Huntington's disease. Neurology. 2009;72(5):426–31.
10. Kherif F, Josse G, Seghier ML, Price CJ. The main sources of intersubject variability in neuronal activation for reading aloud. J Cogn Neurosci. 2009;21(4):654–68.
11. Kawasaki Y, Suzuki M, Kherif F, et al. Multivariate voxel-based morphometry succesfully differentiates schizophrenia patients from healthy controls. Neuroimage. 2007;34(1):235–42.
12. Huber SJ, Shuttleworth EC, Christy JA, Chakeres DW, Curtin A, Paulson GW. Magnetic resonance imaging in dementia of Parkinson's disease. J Neurol Neurosurg Psychiatr. 1989;52(11):1221–7.
13. Laakso MP, Partanen K, Riekkinen P, et al. Hippocampal volumes in Alzheimer's disease, Parkinson's disease with and without dementia, and in vascular dementia: an MRI study. Neurology. 1996;46(3):678–81.
14. Hu MT, White SJ, Chaudhuri KR, Morris RG, Bydder GM, Brooks DJ. Correlating rates of cerebral atrophy in Parkinson's disease with measures of cognitive decline. J Neural Transm. 2001;108(5):571–80.
15. Pereira JB, Ibarretxe-Bilbao N, Marti M-J, et al. Assessment of cortical degeneration in patients with Parkinson's disease by voxel-based morphometry, cortical folding, and cortical thickness. Hum Brain Mapp. 2012;33(11):2521–34.
16. Schwarz ST, Rittman T, Gontu V, Morgan PS, Bajaj N, Auer DP. T1-weighted MRI shows stage-dependent substantia nigra signal loss in Parkinson's disease. Mov Disord. 2011;26(9):1633–8.
17. Sofic E, Riederer P, Heinsen H, et al. Increased iron (III) and total iron content in post mortem substantia nigra of parkinsonian brain. J Neural Transm. 1988;74(3):199–205.
18. Dexter DT, Wells FR, Agid F, et al. Increased nigral iron content in postmortem parkinsonian brain. Lancet. 1987;2(8569):1219–20.
19. Dexter DT, Carayon A, Javoy-Agid F, et al. Alterations in the levels of iron, ferritin and other trace metals in Parkinson's disease and other neurodegenerative diseases affecting the basal ganglia. Brain. 1991;114(Pt 4):1953–75.
20. Graham JM, Paley MN, Grünewald RA, Hoggard N, Griffiths PD. Brain iron deposition in Parkinson's disease imaged using the PRIME magnetic resonance sequence. Brain. 2000;123(Pt 12):2423–31.
21. Martin WRW, Wieler M, Gee M. Midbrain iron content in early Parkinson disease: a potential biomarker of disease status. Neurology. 2008;70(16 Pt 2):1411–7.
22. Sasaki M, Shibata E, Tohyama K, et al. Neuromelanin magnetic resonance imaging of locus ceruleus and substantia nigra in Parkinson's disease. Neuroreport. 2006;17(11):1215–8.
23. Menke RA, Scholz J, Miller KL, et al. MRI characteristics of the substantia nigra in Parkinson's disease: a combined quantitative T1 and DTI study. Neuroimage. 2009;47(2):435–41.
24. Vaillancourt DE, Spraker MB, Prodoehl J, et al. High-resolution diffusion tensor imaging in the substantia nigra of de novo Parkinson disease. Neurology. 2009;72(16):1378–84.
25. Du G, Lewis MM, Styner M, et al. Combined R2* and diffusion tensor imaging changes in the substantia nigra in Parkinson's disease. Mov Disord. 2011;26(9):1627–32.
26. Lyoo CH, Ryu YH, Lee MS. Cerebral cortical areas in which thickness correlates with severity of motor deficits of Parkinson's disease. J Neurol. 2011;258(10):1871–6.
27. Kassubek J, Juengling FD, Hellwig B, Spreer J, Lücking CH. Thalamic grey matter changes in unilateral Parkinsonian resting tremor: a voxel-based morphometric analysis of 3-dimensional magnetic resonance imaging. Neurosci Lett. 2002;323(1):29–32.
28. Amboni M, Cozzolino A, Longo K, Picillo M, Barone P. Freezing of gait and executive functions in patients with Parkinson's disease. Mov Disord. 2008;23(3):395–400.
29. Kostic VS, Agosta F, Pievani M, et al. Pattern of brain tissue loss associated with freezing of gait in Parkinson disease. Neurology. 2012;78(6):409–16.

30. Kostić VS, Agosta F, Petrović I, et al. Regional patterns of brain tissue loss associated with depression in Parkinson disease. Neurology. 2010;75(10):857–63.
31. Blood AJ, Iosifescu DV, Makris N, et al. Microstructural abnormalities in subcortical reward circuitry of subjects with major depressive disorder. PLoS ONE. 2010;5(11):e13945.
32. Kim JW, Lee DY, Choo IH, et al. Microstructural alteration of the anterior cingulum is associated with apathy in Alzheimer disease. Am J Geriatr Psychiatry. 2011;19(7):644–53.
33. Reijnders JSAM, Ehrt U, Weber WEJ, Aarsland D, Leentjens AFG. A systematic review of prevalence studies of depression in Parkinson's disease. Mov Disord. 2008;23(2):183–9; quiz 313.
34. Burton EJ, McKeith IG, Burn DJ, Williams ED, O'Brien JT. Cerebral atrophy in Parkinson's disease with and without dementia: a comparison with Alzheimer's disease, dementia with Lewy bodies and controls. Brain. 2004;127(Pt 4):791–800.
35. Weintraub D, Doshi J, Koka D, et al. Neurodegeneration across stages of cognitive decline in Parkinson disease. Arch Neurol. 2011;68(12):1562–8.
36. Apostolova LG, Beyer M, Green AE, et al. Hippocampal, caudate, and ventricular changes in Parkinson's disease with and without dementia. Mov Disord. 2010;25(6):687–95.
37. Dalaker TO, Larsen JP, Bergsland N, et al. Brain atrophy and white matter hyperintensities in early Parkinson's disease(a). Mov Disord. 2009;24(15):2233–41.
38. Dalaker TO, Larsen JP, Dwyer MG, et al. White matter hyperintensities do not impact cognitive function in patients with newly diagnosed Parkinson's disease. Neuroimage. 2009;47(4):2083–9.
39. Beyer MK, Janvin CC, Larsen JP, Aarsland D. A magnetic resonance imaging study of patients with Parkinson's disease with mild cognitive impairment and dementia using voxel-based morphometry. J Neurol Neurosurg Psychiatr. 2007;78(3):254–9.
40. Bouchard TP, Malykhin N, Martin WRW, et al. Age and dementia-associated atrophy predominates in the hippocampal head and amygdala in Parkinson's disease. Neurobiol Aging. 2008;29(7):1027–39.
41. Martin WRW, Wieler M, Gee M, Camicioli R. Temporal lobe changes in early, untreated Parkinson's disease. Mov Disord. 2009;24(13):1949–54.
42. Camicioli R, Gee M, Bouchard TP, et al. Voxel-based morphometry reveals extra-nigral atrophy patterns associated with dopamine refractory cognitive and motor impairment in parkinsonism. Parkinsonism Relat Disord. 2009;15(3):187–95.
43. Lyoo CH, Ryu YH, Lee MS. Topographical distribution of cerebral cortical thinning in patients with mild Parkinson's disease without dementia. Mov Disord. 2010;25(4):496–9.
44. Sanchez-Castaneda C, Rene R, Ramirez-Ruiz B, et al. Correlations between gray matter reductions and cognitive deficits in dementia with Lewy bodies and Parkinson's disease with dementia. Mov Disord. 2009;24(12):1740–6.
45. Lee JE, Park H-J, Park B, et al. A comparative analysis of cognitive profiles and white-matter alterations using voxel-based diffusion tensor imaging between patients with Parkinson's disease dementia and dementia with Lewy bodies. J Neurol Neurosurg Psychiatr. 2010;81(3):320–6.
46. Braak H, Del Tredici K, Rüb U, de Vos RAI, Jansen Steur ENH, Braak E. Staging of brain pathology related to sporadic Parkinson's disease. Neurobiol Aging. 2003;24(2):197–211.
47. Wattendorf E, Welge-Lüssen A, Fiedler K, et al. Olfactory impairment predicts brain atrophy in Parkinson's disease. J Neurosci. 2009;29(49):15410–3.
48. Rolheiser TM, Fulton HG, Good KP, et al. Diffusion tensor imaging and olfactory identification testing in early-stage Parkinson's disease. J Neurol. 2011;258(7):1254–60.
49. Gattellaro G, Minati L, Grisoli M, et al. White matter involvement in idiopathic Parkinson disease: a diffusion tensor imaging study. AJNR Am J Neuroradiol. 2009;30(6):1222–6.
50. Karagulle Kendi AT, Lehericy S, Luciana M, Ugurbil K, Tuite P. Altered diffusion in the frontal lobe in Parkinson disease. AJNR Am J Neuroradiol. 2008;29(3):501–5.
51. Jubault T, Brambati SM, Degroot C, et al. Regional brain stem atrophy in idiopathic Parkinson's disease detected by anatomical MRI. PLoS ONE. 2009;4(12):e8247.

52. Colosimo C, Riley DE, Wenning GK. Handbook of atypical Parkinsonism. Cambridge: Cambridge University Press; 2011.
53. Stamelou M, Knake S, Oertel WH, Höglinger GU. Magnetic resonance imaging in progressive supranuclear palsy. J Neurol. 2011;258(4):549–58.
54. Dickson DW, Rademakers R, Hutton ML. Progressive supranuclear palsy: pathology and genetics. Brain Pathol. 2007;17(1):74–82.
55. Brenneis C, Seppi K, Schocke M, Benke T, Wenning GK, Poewe W. Voxel based morphometry reveals a distinct pattern of frontal atrophy in progressive supranuclear palsy. J Neurol Neurosurg Psychiatr. 2004;75(2):246–9.
56. Price S, Paviour D, Scahill R, et al. Voxel-based morphometry detects patterns of atrophy that help differentiate progressive supranuclear palsy and Parkinson's disease. Neuroimage. 2004;23(2):663–9.
57. Ling H, O'Sullivan SS, Holton JL, et al. Does corticobasal degeneration exist? A clinicopathological re-evaluation. Brain. 2010;133(Pt 7):2045–57.
58. Boxer AL, Geschwind MD, Belfor N, et al. Patterns of brain atrophy that differentiate corticobasal degeneration syndrome from progressive supranuclear palsy. Arch Neurol. 2006;63(1):81–6.
59. Josephs KA, Whitwell JL, Dickson DW, et al. Voxel-based morphometry in autopsy proven PSP and CBD. Neurobiol Aging. 2008;29(2):280–9.
60. Rizzo G, Martinelli P, Manners D, et al. Diffusion-weighted brain imaging study of patients with clinical diagnosis of corticobasal degeneration, progressive supranuclear palsy and Parkinson's disease. Brain. 2008;131(Pt 10):2690–700.
61. Minnerop M, Specht K, Ruhlmann J, et al. Voxel-based morphometry and voxel-based relaxometry in multiple system atrophy-a comparison between clinical subtypes and correlations with clinical parameters. Neuroimage. 2007;36(4):1086–95.
62. Brenneis C, Egger K, Scherfler C, et al. Progression of brain atrophy in multiple system atrophy. A longitudinal VBM study. J Neurol. 2007;254(2):191–6.
63. Tsukamoto K, Matsusue E, Kanasaki Y, et al. Significance of apparent diffusion coefficient measurement for the differential diagnosis of multiple system atrophy, progressive supranuclear palsy, and Parkinson's disease: evaluation by 3.0-T MR imaging. Neuroradiology. 2012;54(9):947–55.
64. Quattrone A, Nicoletti G, Messina D, et al. MR imaging index for differentiation of progressive supranuclear palsy from Parkinson disease and the Parkinson variant of multiple system atrophy. Radiology. 2008;246(1):214–21.
65. Schulz JB, Skalej M, Wedekind D, et al. Magnetic resonance imaging-based volumetry differentiates idiopathic Parkinson's syndrome from multiple system atrophy and progressive supranuclear palsy. Ann Neurol. 1999;45(1):65–74.
66. Warmuth-Metz M, Naumann M, Csoti I, Solymosi L. Measurement of the midbrain diameter on routine magnetic resonance imaging: a simple and accurate method of differentiating between Parkinson disease and progressive supranuclear palsy. Arch Neurol. 2001;58(7):1076–9.
67. Focke NK, Helms G, Pantel PM, et al. Differentiation of typical and atypical Parkinson syndromes by quantitative MR imaging. AJNR Am J Neuroradiol. 2011;32(11):2087–92.
68. Marsden CD, Obeso JA, Zarranz JJ, Lang AE. The anatomical basis of symptomatic hemidystonia. Brain. 1985;108(Pt 2):463–83.
69. Bhatia KP, Marsden CD. The behavioural and motor consequences of focal lesions of the basal ganglia in man. Brain. 1994;117(Pt 4):859–76.
70. Guehl D, Cuny E, Ghorayeb I, Michelet T, Bioulac B, Burbaud P. Primate models of dystonia. Progress in Neurobiology. 2009;87(2):118–31.
71. Black KJ, Ongür D, Perlmutter JS. Putamen volume in idiopathic focal dystonia. Neurology. 1998;51(3):819–24.
72. Etgen T, Mühlau M, Gaser C, Sander D. Bilateral grey-matter increase in the putamen in primary blepharospasm. J Neurol Neurosurg Psychiatr. 2006;77(9):1017–20.

73. Bradley D, Whelan R, Walsh R, et al. Temporal discrimination threshold: VBM evidence for an endophenotype in adult onset primary torsion dystonia. Brain. 2009;132(Pt 9):2327–35.
74. Obermann M, Yaldizli O, De Greiff A, et al. Morphometric changes of sensorimotor structures in focal dystonia. Mov Disord. 2007;22(8):1117–23.
75. Pantano P, Totaro P, Fabbrini G, et al. A transverse and longitudinal MR imaging voxel-based morphometry study in patients with primary cervical dystonia. AJNR Am J Neuroradiol. 2011;32(1):81–4.
76. Egger K, Mueller J, Schocke M, et al. Voxel based morphometry reveals specific gray matter changes in primary dystonia. Mov Disord. 2007;22(11):1538–42.
77. Granert O, Peller M, Jabusch H-C, Altenmüller E, Siebner HR. Sensorimotor skills and focal dystonia are linked to putaminal grey-matter volume in pianists. J Neurol Neurosurg Psychiatr. 2011;82(11):1225–31.
78. Neychev VK, Gross RE, Lehéricy S, et al. The functional neuroanatomy of dystonia. Neurobiol Dis. 2011;42(2):185–201.
79. Draganski B, Thun-Hohenstein C, Bogdahn U, Winkler J, May A. "Motor circuit" gray matter changes in idiopathic cervical dystonia. Neurology. 2003;61(9):1228–31.
80. Draganski B, Schneider SA, Fiorio M, et al. Genotype-phenotype interactions in primary dystonias revealed by differential changes in brain structure. Neuroimage. 2009;47(4): 1141–7.
81. Garraux G, Bauer A, Hanakawa T, Wu T, Kansaku K, Hallett M. Changes in brain anatomy in focal hand dystonia. Ann Neurol. 2004;55(5):736–9.
82. Delmaire C, Vidailhet M, Elbaz A, et al. Structural abnormalities in the cerebellum and sensorimotor circuit in writer's cramp. Neurology. 2007;69(4):376–80.
83. Delmaire C, Vidailhet M, Wassermann D, et al. Diffusion abnormalities in the primary sensorimotor pathways in writer's cramp. Arch Neurol. 2009;66(4):502–8.
84. Colosimo C, Pantano P, Calistri V, Totaro P, Fabbrini G, Berardelli A. Diffusion tensor imaging in primary cervical dystonia. J Neurol Neurosurg Psychiatr 2005;76(11):1591–3.
85. Fabbrini G, Pantano P, Totaro P, et al. Diffusion tensor imaging in patients with primary cervical dystonia and in patients with blepharospasm. Eur J Neurol. 2008;15(2):185–9.
86. Sadnicka A, Hoffland BS, Bhatia KP, van de Warrenburg BP, Edwards MJ. The cerebellum in dystonia—help or hindrance? Clin Neurophysiol. 2012;123(1):65–70.
87. Ozelius LJ, Bressman SB. Genetic and clinical features of primary torsion dystonia. Neurobiol Dis. 2011;42(2):127–35.
88. Meunier S, Lehéricy S, Garnero L, Vidailhet M. Dystonia: lessons from brain mapping. Neuroscientist. 2003;9(1):76–81.
89. Argyelan M, Carbon M, Niethammer M, et al. Cerebellothalamocortical connectivity regulates penetrance in dystonia. J Neurosci. 2009;29(31):9740–7.
90. Walker FO. Huntington's disease. Lancet. 2007;369(9557):218–28.
91. Aylward E, Mills J, Liu D, et al. Association between age and striatal volume stratified by CAG repeat length in prodromal Huntington's disease. PLoS Curr. 2011;3:RRN1235.
92. Klöppel S, Henley SM, Hobbs NZ, et al. Magnetic resonance imaging of Huntington's disease: preparing for clinical trials. Neuroscience. 2009;164(1):205–19.
93. Ruocco HH, Bonilha L, Li LM, Lopes-Cendes I, Cendes F. Longitudinal analysis of regional grey matter loss in Huntington's disease: effects of the length of the expanded CAG repeat. J Neurol Neurosurg Psychiatry. 2008;79(2):130–5.
94. Rosas HD, Reuter M, Doros G, et al. A tale of two factors: what determines the rate of progression in Huntington's disease? A longitudinal MRI study. Movement Disorders. 2011;26(9):1691–7.
95. Rosas HD, Salat DH, Lee SY, et al. Cerebral cortex and the clinical expression of Huntington's disease: complexity and heterogeneity. Brain. 2008;131(Pt 4):1057–68.
96. Douaud G, Behrens TE, Poupon C, et al. In vivo evidence for the selective subcortical degeneration in Huntington's disease. NeuroImage. 2009;46(4):958–66.
97. Rosas HD, Lee SY, Bender AC, et al. Altered white matter microstructure in the corpus callosum in Huntington's disease: implications for cortical "disconnection." Neuroimage. 2010;49(4):2995–3004.

98. Majid DSA, Stoffers D, Sheldon S, et al. Automated structural imaging analysis detects premanifest Huntington's disease neurodegeneration within 1 year. Movement Disorders. 2011;26(8):1481–8.
99. Mandelli ML, Savoiardo M, Minati L, et al. Decreased diffusivity in the caudate nucleus of presymptomatic Huntington's disease gene carriers: which explanation? AJNR Am J Neuroradiol. 2010;31(4):706–10.
100. Soneson C, Fontes M, Zhou Y, et al. Early changes in the hypothalamic region in prodromal Huntington's disease revealed by MRI analysis. Neurobiol Dis. 2010;40(3):531–43.
101. Nopoulos PC, Aylward EH, Ross CA, et al. Cerebral cortex structure in prodromal Huntington's disease. Neurobiol Dis. 2010;40(3):544–54.
102. Nopoulos PC, Aylward EH, Ross CA, et al. Smaller intracranial volume in prodromal Huntington's disease: evidence for abnormal neurodevelopment. Brain. 2011;134(Pt 1): 137–42.
103. Jurgens CK, Bos R, Luyendijk J, et al. Magnetization transfer imaging in "premanifest" Huntington's disease. J Neurol. 2010;257(3):426–32.
104. Rosas HD, Chen YI, Doros G, et al. Alterations in brain transition metals in Huntington's disease: an evolving and intricate story. Arch Neurol. 2012;69(7):887–93.
105. Deuschl G, Wenzelburger R, Löffler K, Raethjen J, Stolze H. Essential tremor and cerebellar dysfunction clinical and kinematic analysis of intention tremor. Brain. 2000;123(Pt 8): 1568–80.
106. Louis ED, Vonsattel JPG. The emerging neuropathology of essential tremor. Mov Disord. 2008;23(2):174–82.
107. Quattrone A, Cerasa A, Messina D, et al. Essential head tremor is associated with cerebellar vermis atrophy: a volumetric and voxel-based morphometry MR imaging study. AJNR Am J Neuroradiol. 2008;29(9):1692–7.
108. A Cerasa, Messina D, Nicoletti G, et al. Cerebellar atrophy in essential tremor using an automated segmentation method. AJNR Am J Neuroradiol. 2009;30(6):1240–3.
109. Klein JC, Lorenz B, Kang J-S, et al. Diffusion tensor imaging of white matter involvement in essential tremor. Hum Brain Mapp. 2011;32(6):896–904.
110. Saini J, Bagepally BS, Bhatt MD, et al. Diffusion tensor imaging: tract based spatial statistics study in essential tremor. Parkinsonism Relat Disord. 2012;18(5):477–82.
111. Smith SM, Jenkinson M, Johansen-Berg H, et al. Tract-based spatial statistics: voxelwise analysis of multi-subject diffusion data. Neuroimage. 2006;31(4):1487–505.
112. Louis ED. Essential tremors: a family of neurodegenerative disorders? Arch Neurol. 2009;66(10):1202–8.
113. Benito-León J, Alvarez-Linera J, Hernández-Tamames JA, Alonso-Navarro H, Jiménez-Jiménez FJ, Louis ED. Brain structural changes in essential tremor: voxel-based morphometry at 3-T. J Neurol Sci. 2009;287(1-2):138–142.
114. Bagepally BS, Bhatt MD, Chandran V, et al. Decrease in cerebral and cerebellar gray matter in essential tremor: a voxel-based morphometric analysis under 3T MRI. J Neuroimaging. 2012;22(3):275–8.
115. Peterson BS, Staib L, Scahill L, et al. Regional brain and ventricular volumes in Tourette syndrome. Arch Gen Psychiatry. 2001;58(5):427–40.
116. Draganski B, Martino D, Cavanna AE, et al. Multispectral brain morphometry in Tourette syndrome persisting into adulthood. Brain. 2010;133(Pt 12):3661–75.
117. Ludolph AG, Juengling FD, Libal G, Ludolph AC, Fegert JM, Kassubek J. Grey-matter abnormalities in boys with Tourette syndrome: magnetic resonance imaging study using optimised voxel-based morphometry. Br J Psychiatry. 2006;188(5):484–5.
118. Müller-Vahl KR, Kaufmann J, Grosskreutz J, Dengler R, Emrich HM, Peschel T. Prefrontal and anterior cingulate cortex abnormalities in Tourette syndrome: evidence from voxel-based morphometry and magnetization transfer imaging. BMC Neuroscience. 2009;10(1):47.
119. Worbe Y, Gerardin E, Hartmann A, et al. Distinct structural changes underpin clinical phenotypes in patients with Gilles de La Tourette syndrome. Brain. 2010;133(12):3649–60.

120. O'Doherty JP, Hampton A, Kim H. Model-based fMRI and its application to reward learning and decision making. Ann N Y Acad Sci. 2007;1104(1):35–53.
121. Wittfoth M, Bornmann S, Peschel T, et al. Lateral frontal cortex volume reduction in Tourette syndrome revealed by VBM. BMC Neurosci. 2012;13:17.
122. van den Heuvel OA, Remijnse PL, Mataix-Cols D, et al. The major symptom dimensions of obsessive-compulsive disorder are mediated by partially distinct neural systems. Brain. 2009;132(Pt 4):853–68.
123. Haber SN, Knutson B. The reward circuit: linking primate anatomy and human imaging. Neuropsychopharmacology. 2010;35(1):4–26.
124. Ramus SJ, Davis JB, Donahue RJ, Diszenca CB, Waite AA. Interactions between the orbitofrontal cortex and the hippocampal memory system during the storage of long-term memory. Ann N Y Acad Sci. 2007;1121(1):216–31.
125. Paus T. Primate anterior cingulate cortex: where motor control, drive and cognition interface. Nat. Rev Neurosci. 2001;2(6):417–24.
126. Bloch MH, Leckman JF, Zhu H, Peterson BS. Caudate volumes in childhood predict symptom severity in adults with Tourette syndrome. Neurology. 2005;65(8):1253–8.
127. Peterson BS, Thomas P, Kane MJ, et al. Basal ganglia volumes in patients with Gilles de la Tourette syndrome. Arch General Psychiatry. 2003;60(4):415.
128. Peterson B, Riddle MA, Cohen DJ, et al. Reduced basal ganglia volumes in Tourette's syndrome using three-dimensional reconstruction techniques from magnetic resonance images. Neurology. 1993;43(5):941–9.
129. Makki MI, Govindan RM, Wilson BJ, Behen ME, Chugani HT. Altered fronto-striato-thalamic connectivity in children with Tourette syndrome assessed with diffusion tensor MRI and probabilistic fiber tracking. J Child Neurol. 2009;24(6):669–78.
130. Wheeler-Kingshott CAM, Cercignani M. About "axial" and "radial" diffusivities. Magnet Reson Med. 2009;61(5):1255–60.
131. Ferretti A, Babiloni C, Gratta CD, et al. Functional topography of the secondary somatosensory cortex for nonpainful and painful stimuli: an fMRI study. Neuroimage. 2003;20(3):1625–38.
132. Fahim C, Yoon U, Das S, et al. Somatosensory-motor bodily representation cortical thinning in Tourette: effects of tic severity, age and gender. Cortex. 2010;46(6):750–60.
133. Sowell ER, Kan E, Yoshii J, et al. Thinning of sensorimotor cortices in children with Tourette syndrome. Nat Neurosci. 2008;11(6):637–9.
134. Deng H, Gao K, Jankovic J. The genetics of Tourette syndrome. Nat Rev Neurol. 2012;8(4):203–13.

Chapter 3
Diffusion Magnetic Resonance Imaging and Its Applications in Movement Disorders

Jiun-Jie Wang and Yau-Yau Wai

Basic Principles of Diffusion Magnetic Resonance Imaging

Diffusion-Weighted Imaging (DWI)

Diffusion phenomenon is the result of thermal agitation from particles at temperatures above absolute zero degrees. The effect of water diffusion on nuclear magnetic resonance signal is mainly signal attenuation. If the medium is homogeneous, such that the water molecule is free to move, the signal decay curve can be described in a monoexponential manner [1]. Usually, the diffusion coefficient can be calculated from two images with different diffusion weightings, assuming the diffusion signal decay is purely monoexponential. The diffusion weighting of the magnetic resonance (MR) sequence, called "*b*-value" or "*b*-factor", describes the sensitivity of the sequence to the effect of water diffusion.

Typically an echo planar imaging (EPI) sequence is used in the MR diffusion studies due to temporal considerations (e.g., speed of acquisitions). The measured diffusion coefficient is called the "apparent diffusion coefficient" (ADC) because the spatial resolution of MRI is incapable of measuring the diffusion coefficient of individual proton molecules in water. What has been observed is the summary effect from all water protons within the voxel of interest, hence the term "apparent."

Early diffusion studies found that measured ADC in the biological environment is directionally dependent [2]. Therefore, the measured ADC is only meaningful when

J.-J. Wang (✉) · Y.-Y. Wai
Medical Imaging and Radiological Sciences, Chang Gung University,
259 Wen-Hua 1st Road, Taoyuan County, Taiwan
e-mail: jwang@mail.cgu.edu.tw

Medical Imaging and Intervention, Chang Gung Memorial Hospital, Linkou
5 Fu-Hsing Street, Taoyuan County, Taiwan
e-mail: yauwaiwu@ms4.hinet.net

F. B. Nahab, N. Hattori (eds.), *Neuroimaging of Movement Disorders,*
Current Clinical Neurology 44, DOI 10.1007/978-1-62703-471-5_3,

specifying the direction of the applied diffusion-weighting gradient; for example, ADC_x for diffusion-weighted gradient applied in x-direction. In clinical practice, the average from the principle diffusion directions is often reported, which is a reflection of the mean diffusivity (MD) within the voxel of interest.

Diffusion Tensor Imaging (DTI)

Because the water diffusion is directionally constrained in the biological environment, effort has been made to provide a quantitative and rotationally consistent diffusion model in MRI. One of the most successful models is DTI [3–6]. The diffusion tensor is a 3 by 3 matrix, consisting of the diffusion coefficient as measured along different directions (Eq. 3.1).

$$D = \begin{pmatrix} D_{xx} & D_{xy} & D_{xz} \\ D_{yx} & D_{yy} & D_{yz} \\ D_{zx} & D_{zy} & D_{zz} \end{pmatrix} \tag{3.1}$$

The measured ADC is positive and definite. The nature of symmetry reduced the unknowns in the diffusion tensor to 6 (i.e. 3 diagonal components and 3 off-diagonal components). Since one additional image without diffusion weighting and measured at the same echo time is required, the minimum number of images for the full tensor estimation is 7.

It is possible to reconstruct the diffusion tensor with more than the minimally required acquisitions, for example, measurements along more diffusion-encoding directions and/or more different b-values. Many optimization schemes may be employed for the diffusion data acquisition depending on the experimental goals [7–10]. For example, as a rule of thumb, the b-value multiplied by the ADC should be approximately 1.1 [11]. In the brain, because the expected ADC is approximately between 0.6 and 1.0 mm^2/s, a b-value of 1,000 s/mm^2 was often used.

Three eigenvalues (λ_1, λ_2, and λ_3) and 3 eigenvectors (ε_1, ε_2, and ε_3) can be calculated from the diffusion tensor. The eigenvectors point to the 3 orthogonal directions of the principal diffusion where the eigenvalues are the corresponding diffusivities. For purposes of visualization and diagnosis, maps of indices derived from the tensor have been proposed. These indices are usually a reflection of basic tensor properties, relating to either the magnitude or the directional dependence. An ideal index could be quantitative or semiquantitative, rotationally invariant, and without the need to sort the eigenvalues according to the amplitude.

A trace of the diffusion tensor (Trace (D)) is a reflection of the magnitude. By definition Trace (D) is the sum of the diagonal components of the tensor, which is a rotational invariant. Fractional anisotropy (FA) [4] is one of the most clinically used indexes that is related to the directionally dependent diffusion. FA is designed such that when the respective magnitudes of the 3 principal diffusion values are (1, 0, 0), FA equals 1 and means that diffusion occurs only along one axis and is

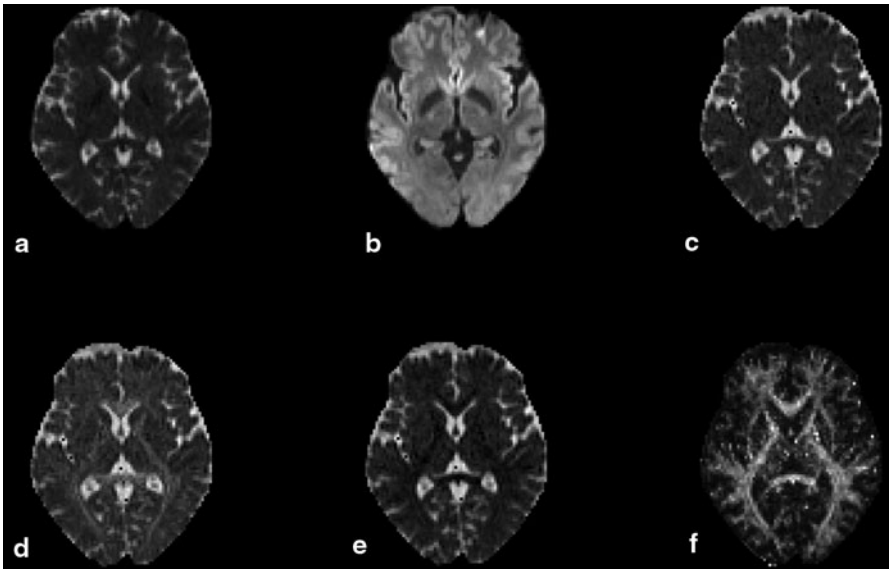

Fig. 3.1 Diffusion MRI of one normal volunteer. The images show: **a** nondiffusion weighted image, **b** diffusion weighted image (b-value = 1,000 mm^2/s), **c** mean diffusivity, **d** axial diffusivity, **e** radial diffusivity, and **f** fractional anisotropy. It should be noted that the contrast in the nondiffusion-weighted image (**a**) is intrinsically T2 weighted. The contrast in diffusion-weighted image (**b**) is potentially negative such that regions with high ADC appear *dark* but *bright* in the mean diffusivity (**c**). The intensity in fractional anisotropy is high in white matter where the water diffusion in the neuron fibers results in increased diffusion anisotropy

fully restricted along all other directions (anisotropic), whereas diffusion values of (1, 1, 1) represent an FA of 0 and indicate that diffusion is isotropic (i.e., unrestricted or equally restricted in all directions).

Song et al. [12] proposed two tensor-derived indexes: axial diffusivity (the largest eigenvalue) and radial diffusivity (RD; the average of the second and third eigenvalues). The diffusion in white matter was often modeled using cylindrical symmetry. The eigenvector corresponding to the largest eigenvalue pointed to the principle direction of the neuron fibers. Therefore, axial diffusivity defined the amplitude of water diffusion along the axial direction of the fiber. RD is the diffusion along the direction orthogonal to the major fiber bundles. The changes of these two indices were often related to the integrity of the neuron fiber. For example, changes in axial diffusivity are often attributed to the axonal damage [13, 14]. An increase of RD is usually related to the loss of myelin sheath integrity [12, 15]. However, it is worth pointing out that the changes of axial diffusivity/RD can be artefactual, especially in regions where fibers cross [16]. Therefore, the interpretation must be exercised with great care. Figure 3.1 demonstrates the various diffusion MRI images obtained from one healthy volunteer.

Tractography

There has been a strong interest in using DTI to perform in vivo tractography, since its invention. The technique assumes the direction of the principal diffusion in DTI is collinear to that in the neuron fibers. A voxel-by-voxel connection can be delineated from a seeding point and propagated along the direction of the principal diffusion. Early work by Conturo et al. [17] successfully demonstrated the fibers along the curvature of the splenium and extended into the occipital and parietal lobes. Various tracking algorithms have since been proposed and many freeware applications are currently available [18–20].

Tractography has been used in presurgical planning to guide surgical margins away from the involvement of neuron fibers for improved surgical outcome [21, 22]. Tractography can be used to differentiate infiltration from cytotoxic edema in order to assess the patient prognosis after successful surgery [23, 24]. It has also been used to visualize neural network integrity and changes in connectivity in neurodegenerative disorders [25, 26].

Instead of visualizing the individual neuron fibers, tract-based spatial statistics (TBSS) identify a common skeleton structure within the white matter [27, 28]. This permits statistical comparison of differences in diffusion properties between two groups of subjects [29, 30].

Diffusion Imaging in Movement Disorders

Morphological studies of neurological movement disorders using MRI commonly report various extents of atrophy in relevant brain regions [31, 32]. Since functional alteration may precede the observable anatomical changes, diffusion imaging was expected to bring new insight into the underlying mechanism of the disease and provide improved diagnosis and prognosis information. In the following section, we will describe recent findings in the major parkinsonian disorders, including idiopathic Parkinson disease (iPD), progressive supranuclear palsy (PSP), and multiple system atrophy (MSA).

Idiopathic Parkinson Disease

The motor symptoms of idiopathic Parkinson disease have been attributed to dopaminergic neuronal death within the basal ganglia. There is a growing interest in imaging Parkinson disease with diffusion MRI, because of the potentially increased extracellular space due to cell death that may be detectible by ADC [33]. In a whole-brain analysis of patients with de novo iPD, an increased FA was noted and was more profound in the akinetic rigid subtype of iPD [34].

Region of interest (ROI)- based studies have usually focused on the basal ganglia. The findings from DTI are still controversial. In a case-control study, Chan et al. [35] reported no significant differences except in substantia nigra where FA was significantly reduced in patients and overlap was present between patients and controls. In contrast, Vaillancourt et al. [36] showed that FA in the rostral part of substantial nigra can separate the patients with iPD from normal, with a sensitivity and specificity of 100 %.

Using a voxel-wise analysis, additional brain regions that could be affected were reported, including decreased FA in bilateral frontal lobes, the supplementary motor area, the presupplementary motor area, and the cingulum [37]. White matter involvement has also been detected in patients using TBSS, which suggests an altered neural network integrity involving basal ganglia regions and extending up to the supplementary motor area in the patients [38].

Progressive Supranuclear Palsy (PSP)

The neuropathology of progressive supranuclear palsy (PSP) is related to neuronal and glial lesions of tau protein, with preferential involvement of the basal ganglia, midbrain, pons, and medulla [39, 40]. In basal ganglia and the surrounding white matter, a reduced FA and an increased MD have been noted; both being related to an increase in RD. This observation was attributed to reduced myelination [41]. DWI can also discriminate patients with PSP from iPD, with an increased ADC located in putamen, globus pallidus, and caudate nucleus in PSP [42].

White matter-tract degeneration was also reported [43], noticeably in the superior cerebellar peduncles and corpus callosum, where the measured FA correlated with disease severity. Similar regions were reported by Knake et al. [44] using TBSS. The changes may be related to an increase of RD and the authors attribute the image findings to axonal and/or myelin alterations.

Multiple System Atrophy (MSA)

Patients of multiple system atrophy (MSA) show varying degrees of atrophy in the central nervous system including the cerebellum, cerebellar peduncles, pons, medulla, and putamen, together with excessive iron deposition within the striatum [45]. DTI studies of the basal ganglia have found increased MD and a reduced FA when compared with normals, particularly in the putamen [46]. ADC is also significantly higher in pons, cerebellum, and putamen [47]. The increased ADC in putamen helped distinguish MSA from iPD and healthy volunteers [48]. ADC values in putamen of patients of the parkinsonian subtype of MSA (MSA-P) were positively correlated with clinical severity as assessed by both the Unified Multiple System Atrophy Rating Scale and the Motor section of the Unified Parkinson's

Disease Rating Scale (UPDRS) [49]. Other regions with increased ADC included the middle cerebellar peduncles and cerebellum. Reductions in FA have also been found in the pyramidal tract, middle cerebellar peduncles, and white matter of the cerebellum [50]. It should be noted that white matter abnormalities were both supra and infratentorial [45]. Patterns of degeneration include progressive involvement of the corticopontocerebellar tract, selective loss of the transverse pontocerebellar tract, and preservation of the corticospinal tracts [51].

Limitations of Diffusion Tensor Imaging (DTI)

Although clinically successful, DTI comes with many limitations [52]. In clinical practice, no accepted model exists regarding changes observed in gray matter. Therefore, it is difficult to interpret the findings involved in cortical or deep gray matter regions, which are particularly relevant to movement disorders [41]. Efforts to better resolve the multiple fiber directions in a voxel of interest have included diffusion spectrum imaging [53] and q-ball imaging [54]. While these newer methods have been successful, the directional resolution was often achieved with prolonged acquisition times.

Diffusion Kurtosis Imaging (DKI)

Diffusion in a biological environment can be significantly different from that of a free and homogeneous medium. Therefore, the distribution of water diffusion maybe deviated from normality. It has been observed that the signal attenuation curve induced by water diffusion is no longer an ideal monoexponential shape, and was often modeled by the weighted sum of two exponential curves, a phenomena referred to as biexponential decay [55]. The observed signal decay was assumed to be a summary effect from different contributions in the intracellular and extracellular compartments.

DKI attempts to quantify the extent of deviation from Gaussian distribution. Kurtosis is a statistical term used to describe the degree of deviation from a Gaussian distribution in a population. If the distribution is more peaked in the center but reduced in both tails, the kurtosis will increase even though the mean remains unchanged. On the other hand, if the distribution is flat in the centre but increased in tails, the kurtosis decreases.

The measured diffusion kurtosis is along the specific gradient direction of interest. Usually, images with multiple different *b*-values are acquired. Both the diffusion coefficient and the diffusion kurtosis can then be calculated using curve fitting. The apparent diffusion kurtosis experiment can be further extended to a full kurtosis tensor in a manner similar to DTI. The diffusion kurtosis tensor is a matrix of 81 elements (3 by 3 by 3 by 3) [56]. Because of symmetry, at least 15 nonlinear diffusion-encoding

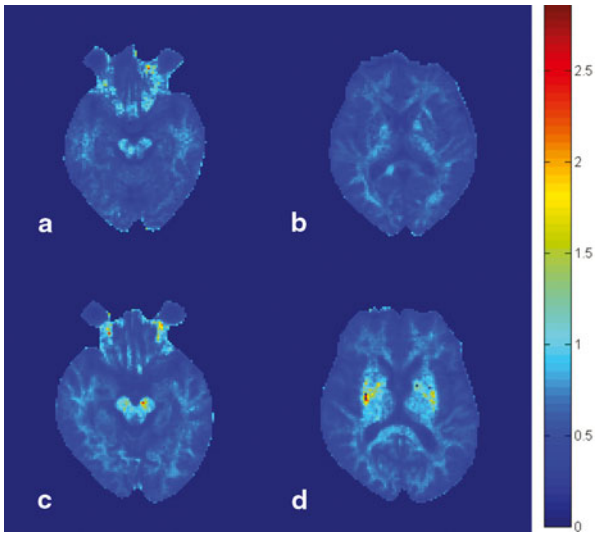

Fig. 3.2 Diffusion kurtosis imaging in the diagnosis of Parkinson disease. The images show the mean diffusion kurtosis from a normal volunteer (**a** and **b**) and a patient with Parkinson disease (**c** and **d**). A significant increase in diffusion kurtosis can be noted in the substantia nigra (**c**) and striatum (**d**), compared with the corresponding locations in the normal volunteer (**a** and **b**, respectively)

directions are required. Indices can be derived from the full kurtosis tensor, including the mean kurtosis, axial kurtosis, radial kurtosis, and kurtosis of FA. Jensen et al. [56] recommend an acquisition scheme for the reconstruction of the full DKI tensor using 3 *b*-values of 0, 1,000, and 2,000 mm^2/s and 30 diffusion-encoding directions.

Diffusion Kurtosis Imaging in Idiopathic Parkinson disease (iPD)

A recent study of iPD using DKI has brought new interest to the topic. Wang et al. [57] showed that patients with probable iPD have a significantly increased diffusion kurtosis in all regions of basal ganglia when compared with the age-matched healthy controls. The mean diffusion kurtosis was calculated from a series of diffusion-weighted images with *b*-values ranging from 0 to 4,000 mm^2/s. The mean kurtosis was compared with the corresponding MD and FA for diagnostic performance. The results indicated that the area under curve from DKI in all regions within basal ganglia outperformed conventional diffusion tensor. The sensitivity and specificity of mean kurtosis values in the substantia nigra were of 87 and 92 %, respectively. The best diagnostic predictors were the ipsilateral substantia nigra and putamen, where the areas under the receiver-operating characteristic (ROC) curves were both 95 %. Although statistically significant, the area under the ROC curve in the corresponding FA was only 65 %.

The study showed that mean kurtosis in all basal ganglia regions were significantly higher in patients with iPD as compared with the healthy subjects and could distinguish these two groups. DKI compares favorable with current dopamine transporter-imaging methods that require the use of radioactive ligands. Figure 3.2

demonstrates the contrast of DKI is good enough for visual diagnosis. The increased sensitivity and specificity of DKI, with it intrinsically non-invasive nature, could compensate for the extended acquisition time when compared to DTI. Using the modern echo planar imaging technique and for a whole brain coverage, this additional time could be less than minutes. In conclusion, DKI can lead to a substantial improvement in the MRI-based diagnosis of iPD.

Conclusions and Future Directions

Diffusion magnetic resonance imaging has been widely used in studies of neurological disorders with demonstrated success, specifically in applications related to white matter. The application of these exciting new methods to neurological movement disorders provide novel ways to explore brain structure for clinical diagnostic purposes and a better understanding of pathophysiology. DKI has provided a preliminary success in the diagnosis of Parkinson disease. In the future, characterization of restricted diffusion in the brain in general and gray matter in particular will be of interest, since it may shed new insights into the microstructural environmental changes that take place in neurodegeneration.

References

1. Stejskal D. Use of spin echoes in a pulsed magnetic-field gradient to study anisotropic, restricted diffusion and flow. J Chem Phys. 1965;43(10):3597–603.
2. Moseley ME, et al. Diffusion-weighted MR imaging of anisotropic water diffusion in cat central nervous system. Radiology. 1990;176(2):439–45.
3. Pierpaoli C, Basser PJ. Toward a quantitative assessment of diffusion anisotropy. Magn Reson Med 1996;36:893–906.
4. Basser PJ, Pierpaoli C. Microstructural and physiological features of tissues elucidated by quantitative-diffusion-tensor MRI. J Magn Reson B. 1996;111(3):209–19.
5. Basser PJ, Mattiello J, LeBihan D. Estimation of the effective self-diffusion tensor from the NMR spin echo. J Magn Reson B. 1994;103(3):247–54.
6. Pierpaoli C, Basser PJ. Toward a quantitative assessment of diffusion anisotropy. Magn Reson Med. 1996;36(6):893–906.
7. Hasan KM, Alexander AL, Narayana PA. Does fractional anisotropy have better noise immunity characteristics than relative anisotropy in diffusion tensor MRI? An analytical approach. Magn Reson Med. 2004;51(2):413–7.
8. Hasan KM, Parker DL, Alexander AL. Comparison of gradient encoding schemes for diffusion-tensor MRI. J Magn Reson Imaging. 2001;13(5):769–80.
9. Conturo TE, et al. Diffusion MRI: precision, accuracy and flow effects. NMR Biomed. 1995;8(7–8):307–32.
10. Wang JJ, et al. Novel diffusion anisotropy indices: an evaluation. J Magn Reson Imaging. 2006;24(1):211–7.
11. Xing D, et al. Optimised diffusion-weighting for measurement of apparent diffusion coefficient (ADC) in human brain. Magn Reson Imaging. 1997;15(7):771–84.
12. Song SK, et al. Demyelination increases radial diffusivity in corpus callosum of mouse brain. Neuroimage. 2005;26(1):132–40.

13. DeBoy CA, et al. High resolution diffusion tensor imaging of axonal damage in focal inflammatory and demyelinating lesions in rat spinal cord. Brain. 2007;130(Pt 8):2199–210.
14. Budde MD, et al. Axial diffusivity is the primary correlate of axonal injury in the experimental autoimmune encephalomyelitis spinal cord: a quantitative pixel-wise analysis. J Neurosci. 2009;29(9):2805–13.
15. Klawiter EC, et al. Radial diffusivity predicts demyelination in ex vivo multiple sclerosis spinal cords. Neuroimage. 2011;55(4):1454–60.
16. Wheeler-Kingshott CA, Cercignani M, About "axial" and "radial" diffusivities. Magn Reson Med. 2009;61(5):1255–60.
17. Conturo TE, et al. Tracking neuronal fiber pathways in the living human brain. Proc Natl Acad Sci U S A. 1999;96(18):10422–7.
18. Tournier D. MRtrix: MR tractography including crossing fibers. Melbourne: Brain Research Institute; 2012.
19. Jiang H, et al. Dti studio: resource program for diffusion tensor computation and fiber bundle tracking. Comput Methods Programs Biomed. 2006;81:106–16. [www.dtistudio.org]
20. P. A. Cook, Y. Bai, S. Nedjati-Gilani, K. K. Seunarine, M. G. Hall, G. J. Parker, D. C. Alexander, Camino: Open-Source Diffusion-MRI Reconstruction and Processing, 14th Scientific Meeting of the International Society for Magnetic Resonance in Medicine, Seattle, WA, USA, p. 2759, May 2006.
21. Romano A, et al. Pre-surgical planning and MR-tractography utility in brain tumour resection. Eur Radiol. 2009;19(12):2798–808.
22. Arfanakis K, Gui M, Lazar M. Optimization of white matter tractography for pre-surgical planning and image-guided surgery. Oncol Rep. 2006;15:1061–4.
23. Talos IF, et al. Volumetric assessment of tumor infiltration of adjacent white matter based on anatomic MRI and diffusion tensor tractography. Acad Radiol. 2007;14(4):431–6.
24. Cha S. Update on brain tumor imaging: from anatomy to physiology. AJNR Am J Neuroradiol. 2006;27(3):475–87.
25. Ciccarelli O, et al. Diffusion-based tractography in neurological disorders: concepts, applications, and future developments. Lancet Neurol. 2008;7(8):715–27.
26. Nilsson C, et al. Tracking the neurodegeneration of parkinsonian disorders—a pilot study. Neuroradiology. 2007;49(2):111–9.
27. Smith SM, et al. Tract-based spatial statistics: voxelwise analysis of multi-subject diffusion data. Neuroimage. 2006;31(4):1487–505.
28. Smith SM, et al. Advances in functional and structural MR image analysis and implementation as FSL. Neuroimage. 2004;23:S208–S19.
29. Chang CC, et al. Clinical significance of the pallidoreticular pathway in patients with carbon monoxide intoxication. Brain. 2011;134(Pt 12):3632–46.
30. Chang CC, et al. Multi-parametric neuroimaging evaluation of cerebrotendinous xanthomatosis and its correlation with neuropsychological presentations. BMC Neurol. 2010;10:59.
31. Ghaemi M, et al. Differentiating multiple system atrophy from Parkinson's disease: contribution of striatal and midbrain MRI volumetry and multi-tracer PET imaging. J Neurol Neurosurg Psychiatry. 2002;73(5):517–23.
32. Burton EJ, et al. Cerebral atrophy in Parkinson's disease with and without dementia: a comparison with Alzheimer's disease, dementia with Lewy bodies and controls. Brain. 2004;127 (Pt 4):791–800.
33. Moffat BA, et al. Functional diffusion map: a noninvasive MRI biomarker for early stratification of clinical brain tumor response. Proc Natl Acad Sci U S A. 2005;102(15):5524–9.
34. Tessa C, et al. A whole-brain analysis in de novo Parkinson disease. AJNR Am J Neuroradiol. 2008;29(4):674–80.
35. Chan LL, et al. Case control study of diffusion tensor imaging in Parkinson's disease. J Neurol Neurosurg Psychiatry. 2007;78(12):1383.
36. Vaillancourt DE, et al. High-resolution diffusion tensor imaging in the substantia nigra of de novo Parkinson disease. Neurology. 2009;72(16):1378.

37. Karagulle Kendi AT, et al. Altered diffusion in the frontal lobe in Parkinson disease. AJNR Am J Neuroradiol. 2008;29(3):501–5.
38. Zhan W, et al. Regional alterations of brain microstructure in Parkinson's disease using diffusion tensor imaging. Mov Disord. 2012;27(1):90–7.
39. Collins SJ, et al. Progressive supranuclear palsy: neuropathologically based diagnostic clinical criteria. J Neurol Neurosurg Psychiatry. 1995;58(2):167–73.
40. Spillantini MG, Bird TD, Ghetti B. Frontotemporal dementia and parkinsonism linked to chromosome 17: a new group of tauopathies. Brain Pathol. 1998;8(2):387–402.
41. Wang JJ, et al. Microstructural changes in patients with progressive supranuclear palsy: a diffusion tensor imaging study. J Magn Reson Imaging. 2010;32(1):69–75.
42. Seppi K, et al. Diffusion-weighted imaging discriminates progressive supranuclear palsy from PD, but not from the Parkinson variant of multiple system atrophy. Neurology. 2003;60(6):922–7.
43. Whitwell JL, et al. Clinical correlates of white matter tract degeneration in progressive supranuclear palsy. Arch Neurol. 2011;68(6):753–60.
44. Knake S, et al. In vivo demonstration of microstructural brain pathology in progressive supranuclear palsy: a DTI study using TBSS. Mov Disord. 2010;25(9):1232–8.
45. Tha KK, et al. Microstructural white matter abnormalities of multiple system atrophy: in vivo topographic illustration by using diffusion-tensor MR imaging. Radiology. 2010;255(2):563–9.
46. Seppi K, et al. Topography of putaminal degeneration in multiple system atrophy: a diffusion magnetic resonance study. Mov Disord. 2006;21(6):847–52.
47. Ito M, et al. Usefulness of combined fractional anisotropy and apparent diffusion coefficient values for detection of involvement in multiple system atrophy. J Neurol Neurosurg Psychiatry. 2007;78(7):722–8.
48. Schocke MF, et al. Diffusion-weighted MRI differentiates the Parkinson variant of multiple system atrophy from PD. Neurology. 2002;58(4):575–80.
49. Pellecchia MT, et al. Diffusion-weighted imaging in multiple system atrophy: a comparison between clinical subtypes. Mov Disord. 2009;24(5):689–96.
50. Wang PS, et al. Use of diffusion tensor imaging to identify similarities and differences between cerebellar and parkinsonism forms of multiple system atrophy. Neuroradiology. 2011;53(7):471–81.
51. Makino T, Ito S, Kuwabara S. Involvement of pontine transverse and longitudinal fibers in multiple system atrophy: a tractography-based study. J Neurol Sci. 2011;303(1–2):61–6.
52. Jones DK, Cercignani M. Twenty-five pitfalls in the analysis of diffusion MRI data. NMR Biomed. 2010;23(7):803–20.
53. Wedeen VJ, et al. Mapping complex tissue architecture with diffusion spectrum magnetic resonance imaging. Magn Reson Med. 2005;54(6):1377–86.
54. Tuch DS, et al. High angular resolution diffusion imaging reveals intravoxel white matter fiber heterogeneity. Magn Reson Med. 2002;48(4):577–82.
55. Clark CA, LeBihan D. Water diffusion compartmentation and anisotropy at high b values in the human brain. Magn Reson Med. 2000;44(6):852–9.
56. Jensen JH, Helpern JA. MRI quantification of non-Gaussian water diffusion by kurtosis analysis. NMR Biomed. 2010;23(7):698–710.
57. Wang JJ, et al. Parkinson disease: diagnostic utility of diffusion kurtosis imaging. Radiology. 2011;261(1):210–7.

Chapter 4
PET/SPECT Imaging During Dynamic Motor Control

Kazumi Iseki and Takashi Hanakawa

Introduction

With the recent development of neuroimaging techniques, we can measure brain activity during a variety of movements in detail. However, when it comes to walking accompanied by locomotion, the imaging modalities that can be applied are limited. Among such modalities, gait activation single-photon emission computed tomography (SPECT) and gait activation positron emission tomography (PET) are valuable tools that enable us to measure brain activity during gross bodily movements. Such imaging studies have provided evidence that not only musculoskeletal and peripheral nervous systems, but also the central nervous system (CNS) consisting of the spinal cord and brain play significant roles in the control of walking movement. In the CNS, the basal ganglia-thalamocortical system is shown to be quite important for the supraspinal control of normal bipedal walking; in particular, the brain activity in the cerebral cortex seems essential. Neuroimaging techniques using radiotracers such as SPECT and PET are applicable for research into the neural substrates involved in gait disorders caused by several diseases. A variety of neural networks are impaired in gait disorders, and it is essential for us to investigate the connectivity among those networks. Further research will be essential for the progression of research on gait.

K. Iseki (✉)
Department of Behavioral Neurology and Cognitive Neuroscience,
Tohoku University Graduate School of Medicine,
2-1, Seiryo-machi, Aoba-ku, Sendai, Miyagi 980-8575, Japan
e-mail: kazumi.iseki@gmail.com

T. Hanakawa
Department of Molecular Imaging, Integrative Brain Imaging Center,
National Center of Neurology and Psychiatry,
4-1-1 Ogawahigashi, Kodaira 187-8511, Japan
e-mail: hanakawa@ncnp.go.jp

F. B. Nahab, N. Hattori (eds.), *Neuroimaging of Movement Disorders,*
Current Clinical Neurology 44, DOI 10.1007/978-1-62703-471-5_4,

Neuroimaging Methods Using Radioactive Tracers

Recent advances in neuroimaging techniques such as functional magnetic resonance imaging (fMRI) allow us to study the functional neuroanatomy of various motor, sensory, cognitive, and emotional processes noninvasively in humans. However, when it comes to the study of walking movement accompanied by locomotion, the modalities that can be applied are quite limited. Neuroimaging methods applying nuclear medicine such as SPECT with ^{99m}Tc-bound perfusion tracers or PET with ^{18}F-deoxyglucose (FDG), enable us to investigate the neural substrates of dynamic movements such as walking. However, the temporal resolution of these methods is low compared with that of other modalities. Thus, unlike experiments using fMRI, it is difficult to measure brain activity during tasks of short duration (order of seconds) with these modalities. Instead, we assume that the total amount of intracranial radioactivity at a certain time after the initiation of the movement would summarize the brain activity associated with the movement performed during that period. Comparison of scans at rest and during a movement task, or between conditions, yields brain activation pattern during that particular task.

There exist some important differences between SPECT and PET. With SPECT, we may apply a split-dose method, and the scanning of two conditions such as rest and gait can be done within a day. After injection, SPECT perfusion radiotracers (^{99m}Tc-ECD or ^{99m}Tc-HMPAO) are trapped in the brain within several minutes and remain stable for hours. Hence, the duration of the movement task can be short in time (a few minutes) to get perfusion images reflecting a certain task condition. Further, we can split a regular dose of perfusion tracers into two fractions, and inject them to examine two different conditions one after another (split-dose method). However, this split-dose method has not been applicable to FDG-PET scanning to date, and the duration of the movement task required to acquire images reflecting glucose metabolism is much longer than that required to acquire SPECT perfusion images. For example, subjects are asked to keep walking for 5 min if we are going to apply the split-dose method for perfusion SPECT imaging [1–3]. On the other hand, subjects kept walking for about 20–30 min [4, 5], when FDG-PET scanning was used. Performing a gait task for such a long time could be quite difficult for patients with severe gait disturbances, and this factor limits the selection of subjects. Also, the scanning of the two conditions need to be done on different days with FDG-PET. Therefore, the conditions of the subjects, which might differ between dates, can potentially influence the result. Nonetheless, there is an advantage of PET scanning over SPECT, in that PET (5–10 mm) has better spatial resolution than SPECT (10–20 mm).

There are several problems with gait activation SPECT/PET studies that should be considered. One is the condition of gait tasks. It would be preferable to ask subjects to walk freely as they do in their normal life, rather than asking them to walk on a treadmill, which is an artificial walking condition. However, the gait activation studies would require a facility with a very long corridor in a secluded place to avoid encountering other people and turning to and fro frequently. This is especially the case

with studies with long task duration such as FDG-PET, and it is not practical in some countries such as Japan under strict radiation control by law. Furthermore, walking might be affected by visual information in such situation [6]. By employing treadmill walking, we are able to inject the tracer during gait conditions while staying beside the treadmill. Hence, the subjects remain in the same area and we do not have to carry the radiotracer and accompany subjects who are walking around. With treadmill walking, it is possible to keep the visual stimuli related to the task consistent among subjects. Further, the use of a treadmill enables us to focus on specialized reactions to visual cues, for example, by placing stimuli onto the belt of the treadmill [1].

Moreover, the amount of task load (walking distance and speeds) may not be consistent among subjects while walking in a corridor. Although this factor can be controlled with treadmill walking by keeping the same speed and task duration, Mishina et al. [5] adjusted the speed of the treadmill according to the ability of patients with cerebellar atrophy when applying gait activation PET.

Despite those advantages, treadmill walking could be regarded as an artificial environment with a settled condition, because the subjects have to match their gait to the moving treadmill. In addition, they have to stay in the same place while making sequential movements, and this condition certainly differs from natural gait movement in which subjects are moving forward with steps to be made. Due to safety concern, subjects who have gait disturbances are asked to hold the bars of the treadmill. In such situations, it is possible that sensory input from the hand might affect brain activity. Furthermore, the observation of the belt, which moves regularly, or the transitive regular movement generated by the treadmill itself, might work as a cue. This could modulate walking behavior and thereby influence the related brain activity. As such, there are a variety of issues need to be considered for gait activation studies. There is no established gold standard and researchers need to choose the task conditions that fit their study considering what they think is most important.

Another point to be considered is that images with absolute values (reflecting quantity of blood flow/perfusion) are not available with gait activation SPECT/PET. Imaging methods for absolute value measurement (e.g., Patlak plot) require us to obtain dynamic images. This procedure requires subjects to stay still during scanning immediately after the injection, and this is impossible for a walking task. Therefore, we are only able to take images with relative values and the lack of absolute value information could restrict possibilities of further analyses.

SPECT Method Gait Activation

Here, we discuss the gait activation SPECT methodology that we have applied in our previous studies. Figure 4.1 summarizes the procedure.

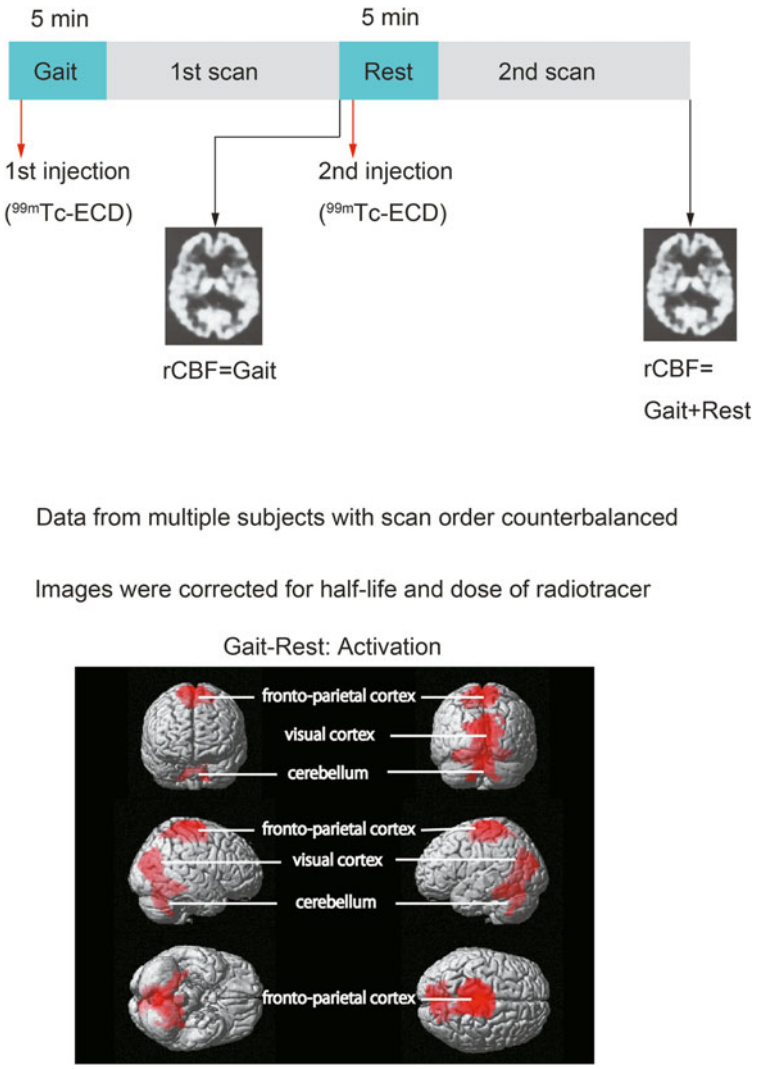

Fig. 4.1 The method of activation SPECT is shown. The task order of the sequence here is gait first followed by rest. The radiotracer (300 MBq of ^{99m}Tc-ECD) was administered when the experimenter judged that the gait of the subjects reached a steady state. The subjects kept walking for 5 min after tracer injection, and were moved onto a scanner bed after task completion. They were positioned under the guidance of a 3D laser-reference system and immobilized using a comfortable restraint device. The subjects remained supine on the scanner bed for the subsequent rest condition. They received additional radiotracer (500 MBq of ^{99m}Tc-ECD) in the resting condition and remained still for 5 min on the scanner bed in a supine position after tracer injection. The first and second doses of radiotracer and the corresponding scan times were adjusted to reduce subtraction errors between the first and second blood flow images. The order of task conditions was counterbalanced across subjects to reduce order effects. Perfusion images were analyzed using statistical parametric mapping (SPM). The images were corrected for the half-life and dose of the tracer, and perfusion images corresponding to the second task condition were created by image subtraction. Increases in cerebral perfusion during the walk condition compared with the rest condition were explored among all subjects, and then for each group separately

Gait Conditions

In our previous studies, we focused on studying subjects with idiopathic Parkinson disease (iPD) [1, 2] and those with vascular parkinsonism ascribed to age-related white matter changes (ARWMC) [3] in comparison to healthy volunteers. Therefore, we adopted a very slow treadmill speed of ~ 0.2 m/s, considering the worst performance among the subjects in the studies listed above. We recognized that walking at this speed might be unnatural for those who usually walk much faster in daily life, but modified conditions in accordance with the needs of the study and the conditions of the subjects.

It is important to control the effects of sensory stimuli as strictly as possible during the experiment. We chose walking on a treadmill, and the subjects were asked to hold the bars attached to a treadmill for safety, so the results might be affected by sensory inputs from upper extremities as described. Subjects were also asked to maintain fixation on a wall marked in front of them to exclude the effect of visual information from the moving treadmill. We considered that such an effect should be taken into account in the rest condition as well, hence the subjects were asked to open their eyes and stare at one point even during the scanning at rest.

SPECT Scanning

Blood pressure and pulse rate should be measured. These measurements should be taken just before the initiation and after the end of walking, and, at the start and end of the first and second SPECT scans. This procedure is necessary because the cerebral blood flow might be influenced by systemic hemodynamic changes. For example, when we are going to make a comparison among groups, such measurements will be necessary to show that the difference in activities acquired is not affected by differences in such hemodynamics at the system level. This would be especially important for studying gait disorders potentially accompanied by orthostatic hypotension.

Then, the subjects are asked to walk on a treadmill to become accustomed to walking in such a specialized environment. We place a venous line in the cubital vein located at the elbow. Subjects are asked to walk on the treadmill, and then the radiotracer (^{99m}Tc-ECD or ^{99m}Tc-HMPAO; Dosing: $\sim$300 MBq) is injected after we deem that the subject has reached a steady gait.

Because the consecutive SPECT and subtraction technique encounters subtraction errors, the values of R_d (administered dose ratio of the second study SPECT against the first) and R_t (acquisition time ratio of the second study SPECT against the first) must be selected carefully [7]. The larger these values, the smaller the subtraction error. As for the gait activation, subject motion occurs between the two SPECT studies, and a large R_d will help savage the rest image by visual assessment without subtraction, because it diminishes the contamination of the first SPECT into the second. However, too large R_d results in longer time intervals between tracer injections.

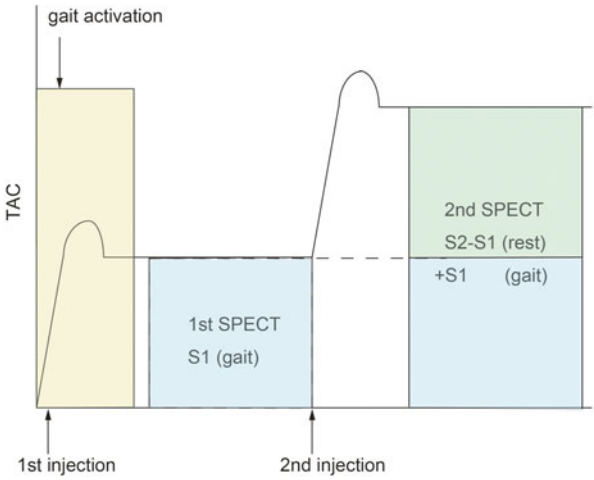

Fig. 4.2 The theory implied in the split-dose method is shown. This is the example with the sequence applying a gait condition followed by rest. The first image (*S1*) represents the activation of gait, and the second image (*S2*) represents that of rest plus gait as shown in the figure. With that, the *S2-S1* should represent the rest. Thus, *S1* and *S2-S1* would be used as representative images of gait and rest, respectively, both of which would be subjected to the group analysis with statistical parametric mapping (SPM) after dose correction. *TAC* time-activity curve

Such time intervals would be limited especially when we use the ^{99m}Tc- HMPAO considering the deterioration in radiochemical purity. Based on these reasons, the R_d ranges from 1 to 4 in proportion to the R_t ranging from 2 to 1/3. For example, we injected 300 MBq for the first injection, and 500 MBq for the second injection. In this way, we can keep the scanning time to be the same between the two occasions. The radioactivity of the radiotracer to be administered is counted each time. For example, when we are going to analyze gait and rest conditions, the amount of radiotracers should be measured just before the first condition (gait or rest). The dosage should be corrected in accordance with the half-life of the tracer, and then adjusted again at the intermediate point between the start and end of the first SPECT scan (A1). After the first scan, the residual amount left in the injector should be counted and adjusted as above (B1). Then, the subtraction of B1 from A1 (A1 − B1) provides the radiotracer dosage injected at the first scan (D1). The same procedure should be repeated for the second condition (rest or gait) as well, and the first amount (A2) and the residual amount left in the injector (B2) should be measured and adjusted to the intermediate point. Then, subtraction of B2 from A2 (A2 − B2) provides the dosage at the second scan (D2). For the first (*S1*) and second (*S2*) images, a dose correction should be applied, i.e., *S1/D1 and S2/D2* should be counted. Calculations of this kind can easily be done using the image calculator option provided with the statistical parametric mapping (SPM) software. Images such as S1/D1 and *(S2/D2-S1/D1)* can be used as a representative image of gait and rest respectively, or vice versa. This methodology is explained in Fig. 4.2.

The task order may induce a sequential effect that might influence the result. Therefore, we counterbalance this effect by applying a gait condition followed by rest in half of the subjects and rest followed by gait in the other half. When applying the former sequence, the image reflecting gait is acquired in supine position after the gait task, and the image reflecting rest is acquired soon afterward with the subject in the same position. In this way, the possibility that the location of the head would be drastically different is minimized. However, with the latter sequence, subjects have to walk on the treadmill after images reflecting rest are acquired, meaning they would need to go back to the scanner, raising the possibility that head position would be different. Thus, caution should be paid to any deviation in brain location. In our facility, we not only used laser pointers to keep the position of the head constant, but also attached tape to parts of the clothes or faces of the subjects to keep subjects in the same position.

Data Analysis

Analysis of the images can be done using SPM (Welcome Department of Cognitive Neurology, Institute of Neurology, University College of London; http://www.fil.ion.ucl.ac.uk/spm/) implemented on MATLAB (The MathWorks Inc., Massachusetts, USA) or similar software. Realignment of the two images, spatial normalization to a SPECT perfusion template, and smoothing are carried out for preprocessing. We adopt full-width at half-maximum (FWHM) of 8–10 mm or even more for a smoothing kernel, considering the spatial resolution of SPECT.

For statistical analyses, comparisons between images during gait and rest are performed for all subjects within a group, and then, between groups (e.g., disease group versus normal volunteer group). Age, gait analysis data, and other parameters might be employed as covariates as necessary. In our experience with healthy subjects, the activation pattern resulting from the contrast between walking and rest conditions mainly consists of three clusters. The first cluster is medial frontoparietal cortex centered at the supplementary motor area (SMA) together with primary sensorimotor cortex; the second is around the visual cortex; and the third is around the cerebellum. This activation pattern is quite robust for gait activation studies with SPECT and consistent across our studies even when we apply a strict threshold like family-wise error (FWE)-corrected $p < 0.05$ as long as we had ten or more subjects.

Identification of coordinates could be done using software such as Talairach Daemon (http://www.talairach.org/), Anatomy Toolbox that can be implemented in SPM, or any other localization software; but it should be noted that the coordinate system in analysis software and a localization tool might be different. The data following SPM analysis are often based on the Montreal Neurological Institute (MNI) template, and localization software might be based on Talairach and Tournoux's template. If this is the case, we may need to use software for the conversion of the coordinates (http://imaging.mrc-cbu.cam.ac.uk/imaging/MniTalairach).

Approaching the Pathophysiology of Gait and Posture Disorders: Applying Activation SPECT and PET

Cerebellum

The cerebellum is well known for its importance in maintaining balance and posture. The cerebellum is also involved in the control of muscle tone and of phases of limb movements, the integration of which is thought to concern interlimb coordination and adaptation to a new walking condition [8, 9]. Furthermore, there exists a locomotor region (CLR) within the cerebellum. Continuous electric stimulation with low intensity in the middle of the hook bundle in the cerebellum increases muscle tone and evokes gait movement on a moving treadmill [10]. Information regarding the activity of the central pattern generator (CPG) including the rhythmic pattern of gait is sent to the cerebellum [11]. Together, the cerebellum seems to play crucial roles in walking as well as maintaining a standing posture.

Several studies applying PET activation protocols have approached the cerebellar mechanisms involved in the control of posture and gait in humans, enabling us to directly investigate brain activity during gait or standing.

Mishina et al. [5] applied FDG-PET to patients with olivopontocerebellar atrophy (OPCA) and control subjects. They found that the pyramis, parts of the cerebellar vermis (the declive-folium-tuber and the culmen), and the thalamus were activated during walking in both groups, suggesting that these substrates play important roles in human gait. Furthermore, they found that gait activation in the cerebellar pyramis was lower in patients compared with normal individuals, suggesting that dysfunction of the cerebellar pyramismay partly explain the pathophysiology of the ataxic gait in OPCA patients. However, the possibility could not be excluded that this finding reflected atrophy rather than functional impairment.

Ouchi et al. [12] applied a radioactive water PET protocol to normal subjects to study the regulatory mechanism of standing. They used a special PET scanner with a mobile gantry, which allowed them to scan the brain while a subject was maintaining a standing posture. Their study revealed that maintaining standing posture compared with maintaining supine posture mainly activated the cerebellar vermis and visual association cortex. Their findings suggest that the cerebellar vermis plays an important role in maintenance of standing posture and that the visual association cortex might process visual information more vigorously while standing than while lying.

Basal Ganglia-Thalamocortical Loop

Outputs from the basal ganglia (BG) control movement via the BG-thalamocortical loop and the BG-brainstem pathway. The BG are deeply involved in the control of movement timing, muscle tone, and gait rhythm.

A representative disease involving dysfunctions of the BG is iPD. The major symptoms of iPD are bradykinesia, increased muscle tone (muscle rigidity), resting tremor, gait disturbance, and postural instability.

Several studies applying activation SPECT or PET have addressed the pathophysiological mechanisms underlying gait disturbance in iPD. Ouchi et al. [13] studied the changes in dopamine transporter (DAT) availability in the BG during walking, using gait activation PET. They found an increase in the level of dopamine release, represented by a reduction in DAT binding in the nigrostriatal projection area, during walking. Furthermore, dopamine release in the putamen, which is usually seen in control subjects, was lacking in iPD subjects; by contrast, dopamine release in the caudate nucleus was increased, which might reflect the pathophysiology or compensatory mechanisms associated with gait disturbance in iPD patients. This study suggests that a shift in dopamine release within the BG might underlie such disturbances.

Hanakawa et al. [2] used gait activation SPECT and noted reduced activation of the medial frontal motor areas, including SMA, during walking in iPD patients.

Moreover, the same group showed that the lateral premotor area was activated when iPD patients showed an improvement of gait by visual cues (paradoxical gait), suggesting that SMA underactivation might be compensated for by the overactivation of the premotor cortex [1].

Similar to iPD, other atypicalparkinsonisms also demonstrate gait dysfunction. An example is vascular parkinsonism (vPD). Individuals with age-related white matter changes may show a form of vPD. Such patients may show gait disorders such as increased stance width with smaller steps, which slightly differs from the gait disorder seen in iPD patients. Gait disorders are so common in patients with vPD that the disease is sometimes called lower body parkinsonism, with accompanying freezing of gait (FOG). The pathophysiology underlying this condition is considered to result from a disconnection between the frontal lobe and the subcortical structures. Iseki et al. [3] showed that dysfunction of the BG-thalamocortical loop might be responsible for the gait disorder in the patients with white matter changes resulting in vPD, using gait activation SPECT. These authors also showed that the lateral premotor area was overactivated in such patients while walking, which supports the compensatory roles of the premotor cortex in gait disturbance as suggested by Hanakawa et al. described above.

The Overall Pattern of Gait Activation SPECT and Other Studies

In the gait activation SPECT studies that we have performed to date [1–3], we have found consistent patterns of activation across studies. Ballanger et al. [14] studied brain activity during the alternating foot movements and found activation of the SMA together with the sensorimotor cortex, as a large cluster. As described above, the visual cortex and cerebellum are involved in maintaining a standing posture, which is essential for gait movement. Taken together, these findings suggest that the SMA is involved in the coordination of lower limb movements together with the

one of the arms and trunk. The cerebellum together with the visual cortex might be involved more in the maintenance of balance. Both elements are required for walking movement. Further, processing of visual input is likely enhanced during standing and walking, and such processes might yield activation in the visual cortex.

La Fougere et al. [4] compared brain activity reflecting walking acquired by FDG-PET with that reflecting imagery of walking acquired by fMRI. The overall activation patterns were similar, verifying the consistency among these gait-related studies.

Other Modalities Applicable for Neuroimaging to Study the Neural Substrates Involved in Movements

With recent developments in the field of neuroimaging, various modalities have become available for the identification of the neural substrates involved in the execution of motor tasks during the scanning procedure. For each modality, there exist advantages and disadvantages for investigations of walking movement, which requires not only the lower limb movement, but also its integration with control of gravity center involving the whole body.

Functional MRI (fMRI) is used to assess brain activity during a variety of movement tasks; it not only has a distinguished spatial resolution, but it also provides considerably high time resolution than PET/SPECT. These advantages of fMRI make it better suited for studies of neural networks or connectivity. However, it is necessary for subjects to maintain a supine position inside MRI scanners unless scanning can be done using a vertical gantry. Therefore, it is difficult to apply such methods to imaging of systemic movement such as gait. Thus, fMRI studies focusing on brain activity during walk-related behavior have primarily used a gait imagery task instead of real gait [6, 15], hypothesizing that the neural substrates involved in these tasks should be shared.

Near-infrared spectroscopy (NIRS) uses reflection of a near-infrared ray to detect relative changes in hemoglobin levels, similar to the blood oxygen level-dependent (BOLD) signal measured by fMRI. The methodology and property of brain-derived signals thus closely resemble fMRI. NIRS enables us to measure brain activity during movement with an upright position while walking, and it provides good temporal resolution. However, NIRS can only cover the surface of the brain, like the cerebral cortex. Thus, it is almost impossible to apply this method to an investigation of the brainstem or BG, both of which are considered to be quite important for movements such as gait.

Conclusion and Future Directions

Dynamic SPECT/PET are indispensable techniques for understanding the neural substrates involved in voluntary movements, especially walking, and the pathophysiology of gait disorders. The future of these technologies will likely combine imaging

with neuro-rehabilitation techniques such as repetitive transcranial magnetic stimulation and brain–computer interfaces to enhance motor impairment, improve response to therapeutics, and optimize outcomes in neurological populations.

References

1. Hanakawa T, Fukuyama H, Katsumi Y, Honda M, Shibasaki H. Enhanced lateral premotor activity during paradoxical gait in Parkinson's disease. Ann Neurol. 1999;45:329–36.
2. Hanakawa T, Katsumi Y, Fukuyama H, et al. Mechanisms underlying gait disturbance in Parkinson's disease: a single photon emission computed tomography study. Brain. 1999;122 (Pt 7):1271–82.
3. Iseki K, Hanakawa T, Hashikawa K, et al. Gait disturbance associated with white matter changes: a gait analysis and blood flow study. Neuroimage. 2010;49:1659–66.
4. La Fougere C, Zwergal A, Rominger A, et al. Real versus imagined locomotion: a [18F]-FDG PET-fMRI comparison. Neuroimage. 2010;50:1589–98.
5. Mishina M, Senda M, Ishii K, Ohyama M, Kitamura S, Katayama Y. Cerebellar activation during ataxic gait in olivopontocerebellar atrophy: a PET study. Acta Neurol Scand. 1999;100:369–76.
6. Iseki K, Hanakawa T, Shinozaki J, Nankaku M, Fukuyama H. Neural mechanisms involved in mental imagery and observation of gait. Neuroimage. 2008;41:1021–31.
7. Oku N, Matsumoto M, Hashikawa K, et al. Carbon dioxide reactivity by consecutive technetium-99m-HMPAO SPECT in patients with a chronically obstructed major cerebral artery. J Nucl Med. 1994;35:32–40.
8. Morton SM, Bastian AJ. Cerebellar contributions to locomotor adaptations during splitbelt treadmill walking. J Neurosci. 2006;26:9107–16.
9. Reisman DS, Block HJ, Bastian AJ. Interlimb coordination during locomotion: what can be adapted and stored? J Neurophysiol. 2005;94:2403–15.
10. Mori S, Matsui T, Kuze B, Asanome M, Nakajima K, Matsuyama K. Stimulation of a restricted region in the midline cerebellar white matter evokes coordinated quadrupedal locomotion in the decerebrate cat. J Neurophysiol. 1999;82:290–300.
11. Vinay L, Padel Y, Bourbonnais D, Steffens H. An ascending spinal pathway transmitting a central rhythmic pattern to the magnocellular red nucleus in the cat. Exp Brain Res. 1993;97:61–70.
12. Ouchi Y, Okada H, Yoshikawa E, Nobezawa S, Futatsubashi M. Brain activation during maintenance of standing postures in humans. Brain. 1999;122(Pt 2):329–38.
13. Ouchi Y, Kanno T, Okada H, et al. Changes in dopamine availability in the nigrostriatal and mesocortical dopaminergic systems by gait in Parkinson's disease. Brain. 2001;124:784–92.
14. Ballanger B, Lozano AM, Moro E, et al. Cerebral blood flow changes induced by pedunculopontine nucleus stimulation in patients with advanced Parkinson's disease: a [(15)O] H2O PET study. Hum Brain Mapp. 2009;30:3901–9.
15. Malouin F, Richards CL, Jackson PL, Dumas F, Doyon J. Brain activations during motor imagery of locomotor-related tasks: a PET study. Hum Brain Mapp. 2003;19:47–62.

Chapter 5
Transcranial Ultrasonography in Movement Disorders

Stefanie Behnke and Daniela Berg

Introduction

The approach to evaluate intracranial structures using ultrasound has been followed for quite some time. Early in the 1960s, one-dimensional sonography ("echoencephalography"; M-mode) was used to assess midline shifts and space-occupying lesions by quantifying dislocation of midline structures that scatter and reflect the ultrasound beam applied through the intact skull. This technique lost its relevance with development, technical improvement, and ubiquitary spread of computed tomography (CT).

Rune Aaslid was the first to have applied ultrasound in *intracranial vascular diagnostics* and examined the circle of Willis using the Doppler effect [1]. He substantiated that a diagnostic ultrasound beam using low frequencies and relatively high energies may penetrate the intact skull. The *two*-dimensional B-mode imaging of the *brain parenchyma* using transcranial ultrasound (TCS) became possible only in the late 1980s. In 1993, Georg Becker and Ulrich Bogdahn described the normal echomorphology of the human brain and thereby opened the door for diagnostic use of TCS by imaging cerebral structures [2]. Early clinical applications included the identification of space-occupying lesions such as intracranial neoplasms [3] and intracerebral hematomas [4] followed by assessment of midline shift in malignant stroke [5], ventricular enlargement, and the estimation of intraventricular pressure [6, 7].

S. Behnke (✉)
Department of Neurology, Saarland University Hospital,
Kirrberger St, 66421 Homburg Saar, Germany
e-mail: s.behnke3@gmx.de

D. Berg
Department of Neurodegeneration, Hertie Institute for Clinical Brain Research,
Hoppe-Seyler-Str. 3, 72076 Tübingen, Germany
e-mail: daniela.berg@uni-tuebingen.de

F. B. Nahab, N. Hattori (eds.), *Neuroimaging of Movement Disorders,*
Current Clinical Neurology 44, DOI 10.1007/978-1-62703-471-5_5,

Table 5.1 Preset technical parameters used for transcranial sonography

Device	High-end duplex sonography devices
Transducer	Phased-array probe
Probe emission frequency	1.8–3.5 MHz
Insonation depth	14–16 cm
Dynamic range	45–55 dB
Contour amplification	Medium to high
Time gain compensation	Adjusted as needed
Image brightness	Adjusted as needed
Postprocessing function	Moderate suppression of low echo signals

The use of TCS in *movement disorders* and the recognition of specific changes in the normal brain echomorphology not educible by routine neuroimaging methods as CT or conventional MRI were introduced in 1995 when Georg Becker described abnormal echogenic signals at the anatomical site of the substantia nigra (SN) in patients with idiopathic Parkinson disease (iPD) [8].

Technical Approach

Device Requirements

For TCS examination of the brain, high-end ultrasound devices similar to those used for transcranial color-coded duplex sonographic assessment of cerebral arteries are used with phased-array low-frequency transducers of 2.0–3.5 MHz. Device parameter settings are provided in Table 5.1.

Until recently, a number of devices from different manufacturers have been used by various publishing workgroups evidencing that sufficient resolution quality may be obtained by different machines [9, 10]. Nevertheless, since image resolution may vary between different devices, consensus guidelines suggest for quantitative assessments the generation of norm values in each ultrasound laboratory by examining a representative population of healthy subjects (see below) [11, 12].

Based on these requirements, sonographic axial resolution of structures in the focus zone reach 0.7–1.0 mm and the lateral resolution is approximately 3 mm depending on the device [13]. Using modern equipment in contemporary high-end machines, resolution in the focus zone has been proven to be even higher (0.6 $\times$ 1.1 mm), thus even exceeding resolution of magnetic resonance imaging (MRI; 1.0 $\times$ 1.0 mm) in a comparative TCS/MRI phantom study [13]. In addition, TCS benefits from the dynamic procedure: movement artifacts may be compensated for by firm pressure of the probe against the temporal bone window and a continuous optimization of probe position.

Fig. 5.1 Transcranial ultrasound examination through the preauricular temporal bone window

Examination Procedure

In general, patients are examined in supine position in a darkened calm room. The probe is pressed firmly on the preauricular bone in the imagined orbitomeatal line (Fig. 5.1). To obtain the best possible image, the probe is slightly tilted upward and downward. Due to insufficient resolution in the near-field of the probe, structures at a depth of less than 2 cm cannot be adequately displayed. The focus zone of low-frequency transducers is between 5 and 7 cm distance from the probe [9]. Based on these circumstances, only near-midline structures are evaluated from the ipsilateral bone window whereas all other brain regions are assessed from the contralateral side to achieve optimized resolution.

Pathological changes of the cerebral echomorphology are described as "*hyperechogenicity*" in case of: (1) abnormally large areas of (physiologically) increased echogenicity with planimetrically measured values out of the limits of a comparative norm collective (i.e., substantia nigra), or (2) in case of an irregular increase of echogenicity compared to the surrounding tissue where under normal conditions isoechogenicity is expected (i.e., basal ganglia). "*Hypoechogenicity*" of a certain brain region is defined as a missing or abnormally small area of regularly increased echogenicity. Here, planimetrically measured values of hyperechogenic regions should fall below clearly defined normative collective percentiles.

Tissue harmonic imaging (THI), meaning the use of harmonic ultrasound reflections, does enhance tissue contrast and resolution. However, use of THI limits sufficient resolution in deeper, frontal, and dorsal areas and produces more artifacts. Moreover, areas of hyperechogenicity seem to be disproportionately large, thus exaggerating some structures [14]. These limitations lead to the convention that all quantitative and semiquantitative assessments of brain structure be achieved exclusively using conventional B-mode.

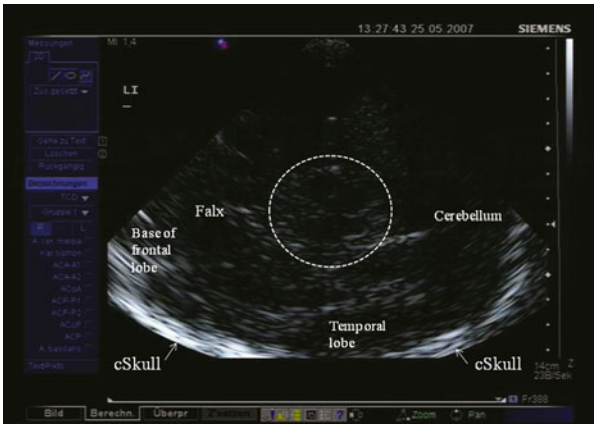

Fig. 5.2 Mesencephalic examination plane. *Encircled*: mesencephalic brainstem. *cSkull* contralateral skull (*arrows*), *LI* insonation from the left side

Examination Planes

Mesencephalic plane—TCS examination starts in the mesencephalic plane (Fig. 5.2). Here the butterfly-shaped mesencephalic brainstem in the center of the image is easy to identify. It exhibits a rather low echogenicity and is surrounded by the hyperechogenic perimesencephalic cisterns. Both hypoechogenic crura cerebri are separated by a prominent hyperechogenic midline structure that divides the butterfly into halves or the two "wings". This so-called "brainstem raphe" widens toward the dorsal proportion of the midbrain where the hyperechogenic signal corresponds to the aqueduct traversing the upper brainstem in a craniocaudal direction. Within the hypoechogenic crus cerebri, a slim line or small patchy oval spot of increased echogenicity is regularly found at the anatomical site of the SN. The adjacent red nucleus (RN) can be identified at the mediorostral end of the SN signal and also exhibits high echogenicity. It is important to selectively look for the RN in order to avoid misinterpretation of the signal of the RN as signal of the SN and to assess both structures separately from each other (inner structures of the midbrain in Fig. 5.3a, b.

Assessment of Inner Structures in the Mesencephalic Plane

Substantia Nigra

After having identified the regularly small SN signal within the midbrain butterfly, position of the probe is minimally varied in order to find the signal in its maximal extent (Fig. 5.4a). This image is frozen immediately and magnified two-fold to four-fold (Fig. 5.4b). It is recommended to freeze the image in order to avoid losing its configuration and extent while zooming it. The magnified SN signal is encircled with the cursor and planimetric measurement is completed automatically by the machine and given in "cm^2" (Fig. 5.4c) [11, 12].

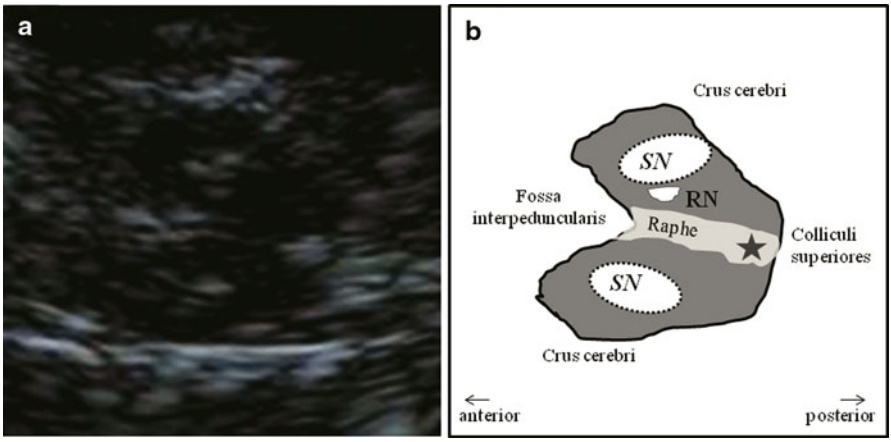

Fig. 5.3 Inner structure of the mesencephalic brainstem (**a**) and corresponding schematic drawing (**b**). *SN* substantia nigra, *RN* red nucleus, *Star* aqueduct

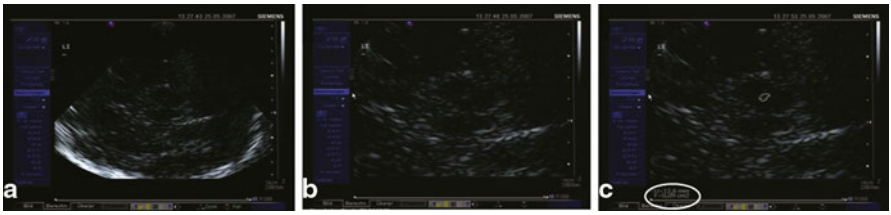

Fig. 5.4 Visualization (**a**), magnification (**b**), and planimetric measurement of the echogenic signal of the substantia nigra (0.09 cm^2) (**c**)

Brainstem Raphe

The hyperechogenic brainstem raphe (see Fig. 5.3a, b) is evaluated with respect to its continuity. Under normal conditions, an undisrupted hyperechogenic line is depictable from the rostral to the dorsal extent of the midbrain. Raphe echogenicity is rated semiquantitatively into normal, interrupted, and not visible at all [11, 12, 15].

Assessment of Inner Structures in the Third Ventricle Plane

By tilting the probe slightly upward, the third ventricle plane is reached (Fig. 5.5a–c). In the center of the image, the third ventricle is easily visible. It appears as two horizontal parallel lines of clear hyperechogenicity where the ultrasound beam meets the borders of ependyma to the cerebrospinal fluid in an orthogonal manner. Both lines enfold an almost anechogenic zone corresponding to the cerebrospinal fluid. In the frontal parts of the image in the elongation of the third ventricle, another

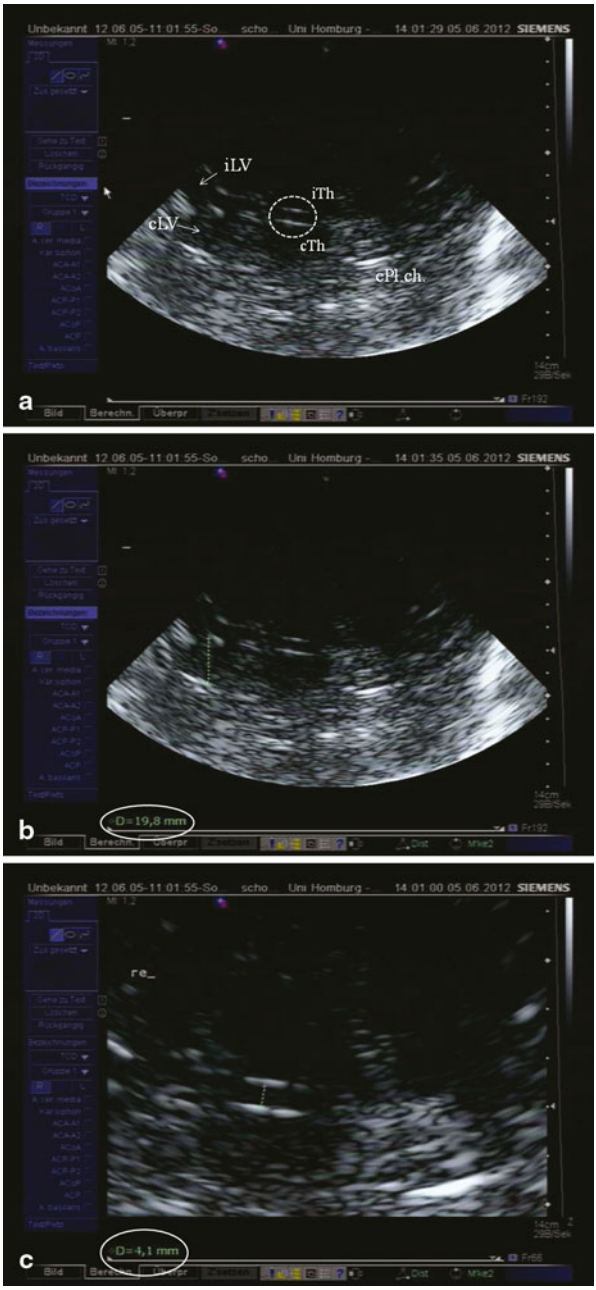

Fig. 5.5 **a** Ventricular or basal ganglia plane. *Encircled* third ventricle, *iTh* ipsilateral thalamus (*arrow*), *cTH* contralateral thalamus (*arrow*), *iLV* ipsilateral lateral ventricle, *cLV* contralateral lateral ventricle, *cPL.ch.* hyperechogenic contralateral Plexus choroideus within the posterior horn of the lateral ventricle. **b** Measurement of the diameter of the frontal horn of the contralateral lateral ventricle (19.8 mm). **c** Measurement of the diameter of the third ventricle (4.1 mm)

two hyperechogenic almost parallel lines are visible and correspond to the septum pellucidum and the lateral wall of the frontal horn of the contralateral lateral ventricle. The posterior horn of the lateral ventricle is visualized as a hyperechogenic area at its anatomical site due to the embedded choroid plexus which is frequently calcified exhibiting an increased echogenicity.

These ventricular structures embrace the basal ganglia area in which the different nuclei are normally isoechogenic to the surrounding parenchyma. Still the thalamus is regularly identifiable due to its location adjacent to the third ventricle and its normally, rather deeply, hypoechogenic echomorphology.

Assessment of the Ventricle Plane

Width of the Third Ventricle

To measure the width of the third ventricle, the two hyperechogenic lines reflecting the ependyma are displayed in their maximal distance from each other, the image is frozen and magnified, and the transverse diameter is measured from the ipsilateral to the contralateral inner layer of hyperechogenic ependyma (see Fig. 5.5b). Measurement is done at the narrowest point. Mean values for the third ventricle have been shown to be 4.8 ± 1.9 mm with an age-related increase. In subjects older than 60 years of age, mean values were 7.6 ± 2.1 mm [7]. Thus, normative values for individuals < 60 years are < 7 mm and > 60 years < 10 mm. Correlation to measurements using CT was high ($r = 0.83$) [7].

Width of the Frontal Horns of the Lateral Ventricles

The contralateral frontal horn is displayed and the image is frozen. Again, the transverse diameter is measured from the ipsilateral to the contralateral inner layer of hyperechogenic ependyma (see Fig. 5.5b) perpendicularly from the septum pellucidum to the tip of the frontal horn (Fig. 5.5c). Mean values for the anterior horn were 16.7 ± 2.3 mm for patients under the age of 60 years, and 19.0 ± 2.9 mm for elderly persons, respectively [7]. Correlation with CT scan measurements were slightly weaker than measurements of the third ventricle, but still sufficiently high ($r = 0.73$) [7].

Changes of Echomorphology of the Basal Ganglia

Since the basal ganglia (caudate and lenticular nucleus) and the thalamus in this plane usually exhibit isoechogenicity, they are not distinguishable from each other. In case

Fig. 5.6 Cella media plane. *CM* cella media, *iTh* ipsilateral thalamus, *iLV* ipsilateral lateral ventricle

of an abnormal increase of echogenicity, it is described according to the anatomic region. To further characterize abnormal findings, it may be manually encircled and planimetrically measured regarding the extent of hyperechogenic area.

Assessment of the Cella Media Plane

When the probe is tilted upward even further, the horizontal part of the lateral ventricle is visualized (Fig. 5.6). Its sonographic aspect is called "cella media." In the cella media plane, measurement of the ventricular width is possible following the same procedure as in the third ventricular plane. This plane has no importance for the ultrasonographic assessment of patients with movement disorders and is thus not commonly used.

Assessment of the Cerebellar Plane

This plane is more rarely used. Nevertheless, it shows interesting changes of echomorphology in a number of diseases affecting the cerebellum. The cerebellum in the posterior fossa is visualized by rotating the probe with its dorsal parts for about 45° downward and tilting it upward for another 10–15°. The resulting cerebral image displays characteristically both the midbrain and the thalamus bilaterally [9]. Dorsal to the brainstem, the hypoechogenic fourth ventricle and the adjacent dentate nucleus (DN) as well as further parts of the cerebellum can be identified. Echogenicity of the DN and the depictable parts of the cerebellar hemispheres have been shown to be increased in patients with spinocerebellar atrophy [16]. The width of the fourth ventricle which presents in the normal case as a comma-shaped hypoechogenic structure may enlarge considerably under pathological conditions. It can

be measured using the perpendicular diameter or the planimetric area [9], normative values, however, are pending. Echogenicity of the DN and the depictable parts of the cerebellar hemispheres have been shown to be increased in some forms of spinocerebellar ataxia [16–18] and Friedreich's ataxia [19].

Limitations

Using TCS in neuroimaging of the brain, one has to keep in mind that parts of the cerebrum are not visualizable by this technique. These are mainly the brain regions near the probe comprising the superficial two centimeters of the ipsilateral temporal lobe, the lower brain parts adjacent to the base of the skull, and the very apical frontoparietal area that is insonable through the preauricular transtemporal bone window. The quality of the temporal bone window itself limits the application of TCS in about 10–20 % of Caucasian subjects age-dependently and gender-dependently with a higher prevalence of bad transcranial insonation qualities in elderly females presumably due to osteoporosis [11, 20]. Besides, ethnicity influences the proportion of insufficient bone windows within a population considerably with up to 60 % of insonable cases in Asian subjects [21, 22].

Examiner experience may limit the quality of TCS assessment substantially since—as always with ultrasound methods—it takes a certain number of examinations until echogenicity and structures are correctly identified and evaluated.

Nevertheless, based on a sufficient experience with the method, correct application following consensus criteria and adequate technical equipment, interrater and intrarater reproducibility has been proven to be high [7, 23–25].

Clinical Application of TCS in Movement Disorders

Parkinson Disease—Typical Findings

Georg Becker was the first to describe changes of the normal echomorphology of the SN in patients with iPD [8]. In his pilot study, he saw a characteristic increase of echogenicity at the anatomical site of the SN within the normally, rather homogenously, hypoechogenic midbrain that he called "SN hyperechogenicity" (SN+; see Fig. 5.7). During the last 15 years, numerous groups were able to reproduce this finding spreading the idea of SN+ as a biomarker of iPD, a thought that had already been formulated by Becker, all over the world [26–34].

Nearly universally, SN+ has been described in various collectives to occur in about 90 % of the examined patients leading to a sensitivity of the presumed iPD biomarker that reached in different studies 86–91 % whereas specificity was 82.4–96 % [30, 34–36]. TCS examination in patients with first motor abnormalities, insufficient for the clinical diagnosis of PD were found to have SN+ in the vast majority

Fig. 5.7 Bilateral hyperechogenicity of the substantia nigra (SN+). *Arrow* brainstem raphe, *Star* aqueduct

of cases cumulating in a high positive predictive value of 92.9 % for the diagnosis of iPD, which was clinically established within another year [36]. Similar positive predictive values from 83 to 100 % were also found by other groups [23, 34, 35, 37].

Important Characteristics of SN+ in iPD

SN+ has been shown to be more prominent contralateral to the clinically more affected body side [22, 26, 38]. Patients with a tremor predominance type were found to exhibit rather asymmetric SN+ whereas patients with akinetic-rigid or equivalent types were more symmetric in their area of SN+ [38]. Early-onset PD had larger SN+ than late-onset PD patients [38, 39]. The area of SN+ has been proven to be independent of age or gender [38]. It does not correlate with disease duration, nor with stage or severity of motor symptoms [38]. Moreover, the intraindividual signal stays stable throughout the course of the disease in follow-up examinations of iPD patients for up to 10 years in spite of disease progression and clinical deterioration [40, 41]. These findings underline that SN+ seems to be rather a trait marker of iPD than a progression marker and may not be used to estimate the extent of neurodegeneration. Comparative imaging studies using radiolabeled tracers have substantiated this view: the area of SN+ did not correlate with [^{18}Fluoro] Dopa positron emission tomography (PET) [42], nor with β-CIT single photon emission computed tomography (SPECT) in most studies [35, 43, 44] or with ^{123}I-MIBG scintigraphy [22, 45]. In contrast to SN+, both [^{18}Fluoro] Dopa PET and β-CIT SPECT findings have been shown to be related to the extent of nigrostriatal impairment and to clinical severity. Also, MIBG

scintigraphy that mirrors sympathetic denervation of the heart in PD correlates with disease severity in later stages [46], which is different from the trait marker SN+.

Consensus criteria have defined a "marked" SN+ as an abnormally large area of increased echogenicity that reaches planimetrically measured values above the 90th percentile of a representative norm collective examined in the same ultrasound laboratory. Values above the 75th percentile represent "moderate" SN+ [11, 12].

Causes of Substantia Nigra Hyperechogenicity

The exact pathophysiological changes underlying SN+ are not fully understood. Animal and postmortem studies emphasize the role of increased iron content and microglial activation: SN echogenicity in rats increased dose-dependently after unilateral injection of iron into the SN compared to the noninjected side [47]. Postmortem examinations in non-Parkinsonian brain tissue samples showed a positive correlation between hyperechogenic SN areas and increasing iron levels and H-ferritin and L-ferritin levels whereas an inverse correlation was found between SN echogenicity and neuromelanin content [48–51]. In a subsequent postmortem study, SN echogenicity correlated with activated microglia [52]. Both phenomena—microglial activation and increased iron content—characterize nigral iPD pathology and are therefore likely to actually play a key role in the formation of SN+. Though there are still open questions, e.g., the understanding of the stability of the echomarker during the course of the disease in spite of ongoing neurodegeneration and the occurrence of SN+ in healthy controls (see the following section).

Monogenetic Parkinsonian Syndromes (gPS)

There is increasing knowledge on mutations in numerous genes leading to hereditary forms of gPS. Although the number of individuals with monogenetic PD assessed by TCS is still limited, it is well established by different groups that both autosomal dominant as well as autosomal recessive forms of PD are associated with SN+. Examples are studies in *PINK 1-associated PD* [53], *DJ-1* associated PD [54], *alpha-synuclein* associated PD [54, 55], and *LRRK2*-associated PD. Interestingly, in some forms of monogenetic PD, SN+ has been described as rather moderate [54, 56]. Still, it was present, similar to mutations in the glucocerebrosidase gene or GBA-associated PD [57], which is the most common genetic risk factor known so far.

Importantly, TCS studies in autosomal dominant as well as in recessive forms of gPS have shown echo changes with SN+ in clinically asymptomatic mutation carriers. For example, in asymptomatic *Parkin* mutation carriers SN+ could be detected even in those subjects with normal [^{18}Fluoro] Dopa PET suggesting that SN+ may indicate preclinical parkinsonism in individuals with a genetically determined risk for PD even before visible effects on the nigrostriatal system [58, 59]. These findings further underline the concept of SN+ as a nigrostriatal vulnerability marker or risk marker for the future development of a Parkinsonian syndrome [60].

Premotor Diagnosis of Idiopathic Parkinson Disease

In the pilot study of Becker et al., two healthy control subjects were found to exhibit SN+ [8]. One of them developed a clinically manifest iPD within a couple of years leading to the question of whether SN+ in iPD may *precede* motor symptoms (*unpublished data*) as could be shown in Parkin-related monogenetic PD years later [58].

Based on these speculations, large collectives of healthy subjects were examined to define the prevalence of SN+ within the normal population. In a first study including more than 300 asymptomatic control subjects of all age groups from 20 to 80 years, SN+ prevalence turned out to be nearly 9 % [48, 50, 51]. Although these individuals had no abnormalities in the neurological and neuropsychological tests, 60 % of an SN+ subgroup examined by [^{18}Fluoro] Dopa PET showed reduced striatal tracer uptake compared to controls without the echofeature (SN−) [48, 50, 51]. Obviously, the echostatus SN+ seems to be associated with a subclinical alteration of the nigrostriatal system. Further evidence for a functional relevance of SN+ in non-Parkinsonian subjects arose from the finding that psychiatric patients who developed neuroleptic-induced parkinsonism had larger echogenic SN areas than those patients treated without extrapyramidal side effects [61]. Moreover, in healthy elderly subjects, SN+ was significantly associated with clinical signs of motor slowing or tremor [24, 62]. In demanding motor tasks such as tap-dancing, subtle motor deficits were visible in SN+ dancers [63]. In conclusion, these findings indicated SN+ as a possible risk marker for the development of Parkinsonian symptoms, which may become clinically evident under challenging conditions.

Also, the finding that SN+ is more frequently found in healthy first-degree relatives of iPD patients compared to individuals without a close family relation to an iPD patient [64] strengthens the hypothesis that the echomarker SN+ represents a risk factor for iPD, since a positive family history doubles the risk for iPD. Based on these findings, the PRIPS multicenter study (Prospective Validation of Risk Factors for the Development of Parkinsonian Syndromes) was initiated to prospectively follow a large cohort of $>$ 1800 healthy individuals aged $>$ 50 years with the aim of correlating future iPD conversion to baseline SN echostatus and other iPD risk and premotor markers. Baseline assessment revealed an association of SN+ with the known iPD risk factors such as male gender and positive family history [65] and with putative iPD premotor symptoms such as hyposmia, cognitive decline, and subtle signs of motor slowing [12, 66–68]. These findings are in line with other cross-sectional studies describing the association of SN+ with a number of premotor markers including olfactory deficits [69, 70], motor slowing [24], depression [71], and REM sleep behavior disorder [72].

Follow-up of the PRIPS cohort after 3 years revealed that 8 of the 11 iPD converters exhibited the echomarker SN+ at baseline (one patient had an insufficient transtemporal bone window) resulting in a 17-fold increased relative risk to develop iPD within a 3-year period in individuals aged 50 years or above with SN+ [73]. This is an extremely high-risk factor, promising for the inclusion of TCS in future assessment batteries for the early (possibly even premotor) diagnosis of PD.

Atypical Parkinsonian Syndromes (aPS)

Differentiation of a diagnosis of iPD from aPS such as multisystem atrophy (MSA) and progressive supranuclear palsy (PSP) is challenging, especially in early disease stages when symptoms overlap and clinical presentation is oligosymptomatic. Nevertheless, an early correct diagnosis is essential for both physicians and patients since therapeutic options and prognosis differ considerably in iPD and aPS.

MRI or SPECT using radiolabeled tracers have been suggested to be of use in the diagnostics of aPS. Still they bear the drawback of limited availability, radiation exposure for the patient, and high cost. Moreover, structural changes on MRI, indicative for aPS, occur rather late in the disease course, as they are signs of neurodegeneration/atrophy.

A number of studies using TCS could prove its utility in differentiating aPS from iPD in clinically suggestive cases [21, 34, 37]. Walter et al. examined 25 patients with aPS with TCS and compared the findings with 25 age-matched iPD patients [34]. He could show that aPS patients rarely exhibit SN+ (only 9 % of aPS patients) which was found in 24 of the 25 iPD patients, as expected. SN+ in the two aPS patients was moderate only but interestingly a hyperechogenicity of the lenticular nucleus (LN+) could be found in more than three quarters of aPS patients in contrast to only one-fifth of iPD patients [34]. These results were substantiated in a large sample of aPS and iPD patients (34 MSA, 21 PSP, 102 iPD) [37]. The combination of a normal or at maximum moderately hyperechogenic SN echomorphology with LN+ predicted MSA or PSP with a positive predictive value of 0.96 whereas SN+ in case of a regularly hypoechogenic presentation of basal ganglia in the ventricular plane indicated iPD with a positive predictive value of 0.91 [37]. In a subsequent study, Walter et al. stressed further that third-ventricle dilatation of more than 10 mm in combination with LN+ indicated PSP [74, 75].

In contrast, patients with corticobasal degeneration (CBD) showed marked SN+ [74] as well as patients with dementia with Lewy bodies (DLB) who were found to exhibit symmetric bilateral marked SN+ [76]. These findings are most important since they revealed that the echomarker SN+ is not an exclusive feature of iPD. Also, some cases of SCA or Huntington's disease may display SN+. Therefore, TCS results should always be placed into the context of clinical and anamnestic data.

Other Indications Where TCS May Be Diagnostically Helpful

Normal Pressure Hydrocephalus (NPH)

Patients with normal pressure hydrocephalus present with the typical triad of cognitive decline, gait disorder, and urinary disturbances. Gait abnormalities are characterized by a gait apraxia leading to severe instability while walking, falls, and especially the fear of falling. Steps are short and of low distance to the floor

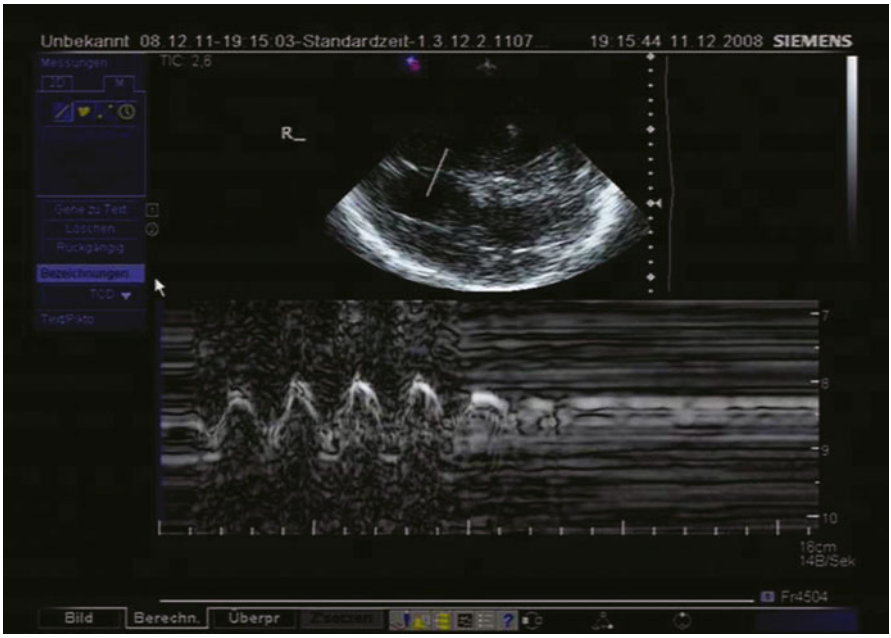

Fig. 5.8 Undulation test in normal pressure hydrocephalus

and posture may be flexed imitating a lower body parkinsonism. Since NPH may be efficiently treated by lumbar puncture and if this is insufficient by surgery, the early correct diagnosis is of utmost importance. TCS may be of special help in these patients since these patients not only do not exhibit SN+ but primarily show marked dilation of the ventricular system [6]. Increased CSF pressure may be additionally visualized by the undulation test described by Becker et al. after having displayed the septum pellucidum separating both frontal horns of the lateral ventricles in the third ventricle plane, the M-mode cursor is in a way that it crosses the septum pellucidum perpendicularly [6]. Pressing the probe firmly on the temporal bone window of the patient, the head is rotated quickly a couple of times about 20° to both sides. The M-mode documents undulating dislocation of the septum pellucidum relative to the ventricular wall while rotating the head in case of normal and low intraventricular pressure [6]. It still undulates once or twice after discontinuation of head rotation (Fig. 5.8). Becker et al. found a loss of undulations when intraventricular pressure exceeded 21 cm H_2O [6].

Essential Tremor (ET)

Differential diagnosis between iPD and ET is usually based on clinical criteria. However, differentiation between tremor dominant PD and ET may be difficult in early stages or in case of atypical presentation. IPD may present with kinetic or

postural tremor, and signs of hypokinesia may be mild, especially in the beginning. In a couple of studies, TCS has proven its potential to help distinguishing ET from iPD cases. Based on the clinical diagnosis, SN+ was found in ET patients only in 8–16 % of cases compared to 75–91 % of iPD patients [35, 77–79]. Interestingly, the prevalence of SN+ in ET was still significantly higher than in normal controls without any tremor who displayed SN only in 3 % [77]. The area of SN+ in ET patients correlated with putative premotor and risk markers, especially with constipation, depression, PD family history, and the number of premotor symptoms [79]. With regard to the hypothesis that SN+ may represent a general risk factor for the future development of iPD, these findings are in accordance with epidemiological studies indicating a higher iPD risk in ET patients compared with the general population [80].

Major Depression

Major depression may lead to considerable loss of voluntary and involuntary movements leaving patients with symmetric but frequently also slightly asymmetric hypomimia, hypophonia, bradykinesia, and a varying number of nonmotor symptoms often associated with iPD such as sleep disturbances, constipation, apathy, and anxiety. TCS studies have provided evidence that depressive patients without concomitant iPD usually do not exhibit SN+ although the echomarker occurs two to three times more often than in nondepressive controls [71]. Since depression has been shown to be a risk factor for the future development of iPD, this finding may further substantiate that SN+ indicates the increased risk for iPD in a number of individuals. Apart from the SN echomorphology, another echofeature has been found in numerous studies in patients with depressive symptoms: the reduced or interrupted echosignal of the mesencephalic brainstem raphe [81]. Since a hypoechogenic raphe signal has been described in depressive iPD patients, too [82], only the combined findings of normal SN echogenicity and hypoechogenic raphe may differentiate primary depression from iPD.

Wilson's Disease

Patients with Wilson's disease may accumulate copper in various body parts, especially in the basal ganglia, cornea, and liver due to a hereditary deficiency of a copper-transporting protein and lack of biliary copper excretion. Following cerebral involvement, patients may present with psychiatric signs but also regularly with extrapyramidal symptoms ranging from dystonic or other hyperkinetic movement disorders, tremor and ataxia, to hypokinesia and even full Parkinsonism. Whereas MRI can detect copper accumulation in the basal ganglia in most of clinically at least moderately affected patients, TCS has proven its capacity to display marked

Fig. 5.9 Hyperechogenicity of the lenticular nucleus (*encircled*) in a patient with Wilson's disease. *iTh* ipsilateral thalamus, *iLV* ipsilateral lateral ventricle, *cLV* contralateral lateral ventricle (diameter = 25.7 mm), *cPL.ch.* hyperechogenic contralateral Plexus choroideus within the posterior horn of the lateral ventricle. Please note that magnetic resonance imaging of the brain in this patient revealed only moderate general atrophy of the cerebrum

echochanges in the basal ganglia with hyperechogenicity especially of the lenticular nucleus even in neurologically asymptomatic patients or in case of normal MRI (Fig. 5.9) [83] diagnosis of young patients with unclear movement disorders or likewise with liver failure of unknown origin.

Restless Legs Syndrome (RLS)

Restless legs syndrome is a common neurologic disorder leading to an irresistible urge to move lower limbs in resting situations that is relieved by movements. In contrast to idiopathic RLS, symptomatic forms occur in pregnancy, associated with iron deficiency, or in patients with polyneuropathy, especially due to renal failure. In RLS patients, SN *hypo*echogenicity has been described in > 80 % of idiopathic as well as in > 70 % symptomatic cases [84, 85]. In idiopathic RLS patients, TCS revealed further frequently hyperechogenicity of the red nucleus (RN+) and reduced brainstem raphe echogenicity which was correlated to periodic limb movements and depressive symptoms, respectively [85]. Combining these specific TCS changes, positive predictive value for RLS was 97 % in case of at least two of these changes of the inner midbrain structure [85].

Dystonia

The exact pathophysiology leading to idiopathic dystonia is still a matter of intense research. Nevertheless, neuroimaging, pathoanatomical, clinical, and especially

electrophysiological studies provide evidence that disinhibition of the frontal motor cortex as a result of basal ganglia and thalamus dysfunction may result in dystonia. Correspondingly, early TCS studies in patients with idiopathic focal and generalized dystonia showed changes of the echomorphology of the basal ganglia with a characteristic hyperechogenicity of the lenticular nucleus (LN+) which is most pronounced in the medial part corresponding to the anatomic site of the globus pallidus internus [86, 87]. LN+ was seen in about 75 % of idiopathic adult onset focal cervical dystonia and in 83 % of upper limb dystonia whereas facial forms of idiopathic dystonia such as blepharospasm or Meige syndrome only displayed LN+ in one third of patients [86, 87]. Most interestingly, nonidiopathic dystonia such as drug-induced forms did not show abnormalities [87]. Recent work by Walter et al. could substantiate these findings by describing LN+ in task-specific focal dystonia in musicians [88].

Postmortem examination of brain tissue of dystonic patients have pointed toward a copper accumulation in the LN as cause for the abnormally increased echogenicity [89] suggesting disturbances of cerebral copper metabolism to be involved in dystonia [90]. Accordingly, further analysis showed reduced Menkes protein, a copper transporting protein, in this tissue [91] as well as reduced Menkes mRNA copies and lower copper levels in leukocytes of patients with idiopathic adult-onset cervical dystonia [92]. Since copper modulates synaptic function and neurotransmission, it may play a key role in the pathogenesis of primary dystonia [51]. Although, final understanding of dystonia pathophysiology is still to be awaited, dystonia is an impressive example of TCS contributing not only to diagnosis and differential diagnosis but also to reappraisal of current concepts and to new perspectives of pathophysiological knowledge.

Conclusions and Future Directions

Since the first description of an enlarged area of SN hyperechogenicity as a typical sign for Parkinson disease in 1995, a large number of papers have been published witnessing the value of TCS in the diagnosis and differential diagnosis of movement disorders. TCS is fairly easy to apply and quick to perform even in agitated or hyperkinetic patients and it is increasingly used with good interrater and intrarater reliability. Because of specific underlying physical principals, information can be derived from this technique that differs from the aspects depicted, for example, by CT or MRI. Thus, it may be regarded as a supplementary tool to other neuroimaging methods. Like other neuroimaging techniques, the method entails some limitations including, for example, an insufficient bone window in about 10–20 % of the Caucasian population, nonspecificity of typical ultrasound-features such as SN or lentiform nucleus hyperechogenicity and difficulties in objectifying and quantifying observations. It is important to take these limitations seriously and to stick to applications which are proposed for clinical as well as for research purposes. On the other hand, it should be considered and approached, that many of the technical limitations can at least in part be overcome, as testified by the development of the method in the last years.

Therefore, further effort needs to be put into the improvement of the method. Doing so, new and even broader applications can be expected in the future. One example for a new field of application is the intraoperative and postoperative monitoring of the placement of brain electrodes, another may be widening of the technique to other medical fields such as psychiatry as already done in depression or extrapyramidal symptoms induced by neuroleptic therapy.

References

1. Aaslid R, Markwalder TM, Nornes H. Noninvasive transcranial Doppler ultrasound recording of flow velocity in basal cerebral arteries. J Neurosurg. 1982;57:769–74.
2. Becker G, Bogdahn U. Transcranial color-coded real-time sonography. In: Babikian VL, Wechsler LR, editors. Transcranial doppler ultrasonography. St. Louis, MO: Mosby Yearbook; 1993. p. 51–60.
3. Becker G, Perez J, Krone A, Demuth K, Lindner A, Hofmann E, Winkler J, Bogdahn U. Transcranial color-coded real-time sonography in the evaluation of intracranial neoplasms and arteriovenous malformations. Neurosurgery. 1992;31(3):420–8.
4. Seidel G, Kaps M, Dorndorf W. Transcranial color-coded duplex sonography of intracerebral hematomas in adults. Stroke. 1993;24:1519–27.
5. Gerriets T, Stolz E, Modrau B, Fiss I, Seidel G, Kaps M. Sonographic monitoring of midline shift in hemispheric infarctions. Neurology. 1999;52(1):45–9.
6. Becker G, Bogdahn U, Strassburg HM, Lindner A, Hassel W, Meixensberger J, Hofmann E. Identification of ventricular enlargement and estimation of intracranial pressure by transcranial color-coded real-time sonography. J Neuroimaging. 1994;4:17–22.
7. Seidel G, Kaps M, Gerriets T, Hutzelmann A. Evaluation of the ventricular system in adults by transcranial duplex sonography. J Neuroimaging. 1995;5:105–8.
8. Becker G, Seufert J, Bogdahn U, Reichmann H, Reiners K. Degeneration of substantia nigra in chronic Parkinson's disease visualized by transcranial color-coded real-time sonography. Neurology. 1995;45:182–4.
9. Skoloudík D, Walter U. Method and validity of transcranial sonography in movement disorders. Int Rev Neurobiol. 2010;90:7–34.
10. Godau J, Berg D. Role of transcranial ultrasound in the diagnosis of movement disorders. Neuroimaging Clin N Am. 2010;20:87–101.
11. Walter U, Behnke S, Eyding J, Niehaus L, Postert T, Seidel G, Berg D. Transcranial brain parenchyma sonography in movement disorders: state of the art. Ultrasound Med Biol. 2007;33(1):15–25.
12. Berg D. Hyperechogenicity of the substantia nigra: pitfalls in assessment and specificity for Parkinson's disease. J Neural Transm. 2010;118:453–61.
13. Walter U, Kanowski M, Kaufmann J, Grossmann A, Benecke R, Niehaus L. Contemporary ultrasound systems allow high-resolution transcranial imaging of small echogenic deep structures similarly as MRI: a phantom study. Neuroimage 2008;40(2):551–8.
14. Puls I, Berg D, Mäurer M, Schliesser M, Hetzel G, Becker G. Transcranial sonography of the brain parenchyma: comparison of B-mode imaging and tissue harmonic imaging. Ultrasound Med Biol. 2000;26:189–94.
15. Berg D, Behnke S, Walter U. Application of transcranial sonography in extrapyramidal disorders: updated recommendations. Ultraschall Med. 2006;27:12–9.
16. Postert T, Eyding J, Berg D, Przuntek H, Becker G, Finger M, Schöls L. Transcranial sonography in spinocerebellar ataxia type 3. J Neural Transm Suppl. 2004;68:123–33.
17. Mijajlović M, Dragasević N, Stefanova E, Petrović I, Svetel M, Kostić VS. Transcranial sonography in spinocerebellar ataxia type 2. J Neurol. 2008;255:1164–7.

18. Krogias C, Postert T, Eyding J. Transcranial sonography in ataxia. Int Rev Neurobiol. 2010;90:217–35.
19. Synofzik M, Godau J, Lindig T, Schöls L, Berg D. Transcranial sonography reveals cerebellar, nigral, and forebrain abnormalities in Friedreich's ataxia. Neurodegener Dis. 2011;8:470–5.
20. Nedelmann M, Stolz E, Gerriets T, Baumgartner RW, Malferrari G, Seidel G, Kaps M, TCCS Consensus Group. Consensus recommendations for transcranial color-coded duplex sonography for the assessment of intracranial arteries in clinical trials on acute stroke. Stroke. 2009;40(10):3238–44.
21. Okawa M, Miwa H, Kajimoto Y, Hama K, Morita S, Nakanishi I, Kondo T. Transcranial sonography of the substantia nigra in Japanese patients with Parkinson's disease or atypical parkinsonism: clinical potential and limitations. Intern Med. 2007;46(18):1527–31.
22. Kajimoto Y, Miwa H, Okawa-Izawa M, Hironishi M, Kondo T. Transcranial sonography of the substantia nigra and MIBG myocardial scintigraphy: complementary role in the diagnosis of Parkinson's disease. Parkinsonism Relat Disord. 2009;15:270–2.
23. Prestel J, Schweitzer KJ, Hofer A, Gasser T, Berg D. Predictive value of transcranial sonography in the diagnosis of Parkinson's disease. Mov Disord. 2006;21:1763–5.
24. Behnke S, Double KL, Duma S, Broe GA, Guenther V, Becker G, et al. Substantia nigra echomorphology in the healthy very old: correlation with motor slowing. Neuroimage. 2007;34:1054–9.
25. Van de Loo S, Walter U, Behnke S, Hagenah J, Lorenz MW, Sitzer M, Hilker R, Berg D. Reproducibility and diagnosis accuracy of substantia nigra sonography for the diagnosis of Parkinson's disease. J Neurol Neurosurg Psychiatry. 2010;81(10):1087–92.
26. Berg D, Siefker C, Becker G. Echogenicity of the substantia nigra in Parkinson's disease and its relation to clinical findings. J Neurol. 2001;8:684–9.
27. Walter U, Wittstock M, Benecke R, Dressler D. Substantia nigra echogenicity is normal in non-extrapyramidal cerebral disorders but increased in Parkinson's disease. J Neural Transm. 2002;109:191–6.
28. Huang YW, Jeng JS, Tsai CF, Chen LL, Wu RM. Transcranial imaging of substantia nigra hyperechogenicity in a Taiwanese cohort of Parkinson's disease. Mov Disord. 2007;22:550–5.
29. Kim JY, Kim ST, Jeon SH, Lee WY. Midbrain transcranial sonography in Korean patients with Parkinson's disease. Mov Disord. 2007;22:1922–6.
30. Ressner P, Skoloudik D, Hlustik P, Kanovsky P. Hyperechogenicity of the substantia nigra in Parkinson's disease. J Neuroimaging. 2007;17(2):164–7.
31. Tsai CF, Wu RM, Huang YW, Chen LL, Yip PK, Jeng JS. Transcranial color-coded sonography helps differentiation between idiopathic Parkinson's disease and vascular parkinsonism. J Neurol. 2007;254:501–7.
32. Vlaar AM, Bouwmans A, Mess WH, Tromp SC, Weber WE. Transcranial duplex in the differential diagnosis of parkinsonian syndromes: a systematic review. J Neurol. 2009;256:530–8.
33. Mehnert S, Reuter I, Schepp K, Maaser P, Stolz E, Kaps M. Transcranial sonography for diagnosis of Parkinson's disease. BMC Neurol. 2010;21:10–9.
34. Walter U, Niehaus L, Probst T, Benecke R, Meyer BU, Dressler D. Brain parenchyma sonography discriminates Parkinson's disease and atypical parkinsonian syndromes. Neurology. 2003;60:74–7.
35. Doepp F, Plotkin M, Siegel L, Kivi A, Gruber D, Lobsien E, Kupsch A, Schreiber SJ. Brain parenchyma sonography and 123I-FP-CIT SPECT in Parkinson's disease and essential tremor. Mov Disord. 2008;23(3):405–10.
36. Gaenslen A, Unmuth B, Godau J, Liepelt I, Di Santo A, Schweitzer KJ, Gasser T, Machulla HJ, Reimold M, Marek K, Berg D. The specificity and sensitivity of transcranial ultrasound in the differential diagnosis of Parkinson's disease: a prospective blinded study. Lancet Neurol. 2008;7:417–24.
37. Behnke S, Berg D, Naumann M, Becker G. Differentiation of Parkinson's disease and atypical parkinsonian syndromes by transcranial ultrasound. J Neurol Neurosurg Psychiatry. 2005;76:423–5.

38. Walter U, Dressler D, Wolters A, Wittstock M, Benecke R. Transcranial brain sonography findings in clinical subgroups of idiopathic Parkinson's disease. Mov Disord. 2007;22:48–54.
39. Schweitzer KJ, Hilker R, Walter U, Burghaus L, Berg D. Substantia nigra hyperechogenicity as a marker of predisposition and slower progression in Parkinson's disease. Mov Disord. 2006;21(1):94–8.
40. Berg D, Merz B, Reiners K, Naumann M, Becker G. Five year follow-up study of hyperechogenicity of the substantia nigra in Parkinson's disease. Mov Disord. 2005;20:383–5.
41. Behnke S, Runkel A, Al-Sibai Kassar H, Ortmann M, Guidez D, Dillmann U, Fassbender K, Spiegel J. Long-term course of substantia nigra hyperechogenicity in Parkinson's disease. Mov Disord. 2012. doi:10.1002/mds.25193.
42. Behnke S, Schröder U, Dillmann U, Fuß G, Buchholz HG, Schreckenberger M, et al. Hyperechogenicity of the substantia nigra in healthy controls is related to MRI changes and to neuronal loss as determined by F-Dopa PET. Neuroimage. 2009;47:1237–43.
43. Spiegel J, Hellwig D, Möllers MO, Behnke S, Jost W, Fassbender K, Samnick S, Dillmann U, Becker G, Kirsch CM. Transcranial sonography and [123I]FP-CIT SPECT disclose complementary aspects of Parkinson's disease. Brain. 2006;129:1188–93.
44. Lobsien E, Schreiner S, Plotkin M, Kupsch A, Schreiber SJ, Doepp F. No correlation of substantia nigra echogenicity and nigrostriatal degradation in Parkinson's disease. Mov Disord. 2012;27:450–3.
45. Behnke S, Hellwig D, Bürmann J, Runkel A, Farmakis G, Kirsch CM, Fassbender K, Becker G, Dillmann U, Spiegel J. Evaluation of transcranial ultrasound findings and MIBG cardiac scintigraphy in the diagnosis of idiopathic Parkinson's disease. (Submitted).
46. Nagayama H, Hamamoto M, Ueda M, Nagashima J, Katayama Y. Reliability of MIBG myocardial scintigraphy in the diagnosis of Parkinson's disease. J Neurol Neurosurg Psychiatry. 2005;76:249–51.
47. Berg D, Grote C, Rausch WD, Maurer M, Wesemann W, Riederer P, Becker G. Iron accumulation of the substantia nigra in rats visualized in ultrasound. Ultrasound Med Biol. 1999;25:901–4.
48. Berg D, Becker G, Zeiler B, et al. Vulnerability of the nigrostriatal system as detected by transcranial ultrasound. Neurology. 1999;53:1026–31.
49. Zecca L, Berg D, Arzberger T, Ruprecht P, Rausch WD, Musicco M, Tampellini D, Riederer P, Gerlach M, Becker G. In vivo detection of iron and neuromelanin by transcranial sonography: a new approach for early detection of substantia nigra damage. Mov Disord. 2005;20(10): 1278–85.
50. Berg D, Roggendorf W, Schroder U, Klein R, Tatschner T, Benz P, Tucha O, Preier M, Lange KW, Reiners K, Gerlach M, Becker G. Echogenicity of the substantia nigra: association with increased iron content and marker of susceptibility to nigrostriatal injury. Arch Neuro. 2002;59:999–1005.
51. Berg D, Becker G. Perspectives of B-mode transcranial ultrasound. Neuroimage. 2002;15(3):463–73.
52. Berg D, Godau J, Riederer P, Gerlach M, Arzberger T. Microglia activation is related to substantia nigra echogenicity. J Neural Transm. 2010;117:1287–92.
53. Hagenah JM, Becker B, Brüggemann N, Djarmati A, Lohmann K, Sprenger A, Klein C, Seidel G. Transcranial sonography findings in a large family with homozygous and heterozygous PINK1 mutations. J Neurol Neurosurg Psychiatry. 2008;79:1071–4.
54. Schweitzer KJ, Brüssel T, Leitner P, Krüger R, Bauer P, Woitalla D, Tomiuk J, Gasser T, Berg D. Transcranial ultrasound in different monogenetic subtypes of Parkinson's disease. J Neurol. 2007;254(5):613–6.
55. Brueggemann N, Odin P, Gruenewald A, Tadic V, Hagenah J, Seidel G, Lohmann K, Klein C, Djarmati A. Re: Alpha-synuclein gene duplication is present in sporadic Parkinson disease. Neurology. 2008;71:1294.
56. Berg D, Schweitzer KJ, Leitner P, Zimprich A, Lichtner P, Belcredi P, Brüssel T, Schulte C, Maass S, Nägele T, Wszolek ZK, Gasser T. Type and frequency of mutations in the LRRK2 gene in familial and sporadic Parkinson's disease. Brain. 2005;128:3000–11.

57. Brockmann K, Srulijes K, Hauser AK, Schulte C, Csoti I, Gasser T, Berg D. GBA-associated PD presents with nonmotor characteristics. Neurology. 2011;77(3):276–80.
58. Walter U, Klein C, Hilker R, Benecke R, Pramstaller PP, Dressler D. Brain parenchyma sonography detects preclinical parkinsonism. Mov Disord. 2004;19(12):1445–9.
59. Hagenah JM, König IR, Becker B, Hilker R, Kasten M, Hedrich K, Pramstaller PP, Klein C, Seidel G. Substantia nigra hyperechogenicity correlates with clinical status and number of Parkin mutated alleles. J Neurol. 2007;254:1407–13.
60. Brockmann K, Hagenah J. TCS in monogenic forms of Parkinson's disease. Int Rev Neurobiol. 2010;90:157–64.
61. Berg D, Jabs B, Merschdorf U, Beckmann H, Becker G. Echogenicity of substantia nigra determined by transcranial ultrasound correlates with severity of Parkinsonian symptoms induced by neuroleptic therapy. Biol Psychiatry. 2001;50:463–7.
62. Berg D, Siefker C, Ruprecht-Dörfler P, Becker G. Relationship of substantia nigra echogenicity and motor function in elderly subjects. Neurology. 2001;56:13–7.
63. Ruprecht-Doerfler P, Klotz P, Becker G, Berg D. Substantia nigra hyperechogenicity correlates with subtle motor dysfunction in tap dancers. Parkinsonism Relat Disord. 2007;6:363–4.
64. Ruprecht-Dörfler P, Berg D, Tucha O, Benz P, Meier-Meitinger M, Alders GL, Lange KW, Becker G. Echogenicity of the substantia nigra in relatives of patients with sporadic Parkinson's disease. Neuroimage. 2003;18(2):416–22.
65. Schweitzer KJ, Behnke S, Liepelt I, Wolf B, Grosser C, Godau J, et al. Cross-sectional study discloses a positive family history for Parkinson's disease and male gender as epidemiological risk factors for substantia nigra hyperechogenicity. J Neural Transm. 2007;114:1167–71.
66. Liepelt I, Wendt A, Schweitzer KJ, Wolf B, Godau J, Gaenslen A, Bruessel T, Berg D. Substantia nigra hyperechogenicity assessed by transcranial sonography is related to neuropsychological impairment in the elderly population. J Neural Transm. 2008;115:993–9.
67. Liepelt I, Behnke S, Schweitzer K, Wolf B, Godau J, Wollenweber F, Dillmann U, Gaenslen A, Di Santo A, Maetzler W, Berg D. Pre-motor signs of PD are related to SN hyperechogenicity assessed by TCS in an elderly population. Neurobiol Aging. 2011;32:1599–606.
68. Liepelt-Scarfone I, Behnke S, Godau J, Schweitzer KJ, Wolf B, Gaenslen A, Berg D. Relation of risk factors and putative premotor markers for Parkinson's disease. J Neural Transm. 2011;118:579–85.
69. Sommer U, Hummel T, Corman K, Mueller A, Frasnelli J, Krop J, Reichmann H. Detection of presymptomatic Parkinson's disease: combining smell tests, transcranial sonography, and SPECT. Mov Disord. 2004;19:1196–202.
70. Haehner A, Hummel T, Hummel C, Sommer U, Junghanns S, Reichmann H. Olfactory loss may be a first sign of idiopathic Parkinson's disease. Mov Disord. 2007;22:839–42.
71. Walter U, Hoeppner J, Prudente-Morrissey L, et al. Parkinson's disease-like midbrain sonography abnormalities are frequent in depressive disorders. Brain. 2007;130:1799–807.
72. Stockner H, Iranzo A, Seppi K, Serradell M, Gschliesser V, Sojer M, Valldeoriola F, Molinuevo JL, Frauscher B, Schmidauer C, Santamaria J, Högl B, Tolosa E, Poewe W. Midbrain hyperechogenicity in idiopathic REM sleep behavior disorder. Mov Disord. 2009;24:1906–9.
73. Berg D, Seppi K, Behnke S, Liepelt I, Schweitzer K, Stockner H, Wollenweber F, Gaenslen A, Mahlknecht P, Spiegel J, Godau J, Huber H, Srulijes K, Kiechl S, Bentele M, Schubert T, Hiry T, Probst M, Schneider V, Klenk J, Sawires M, Willeit J, Maetzler W, Fassbender K, Gasser T, Poewe W. Enlarged substantia nigra hyperechogenicity and risk for Parkinson disease. 37 months three-centre study of 1847 elderly. Arch Neurol. 2011;68:932–7.
74. Walter U, Dressler D, Wolters A, Probst T, Grossmann A, Benecke R. Sonographic discrimination of corticobasal degeneration vs progressive supranuclear palsy. Neurology. 2004;63(3):504–9.
75. Walter U, Dressler D, Probst T, Wolters A, Abu-Mugheisib M, Wittstock M, Benecke R. Transcranial brain sonography findings in discriminating between parkinsonism and idiopathic Parkinson disease. Arch Neurol. 2007;64:1635–40.
76. Walter U, Dressler D, Wolters A, Wittstock M, Greim B, Benecke R. Sonographic discrimination of dementia with Lewy bodies and Parkinson's disease with dementia. J Neurol. 2006;253(4):448–54.

77. Stockner H, Sojer M, Sepi K, Mueller J, Wenning GK, Schmidauer C, Poewe W. Midbrain sonography in patients with essential tremor. Mov Disord. 2007;22(3):414–7.
78. Budisic M, Trkanjec Z, Bosnjak J, Lovrencic-Huzjan A, Vukovic V, Demarin V. Distinguishing Parkinson's disease and essential tremor with transcranial sonography. Acta Neurol Scand. 2009;119(1):17–21.
79. Kim JS, Oh YS, Kim YI, Koo JS, Yang DW, Lee KS. Transcranial sonography (TCS) in Parkinson's disease (PD) and essential tremor (ET) in relation with putative premotor symptoms of PD. Arch Gerontol Geriatr. 2012;54(3):436–9.
80. Koller WC, Busenbark K, Miner K. The relationship of essential tremor to other movement disorders: report on 678 patients. Essential Tremor Study Group. Ann Neurol. 1994;35:717–23.
81. Becker G, Becker T, Struck M, et al. Reduced echogenicity of brainstem raphe specific to unipolar depression: a transcranial color-coded real-time sonography study. Biol Psychiatry. 1995;38:180–4.
82. Berg D, Supprian T, Hofmann E, et al. Depression in Parkinson's disease: brainstem midline alteration on transcranial sonography and magnetic resonance imaging. J Neurol. 1999;246:1186–93.
83. Walter U, Krolikowski K, Tarnacka B, Benecke R, Czlonkowska A, Dressler D. Sonographic detection of basal ganglia lesions in asymptomatic and symptomatic Wilson disease. Neurology. 2005;64(10):1726–32.
84. Godau J, Schweitzer KJ, Liepelt I, et al. Substantia nigra hypoechogenicity: definition and findings in restless legs syndrome. Mov Disord. 2007;22:187–92.
85. Godau J, Wevers AK, Gaenslen A, et al. Sonographic abnormalities of brainstem structures in restless legs syndrome. Sleep Med. 2008;9:782–9.
86. Becker G, Naumann M, Scheubeck M, Hofmann E, Deimling M, Lindner A, Gahn G, Reiners C, Toyka KV, Reiners K. Comparison of transcranial sonography, magnetic resonance imaging, and single photon emission computed tomography findings in idiopathic spasmodic torticollis. Mov Disord. 1997;12(1):79–88.
87. Naumann M, Becker G, Toyka KV, Supprian T, Reiners K. Lenticular nucleus lesion in idiopathic dystonia detected by transcranial sonography. Neurology. 1996;47:1284–90.
88. Walter U, Buttkus F, Benecke R, Grossmann A, Dressler D, Altenmüller E. Sonographic alteration of lenticular nucleus in focal task-specific dystonia of musicians. Neurodegener Dis. 2012;9(2):99–103.
89. Becker G, Berg D, Rausch WD, Lange HK, Riederer P, Reiners K. Increased tissue copper and manganese content in the lentiform nucleus in primary adult-onset dystonia. Ann Neurol. 1999;46(2):260–3.
90. Becker G, Berg D, Francis M, Naumann M. Evidence for disturbances of copper metabolism in dystonia: from the image towards a new concept. Neurology. 2001;57(12):2290–4.
91. Berg D, Weishaupt A, Francis MJ, Naoyuki M, Yang X-L, Goodyer ID, Naumann M, Koltzenburg M, Reiners K, Becker G. Changes of copper transporting proteins and ceruloplasmin in the lentiform nuclei in primary adult-onset dystonia. Ann Neurol. 2000;47:827–30.
92. Kruse N, Berg D, Francis MJ, Naumann M, Rausch WD, Reiners K, Rieckmann P, Weishaupt A, Becker G. Reduction of Menkes mRNA and copper in leukocytes of patients with primary adult-onset dystonia. Ann Neurol. 2001;49:405–8.

Chapter 6
Applications of Near-Infrared Spectroscopy in Movement Disorders

Masahito Mihara, Noriaki Hattori and Ichiro Miyai

Introduction

Movement disorders are neurological conditions that affect the regulation of movement, including excessive and/or involuntary movement as well as slowed and/or absent voluntary movement. Recent advances in functional neuroimaging techniques, including positron emission tomography (PET) and functional magnetic resonance imaging (fMRI), have enabled us to investigate underlying neuronal mechanisms of motor and cognitive control. Among these functional neuroimaging techniques, functional near-infrared spectroscopy (fNIRS) has drawn attention because this system is relatively robust for subjects' motion and available for various tasks including standing, walking, and reaching. In this chapter, we introduce the clinical applications of NIRS and discuss future possible applications.

Principles of Functional NIRS

Near-infrared light, especially with a wavelength between 700 and 900 nm can penetrate through biological tissues including scalp and skull bone, and is absorbed by biological chromophores such as hemoglobin, myoglobin, and cytochrome oxidase

M. Mihara (✉)
Department of Neurology, Graduate School of Medicine, Osaka University,
2-2, D-4 Yamadaoka, Suita, Osaka 565-0871, Japan
e-mail: mihara@neurol.med.osaka-u.ac.jp

N. Hattori
Neurorehabilitation Research Institute, Morinomiya Hospital,
2-1-88, Morinomiya, Joto-ku, Osaka 536-0025, Japan
e-mail: hattori@omichikai.or.jp

I. Miyai
Morinomiya Hospital, 2-1-88, Morinomiya, Joto-ku, Osaka 536-0025, Japan
e-mail: miyai@omichikai.or.jp

F. B. Nahab, N. Hattori (eds.), *Neuroimaging of Movement Disorders,*
Current Clinical Neurology 44, DOI 10.1007/978-1-62703-471-5_6,

in underlying brain tissues. Considering that myoglobin concentration is much less than hemoglobin in the brain tissue, and change in the redox state of cytochrome oxidase only occurs in severely hypoxic conditions, near-infrared light is absorbed mainly by hemoglobin when it is used as a functional brain-imaging tool. In continuous wave NIRS systems, widely used in commercially available instruments, measurement of the transmitted intensity and calculation of the relative concentration changes in hemoglobin are performed according to the modified Beer–Lambert law (MBLL) for highly scattering media [1]. Under the assumption that the light attenuation by scattering is constant, MBLL is denoted as

$$\Delta A_{\lambda 1} = (\varepsilon_{\lambda 1}^{OxyHb} \cdot \Delta C^{OxyHb} + \varepsilon_{\lambda 1}^{DeoxyHb} \cdot \Delta C^{DeoxyHb}) \cdot L$$

Where, ε_{λ} is the extinction coefficient at a given wavelength λ, L is the optical path length, and $\triangle C$ is the change in concentration of each chromophore. If simultaneous measurement with multiple wavelengths is used and optical path length is considered, the product of concentration change of chromophere and optical path length are calculated by solving the simultaneous equations. However, it should be noted that the precise measurement of optical path length is impossible with the continuous-wave NIRS system. Therefore, calculated measures were usually denoted in arbitrary units such as millimolar-millimeter (mM × mm) [2]. The distribution of near-infrared light paths between an illuminator and detector is predicted to become "banana-shaped" [3], requiring particular interoptodes distances for propagation of near-infrared light to the cerebral cortex. Generally, at least 2 cm of distance is required for cortical propagation.

In the brain tissue, regional brain activation is accompanied by increase in regional blood flow [4] that exceeds the regional oxygen consumption. Therefore, the regional increase in oxygenated hemoglobin (OxyHb), accompanied by a relative decrease in deoxygenated hemoglobin (DeoxyHb), are observed when regional cortical activation occurs. Similarly to fMRI and PET, fNIRS detects cortical activation in an indirect manner; that is, task-related increases in the OxyHb signal and/or task-related decrease in the DeoxyHb rather than by direct measurement of neuronal activity.

Potential Advantages and Shortcomings of Functional NIRS

There are several potential advantages to fNIRS in investigating human brain activity. First, NIRS measurement requires the tight contact between the scalp and optodes during measurement. If contact is maintained, minor head and truncal motion are cancelled and less onerous constraints are required. Second, unlike other neuroimaging modalities, NIRS systems are relatively small and less complex in design. Finally, such systems are noninvasive and safe since they utilize only low-power near-infrared laser. Consequently, NIRS systems enable us to measure cortical activation in daily life actions such as standing and walking. Based on these characteristics, it is thought

that NIRS is an ideal neuroimaging tool for clinical investigation in areas such as pediatric neurology and rehabilitation medicine.

Despite these potential advantages, there are several shortcomings of NIRS as a tool for functional neuroimaging. First, because of the limited propagation of near-infrared light from the scalp, it is difficult to measure brain activation of deep brain structures including basal ganglia, brain stem, and cerebellum. Second, NIRS has relatively poor spatial resolution of a few centimeters. Therefore, spatial registration using other modalities such as high-resolution 3D structural MRI scans or other standard references are necessary [5]. Third, the continuous-wave NIRS systems most commonly used only to measure relative changes in hemoglobin concentration; they cannot measure absolute changes because precise optical path length cannot be determined with continuous-wave NIRS system. Finally, the NIRS signal changes reflect not only the brain tissue, but also other signals including skin tissue beneath optodes [6]. Till date, several methodologies have been proposed to avoid or cancel the nonbrain artifact [7, 8], but there is no "gold standard" for this problem. Therefore, researchers should be cautious about contamination of these nonbrain signals in interpreting the results from NIRS measurement.

Application of Functional NIRS to Locomotion and Postural Control Study in Healthy Humans

Habitual bipedal standing and locomotion in humans is highly advantageous because it helps to maximize dexterity of hands for developing tools. However, as a tradeoff for this advantage, unstable nature of bipedal standing increases the tendency to fall, leading to severe injuries. Actually, one community-based study revealed that more than one-third of people older than the age of 65 years fell at least once a year and that the proportion increased to 50 % by the age of 80 [9]. Accumulated results from studies of quadruped animals [10, 11], suggest that multiple automated and reflective actions regulated by the subcortical structures contribute to balance control. However, since balance control in bipedal standing requires more complex and sophisticated sensorimotor coordination than in quadruped standing, it is plausible that not only subcortical structures, but also well-evolved cerebral cortices are involved in balance control during bipedal standing in humans [12]. In line with this notion, recent studies suggested that the cerebral cortex was involved in human balance control [13–15]. Compared with conventional neuroimaging techniques such as fMRI or PET, fNIRS is relatively robust for subjects' motion and seems to be suitable for investigating cortical involvement in postural control.

Using a multichannel NIRS system, Miyai et al. [16] reported successful measurement of cortical activation during locomotion. They used a weight-balancer system to avoid excessive motion artifacts during a locomotor task, and could measure task-related hemoglobin signal changes from the frontoparietal skull surface during gait on a treadmill (Fig. 6.1).

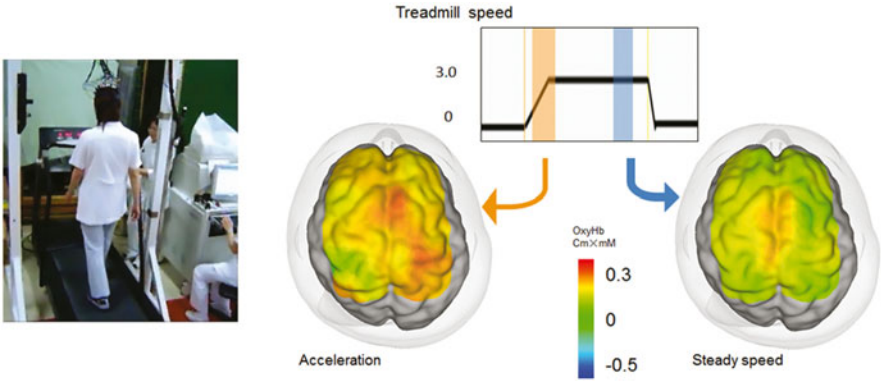

Fig. 6.1 Measurement of cortical activation during walking using NIRS system. **a** Subject performing a locomotor task on the treadmill. **b** T Cortical activation map based on the OxyHb signal changes during gait on the treadmill at 3 km/h. Broad cortical area is activated in acceleration phase, whereas only medial aspect of motor-related cortices are activated in steady speed phase

In healthy subjects, symmetrical activation in the medial sensorimotor cortex and supplementary motor area were observed during treadmill gait (see Fig. 6.1). These findings were consistent with results from a study using single-photon emission tomography [17]. Furthermore, it was also suggested that the various cortical areas play different roles in locomotor control. For example, the prefrontal cortex activated mainly during the acceleration phase of locomotion and gradually decreased at a steady speed (see Fig. 6.1, [18]). It was also revealed that the prefrontal activation change was more prominent at the higher locomotor speed, but cortical activation in the sensorimotor cortex was not associated with gait speed. Therefore, it was suggested that the prefrontal cortex was more involved in the adaptation of locomotion, but medial sensorimotor cortex was involved in the stable gait.

As for maintaining standing posture, Mihara et al. [19] reported cortical activation was associated with predictable and unpredictable postural perturbations. During the experiment, subjects were asked to maintain upright posture on the platform against the brisk forward and backward translation of the platform. Statistical analyses using general linear model with least square estimation revealed significant task-related OxyHb increases in the bilateral prefrontal cortices regardless of preceding warning cues. In the predictable condition, the supplementary motor area and the parietal association cortices were activated along with the prefrontal cortex (Fig. 6.2).

Based upon the findings from these previous studies of postural control, the prefrontal cortex appears to be involved in the attentional processing of postural maintenance against external perturbation [20], whereas the supplementary motor area and parietal association cortical activations were more prominent preceding warning cues, suggesting that the latter areas are involved in the intentional control of posture.

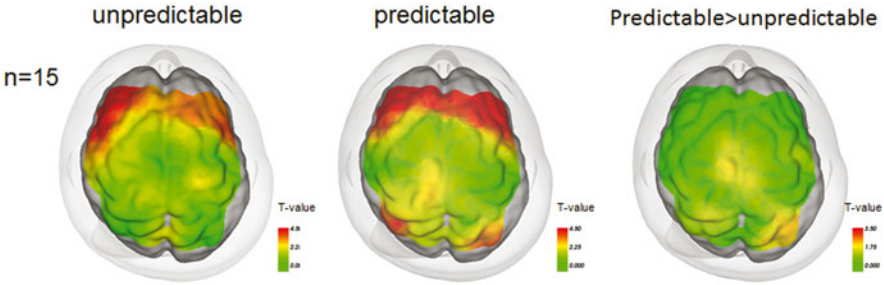

Fig. 6.2 Cortical activation associated with the postural perturbation in healthy subjects. Cortical activation mapping based on the task-related OxyHb signal increase. In the unpredictable condition, task-related OxyHb signal increase as prominent in the bilateral prefrontal cortex (*left*). In the predictable condition, postural perturbation evoked task-related OxyHb signal increase in the supplementary motor area and parietal association cortex as well as the bilateral prefrontal cortex (*middle*). *SMA* supplementary motor area, *PFC* prefrontal cortex

Application of Functional NIRS Study for Investigating Postural and Gait Impairment After Neurologic Disorders

Patients with stroke or movement disorders, including idiopathic Parkinson disease (iPD) and spinocerebellar ataxia (SCA), show balance impairment and impacts on activities of daily living. In the field of rehabilitation medicine, balance impairment is one of the main therapeutic targets. As described in the previous section, fNIRS can monitor activation of the cortical networks that are vital for postural control. Figure 6.3 shows the correlation between balance function and task-related OxyHb signal changes associated with the unpredicted postural perturbation in hemiplegic stroke patients with a subcortical lesion. Significant correlation between balance function and cortical activation was observed in several cortical areas including the supplementary motor area and affected prefrontal cortex [21]. These results suggest that the recovery of balance is associated with changes in cortical activation, as the upper and lower limb recover after stroke [22−25].

Functional NIRS measurements can be useful as surrogate markers of balance recovery after rehabilitation. Figure 6.4 illustrates two patients with Parkinson disease who received 4 weeks of inpatient rehabilitation and medication adjustments. Cortical activation associated with the postural perturbation increased in widespread cortical areas including the prefrontal cortex and supplementary motor area in both patients. Considering the subcortical nature of the iPD, increased cortical activation may serve a compensatory role for the subcortical dysfunction. Although there are several issues to be elucidated, these results imply that fNIRS could be used as the surrogate marker of the functional recovery or reorganization after rehabilitative interventions in various neurological disorders.

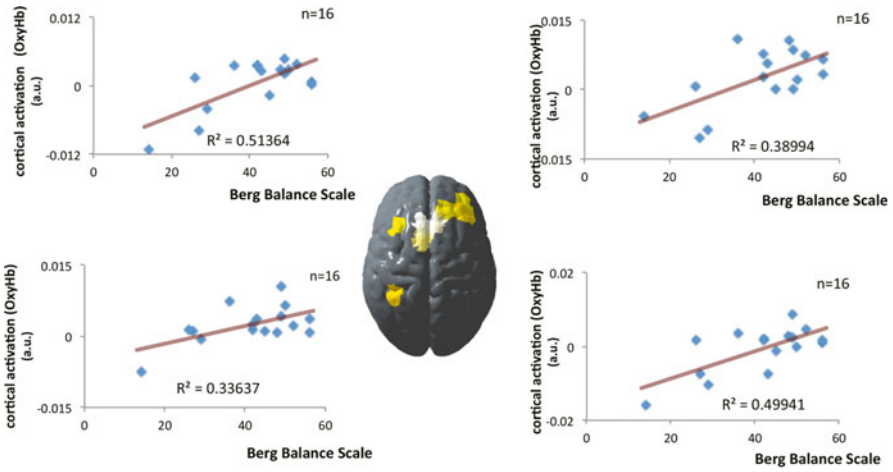

Fig. 6.3 Correlation between balance function and task-related OxyHb signal changes. Cortical region in which a significant correlation between balance function and task-related OxyHb signal changes was observed. Note that the *left* side of the figure represents the unaffected side of the patients. Each scatter plot represents the correlation between OxyHb signal changes and individual balance functions. *BBS* Berg balance scale

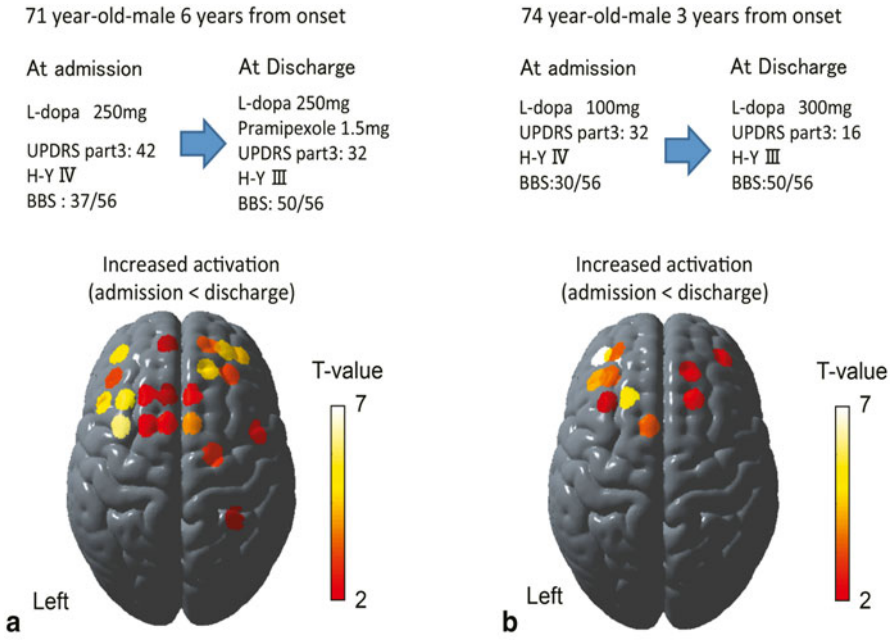

Fig. 6.4 Cortical activation change along with the balance recovery in PD patients. Postural perturbation-related cortical activation mapping change between at admission and at discharge based on the task-related OxyHb signal increase in two PD cases with inpatients rehabilitation. In both cases, cortical activation was increased as the recovery of balance function in widespread cortical area including the bilateral prefrontal, premotor, and supplementary motor area. *BBS* Berg balance scale

Functional NIRS as the Tool for Motor-Learning Studies

Motor learning is vital for the acquisition of motor skills in the daily lives of both healthy individuals and those with neurological disorders. Motor learning comprises motor sequence learning and motor adaptation in experimental settings [26]. Motor sequence learning is assessed by incremental acquisition of movements with repetitions whereas motor adaptation refers to ability to compensate for environmental changes. Till date, most human studies regarding motor sequence learning used PET or fMRI and investigated the neural mechanisms underlying learning of sequential movements of fingers or the feet in a supine position. However, motor learning usually occurs under postural control since most movements are executed while subjects are sitting or standing in a daily situation. As described above, because of less postural restriction, fNIRS is better suited for investigating the motor learning in daily circumstances.

Using fNIRS, Hatakenaka et al. [27] studied the cortical activation change during the pursuit rotor (PR) task in healthy subjects. A pursuit rotor (PR) is one of the tools used to evaluate motor sequence learning by measuring ability to keep a stylus on a rotating target. In the PR task, there is no need for precise control of finger movements, but it requires motor control of proximal parts of the upper extremity including the shoulder and elbow as well as postural control for sitting [28]. In this study, 18 right-handed healthy subjects performed eight repetitions of 30-s PR tasks followed by 30-s rest periods. Motor skill gains were evaluated by contact time of stylus and target. During eight repetitions of PR tasks, cortical activation in the frontoparietal cortices was evaluated with fNIRS.

Task-related OxyHb increases were observed in the sensorimotor cortices, prefrontal cortex, and premotor cortex as task performance improved. Interestingly, the center of task-related OxyHb increase was observed in the presupplementary motor area initially, but it shifted caudally to the supplementary motor area with cycle repetitions. These data suggest a different cortical role between presupplementary area and supplementary motor area in motor skill-learning process.

Functional NIRS was also used to investigate the adaptation-learning process. We investigated the cortical activation changes during the adaptation of reaching with robotic devices using a 3D virtual-reality (VR) system in which the limb coordination patterns are altered [29]. In this study, seven right-handed healthy subjects participated. The upper limb training system used was mediated by electro-rheological fluid actuators with 3-degrees of free movement range [30]. The subjects are given visual feedback of the position and the movement of the gripping handle of the robot arm as the colored ball (Object) in the 3D VR space on the 13′-monitor (Fig. 6.5a). The experiment consisted of 16 cycles of alternating 12-s rest and 8-s task periods. In the rest period, the floating target (Target) was fixed at the near-lower-left corner (home position) of the VR space. In the reaching task period, the Target moved from the home position to the far-upper-right corner, and then returned to the home position in 8 s, and subjects were asked to follow the Target by moving the robot arm. The distance between the Object and the Target was indicated as color of the Object. The mean distance in each cycle was calculated as a performance measure.

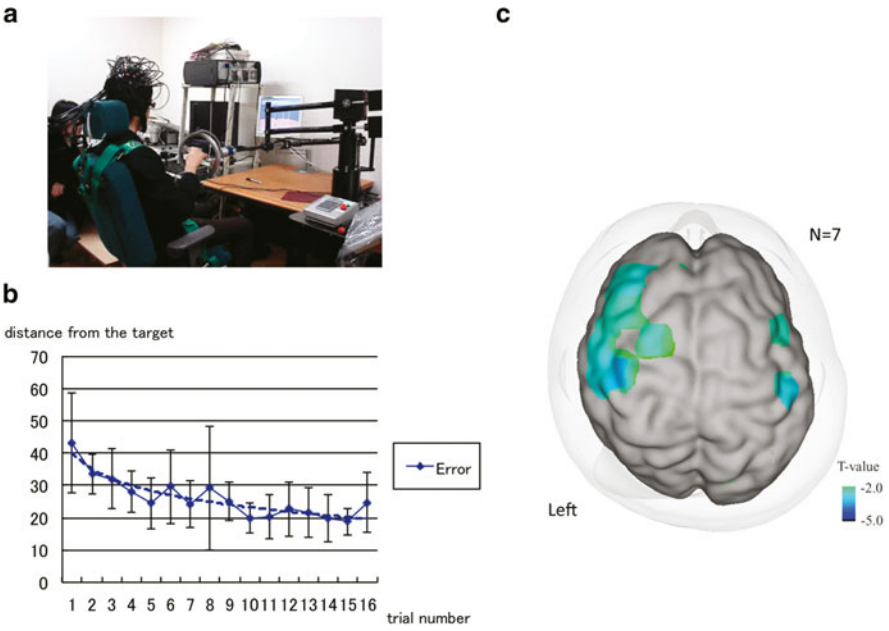

Fig. 6.5 Adaptation-learning task with the 3D robotic rehabilitation system. **a** Experimental setting of robotic rehabilitation system with functional NIRS. In a virtual reality space, subjects were asked to follow the target. **b** Averaged distance from the handle position and the target. Averaged distance gradually reduced with cycle repetitions, indicating that the subjects could adapt to the visuomotor reaching task. **c** Significant correlations between error and cortical activation. Cortical activation in the *left* premotor cortex was increased as the adaptation-learning improved

Cortical activation was measured as oxygenated hemoglobin signal change using a 50-channel fNIRS system from the frontoparietal area. Task-related cortical activation of each subject was modeled using the two orthogonal covariates [31]. The first was the Task covariate modeled as a box-car function in all task periods and the second was the Error covariate that comprised a box-car function scaled by the mean distance. The Error covariate was mean corrected and orthogonalized with respect to the first covariate. Both covariates were convolved with the canonical hemodynamic response function and used in a GLM analysis. Group analysis was performed using the random-effects model.

Mean distance for the seven subjects gradually reduced with cycle repetitions, indicating that the subjects learned to adapt to the visuomotor reaching task in VR space. Group analysis of fNIRS signals showed significant main effects in the bilateral prefrontal, bilateral premotor, and left primary sensorimotor area. Significant negative correlations to the Error covariate were also found in the left prefrontal and premotor area (see Fig. 6.5). Although broad cortical networks were involved in the visuomotor adaption learning of reaching task, the prefrontal and premotor area were primarily involved in the early stage of the adaptation process.

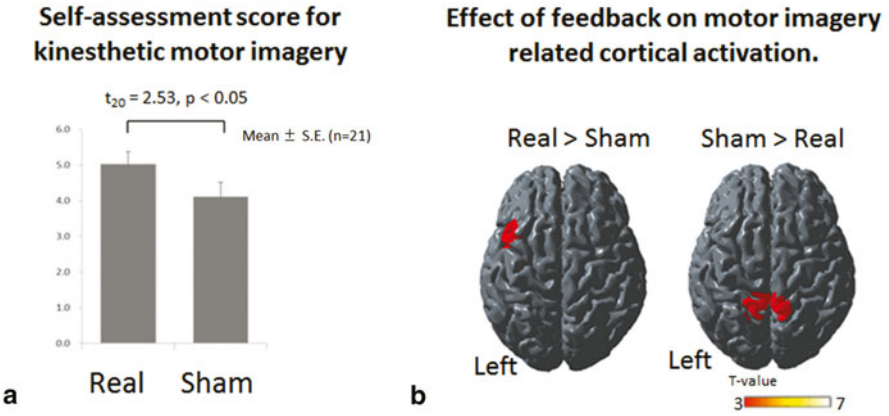

Fig. 6.6 Neurofeedback effect on the motor imagery and imagery-related cortical activation. **a** Self-assessment score for kinesthetic motor imagery after Real and Sham feedback. Feedback of contralateral motor area increased kinesthetic motor imagery score. **b** Effect of feedback on motor imagery-related cortical activation. Neurofeedback increased activation in the contralateral motor-related cortex and decreased medial parietal cortex

Therapeutic Application of Functional NIRS in Rehabilitation Field

There has been much interest in developing brain–computer interface (BCI) technology to improve activities of daily life and to restore function in patients with stroke and neurodegenerative disorders [32, 33]. One primary purpose for the development of BCI systems is to substitute for the lost function of neuromuscular output. In order to restore interaction between the brain and outer environment, the BCI system requires detection of brain signals, decoding the information from these signals, and output to an appropriate interface device. Among number of techniques for detecting brain activity have been employed, fNIRS has attracted attention because of its portability and noninvasiveness. Although clinical usage of BCI in the rehabilitation field remains limited at this time, decoding techniques are improving. Sitaram et al. [34] reported that right/left finger motor imagery could be classified with an average of 89 % accuracy applying a pattern recognition algorithm using hidden Markov Model on multichannel NIRS data.

In addition, BCI could be used as the tool for augmenting cortical plasticity. Use of electroencephalography (EEG) signals as feedback to a subject has been known to alter brain activity itself (neurofeedback). According to this notion, we have developed a NIRS-mediated neurofeedback system [35]. We investigated the effect of our neurofeedback system with 21 healthy subjects using a motor imagery task of right finger movement. Neurofeedback from the contralateral motor-related area successfully improved the motor imagery-related cortical activation in the contralateral premotor area as well as the subjective score of motor imagery (Fig. 6.6).

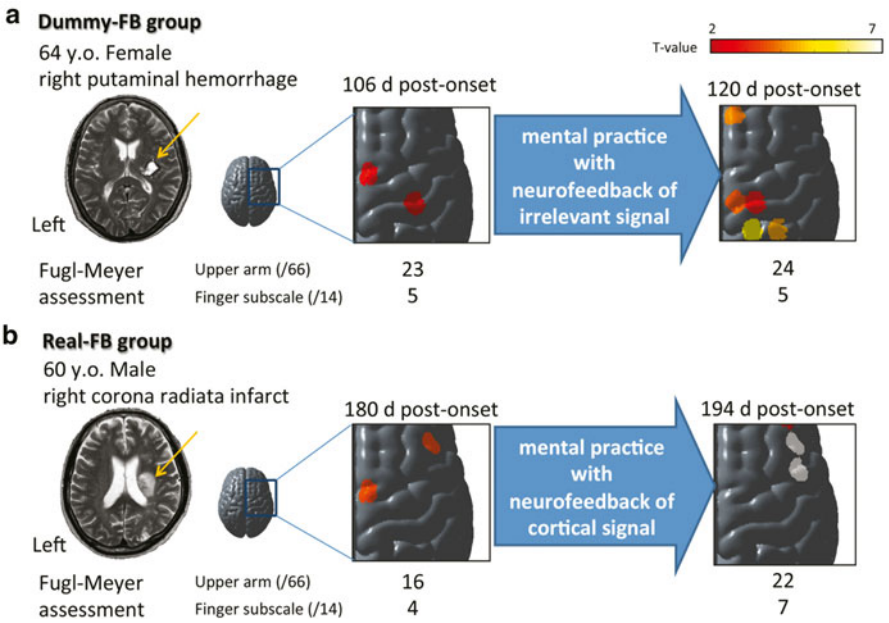

Fig. 6.7 Effect of neurofeedback of the premotor activation during mental practice with motor imagery. We applied the motor imagery-based training combined with neurofeedback of the premotor activation or irrelevant signal during mental practice. Patients who were provided irrelevant signal feedback during mental practice (**a** dummy-FB group), showed insignificant motor cortical activation change during motor imagery and also showed trivial functional recovery of upper limb. Whereas, patients who were provided the premotor activation signal during mental practice (**b** real-FB group), showed significant increases in the motor imagery-related cortical activation and also showed significant functional recovery through mental practice

We also applied this system to stroke rehabilitation, and showed the potential usefulness of the NIRS-mediated neurofeedback on functional recovery after stroke [36]. As shown in the Fig. 6.7, our preliminary results showed that the neurofeedback augments the effect of the mental practice with motor imagery for the upper limb function. These findings hold promise for the therapeutic implementation of NIRS-mediated neurofeedback for patients with stroke or movement disorders.

Conclusion and Future Directions

Functional NIRS provides unique advantages as a tool for neuroimaging. Despite several shortcomings, including difficulty in measuring hemoglobin oxygenation changes in deep brain structures and poor spatial resolution, it has characteristic advantages including the ability to measure cortical activation under daily life circumstances. In addition to the measurement of cortical activation,with further advances in data analysis, fNIRS could be applied as a tool for treatment augmenting rehabilitation.

References

1. Cope M, Delpy DT, Reynolds EO, Wray S, Wyatt J, van der Zee P. Methods of quantitating cerebral near infrared spectroscopy data. Adv Exp Med Biol. 1988;222:183–89.
2. Maki A, Yamashita Y, Ito Y, Watanabe E, Mayanagi Y, Koizumi H. Spatial and temporal analysis of human motor activity using noninvasive NIR topography. Med Phys. 1995 Dec;22(12):1997–2005.
3. Gratton G, Maier JS, Fabiani M, Mantulin WW, Gratton E. Feasibility of intracranial near-infrared optical scanning. Psychophysiology. 1994 Mar;31(2):211–5.
4. Fox PT, Raichle ME. Focal physiological uncoupling of cerebral blood flow and oxidative metabolism during somatosensory stimulation in human subjects. Proc Natl Acad Sci U S A. 1986 Feb;83(4):1140–4.
5. Okamoto M, Dan H, Sakamoto K, et al. Three-dimensional probabilistic anatomical cranio-cerebral correlation via the international 10–20 system oriented for transcranial functional brain mapping. Neuroimage. 2004 Jan;21(1):99–111.
6. Takahashi T, Takikawa Y, Kawagoe R, Shibuya S, Iwano T, Kitazawa S. Influence of skin blood flow on near-infrared spectroscopy signals measured on the forehead during a verbal fluency task. Neuroimage. 2011 Aug 1;57(3):991–1002.
7. Kohno S, Miyai I, Seiyama A, et al. Removal of the skin blood flow artifact in functional near-infrared spectroscopic imaging data through independent component analysis. J Biomed Opt. 2007 Nov–Dec;12(6):062111.
8. Yamada T, Umeyama S, Matsuda K. Multidistance probe arrangement to eliminate artifacts in functional near-infrared spectroscopy. J Biomed Opt. 2009;14(6):064034.
9. O'Loughlin JL, Robitaille Y, Boivin JF, Suissa S. Incidence of and risk factors for falls and injurious falls among the community-dwelling elderly. Am J Epidemiol. 1993 Feb 1;137(3):342–54.
10. Armstrong DM. The supraspinal control of mammalian locomotion. J Physiol. 1988 Nov;405:1–37.
11. Drew T, Prentice S, Schepens B. Cortical and brainstem control of locomotion. Prog Brain Res. 2004;143:251–61.
12. Nielsen JB. How we walk: central control of muscle activity during human walking. Neuroscientist. 2003 Jun;9(3):195–204.
13. Dietz V, Quintern J, Berger W. Cerebral evoked potentials associated with the compensatory reactions following stance and gait perturbation. Neurosci Lett. 1984 Sep 7;50(1–3):181–6.
14. Quant S, Maki BE, McIlroy WE. The association between later cortical potentials and later phases of postural reactions evoked by perturbations to upright stance. Neurosci Lett. 2005 Jun 24;381(3):269–74.
15. Slobounov S, Hallett M, Stanhope S, Shibasaki H. Role of cerebral cortex in human postural control: an EEG study. Clin Neurophysiol. 2005 Feb;116(2):315–23.
16. Miyai I, Tanabe HC, Sase I, et al. Cortical mapping of gait in humans: a near-infrared spectroscopic topography study. Neuroimage. 2001 Nov;14(5):1186–92.
17. Fukuyama H, Ouchi Y, Matsuzaki S, et al. Brain functional activity during gait in normal subjects: a SPECT study. Neurosci Lett. 1997 Jun 13;228(3):183–6.
18. Suzuki M, Miyai I, Ono T, et al. Prefrontal and premotor cortices are involved in adapting walking and running speed on the treadmill: an optical imaging study. Neuroimage. 2004 Nov;23(3):1020–6.
19. Mihara M, Miyai I, Hatakenaka M, Kubota K, Sakoda S. Role of the prefrontal cortex in human balance control. Neuroimage. 2008 Nov 1;43(2):329–36.
20. Woollacott M, Shumway-Cook A. Attention and the control of posture and gait: a review of an emerging area of research. Gait Posture. 2002;16:1–14.
21. Mihara M, Miyai I, Hattori N, et al. Cortical control of postural balance in patients with hemiplegic stroke. Neuroreport. 2012 Mar 28;23(5):314–9.
22. Calautti C, Baron JC. Functional neuroimaging studies of motor recovery after stroke in adults: a review. Stroke. 2003 Jul;34(6):1553–66.

23. Enzinger C, Dawes H, Johansen-Berg H, et al. Brain activity changes associated with treadmill training after stroke. Stroke. 2009 Jul;40(7):2460–7.
24. Luft AR, Forrester L, Macko RF, et al. Brain activation of lower extremity movement in chronically impaired stroke survivors. Neuroimage. 2005 May 15;26(1):184–94.
25. Ward NS, Brown MM, Thompson AJ, Frackowiak RS. Neural correlates of motor recovery after stroke: a longitudinal fMRI study. Brain. 2003 Nov;126(Pt 11):2476–96.
26. Doyon J, Benali H. Reorganization and plasticity in the adult brain during learning of motor skills. Curr Opin Neurobiol. 2005 Apr;15(2):161–7.
27. Hatakenaka M, Miyai I, Mihara M, Sakoda S, Kubota K. Frontal regions involved in learning of motor skill—a functional NIRS study. Neuroimage. 2007 Jan 1;34(1):109–16.
28. Grafton ST, Mazziotta JC, Presty S, Friston KJ, Frackowiak RS, Phelps ME. Functional anatomy of human procedural learning determined with regional cerebral blood flow and PET. J Neurosci. 1992 Jul;12(7):2542–8.
29. Mihara M, Miyai I, Haraguchi M, et al. Cortical network involved in the adaptation learning of reaching using 3-dimensional robotic rehabilitation system: a functional near-infrared spectroscopic study. Neuroimage. 2009;47(Suppl 1):S170.
30. Furusho J, Koyanagi K, Imada Y, et al. A 3-D rehabilitation system for upper limbs. Developed in a 5-year NEDO project and its clinical testing. Paper presented at: IEEE 9th International Conference on Rehabilitation Robotics; 2005.
31. Buchel C, Holmes AP, Rees G, Friston KJ. Characterizing stimulus-response functions using nonlinear regressors in parametric fMRI experiments. Neuroimage. 1998 Aug;8(2):140–8.
32. Daly JJ, Wolpaw JR. Brain-computer interfaces in neurological rehabilitation. Lancet Neurol. 2008 Nov;7(11):1032–43.
33. Dobkin BH. Brain-computer interface technology as a tool to augment plasticity and outcomes for neurological rehabilitation. J Physiol. 2007 Mar 15;579(Pt 3):637–42.
34. Sitaram R, Zhang H, Guan C, et al. Temporal classification of multichannel near-infrared spectroscopy signals of motor imagery for developing a brain-computer interface. Neuroimage. 2007 Feb 15;34(4):1416–27.
35. Mihara M, Miyai I, Hattori N, et al. Neurofeedback using real-time near-infrared spectroscopy enhances motor imagery related cortical activation. PLoS One. 2012;7(3):e32234.
36. Mihara M, Hattori N, Hatakenaka M, et al. Near-infrared spectroscopy-mediated neurofeedback enhances efficacy of motor imagery-based training in poststroke victims: a pilot study. Stroke. 2013;44(4):1091–1098.

Chapter 7
Structural MRI in Idiopathic Parkinson Disease and Parkinsonism

Christoph Mueller, Klaus Seppi and Werner Poewe

Introduction

Parkinson disease (PD) is a slowly progressive neurodegenerative disorder, which is currently defined by the presence of bradykinesia and additional cardinal motor features including rigidity, rest tremor, and, later in the disease course, postural instability. The critical pathology underlying the cardinal motor symptoms of idiopathic PD (iPD) is cell loss with Lewy body inclusions in the substantia nigra (SN) resulting in striatal dopamine deficiency. In addition, alpha-synuclein pathology and neuronal loss are present in multiple sites in the central nervous system (CNS) as well as in the peripheral autonomic nervous system, causing a broad spectrum of nonmotor symptoms. Despite published consensus operational criteria for the diagnosis of iPD, clinical distinction from other types of neurodegenerative parkinsonism, including multiple system atrophy (MSA), progressive supranuclear palsy (PSP), dementia with Lewy bodies (DLB), or corticobasal syndrome (CBS) can be difficult on clinical grounds alone, particularly in early stages of the disease. Even in the hands of experienced neurologists, erroneous clinical diagnosis of parkinsonian syndromes may occur in up to one quarter of patients suffering from parkinsonian symptoms [1]. For this reason, the primary diagnosis has to be reevaluated in many patients over the years. In recent years, structural imaging using magnetic resonance imaging (MRI) has been explored as a tool to enhance diagnostic accuracy in differentiating iPD from other types of parkinsonisms.

C. Mueller (✉) · K. Seppi · W. Poewe
Department of Neurology, Innsbruck Medical University,
Anichstrasse 35, Innsbruck, A-6020 Austria
e-mail: christoph.mueller@i-med.ac.at

K. Seppi
e-mail: klaus.seppi@i-med.ac.at

W. Poewe
e-mail: werner.poewe@i-med.ac.at

F. B. Nahab, N. Hattori (eds.), *Neuroimaging of Movement Disorders,*
Current Clinical Neurology 44, DOI 10.1007/978-1-62703-471-5_7,

Role of Structural MRI in Diagnosing Parkinsonism

Neurodegenerative processes within the CNS, characterized by cell loss, microglial proliferation, astroglial reaction, or increased age-related deposition of iron may lead to signal changes in affected brain areas. Structural MRI is able to provide additional information on regional changes in tissue volume and offers the possibility for measuring macroscopic cerebral lesions in a quantitative way.

Because of its high spatial and contrast resolution, conventional MRI (cMRI) at 1.5 T with assessment of T1-weighted, T2-weighted, and proton-density-weighted sequences offers in vivo visualization of configuration changes in the range of CNS structures with some regional distribution patterns typical for some parkinsonian syndromes. Atrophy patterns are better demonstrated by T1-weighted images, displaying anatomical details and a good gray and white matter contrast. T2-weighted sequences are more sensitive to changes in tissue properties; increased T2 signals reflect degeneration, demyelination, or gliosis of the affected white matter tracts. On the other hand, a decreased T2 signal is generally restricted to the subcortical gray matter nuclei and may point toward a deposit of paramagnetic substances. The sensitivity of signal changes due to iron deposition can be increased by using T2*-weighted gradient-echo sequences. In iPD or healthy controls, a hyperintense putaminal rim on T2-weighted images at 1.5 T has rarely been reported. However, on T2-weighted images at 3.0 T, a hyperintense putaminal rim seems to be a nonspecific, normal finding [2]. MR scanning at 1.5 T field strength is the most commonly used technique applied in routine clinical practice and from which most data are obtained. Thus, when discussing signal changes, the authors refer to 1.5 T field strengths.

Structural MRI in iPD versus MSA, PSP, and CBD

Structural MRI has gained great potential for the differential diagnosis of neurodegenerative parkinsonisms in the last few years. cMRI may show signal changes in the basal ganglia or further supratentorial and infratentorial structures, as well as characteristic patterns of atrophy and features for the discrimination of atypical parkinsonian syndromes (aPS) and iPD (Figs. 7.1 and 7.2).

Parkinson Disease

In early iPD patients, cMRI does not indicate disease-specific changes. Therefore, its main role is detecting or ruling out other underlying pathologies causing nonneurodegenerative symptomatic parkinsonisms. Structural brain imaging using MRI is usually normal in patients with uncomplicated iPD. In more advanced stages of the disease, signal changes in the area of the SN such as hyperintensities in T2-weighted sequences, or smudging of the red nucleus borders toward the SN, may occur. When

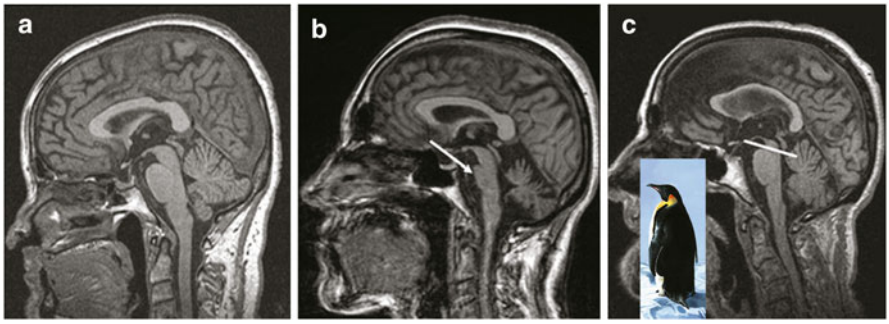

Fig. 7.1 Midsagittal T1-weighted MR images in a patient with PD (**a**), a patient with MSA-P (MSA with predominant parkinsonism) (**b**), and a patient with PSP (**c**). **a** No pontine or midbrain atrophy in the patient with PD. **b** Pontine atrophy (*arrow*) without midbrain atrophy in the MSA-P patient. **c** Midbrain atrophy without pontine atrophy (divided by the *white line*) forming the silhouette of the "penguin" or "hummingbird" sign with the shapes of midbrain tegmentum (bird's head—*above* the *white line*) and pons (bird's body—*below* the *white line*). (© M. Schocke, K. Seppi. Department of Radiology, Department of Neurology. Innsbruck Medical University)

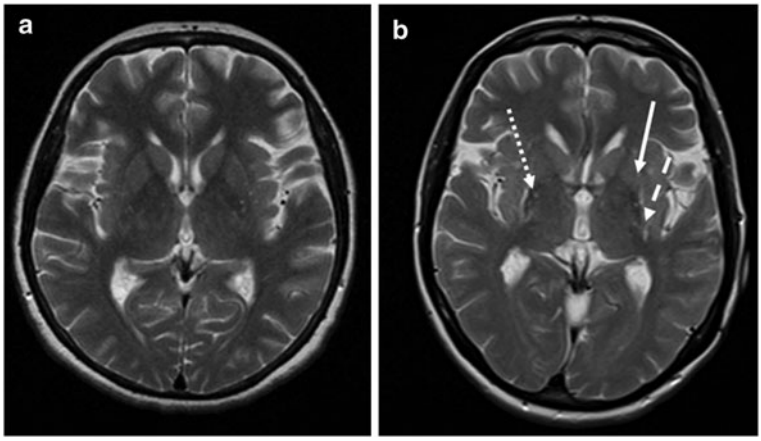

Fig. 7.2 Axial T2-weighted MR images at the striatal level in a patient with PD (**a**) and a patient with MSA-P (**b**). The image appears normal in the PD patient, whereas there is putaminal atrophy (*arrow*), putaminal hypointensity (*dotted arrow*), and a putaminal hyperintense rim (*dashed arrow*) in the patient with MSA-P. (© M. Schocke, K. Seppi. Department of Radiology, Department of Neurology. Innsbruck Medical University)

using the inversion recovery ratio, signal loss in the SN has also been reported in patients with iPD [3–5]. Some studies were able to completely discriminate between iPD patients and healthy controls [3], whereas other authors found an overlap between normal and iPD values in their results [4, 5]. A recent study using 3-dimensional 7.0 T and T2*-weighted gradient-echo sequences could definitively visualize anatomical alterations occurring in the SN of iPD patients, depicting undulated boundaries

between the SN and crus cerebri [6]. By using voxel-based morphometry (VBM), an operator-independent and automated detection of significant volume differences in the whole brain involving voxel-wise statistical analysis of preprocessed structural MR images, gray matter loss of frontal cortical areas could be revealed in advanced iPD patients (see Chap. 3 for a more in-depth review).

Multiple System Atrophy

Multiple system atrophy is an adult-onset, sporadic, progressive neurodegenerative disorder characterized by an increase of alpha-synuclein in oligodendroglia and neuronal loss in multiple areas of the CNS. It is clinically characterized by the variable combination of autonomic failure, parkinsonian symptoms, cerebellar ataxia, and pyramidal signs. Diagnosis during life is often difficult, especially in early stages of the disease, and distinction between MSA-P *(MSA with predominant parkinsonism)* and iPD can be impossible on clinical grounds alone. Nevertheless, an early differentiation between MSA and iPD is essential because of specific therapeutic needs and higher morbidity and mortality of patients with MSA.

Structural MRI in patients with MSA frequently shows characteristic abnormalities in the striatum, brain stem, and cerebellum. The most striking imaging features using cMRI at 1.5 T include putaminal atrophy, hypointensity of the putamen in T2-weighted sequences, and "slit-like" marginal hyperintensity. In addition, abnormalities such as atrophy of the lower brain stem, middle cerebellar peduncle (MCP), and cerebellum, as well as hyperintensities in the pons, MCP, and cerebellum are found in patients with MSA (see Figs. 7.1 and 7.2). Although putaminal atrophy seems to be quite specific and appears to distinguish between MSA and iPD, T2 putaminal hypointensity and hyperintense putaminal rim may also occur in iPD patients. Infratentorial features including atrophy of the pons, lower brain stem, MCPs, medulla, inferior olives, and cerebellum could favor a diagnosis like MSA-C *(MSA with predominant cerebellar ataxia)*. An interesting pattern occasionally resembling the "hot cross bun" sign. This sign comprises T2 signal hyperintensities within the pons and both MCPs, reflects degeneration of pontocerebellar fibers (Fig. 7.3), whereas the median raphe, transverse pontocerebellar fibers ventral to the tegmentum,and anterior and anterolateral contours of the pons show no signal changes. Highly indicating for MSA, this impressive pattern may also be rarely found in nonneurodegenerative parkinsonism [7] and even in patients with spinocerebellar ataxia (SCA) [8].

When comparing MSA-P with MSA-C, the structural and signal changes at 1.5 T mentioned above appear more often and earlier in MSA-P than in MSA-C; on the other hand, infratentorial abnormalities seem to appear more often and earlier in MSA-C than in MSA-P. Overall, putaminal and infratentorial findings detected by MRI at 1.5 T demonstrate high specificity for distinguishing MSA from iPD and healthy controls, while specificity of the putaminal changes is inadequate to differentiate MSA from other forms of aPS. Especially in the early course of the disease,

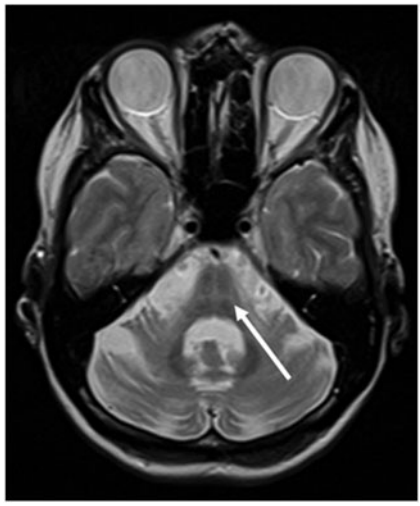

Fig. 7.3 Axial T2-weighted MR image in a patient with MSA-P demonstrating the "hot cross bun" sign (*arrow*) in the basis pontis. (© M. Schocke, K. Seppi. Department of Radiology, Department of Neurology. Innsbruck Medical University)

sensitivity of the above-mentioned findings is suboptimal and inconsistent in the literature. Sensitivity of signal alterations can be somewhat improved by modifying technical aspects such as spatial resolution by using thinner slices or modifying relaxation contrast by using T2*-weighted gradient-echo sequences.

By applying VBM in patients with MSA, basal ganglia and further infratentorial structures show volume loss, and atrophy is even detectable in several cortical regions. Interestingly, callosal thickness declines over time more pronounced in MSA patients, showing a marked loss of volume mainly in the isthmus. An MCP width, using a cutoff value of 8 mm, is shown to be significantly smaller in patients with MSA compared with iPD patients and healthy controls. Furthermore, the area of the pons measured on midsagittal T1-weighted MR images is smaller in patients with MSA-P than in those with iPD or control subjects. By using voxel-based relaxometry (VBR), signal abnormalities can be demonstrated in the cerebellum and brain stem reflecting infratentorial brain atrophy in MSA-C. Using magnetic resonance volumetry, significant reductions in whole brain, striatal, brain stem, and cerebellar volumes are seen in MSA.

Progressive Supranuclear Palsy

Progressive supranuclear palsy is clinically characterized by poorly levodopa-responsive parkinsonism with supranuclear vertical gaze palsy, postural instability, and falling early in the disease course. The parkinsonian variant of PSP (PSP-P) initially may closely mimic iPD with preserved levodopa responsiveness and a lack of characteristic features, like early falls or vertical gaze palsy. The pathological hallmarks of PSP are tau-positive neuronal inclusions and cell loss particularly in the SN, globus pallidus (GP), pons, and subthalamic nucleus.

Common findings on cMRI in patients with PSP include atrophy of the midbrain with enlargement of the third ventricle and tegmental atrophy, as well as T2 signal increase in the midbrain and the inferior olives, and atrophy of frontal and temporal lobes. Putaminal tissue loss, atrophy of the superior cerebellar peduncle (SCP), and the mammillary bodies are also commonly detected. Furthermore, the following indirect parameters of midbrain atrophy may assist in the differential diagnosis of PSP: shortened anteroposterior midbrain diameter, dilatation of the third ventricle, and abnormal superior profile of the midbrain, depicting a flat or concave contour versus convex aspect in healthy people. On midsagittal MR images, these features can create a specific architecture referred to as the "penguin" silhouette or the "hummingbird" sign, with the shape of the midbrain tegmentum resembling the bird's head and the pons resembling the bird's body (see Fig. 7.1c). In axial sections, the reduced anteroposterior midbrain diameter with a selective atrophy of the midbrain tegmentum and with a relative sparing of midbrain tectum and cerebellar peduncles can form the so-called "morning glory flower sign" of "Mickey mouse sign." Values with 14 mm and lower appear to be quite specific for PSP compared with healthy controls, iPD patients, and MSA-P patients. This metric has been suggested to separate adequately between PSP and non-PSP [9], but recent studies could not confirm these postulated results, presenting overlapping values [10–12]. Another helpful imaging-dependent tool for the differentiation between PSP and non-PSP is the planimetric measurement of the pontine and midbrain area, as well as the width of SCPs and MCPs. The MR parkinsonism index (MRPI) is calculated as the product of the ratio of pons area to midbrain area in midsagittal expanse multiplied by the ratio of the width of MCPs and SCPs ([area pons/area midbrain] $\times$ [width MCP/width SCP]) [10]. Both a decreased midbrain-to-pontine area ratio (m/p-ratio) as well as an increased MRPI seem to be helpful in distinguishing PSP from MSA, iPD, and controls, achieving diagnostic accuracy values ranging between 80 and 100 %. By comparing the diagnostic accuracy of the MRPI and the m/p-ratio, the MRPI seems to better differentiate PSP from MSA-P, whereas the m/p-ratio is a better discriminator between PSP and iPD [13].

By applying VBM in patients with PSP, gray matter loss is pronounced in frontotemporal cortical areas including the prefrontal cortex and the insular region, whereas white matter loss is found in the midbrain, comprising cerebral peduncles and central midbrain structures. One study tested the clinical utility of the VBM results as a guide for the differential diagnosis of PSP from iPD and controls by allocating the subject to either PSP or "non-PSP," on the basis of the presence or absence of the midbrain tissue loss. A sensitivity of 83 % and a specificity of 79 %was achieved for discrimination between the two disorders [14].

Corticobasal Degeneration

Corticobasal degeneration (CBD) is an adult-onset, tau-positive, progressive parkinsonian syndrome. Its clinical appearance as CBS presents strikingly asymmetric

features and additional signs and symptoms referable to both cerebral cortex and basal ganglia. The most prominent clinical features in patients with CBS are apraxia, cortical sensory loss, and involuntary movements, which have been referred to as alien hand; extrapyramidal signs may consist in parkinsonian symptoms or dystonia.

In patients with CBD, only few studies have investigated the role of cMRI, depicting cortical atrophy and hyperintense signal changes in the motor cortex or subcortical white matter on T2-weighted images. Furthermore, significantly greater T2-weighted signal hypointensity in the putamen and the GP are common. Although mostly described as frontoparietal and asymmetric, cortical atrophy may also affect other parts of the brain and may even occur in a symmetric pattern. Koyama et al. [15] were able to demonstrate atrophy in the corpus callosum and bulk loss in the cerebral peduncles with ipsilateral pattern of atrophy to the dominant atrophic cerebral hemisphere, whereas signal intensity changes in the cerebral peduncles are absent. Increased T2-weighted lenticular signal hypointensity, ventricular enlargement, and asymmetric cortical atrophy have been suggested as supportive MRI diagnostic findings in patients with CBD, although none of these MRI abnormalities are specific for the disease. A summary of typical MRI patterns for the differential diagnosis of neurodegenerative parkinsonism using 1.5 T are shown in Tables 7.1 and 7.2.

Structural MRI in DLB and PD Dementia

Dementia with Lewy bodies and PD with dementia (PDD) are considered two manifestations of a clinical and pathological spectrum. DLB and PDD are differentiated from other dementia subtypes by the presence of Lewy body pathology, which is commonly detectable in neocortical and limbic areas as well as in brain stem nuclei. DLB and PDD have a similar clinical phenotype, presenting a considerable overlap of symptoms. Features include spontaneous motor parkinsonism, recurrent visual hallucinations, and fluctuating subcortical and cortical neuropsychological deficits with prominent attention dysfunction and impairment of executive function, visuospatial function, and aspects of language and memory retrieval. The separation between DLB and PDD is based on the duration of motor symptoms relative to the development of cognitive impairment, using a simple 1-year rule: onset of dementia within 1 year of parkinsonism favors DLB, whereas more than 12 months of parkinsonism before dementia onset points toward PDD. However, in clinical routine, differential diagnosis of DLB and PDD and other dementia subtypes such as Alzheimer disease (AD) can still be challenging.

MRI routine sequences of patients with DLB and PDD often show whole brain atrophy with a diffuse pattern of gray matter atrophy in the temporal, parietal, middle, and inferior frontal gyri and the occipital lobes. A robust MR finding in DLB and PDD is a relative preservation of the medial temporal lobe when compared with AD (Fig. 7.4). Moreover, the absence of medial temporal atrophy is highly specific for separating DLB/PDD from AD with insufficient sensitivity, but no conventional MR features could be established to distinguish DLB and PDD. In

Table 7.1 Signal and structural changes in MSA and PSP using cMRI at 1.5 T

MSA-P	PSP
Supratentorial changes and abnormalities	
Putaminal atrophy	Putaminal atrophy
Putaminal hypointensity	Atrophy of frontal and temporal lobe
"Slit-like" marginal hyperintensity (putaminal hyperintense rim)	
Infratentorial changes and abnormalities	
Atrophy and/or hyperintensities of lower brain stem, MCP, and cerebellum	Atrophy and/or hyperintensity of the midbrain • Shortened anteroposterior midbrain diameter < 14 mm (eventually Mickey mouse sign) • Abnormal superior profile of the midbrain (flat or concave contour) • "Hummingbird" sign or "penguin" silhouette
Atrophy and/or hyperintensity in the pons (possible "hot cross bun" sign)	
	Enlargement of the third ventricle
	Atrophy and/or hyperintensity of SCP

Signal changes (hyperintensities and hypointensities) are referred to T2-weighted sequences
cMRI conventional magnetic resonance imaging, *T* Tesla, *MSA-P* Parkinson variant of multiple system atrophy, *PSP* progressive supranuclear palsy, *MCP* middle cerebellar peduncle, *SCP* superior cerebellar peduncle

addition, sometimes gray matter loss may be identified around the third ventricle, representing the hypothalamus. These findings were supported by a prospective MRI study with pathological verification [16]; the neuropathological correlates of medial temporal atrophy include senile plaques and neurofibrillary tangles, but not Lewy body-associated pathology.

In summary, DLB and PDD share similar patterns of MRI changes, showing structural preservation of the medial temporal lobe, one of the main distinguishing criteria compared with AD. This imaging feature could be a diagnostic marker for the differentiation of DLB and AD and is indeed part of the consensus criteria for the clinical diagnosis of DLB.

Structural MR Changes in Secondary Parkinsonism

Structural lesions causing symptomatic parkinsonism include space-occupying masses in the region of the basal ganglia and brain stem and strategic microvascular or macrovascular lesions, as well as normal pressure hydrocephalus (NPH) or medication-induced parkinsonism. Furthermore, rare diseases such as Huntington's disease (HD), Wilson disease, or NBIA syndromes (neurodegeneration with brain iron accumulation) can cause parkinsonism (Table 7.3). Because of similar clinical

Table 7.2 Characteristic MRI patterns for the differential diagnosis of neurodegenerative parkinsonism using 1.5 T

	iPD	MSA (-P)	PSP
cMRI			
Normal	++	−	−
Putaminal atrophy	−	++	++
Putaminal hyperintense rim	+	++	+
Putaminal hypointensity	−	++	−
Atrophy of pons and vermis cerebellaris	−	++	+
Signal changes in the pons (hot cross bun sign) or MCPs	−	++	−
Midbrain atrophy (Mickey Mouse sign and penguin silhouette in PSP patients)	−	−	++
MRI planimetry			
Decreased anteroposterior midbrain diameter	−	+	++
Decreased ratio of midbrain and pons area	−	+	+++
Abnormal MRPI (> 15 in patients with PSP)	+	−	+++
DWI			
Increased putaminal diffusivity	−	+++	++
Increased diffusivity of SCP	−	−	+++

MRPI = (area pons/area midbrain) × (width MCP/width SCP)
− < 20 %, + 20–50 %, ++ 50–70 %, +++ 70–90 %, ++++ > 90 %. Signal changes (hyperintensities and hypointensities) are referred to T2-weighted sequences
cMRI conventional magnetic resonance imaging, *T* Tesla, *iPD* idiopathic Parkinson disease, *MSA* multiple system atrophy, *PSP* progressive supranuclear palsy, *MCP* middle cerebellar peduncle, *MRPI* MR parkinsonism index, *DWI* diffusion weighted imaging, *SCP* superior cerebellar peduncle

presentations, these syndromes require diagnostic work-up including evaluation of structural imaging.

Vascular Parkinsonism

Vascular parkinsonism (vPD) is a heterogeneous clinical entity and may arise because of cerebral vascular disease (CVD) with lacunar infarction of the brain, affecting the external part of the GP, the ventrolateral thalamus, or in some cases, the SN itself (Fig. 7.5). Structural cMRI may depict focal patterns, showing lacunar infarctions in the basal ganglia, frontal lobe infarctions, vascular changes in subcortical and periventricular white matter, and the brain stem. An important diagnostic criterion is a temporal correlation between the occurrence of motor symptoms

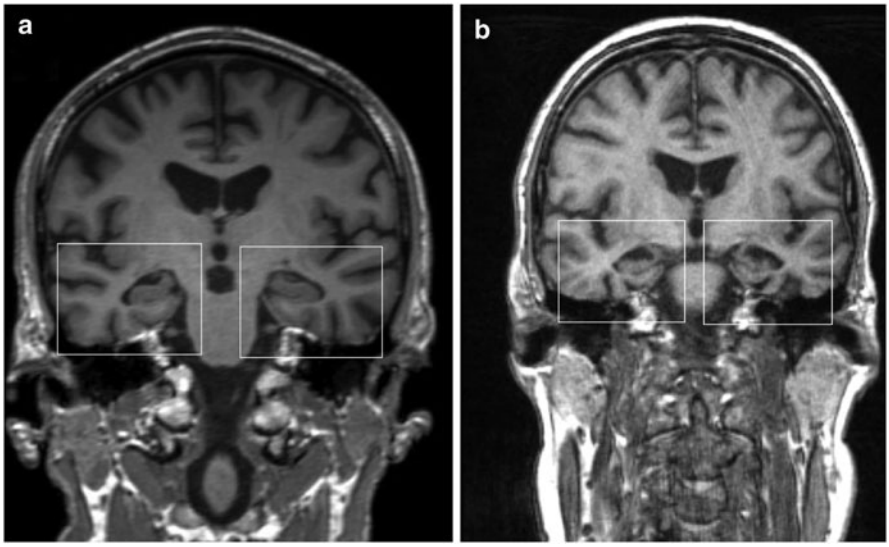

Fig. 7.4 Coronary MR image in a patient with dementia with Lewy bodies (disease duration 1.5 years) showing relative preservation of the medial temporal lobe (**a**), and coronary MR image in a patient with Alzheimer disease (disease duration 2 years) depicting marked atrophy of medial temporal lobe and hippocampus formation (**b**). (© M. Schocke, K. Seppi. Department of Radiology, Department of Neurology. Innsbruck Medical University)

and vascular lesions. Subcortical microangiopathic lesions with diffuse periventicular signal alterations may be associated with lower body parkinsonism, which is characterized by slow progressive gait problems with freezing and falls, usually if vascular lesions are present also in the basal ganglia [17]. Because white matter changes are common in the elderly population and highly nonspecific, other causes for parkinsonism have to be considered, if the clinical picture is not typical for vPD. In some patients, rapidly progressive parkinsonism and even fluctuating parkinsonian syndromes may be caused by dural arteriovenous fistulas, showing white matter hyperintensities of thalamus and basal ganglia [18, 19] and diffuse dilated medullar and cortical veins [20], respectively.

Normal Pressure Hydrocephalus

Normal pressure hydrocephalus is a chronic neurological disorder in adults characterized by a classical triad with difficulties in walking, cognitive impairment, and bladder dysfunction, whereas further concomitant parkinsonian-like features can be

Table 7.3 MRI findings for differential diagnosis in symptomatic parkinsonism

Entity	Typical MRI findings (may vary)
1. Vascular parkinsonism	Lacunar infarctions in the basal ganglia, frontal lobe infarctions, subcortical microangiopathic lesions with diffuse periventricular signal alterations
2. Normal pressure hydrocephalus	Enlargement of lateral cerebral ventricles, ballooning of anterior horn of lateral ventricle, periventricular T2 signal alterations
3. Toxic-induced parkinsonism	
3.1 Manganese	Hyperintensities in the GP, increasing signals in T1-weighted sequences in the striatum and SN
3.2 Ephedrone (methcathinone)	Increased bilateral and symmetric T1-signal intensity in the GP and hyperintensities in the SN, no signal abnormalities on T2-weighted images
3.3 Carbon monoxide	Transient bilateral symmetric lesions in the GP with hyperintensities in T2-weighted images
3.4 Cyanide	Symmetric hyperintense signal changes in the GP, putamen, caudate nucleus, and white matter areas in T2-weighted images and FLAIR-sequences, lesions in the basal ganglia displaying T1 signal increase with contrast enhancement
3.5 Methanol	T2 signal increase and T1 signal decrease in the area of the putamen
4. Huntongton disease (Westphal variant)	Progressive bilateral atrophy of the striatum and caudate nucleus with enlarged anterior horn of lateral ventricle; in the later course, widespread atrophy throughout the cortex; extend of white matter loss is relatively greater and earlier detectable
5. Wilson disease	Atrophy of the midbrain, brain stem, and cerebellum; marked T2 hypointensity in the GP, symmetric T2 hyperintensity in the striatum, lateral thalamus, white matter, and dorsal brain stem; "face of the giant panda": T2-weighted axial MRI with normal signal at the red nuclei (eyes) and lateral aspects of the SN (ears) with signal increase at the tegmentum and hypointense superior colliculi
6. Neurodegeneration with iron accumulation (NBIA)	
6.1 Pantothenate kinase-associated neurodegeneration (PKAN)	Decreased signal in T2-weighted sequences in the GP, putamen, caudate nucleus, and thalamus; "eye of the tiger" sign: high signal in the center of the GP and T2 hypointensity of the surrounding area
6.2 Aceruloplasminemia and neuroferritinopathy	T2 hypointensity in the GP, SN, striatum, thalamus, and dentate nucleus
7. Cerebral masses	Characteristic structural imaging according to the CNS tumors' entity
8. Multiple sclerosis	T1-weighted hypointense lesions ("black holes") and hyperintensities in T2-weighted sequences in the SN and basal ganglia

GP globus pallidus, *MRI* magnetic resonance imaging, *SN* substantia nigra, *NBIA* neurodegeneration with iron accumulation, *PKAN* pantothenate kinase-associated neurodegeneration, *CNS* central nervous system

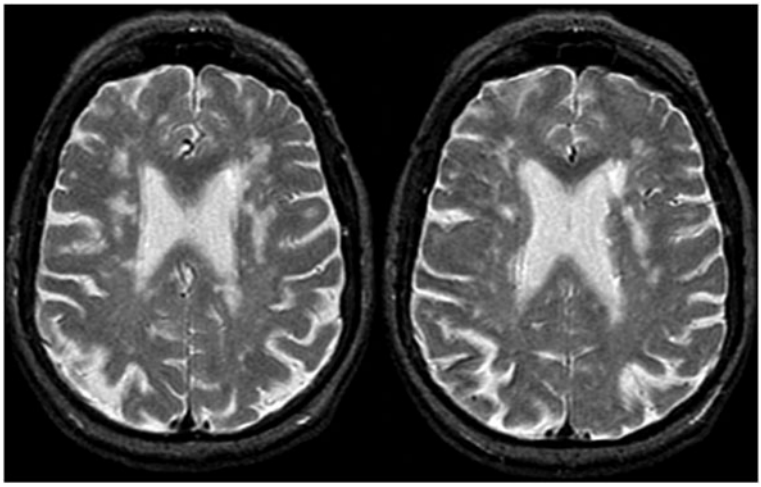

Fig. 7.5 Axial T2-weighted MR images in a patient with vascular parkinsonism due to multiple vascular lesions in the basal ganglia and subcortical arteriosclerotic encephalopathy. (© M. Schocke, K. Seppi. Department of Radiology, Department of Neurology. Innsbruck Medical University)

missing. Structural cMRI may display enlargement of lateral cerebral ventricles, ballooning of anterior horn of lateral ventricle, and periventricular T2 signal alterations (Fig. 7.6).

Toxic Parkinsonism

Chronic intoxication with manganese, "manganism," is believed to be the most common reason for the development of toxic-induced parkinsonism. Within the brain, manganese accumulates in the area of the SN and GP. Characteristic changes in cMRI can be identified as hyperintensities in the GP as well as, depending on severity and disease stage, increasing signals in T1-weighted sequences in the striatum and SN. Liver failure or chronic liver cirrhosis may cause acquired hepatocerebral degeneration with a clinical presentation of cognitive deficits, ataxia, dysarthria, and parkinsonism. MRI patterns generally consist of signal hyperintensity on T1-weighted images in the pallidum, but may also be seen in the putamen, the caudate nucleus, the internal capsule, the mesencephalon, and the cerebellum. Recent evidence suggests manganese as a crucial factor in the pathogenesis of acquired hepatocerebral degeneration, and the MRI abnormalities are believed to reflect local manganese accumulation. This is also the case in patients with ephedrone (methcathinone) abuse. Addicts use a protocol of ephedrine synthesis from the decongestant pseudoephedrine that is associated with the exposure of high quantities of manganese acid. Conventional MRI reveals increased bilateral and symmetric T1-signal

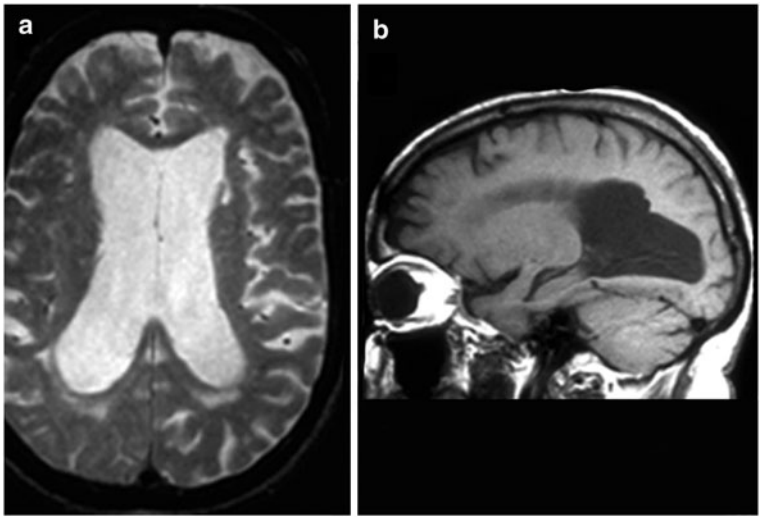

Fig. 7.6 Axial T2-weighted MR image (**a**) and sagittal T1-weighted MR image (**b**) in a patient with normal pressure hydrocephalus. Characteristic enlargement of the lateral ventricles and periventricular signal alterations. (© M. Schocke, K. Seppi. Department of Radiology, Department of Neurology. Innsbruck Medical University)

intensity in the GP, including hyperintensities of the SN in some of the patients, whereas there are no signal abnormalities on T2-weighted images [21].

In patients with parkinsonism due to acute intoxication with carbon monoxide, cMRI depicts transient bilateral symmetric lesions in the GP with hyperintensities in T2-weighted images. Toxic parkinsonism as a result of cyanide intoxication appears in MR images with symmetric hyperintense signal changes in the GP, putamen, and caudate nucleus as well as in white matter areas in T2-weighted images and FLAIR-sequences including lesions in the basal ganglia displaying T1 signal increase with contrast enhancement. In patients with parkinsonian syndromes due to methanol intoxication, cMRI shows T2 signal increase and T1 signal decrease in the area of the putamen, considering nonhemorrhagic necrosis, whereas a marked edema could be displayed in the beginning.

Huntington's Disease

Parkinsonism and dystonia are typical signs in juvenile Huntington's Disease (HD, Westphal variant). There is progressive bilateral atrophy of the striatum and caudate nucleus with enlarged anterior horn of lateral ventricle (Fig. 7.7) on structural MRI in patients with juvenile HD. Later in the course of disease, structural MRI may depict widespread volume loss throughout the cortex. Additionally, in contrast to gray matter, the extent of white matter loss is relatively greater and is detectable earlier in the course of HD.

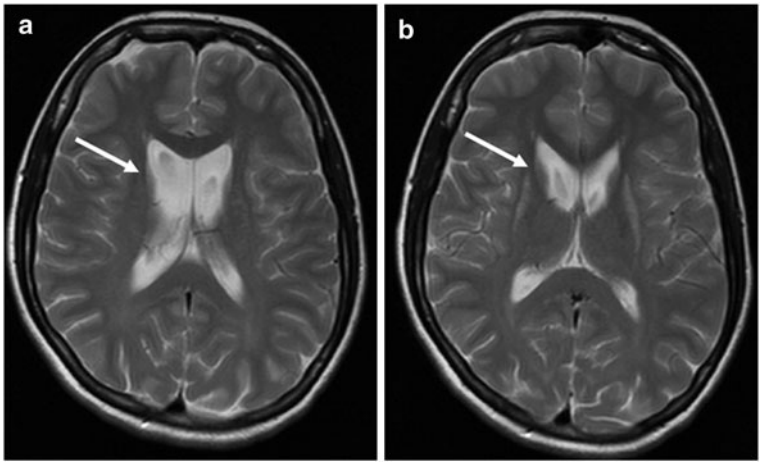

Fig. 7.7 Axial T2-weighted MR images (**a** and **b**) in a patient with Westphal variant of HD demonstrating characteristic atrophy of caudate nucleus (*arrows*). (© M. Schocke, K. Seppi. Department of Radiology, Department of Neurology. Innsbruck Medical University)

Wilson Disease

Wilson disease is an autosomal recessive genetic disorder characterized with accumulation of copper in several tissues; neurological symptoms include: dysarthria, extrapyramidal symptoms with tremor, bradykinesia or impairment of gait, and retraction of the upper lips, so-called "risus sardonicus," and impairment of handwriting. Specific MR features may vary, reflecting differences in clinical presentation and the variability in the location and dimension of copper deposition. Characteristic MR findings include marked T2 hypointensity in the GP, T2 signal increase as well as decrease in the putamen, or symmetric T2 hyperintensity in the striatum, lateral thalamus, white matter, and dorsal brain stem. Furthermore, atrophy of the midbrain, brain stem, and cerebellum are common. MRI may also demonstrate the pathognomonic "face of the giant panda" pattern; T2-weighted axial MRI with normal signal at the red nuclei (eyes) and lateral aspects of the SN (ears), signal increase at the tegmentum, and hypointense superior colliculi (Fig. 7.8).

Neurodegeneration with Brain Iron Accumulation

The term neurodegeneration with brain iron accumulation (NBIA) includes a cluster of progressive extrapyramidal diseases characterized by radiographic evidence of focal iron deposition, especially in the basal ganglia. NBIA includes entities such as pantothenate kinase-associated neurodegeneration (PKAN, NBIA-1), formerly known as Hallervorden–Spatz syndrome, aceruloplasminemia, and neuroferritinopathy. The classic MR feature of NBIAs reveals decreased signal in T2-weighted

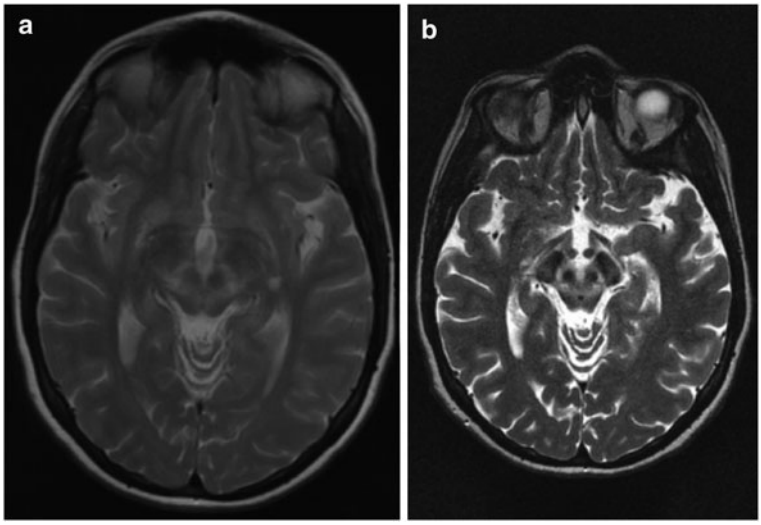

Fig. 7.8 Axial T2-weighted MR images (**a** and **b**) in a patient with Wilson disease. "Face of the giant panda" with normal signal at the red nuclei (*eyes*) and lateral aspects of the Substantia nigra (*ears*) and high signal at the tegmentum. (© K. Seppi, M. Schocke. Department of Neurology, Department of Radiology. Innsbruck Medical University)

sequences corresponding to the locus of iron deposition. In patients with PKAN, these signal changes are basically located in the GP and SN pars reticularis; in patients with aceruloplasminemia and neuroferritinopathy, T2 hypointensity also depicts itself in the striatum, thalamus, and dentate nucleus (Fig. 7.9). Furthermore, a pattern seen in patients with NBIA-1 and neuroferritinopathy is the so-called "eye-of-the-tiger sign," which links high signal increase in the center of the GP and T2 hypointensity of the surrounding area.

Space Occupying Lesions

Parkinsonism due to cerebral masses may occur in patients with CNS tumors and arises from tumor invasion or secondary effects of distant space-occupying lesions on the extrapyramidal system. Meningiomas situated in the frontal or temporal lobe may lead to rest tremor and even bradykinesia and rigidity. Structural imaging depicts the characteristic patterns of the underlying pathology (Fig. 7.10).

Multiple Sclerosis

Parkinsonism due to multiple sclerosis (MS) is a rarely reported condition [22]. Besides the common distribution of MS plaques, demyelinating lesions can be found

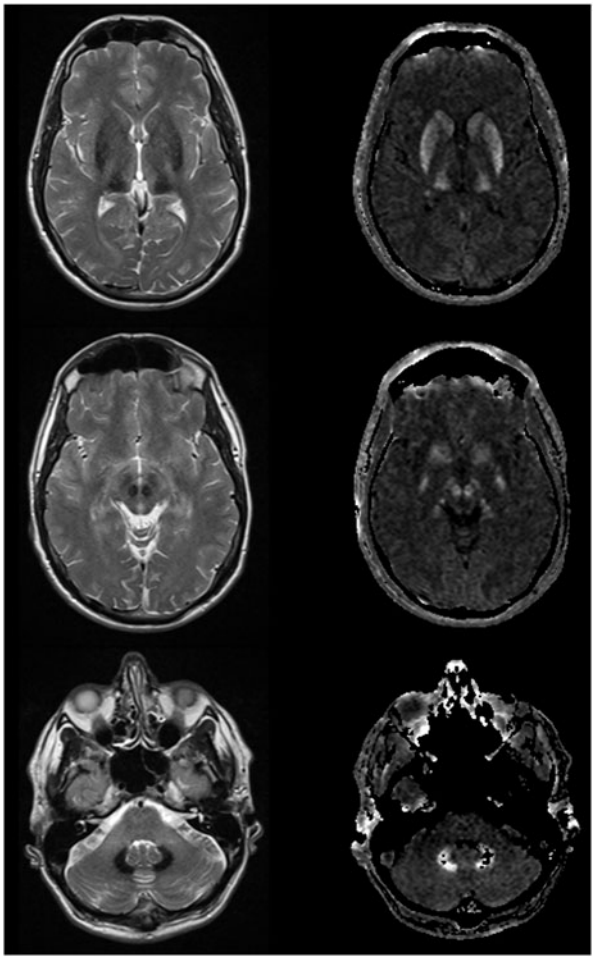

Fig. 7.9 Axial T2-weighted MR images (*left column*) with corresponding R2* maps (*right column*) in a patient with aceruloplasminemia. T2 hypointensities in the striatum, thalamus, substantia nigra, red nucleus, and dentate nucleus with signal increase in R2* maps. (© M. Schocke. Department of Radiology, Innsbruck Medical University)

in the striatum, GP, thalamus, and brain stem. MRI may demonstrate involvement of the SN and basal ganglia, depicting T1-weighted hypointense lesions ("black holes") and hyperintensities in T2-weighted sequences [23]. However, there is still an open debate whether MS lesions can cause parkinsonism or are just a coincidental finding [24].

Infections

Parkinsonism may also be due to infectious diseases including HIV and its complications, opportunistic infections, such as toxoplasmosis (Fig. 7.11), syphilis, or others, such as cerebral abscesses in the basal ganglia, encephalitis, or Creutzfeldt–Jakob

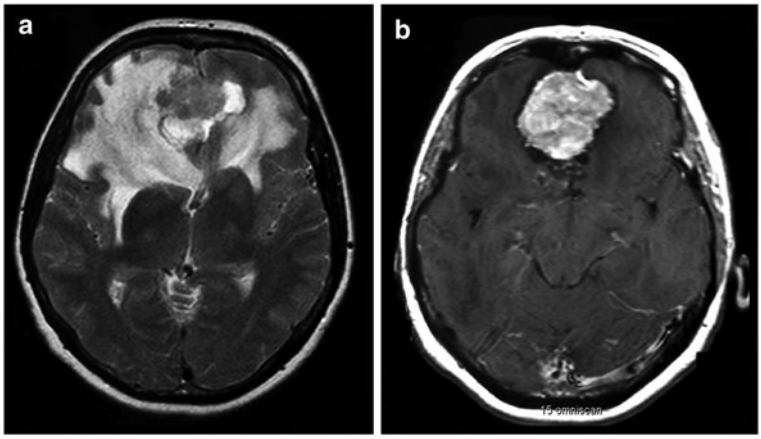

Fig. 7.10 Axial T2-weighted (**a**) and T1-weighted contrast-enhanced (**b**) MR images in a patient with symptomatic parkinsonism due to a meningioma of the olfactory nerve. Displacement of the right basal ganglia because of the space-occupying lesion in the frontal lobe. (© W. Pirker, Department of Neurology, University Hospital Vienna)

disease. Structural brain imaging with MRI shows abnormalities and signal changes due to the underlying cause.

Role of Structural MRI in Assessing Disease Progression in Neurodegenerative Parkinsonism

The longitudinal assessment of serial MRI-derived parameters offers the opportunity for robust inferences regarding the progression of an underlying disease. In the field of movement disorders and, in particular, neurodegenerative parkinsonism, serial MRI offers the possibility to measure macroscopic progression of cerebral lesions in a noninvasive way in vivo. A recent study reported a significant and stage-dependent decrease of SN signal in iPD patients using a modified T1-weighted MRI sequence with magnetization transfer effect at 3.0 T [25]. Similarly, proton transverse relaxation rates in the lateral SN pars compacta as a measure of iron content showed a significant and stage-dependent increase in iPD patients [26]. Automated methods for the longitudinal assessment of volumetric MR studies are based on an automated definition of tissue type in each voxel, thus being operator-independent. While VBM is applied to groups of scans rather than individual scan pairs highlighting atrophy patterns shared across patients over time, methods using registration of serial imaging are applied to individual scan pairs with accurate registration of follow-up and baseline scan, thus determining rates of atrophy rather than atrophy patterns [27].

Several longitudinal MRI studies using registration of serial imaging applied to individual scan pairs with accurate registration of follow-up and baseline scan have

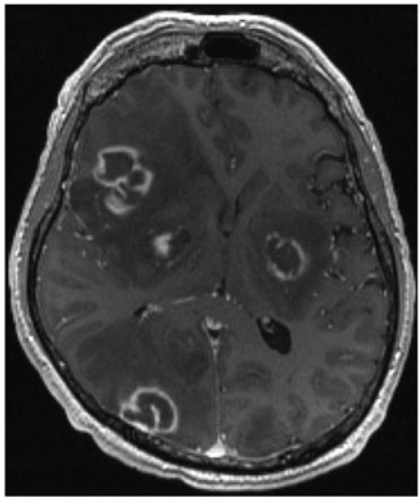

Fig. 7.11 Axial T1-weighted contrast-enhanced MR image showing multiple contrast-enhancing cerebral lesions including the basal ganglia in a patient with cerebral toxoplasmosis due to AIDS. (© M. Schocke, K. Seppi. Department of Radiology, Department of Neurology. Innsbruck Medical University)

found very small or no yearly atrophy rates of up to 1 % in iPD compared with controls [28–30]. However, another study showed small clusters of gray matter loss, involving limbic, paralimbic, and neocortical associative temporooccipital regions in iPD patients without dementia followed over 25 months [31].

A number of characteristic cMRI features have been reported for patients with MSA and PSP, showing a considerable overlap; several imaging studies revealed progression markers for these entities [28, 30, 32]. One study assessed annual whole and regional brain atrophy rates in 12 patients with iPD, 24 with PSP, 11 with MSA-P, and 18 healthy controls. Annual regional atrophy rates in PSP were greatest in the midbrain and the SCP, showing rates of 1.5 and 4.0 % per year, respectively. These declines were significantly greater than those in iPD and controls. Moreover, midbrain and SCP atrophy rates were significantly higher than whole brain atrophy rates in PSP. Additionally, in patients with PSP, these regional atrophy rates show a high association with worsening of clinical parameters such as cognitive, frontal executive, and motor function. Annual regional atrophy rates in MSA-P were greatest in the pons and cerebellum, depicting values of up to 3.2 and 1.9 % atrophy per year, which was reported significantly different to those in iPD and controls. Moreover, pontine and cerebellar atrophy rates were significantly higher than whole brain atrophy rates in MSA-P. Annual atrophy rates come to 0.6 % in iPD, 0.4 % in healthy controls, 1.0 % in MSA-P, and 1.2 % in PSP. Although higher in MSA-P and PSP compared with iPD and controls in this study, the difference of the annual atrophy rates was significant only for the comparison of PSP versus healthy controls.

A significant increase of putaminal diffusivity over time has been demonstrated in two longitudinal DWI studies [33, 34]. Seppi et al. could show a significant increase of the Trace (D) in the putamen of 10 MSA-P patients. On the other hand, none of the Trace (D) values in the basal ganglia regions in 10 iPD patients changed significantly at follow-up compared with baseline. The rate of cerebral atrophy in DLB and PDD

has been assessed in several longitudinal MR studies [29, 35, 36], showing an overall brain atrophy rate of up to 1.4 % per year, slightly less than in AD with 2 % per year. In summary, cMRI may be a sensitive, reliable, and reproducible technique relative to clinical measures for assessing the progression of neurological diseases [37]. However, despite many potential candidates for assessing disease progression in iPD and aPS, sensitivity is still insufficient and minor structural changes are quite difficult to detect. In addition, currently established MR markers mainly focus on advanced disease stages and little is known about changes during the early course of the diseases.

Future Developments

Over the past two decades, MRI has become a well-established method that is used in clinical routine for diagnostic work-up in the field of movement disorders, providing specific information that point toward the diagnosis of a neurodegenerative condition. However, the role of MRI has progressed from excluding symptomatic parkinsonism due to other pathologies to distinguishing iPD from aPS. Specific changes in the basal ganglia and infratentorial structures have been shown especially in aPS, not only by cMRI but also by different advanced MRI techniques. Because of the limitations of cMRI regarding the diagnosis of neurodegenerative parkinsonism, new MRI techniques have been studied extensively, evaluating specific markers for diagnostic issues.

High-Field MRI

Newer quantitative imaging techniques at high field (3.0 T) and ultrahigh field (7.0 T) have recently been applied in patients with iPD and have shown promising results in detecting abnormalities in the SN and nigrostriatal pathway using diffusion tensor imaging (DTI), relaxometry, 1H-MRSI, and multimodal imaging in patients with iPD. Advances in high-field MRI technology with 3.0 T or higher field strengths have increased interest in such systems, and MRI at 3.0 T has rapidly gained acceptance in the MR community for both research and clinical applications in the last few years. The most straightforward advantage of high-field MRI is the increased signal-to-noise ratio (SNR) that scales linearly with the field strength. Increased SNR can be invested into decreased acquisition time, increased spatial resolution, or a combination of both. Spectacular anatomic delineation that is provided by high-definition scanning may improve sensitivity to smaller lesions. Furthermore, high-field MRI leads to a better gray-to-white-matter contrast, showing sharp images and smooth transitions between the different brain structures. MRI studies at 1.5 T have shown that morphological changes including volume loss in the basal ganglia or signal changes in the SN can be detected in advanced iPD. This raises the possibility that

Table 7.4 Findings with quantitative imaging techniques implemented on high-field (3.0 T) and ultrahigh-field (7.0 T) MR systems in iPD

MRI findings	MRI technique	Reference
Decreased R2* in lateral SN controlateral	Gradient-echo sequence for proton transversal relaxation rate (R2*) at 3.0 T (iron-sensitive sequence)	Martin et al. [26]
Decreased SN volume	Combined SN volumetry with DTI of SN at 3.0 T (VCDR[a])	Menke et al. [38]
Decreased VCDR[b]		
Decreased SN volume + decreased VCDR		
Decreased T2* in SN bilateral	T1-weighted 3D gradient-echo sequence and T2*-weighted multiecho technique at 3.0 T	Baudrexel et al. [41]
Decreased T1 in SN controlateral		
Increased R2* in the SN	Multimodal MRI study at 3.0 T using a combination of different MR markers including volumetry, mean R2*, mean diffusivity, and FA applied in six deep gray matter structures (SN, red nucleus, thalamus, putamen, caudate, pallidum)	Péran et al. [39]
Reduced FA in the SN		
Increased mean diffusivity in the putamen or caudate nucleus		
Decreased NAA/Cr ratio of rostral SN	3D-MRSI of the SN at 3.0 T	Gröger et al. [42]
Increased NAA/Cr ratio of caudal SN		
Decreased rostral-to-caudal ratios of the NAA/Cr ratio		
Significant increase of SAD in iPD versus controls with only a small overlap of SAD values between iPD patients and controls, significant correlation of SAD with UPDRS	T2*-weighted gradient-echo sequence at 7.0 T, aligned with AC–PC line to delineate shapes and boundaries of SN and calculation of SAD[c]	Cho et al. [43]
Better discrimination of combined use of transverse relaxation rate and FA values in the SN compared with transverse relaxation rate or FA alone	Multimodal imaging using a combination of transverse relaxation rate and FA values in the SN at 3.0 T	Du et al. [40]
Undulated lateral surface of SN, rostral > caudal and medial	3D T2*-weighted gradient-echo sequence at 7.0 T of the SN	Kwon et al. [6]

Table 7.4 (continued)

MRI findings	MRI technique	Reference
Decreased T2* at dorsomedial surface of lateral SN		

T Tesla, *MR* magnetic resonance, *iPD* idiopathic Parkinson disease, *R2** relaxation rates = 1/T2*, *SN* substantia nigra, *DTI* diffusion tensor imaging, *FA* fractional anisotropy, *VCDR* voxels for all connectivity-defined subregions, *3D-MRSI* three-dimensional magnetic resonance spectroscopic imaging, *NAA/Cr* N-acetylaspartate-to-creatine ratio, *AC–PC* anterior commissure, posterior commissure, *SAD* sum of absolute differences, *UPDRS* unified Parkinson's disease rating scale

[a]VCDR is a DTI marker representing the numbers of voxels for all connectivity-defined subregions within the SN thresholded at 10 % of the maximum connection probability

[b]Reduced left and right SN to ipsilateral thalamus VCDRs

[c]Quantification of shapes and boundaries of SN via an undulation value, which has been termed sum of absolute differences (SAD) with higher values in PD and lower values in controls. For exact calculation of SAD, see Cho et al. [43]

greater sensitivity of MRI at higher magnetic fields complemented by higher tissue contrast may lead to more robust findings of structural abnormalities in early iPD. Because of the increased SNR and impressive anatomic delineation that is provided by high-field scanning, sensitivity of atrophy measures may increase, especially at a group level when using VBM. Signal changes on T2-weighted images at 1.5 T in the basal ganglia as well as in infratentorial structures have been reported for all aPS. These signal changes are important pointers toward the suspected diagnosis of atypical parkinsonism, but as discussed earlier, they are not transferable to 3.0 T scanners. A pilot study using ultrahigh-field MRI with 7.0 T has demonstrated that the increased SNR may help to better delineate the SN when using T2*-weighted gradient-echo sequences. Within a small group of 10 iPD patients, Cho et al. assessed shapes and boundaries of the SN. While controls had a smooth "arch" shape lateral boundary of the SN, in iPD patients, it was serrated. By quantifying these differences of the lateral boundaries of the SN via an undulation value, iPD patients had significant higher values compared with the controls with only a small overlap of the individual values between the groups. Table 7.4 summarizes important studies on the use of high-field MRI in iPD patients.

Multimodal Imaging

Multimodal imaging is an approach to measure MR parameters sensitive to complementary tissue characteristics. Menke et al. [38] investigated volumetry and DTI of the SN and found a loss of volume of the SN as well as a decrease of voxels for all connectivity-defined subregions (VCDR), a special DTI marker representing the numbers of voxels for all connectivity-defined subregions within the SN, using a cutoff at 10 % of the maximum connection probability. Péran et al. [39] described a multimodal MR study at 3.0 T, investigating volumetry, mean R2*, mean diffusivity (MD), and fractional anisotropy (FA) in six different brain regions. These included SN, nucleus ruber, thalamus, putamen, caudate nucleus, and GP in 30 early iPD

patients. Results showed an increase of R2* in the SN, an increase of MD in putamen and caudate nucleus, and a decreased FA in the SN. Interestingly, best discrimination of iPD from controls was achieved by combing these three different magnetic resonance parameters. In a further multimodal study, combined use of transverse relaxation rate and FA measures in the SN of iPD had high accuracy in differentiating patients with iPD from controls [40]. In these studies, combination of different markers sensitive to complementary tissue characteristics provided better discrimination compared with the markers alone.

Conclusions and Future Directions

Magnetic resonance imaging has a considerable role in the diagnosis of patients with parkinsonism. Conventional MRI excludes symptomatic causes of parkinsonism but, to date, does not show any specific findings in iPD. In other neurodegenerative forms of parkinsonism including PSP, MSA, and CBD, MRI reveals characteristic patterns of regional atrophy combined with signal changes of microstructural changes in the basal ganglia, pons, middle and superior cerebellar peduncles, and cerebral subcortical white matter. A combination of the clinical features with structural imaging using MRI is recommended for optimization of the diagnostic algorithm in movement disorders. Further developments and advanced MR imaging techniques could add diagnostic information and could lead to an earlier diagnosis in patients with iPD, additionally distinguishing iPD from aPS.

References

1. Hughes AJ, Daniel SE, Kilford L, Lees AJ. Accuracy of clinical diagnosis of idiopathic Parkinson's disease: a clinico-pathological study of 100 cases. J Neurol Neurosurg Psychiatry. 1992 Mar;55(3):181–4.
2. Lee WH, Lee CC, Shyu WC, Chong PN, Lin SZ. Hyperintense putaminal rim sign is not a hallmark of multiple system atrophy at 3 T. AJNR Am J Neuroradiol. 2005 Oct;26(9):2238–42.
3. Hutchinson M, Raff U, Lebedev S. MRI correlates of pathology in parkinsonism: segmented inversion recovery ratio imaging (SIRRIM). Neuroimage. 2003 Nov;20(3):1899–902.
4. Minati L, Grisoli M, Carella F, De Simone T, Bruzzone MG, Savoiardo M. Imaging degeneration of the substantia nigra in Parkinson disease with inversion-recovery MR imaging. AJNR Am J Neuroradiol. 2007 Feb;28(2):309–13.
5. Hu MT, White SJ, Herlihy AH, Chaudhuri KR, Hajnal JV, Brooks DJ. A comparison of (18) F-dopa PET and inversion recovery MRI in the diagnosis of Parkinson's disease. Neurology. 2001 May;56(9):1195–200.
6. Kwon DH, Kim JM, Oh SH, et al. Seven-Tesla magnetic resonance images of the substantia nigra in Parkinson disease. Ann Neurol. 2012 Feb;71(2):267–77.
7. Muqit MM, Mort D, Miskiel KA, Shakir RA. "Hot cross bun" sign in a patient with parkinsonism secondary to presumed vasculitis. J Neurol Neurosurg Psychiatry. 2001 Oct;71(4):565–6.
8. Lee YC, Liu CS, Wu HM, Wang PS, Chang MH, Soong BW. The 'hot cross bun' sign in the patients with spinocerebellar ataxia. Eur J Neurol. 2009 Apr;16(4):513–6.

9. Warmuth-Metz M, Naumann M, Csoti I, Solymosi L. Measurement of the midbrain diameter on routine magnetic resonance imaging: a simple and accurate method of differentiating between Parkinson disease and progressive supranuclear palsy. Arch Neurol. 2001 Jul;58(7):1076–9.
10. Quattrone A, Nicoletti G, Messina D, et al. MR imaging index for differentiation of progressive supranuclear palsy from Parkinson disease and the Parkinson variant of multiple system atrophy. Radiology. 2008 Jan;246(1):214–21.
11. Righini A, Antonini A, De Notaris R, et al. MR imaging of the superior profile of the midbrain: differential diagnosis between progressive supranuclear palsy and Parkinson disease. AJNR Am J Neuroradiol. 2004 Jun–Jul;25(6):927–32.
12. Cosottini M, Ceravolo R, Faggioni L, et al. Assessment of midbrain atrophy in patients with progressive supranuclear palsy with routine magnetic resonance imaging. Acta Neurol Scand. 2007 Jul;116(1):37–42.
13. Hussl A, Mahlknecht P, Scherfler C, et al. Diagnostic accuracy of the magnetic resonance parkinsonism index and the midbrain-to-pontine area ratio to differentiate progressive supranuclear palsy from Parkinson's disease and the Parkinson variant of multiple system atrophy. Mov Disord. 2010 Oct;25(14):2444–9.
14. Price S, Paviour D, Scahill R, et al. Voxel-based morphometry detects patterns of atrophy that help differentiate progressive supranuclear palsy and Parkinson's disease. Neuroimage. 2004 Oct;23(2):663–9.
15. Koyama M, Yagishita A, Nakata Y, Hayashi M, Bandoh M, Mizutani T. Imaging of corticobasal degeneration syndrome. Neuroradiology. 2007 Nov;49(11):905–12.
16. Burton EJ, Barber R, Mukaetova-Ladinska EB, et al. Medial temporal lobe atrophy on MRI differentiates Alzheimer's disease from dementia with Lewy bodies and vascular cognitive impairment: a prospective study with pathological verification of diagnosis. Brain. 2009 Jan;132(Pt 1):195–203.
17. Rektor I, Rektorová I, Kubová D. Vascular parkinsonism—an update. J Neurol Sci. 2006 Oct;248(1–2):185–91.
18. Netravathi M, Pal PK, Bharath RD, Ravishankar S. Intracranial dural arteriovenous fistula presenting as parkinsonism and cognitive dysfunction. J Clin Neurosci. 2011 Jan;18(1):138–40.
19. Miura S, Noda K, Shiramizu N, et al. Parkinsonism and ataxia associated with an intracranial dural arteriovenous fistula presenting with hyperintense basal ganglia in T1-weighted MRI. J Clin Neurosci. 2009 Feb;16(2):341–3.
20. Kajitani M, Yagura H, Kawahara M, et al. Treatable fluctuating parkinsonism and dementia in a patient with a dural arteriovenous fistula. Mov Disord. 2007 Feb;22(3):437–9.
21. Stepens A, Logina I, Liguts V, et al. A Parkinsonian syndrome in methcathinone users and the role of manganese. N Engl J Med. 2008 Mar;358(10):1009–17.
22. Tranchant C, Bhatia KP, Marsden CD. Movement disorders in multiple sclerosis. Mov Disord. 1995 Jul;10(4):418–23.
23. Zivadinov R, Cox JL. Neuroimaging in multiple sclerosis. Int Rev Neurobiol. 2007;79:449–74.
24. Folgar S, Gatto EM, Raina G, Micheli F. Parkinsonism as a manifestation of multiple sclerosis. Mov Disord. 2003;18(1):108–10.
25. Schwarz ST, Rittman T, Gontu V, Morgan PS, Bajaj N, Auer DP. T1-weighted MRI shows stage-dependent substantia nigra signal loss in Parkinson's disease. Mov Disord. 2011 Aug;26(9):1633–8.
26. Martin WR, Wieler M, Gee M. Midbrain iron content in early Parkinson disease: a potential biomarker of disease status. Neurology. 2008 Apr;70(16 Pt 2):1411–7.
27. Wild EJ, Fox NC. Serial volumetric MRI in Parkinsonian disorders. Mov Disord. 2009;24(Suppl 2):S691–8.
28. Paviour DC, Price SL, Jahanshahi M, Lees AJ, Fox NC. Longitudinal MRI in progressive supranuclear palsy and multiple system atrophy: rates and regions of atrophy. Brain. 2006 Apr;129(Pt 4):1040–49.
29. Burton EJ, McKeith IG, Burn DJ, O'Brien JT. Brain atrophy rates in Parkinson's disease with and without dementia using serial magnetic resonance imaging. Mov Disord. 2005 Dec;20(12):1571–6.

30. Brenneis C, Egger K, Scherfler C, et al. Progression of brain atrophy in multiple system atrophy. A longitudinal VBM study. J Neurol. 2007 Feb;254(2):191–6.
31. Ramírez-Ruiz B, Martí MJ, Tolosa E, et al. Longitudinal evaluation of cerebral morphological changes in Parkinson's disease with and without dementia. J Neurol. 2005 Nov;252(11): 1345–2.
32. Paviour DC, Price SL, Lees AJ, Fox NC. MRI derived brain atrophy in PSP and MSA-P. Determining sample size to detect treatment effects. J Neurol. 2007 Apr;254(4):478–81.
33. Seppi K, Schocke MF, Mair KJ, et al. Progression of putaminal degeneration in multiple system atrophy: a serial diffusion MR study. Neuroimage. 2006 May;31(1):240–5.
34. Pellecchia MT, Barone P, Vicidomini C, et al. Progression of striatal and extrastriatal degeneration in multiple system atrophy: a longitudinal diffusion-weighted MR study. Mov Disord. 2011 Jun;26(7):1303–9.
35. Seppi K, Rascol O. Dementia with Lewy bodies and Parkinson disease with dementia: can MRI make the difference? Neurology. 2007 Aug;69(8):717–8.
36. Watson R, Blamire AM, O'Brien JT. Magnetic resonance imaging in lewy body dementias. Dement Geriatr Cogn Disord. 2009;28(6):493–506.
37. Ciumas C, Montavont A, Ryvlin P. Magnetic resonance imaging in clinical trials. Curr Opin Neurol. 2008 Aug;21(4):431–6.
38. Menke RA, Scholz J, Miller KL, et al. MRI characteristics of the substantia nigra in Parkinson's disease: a combined quantitative T1 and DTI study. Neuroimage. 2009 Aug;47(2):435–41.
39. Péran P, Cherubini A, Assogna F, et al. Magnetic resonance imaging markers of Parkinson's disease nigrostriatal signature. Brain. 2010 Nov;133(11):3423–33.
40. Du G, Lewis MM, Styner M, et al. Combined R2* and diffusion tensor imaging changes in the substantia nigra in Parkinson's disease. Mov Disord. 2011 Aug;26(9):1627–32.
41. Baudrexel S, Nürnberger L, Rüb U, et al. Quantitative mapping of T1 and T2* discloses nigral and brainstem pathology in early Parkinson's disease. Neuroimage 2010;51(2):512–20.
42. Gröger A, Chadzynski G, Godau J, Berg D, Klose U. Three-dimensional magnetic resonance spectroscopic imaging in the substantia nigra of healthy controls and patients with Parkinson's disease. Eur Radiol 2011;21(9):1962–9.
43. Cho ZH, Oh SH, Kim JM, et al. Direct visualization of Parkinson's disease by in vivo human brain imaging using 7.0T magnetic resonance imaging. Mov Disord 2011;26(4):713–718.

Chapter 8
Dopamine Imaging in Idiopathic Parkinson Disease and Other Parkinsonisms

Yen F. Tai and Nicola Pavese

Introduction

Idiopathic Parkinson disease (iPD) is a progressive neurodegenerative disorder characterised clinically by asymmetric tremor, bradykinesia, rigidity and later postural instability. The pathological hallmark of iPD is the formation of proteinaceous intraneuronal Lewy body inclusions and Lewy neurites, which are found in the lower brainstem nuclei and anterior olfactory structures at the earliest stage of the disease. These then progress to involve the substantia nigra and other basal nuclei of the midbrain and forebrain, before finally affecting the neocortex [1].

One major pathological feature of iPD is the loss of dopaminergic projection neurons in the pars compacta of substantia nigra (SNc)[2]. The greatest loss occurs in the ventrolateral tier of pars compacta, with lesser involvement in the ventromedial and dorsal tiers. This unique pattern of cell loss in the SNc results in a corresponding loss of its striatal terminals with caudal putamen being most affected, followed by rostral putamen and caudate nucleus. It was estimated that at the onset of symptoms, there is a greater than 50 % loss of dopaminergic neurons in SNc and 80 % loss of striatal dopamine [3].

Using various positron emission tomography (PET) and single-photon emission computed tomography (SPECT) radiotracers as discussed further, researchers have been able to study in vivo the pre-synaptic and post-synaptic dopaminergic functions

N. Pavese (✉)
Centre for Neuroscience,
Hammersmith Hospital Campus,
Imperial College London, DuCane Road,
London W12 ONN, UK
e-mail: nicola.pavese@imperial.ac.uk

Y. F. Tai
Department of Neurology,
Imperial College Healthcare NHS Trust,
Fulham Palace Road, London W6 8RF, UK
e-mail: yen.tai@imperial.ac.uk

F. B. Nahab, N. Hattori (eds.), *Neuroimaging of Movement Disorders,*
Current Clinical Neurology 44, DOI 10.1007/978-1-62703-471-5_8,

in humans. In this chapter, we will provide an overview of the clinical and research applications of dopamine imaging in patients with parkinsonisms.

In Vivo Imaging of Dopaminergic System Using PET and SPECT

In healthy individuals, the striatal dopamine levels are tightly regulated by several processes. Dihydroxyphenylalanine (DOPA) is converted by aromatic amino acid decarboxylase (AADC) into dopamine in the dopaminergic neurons. Dopamine is then packaged into synaptic vesicles by type 2 vesicular monoamine transporters (VMAT2). Following a signal to release dopamine, depolarisation occurs and dopamine is released into the synaptic cleft, where it interacts with pre-synaptic and post-synaptic dopamine receptors. The concentration of this synaptic dopamine is regulated by pre-synaptic plasma membrane dopamine transporter (DAT), which re-uptake synaptic dopamine into dopamine nerve terminals. The remaining dopamine in the synapse is broken down by the enzyme catechol *O*-methyltransferase. The synaptic dopamine also binds to inhibitory pre-synaptic dopamine autoreceptors, and this provides a negative feedback to the terminals and cell bodies to reduce synthesis and release of dopamine. The firing rate and pattern of dopaminergic neurons can vary between 'tonic' low-frequency to brief high-frequency 'phasic' bursts of action potential. The latter is important for reward-based learning and selection of habitual motor programme [4].

Based on the above understanding of dopamine metabolism, a number of PET and SPECT radiotracers targeting AADC, DAT and VMAT2 have been developed to allow in vivo imaging of pre-synaptic dopaminergic function (Table 8.1).

^{18}F-6-fluorodopa (^{18}F-dopa) is a PET tracer that is taken up by dopaminergic neurons, where it is converted by AADC into ^{18}F-Dopamine. This is stored in the synaptic vesicles and transported to pre-synaptic terminals before being released. The influx constants (Ki) of ^{18}F-dopa therefore reflects DOPA transport into the dopaminergic terminals, AADC activity and dopamine storage capacity [5]. Striatal ^{18}F-dopa influx constants (Ki) correlated with nigral dopaminergic cell density in a human post-mortem study [6].

Several PET ligands (^{11}C-CFT, ^{18}F-CFT, ^{18}F-FP-CIT, ^{11}C-methylphenidate and ^{11}C-RTI-32) and SPECT tracers (such as ^{123}I-β-CIT, ^{123}I-FP-CIT, ^{123}I-altropane and ^{99m}Tc-TRODAT-1) are now available to measure DAT availability as an indicator of pre-synaptic dopaminergic function. ^{11}C-dihydrotetrabenazine (^{11}C-DTBZ) is a PET tracer that binds to VMAT2. SPECT (^{123}I-IBZM) and PET (^{11}C-raclopride, ^{11}C-NMSP) tracers that bind to dopamine D2 receptors are also available to image post-synaptic dopaminergic functions.

Due to its expense, PET is generally available only as a research tool. By contrast, several DAT SPECT tracers such as ^{123}I-β-CIT and ^{123}I-FP-CIT are now commercially available for diagnostic use in clinical settings.

Table 8.1 SPECT and PET radiotracers used in dopaminergic imaging

	SPECT	PET
Presynaptic		
AADC activity and vesicular storage of ^{18}F-dopamine		^{18}F-dopa
DAT	^{123}I-β-CIT	^{11}C-CFT
	^{123}I-FP-CIT	^{18}F-CFT
	^{123}I-altropane	^{18}F-FP-CIT
	^{99m}Tc-TRODAT-1	^{11}C-methylphenidate
		^{11}C-RTI-32
VMAT-2		^{11}C-DTBZ
Postsynaptic		
D2 receptor	^{123}I-IBZM	^{11}C-raclopride
		^{11}C-NMSP

SPECT single-photon emission computed tomography, *PET* positron emission tomography, *AADC* aromatic amino acid decarboxylase, *DAT* dopamine transporter, *VMAT-2* type 2 vesicular monoamine transporters

Imaging Pre-synaptic Dopaminergic Function in Parkinson Disease

In iPD, the loss of nigrostriatal dopaminergic projection is consistently reflected by the above PET and SPECT pre-synaptic dopaminergic markers as asymmetric reduction of tracer uptake or binding in the putamen, greatest in the side contralateral to the clinically more affected limbs [7–9]. There is also a caudal–rostral gradient loss of uptake/binding, starting from caudal putamen, and eventually progressing to rostral putamen (Fig. 8.1), reflecting the regional selectivity of iPD pathology in the SNc as described above. The caudate nucleus is also affected in the later stages. The nigrostriatal dopaminergic dysfunction as measured by PET or SPECT correlated with the clinical severity of iPD as measured with Unified Parkinson's Disease Rating Scale (UPDRS). More specifically, it correlated with the degree of rigidity and bradykinesia, but not tremor [9–13]. This indicates that tremor is either mediated by non-nigrostriatal and/or non-dopaminergic pathways. The latter would be in keeping with the clinical findings that bradykinesia and rigidity are more responsive than tremor to levodopa treatment [14].

^{18}F-dopa PET has detected extrastriatal reductions in ^{18}F-dopa uptake in iPD, such as in hypothalamus, globus pallidus and subthalamic nucleus, reflecting advancing iPD pathology [15]. However, studies have also identified regions of increased ^{18}F-dopa uptake in dorsolateral prefrontal cortex, anterior cingulate, and globus pallidus interna (GPi) of patients with early iPD compared with both normal controls and patients with more advanced disease [16–18]. It is likely that these increases in extrastriatal ^{18}F-dopa uptake in early PD reflect a compensatory upregulation of AADC activity to maintain dopaminergic output. For example, Whone et al. [18] reported a 40 % increase in GPi ^{18}F-dopa uptake in early iPD when there is relative clinical

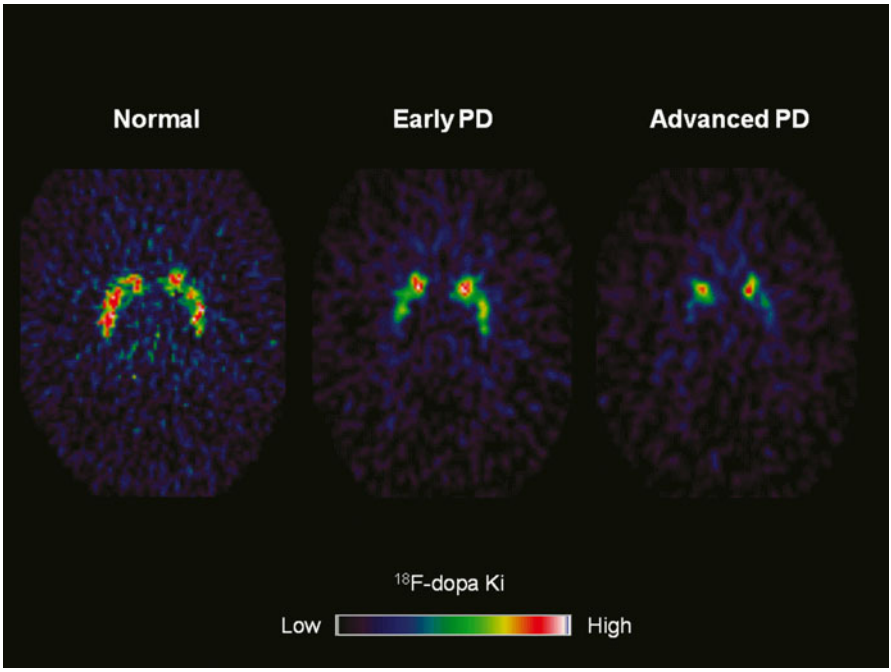

Fig. 8.1 ^{18}F-dopa PET parametric images showing progressive and asymmetric reduction in striatal ^{18}F-dopa influx constants (Ki) in idiopathic Parkinson disease (iPD). There is a caudal–rostral gradient in nigrostriatal dysfunction, with the caudal putamen being most affected, followed by rostral putamen and caudate nucleus

stability. This is likely to arise from the upregulation of nigropallidal projection to normalise basal ganglia output to the ventral thalamus and motor cortex. The loss of the upregulation of GPi signal coincided with the onset of more rapid clinical progression and development of motor complications.

Lee et al. [19] studied 35 iPD patients using three pre-synaptic dopaminergic PET tracers, ^{11}C-DTBZ, ^{18}F-Dopa and ^{11}C-methylphenidate. They showed that in iPD, the striatal terminal AADC activity appears to be relatively upregulated and DAT binding relatively downregulated compared with VMAT2 density. These are interpreted by the authors as evidence of compensatory mechanisms of the surviving dopaminergic terminals to enhance dopamine transmission in the denervated striatum. As the disease progresses, these compensatory mechanisms are lost [15, 20].

Dopamine Imaging as a Diagnostic Tool in Parkinsonism

When a patient presents with the classical signs of iPD, the diagnosis is usually fairly straightforward. However, distinguishing iPD from other degenerative and non-degenerative forms of parkinsonism can be difficult especially in the initial stages.

One post-mortem study reported that 24 % of patients diagnosed with iPD in life turned out to have an alternative diagnosis [21]. In an epidemiological study, around 20 % of patients with iPD in the community were misdiagnosed [22]. Making the correct diagnosis would enable the appropriate treatment of the underlying condition and avoid exposing the patients unnecessarily to medications that might not be effective or have significant side effects. It is also important for correct prognostication.

Numerous studies have been performed to validate the diagnostic accuracy of SPECT or PET in parkinsonism and its mimics, but most are slightly limited by the fact that they use clinical diagnosis as the gold standard.

One multi-centre study looked at the accuracy of visual assessment of ^{123}I-FP-CIT SPECT imaging in differentiating patients with degenerative parkinsonism from essential tremor (ET). Scans with normal DAT binding were classified as ET whilst abnormal scans were classified as having degenerative parkinsonism, and clinical diagnosis is the gold standard. Visual assessment of DAT SPECT achieved a sensitivity of 97 % for the diagnosis of parkinsonism, and a specificity of 100 % for ET [23]. In a prospective ^{123}I-FP-CIT SPECT study, patients in whom there was initial diagnostic uncertainty as to whether they have degenerative or non-degenerative parkinsonism received SPECT at baseline and serial clinical assessments over 3 years, with the eventual clinical diagnosis being used as the gold standard. Baseline ^{123}I-FP-CIT SPECT diagnosed degenerative parkinsonism with a sensitivity of 78 % and specificity of 97 %, versus baseline clinical diagnosis which has sensitivity and specificity of 93 and 46 %, respectively [24]. The authors concluded that degenerative parkinsonism is over diagnosed clinically at baseline and that DAT SPECT can help improve the diagnostic accuracy.

Approximately 10–15 % of patients diagnosed with iPD and recruited into clinical trials have scans without evidence of dopaminergic deficit (SWEDDs) [25]. These patients respond poorly to dopaminergic medications and do not display progression on serial DAT SPECT. Some of these patients have signs of dystonia or components of their arm tremor that are compatible with dystonic tremor [26].

Differing patterns of pre-synaptic dopaminergic involvement have been reported in patients with atypical neurodegenerative parkinsonism [27, 28]. Diffuse loss of nigrostriatal dopaminergic projection is seen in multiple system atrophy (MSA) and progressive supranuclear palsy (PSP), as reflected by the symmetrical loss of ^{18}F-dopa uptake in the entire striatum. Patients with corticobasal degeneration (CBD) show equivalent reduction in ^{18}F-dopa uptake of caudate and putamen, but the striatum opposite the most affected limbs has the greatest reduction. However, accuracy of ^{18}F-Dopa PET and DAT SPECT in distinguishing the various forms of degenerative parkinsonism on an individual patient basis is rather low [29, 30].

Post-synaptic D2 imaging with ^{11}C-raclopride PET may help further distinguish iPD from the atypical parkinsonisms. Striatal D2 receptors binding is normal or slightly upregulated in patients with early iPD, but it is significantly reduced in patients with atypical parkinsonism. However, in more advanced cases of iPD especially following long-term treatment with dopaminergic medications, the D2 receptors can become downregulated [31, 32].

Cognitive impairment is a significant cause of morbidity in iPD and the average prevalence of dementia in iPD patients is up to 40 % [33, 34]. For practical purpose, patients who develop dementia within 1 year of onset of iPD motor symptoms are classified as dementia with Lewy Bodies (DLB), whereas those who develop dementia more than 1 year after onset of motor symptoms are classified as PD with dementia (PDD). Many authors, however, consider these two conditions as representing different spectrum of the same underlying pathological process, i.e., Lewy Body disorders [35]. Distinguishing patients with DLB and Alzheimer's disease (AD) can be difficult in some patients. Both of these conditions respond to cholinesterase inhibitors but patients with DLB have marked sensitivity to neuroleptics and this group of medications should be avoided if possible. One study compared the accuracy of clinicians and ^{123}I-FP-CIT SPECT in diagnosing DLB, using post-mortem findings as the gold standard. The sensitivity and specificity of an initial clinical diagnosis of DLB was 75 and 42 %, respectively. Using ^{123}I-FP-CIT SPECT, the sensitivity and specificity improved to 88 and 100 %, respectively [36]. In a phase III multi-centre study, ^{123}I-FP-CIT SPECT was able to diagnose clinically probable DLB with a sensitivity of 77.7 % and a specificity of 90.4 % when measured against clinical diagnosis established by a consensus clinical panel [37]. The International Consensus Criteria for DLB has now recommended reduced striatal pre-synaptic dopaminergic markers, including DAT, on SPECT/PET as a suggestive feature for the diagnosis of DLB [38]. Dopaminergic imaging is not able to distinguish between PDD and DLB as they both exhibit nigrostriatal dopaminergic dysfunction.

Dopaminergic imaging has also been used to differentiate neurodegenerative from non-neurodegenerative forms of parkinsonism. Drug-induced parkinsonism is usually caused by the use of anti-dopaminergic agents such as neuroleptics or anti-emetics. It can be difficult to distinguish it clinically from iPD. Pre-synaptic dopamine imaging is usually normal in these patients unless they have concomitant iPD or degenerative parkinsonism where the symptoms have been unmasked or worsened by the use of anti-dopaminergic agents [39, 40]. Most patients with vascular parkinsonism have normal striatal pre-synaptic dopamine binding [41] though some may have reduced binding [42, 43]. In those that display a reduction, the pattern is usually more symmetrical and diffuse than that of iPD. Dopamine imaging is also helpful in evaluating patients with suspected psychogenic parkinsonisms. An abnormal pre-synaptic dopamine PET/SPECT is highly suggestive of an organic aetiology [44].

The United States Food and Drug Administration (FDA) has recently approved the use of ^{123}I-FP-CIT SPECT (DaTscan^{TM}) for the detection of dopamine transporters in patients with suspected parkinsonism syndromes, and the decision was largely based on two prospective phase III diagnostic studies discussed above [23, 24]. Re-analyzing data from these two studies, however, one recent report concluded that the clinical diagnostic accuracy of PD is very similar to that achieved by DAT SPECT [45]. The author of the study cautioned against routine use of DAT SPECT for the diagnosis of iPD.

In patients with classical signs of iPD and good levodopa responsiveness, DAT SPECT probably has little to add to clinical diagnosis. We feel that DAT SPECT is

of most value clinically when used (1) in patients with indeterminate tremor (e.g., to distinguish atypical ET or SWEDDs from tremor-dominant iPD); (2) to differentiate degenerative forms of parkinsonism from the non-degenerative forms (particularly drug-induced and vascular parkinsonism); and (3) to identify patients with mixed pathology, e.g., AD and DLB, or drug-induced parkinsonism and iPD.

Detecting Subclinical Dopaminergic Dysfunction in High-Risk Patients

PET and SPECT have been able to detect subclinical dopaminergic dysfunction in subjects at high risk for iPD. Studying these subjects can provide important insight into the preclinical phase of iPD, and enable trials of putative neuroprotective agents to delay or even prevent disease onset. One longitudinal PET study investigated the role of inheritance in sporadic iPD by investigating twin pairs who were clinically discordant for iPD at baseline. Subclinical nigrostriatal dopaminergic dysfunction was found in 55 % of monozygotic twin pairs, versus only 18 % in dizygotic pairs. All the 18 asymptomatic monozygotic co-twins showed deterioration in striatal ^{18}F-Dopa uptake over 7 years, and four of them developed clinical iPD [46].

Interestingly, two PET studies have demonstrated reduced striatal ^{18}F-Dopa uptake in asymptomatic carriers of a single *parkin* mutation, which causes autosomal recessive parkinsonism[47, 48]. Longitudinal studies are required to establish whether these subjects will progress to clinical iPD.

^{123}I-β-CIT SPECT has been used to evaluate dopamine terminal integrity in asymptomatic relatives of iPD patients. Among those with idiopathic hyposmia, a known risk factor for PD, 17.5 % had reduced striatal ^{123}I-β-CIT binding, and half of these 17.5 % converted to clinical iPD over a 2-year follow-up [49].

Asymptomatic carriers of the Leucine-rich repeat kinase 2 (LRRK2) mutation, an autosomal dominant form of parkinsonism, have been found to display compensatory changes similar to those seen in early iPD patients, with downregulation of DAT binding and upregulation of AADC activity, probably as an attempt to delay the onset of parkinsonian symptoms [50]. Some of these subjects showed progressive reduction in pre-synaptic dopaminergic function, with DAT being the most sensitive indicator. Reduction in AADC activity as evidenced by abnormal ^{18}F-dopa uptake is associated with the emergence of clinical symptoms [51].

Using Dopamine Imaging to Measure Disease Progression and Effects of Putative Neuroprotective Agents in Parkinson Disease

PET and SPECT have been employed to monitor the progression of nigrostriatal degeneration in iPD. Using serial ^{18}F-dopa PET, the mean annual rate of reduction in striatal uptake in iPD is reported to be 8–12 % in the putamen and 4–6 % in the caudate

nucleus, compared with 0.5 and 0.7 % in the putamen and caudate respectively in healthy volunteers [15, 52–54]. Extrastriatal involvement is detected only at a later stage of iPD and the annual rates of reduction in ^{18}F-dopa uptake in these regions are slower than that seen in the putamen, with 7.7 % in the GPi, 6.1 % in the hypothalamus, 4.9 % in the ventral striatum, and 2.4 % in the globus pallidus externa. The authors found no correlation between the rates of reduction of ^{18}F-dopa uptake in the putamen and extrastriatal regions, suggesting that the degenerative processes affecting nigrostriatal and extrastriatal structures may occur independently [15]. One of the longitudinal PET studies also looked at the absolute, rather than the percentage, decline in striatal ^{18}F-Dopa Ki in iPD and found that the rate of decline is the same in all striatal subregions [54].

In a multi-tracer longitudinal PET study, ^{11}C-DTBZ, ^{18}F-Dopa and ^{11}C-methylphenidate PET were used to investigate the rate of progression of nigrostriatal dopaminergic dysfunction in iPD. The authors also found that the decline in nigrostriatal dysfunction affects all striatal subregions at a similar rate and the anteroposterior gradient of reduced tracer uptake/binding in the putamen is preserved as the disease progresses [55]. Findings from this paper and another study [56] also reveal a negative exponential progression in nigrostriatal dopaminergic dysfunction, with a higher rate of cell loss in the earlier stage of the disease.

Dopamine imaging with PET/SPECT has been used as a marker of disease outcome in many disease modifying trials in iPD. Parkinson disease patients taking dopamine agonists such as ropinirole [57] or pramipexole [58] showed a significantly slower decline in nigrostriatal function, as measured with ^{18}F-Dopa PET and ^{123}I-FP-CIT SPECT, respectively, compared with patients assigned to levodopa. However, the latter group of patients have better clinical scores as measured using UPDRS compared with patients taking dopamine agonists. In another study that assessed the effects of levodopa on iPD disease progression, although levodopa improved the clinical status of de novo iPD patients, these patients showed a greater reduction in striatal ^{123}I-FP-CIT SPECT compared with patients taking placebo even after a 2-week washout period [59]. Numerous theories have been proposed to explain this apparent discordance between clinical and imaging outcomes. If the imaging markers indeed reflect the true biological state of the nigrostriatal dopaminergic neurons, it is possible that dopamine agonists are neuroprotective and levodopa is neurotoxic to dopaminergic neurons, and the better clinical outcome seen in patients taking levodopa is due to the greater symptomatic effect of the medication. However, levodopa and dopamine agonists may have direct and differential effects on the imaging markers, with the former acting to depress DAT binding and AADC activity. Further studies are required to discover and validate a truly objective biological marker. Nevertheless, current PET/SPECT markers still have a role to play in demonstrating dopaminergic neuron survival in neurorestorative studies such as fetal neural transplantation [60] and infusion of neurotrophic factors [61].

Assessment of Synaptic Dopamine Release with ^{11}C-Raclopride PET

^{11}C-raclopride PET, which reflects post-synaptic D2/D3 status, is sensitive to competition with endogenous dopamine and has been used to measure changes in extracellular dopamine levels induced by pharmacological challenges, motor and behavioural tasks. Animal microdialysis studies have confirmed that a 10 % reduction in striatal ^{11}C-raclopride binding reflects a fivefold increase in synaptic dopamine levels [62]. This method provides an innovative approach to study the motor and behavioural manifestations of iPD, including dopamine dysregulation syndrome (DDS) and impulse control disorder which are thought to be related to sensitisation of the dopamine pathways mediating reward.

Several papers have assessed changes in synaptic levels of dopamine induced by exogenous levodopa in iPD patients [63–66]. A common observation in these studies is that striatal reductions in ^{11}C-raclopride binding following levodopa administration become larger as disease progresses and the motor disability increases. This increasing amplitude of the synaptic dopamine response to levodopa with disease severity might reflect the progressive degeneration of dopaminergic terminals and the subsequent loss of the capacity to store dopamine within the synaptic vesicles. This would in turn result in a more pulsatile dopamine release in the synaptic cleft, which could eventually contribute to the emergence of fluctuating motor responses and peak-dose dyskinesias. This view is supported by the observation that larger reductions in putaminal ^{11}C-raclopride binding after a single oral dose of levodopa (250 mg levodopa/25 mg carbidopa) are associated with higher dyskinesia scores in patients with advanced iPD [66].

Individual improvements in UPDRS score induced by a single oral dose of levodopa were also found to correlate significantly with reductions in putaminal ^{11}C-raclopride binding potential. Interestingly, improvements in rigidity and bradykinesia correlated well with putaminal dopamine release, but this was not the case for tremor or axial symptoms. In summary, these findings suggest that parkinsonian tremor and axial symptoms presumably occur via extrastriatal mechanisms and confirm the common clinical observations that these symptoms are often not very responsive to levodopa therapy [66].

DDS is a complication of dopaminergic treatment in iPD. Patients with DDS develop a harmful pattern of compulsive use of dopaminergic drugs, taking doses in excess of those required to control their motor symptoms.

A ^{11}C-raclopride PET study has provided evidence that DDS in iPD patients is associated with the sensitisation of the ventral striatal system circuitry which is implicated in reward and motivation [67]. Compared with iPD patients without compulsive use of their medication, iPD patients with DDS showed significantly greater reductions in ventral striatum ^{11}C-raclopride binding after levodopa administration, indicating enhanced dopamine release. Additionally, in agreement with the incentive-sensitisation theory of addiction, ventral striatal dopamine release in DDS patients correlated with self-reported compulsive drug “wanting” but not “liking.”

Enhanced dopaminergic transmission in the ventral striatum has also been reported in iPD patients who developed pathological gambling following treatment with dopamine agonists. When performing a gambling task, these iPD patients showed greater decreases in ^{11}C-raclopride binding in the ventral striatum than control patients without pathological gambling [68]. Similarly, a group of iPD patients with a variety of impulsive-compulsive behaviours, including hypersexuality, binge eating, punding, compulsive use of dopamine replacement therapy, compulsive buying and pathological gambling, showed greater decreases in ventral striatal ^{11}C-raclopride binding than iPD patients without impulsive-compulsive behaviour following exposure to a variety of reward-related cues [69].

Taken together, these findings suggest that both addictions and impulsive-compulsive behaviour in iPD might arise due to aberrant sensitisation of the ventral striatal reward system in susceptible individuals.

Conclusions and Future Directions

Dopamine imaging using PET and SPECT provides a useful diagnostic aid in patients with indeterminate tremor or parkinsonism. It can improve diagnostic accuracy and identify the correct patient groups to be recruited into clinical trials. PET/SPECT imaging also helps us understand the pathogenic mechanisms in iPD. In particular, measuring striatal dopamine release under different pharmacological and behavioural challenges allows us to study the motor and behavioural correlates of iPD. Its ability to detect subclinical dopaminergic dysfunction in subjects at high risk of developing clinical parkinsonism might be particularly useful if an effective neuroprotective agent becomes available which can delay disease onset. Although queries remain about its true objectivity in measuring disease outcome in neuroprotective studies, PET/SPECT still has a role as an imaging marker in neurorestorative trials such as fetal transplantation.

References

1. Braak H, Del Tredici K, Rub U, de Vos RA, Jansen Steur EN, Braak E. Staging of brain pathology related to sporadic Parkinson's disease. Neurobiol Aging. 2003;24:197–211.
2. Bernheimer H, Birkmayer W, Hornykiewicz O, Jellinger K, Seitelberger F. Brain dopamine and the syndromes of Parkinson and Huntington's. Clinical, morphological and neurochemical correlations. J Neurol Sci. 1973;20:415–55.
3. Fearnley JM, Lees AJ. Ageing and Parkinson's disease: substantia nigra regional selectivity. Brain. 1991;114:2283–301.
4. Rice ME, Patel JC, Cragg SJ. Dopamine release in the basal ganglia. Neuroscience. 2011;198:112–37.
5. Brooks DJ. Imaging end points for monitoring neuroprotection in Parkinson's disease. Ann Neurol. 2003;53:S110–8; discussion S8–9.

6. Snow BJ, Tooyama I, McGeer EG, et al. Human positron emission tomographic [18F]fluorodopa studies correlate with dopamine cell counts and levels. Ann Neurol. 1993;34:324–30.
7. Leenders KL, Palmer AJ, Quinn N, et al. Brain dopamine metabolism in patients with Parkinson's disease measured with positron emission tomography. J Neurol Neurosurg Psychiatry. 1986;49:853–60.
8. Frey KA, Koeppe RA, Kilbourn MR, et al. Presynaptic monoaminergic vesicles in Parkinson's disease and normal aging. Ann Neurol. 1996;40:873–84.
9. Seibyl JP, Marek KL, Quinlan D, et al. Decreased single-photon emission computed tomographic [123I]beta-CIT striatal uptake correlates with symptom severity in Parkinson's disease. Ann Neurol. 1995;38:589–98.
10. Brucke T, Asenbaum S, Pirker W, et al. Measurement of the dopaminergic degeneration in Parkinson's disease with [123I] beta-CIT and SPECT. Correlation with clinical findings and comparison with multiple system atrophy and progressive supranuclear palsy. J Neural Transm-Supp. 1997;50:9–24.
11. Pirker W. Correlation of dopamine transporter imaging with parkinsonian motor handicap: how close is it? Mov Disord. 2003;18(Suppl 7):S43–51.
12. Brooks DJ, Salmon EP, Mathias CJ, et al. The relationship between locomotor disability, autonomic dysfunction, and the integrity of the striatal dopaminergic system in patients with multiple system atrophy, pure autonomic failure, and Parkinson's disease, studied with PET. Brain. 1990;113 (Pt 5):1539–52.
13. Vingerhoets FJ, Schulzer M, Calne DB, Snow BJ. Which clinical sign of Parkinson's disease best reflects the nigrostriatal lesion? Ann Neurol. 1997;41:58–64.
14. Lang AE, Lozano AM. Parkinson's disease. Second of two parts. N Engl J Med. 1998;339:1130–43.
15. Pavese N, Rivero-Bosch M, Lewis SJ, Whone AL, Brooks DJ. Progression of monoaminergic dysfunction in Parkinson's disease: a longitudinal 18F-dopa PET study. Neuroimage. 2011;56:1463–8.
16. Rakshi JS, Uema T, Ito K, et al. Frontal, midbrain and striatal dopaminergic function in early and advanced Parkinson's disease A 3D [(18)F]dopa-PET study. Brain. 1999;122 (Pt 9):1637–50.
17. Kaasinen V, Nurmi E, Bruck A, et al. Increased frontal [(18)F]fluorodopa uptake in early Parkinson's disease: sex differences in the prefrontal cortex. Brain. 2001;124:1125–30.
18. Whone AL, Moore RY, Piccini PP, Brooks DJ. Plasticity of the nigropallidal pathway in Parkinson's disease. Ann Neurol. 2003;53:206–13.
19. Lee CS, Samii A, Sossi V, et al. In vivo positron emission tomographic evidence for compensatory changes in presynaptic dopaminergic nerve terminals in Parkinson's disease. Ann Neurol. 2000;47:493–503.
20. Nandhagopal R, Kuramoto L, Schulzer M, et al. Longitudinal evolution of compensatory changes in striatal dopamine processing in Parkinson's disease. Brain. 2011;134:3290–8.
21. Hughes AJ, Daniel SE, Kilford L, Lees AJ. Accuracy of clinical diagnosis of idiopathic Parkinson's disease: a clinico-pathological study of 100 cases. J Neurol Neurosurg Psychiatry. 1992;55:181–4.
22. Schrag A, Ben-Shlomo Y, Quinn N. How valid is the clinical diagnosis of Parkinson's disease in the community? J Neurol Neurosurg Psychiatry. 2002;73:529–34.
23. Benamer TS, Patterson J, Grosset DG, et al. Accurate differentiation of parkinsonism and essential tremor using visual assessment of [123I]-FP-CIT SPECT imaging: the [123I]-FP-CIT study group. Mov Disord. 2000;15:503–10.
24. Marshall VL, Reininger CB, Marquardt M, et al. Parkinson's disease is overdiagnosed clinically at baseline in diagnostically uncertain cases: a 3-year European multicenter study with repeat [123I]FP-CIT SPECT. Mov Disord. 2009;24:500–8.
25. Marek KL, Jennings DL, Seibyl JP, Parkinson Study Group. Long-term follow-up of patients with scans without evidence of dopaminergic deficit (SWEDD) in the ELLDOPA study. Neurology. 2005;64:A274-A.

26. Schneider SA, Edwards MJ, Mir P, et al. Patients with adult-onset dystonic tremor resembling parkinsonian tremor have scans without evidence of dopaminergic deficit (SWEDDs). Mov Disord. 2007;22:2210–5.
27. Brooks DJ, Ibanez V, Sawle GV, et al. Differing patterns of striatal 18F-dopa uptake in Parkinson's disease, multiple system atrophy, and progressive supranuclear palsy. Ann Neurol. 1990;28:547–55.
28. Brooks DJ. PET studies on the early and differential diagnosis of Parkinson's disease. Neurology. 1993;43:S6–16.
29. Burn DJ, Sawle GV, Brooks DJ. Differential diagnosis of Parkinson's disease, multiple system atrophy, and Steele-Richardson-Olszewski syndrome: discriminant analysis of striatal 18F-dopa PET data. J Neurol Neurosurg Psychiatry. 1994;57:278–84.
30. Vlaar AM, de Nijs T, Kessels AG, et al. Diagnostic value of 123I-ioflupane and 123I-iodobenzamide SPECT scans in 248 patients with parkinsonian syndromes. European Neurology. 2008;59:258–66.
31. Antonini A, Leenders KL, Vontobel P, et al. Complementary PET studies of striatal neuronal function in the differential diagnosis between multiple system atrophy and Parkinson's disease. Brain. 1997;120(Pt 12):2187–95.
32. Brooks DJ, Ibanez V, Sawle GV, et al. Striatal D2 receptor status in patients with Parkinson's disease, striatonigral degeneration, and progressive supranuclear palsy, measured with 11C-raclopride and positron emission tomography. Ann Neurol. 1992;31:184–92.
33. Cummings JL. Intellectual impairment in Parkinson's disease: clinical, pathologic, and biochemical correlates. J Geriatr Psychiatry Neurol. 1988;1:24–36.
34. Aarsland D, Tandberg E, Larsen JP, Cummings JL. Frequency of dementia in Parkinson disease. Arch Neurol. 1996;53:538–42.
35. Lippa CF, Duda JE, Grossman M, et al. DLB and PDD boundary issues: diagnosis, treatment, molecular pathology, and biomarkers. Neurology. 2007;68:812–9.
36. Walker Z, Jaros E, Walker RW, et al. Dementia with Lewy bodies: a comparison of clinical diagnosis, FP-CIT single photon emission computed tomography imaging and autopsy. J Neurol Neurosurg Psychiatry. 2007;78:1176–81.
37. McKeith I, O'Brien J, Walker Z, et al. Sensitivity and specificity of dopamine transporter imaging with 123I-FP-CIT SPECT in dementia with Lewy bodies: a phase III, multicentre study. Lancet Neurol. 2007;6:305–13.
38. McKeith IG, Dickson DW, Lowe J, et al. Diagnosis and management of dementia with Lewy bodies: third report of the DLB Consortium. Neurology. 2005;65:1863–72.
39. Burn DJ, Brooks DJ. Nigral dysfunction in drug-induced parkinsonism: an 18F-dopa PET study. Neurology. 1993;43:552–6.
40. Tolosa E, Coelho M, Gallardo M. DAT imaging in drug-induced and psychogenic parkinsonism. Mov Disord. 2003;18(Suppl 7):S28–33.
41. Gerschlager W, Bencsits G, Pirker W, et al. [123I]beta-CIT SPECT distinguishes vascular parkinsonism from Parkinson's disease. Mov Disord. 2002;17:518–23.
42. Zijlmans J, Evans A, Fontes F, et al. [123I] FP-CIT SPECT study in vascular parkinsonism and Parkinson's disease. Mov Disord. 2007;22:1278–85.
43. Lorberboym M, Djaldetti R, Melamed E, Sadeh M, Lampl Y. 123I-FP-CIT SPECT imaging of dopamine transporters in patients with cerebrovascular disease and clinical diagnosis of vascular parkinsonism. J Nucl Med. 2004;45:1688–93.
44. Benaderette S, Zanotti Fregonara P, Apartis E, et al. Psychogenic parkinsonism: a combination of clinical, electrophysiological, and [(123)I]-FP-CIT SPECT scan explorations improves diagnostic accuracy. Mov Disord. 2006;21:310–7.
45. de la Fuente-Fernandez R. Role of DaTSCAN and clinical diagnosis in Parkinson disease. Neurology. 2012;78:696–701.
46. Piccini P, Burn DJ, Ceravolo R, Maraganore D, Brooks DJ. The role of inheritance in sporadic Parkinson's disease: evidence from a longitudinal study of dopaminergic function in twins. Ann Neurol. 1999;45:577–82.

47. Khan NL, Scherfler C, Graham E, et al. Dopaminergic dysfunction in unrelated, asymptomatic carriers of a single parkin mutation. Neurology. 2005;64:134–6.
48. Hilker R, Klein C, Hedrich K, et al. The striatal dopaminergic deficit is dependent on the number of mutant alleles in a family with mutations in the parkin gene: evidence for enzymatic parkin function in humans. Neurosci Lett. 2002;323:50–4.
49. Ponsen MM, Stoffers D, Booij J, van Eck-Smit BL, Wolters E, Berendse HW. Idiopathic hyposmia as a preclinical sign of Parkinson's disease. Ann Neurol. 2004;56:173–81.
50. Adams JR, van Netten H, Schulzer M, et al. PET in LRRK2 mutations: comparison to sporadic Parkinson's disease and evidence for presymptomatic compensation. Brain. 2005; 128:2777–85.
51. Nandhagopal R, Mak E, Schulzer M, et al. Progression of dopaminergic dysfunction in a LRRK2 kindred: a multitracer PET study. Neurology. 2008;71:1790–5.
52. Vingerhoets FJ, Snow BJ, Lee CS, Schulzer M, Mak E, Calne DB. Longitudinal fluorodopa positron emission tomographic studies of the evolution of idiopathic parkinsonism. Ann Neurol. 1994;36:759–64.
53. Morrish PK, Rakshi JS, Bailey DL, Sawle GV, Brooks DJ. Measuring the rate of progression and estimating the preclinical period of Parkinson's disease with [18F]dopa PET. J Neurol Neurosurg Psychiatry. 1998;64:314–9.
54. Nurmi E, Ruottinen HM, Bergman J, et al. Rate of progression in Parkinson's disease: a 6-[18F]fluoro-L-dopa PET study. Mov Disord. 2001;16:608–15.
55. Nandhagopal R, Kuramoto L, Schulzer M, et al. Longitudinal progression of sporadic Parkinson's disease: a multi-tracer positron emission tomography study. Brain. 2009;132:2970–9.
56. Hilker R, Schweitzer K, Coburger S, et al. Nonlinear progression of Parkinson disease as determined by serial positron emission tomographic imaging of striatal fluorodopa F 18 activity. Arch Neurol. 2005;62:378–82.
57. Whone AL, Watts RL, Stoessl AJ, et al. Slower progression of Parkinson's disease with ropinirole versus levodopa: the REAL-PET study. Ann Neurol. 2003;54:93–101.
58. Parkinson Study Group. Dopamine transporter brain imaging to assess the effects of pramipexole vs. levodopa on Parkinson disease progression. J Am Med Assoc. 2002;287:1653–61.
59. Fahn S, Oakes D, Shoulson I, et al. Levodopa and the progression of Parkinson's disease. N Engl J Med. 2004;351:2498–508.
60. Lindvall O, Brundin P, Widner H, et al. Grafts of fetal dopamine neurons survive and improve motor function in Parkinson's disease. Science. 1990;247:574–7.
61. Gill SS, Patel NK, Hotton GR, et al. Direct brain infusion of glial cell line-derived neurotrophic factor in Parkinson disease. Nat Med. 2003;9:589–95. (Epub 2003 Mar 31).
62. Breier A, Su TP, Saunders R, et al. Schizophrenia is associated with elevated amphetamine-induced synaptic dopamine concentrations: evidence from a novel positron emission tomography method. Proc Natl Acad Sci U S A. 1997;94:2569–74.
63. Tedroff J, Pedersen M, Aquilonius SM, Hartvig P, Jacobsson G, Langstrom B. Levodopa-induced changes in synaptic dopamine in patients with Parkinson's disease as measured by [11C]raclopride displacement and PET. Neurology. 1996;46:1430–6.
64. de la Fuente-Fernandez R, Lu JQ, Sossi V, et al. Biochemical variations in the synaptic level of dopamine precede motor fluctuations in Parkinson's disease: PET evidence of increased dopamine turnover. Ann Neurol. 2001;49:298–303.
65. de la Fuente-Fernandez R, Sossi V, Huang Z, et al. Levodopa-induced changes in synaptic dopamine levels increase with progression of Parkinson's disease: implications for dyskinesias. Brain. 2004;127:2747–54. (Epub 2004 Aug 25).
66. Pavese N, Evans AH, Tai YF, et al. Clinical correlates of levodopa-induced dopamine release in Parkinson disease: a PET study. Neurology. 2006;67:1612–7.
67. Evans AH, Pavese N, Lawrence AD, et al. Compulsive drug use linked to sensitized ventral striatal dopamine transmission. Ann Neurol. 2006;59:852–8.
68. Steeves TD, Miyasaki J, Zurowski M, et al. Increased striatal dopamine release in Parkinsonian patients with pathological gambling: a [11C] raclopride PET study. Brain. 2009;132:1376–85.
69. O'Sullivan SS, Wu K, Politis M, et al. Cue-induced striatal dopamine release in Parkinson's disease-associated impulsive-compulsive behaviours. Brain. 2011;134:969–78.

Chapter 9
Functional MRI in Idiopathic Parkinson Disease and Parkinsonism

Tao Wu and Mark Hallett

Basic Overview of Functional MRI

Early functional neuroimaging studies commonly employed positron emission tomography (PET) or single-photon emission computed tomography (SPECT). However, their popular use is restricted due to the limitation of these techniques, which include limited temporal and spatial resolution, and the exposure of human subjects to radioactivity. The development of fMRI in the 1990s provides a useful technique that already has replaced PET or SPECT in many neuroscientific or neurological research areas. Advantages of fMRI compared with PET are that the scanners are widely available, provide superior temporal and spatial resolution, utilize no ionizing radiation thereby allowing a single subject to be scanned repeatedly, and allowing more subjects to be recruited to increase statistical power. Broadly defined, fMRI includes all MRI methods that detect neural functional changes, including the measurement of blood oxygen level-dependent (BOLD) contrast, perfusion, and diffusion imaging. The term fMRI does, however, usually refer specifically to the use of BOLD signal to indirectly characterize neural function, a method developed in the early 1990s [1] which detects blood-level changes of oxygen saturation. During neuronal activity, cerebral blood flow (CBF) and cerebral blood volume (CBV) increase, and the ratio of oxyhemoglobin to deoxyhemoglobin increases. Oxyhemoglobin is diamagnetic, whereas deoxyhemoglobin is paramagnetic. An area with more oxygenated blood is more intense on T2*-weighted images [2]. Following this chapter, we mainly discuss the applications of BOLD fMRI in idiopathic Parkinson disease (iPD) and other types of parkinsonism, and give a brief introduction to the use of perfusion MRI.

T. Wu (✉)
Department of Neurobiology, Xuanwu Hospital,
45 Changchun Street, Bejing 100053, China
e-mail: wutao69@gmail.com

M. Hallett
Human Motor Control Section, National Institute of Neurological Disorders and Stroke, National Institutes of Health, Building 10, Room 7D37, 10 Center Drive, Bethesda, MD 20892-1428, USA
e-mail: hallettm@ninds.nih.gov

F. B. Nahab, N. Hattori (eds.), *Neuroimaging of Movement Disorders,*
Current Clinical Neurology 44, DOI 10.1007/978-1-62703-471-5_9,

Bold Functional MRI in Idiopathic Parkinson Disease

Functional MRI Studies of Motor Deficits in Idiopathic PD

Idiopathic PD is primarily a movement disorder. Therefore, numerous fMRI studies have investigated the neural correlates of motor deficits in iPD. The most common and possibly most important findings of these studies are the hypoactivation of the rostral supplementary motor area (pre-SMA) and striatum and hyperactivation of other motor regions such as the lateral premotor cortex, parietal cortex, and cerebellum in iPD patients compared with normal subjects during performance of various movements (Fig. 9.1, [3–8]). Levodopa administration can relatively normalize the dysfunction of the pre-SMA [4, 5] and decrease the overactivation of some other motor areas [4]. However, some reported iPD modulations of brain activations have been controversial; for example, both increased [3, 4] and decreased [5, 9] activity of the primary motor cortex (M1) have been observed. The basis for these inconsistent findings remains unclear but may be due to the use of different motor tasks, different disease phenotypes, or severity of the patients being studied.

The increased activity in the pre-SMA is highly correlated with improved motor performance. The pre-SMA is suggested to be critical in planning and decision-making of movements and might play a primary role in the preparation of self-initiated movements [10–12]. The pre-SMA is also one of the main target regions receiving projections from the basal ganglia motor circuit [13]. These results indicate that the dysfunction of pre-SMA, due to a deficit of the nigrostriatal dopamine system, is an important reason contributing to the akinesia in iPD. The hyperactivity in the premotor cortex, parietal cortex, and cerebellum is likely compensatory. iPD patients need recruitment of other motor circuits to compensate for the functional deficits of the striatum in order to overcome their difficulty in performing movements [3, 6, 7, 14–16].

The motor deficits in iPD appear not only during motor execution, but also in the motor learning process. BOLD fMRI studies of motor learning commonly found that iPD patients have dysfunction in frontostriatal motor circuits, especially with decreased activity in the prefrontal cortex, but with compensatory hyperactivation in the parietal and premotor cortices and cerebellum [17–19]. The difficulty of iPD patients in motor learning is made more obvious when they try to shift learned movements to the automatic stage. It has been shown that iPD patients need greater activity in the cerebellum, premotor area, parietal cortex, precuneus, and prefrontal cortex compared with normal subjects while performing automatic movements. They require more brain activity to compensate for basal ganglia dysfunction in order to perform automatic movements [6].

Functional MRI has also been used to investigate the deficits of iPD patients in more complex coordination motor tasks. For example, iPD patients have difficulty in performing bimanual movements, especially antiphase movements [20]. Antiphase bimanual movements are when both hands perform the same movement with a phase shift of 180° between the two hands (i.e., one hand flexes while the other extends).

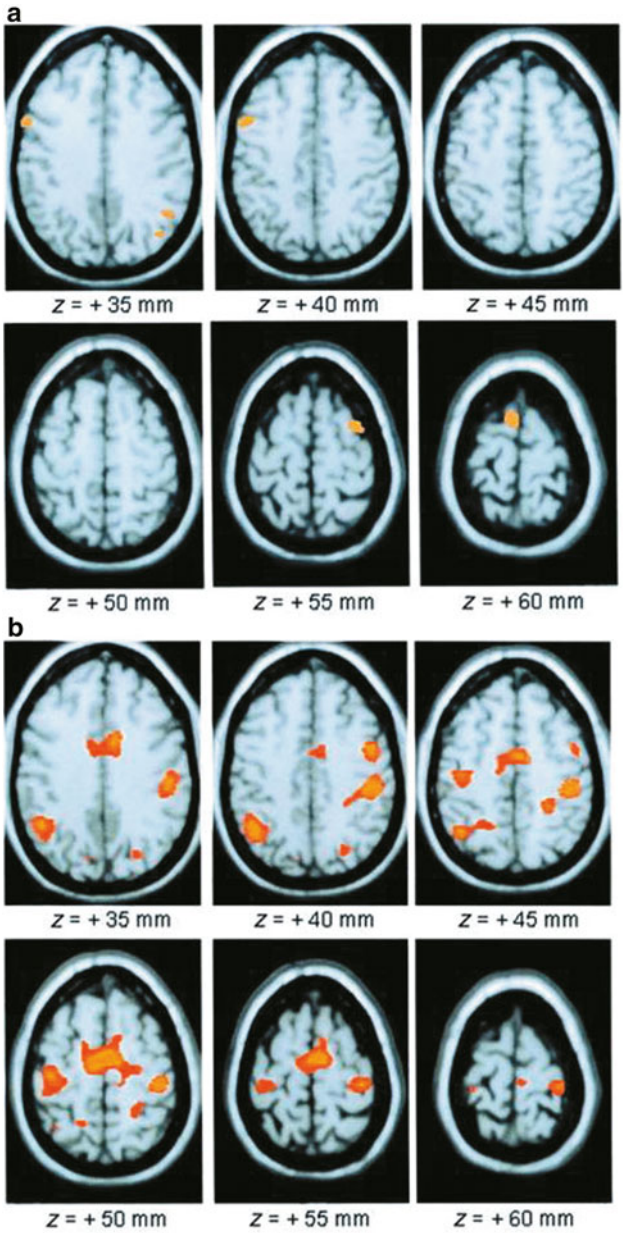

Fig. 9.1 **a** Areas of relative overactivity in normal controls compared with patients with idiopathic Parkinson disease (iPD) during a complex sequential righthand movement (z = location of area of activation above commissural plane; threshold = $p < 0.01$). **b** Areas of relative overactivity in patients with iPD compared with normal controls during a complex sequential right-hand movement, superimposed onto a stereotaxically normalized MRI brain scan (z = location of area of activation above commissural plane; threshold = $p < 0.001$). (Modified from Sabatini et al. [3] with permission from Oxford University Press)

A recent study found that the SMA was more activated during antiphase movement than inphase movement in controls, but not in iPD patients. In performing antiphase movements, iPD patients showed less activity in the basal ganglia and SMA, and had more activation in the M1, premotor cortex, and cerebellum compared with normal subjects. These findings suggest that dysfunction of the SMA and basal ganglia, abnormal interactions of brain networks, and disrupted attentional networks are important reasons contributing to the difficulty in performing bimanual antiphase movements. More brain activity and stronger connectivity are required in some brain regions to compensate for dysfunction of the supplementary motor area and basal ganglia in order to perform bimanual movements correctly [8].

Idiopathic PD patients also have more difficulty in performing two different tasks simultaneously (dual task). Wu and Hallett [21] found that iPD subjects can execute some simple dual motor and cognitive tasks correctly, but needed greater activity in the cerebellum, premotor area, parietal cortex, precuneus, and prefrontal cortex compared with controls. These fMRI findings suggest that the problem in performing dual tasks in iPD is due to limited attentional resources, defective central executive function, and less automaticity in performing the tasks.

More recently, fMRI has been used to investigate the alterations in connectivity of motor circuits. Since iPD affects large-scale brain networks, examination of network interactions may provide more valuable information in understanding pathophysiological changes than simply investigating local brain activity. The method used to explore network integration is analysis of functional or effective connectivity. Functional connectivity is defined as the degree of temporal correlation between spatially remote brain regions, whereby areas having more similar blood flow responses over time are considered to be more "functionally connected." Effective connectivity expands on this by predicting the direction of information flow between two regions and is defined as the influence one neuronal system exerts over another [22]. These methods are increasingly being used to investigate iPD-induced modifications of brain networks [23–31]. The primary finding of these studies is that in addition to regional activation changes, the connectivity of brain networks also has iPD-related modifications during the performance of various motor tasks. For example, using structural equation modeling (SEM) [23], psychophysiological interaction (PPI) [30, 31], and dynamic causal modeling (DCM) [24], investigators have identified that iPD patients fail to modulate effective connectivity between prefrontal cortex, premotor cortex, and SMA. During the performance of self-initiated movement, the connectivity of striatal motor circuits is weakened, which might contribute to the impairment in performing self-initiated movements in iPD. Meanwhile, the connections between corticocerebellar motor regions are strengthened and may help compensate for basal ganglia dysfunction ([31], Fig. 9.2). While the use of fMRI activation maps to measure the amplitude of blood flow responses may provide valuable information about regional brain changes, connectivity analyses may be a more sensitive method to detect neural changes in iPD [32].

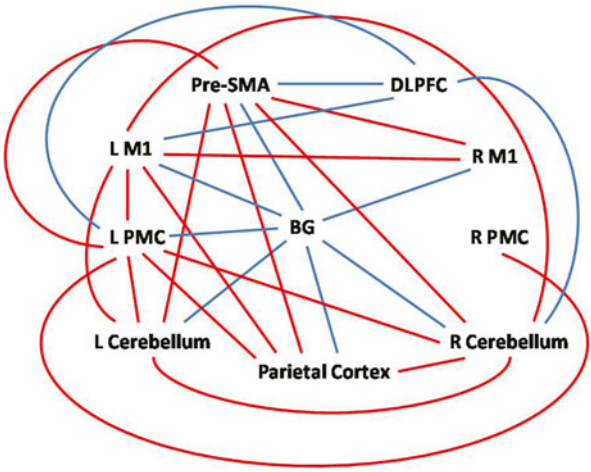

Fig. 9.2 Differences of effective connectivity between iPD patients and healthy controls among the basal ganglia, rostral supplementary motor area (*pre-SMA*), bilateral primary motor cortex (*M1*), bilateral premotor cortex (*PMC*), bilateral cerebellum, dorsolateral prefrontal cortex (DLPFC), and parietal cortex. *Red*/*blue* lines indicate increased/decreased connectivity between the two brain regions in iPD patients compared with healthy controls. (Modified from Wu et al. [31] with permission from Elsevier)

Functional MRI Studies of Nonmotor Symptoms of Idiopathic PD

Besides motor symptoms, most iPD patients present with nonmotor symptoms (e.g., cognitive, emotional, or olfactory impairments). These problems can predate the onset of motor symptoms, and may be due to degeneration outside the basal ganglia, although dysfunction of the basal ganglia also contributes to some nonmotor symptoms. The basal ganglia were classically regarded as motor structures. However, in recent years, it has been recognized that the basal ganglia have an important role in diverse functions, including cognitive and emotional control. Using fMRI and functional connectivity methods, Di Martino et al. [33] provided evidence for the hypothesized motor (dorsal putamen), cognitive (ventral putamen, dorsal caudate, superior ventral striatum), and affective (inferior ventral striatum) subdivisions of the striatum.

Cognitive deficits are very common in iPD. fMRI studies revealed that cognitively impaired PD patients had significantly less activation in the prefrontal cortex compared with unimpaired patients or healthy controls [34–36]. Some studies observed compensatory hyperactivation in the inferior frontal and posterolateral temporal-parietal areas in iPD patients [34]. Monchi et al. [37] have developed a card-sorting task to study the role of the caudate nucleus in executive processes, and shown that the caudate nucleus is specifically required when a set-shift must be planned. Using this task, the same group [38] observed increased cortical activation in iPD patients

compared with the control group in the condition not specifically requiring the caudate nucleus, whereas decreased cortical activation was observed in the patients in the condition significantly involving the caudate nucleus. In addition, this study provided evidence that not only the nigrostriatal, but also the mesocortical dopaminergic pathway may play a significant role in the cognitive deficits in PD. van Eimeren et al. [28] examined the integrity of the so-called "default mode network" (DMN). The DMN is a network showing consistent task-related deactivations, and includes the medial prefrontal cortex, anterior cingulate cortex, posterior cingulate cortex, precuneus, and inferior parietal lobe [39, 40]. The functional role of this network is thought to facilitate cognitive performance by allocating neural resources to critical brain regions. iPD patients showed less deactivation of the posterior cingulate cortex and the precuneus compared with controls during performing a card-sorting task, while medial prefrontal cortex and the rostral ventromedial caudate nucleus were functionally disconnected. The malfunctioning of the DMN may contribute to the executive deficits in iPD.

Impulse control disorders, including gambling or compulsive shopping, are frequently observed in iPD patients treated with dopamine agonists [41]. A couple of recent fMRI studies [42, 43] found that during performance of a probabilistic learning task in which participants had to learn whether a symbol was associated with reward or loss [42], iPD patients with impulse control disorders showed an increased striatal prediction error signal in the gain condition after intake of dopamine agonists. This enhanced response in ventral striatum signaled a better than expected outcome for chosen actions and suggesting this might bias behavioral decisions in these patients. When performing a risk-taking task, iPD patients with impulse control disorders made more risky choices in the gain condition along with decreased orbitofrontal cortex and anterior cingulate activations [43]. The opposite pattern was found in iPD patients without these symptoms. Dopamine agonists have also been shown to decrease activation in the ventral striatum and biased decisions toward greater risk in iPD patients with impulse control disorders.

Hallucinations are also present in some iPD patients. Patients with visual hallucinations showed greater activation in the inferior frontal gyrus and the caudate nucleus, and less activation in the parietal lobe and cingulate gyrus compared with patients without hallucinations during stroboscopic (flashing) visual stimulation. During kinematic (apparent motion) stimulation, iPD subjects with hallucinations showed greater activation in the superior frontal gyrus, and less activation in area V5/MT, parietal cortices, and cingulate gyrus compared with iPD subjects with no hallucinations. These results indicate iPD patients with chronic visual hallucinations respond to visual stimuli with greater frontal and subcortical activation and less visual cortical activation than those without hallucinations. Shifting visual circuitry from posterior to anterior regions associated primarily with attention processes suggests altered network organization may play a role in the pathophysiology of visual hallucinations in iPD [44].

Depression is the most frequent psychiatric disorder in iPD. Using an event-related parametric emotional perception paradigm, Cardoso et al. [45] showed decreased activation in the left mediodorsal thalamus and medial prefrontal cortex in iPD patients

with depression compared with those without depression. These findings highlight the importance of limbic thalamus in iPD depression.

Olfactory impairment can be a premotor symptom in iPD. An event-related fMRI during an odor-detection task found olfactory-induced hyperactivation in piriform and orbitofrontal cortices in iPD patients [46]. The authors defined trials without olfactory stimulation as noise trials and trials with olfactory stimulation as signal trials, referring to the fact that additional information, namely the signal, is superimposed upon the noise. They found that while orbitofrontal areas seem to be unable to discriminate between signal and noise, primary olfactory cortex shows preserved discriminatory ability. These results support a complex network dysfunction that exceeds structural pathology observed in the olfactory bulb and mesolimbic cortices.

Use of Resting-State Functional MRI in Idiopathic PD

In recent years, the use of so-called resting-state fMRI (RS-fMRI) methodology has been developed to measure neural functional connectivity based on the presence of spontaneous low-frequency fluctuations of BOLD signal [47]. Compared with the conventional task-based fMRI method, RS-fMRI can circumvent task-related confounds, increase the signal-to-noise ratio, and expand patient populations [48]. RS-fMRI has been used to investigate iPD-related spontaneous neural activity. Wu et al. [49] used regional homogeneity (ReHo), a method to analyze the BOLD signal of the brain to examine changes in the iPD brain during rest. ReHo [50] assumes that within a functional cluster, the hemodynamic characteristics of every voxel would be similar or synchronous with that of each other, and such similarity could be changed or modulated by different conditions. The authors observed decreased ReHo in the putamen, thalamus, SMA, and increased ReHo in the cerebellum, M1, and premotor area in iPD patients compared with healthy controls (Fig. 9.3). The ReHo in the off-levodopa condition was negatively correlated with the Unified Parkinson's Disease Rating Scale (UPDRS) in the putamen, and was positively correlated with the UPDRS in the cerebellum. Administration of levodopa relatively normalized ReHo. These findings demonstrate that there are iPD-related specific changes of neural activity in the resting state. Moreover, some of these changes are secondary to dopamine deficiency, and relate to the severity of the disease.

The amplitudes of the spontaneous low-frequency fluctuations (ALFF) have also been explored in iPD [51]. Findings include decreased amplitudes of BOLD in the SMA, mesial prefrontal cortex, right middle frontal gyrus, left cerebellum, and increased amplitudes in the right cerebellum. These patterns were able to distinguish between iPD patients and healthy controls with 92 % sensitivity and 87 % specificity [52]. These findings suggest that RS-fMRI has the potential to be developed as a biomarker of iPD.

Resting-state fMRI has also been used to evaluate activity patterns associated with the presence of apathy or depression in iPD [53]. The authors found that the apathy score was best predicted by ALFF signal in the left supplementary motor

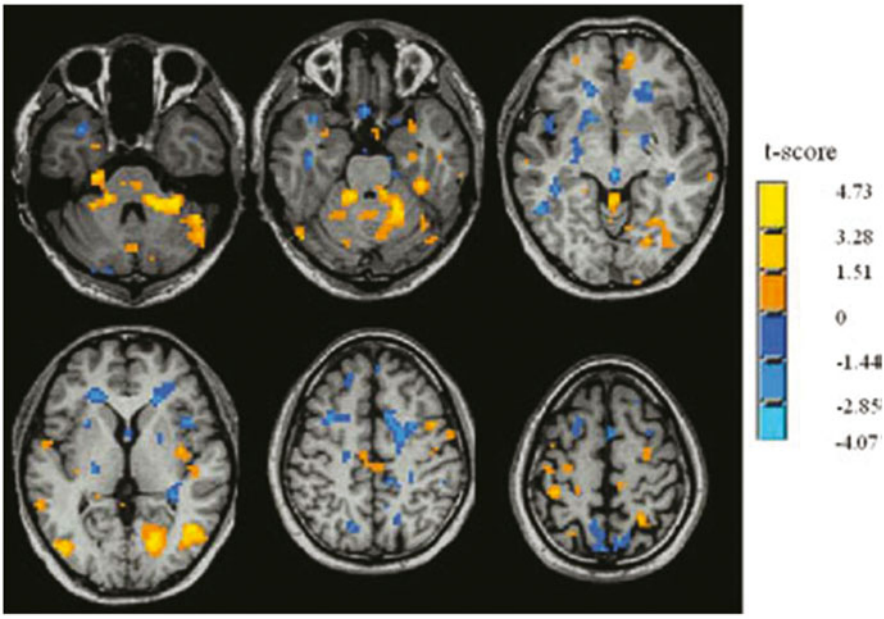

Fig. 9.3 Idiopathic Parkinson disease-related changes of regional homogeneity (ReHo) shown as a comparison of Kendall's coefficient of concordance (KCC) maps between patients with iPD in the off state and controls (two-sample *t* test; $p < 0.05$, corrected) in the resting state. *t*-score bars are shown on the right. Hot and cold *colors* indicate iPD-related ReHo increases and decreases, respectively. (Modified from Wu et al. [49] with permission from John Wiley and Sons)

cortex, the right orbitofrontal cortex, and the right middle frontal cortex, whereas depression score is best predicted by ALFF signal in the right subgenual cingulate. Disease severity was best predicted by ALFF signal in the right putamen.

Resting-state fMRI has been proved well suited for network connectivity studies in iPD. A RS-fMRI study with a network model based on graph theory compared the functional connectivity in the motor network between iPD patients and healthy controls [54]. Patients off medication had decreased connectivity in the SMA, left dorsolateral prefrontal cortex, and left putamen, and increased connectivity in the left cerebellum, left M1, and left parietal cortex. Administration of levodopa relatively normalized these connectivity patterns in patients. Using multiple regression analyses, Helmich et al. [55] investigated striatal connectivity in iPD patients. They found that the posterior putamen had reduced coupling with the inferior parietal cortex, but had increased connectivity with the anterior putamen in iPD. They concluded that dopamine depletion lead to a remapping of cerebral connectivity that reduced the spatial segregation between different corticostriatal loops, which might contribute to the abnormal sensorimotor integration in iPD. RS-fMRI has also been used to identify iPD-related changes in the connectivity profile of cortical motor areas [56] and the subthalamic nucleus [57]. A recent RS-fMRI study found that iPD with dementia is associated with selective disruption of corticostriatal connectivity [58].

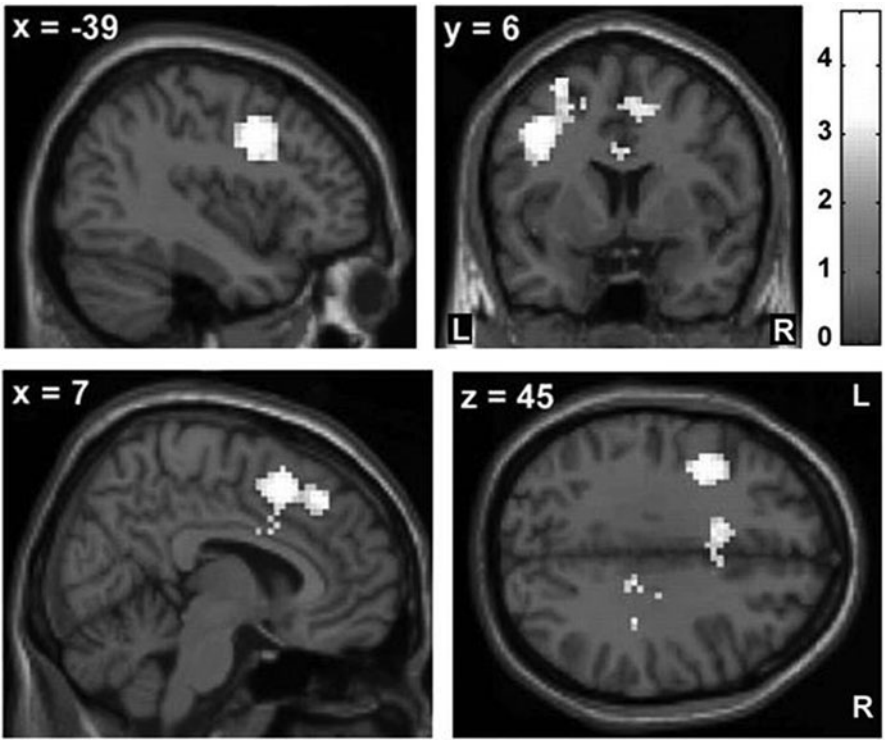

Fig. 9.4 The *z*-score maps delineate voxels with relative overactivity during internally selected movements in asymptomatic carriers of a single mutant Parkin allele relative to healthy noncarriers ($p < 0.05$, corrected at the cluster level). Asymptomatic carriers showed increased activity in the rostral cingulate motor area (rCMA) and adjacent rostral supplementary motor area (SMA) as well as the left dorsal premotor cortex (PMd). (Modified from Buhmann et al. [61] with permission from Oxford University Press)

Functional MRI in Preclinical Idiopathic PD

The neurodegenerative process in iPD begins years before the onset of any clinical symptoms [59] and the development of dopaminergic degeneration [60]. As a reliable method to identify individuals at risk for developing sporadic PD is not yet available, an alternative approach is to use asymptomatic genetic mutation carriers to study pathophysiological changes of preclinical iPD. fMRI studies have reported neural changes in some types of asymptomatic mutation carriers such as Parkin and PINK1 [61–63]. These studies have found additional recruitment of SMA, cingulate motor area, and premotor cortex in asymptomatic mutation carriers compared with healthy controls during motor tasks. In addition, the cingulate motor area had a stronger influence on activity in the basal ganglia in asymptomatic mutation carriers compared with controls (Fig. 9.4). These results might reflect a compensatory reorganization of striatocortical motor loops to maintain motor function in the preclinical stage.

Use of Perfusion MRI in Idiopathic PD

Arterial spin labeling (ASL) is a noninvasive MRI perfusion method that quantitatively measures CBF per unit of tissue mass [64]. ASL eliminates expensive, potentially harmful radioactive materials and long preparation times and requires shorter scan times than radiotracer methods. It is an easily repeatable addition to routine MRI scanning that produces absolute perfusion images. Melzer et al. [65] used pseudo-continuous ASL and principal component analysis to derive an iPD-related perfusion network via logistic regression. They found an iPD-related pattern of decreased perfusion in the posterior parieto-occipital cortex, precuneus and cuneus, and middle frontal gyri compared with healthy controls. Perfusion was preserved in globus pallidus, putamen, anterior cingulate, and postcentral and precentral gyri. Both motor and cognitive statuses were significant factors related to network score. Another study compared the iPD-related spatial covariance pattern (PDRP) derived from continuous ASL perfusion MRI with the corresponding 18F-fluorodeoxyglucose PET (FDG-PET) values. The PDRP expression was abnormally elevated in patients scanned with either modality, and the values from ASL-MRI and FDG-PET were highly intercorrelated ($p < 0.0001$). Perfusion MRI methods can be used for accurate quantification of disease-related covariance patterns [66]. These results suggest that perfusion MRI has potential to be a functional biomarker of PD.

Functional MRI in Atypical Parkinsonism

Functional MRI has also been used to investigate neural changes in atypical parkinsonian disorders (aPD) such as multiple system atrophy (MSA), progressive supranuclear palsy (PSP), and dementia with Lewy bodies (DLB). These studies have found disorder-specific activity or connectivity patterns that may help to distinguish iPD from aPD. You et al. [67] found that MSA patients had decreased ReHo in the left M1, posterior cingulate cortex, left lateral prefrontal cortex, and right inferior parietal lobule, and had increased ReHo in the right M1, bilateral premotor cortices, bilateral SMA, medial prefrontal cortex, and left inferior parietal lobule.

Whitwell et al. [68] found reduced functional connectivity between the thalamus and premotor cortex, and the SMA, striatum, and cerebellum. Reduced connectivity in the basal ganglia network, DMN, and subcortical salience networks were also present in patients with PSP. SMA functional connectivity correlated with SMA volume and measures of cognitive and motor dysfunction, while thalamic connectivity correlated with degeneration of superior cerebellar peduncles. These results suggest that PSP is associated with disrupted thalamocortical connectivity that is associated with degeneration of the dentatorubrothalamic tracts and the presence of cortical atrophy. Zwergal et al. [69] used mental imagery of standing during fMRI, and revealed a reduced activation of the mesencephalic brainstem tegmentum and the thalamus in PSP patients with postural instability and falls. The results give support to the hypothesis that reduced thalamic activation via the ascending brainstem projections may cause postural imbalance in PSP.

Both DLB and iPD are associated with deposition of α-synuclein-containing Lewy bodies and Lewy neurites within brainstem, limbic, and cortical neurons. Despite a common molecular substrate, iPD and DLB show important differences with regard to the onset timing and severity of symptoms [70]. The differences of structural networks between iPD and DLB have been measured using diffusion tensor imaging [71]. Whether differences in regional activation or network connectivity patterns can distinguish iPD from DLB has not been examined using fMRI, though some studies have identified DLB-specific patterns of functional network connectivity. In DLB patients, Galvin et al. [72] found increased connectivity between the precuneus and regions in the dorsal attention network and the putamen, along with decreased connectivity between the precuneus and other task-negative default regions and visual cortices. Kenny et al. [73] observed increased connectivity between the right posterior cingulate cortex and other brain areas compared with controls.

Limitations and Prospect

Functional MRI is unable to directly detect the dysfunction of nigrostriatal dopamine system, which might limit its clinical application. It is sensitive to motion artifact, making it difficult to study patients who have severe tremor. In addition, the BOLD fMRI method relies on neurovascular coupling to produce a detectable signal. This indirect coupling to the neuronal response may impede absolute determination of functional activity from the BOLD signal. The pathophysiological nature of some fMRI findings in iPD remains debatable. For example, whether the hyperactivation in iPD patients is a compensatory effect or a pathological dysfunction remains unclear. In addition, some fMRI studies have reported inconsistent findings. For example, observed PD modulations of primary motor cortex are controversial. Both increased [3, 4] and decreased [5] activity of primary motor cortex has been reported. Therefore, although some findings are promising, and might even detect abnormalities in the early stages of iPD, fMRI is still far from being a standard method in the routine clinical investigations and requires further development.

Conclusions and Future Directions

Functional MRI methods provide a relatively inexpensive and noninvasive means of measuring regional brain function, and are now increasingly used in investigating parkinsonian disorders. The most promising achievement of fMRI is that it has provided important information on iPD-related functional and pathophysiological changes. At present, fMRI is mainly restricted to research studies, and is far from being a method in routine clinical investigations. However, some fMRI approaches such as RS-fMRI show potential as biomarkers of PD. In the future, one direction of fMRI research concerns iPD-related pathophysiological changes, which will enhance our understanding of symptomatic onset and development. Additional research

should focus on increasing efforts to develop fMRI as a neuroimaging biomarker for early diagnosis of iPD; and this might well require further technical and methodological improvements. These developments have the potential to improve early diagnosis, better evaluate disease progression, differentiate iPD from other parkinsonisms on an individual basis, and may guide novel targets for future therapies.

References

1. Ogawa S, Lee TM, Kay AR, Tank DW. Brain magnetic resonance imaging with contrast dependent on blood oxygenation. Proc Natl Acad Sci U S A. 1990;87:9868–72.
2. Ogawa S, Menon RS, Tank DW, Kim SG, Merkle H, Ellermann JM, Ugurbil K. Functional brain mapping by blood oxygenation level-dependent contrast magnetic resonance imaging. A comparison of signal characteristics with a biophysical model. Biophys J. 1993;64:803–12.
3. Sabatini U, Boulanouar K, Fabre N, Martin F, Carel C, Colonnese C, Bozzao L, Berry I, Montastruc JL, Chollet F, Rascol O. Cortical motor reorganization in akinetic patients with Parkinson's disease: a functional MRI study. Brain. 2000;123:394–403.
4. Haslinger B, Erhard P, Kampfe N, Boecker H, Rummeny E, Schwaiger M, Conrad B, Ceballos-Baumann AO. Event-related functional magnetic resonance imaging in Parkinson's disease before and after levodopa. Brain. 2001;124:558–70.
5. Buhmann C, Glauche V, Sturenburg HJ, Oechsner M, Weiller C, Buchel C. Pharmacologically modulated fMRI—cortical responsiveness to levodopa in drug-naïve hemiparkinsonian patients. Brain. 2003;126:451–61.
6. Wu T, Hallett M. A functional MRI study of automatic movements in patients with Parkinson's disease. Brain. 2005;128:2250–9.
7. Yu H, Sternad D, Corcos DM, Vaillancourt DE. Role of hyperactive cerebellum and motor cortex in Parkinson's disease. Neuroimage. 2007;35(1):222–33.
8. Wu T, Wang L, Hallett M, Li K, Chan P. Neural correlates of bimanual anti-phase and in-phase movements in Parkinson's disease. Brain. 2010;133:2394–409.
9. Tessa C, Lucetti C, Diciotti S, Paoli L, Cecchi P, Giannelli M, Baldacci F, Ginestroni A, Vignali C, Mascalchi M, Bonuccelli U. Hypoactivation of the primary sensorimotor cortex in de novo Parkinson's disease: a motor fMRI study under controlled conditions. Neuroradiology. 2012;554(3):261–8.
10. Deiber MP, Passingham RE, Colebatch JG, Friston KJ, Nixon PD, Frackowiak RS. Cortical areas and the selection of movement: a study with positron emission tomography. Exp Brain Res. 1991;84:393–402.
11. Jenkins IH, Jahanshahi M, Jueptner M, Passingham RE, Brooks DJ. Self-initiated versus externally triggered movements. II. The effect of movement predictability on regional cerebral blood flow. Brain. 2000;123:1216–28.
12. Cunnington R, Windischberger C, Deecke L, Moser E. The preparation and execution of self-initiated and externally-triggered movement: a study of event-related fMRI. Neuroimage. 2002;15:373–85.
13. Schell GR, Strick PL. The origin of thalamic inputs to the arcuate premotor and supplementary motor areas. J Neurosci. 1984;4:539–60.
14. Rascol O, Sabatini U, Fabre N, Brefel C, Loubinoux I, Celsis P, Senard JM, Montastruc JL, Chollet F. The ipsilateral cerebellar hemisphere is overactive during hand movements in akinetic parkinsonian patients. Brain. 1997;120:103–10.
15. Catalan MJ, Ishii K, Honda M, Samii A, Hallett M. A PET study of sequential finger movements of varying length in patients with Parkinson's disease. Brain. 1999;122:483–95.
16. Appel-Cresswell S, de la Fuente-Fernandez R, Galley S, McKeown MJ. Imaging of compensatory mechanisms in Parkinson's disease. Curr Opin Neurol. 2010;23:407–12.

17. Werheid K, Zysset S, Müller A, Reuter M, von Cramon DY. Rule learning in a serial reaction time task: an fMRI study on patients with early Parkinson's disease. Brain Res Cogn Brain Res. 2003;16:273–84.
18. Mallol R, Barrós-Loscertales A, López M, Belloch V, Parcet MA, Avila C. Compensatory cortical mechanisms in Parkinson's disease evidenced with fMRI during the performance of pre-learned sequential movements. Brain Res. 2007;1147:265–71.
19. Bédard P, Sanes JN. On a basal ganglia role in learning and rehearsing visual-motor associations. Neuroimage. 2009;47(4):1701–10.
20. Ponsen MM, Daffertshofer A, van den Heuvel E, Wolters ECH, Beek PJ, Berendse HW. Bimanual coordination dysfunction in early, untreated Parkinson's disease. Parkinsonism Relat Disord. 2006;12:246–52.
21. Wu T, Hallett M. Neural correlates of dual task performance in patients with Parkinson's disease. J Neurol Neurosurg Psychiatry. 2008;79:760–6.
22. Friston KJ. Functional and effective connectivity in neuroimaging: a synthesis. Hum Brain Mapp. 1994;2:56–78.
23. Rowe J, Stephan KE, Friston K, Frackowiak R, Lees A, Passingham R. Attention to action in Parkinson's disease: impaired effective connectivity among frontal cortical regions. Brain. 2002;125:276–89.
24. Rowe JB, Hughes LE, Barker RA, Owen AM. Dynamic causal modelling of effective connectivity from fMRI: are results reproducible and sensitive to Parkinson's disease and its treatment? Neuroimage. 2010;52:1015–26.
25. Helmich RC, de Lange FP, Bloem BR, Toni I. Cerebral compensation during motor imagery in Parkinson's disease. Neuropsychologia. 2007;45:2201–15.
26. Helmich RC, Aarts E, de Lange FP, Bloem BR, Toni I. Increased dependence of action selection on recent motor history in Parkinson's disease. J Neurosci. 2009;29:6105–13.
27. Palmer SJ, Eigenraam L, Hoque T, McCaig RG, Troiano A, McKeown MJ. Levodopa-sensitive, dynamic changes in effective connectivity during simultaneous movements in Parkinson's disease. Neuroscience. 2009;158:693–704.
28. van Eimeren T, Monchi O, Ballanger B, Strafella AP. Dysfunction of the default mode network in Parkinson disease. A functional magnetic resonance imaging study. Arch Neurol. 2009;66:877–83.
29. Jahanshahi M, Jones CR, Zijlmans J, Katzenschlager R, Lee L, Quinn N, Frith CD, Lees AJ. Dopaminergic modulation of striato-frontal connectivity during motor timing in Parkinson's disease. Brain. 2010;133:727–45.
30. Wu T, Chan P, Hallett M. Effective connectivity of neural networks in automatic movements in Parkinson's disease. Neuroimage. 2010;49:2581–87.
31. Wu T, Wang L, Hallett M, Chen Y, Li K, Chan P. Effective connectivity of brain networks during self-initiated movement in Parkinson's disease. Neuroimage. 2011;55:204–15.
32. Palmer SJ, Li J, Wang ZJ, McKeown MJ. Joint amplitude and connectivity compensatory mechanisms in Parkinson's disease. Neuroscience. 2010;166:1110–8.
33. Di Martino A, Scheres A, Margulies DS, Kelly AM, Uddin LQ, Shehzad Z, Biswal B, Walters JR, Castellanos FX, Milham MP. Functional connectivity of human striatum: a resting state FMRI study. Cereb Cortex. 2008;18:2735–47.
34. Grossman M, Cooke A, DeVita C, Lee C, Alsop D, Detre J, Gee J, Chen W, Stern MB, Hurtig HI. Grammatical and resource components of sentence processing in Parkinson's disease: an fMRI study. Neurology. 2003;60:775–81.
35. Lewis SJ, Dove A, Robbins TW, Barker RA, Owen AM. Cognitive impairments in early Parkinson's disease are accompanied by reductions in activity in frontostriatal neural circuitry. J Neurosci. 2003;23:6351–6.
36. Monchi O, Petrides M, Doyon J, Postuma RB, Worsley K, Dagher A. Neural bases of set-shifting deficits in Parkinson's disease. J Neurosci. 2004;24:702–10.
37. Monchi O, Petrides M, Strafella AP, Worsley K, Doyon J. Functional role of the basal ganglia in planning and execution of actions. Ann Neurol. 2006;59:257–64.

38. Monchi O, Petrides M, Mejia-Constain B, Strafella AP. Cortical activity in Parkinson's disease during executive processing depends on striatal involvement. Brain. 2007;130:233–44.
39. Raichle ME, MacLeod AM, Snyder AZ, Powers WJ, Gusnard DA, Shulman GL. A default mode of brain function. Proc Natl Acad Sci U S A. 2001;98:676–82.
40. Greicius MD, Krasnow B, Reiss AL, Menon V. Functional connectivity in the resting brain: a network analysis of the default mode hypothesis. Proc Natl Acad Sci U S A. 2003;100:253–8.
41. Voon V, Dalley JW. Parkinson disease: impulsive choice-Parkinson disease and dopaminergic therapy. Nat Rev Neurol. 2011;7:541–2.
42. Voon V, Pessiglione M, Brezing C, Gallea C, Fernandez, HH, Dolan RJ, Hallett M. Mechanisms underlying dopamine-mediated reward bias in compulsive behaviors. Neuron. 2010;65: 135–42.
43. Voon V, Gao J, Brezing C, Symmonds M, Ekanayake V, Fernandez H, Dolan RJ, Hallett M. Dopamine agonists and risk: impulse control disorders in Parkinson's disease. Brain. 2011;134:1438–46.
44. Stebbins GT, Goetz CG, Carrillo MC, Bangen KJ, Turner DA, Glover GH, Gabrieli JD. Altered cortical visual processing in PD with hallucinations: an fMRI study. Neurology. 2004;63: 1409–16.
45. Cardoso EF, Maia FM, Fregni F, Myczkowski ML, Melo LM, Sato JR, Marcolin MA, Rigonatti SP, Cruz AC Jr, Barbosa ER, Amaro E Jr. Depression in Parkinson's disease: convergence from voxel-based morphometry and functional magnetic resonance imaging in the limbic thalamus. Neuroimage. 2009;47:467–72.
46. Moessnang C, Frank G, Bogdahn U, Winkler J, Greenlee MW, Klucken J. Altered activation patterns within the olfactory network in Parkinson's disease. Cereb Cortex. 2011;221:1246–53.
47. Biswal B, Yetkin FZ, Haughton VM, Hyde JS. Functional connectivity in the motor cortex of resting human brain using echo-planar MRI. Magn Reson Med. 1995;34:537–41.
48. Fox MD, Greicius M. Clinical applications of resting state functional connectivity. Front Syst Neurosci. 2010;4:19.
49. Wu T, Long X, Zang Y, Wang L, Hallett M, Li K, Chan P. Regional homogeneity changes in patients with Parkinson's disease. Hum Brain Mapp. 2009;30:1502–10.
50. Zang YF, Jiang TZ, Lu YL, He Y, Tian LX. Regional homogeneity approach to fMRI data analysis. Neuroimage. 2004;22:394–400.
51. Zang YF, He Y, Zhu CZ, Cao QJ, Sui MQ, Liang M, Tian LX, Jiang TZ, Wang YF. Altered baseline brain activity in children with ADHD revealed by resting-state functional MRI. Brain Dev. 2007;29(2):83–91.
52. Skidmore FM, Yang M, Baxter L, von Deneen KM, Collingwood J, He G, White K, Korenkevych D, Savenkov A, Heilman KM, Gold M, Liu Y. Reliability analysis of the resting state can sensitively and specifically identify the presence of Parkinson disease. Neuroimage. 2011 Sep 6. (in press).
53. Skidmore FM, Yang M, Baxter L, von Deneen KM, Collingwood J, He G, Tandon R, Korenkevych D, Savenkov A, Heilman KM, Gold M, Liu Y. Apathy, depression, and motor symptoms have distinct and separable resting activity patterns in idiopathic Parkinson disease. Neuroimage 2011 Jul 14. (in press).
54. Wu T, Wang L, Chen Y, Zhao C, Li K, Chan P. Changes of functional connectivity of the motor network in the resting state in Parkinson's disease. Neurosci Lett. 2009;460:6–10.
55. Helmich RC, Derikx LC, Bakker M, Scheeringa R, Bloem BR, Toni I. Spatial remapping of cortico-striatal connectivity in Parkinson's disease. Cereb Cortex. 2010;20:1175–86.
56. Wu T, Long X, Wang L, Hallett M, Zang Y, Li K, Chan P. Functional connectivity of cortical motor areas in the resting state in Parkinson's disease. Hum Brain Mapp. 2011;32:1443–57.
57. Baudrexel S, Witte T, Seifried C, von Wegner F, Beissner F, Klein JC, Steinmetz H, Deichmann R, Roeper J, Hilker R. Resting state fMRI reveals increased subthalamic nucleus-motor cortex connectivity in Parkinson's disease. Neuroimage 2011;55:1728–38.
58. Seibert TM, Murphy EA, Kaestner EJ, Brewer JB. Interregional correlations in Parkinson disease and Parkinson-related dementia with resting functional MR imaging. Radiology. 2012 Apr;263(1):226–34.

59. Braak H, Del TK, Rub U, de Vos RA, Jansen Steur EN, Braak E. Staging of brain pathology related to sporadic Parkinson's disease. Neurobiol Aging. 2003;24:197–211.
60. Fearnley JM, Lees AJ. Ageing and Parkinson's disease: substantia nigra regional selectivity. Brain. 1991;14:2283–230.
61. Buhmann C, Binkofski F, Klein C, Büchel C, van Eimeren T, Erdmann C, Hedrich K, Kasten M, Hagenah J, Deuschl G, Pramstaller PP, Siebner HR. Motor reorganization in asymptomatic carriers of a single mutant Parkin allele: a human model for presymptomatic parkinsonism. Brain. 2005;128:2281–90.
62. van Nuenen BF, Weiss MM, Bloem BR, Reetz K, van Eimeren T, Lohmann K, Hagenah J, Pramstaller PP, Binkofski F, Klein C, Siebner HR. Heterozygous carriers of a Parkin or PINK1 mutation share a common functional endophenotype. Neurology. 2009;72:1041–7.
63. van Eimeren T, Binkofski F, Buhmann C, Hagenah J, Strafella AP, Pramstaller PP, Siebner HR, Klein C. Imaging movement-related activity in medicated Parkin-associated and sporadic Parkinson's disease. Parkinsonism Relat Disord. 2010;16:384–7.
64. Detre JA, Leigh JS, Williams DS, Koretsky AP. Perfusion imaging. Magn Reson Med. 1992;23:37–45.
65. Melzer TR, Watts R, MacAskill MR, Pearson JF, Rüeger S, Pitcher TL, Livingston L, Graham C, Keenan R, Shankaranarayanan A, Alsop DC, Dalrymple-Alford JC, Anderson TJ. Arterial spin labelling reveals an abnormal cerebral perfusion pattern in Parkinson's disease. Brain. 2011;134:845–55.
66. Ma Y, Huang C, Dyke JP, Pan H, Alsop D, Feigin A, Eidelberg D. Parkinson's disease spatial covariance pattern: noninvasive quantification with perfusion MRI. J Cereb Blood Flow Metab. 2010;30:505–9.
67. You H, Wang J, Wang H, Zang YF, Zheng FL, Meng CL, Feng F. Altered regional homogeneity in motor cortices in patients with multiple system atrophy. Neurosci Lett. 2011;502(1):18–23.
68. Whitwell JL, Avula R, Master A, Vemuri P, Senjem ML, Jones DT, Jack CR Jr, Josephs KA. Disrupted thalamocortical connectivity in PSP: a resting-state fMRI, DTI, and VBM study. Parkinsonism Relat Disord. 2011;17:599–605.
69. Zwergal A, la Fougère C, Lorenzl S, Rominger A, Xiong G, Deutschenbaur L, Linn J, Krafczyk S, Dieterich M, Brandt T, Strupp M, Bartenstein P, Jahn K. Postural imbalance and falls in PSP correlate with functional pathology of the thalamus. Neurology. 2011;77(2):101–9.
70. McKeith IG, Dickson DW, Lowe Emre M, O'Brien JT, Feldman H, Cummings J, Duda JE, Lippa C, Perry EK, Aarsland D, Arai H, Ballard CG, Boeve B, Burn DJ, Costa D, Del Ser T, Dubois B, Galasko D, Gauthier S, Goetz CG, Gomez-Tortosa E, Halliday G, Hansen LA, Hardy J, Iwatsubo T, Kalaria RN, Kaufer D, Kenny RA, Korczyn A, Kosaka K, Lee VM, Lees A, Litvan I, Londos E, Lopez OL, Minoshima S, Mizuno Y, Molina JA, Mukaetova-Ladinska EB, Pasquier F, Perry RH, Schulz JB, Trojanowski JQ, Yamada M; Consortium on DLB. Diagnosis and management of dementia with Lewy bodies: third report of the DLB Consortium. Neurology. 2005;65:1863–72.
71. Lee JE, Park HJ, Park B, Song SK, Sohn YH, Lee JD, Lee PH. A comparative analysis of cognitive profiles and white-matter alterations using voxel-based diffusion tensor imaging between patients with Parkinson's disease dementia and dementia with Lewy bodies. J Neurol Neurosurg Psychiatry. 2010;81:320–26.
72. Galvin JE, Price JL, Yan Z, Morris JC, Sheline YI. Resting bold fMRI differentiates dementia with Lewy bodies vs. Alzheimer disease. Neurology. 2011;76:1797–803.
73. Kenny ER, Blamire AM, Firbank MJ, O'Brien JT. Functional connectivity in cortical regions in dementia with Lewy bodies and Alzheimer's disease. Brain. 2012;135:569–81.

Chapter 10
Neuromelanin Imaging in Parkinson Disease

Makoto Sasaki, Fumio Yamashita and Kohsuke Kudo

Introduction

Neuromelanin is a black pigment that is mainly present in the substantia nigra pars compacta (SNc) and locus ceruleus (LC) of the human brain. These nuclei can be identified as evident black or blue areas in gross specimens, but neuroimaging techniques used to visualize these nuclei in vivo are not well developed. Recent development of some magnetic resonance imaging (MRI) techniques that can capture contrast as a result of neuromelanin enables direct visualization of the SNc and LC [1–3]. In this chapter, we describe the imaging techniques, normal findings, and clinical applications of neuromelanin-sensitive MRI.

Neuroimaging Techniques for Visualizing Neuromelanin

Neuromelanin as a Paramagnetic Agent

Neuromelanin, a dark polymer pigment, is structurally similar but not identical to peripheral melanins and consists of eumelanin, pheomelanin, cysteinyldopa, and a small amount of lipid/protein components [4, 5]. Neuromelaninis a byproduct of catecholamine metabolism and is mainly present within the dopaminergic neurons of the SNc and noradrenergic neurons of the LC. It has been shown that neuromelanin plays an important role in protecting these neurons against toxic metabolites and

M. Sasaki (✉) · F. Yamashita · K. Kudo
Division of Ultrahigh Field MRI, Institute for Biomedical Sciences,
Iwate Medical University, 19-1 Uchimaru, Morioka, 020-8505, Japan
e-mail: masasaki@iwate-med.ac.jp

F. Yamashita
e-mail: fyamashi@iwate-med.ac.jp

K. Kudo
e-mail: kokudo@iwate-med.ac.jp

F. B. Nahab, N. Hattori (eds.), *Neuroimaging of Movement Disorders,*
Current Clinical Neurology 44, DOI 10.1007/978-1-62703-471-5_10,

Table 10.1 Scan parameters of neuromelanin-sensitive T1-weighted imaging

MRI sequence	Fast spin-echo
Repetition time (TR)	600 ms
Effective echo time (TE)	14 ms
Slice thickness	2.5 mm
Interslice gap	1.0 mm
Number of slices	10
Field of view (FOV)	22 cm
Matrix size	512 × 320
Echo trains	2
Number of excitations	8
Acquisition time	12 min

oxidative stress and interacts with α-synuclein [6, 7]. Similar to peripheral melanins, neuromelanin acts as a paramagnetic agent when bound to metals such as iron and copper during MRI [8]. Longitudinal and transverse relaxivities (R1 and R2) of neuromelanin have been reported to be approximately 1.0 $mM^{-1}s^{-1}$ and 1.3 $mM^{-1}s^{-1}$, respectively [9], indicating that neuromelanin mainly possesses T1-shortening effects and can be visualized on T1-weighted imaging (T1WI).

T1-Weighted Fast Spin-Echo Imaging at 3 T

Conventional T1WI with either spin-echo or gradient-echo (GRE) techniques show minimal neuromelanin-related signal changes even in the SNc and LC. A recent study reported that high-resolution two-dimensional (2D) fast spin-echo (FSE) T1WI at 3 T can depict these nuclei as high-signal areas [1]. In this technique, T1-shortening effects of intraneuronal neuromelanin become conspicuous due to the additive effects of high signal-to-noise ratio, high spatial resolution, T1 prolongation of the brain tissue, and the augmentation of inherent magnetization transfer contrast (MTC) effects of multislice FSE; all these are characteristic features of MRI at 3 T. The scanning parameters of neuromelanin-sensitive T1WI are provided in Table 10.1. The distribution of high-signal areas on images obtained using these parameters correlated well with the distribution of neuromelanin-containing neurons of SNc and LC [10], indicating that this technique can be used to directly visualize and detect changes in these nuclei (Fig. 10.1a, b).

T1-Weighted Three-Dimensional Gradient Echo Imaging with Magnetization Transfer Contrast

Neuromelanin-sensitive 2D-FSE T1WI has several limitations such as relatively low spatial resolution, long acquisition time, limited coverage, and signal nonuniformity due to B1 heterogeneity [1]. These technical issues can cause substantial errors in

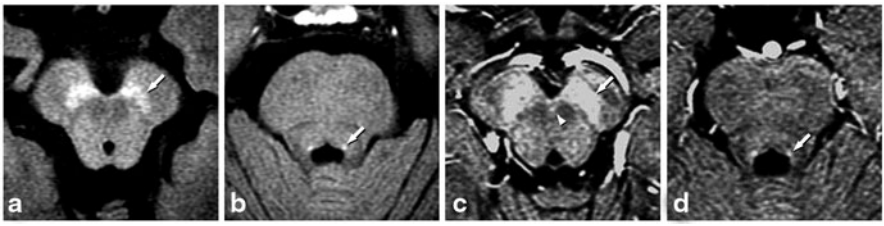

Fig. 10.1 Neuromelanin-sensitive magnetic resonance imaging of the substantia nigra and locus ceruleus (LC). **a**, **b** Two-dimensional (2D) fast spin-echo (FSE) images obtained at 3 T; **c**, **d** three-dimensional (3D) spoiled gradient-echo (GRE) images with magnetization transfer contrast pulse at 3 T; **a**, **c**: axial sections at the level of the midbrain; **b**, **d** axial sections at the level of the upper pons. Neuromelanin-sensitive images obtained by either 2D-FSE or 3D-GRE techniques clearly depict the high-signal areas at locations that correlate well with the locations of the substantia nigra pars compacta (**a**, **c**; *arrows*) and LC (**b**, **d**; *arrows*). On the 3D-GRE image, a punctate hyperintense area is seen at the midline of the midbrain tegmentum, indicating the ventral tegmental area (**c**, *arrowhead*)

the qualitative and quantitative assessment of the signal alterations in the SNc and LC in Parkinson disease and other related disorders.

Three-dimensional (3D) spoiled GRE technique with MTC pulse, also used for source imaging in magnetic resonance angiography, is sensitive to neuromelanin-related contrast [3]. This technique can obtain high-resolution volume images with minimal signal inhomogeneity during a short acquisition (< 10 min) and can overcome the limitations of the 2D-FSE technique (Fig. 10.1c, d). In addition, this method can be used for visualizing the SNc and LC at both 3 and 1.5 T [3].

Normal Image Findings of Neuromelanin-Containing Nuclei

Substantia Nigra

Axial neuromelanin-sensitive images show distinct band-like high-signal areas in the posteromedial part of the crus cerebri, mainly at the level of the lower midbrain (see Fig. 10.1a) [1, 11]. Horizontal and vertical distributions of the hyperintense areas correspond well with that of neuromelanin-containing neurons in gross specimens, but are substantially different from the distribution of low-signal-intensity areas on T2-weighted images and gray matter signal areas on proton-density-weighted or short inversion–time inversion recovery images [11]. Thus, compared with other structural imaging techniques, neuromelanin-sensitive MRI is more appropriate for direct assessment of the SNc. Sometimes, 3D-GRE images show a punctate hyperintense area at the midline of the midbrain tegmentum, indicating dopaminergic neurons of the ventral tegmental area (see Fig. 10.1c).

Locus Ceruleus (LC)

The LC is one of the gray matter structures that are "invisible" on conventional MRI but can be visualized as a pair of rod-shaped hyperintense areas along the lateral edge of the fourth ventricle floor in the upper pontine tegmentum by using neuromelanin-sensitive imaging techniques (see Fig. 10.1b, d) [1, 11]. Distribution of the hyperintense areas is identical to that of the LC in gross specimens [10]. In addition, rostrocaudal variations in the signal intensity have been reported to be closely related to the variations in the number of the neuromelanin-containing neurons [12], suggesting that the degree of signal intensity can reflect neuronal number and/or intraneuronal neuromelanin content.

Neuromelanin-Sensitive Imaging for Evaluating the Changes that Occur in Neurodegenerative Diseases

Idiopathic Parkinson Disease (iPD)

Neuromelanin-sensitive imaging techniques have been mainly utilized for evaluating the pathological changes in the SNc or LC of patients with iPD, because conventional MRI techniques fail to detect significant changes related to the principal pathological changes in iPD, i.e., neuronal depletion of the SNc and LC [11, 13]. Several studies have shown significant signal attenuation and/or volume reduction of hyperintense SNc areas on neuromelanin-sensitive images of iPD patients, indicating degeneration of dopaminergic neurons (Fig. 10.2b) [1, 2, 14]. In addition, such changes were more pronounced in the later stages than in the early stages of the disease, reflecting pathological progression of iPD [2]. Significant signal decrease in the LC areas was also seen in iPD (see Fig. 10.2d) [1]. Thus, neuromelanin-sensitive MRI can be used to visualize degenerative changes in the neuromelanin-containing neurons occurring in iPD. However, the performance of neuromelanin-sensitive MRI in terms of early and differential diagnoses is not known and should be evaluated in further investigations.

Other Neurological and Psychiatric Disorders

A few investigations have used neuromelanin imaging to assess other parkinsonian and psychiatric disorders. A significant decrease in the volume of hyperintense SNc areas was noted in patients with multiple system atrophy (MSA), progressive supranuclear palsy (PSP), and corticobasal syndrome (CBS), but this finding could not be used to discriminate these disorders from iPD [15]. Signal attenuation for the

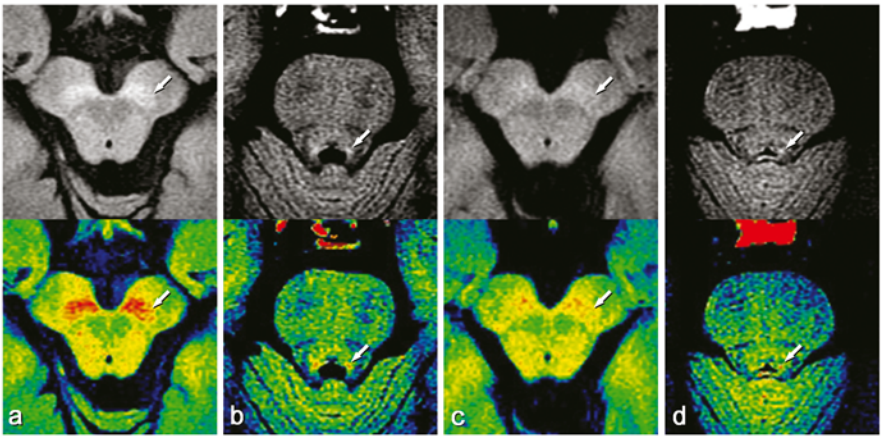

Fig. 10.2 Neuromelanin-sensitive imaging of patients with idiopathic Parkinson disease. **a**, **b** Images of a 60-year-old healthy woman; **c**, **d** images of a 57-year-old woman with early-stage Parkinson disease (Hoehn-Yahr II); **a**, **c** axial images at the level of the lower midbrain; **b**, **d** axial images at the level of the upper pons; *upper row*: gray-scale images; *lower row*: color-coded images. Window level and width were set as a signal intensity of the midbrain tegmentum and 70 % of that (**a**, **c**), or were set as that of the pontine tegmentum and 35 % of that (**b**, **d**). Signal intensities of the substantia nigra pars compacta and locus ceruleus are evidently lower for the patient with Parkinson disease (**c**, **d**; *arrows*) than for the healthy subject (**a**, **b**)

LC, particularly in its rostral two-thirds, was observed for depressive patients suggesting dysfunction of the ascending noradrenergic system [12]. On the other hand, signal augmentation for the SNc was observed in patients with schizophrenia, which may reflect an increase in the dopamine activity [16]. Further, a recent report showed that color-coded MR images could be visually assessed to discriminate depressive patients from healthy individuals with relatively high sensitivity and specificity [17].

Summary and Future Directions

Neuromelanin-sensitive imaging by using specific MRI techniques shows promise for use in direct assessment of pathological and functional changes in the neuromelanin-containing neurons of the SNc and LC. However, further technical improvement and clinical investigations are needed to establish the clinical significance of this imaging in terms of preclinical, early, and differential diagnoses as well as evaluation of surrogate markers for clinical severity and drug response.

Acknowledgments This work was partly supported by a grant-in-aid for Advanced Medical Science Research from the Ministry of Education, Culture, Sports, Science, and Technology of Japan.

References

1. Sasaki M, Shibata E, Tohyama K, et al. Neuromelanin magnetic resonance imaging of locus ceruleus and substantia nigra in Parkinson's disease. Neuroreport. 2006;31:1215–8.
2. Schwarz ST, Rittman T, Gontu V, et al. T1-weighted MRI shows stage-dependent substantia nigra signal loss in Parkinson's disease. Mov Disord. 2011;26:1633–8.
3. Nakane T, Nihashi T, Kawai H, et al. Visualization of neuromelanin in the substantia nigra and locus ceruleus at 1.5 T using a 3D-gradient echo sequence with magnetization transfer contrast. Magn Reson Med Sci. 2008;7:205–21.
4. Fedorow H, Tribl F, Halliday G, et al. Neuromelanin in human dopamine neurons: comparison with peripheral melanins and relevance to Parkinson's disease. Prog Neurobiol. 2005; 75:109–24.
5. Zecca L, Tampellini D, Gerlach M, et al. Substantia nigra neuromelanin: structure, synthesis, and molecular behaviour. Mol Path. 2001;54:414–8.
6. Zecca L, Zucca FA, Wilms H, et al. Neuromelanin of the substantia nigra: a neuronal black hole with protective and toxic characteristics. Trends Neurosci. 2003;26:578–80.
7. Fasano M, Bergamasco B, Lopiano L. Modifications of the iron-neuromelanin system in Parkinson's disease. J Neurochem. 2006;96:909–16.
8. Tosk JM, Holshouser BA, Aloia RC, et al. Effects of the interaction between ferric iron and L-dopa melanin on T1 and T2 relaxation times determined by magnetic resonance imaging. Magn Reson Med. 1992;26:40–5.
9. Enochs WS, Petherick P, Boqdanova A, et al. Paramagnetic metal scavenging by melanin: MR imaging. Radiology. 1997;204:417–23.
10. Shibata E, Sasaki M. Imaging of neuromelanin. In: Naidich TP, Duvernoy HM, Delman BN, et al. editors. Duvernoy's atlas of the human brain stem and cerebellum. Wien, Springer; 2009. p. 475–482.
11. Sasaki M, Shibata E, Tohyama K, et al. Monoamine neurons in the human brain stem: anatomy, magnetic resonance imaging findings, and clinical implications. Neuroreport. 2008; 19:1649–54.
12. Shibata E, Sasaki M, Tohyama K, et al. Reduced signal of locus ceruleus in depression in quantitative neuromelanin magnetic resonance imaging. Neuroreport. 2007;18:415–8.
13. Lehericy S, Sharman MA, Santos CL, et al. Magnetic resonance imaging of the substantia nigra in Parkinson's disease. Mov Disord. 2012;27:822–30.
14. Kashihara K, Shinya T, Higaki F. Reduction of neuromelanin-positive nigral volume in patients with MSA, PSP and CBD. Intern Med. 2011;50:1683–7.
15. Kashihara K, Shinya T, Higaki F. Neuromelanin magnetic resonance imaging of nigral volume loss in patients with Parkinson's disease. J Clin Neurosci. 2011;18:1093–6.
16. Shibata E, Sasaki M, Tohyama K, et al. Use of neuromelanin-sensitive MRI to distinguish schizophrenic and depressive patients and healthy individuals based on signal alterations in the substantia nigra and locus ceruleus. Biol Psychiatry. 2008;64:401–6.
17. Sasaki M, Shibata E, Ohtsuka K, et al. Visual discrimination among patients with depression and schizophrenia and healthy individuals using semiquantitative color-coded fast spin-echo T1-weighted magnetic resonance imaging. Neuroradiology. 2010;52:83–9.

Chapter 11
Neuroimaging of Dystonia

Silvina G. Horovitz and Mark Hallett

Introduction

The primary dystonias are movement disorders characterized by involuntary muscle contractions that produce abnormal posture of a specific body part. While there can be debilitating dysfunction of movement, no specific pathology has been identified. Neuroimaging plays a role in trying to define where pathology might be, although, in general, the findings are subtle. Neuroimaging does not presently have a clinical role except to rule out secondary dystonias, in which dystonia is a result of defined central nervous system lesions. When primary dystonia presents in childhood, it is most frequently generalized, and when it presents in adult life, it is most frequently focal, affecting only one or few body parts. The prevalence of dystonias was estimated to be 0.5/100,000 for the general population and 6/100,000 for the Ashkenazi Jewish population [1]. A random sample of individuals aged 50 and older suggested prevalence could be as high as 732/100,000 for older populations [2].

The most common childhood generalized dystonia is DYT1, in which symptoms usually start in the legs. DYT1 dystonia may manifest in young adulthood and more rarely in adult life [3]. DYT1 has a penetrance of only 30 %. One can compare manifesting and nonmanifesting carriers to noncarrier dystonia patients and healthy controls to separate genetic traits from disease traits. There are four common primary focal dystonias, and, while there is likely some genetic basis, they usually are sporadic. Named for the body part affected, these common adult onset dystonias are blepharospasm, cervical dystonia, spasmodic dysphonia, and focal hand dystonia. Most imaging information with regard to primary dystonias relates to these five conditions, and this chapter will emphasize them.

S. G. Horovitz (✉) · M. Hallett
Human Motor Control Section, Medical Neurology Branch,
National Institute of Neurological Disorders and Stroke, National Institute of Health,
Building 10, Room 7D37, 10 Center Drive, Bethesda, MD 20892-1428, USA
e-mail: silvina.horovitz@nih.gov

M. Hallett
e-mail: hallettm@ninds.nih.gov

F. B. Nahab, N. Hattori (eds.), *Neuroimaging of Movement Disorders,*
Current Clinical Neurology 44, DOI 10.1007/978-1-62703-471-5_11,

Clinical Overview of Primary Dystonias

Blepharospasm, also called benign essential blepharospasm, presents as an involuntary eye closure due to either spasms of the orbicularis oculi or a contraction failure of the levator palpebrae muscles (previously called apraxia of eyelid opening) [4, 5]. It is more prominent in females (2.8:1); 93 % of a patient series in the USA were white; median age of diagnosis was 53 years [6].

Cervical dystonia (CD), also called spasmodic torticollis, manifests with an abnormal twisting and squeezing of the neck muscles that can extend to the shoulders, producing an awkward neck and head posture. It affected 0.28 % of the population in a general population questionnaire, where it was more prominent in females (79 %) and whites (92 %) [7].

Spasmodic dysphonia (SD) is a vocal dysfunction marked by uncontrolled voice breaks and effort while speaking due to spasms in the vocal cords. Most commonly, the adductor muscles are affected, interfering with vowel sounds; when the abductor muscles are affected, it interrupts voice onset after voiceless consonants [8]. These patients have no problems with other laryngeal functions such as breathing or swallowing. It is more prominent in females (60–80 %) [9, 10], and has a 0.98 % prevalence in the general population seeking medical care [10].

Focal hand dystonia commonly presents as an occupational cramp with cocontraction of antagonist hand muscles when performing a very well-learned and practiced task such as writing or playing a musical instrument. The same hand can perform other tasks without being affected; thus, focal hand dystonia is often task-specific. It has a high prevalence in musicians (1/500), is more prominent in males, and onset is in young adulthood [11]. Even when presenting as a specific and focal disorder, focal hand dystonia can generalize to other tasks and involve more widespread muscles.

Using Neuroimaging to Understand Dystonia Pathophysiology

Several lines of evidence indicate that there are likely deficits of the basal ganglia, thalamus, sensorimotor cortices, and cerebellum of patients. However, there is no overt pathology or biomarker for the primary dystonias. This chapter will present findings from imaging studies of each of the five types of dystonias in an attempt to better understand the disorder as a group and its different manifestations. These studies use different imaging modalities, aiming to understand the structural and functional deficits the patients might have. Structural changes in gray matter are studied with T1-weighted MRI images and morphometric techniques [12]. Changes in white matter are measured with diffusion tensor imaging (DTI) [13] and the structural connectivity is modeled using tractography methods [14, 15].Changes in blood flow, function, and metabolism are measured with radioligands in positron emission tomography (PET) [16]. Metabolic changes are measured with magnetic resonance spectroscopy (MRS) [17]. Functional magnetic resonance imaging (fMRI) is used to analyze brain function [18] and connectivity [19].

DYT1

One of the core regions-of-interest (ROI) in dystonias is the basal ganglia. Using voxel-based morphometry (VBM), Draganski et al. [20] compared the size of gray matter structures in manifesting and nonmanifesting carriers of the DYT1 gene to healthy volunteers and non-DYT1 carrier dystonia patients. They found an interaction between putamen size and the disorder. Nonmanifesting DYT1 carriers and non-DYT1 carrier primary dystonia patients have enlarged basal ganglia volumes. In manifesting DYT1 carriers, basal ganglia size was inversely proportional to severity of dystonia symptoms. Interestingly, the manifesting carriers, on average, did not differ in basal ganglia size from the healthy volunteers. These results suggest two different mechanisms for the changes in basal ganglia size. For DYT1 carriers, enlarged basal ganglia might be a compensatory mechanism preventing the manifestation of the dystonia. Furthermore, the enlarged basal ganglia in non-DYT1 carrier dystonia patients could either be a compensatory mechanism as well, since dystonic symptoms are not severe for this group and onset is late in life, or could be part of the disease pathological process. Consequently, the dystonia trait is not directly related to basal ganglia size.

DTI studies showed that some deficits are related to the presence of the DYT1 gene while others are related to the dystonia itself. Manifesting and nonmanifesting DYT1 carriers differed from noncarrier healthy controls in the fractional anisotropy (FA) values of the precentral cortex [21], basal ganglia, supplementary motor area (SMA), and cerebellum [22]. Both groups of DYT1 carriers had decreased integrity of the proximal segment of the cerebellar-thalamo-cortical pathway, as evidenced by a reduced FA. Penetrance was reflected in a trend in the distal portion of these fibers, where nonmanifesting carriers had lower FA than healthy volunteers, and manifesting carriers had values in between the other two groups [23]. The authors proposed a model where the difference in integrity of the proximal and distal sections of the pathway represented cerebello-cortical inhibition and suggested this measure as a marker of penetrance.

In the same study, all DYT1 carriers displayed a positive correlation between cerebellar connectivity and cerebellar regional blood flow response to a motor task. Conversely, there was an inverse correlation between their cerebellar connectivity and the thalamus, sensorimotor cortex, and SMA regional cerebral blood flow (rCBF) change elicited by the task [23]. These findings suggest that structure and function of the different components of the cerebellar-thalamo-cortical loop are affected and interrelated.^{18}F-fluorodeoxyglucose (FDG) PET studies indicated that DYT1 carriers, irrespective of penetrance, have increased resting glucose metabolism in basal ganglia, SMA, and cerebellum [21, 24, 25]. Manifesting DYT1 carriers also had increased activity in pre-SMA and parietal association areas [21]. These findings are in concordance with the DTI studies, where cerebellar changes were related to the presence of the DYT1 gene, and distal or cortical changes depended on the penetrance.

Dystonic patients, despite genetic status, had a decreased number of GABAa receptors, measured with ^{11}C-flumazenil, in the bilateral sensorimotor cortex, left

premotor cortex, and left anterior cingulate cortex when compared with healthy volunteers; there was no difference in GABAa receptors between carrier and noncarrier patients [26]. These results support the concept of inhibition as a major factor in disease manifestation [27]. D2 receptors, measured with ^{11}C raclopride, were decreased in the striatum of nonmanifesting DYT1 carriers [28]. In another study, manifesting and nonmanifesting carriers had similarly decreased D2 receptors in the caudate nucleus, putamen, and thalamic nucleus [29]. Secondary dystonias may occur at peaks and troughs of dopamine in idiopathic Parkinson disease (iPD) patients, suggesting a pharmacological effect of dopamine in the manifestation of dystonic symptoms [30]. However, for DYT1 carriers, dopamine receptor levels do not appear to explain the manifestation.

There is evidence that some of the clinical deficits seen in manifesting carriers are also present in nonmanifesting carriers, even if subtle. For example, nonmanifesting carriers had impaired right hand sequence-learning skills, when compared with healthy controls. The behavioral deficit was accompanied by increased $H_2{}^{15}O$ PET signal in the right SMA, left lateral premotor cortex, and inferior parietal cortex. During a kinematically controlled motor task, the nonmanifesting carriers had an increased signal in the left sensorimotor cortex, left premotor cortex, SMA, ventral thalamus, posterior cerebellum, and inferior occipital cortex that could indicate a compensatory mechanism since the performance is not affected in this group [31]. Patients also had diminished activation of their dorsolateral prefrontal, motor cingulate, and dorsal premotor cortices [32]. The nonmanifesting carriers' cerebellar activity was increased during sequence learning [32], but decreased in during motor execution [31].

Since the penetrance of the DYT1 mutation is reduced, there must be other factors involved in manifestation of the dystonia besides this gene. Structural imaging studies show several metrics where manifesting and nonmanifesting carriers differ. Deficits are not always more pronounced in the manifesting carriers. On the contrary, putaminal size [20] and cerebellar-thalamo-cortical pathway connectivity [23] show larger differences in nonmanifesting subjects, suggesting compensatory mechanisms may be at play. Cerebellar abnormalities appear to be similar in manifesting and nonmanifesting DYT1 carriers, so these might be a direct gene effect. Basal ganglia, thalamic, and cortical changes depend on the penetrance; therefore, they reflect an interplay of compensation and manifestation mechanisms.

Blepharospasm

Blepharospasm was thought to be solely a basal ganglia disorder, but now there is evidence from electrophysiology and imaging indicating that the cerebral cortex also plays an important role in the genesis and manifestation of the disorder. In a number of VBM studies, blepharospasm patients had gray matter changes in the putamen [33, 34],inferior parietal cortex (BA40) [33], thalamus, head of caudate, and cerebellum [34]. Recent studies report additional changes at the cortical level, including

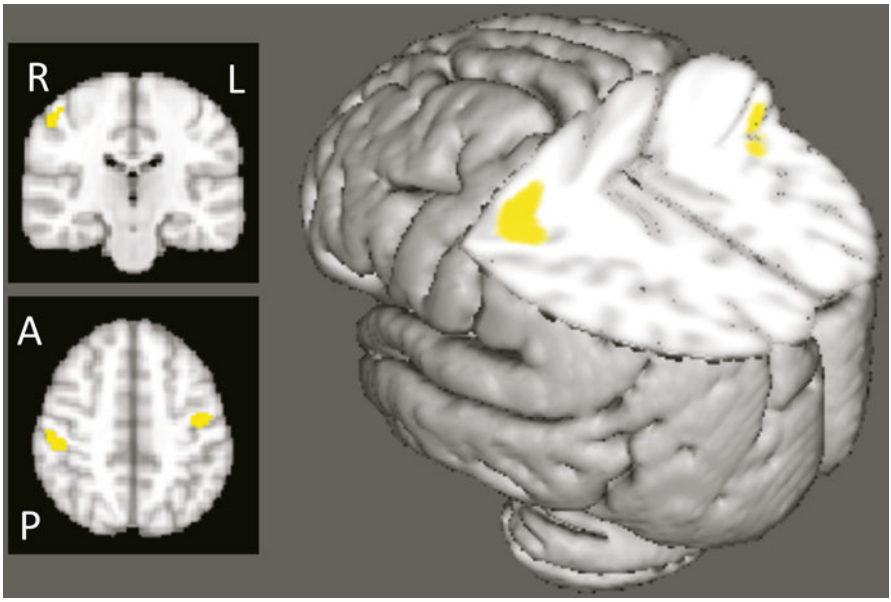

Fig. 11.1 Gray matter volume changes in blepharospasm patients. Significant differences in gray volume, detected using voxel-based morphometry are seen in the sensorimotor area (data from [37]). Regions are shown on *axial* and *coronal* slices and on a 3D reconstructed brain

the right middle frontal gyrus, left superior temporal gyrus, left postcentral gyrus [35], bilateral sensorimotor area, and cingulate gyrus (Fig. 11.1) [36, 37]. Suzuki et al. [38] found a strong correlation between the changes in gray matter volume of the sensorimotor cortex and the duration and activity index indicative of severity, suggesting that the changes might be secondary to the disorder. The variability in the different studies is striking and may be due to differences in imaging sequences or the populations studied. White matter of healthy volunteers and blepharospasm patients had similar FA and mean diffusivity (MD) values [37, 39]. However, the peak connectivity of the corticobulbar tract was lower in blepharospasm patients than in healthy controls [37]. Fiber tracking from a single subject is shown in Fig. 11.2.

Similar to the changes in gray matter, metabolic changes in the resting state were seen in several areas known to be related to blink production and control. Glucose metabolism, measured with ^{18}F-FDG PET, was increased in cortical regions, including inferior frontal gyri, right posterior cingulate gyrus, left middle occipital gyrus, right fusiform gyrus, and left anterior cingulate gyrus. Subcortical areas were also affected, with increased metabolism in the right caudate and decreased in the left inferior cerebellar hemisphere and thalamus [40]. Glucose hypermetabolism in the thalamus and pons was observed in patients treated with botulinum toxin, suggesting these changes are intrinsic to the disorder and not dependent on sensory feedback from the eyelid spasms [41]. In another study, however, metabolic changes in the

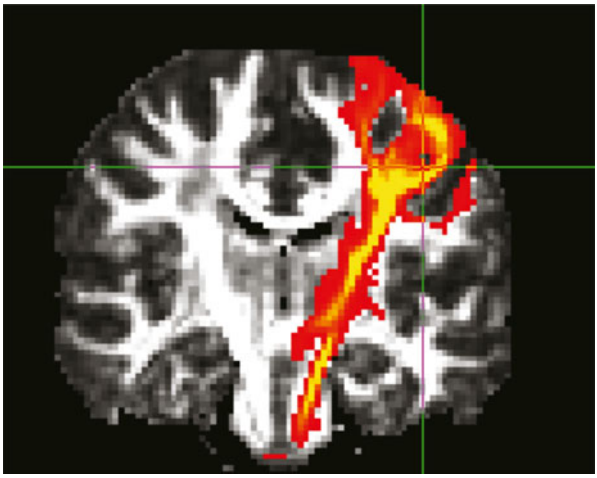

Fig. 11.2 Probabilistic tractography on individual subject data (data from [37]). Left corticobulbar bundle traced on diffusion-weighted images using the motor region shown in Fig. 12.1 as the initiation point and the pons as the endpoint

thalamus correlated with disease severity [36]. Thalamic hypermetabolism (in ventral anterior (VA) and ventral lateral (VL)) was more pronounced in blepharospasm patients with photophobia compared with those without photophobia. Nonphotophobic blepharospasm patients also had decreased metabolism in their midbrain [42].

Some metabolic studies have explored changes in different brain states. rCBF, measured with $H_2{}^{15}O$ PET, was decreased in the primary sensorimotor area in response to lower face stimulation [43]. The sleep–wake cycle also affects metabolism in patients. During wakefulness, there was increased metabolism in the cerebellum and pons. During sleep, when blepharospasm movements are suppressed, there was decreased metabolism in the superior-medial frontal cortex, an area associated with eyelid control [44]. These studies showed that metabolism is sensitive to the precise state of the patient and likely the frequency of eye blinking; this may explain some of the variability of the metabolic studies done "at rest."

There are suggestions of abnormal sensory integration and basal ganglia function with studies not focused on eyelid control. fMRI studies of blepharospasm patients evaluated brain activity elicited by nondystonic motor tasks. During handgrip, the thalamus, caudate nucleus, putamen, and globus pallidus were more active in patients than in controls [45]. During whistling, blepharospasm patients have increased activity in the postcentral cortex and caudal supplementary motor cortex bilaterally, left dorsolateral prefrontal cortex, and left paravermal cerebellum [46]. Using fMRI, activation with patients' blink spasms was compared with healthy volunteers' volitional blinks. Blink spasms increased activation in the putamen [47]; when patients

added volitional blinks to their spasms, cortical areas related to blink production (anterior visual cortex, anterior cingulate, primary motor cortex, thalamus, and superior cerebellum) were more active than in the controls [48]. Forehead stimulation produced increased activation in the putamen that was reversed by botulinum toxin treatment [49].

There is great variability in the results from the different imaging modalities and even within modalities. The variability maybe, in part, due to the inhomogeneity of the population sampled and the different sensitivity of each modality utilized. In addition, different imaging parameters or processing methods used within the same modality can lead to different results. However, put together, these studies find structural, functional, and metabolic deficits in areas seen to produce secondary blepharospasm, such as thalamus [50], basal ganglia [51], cortical areas involved in blink control such as sensorimotor cortex and anterior cingulate among others, and in the cerebellum, an area thought to have a role in dystonia [52].

Cervical Dystonia

One goal of neuroimaging studies is to find the sites of pathology. Neuropathology studies, which would be the most direct method, in all the primary dystonias are few and findings are scarce. A report from four postmortem brains showed subtle changes in the midbrain and cerebellum [53], with absence of anomalies in other brain areas presumed affected in dystonias such as basal ganglia, thalamus, or cerebral cortex. Another postmortem study showed increased concentrations of copper and manganese in the putamen of dystonia patients [54]. Transcranial sonography of the lentiform nucleus of CD patients showed a slight hyperechogenicity contralateral to the head deviation in 9 of 10 subjects [55].

A VBM study reported that CD patients have increased gray matter volume in the thalamus, caudate head bilaterally, superior temporal lobe, and left cerebellum and decreased gray matter in bilateral putamen [34]. Trends toward significant changes were also seen in the globus pallidus, bilateral orbitofrontal cortex, SMA, medial frontal gyrus, and cingulate cortex [56]. Another study reproduced the left caudate and putamen findings and found additional changes in the bilateral premotor and primary sensorimotor cortices [57]. While no correlations were found with disease duration, severity, or age in a cross-sectional study, the left sensorimotor cortex was further reduced when patients were tested/retested 5 years after [57]. The different results between cross-sectional and longitudinal studies highlight the great degree of variability existent across subjects. Additional longitudinal studies of dystonia are needed, since they allow for more controlled evaluation of these changes.

White matter in patients also shows some alterations. Based on small ROI drawn in the white matter between putamen and thalamus, Blood et al. [58] reported that patients had more asymmetry than controls in the FA values. These changes were reversed after botulinum toxin treatment, suggesting the abnormalities were related to the symptoms and that the connection between basal ganglia and thalamus displays

plasticity. Another study found no changes in FA, but reported increased MD in the white matter adjacent to pallidum, caudate, and putamen bilaterally in patients [59]. In an ROI analysis, another study found that FA in CD patients was significantly reduced in the body of the corpus callosum and bilateral putamen. MD was reduced in the right caudate, left putamen, bilateral prefrontal cortex, and left supplementary motor cortex [39]. ROI analyses, while less specific on the location, increase the power and compensate for variability between subjects, both in anatomy and in the manifestation of the dystonia, thus, providing more robust results. In line with the midbrain-cerebellum changes seen in postmortem brains, tractography showed altered connections between the pallidal output fibers and the brainstem [60]. There was a right/left hemisphere asymmetry in the tracts, in accordance with the asymmetric clinical manifestation of the disorder.

Using single-voxel proton magnetic resonance spectroscopy (^{1}H-MRS), basal ganglia NAA/Cr and NAA/Cho were reduced in patients [61]. NAA/Cr is a marker of neuronal integrity, and NAA/Cho a possible indicator of membrane dysfunction, suggesting, in this situation, loss of dopaminergic terminals or abnormal function of the striatal neurons. Because drugs that block dopamine receptors can produce dystonia, particularly of the head and neck, it is believed that the dopaminergic pathways can be involved in the etiology of the disorder. Indeed, an ^{11}C-N-methyl-spiperone PET study showed that while there were no significant differences between healthy controls and patients, patients had a trend toward higher tracer uptake in the hemisphere contralateral to the symptoms [62]. Using ^{123}I iodobenzamide SPECT, there were no differences in radiotracer uptake in basal ganglia between healthy controls and patients, but an interstriatal analysis showed that the basal ganglia contralateral to the direction of the torticollis had a higher binding to D2 receptors than the ipsilateral one [63]. A SPECT study compared the presynaptic striatal dopamine receptors, measured as ^{123}I beta-CIT binding, with the postsynaptic dopamine receptors, measured with ^{123}I-epidepride [64]. While the presynaptic receptor binding was similar for healthy controls and patients, the postsynaptic binding was lower in the CD group. The decreased postsynaptic D2 receptors could explain the lack of inhibition of the thalamo-cortical (indirect) pathway, and also explain the relative increased number of presynaptic receptors seen in other studies [63].

Patients' glucose metabolism, measured with ^{18}F-FDG PET, was increased in the basal ganglia-thalamo-cortical loop, including the basal ganglia, thalamus, premotor and motor cortex, and cerebellum [65], and bilaterally in sensorimotor areas when compared with controls [66]. A recent exploratory study showed that most of the sensorimotor differences were reverted when symptoms were alleviated following epidural premotor cortical stimulation [66]. These results are in line with the notion of CD being a disorder not only of the basal ganglia, but rather representing a more complex association with the sensorimotor network, including sensorimotor cortex, thalamus, and cerebellum.

fMRI studies have shown that nondystonic tasks impair activity in CD patients. As seen in blepharospasm patients, basal ganglia activity was altered during handgrip in CD patients. CD patients' handgrip resulted in increased activity in basal ganglia,

caudate nucleus, putamen, and thalamus [45]. On the other hand, patients' movement imagery produced less activity than healthy volunteers in bilateral parietal, left premotor, and anterior cingulate cortices; movement execution showed impaired activation in the ipsilateral putamen, insula, and cingulate cortex [67]. As a response to passive movement of nondystonic areas, CD patients showed increased activation in primary and secondary sensory cortices contralateral to the stimulation, cingulate cortex, and bilateral cerebellum [68]. Several studies explored the correlation between botulinum toxin and fMRI activity. SMA activity in response to passive movements was positively correlated with botulinum toxin dosage and negatively correlated with the Toronto Western Spasmodic Torticollis Rating Scale (TWSTRS) score, suggesting a general disinhibition of the somatosensory system [68]. Similar results are seen during finger tapping, where SMA was abnormally hypoactive in CD patients, and improved toward normal after botulinum toxin treatment [69]. In response to median nerve stimulation, secondary somatosensory and insular cortices were less active in CD patients; however, these changes were reverted 4 weeks after botulinum toxin treatment [70]. These functional findings reinforce the notion of CD as a disorder of the sensorimotor system extending beyond the representation of the affected area. They also show that changes in symptoms, even induced peripherally by botulinum toxin, affect not only primary sensory areas, but also the secondary sensory association areas, SMA, and insula. The abnormalities in these areas are presumably not indicators of the underlying etiological pathology since they revert with botulinum toxin treatment.

Spasmodic Dysphonia

As in the other primary dystonias, there are no consistent radiological findings to explain SD, supporting the idea it is a heterogeneous voice disorder [71]. Similar to other primary dystonias, in addition to basal ganglia involvement, cortical contribution has been suspected. SD patients show changes in cortical thickness, gray matter volume and function in areas related to speech control, including the laryngeal sensorimotor cortex, inferior frontal gyrus, superior and middle temporal cortices, supramarginal gyri, and cerebellum [72]. In these patients, DTI findings indicate patients have decreased FA in the genu of the right internal capsule, a site confirmed in one histopathological examination, and increased MD bilaterally in the lentiform nucleus, ventral thalamus, and cerebellum. These changes correlated positively with severity of the clinical symptoms [73].

While no resting metabolism data are available in SD patients, there are several functional studies with PET and fMRI that found cortical, thalamic, basal ganglia, and cerebellar deficits. An early $H_2{}^{15}O$ PET case study suggested a reduction in SMA during phonation [74]. However, during speech-related activity, patients had hyperactivity in a network including the right dorsal precentral gyrus, cerebellar hemisphere and vermis, primary auditory cortex, anterior cingulate, and anterior insula [75]. The unimodal and heteromodal association areas, including the posterior

supramarginal area and posterior middle temporal gyri and the dorsal postcentral gyrus, were hypoactive in the same patients [75]. These changes reverted after botulinum toxin treatment [75]. The improvement provided by the treatment correlated with increased sensorimotor activity and decreased activity in areas unrelated to motor control. The decreases in posterior auditory association cortex and the right ventral precentral gyrus and increases in SMA proper, heteromodal sensory areas (anterior middle temporal gyrus), and periaqueductal gray matter were not affected by the treatment, thus, considered traits of the disorder. During narrative whispering, increased activity was limited to the SMA proper. Treatment produced changes in the pre-SMA, right dorsal precentral gyrus, caudate, anterior putamen, ventral thalamus, pulvinar, cerebellar hemisphere, and vermis. Therefore, basal ganglia function is not particularly different between healthy volunteers and SD patients, but it is one of the areas where botulinum toxin treatment shows a marked effect.

SD patients showed increased extent of activation in the primary sensorimotor cortex, insula, and superior temporal gyrus during symptomatic and asymptomatic tasks and decreased activation extent in the basal ganglia, thalamus, and cerebellum only during asymptomatic tasks. The extent of activation in the primary sensorimotor cortex and ventral thalamus during a symptomatic task, and in the inferior temporal cortex and cerebellum during symptomatic and asymptomatic voice production, was greater in patients with the abductor form of dysphonia than for those with the adductor form [76].

All aspects of the speech control system [77], including unimodal and heteromodal cortices, basal ganglia, and SMA, have altered function and structure in SD. Pathways extending from the motor cortex to the midbrain are also affected.

Focal Hand Dystonia

Among all the dystonias, focal hand is the most studied one using imaging techniques. Most studies find deficits in the sensory and motor circuits. The gray matter volumes as assessed with VBM of the basal ganglia [78] and the sensorimotor cortices [79] of focal hand dystonia patients differ from those of healthy volunteers. Some of the structural changes are shared with other dystonia types. For example, the volume of the globus pallidus internus and the orbitofrontal cortex are less in dystonic patients than healthy volunteers, but these changes are not specific to focal hand dystonia [56]. Volume changes might be related to plasticity. Evidence for this is that the volume of the middle section of the putamen gray matter in pianists, with and without dystonia, covaries with the variability of their keystroke timing during scale playing. Patients have more variability, and the volume of the middle section of the right putamen is larger in patients than in healthy piano players [80].

Plasticity of the morphological changes is also observed in the white matter. FA values of the corticospinal tract were shown to be larger for musicians than nonmusicians [81], suggesting that practice can effect changes independent of disease. An ROI comparison of FA values of the small white matter region between the basal

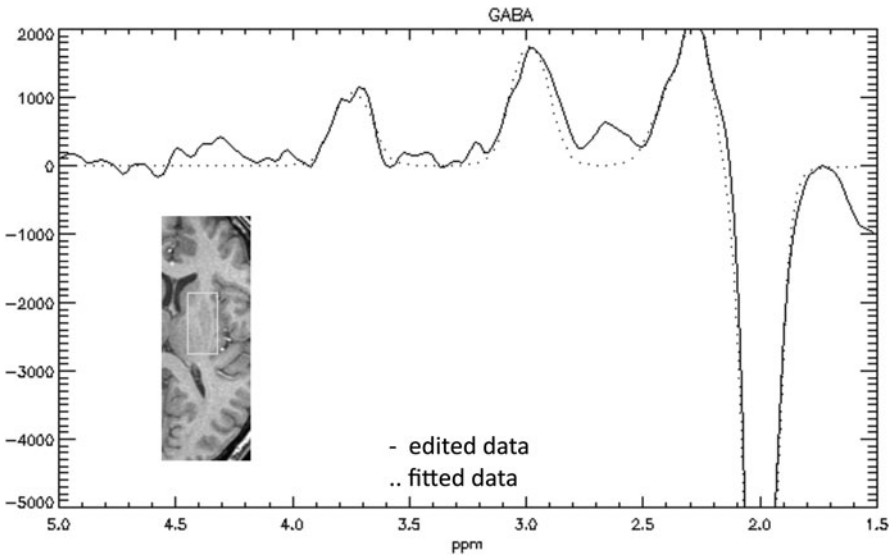

Fig. 11.3 Magnetic resonance spectroscopy. Example of the spectra for GABA (g (gamma)-aminobutyric acid) edited signal from a single subject (data from [85]). *Inset* brain section shows voxel location. *Trace* shows edited MRS with the GABA peak at 3.0 ppm, and the inverted NAA peak at 2.0 ppm

ganglia and thalamus showed left/right asymmetry in two patients with focal hand dystonia before treatment that reversed after botulinum toxin treatment [58]. Writer's cramp patients had increased FA values bilaterally in the posterior limb of the internal capsule and adjacent structures, involving tracts connecting primary sensorimotor areas and subcortical structures [82].

Sensorimotor cortex and basal ganglia of patients were reported to have reduced levels of GABA measured with MRS [83]. This would be in accordance with the concept of reduced inhibition seen in electrophysiological studies [84]. However, the voxel size for GABA MRS is rather large (on the order of tens of cubic centimeters), making it difficult to detect signals when different tissues are part of the region of observation (Fig. 11.3). An attempt to confirm these findings in a second MRS study with improved technique observed only a trend [85]. MRS showed no differences in N-acetylaspartate/creatine or lactate/creatine in the lentiform nucleus [85, 86] or the sensorimotor area [85].

Several studies looked at CBF and metabolism during performance of tasks that generate or do not generate dystonic postures. During a writing task, writer's cramp patients had impaired activation in the contralateral primary motor cortex and enhanced frontal activation. Improvements in writing, seen after botulinum toxin treatment, were accompanied by increases in parietal cortex and caudal SMA activations; however, the impairment persisted in the primary motor cortex [87]. In another study, the primary sensory cortex was overactive in writer's cramp patients

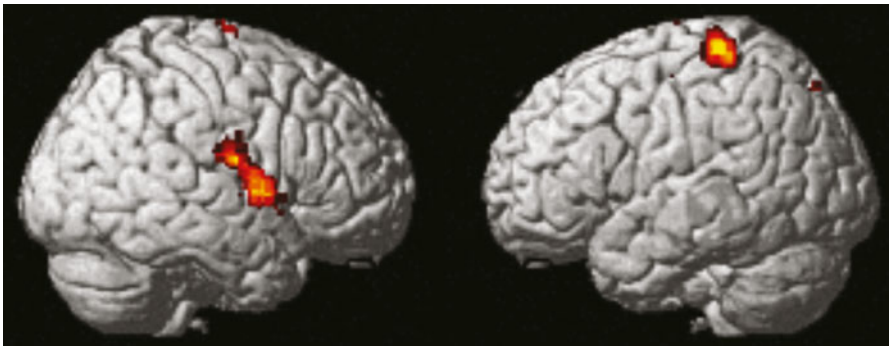

Fig. 11.4 [^{15}O] H_2O PET in focal hand dystonia patients (data from [88]). Regional cerebral blood flow in primary and secondary sensory areas correlates with patients' subjective dystonia score

during a writing task. This change in rCBF, measured with $H_2{}^{15}O$ PET, correlated with subjective patients' scores (Fig. 11.4). The activity in the primary sensory and motor cortices correlated with electromyography (EMG) activity during writing. The sensory changes suggested a possible dysfunction of sensory feedback [88]. When vibrotactile stimulation was applied to either arm, the rCBF response, measured with $H_2{}^{15}O$ PET, was decreased bilaterally in sensorimotor cortices and SMA, even though patients had unilateral symptoms. These changes did not depend on muscle cocontraction, since healthy volunteers had even larger responses when stimulation was applied during muscle contraction [89, 90]. Putamen rCBV measured with $C^{15}O$, rCBF, and $H_2{}^{15}O$ show no functional alteration in patients; however, D_2 binding measured with ^{18}F-spiperone is decreased in patients [91]. Nevertheless, ^{18}F-N-methyl-benperidol (NMB), a more selective D2 receptor that excludes serotonin receptors (5-HT_{2A}), failed to reproduce D2 receptor changes [92]. These results indicate a complex mechanism for the disorder where there are subclinical brain deficits and unclear neurotransmitter alterations.

Several fMRI studies compared task performance and brain activations between healthy volunteers and focal hand dystonia patients. They found differences in brain activity even when performance was matched [93–95]. A comparison between guitar players with and without dystonia found the patients' group to have increased activity in the contralateral sensorimotor cortex and decreased activity bilaterally in the premotor areas when performing hand movements, irrespective of whether the task triggered dystonia or not [94]. Extension or relaxation of the wrist resulted in decreased activation of the sensorimotor cortex and the SMA in writers' cramp patients compared with controls, suggesting deficits both in inhibitory and excitatory mechanisms [95]. When patients tried to control an isolated finger movement, they had less activation in the primary sensory area, associative parietal areas, and right sensorimotor area of the cerebellum than when they were moving two fingers together (Fig. 11.5). These decreases were significantly more pronounced in patients than in healthy volunteers. Nevertheless, patients had increased functional connectivity between the left posterior putamen, left sensorimotor cortex, and left cerebellum. The left anterior putamen connectivity also differed in the bilateral SMA, bilateral

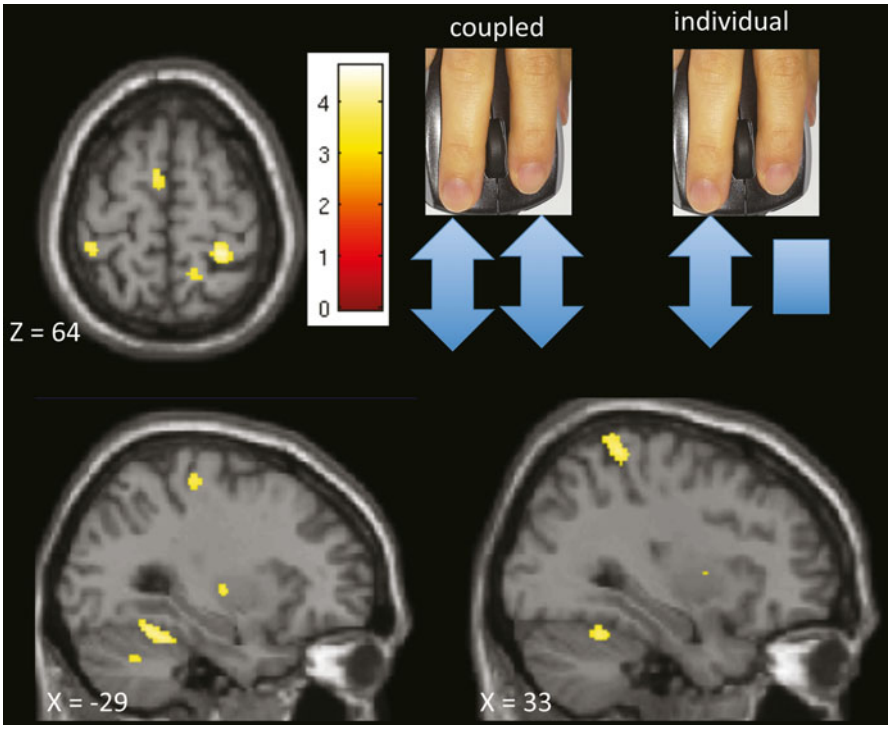

Fig. 11.5 fMRI study of focal hand dystonia (FHD) patients (data from [93]). Compared with healthy volunteer activations, FHD patients show widespread deficits when controlling individual finger movements compared with performing the same movement with both fingers. Healthy volunteers have more activation in the supplementary motor area (SMA), cerebellum, bilateral putamen and bilateral sensory cortex when performing different tasks with each finger (individual task) than when both fingers do the same. Patients show less difference in these areas, suggesting lack of surround inhibition in the FHD

motor cingulate area, left primary motor area, premotor cortex, and left cerebellum, suggesting a compensatory mechanism [93].

Somatosensory finger representation is less demarcated in patients than in controls. It differs between dystonic musicians and healthy nonmusician controls, with patients having smaller distances between individual finger representation [96]. Sensory representation of the fingers had lower spatial separation for patients; the order of the representation was also reversed in the secondary sensory cortex and posterior parietal cortex in patients compared with controls [97]. Another study showed that digits involved in writing (D1, D2, and D3) had smaller interdigit separation in area 3b and overlapping activity, while the distance for asymptomatic digits was preserved. The cluster location, closer to the symptomatic digits, suggested that dystonic symptoms could arise from reduced cortical spacing. In another study, sensory input elicited a lower response in patients' area 3a [98]. Somatotopy is also affected in patients' basal ganglia. Another fMRI study showed that, in patients, the representation

of hand, lip, and toe movements was disorganized in the left putamen, contralateral to the affected side, and to a lesser extent, on the ipsilateral side [99]. Moreover, while the brain response to sensory stimulation of individual fingers predicts the activation from combined stimulation with a 12 % error for the healthy controls, prediction error is 30 % for patients, suggesting a nonlinear interaction [100].

Repetitive transcranial magnetic stimulation (rTMS) of patients' primary sensory cortices can produce a subjective benefit in writing quality. In one study, these improvements were paralleled by bilateral increases in the blood oxygen level-dependent (BOLD) signal on fMRI in the primary sensory cortex, parietal cortex, and SMA. There were neither behavioral nor imaging changes after sham stimulation [101]. Basal ganglia also have abnormal responses to motor tasks. One study showed that after performing a motor task, BOLD signal in the motor area returned to baseline; however, the basal ganglia activation level remained elevated in patients [102]. In another study, basal ganglia and thalamus were hyperactive during tactile stimulation of the index finger of writer's cramp patients, suggesting a deficit in the center-surround inhibition within their circuits. Basal ganglia and thalamus interaction is also affected in musicians with focal hand dystonia; they were active in healthy volunteers, but not in patients during finger tapping [103]. Basal ganglia and thalamic deficits may lead to compensation with augmented activations in cerebellum and cortical areas. This was seen in a study showing increased activity in the posterior vermis, right paramedian cerebellar hemisphere, and dorsal pons, which correlated with disease severity [104]. Patients also had hyperactivity in areas of the visual cortex, anterior insula, and intraparietal sulcus.

Several studies compared finger tapping in healthy volunteers and focal hand dystonia patients. One of them found that while cerebellum and contralateral sensorimotor and premotor areas were active in both groups, ipsilateral activation in the premotor area was larger in patients during tapping with the affected hand, and left cerebellar activation was reduced in patients when tapping with either hand [103]. Another study reported that the execution of simple or complex finger-tapping activates primary motor cortex, primary sensory cortex, SMA, left insula, and bilateral cerebellum. In this study, musicians and writer's cramp patients activated the same network as controls, but to a lower level for both the symptomatic and nonsymptomatic hands [105]. To avoid confounds due to symptomatic task execution in focal hand dystonia patients, a couple of studies explored motor imagery of different hand movements in patients and healthy controls. One study compared imagery of grasping a pencil and writing with grasping the same pencil to sharpen it. Writing imagery produced larger activation than sharpening imagery in the left dorsal premotor area, an area involved in task planning. But, when the grasping was evaluated, healthy volunteers used more of the ventral premotor cortex, while focal hand dystonia patients relied on the dorsal premotor cortex [106]. A second study compared the imagery of writing from a kinesthetic perspective with the observation of a hand performing the movement subjects were asked to imagine. In patients, writing imagery produced an activation deficit of the left sensorimotor cortex, mesial SMA, and left premotor cortex, bilateral putamen, and bilateral thalamus when compared with the writing observation condition [107]. As in the other dystonias, focal hand dystonia affects

structure and function of the components of the motor control circuit and the sensory networks. These alterations are observed as structural changes in white and gray matter. Functional changes are seen not only for tasks triggering dystonia, but also for a variety of tasks not related to the dystonia.

Conclusions and Future Directions

The basal ganglia, originally thought to be the sole origin of dystonia, can now be seen as one player in a more widespread dysfunction. Involvement of the cerebral cortex, in particular, sensorimotor, SMA, and parietal association areas, are consistent in all the primary dystonias. The cerebellum is also affected in all the dystonias discussed here. Unfortunately, there is a large variability of results found in imaging studies across groups and modalities. There are a number of reasons for this, including variation in patient characteristics, MRI hardware, and sequences employed; but, some results are also likely false positives due to small sample sizes. Till date, imaging has not produced a biomarker of dystonia, but has been helpful in expanding our understanding of the brain areas affected. Electrophysiology and imaging studies support the concepts of surround inhibition, compensation, and network imbalance as mechanisms for the disorder. Basal ganglia-thalamo-cortical, cerebellar-thalamo-cortical circuits, and the communication between sensory and motor areas seem to play key roles. What is not yet clear is which of the observed changes are the root causes of the dystonia and which ones are consequences. The ability to study manifesting and nonmanifesting carriers of the DYT1 gene or musicians with and without dystonia is helping to separate the plasticity that compensates for a deficit from the maladaptive plasticity that could result in dystonia. As noted at the outset, the main clinical role for neuroimaging in dystonia, at present, is to identify a secondary cause.

Key elements for further advances in understanding the pathophysiology of dystonias will come from multimodal strategies, where neuroimaging is expected to keep playing a pivotal role. Current studies pinpointed areas of interest, which not only can be studied with pathology, but also guide new imaging studies. It is expected that images obtained at high magnetic field (7 T or higher) will provide an increased signal-to-noise ratio and allow for higher resolution that could help solve the discrepancies seen in morphometric studies. High-order fields also will have an impact on what can be learned from MRS studies.

Another aspect that will improve our understanding the dystonias is having larger populations and longitudinal studies. The latter will be fundamental to delineate which features are causal and which are consequences of the disorder. Finally, as the dystonias are focal and action related, dynamic studies, either based on PET with new radioligands or on more specific fMRI designs, will clarify our understanding of network interactions.

References

1. Muller U, Kupke KG. The genetics of primary torsion dystonia. Hum Genet. 1990;84:107–15.
2. Muller J, Kiechl S, Wenning GK, et al. The prevalence of primary dystonia in the general community. Neurology. 2002;59:941–3.
3. Muller U. The monogenic primary dystonias. Brain. 2009;132:2005–25.
4. Hallett M. Blepharospasm: recent advances. Neurology. 2002;59:1306–12.
5. Hallett M, Evinger C, Jankovic J, Stacy M. Update on blepharospasm: report from the BEBRF International Workshop. Neurology. 2008;71:1275–82.
6. Peckham EL, Lopez G, Shamim EA, et al. Clinical features of patients with blepharospasm: a report of 240 patients. Eur J Neurol. 2011;18:382–6.
7. Jankovic J, Tsui J, Bergeron C. Prevalence of cervical dystonia and spasmodic torticollis in the United States general population. Parkinsonism Relat Disord. 2007;13:411–6.
8. Ludlow CL. Spasmodic dysphonia: a laryngeal control disorder specific to speech. J Neurosci. 2011;31:793–7.
9. Adler CH, Edwards BW, Bansberg SF. Female predominance in spasmodic dysphonia. J Neurol Neurosurg Psychiatry. 1997;63:688.
10. Cohen SM, Kim J, Roy N, Asche C, Courey M. Prevalence and causes of dysphonia in a large treatment-seeking population. Laryngoscope. 2012;122:343–8.
11. Bartolome FM, Fanjul S, Cantarero S, Hernandez J, Garcia Ruiz PJ. Primary focal dystonia: descriptive study of 205 patients. Neurologia. 2003;18:59–65.
12. Ashburner J, Friston KJ. Voxel-based morphometry-the methods. Neuroimage. 2000;11: 805–21.
13. Pierpaoli C, Basser PJ. Toward a quantitative assessment of diffusion anisotropy. Magn Reson Med. 1996;36:893–906.
14. Behrens TE, Berg HJ, Jbabdi S, Rushworth MF, Woolrich MW. Probabilistic diffusion tractography with multiple fibre orientations: what can we gain? Neuroimage. 2007;34:144–55.
15. Behrens TE, Woolrich MW, Jenkinson M, et al. Characterization and propagation of uncertainty in diffusion-weighted MR imaging. Magn Reson Med. 2003;50:1077–88.
16. Fox PT, Mintun MA, Raichle ME, Herscovitch P. A noninvasive approach to quantitative functional brain mapping with H2 (15)O and positron emission tomography. J Cereb Blood Flow Metab. 1984;4:329–33.
17. De Graaf RA. In vivo NMR spectroscopy: principles and techniques. Chichester: Wiley; 1998.
18. Bandettini PA, Wong EC, Hinks RS, Tikofsky RS, Hyde JS. Time course EPI of human brain function during task activation. Magn Reson Med. 1992;25:390–7.
19. Biswal B, Yetkin FZ, Haughton VM, Hyde JS. Functional connectivity in the motor cortex of resting human brain using echo-planar MRI. Magn Reson Med. 1995;34:537–41.
20. Draganski B, Schneider SA, Fiorio M, et al. Genotype-phenotype interactions in primary dystonias revealed by differential changes in brain structure. Neuroimage. 2009;47:1141–7.
21. Carbon M, Su S, Dhawan V, Raymond D, Bressman S, Eidelberg D. Regional metabolism in primary torsion dystonia: effects of penetrance and genotype. Neurology. 2004;62:1384–90.
22. Carbon M, Argyelan M, Eidelberg D. Functional imaging in hereditary dystonia. Eur J Neurol. 2010;17(Suppl 1):58–64.
23. Argyelan M, Carbon M, Niethammer M, et al. Cerebellothalamocortical connectivity regulates penetrance in dystonia. J Neurosci. 2009;29:9740–7.
24. Eidelberg D. Abnormal brain networks in DYT1 dystonia. Adv Neurol. 1998;78:127–33.
25. Trost M, Carbon M, Edwards C, et al. Primary dystonia: is abnormal functional brain architecture linked to genotype? Ann Neurol. 2002;52:853–6.
26. Garibotto V, Romito LM, Elia AE, et al. In vivo evidence for GABA(A) receptor changes in the sensorimotor system in primary dystonia. Mov Disord. 2011;26:852–7.
27. Hallett M. Pathophysiology of dystonia. J Neural Transm Suppl. 2006;70:485–8.
28. Asanuma K, Ma Y, Okulski J, et al. Decreased striatal D2 receptor binding in non-manifesting carriers of the DYT1 dystonia mutation. Neurology. 2005;64:347–9.

29. Carbon M, Niethammer M, Peng S, et al. Abnormal striatal and thalamic dopamine neurotransmission: genotype-related features of dystonia. Neurology. 2009;72:2097–103.
30. Hallett M. The neurophysiology of dystonia. Arch Neurol. 1998;55:601–3.
31. Ghilardi MF, Carbon M, Silvestri G, et al. Impaired sequence learning in carriers of the DYT1 dystonia mutation. Ann Neurol. 2003;54:102–9.
32. Carbon M, Ghilardi MF, Argyelan M, Dhawan V, Bressman SB, Eidelberg D. Increased cerebellar activation during sequence learning in DYT1 carriers: an equiperformance study. Brain. 2008;131:146–54.
33. Etgen T, Muhlau M, Gaser C, Sander D. Bilateral grey-matter increase in the putamen in primary blepharospasm. J Neurol Neurosurg Psychiatry. 2006;77:1017–20.
34. Obermann M, Yaldizli O, De Greiff A, et al. Morphometric changes of sensorimotor structures in focal dystonia. Mov Disord. 2007;22:1117–23.
35. Martino D, Di Giorgio A, D'Ambrosio E, et al. Cortical gray matter changes in primary blepharospasm: a voxel-based morphometry study. Mov Disord. 2011;26:1907–12.
36. Murai H, Suzuki Y, Kiyosawa M, et al. Positive correlation between severity of blepharospasm and thalamic glucose metabolism. Case Report Ophthalmol. 2011;2:50–4.
37. Horovitz SG, Ford A, Najee-ullah MA, Ostuni JL, Hallett M. Anatomical correlates of blepharospasm. Transl Neurodegener. 2012;1:12.
38. Suzuki Y, Kiyosawa M, Wakakura M, Mochizuki M, Ishii K. Gray matter density increase in the primary sensorimotor cortex in long-term essential blepharospasm. Neuroimage. 2011;56:1–7.
39. Fabbrini G, Pantano P, Totaro P, et al. Diffusion tensor imaging in patients with primary cervical dystonia and in patients with blepharospasm. Eur J Neurol. 2008;15:185–9.
40. Kerrison JB, Lancaster JL, Zamarripa FE, et al. Positron emission tomography scanning in essential blepharospasm. Am J Ophthalmol. 2003;136:846–52.
41. Suzuki Y, Mizoguchi S, Kiyosawa M, et al. Glucose hypermetabolism in the thalamus of patients with essential blepharospasm. J Neurol. 2007;254:890–6.
42. Emoto H, Suzuki Y, Wakakura M, et al. Photophobia in essential blepharospasm-a positron emission tomographic study. Mov Disord. 2010;25:433–9.
43. Feiwell RJ, Black KJ, McGee-Minnich LA, Snyder AZ, MacLeod AM, Perlmutter JS. Diminished regional cerebral blood flow response to vibration in patients with blepharospasm. Neurology. 1999;52:291–7.
44. Hutchinson M, Nakamura T, Moeller JR, et al. The metabolic topography of essential blepharospasm: a focal dystonia with general implications. Neurology. 2000;55:673–7.
45. Obermann M, Yaldizli O, de Greiff A, et al. Increased basal-ganglia activation performing a non-dystonia-related task in focal dystonia. Eur J Neurol. 2008;15:831–8.
46. Dresel C, Haslinger B, Castrop F, Wohlschlaeger AM, Ceballos-Baumann AO. Silent event-related fMRI reveals deficient motor and enhanced somatosensory activation in orofacial dystonia. Brain. 2006;129:36–46.
47. Schmidt KE, Linden DE, Goebel R, Zanella FE, Lanfermann H, Zubcov AA. Striatal activation during blepharospasm revealed by fMRI. Neurology. 2003;60:1738–43.
48. Baker RS, Andersen AH, Morecraft RJ, Smith CD. A functional magnetic resonance imaging study in patients with benign essential blepharospasm. J Neuroophthalmol. 2003;23:11–5.
49. Dresel C, Bayer F, Castrop F, Rimpau C, Zimmer C, Haslinger B. Botulinum toxin modulates basal ganglia but not deficient somatosensory activation in orofacial dystonia. Mov Disord. 2011;26:1496–502.
50. Lee MS, Marsden CD. Movement disorders following lesions of the thalamus or subthalamic region. Mov Disord. 1994;9:493–507.
51. Larumbe R, Vaamonde J, Artieda J, Zubieta JL, Obeso JA. Reflex blepharospasm associated with bilateral basal ganglia lesion. Mov Disord. 1993;8:198–200.
52. Sadnicka A, Hoffland BS, Bhatia KP, van de Warrenburg BP, Edwards MJ. The cerebellum in dystonia—help or hindrance? Clin Neurophysiol. 2012;123:65–70.
53. Zerrate MC, Pardo CA, Jinnah HA. Neuropathology in idiopatic cervical dystonia. Mov Disord. 2007;22:1.

54. Becker G, Berg D, Rausch WD, Lange HK, Riederer P, Reiners K. Increased tissue copper and manganese content in the lentiform nucleus in primary adult-onset dystonia. Ann Neurol. 1999;46:260–3.
55. Becker G, Naumann M, Scheubeck M, et al. Comparison of transcranial sonography, magnetic resonance imaging, and single photon emission computed tomography findings in idiopathic spasmodic torticollis. Mov Disord. 1997;12:79–88.
56. Egger K, Mueller J, Schocke M, et al. Voxel based morphometry reveals specific gray matter changes in primary dystonia. Mov Disord. 2007;22:1538–42.
57. Pantano P, Totaro P, Fabbrini G, et al. A transverse and longitudinal MR imaging voxel-based morphometry study in patients with primary cervical dystonia. AJNR Am J Neuroradiol. 2011;32:81–4.
58. Blood AJ, Tuch DS, Makris N, Makhlouf ML, Sudarsky LR, Sharma N. White matter abnormalities in dystonia normalize after botulinum toxin treatment. Neuroreport. 2006;17:1251–5.
59. Bonilha L, de Vries PM, Vincent DJ, et al. Structural white matter abnormalities in patients with idiopathic dystonia. Mov Disord. 2007;22:1110–6.
60. Blood AJ, Kuster JK, Woodman SC, et al. Evidence for altered basal ganglia-brainstem connections in cervical dystonia. PLoS One. 2012;7:e31654.
61. Federico F, Lucivero V, Simone IL, et al. Proton MR spectroscopy in idiopathic spasmodic torticollis. Neuroradiology. 2001;43:532–6.
62. Leenders K, Hartvig P, Forsgren L, et al. Striatal [11C]-N-methyl-spiperone binding in patients with focal dystonia (torticollis) using positron emission tomography. J Neural Transm Park Dis Dement Sect. 1993;5:79–87.
63. Hierholzer J, Cordes M, Schelosky L, et al. Dopamine D2 receptor imaging with iodine-123-iodobenzamide SPECT in idiopathic rotational torticollis. J Nucl Med. 1994;35:1921–7.
64. Naumann M, Pirker W, Reiners K, Lange KW, Becker G, Brucke T. Imaging the pre- and postsynaptic side of striatal dopaminergic synapses in idiopathic cervical dystonia: a SPECT study using [123I] epidepride and [123I] beta-CIT. Mov Disord. 1998;13:319–23.
65. Galardi G, Perani D, Grassi F, et al. Basal ganglia and thalamo-cortical hypermetabolism in patients with spasmodic torticollis. Acta Neurol Scand. 1996;94:172–6.
66. Lalli S, Piacentini S, Franzini A, et al. Epidural premotor cortical stimulation in primary focal dystonia: clinical and (18) F-fluoro deoxyglucose positron emission tomography open study. Mov Disord. 2012;27:533–8.
67. de Vries PM, Johnson KA, de Jong BM, et al. Changed patterns of cerebral activation related to clinically normal hand movement in cervical dystonia. Clin Neurol Neurosurg. 2008;110:120–8.
68. Obermann M, Vollrath C, de Greiff A, et al. Sensory disinhibition on passive movement in cervical dystonia. Mov Disord. 2010;25:2627–33.
69. Opavsky R, Hlustik P, Otruba P, Kanovsky P. Sensorimotor network in cervical dystonia and the effect of botulinum toxin treatment: a functional MRI study. J Neurol Sci. 2011;306:71–5.
70. Opavsky R, Hlustik P, Otruba P, Kanovsky P. Somatosensory cortical activation in cervical dystonia and its modulation with botulinum toxin: an FMRI study. Int J Neurosci. 2012;122:45–52.
71. Schaefer S, Freeman F, Finitzo T, et al. Magnetic resonance imaging findings and correlations in spasmodic dysphonia patients. Ann Otol Rhinol Laryngol. 1985;94:595–601.
72. Simonyan K, Ludlow CL. Abnormal structure-function relationship in spasmodic dysphonia. Cereb Cortex. 2012;22:417–25.
73. Simonyan K, Tovar-Moll F, Ostuni J, et al. Focal white matter changes in spasmodic dysphonia: a combined diffusion tensor imaging and neuropathological study. Brain. 2008;131:447–59.
74. Hirano S, Kojima H, Naito Y, et al. Cortical dysfunction of the supplementary motor area in a spasmodic dysphonia patient. Am J Otolaryngol. 2001;22:219–22.
75. Ali SO, Thomassen M, Schulz GM, et al. Alterations in CNS activity induced by botulinum toxin treatment in spasmodic dysphonia: an $H_2{}^{15}O$ PET study. J Speech Lang Hear Res. 2006;49:1127–46.

76. Simonyan K, Ludlow CL. Abnormal activation of the primary somatosensory cortex in spasmodic dysphonia: an fMRI study. Cereb Cortex. 2010;20:2749–59.
77. Hickok G, Poeppel D. The cortical organization of speech processing. Nat Rev Neurosci. 2007;8:393–402.
78. Black KJ, Ongur D, Perlmutter JS. Putamen volume in idiopathic focal dystonia. Neurology. 1998;51:819–24.
79. Garraux G, Bauer A, Hanakawa T, Wu T, Kansaku K, Hallett M. Changes in brain anatomy in focal hand dystonia. Ann Neurol. 2004;55:736–9.
80. Granert O, Peller M, Jabusch HC, Altenmuller E, Siebner HR. Sensorimotor skills and focal dystonia are linked to putaminal grey-matter volume in pianists. J Neurol Neurosurg Psychiatry. 2011;82:1225–31.
81. Imfeld A, Oechslin MS, Meyer M, Loenneker T, Jancke L. White matter plasticity in the corticospinal tract of musicians: a diffusion tensor imaging study. Neuroimage. 2009;46: 600–7.
82. Delmaire C, Vidailhet M, Wassermann D, et al. Diffusion abnormalities in the primary sensorimotor pathways in writer's cramp. Arch Neurol. 2009;66:502–8.
83. Levy LM, Hallett M. Impaired brain GABA in focal dystonia. Ann Neurol. 2002;51:93–101.
84. Hallett M. Pathophysiology of writer's cramp. Hum Mov Sci. 2006;25:454–63.
85. Herath P, Gallea C, van der Veen JW, Horovitz SG, Hallett M. In vivo neurochemistry of primary focal hand dystonia: a magnetic resonance spectroscopic neurometabolite profiling study at 3 T. Mov Disord. 2010;25:2800–8.
86. Naumann M, Warmuth-Metz M, Hillerer C, Solymosi L, Reiners K. 1H magnetic resonance spectroscopy of the lentiform nucleus in primary focal hand dystonia. Mov Disord. 1998;13:929–33.
87. Ceballos-Baumann AO, Sheean G, Passingham RE, Marsden CD, Brooks DJ. Botulinum toxin does not reverse the cortical dysfunction associated with writer's cramp. A PET study. Brain. 1997;120(Pt 4):571–82.
88. Lerner A, Shill H, Hanakawa T, Bushara K, Goldfine A, Hallett M. Regional cerebral blood flow correlates of the severity of writer's cramp symptoms. Neuroimage. 2004;21:904–13.
89. Tempel LW, Perlmutter JS. Abnormal vibration-induced cerebral blood flow responses in idiopathic dystonia. Brain. 1990;113(Pt 3):691–707.
90. Tempel LW, Perlmutter JS. Abnormal cortical responses in patients with writer's cramp. Neurology. 1993;43:2252–7.
91. Perlmutter JS, Stambuk MK, Markham J, et al. Decreased [18F] spiperone binding in putamen in idiopathic focal dystonia. J Neurosci. 1997;17:843–50.
92. Karimi M, Moerlein SM, Videen TO, et al. Decreased striatal dopamine receptor binding in primary focal dystonia: a D2 or D3 defect? Mov Disord. 2011;26:100–6.
93. Moore RD, Gallea C, Horovitz SG, Hallett M. Individuated finger control in focal hand dystonia: an fMRI study. Neuroimage. 2012;61:823–31.
94. Pujol J, Roset-Llobet J, Rosines-Cubells D, et al. Brain cortical activation during guitar-induced hand dystonia studied by functional MRI. Neuroimage. 2000;12:257–67.
95. Oga T, Honda M, Toma K, et al. Abnormal cortical mechanisms of voluntary muscle relaxation in patients with writer's cramp: an fMRI study. Brain. 2002;125:895–903.
96. Elbert T, Candia V, Altenmuller E, et al. Alteration of digital representations in somatosensory cortex in focal hand dystonia. Neuroreport. 1998;9:3571–5.
97. Butterworth S, Francis S, Kelly E, McGlone F, Bowtell R, Sawle GV. Abnormal cortical sensory activation in dystonia: an fMRI study. Mov Disord. 2003;18:673–82.
98. Nelson AJ, Blake DT, Chen R. Digit-specific aberrations in the primary somatosensory cortex in writer's cramp. Ann Neurol. 2009;66:146–54.
99. Delmaire C, Krainik A, Tezenas du Montcel S, et al. Disorganized somatotopy in the putamen of patients with focal hand dystonia. Neurology. 2005;64:1391–6.
100. Sanger TD, Pascual-Leone A, Tarsy D, Schlaug G. Nonlinear sensory cortex response to simultaneous tactile stimuli in writer's cramp. Mov Disord. 2002;17:105–11.

101. Havrankova P, Jech R, Walker ND, et al. Repetitive TMS of the somatosensory cortex improves writer's cramp and enhances cortical activity. Neuro Endocrinol Lett. 2010;31:73–86.
102. Blood AJ, Flaherty AW, Choi JK, et al. Basal ganglia activity remains elevated after movement in focal hand dystonia. Ann Neurol. 2004;55:744–8.
103. Kadota H, Nakajima Y, Miyazaki M, et al. An fMRI study of musicians with focal dystonia during tapping tasks. J Neurol. 2010;257:1092–8.
104. Peller M, Zeuner KE, Munchau A, et al. The basal ganglia are hyperactive during the discrimination of tactile stimuli in writer's cramp. Brain. 2006;129:2697–708.
105. Wu CC, Fairhall SL, McNair NA, et al. Impaired sensorimotor integration in focal hand dystonia patients in the absence of symptoms. J Neurol Neurosurg Psychiatry. 2010;81: 659–65.
106. Delnooz CC, Helmich RC, Medendorp WP, Van de Warrenburg BP, Toni I. Writer's cramp: increased dorsal premotor activity during intended writing. Hum Brain Mapp. 2013;34: 613–25.
107. Castrop F, Dresel C, Hennenlotter A, Zimmer C, Haslinger B. Basal ganglia-premotor dysfunction during movement imagination in writer's cramp. Mov Disord. 2012;27:1432–9.

Chapter 12
Neuroimaging in Essential Tremor

Corneliu C. Luca and Fatta B. Nahab

Introduction

Essential tremor (ET) is one of the most common neurological disorders with a prevalence of 0.9 % in the general population that increases with age, with an estimated 4.6 % of individuals above 65 having the diagnosis [1]. Clinical onset is bimodal, with some manifesting symptoms early in life, while others report tremors beginning in late life. In contradistinction to the rest tremors of idiopathic Parkinson disease (iPD), ET is characterized by action tremors that occur during movement. Further distinctions in tremor type include separation of tremors during fixed antigravity body movements, referred to as postural tremors, from tremors occurring during dynamic movements called kinetic tremors. Tremors most frequently involve the upper extremities, head and voice in decreasing frequency, with an unclear relationship between action tremors of the lower limbs and orthostatic tremors that are only elicited during standing [2].

Recent developments in the understanding of the ET suggest that it is a slowly evolving degenerative process with associated nonmotor symptoms such as cognitive dysfunction, anxiety, depression, and hearing loss [3]. Neuropathological data is compatible with the presence of cerebellar degeneration and characteristic axonal swelling in the Purkinje cells (torpedoes) [4], together with less consistent findings of Lewy body pathology in the brainstems of ET patients. However, these findings have not been replicated by other groups [5]. There is a strong genetic component in the pathogenesis of ET. LINGO-1 gene mutations have been associated with the

C. C. Luca (✉)
Department of Neurology, Miller School of Medicine, University of Miami, 1150 NW 14th Street, PAC Suite 401, Miami, FL 33136, USA
e-mail: cluca@med.miami.edu

F. B. Nahab
Department of Neuroscience, University of California, San Diego, 8950 Villa La Jolla Drive, Suite C112, La Jolla, CA 92037, USA
e-mail: fnahab@ucsd.edu

F. B. Nahab, N. Hattori (eds.), *Neuroimaging of Movement Disorders,* Current Clinical Neurology 44, DOI 10.1007/978-1-62703-471-5_12,

disease [6]; however, the great majority of cases have not been linked with the gene defect suggesting the disease has a multifactorial etiology.

Clinical Diagnosis

Diagnosis of ET is done clinically based on medical history and the results of a neurologic examination [7]. Supporting factors include a strong family history of action tremors, presence of a 5–7 Hz action tremor that increases with stress, and reduction of tremor amplitude with alcohol consumption. Therapies for ET remain limited due to the lack of understanding of pathophysiological mechanisms. Response to primidone and propranolol is often seen; however, 30 % of patients do not respond to these treatments [8]. Recent published guidelines for ET treatment suggested that besides primidone and propranolol that are established as effective (level A), alprazolam, atenolol, gabapentin, sotalol, and topiramate are probably effective (level B) [9]. Deep brain stimulation (DBS) of the thalamic nucleus ventrointermedius (Vim) has also been shown to be efficacious and is recommended in patients with significant impairment in activities of daily living (ADLs) that do not respond to pharmacological therapies.

Pathophysiology

The pathophysiology of ET is not completely understood, but clinical and imaging studies point to cerebellar involvement. The tremor is thought to be mediated by neuronal loops that involve cerebello-thalamo-cortical (CTC) pathways (reviewed in [10]). Current hypotheses about the source of tremor generation in ET suggest that neuronal pacemakers located within subcortical structures, most likely in the cerebellar circuit, are responsible for tremor oscillations. However, there has been no report of direct recording of neuronal discharges from the cerebellum itself in patients with ET; particularly, since DBS of cerebellar structures has never been performed clinically [11]. The thalamus also plays an important role in tremor generation. The Vim nucleus is the main cerebellar receiving area and the current DBS target for ET, whereas nucleus ventralisoralis posterior (Vop) is the main pallidal-receiving area. Direct brain recordings of local field potentials from Vim and Vop of patients with ET find coherence with electromygraphic (EMG) recordings of tremor at the site of tremor [12]. The role of cortex in ET has also been studied using a number of noninvasive techniques in humans. Electrophysiological studies examining the relationship between EMG tremor oscillations and electroencephalography (EEG) have shown the presence of cortico-muscular coherence at the tremor frequency [13]. Magnetoencephalography (MEG) studies have shown coherence with tremor in the contralateral primary motor cortex, premotor cortex, thalamus, brainstem, and ipsilateral cerebellum [14].

Overview of Neuroimaging in Essential Tremor (ET)

Functional imaging studies such as single-photon emission computed tomography (SPECT), positron emission tomography (PET), and functional magnetic resonance imaging (fMRI) have been used to explore the metabolic and hemodynamic changes that develop in the ET brain and the neural networks involved. These metabolic and hemodynamic techniques correlate indirectly with neuronal activity and synaptic activity, permitting the study of network changes noninvasively. Determining the best method to use requires an in-depth understanding of the strengths and limitations of the various techniques, including the need for high temporal resolution, high spatial resolution, or some intermediate technique providing a balance.

In some cases, there is a clinical overlap between ET and iPD, with patients evolving from a typical ET tremor to a combination of action and resting tremors and/or other findings consistent with iPD such as rigidity or bradykinesia. In contrast to iPD, ET patients show little or no loss of dopaminergic innervation, suggesting different pathophysiologic mechanisms for the two disorders. However, there is growing evidence of overlap between ET and iPD, based on shared clinical features, epidemiology, imaging, and pathological findings. Due to clinical heterogeneity in some cases where it is difficult to separate ET from iPD, imaging techniques are available to clinically evaluate presynaptic dopaminergic function. Furthermore, the overlap between ET and iPD is likely contributing to the presence of PD cases associated with so-called "scans without evidence of dopamine deficiency" or "SWEDD" [15]. The next section will discuss both the practical applications of imaging in ET and research-oriented methods that are providing a better understanding of ET pathophysiology.

The use of structural neuroimaging for ET in clinical practice is mainly indicated when atypical features are present, possibly from an alternate diagnosis. Functional neuroimaging using SPECT with [^{123}I]-FP-CIT scan has gained clinical approval for differentiation of ET tremor from PD tremor in spite of controversies regarding the need or utility of such a method [16]. The need for precise identification of thalamic structures involved in ET tremor control for effective DBS targeting has led to a recent explosion in the use of both structural and functional imaging techniques for this application. However, the vast majority of neuroimaging techniques applied to ET continue to be used solely for research purposes.

Structural Magnetic Resonance Imaging (MRI) Findings in Essential Tremor (ET)

Based on clinical and pathological findings, abnormal CTC pathways have been implicated in the pathogenesis of ET. Before the era of computational neuroanatomy, manual and semiautomated methods were qualitatively used to evaluate the ET brain. The use of conventional MRI T2-weighted imaging showed atrophy of dentate and red nuclei, along with changes in signal intensity in the cerebello-rubral thalamic

tracts in a group of 7 patients with ET [17]. Diffusion-weighted imaging (DWI) typically shows increased water apparent diffusion coefficient (ADC) changes in brain areas where neuronal or axonal losses occur as a consequence of ischemia, inflammation, or neurodegeneration. DWI has therefore been used in patients with ET to look for evidence of tissue abnormalities. In a comparative study of 10 ET patients and 10 matched controls [18], the ADC values assessed in various regions of interest (ROIs) were similar in both ET patients and controls. It is difficult, however, to draw conclusions since exploratory neuroimaging studies are frequently limited by relatively low statistical power due to small sample sizes and poor sensitivity of the methods.

T1-weighted MRI is widely used in more objective and quantitative brain morphometry studies due to its ability to provide contrast between gray and white matter in most cortical areas. However, in subcortical areas with increased iron content, contrast decreases significantly and can create difficulty in the tissue classification algorithms. In the case of ET, thalamic nuclei morphology has been explored extensively due to the need for precise targeting during DBS. High-field MRI at 4.7 T has been used to better define the thalamic nuclei using automated segmentation [19]. Progress in the mapping of basal ganglia and thalamic nuclei has been made with the development of 7 T MRI that offers high spatial resolution and clear delineation of globus palidus pars externa (GPe), globus palidus pars interna (GPi), subthalamic nucleus (STN), and substantianigra (SN). This method enabled precise characterization of white matter tracts that comprise the basal ganglia and thalamic circuitry, and allowed the reconstruction of white matter pathways and their connectivity [20]. High-field imaging provides new tools that can be used to investigate alterations in basal ganglia and thalamic connectivity in patients with ET and other movement disorders.

Anatomical Variability in Essential Tremor (ET)

Voxel-based morphometry (VBM) is a fully automated approach that assesses regional differences between groups of subjects in both white and gray matter. Various preprocessing steps are carried out to ensure uniformity across subjects, including differences in brain size and appearance. While VBM has been used to search for regional brain changes in many neurological disorders, only a handful of studies have been done in ET. Furthermore, results from these studies have been contradictory. Some studies found evidence of cerebellar atrophy [21], including the anterior vermis [22], and reduced gray matter volumes of subcortical structures [21], while other studies using similar techniques found no differences [23]. Benito-León et al. [24] observed white matter changes in patients with ET versus controls in multiple regions, including right cerebellum, left medulla, right parietal lobe, and right limbic lobe; gray matter changes were found in bilateral cerebellum, bilateral parietal lobes, right frontal lobe, and right insula suggesting widespread neurodegeneration. Similar findings demonstrating widespread gray matter atrophy in bilateral posterior

cerebellum, vermis, insular regions, bilateral frontal, and temporal lobes have been reported in a recent VBM study also performed using 3 T MRI [25]. The studies reported here illustrate the limitations associated with VBM and similar techniques that may produce different results depending on the exact methodological approaches, hardware utilized, or even biological differences within the study population, making it more challenging to identify generalizable information about the pathophysiology of ET [26].

White Matter Integrity in Essential Tremor (ET)

Diffusion tensor imaging (DTI) has been used extensively for evaluation of brain white matter structure. DTI provides an indirect measure of neuronal integrity, particularly the white matter, based on the degree of restriction imposed on the diffusion of water molecules by various structures within the brain and referred to as "anisotropy." White matter pathology disrupts the orderly orientation of myelinated (hydrophobic) axons, and leads to a reduction in tissue anisotropy. The anisotropy and diffusion of different brain tissues are measured by fractional anisotropy (FA) and mean diffusivity (MD), respectively.

Using regions of interest (ROI) analysis, Klein found an increased MD bilaterally in the inferior cerebellar peduncles and reduced FA in the right inferior cerebellar peduncles [27]. Whole-brain analyses with tract-based spatial statistics (TBSS) detected increased MD in white matter fibers of ET patients predominantly in the left parietal region, while there was no significant FA differences in these areas between ET patients and controls. Nicoletti et al. [28] assessed 25 patients with ET, 15 with iPD and 15 controls and found reduced FA values in the dentate nucleus and superior cerebellar peduncle of patients with ET. MD values were increased in the superior cerebellar peduncle of the ET group compared with iPD patients and healthy controls. These studies suggest that neurodegenerative pathology of cerebellar structures may play a role in ET. Further evidence for axonal injury of cerebral and cerebellar white matter fibers in patients with ET has been provided by a recent study performed by Saini et al. [29]. Using DTI in 22 ET and 17 controls, an increase of MD and radial diffusivity in right frontoparietal white matter was found. Axial diffusivity was increased in bilateral cerebral hemispheres, thalamus, brainstem, and cerebellum, whereas FA was unchanged. The basis for the variability of white matter changes observed in this and prior DTI studies is poorly understood. Furthermore, little is currently known about the relationship between various DTI measures and brain structural integrity. Some authors attribute this asymmetry to handedness or tremor laterality. Since there is some correlation between the white matter changes and tremor severity, it has been speculated that the white matter abnormalities detected by DTI reflect secondary degeneration of afferent fibers due to Purkinje cell loss in the cerebellum [28]. However, Saini et al. [29] found no correlation between white matter changes and tremor severity, raising the possibility that changes in brain

seen with DTI are secondary to a neurodegenerative process that is independent of tremor.

Despite findings of widespread white matter abnormalities in ET, studies till date have failed to show a consistent pattern that explains the mechanism of tremor generation. Possible reasons for these discrepancies are small sample size, limited phenotypic characterization of subjects, and methodological differences. In order to overcome these limitations, large longitudinal studies of well-characterized patients are needed to assess if the changes in cerebellum and subcortical structures correlate with tremor severity, and if these changes are primary or secondary to cerebellar degeneration.

Another emergent application of imaging in ET is the use of DTI to better define the thalamic nuclei for accurate lead placement in patients undergoing DBS. Current targeting methods for DBS rely extensively on anatomical atlases in order to select the location for electrode placement. While such methods are helpful, they are not able to account for anatomical variations across individuals. The use of DTI to improve targeting of thalamic nuclei, based on the characteristic fiber orientations of corticothalamic and thalamocortical striations within each nucleus, is now being explored [30, 31]. The assessment of structural connectivity of a brain region also provides information about its remote connectional partners and, hence, its function. Using diffusion tractography probabilistic connectivity, unique patterns of cortical connectivity have been identified between the motor cortex and thalamic nuclei. Based on these connectivity patterns, the location of Vim and ventralisoralis anterior (Voa) nuclei can be determined individually for each patient. Tractogram signal intensity was found to be highest in the primary motor cortex when Vim seeding was used, while dorsolateral prefrontal cortex and supplementary motor area (SMA) showed highest intensity after nucleus Vop seeding [32, 33].

The effectiveness of tremor control has been found to be maximal when stimulating target thalamic regions with the greatest structural connectivity to SMA and premotor cortex (PMC) [34]. However, based on the structural connectivity between thalamus and area M1, it has been proposed that the primary motor cortex is essential in the successful stimulation for tremor treatment in patients with ET [35], providing further evidence for the importance of thalamo-cortical loops in tremor control. Moreover, recent studies showed that beside M1, SMA, and PMC, cerebellar structures are important in tremor controls. Coenen et al. [36] used DTI to target the dentato-rubro-thalamic tract for DBS and showed good tremor control after stimulation. These findings suggest that thalamocortical and cerebellothalamic projections converge around the tremor-suppressive and electrophysiologically defined Vim site in humans. DTI used in conjunction with DBS has also proven useful for guiding tremor therapies to the CTC circuit. The future integration of DTI tractography into surgical planning holds promise for improved stereotactic planning and outcomes, while continuing to increase understanding of ET pathophysiology. Prospective, randomized, and blinded trials evaluating the superiority of high-resolution DTI-based targeting compared with current anatomical atlas-based methods will however be needed before wide-scale adoption of these more complex techniques become the standard of care. Patients undergoing DBS electrode placement also provide a rare

opportunity for direct functional validation of DTI data in humans, because the stimulation target and the seed region for probabilistic tractography represents a region that is functionally and putatively anatomically congruent across subjects.

Functional Magnetic Resonance Imaging (fMRI)

Functional MRI (fMRI) is a useful technique for exploring brain dysfunctions in neurological disorders and has been successfully employed for characterizing neural networks. The technique most commonly used in fMRI studies is based on the principle of blood oxygen level-dependent (BOLD) contrast changes. BOLD-fMRI uses the different magnetic properties of oxygenated and deoxygenated hemoglobin to identify regional blood flow changes in the brain. BOLD changes during voluntary movements have been associated mainly with activation in the contralateral sensorimotor cortex, subcortical regions, and ipsilateral cerebellum, together with significant deactivation in the ipsilateral sensorimotor cortex subcortical regions, and contralateral cerebellum [37].

Till date, there are only a handful of fMRI studies that evaluate BOLD changes related with ET. Subjects with ET manifesting tremors during fMRI not only show contralateral activation of the primary motor and primary sensory areas, globus pallidus, and thalamus, but also bilateral activation of the dentate nucleus, cerebellar hemispheres, and red nucleus [38]. Subjects with writing tremor similarly show bilateral cerebellar hemisphere activation, along with marked activation of the left sensorimotor cortex (S1, M1) [39].

The functional changes in sensorimotor cortex secondary to ET were investigated using fMRI in patients undergoing Vim thalamotomy. Activation in the sensorimotor cortex and SMA that are normally evoked by wrist passive movement were preserved after thalamotomy; however, activation at the fundus of the central sulcus (Brodmann area 3a) was significantly decreased. These findings suggested that area 3 may be responsible for tremor generation, since disruption of the thalamocortical pathway produces significant decrease in its activation [40]. However, it is unclear whether these changes represent a primary effect or simply mirror the reduction in tremor post-DBS.

During verbal working memory task, patients with ET show altered functional connectivity between cerebellum and regions implicated in attention (dorsolateral prefrontal cortex, inferior parietal lobule and thalamus) [41]. Also, fronto-parietal overactivation is present in patients with ET during a Stroop task [42], suggesting that ET patients require additional cognitive effort to achieve comparable performance levels on test of attentional control.

An intrinsic limitation to the performance of fMRI in a population being asked to manifest tremor in the confined space of an MRI scanner is the task-correlated motion artifact that is generated. Additional confounds are also of concern when attempting to compare subjects with ET manifesting involuntary tremors, with controls often asked to mimick tremors since the performance is inevitably different.

One way these confounds can be avoided is with the exploration of brain network connectivity at rest. Such resting-state fMRI (RS-fMRI) techniques dramatically limit motion artifacts and task performance confounds. However, this technique assumes that the observed fMRI changes are trait specific and not state specific. In other words, affected brain networks remain dysfunctional whether or not tremors are present. Anderson et al. [43] assessed functional connectivity during RS-fMRI between different brain regions and showed that connectivity between the primary motor cortex, cerebellar motor cortex, and thalamus is greatest in the thalamic voxels located within 3 mm of clinically optimized targets for deep brain stimulation in ET. In another study, fMRI connectivity between the cerebellum and the motor network was analyzed in ET patients before and after repetitive transcranial magnetic stimulation (rTMS) applied to the posterior cerebellar cortex [44]. rTMS represents a valid tool for modulating the cerebello-cortical output. At baseline, the cerebellar vermis of patients with ET showed impaired functional connectivity with the rest of the CTC. rTMS over the cerebellum significantly reduced the tremor amplitude and restored the abnormal information functional connectivity in the motor cortex in line with the current view that the pacemaker responsible for ET is present in the cerebellar network. In our own work, preliminary data shows increased connectivity between brainstem and cerebellar structures at rest (no tremor present) in ET subjects compared with controls (Fig. 12.1, unpublished results). The structural and functional imaging studies presented above support the idea that ET is associated with abnormalities in the CTC network and therapies should specifically target this loop.

Positron Emission Tomography (PET)

PET is a sensitive imaging technique involving the intravenous injection of radiolabeled ligands binding to specific molecular targets. PET can provide information about the regional distribution and affinity of receptors in the brain or cerebral metabolism noninvasively and with high sensitivity in the living brain. The regional cerebral metabolic rate of glucose can be assessed using [^{18}F]-fluoro-2-deoxyglucose (FDG). Using FDG PET, Hallett and Dubinsky [45] demonstrated increased activation in medullary structures and thalamus in ET patients, but not in the cerebellum. Other PET studies have used ^{15}O-labeled water to measure regional cerebral blood flow and showed an increased flow bilaterally in the cerebellum with normal olivary activity in the ET group [46]. A variety of PET studies have demonstrated involvement of the motor system in ET, including contralateral thalamus, striatum, sensorimotor, and premotor cortex, as well as the red nucleus and parietal cortex [47–49].

Functional brain imaging with PET and 6-[^{18}F]-fluoro-L-dopa (FDOPA) is commonly used to assess the nigrostriatal dopamine system in iPD. In ET, most studies have not shown significant changes in striatal FDOPA uptake. However, one study by Brooks et al. [50] showed a 10–13 % reduction in FDOPA uptake in the striatum

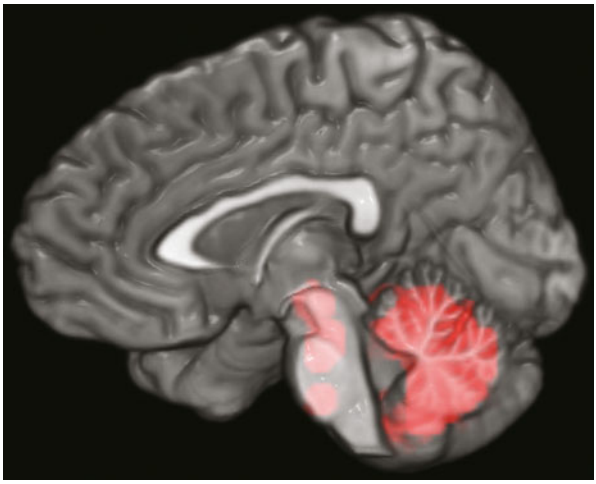

Fig. 12.1 Conjunction analysis of resting-state fMRI-based connectivity map demonstrating greater connectivity in brainstem and cerebellar structures in ET subjects compared with controls despite the absence of tremor in both groups

of patients with ET when compared with controls, suggesting in some cases an overlap between the ET- and iPD-associated nigrostriatal degeneration. The pattern of striatal uptake loss varied by disorder, with predominant loss in caudate in ET and tremor-dominant iPD, while predominately reduced uptake in the putamen was seen in akinetic-rigid iPD.

PET has also been used to assess changes in the oscillatory brain network of ET after DBS. PET studies in patients with ET during tremor-suppressive Vim DBS demonstrated increased regional cerebral blood flow (rCBF) in the ipsilateral primary motor cortex [51] and in the ipsilateral supplementary motor area [52]. Vim DBS was also shown to normalize reduced cerebellar inhibition on the M1 area [53], though it remains unclear whether these findings simply reflected the reduction in tremors post-DBS.

The hyperactivity in the CTC circuits have led to the hypothesis that disturbance in γ-aminobutyric acid (GABA), an inhibitory neurotransmitter in the CNS, is responsible for ET [54]. This is supported by the tremor suppression properties of GABAergic medications, and by decreased GABA receptor densities in the dentate nucleus of ET patients [55]. GABAergic function has been assessed using [^{11}C]-flumazenil PET, a benzodiazepine receptor sites ligand, in a group of 8 patients with bilateral ET, as compared with 11 healthy controls. Significant increases in [^{11}C]-flumazenil binding at the GABA(A) receptor concentrations were found in the cerebellum, ventrolateral thalamus, and lateral premotor cortex of the ET group. This impaired GABA function is thought to reflect an overactivity of the CTC circuits seen in ET [56].

While PET provides unique contributions not afforded by MRI, certain limitations continue to limit its widespread utility. These include relatively low spatial resolution, exposure to ionizing radiation, the need for an extensive infrastructure to synthesize the tracers, and the short half-life of the radionucleotides used. Furthermore, PET cannot provide anatomical information by itself and is often combined with computed

tomography in order to show both metabolic functions and accurate anatomical structures.

Single-Photon Emission Computed Tomography (SPECT)

Similarities exist between PET and SPECT-based nuclear-imaging methods, though it is important to understand some basic differences. Whereas PET imaging detects the indirect production of opposite pairs of gamma rays emitted by a positron decay, SPECT imaging directly measures the gamma radiation emitted by the radiotracer. These differences have direct clinical consequences, with SPECT imaging having reduced sensitivity compared with PET. Advantages to SPECT include longer half-life radiotracers, lower cost, and reduced infrastructure required. Among a variety of SPECT radiotracers are cocaine analogues such as [^{123}I]-β-CIT, [^{123}I]-FP-CIT, and [^{18}F]-DOPA. These radioligands label the presynaptic dopamine transporters and are used to quantify nigrostriatal degeneration. SPECT imaging has significant clinical value for the differentiation of patients with ET from patients with iPD based on the consistent findings of decreased ligand binding in the case of iPD.

Striatal [^{123}I]-β-CIT binding in patients with ET was evaluated with the purpose of identifying a subclinical dopaminergic nigrostriatal loss in ET. The binding of β-CIT was shown to be in the normal range in ET patients in accordance with findings from FDOPA PET studies, suggesting that this technique can successfully distinguish between ET and early iPD [57].

[^{123}I]-Ioflupane SPECT has also been used to evaluate dopamine transporter (DAT) binding in ET. Multiple studies report that **DAT**-SPECT can distinguish parkinsonism from ET given the consistent decrease in DAT ligand binding in PD. However, the DAT binding in ET was found to be reduced by 15 % in putamen and 21 % in caudate when compared with healthy subjects. This suggests that some ET patients may present mild abnormalities of striatal dopamine transporters, similar to those seen in iPD [58]. In a follow up study that assessed DAT uptake loss over time, the annual decline of DAT binding was 7.5 % in PD patients. The DAT binding was not changed in the putamen of ET patients, but showed mild reductions in the caudate nucleus [59]. Currently, the clinical utility of [^{123}I]-Ioflupane SPECT is limited to cases when there is clinical uncertainty regarding the diagnosis of ET. Furthermore, a limitation of these studies remains the lack of a validated quantitative measure to apply clinically. Attempts to develop such a measure suggest that a striatal asymmetry index is useful in differentiating iPD from other disorders.

Magnetic Resonance Spectroscopy (MRS)

MRS is a powerful method for direct and noninvasive identification of major metabolites in the brain. MRS can make in vivo inferences about the neuropathology of ET

by characterizing the relative proportions of different brain metabolites. Furthermore, measurement of concentration and synthesis rates of specific biochemical compounds can be obtained, with spatial localization, in defined areas in the brain. Typically, ^{1}H-MRS can detect metabolites reflecting neuronal density and integrity, markers of energy metabolism or inflammation, as well as neurotransmitters (see Chap. 1 for additional details). In the setting of ET, MRS studies have detected a selective reduction of the neuronal marker N-acetyl-aspartate (NAA) in the cerebellum that correlates with the severity of tremor [60, 61]. The reduction in cerebellar NAA/Creatine (Cr) represents neuronal damage or loss and suggests, similar to other imaging studies, that ET may be a neurodegenerative disease that affects the cerebellum.

Magnetoencephalography (MEG)

MEG is a method used for mapping brain activity by recording magnetic fields occurring naturally in the brain, using superconducting quantum interference devices (SQUIDS). The availability of MEG systems and modern spatial filter-based analysis tools permits the analysis of oscillatory cerebral networks in ET and has the potential to provide new insights into the physiological mechanisms of motor control and pathophysiological mechanisms of tremor disorders.

Using a localization technique called dynamic imaging of coherent sources (DICS) to identify cerebral areas coherent with the EMG signal at tremor frequency (5–7 Hz), patients with ET showed coherence to the contralateral primary motor cortex, premotor cortex, thalamus, brainstem, and ipsilateral cerebellum [14]. MEG-EEG dynamic coherence is able to distinguish changes in the tremor network between the ET patients and voluntary mimicked tremors. Muthuraman et al. [62] identified symmetric and direct connections between thalamic regions and motor cortex, forming thalamocortical loops responsible for pathologic oscillations and providing further evidence regarding the tremor network in ET. These observations lead to the conclusion that the inferior olive, cerebellar nuclei, and the thalamus are key structures in the tremor network with cortical motor regions being intermittently entrained in the tremor rhythm in thalamocortical loops [63].

Transcranial Sonography (TCS)

TCS allows high-resolution imaging of deep brain structures and is able to identify increased echogenicity of substantianigra in iPD. Substantia nigra hyperechogenicity (SN+) on TCS is defined as an enlargement of the echogenic area of the SN in the brainstem. Previous studies have demonstrated that SN+ is associated with increased vulnerability of the nigrostriatal dopaminergic system and a risk factor for iPD. Most of the studies published thus far have shown that SN+ is a typical finding in about

90 % of patients with iPD, but not in patients with ET [64]. In ET patients, the prevalence of SN+ is in the range of healthy control subjects or slightly above [65], which may indicate an increased risk for iPD in the subgroup of ET patients. Further studies are needed to establish whether this same subgroup of ET with SN+ may go on to develop iPD. Midbrain sonography shows SN+ in 13 % of patients with ET, 91 % of PD patients, and 10 % of healthy subjects [66].

TCS sensitivity and specificity has also recently been examined alongside [^{123}I]-FP-CIT SPECT to differentiate iPD from ET. Findings showed sensitivity and specificity of TCS for detection of iPD were 86 and 93 %, respectively, suggesting that TCS can reliably differentiate between ET and iPD [67].

Conclusions and Future Directions

The exploration of structural and functional correlates of ET using neuroimaging has led to significant progress in the past decade. Findings till date implicate both cortical, subcortical, brainstem, and cerebellar areas in the ET brain. These widespread changes also provide support for ET being a neurodegenerative disorder, though this remains highly controversial. Despite the consistent findings of cerebellar involvement in ET, much work remains in trying to separate those brain changes that are a direct consequence of ET from more nonspecific changes seen during the process of generating a tremor. Furthermore, ET is a highly heterogeneous disorder with varying age of onset, heredity, and phenotype. Future studies of ET will need to markedly extend phenotypic–genotypic characterization and classification while combining various imaging modalities to achieve both high spatial and temporal resolutions. Achieving these objectives will provide a better understanding of clinical-genetic-imaging correlations, and ultimately shed light on the molecular basis underlying ET.

References

1. Louis ED, Ferreira JJ. How common is the most common adult movement disorder? Update on the worldwide prevalence of essential tremor. Mov Disord. 2010;25(5):534–41.
2. Deuschl G, Raethjen J, Hellriegel H, Elble R. Treatment of patients with essential tremor. Lancet Neurol. 2011;10(2):148–61.
3. Chandran V, Pal PK. Essential tremor: beyond the motor features. Parkinsonism Relat Disord. 2012;18(5):407–13.
4. Louis ED, Faust PL, Vonsattel J-G, et al. Neuropathological changes in essential tremor: 33 cases compared with 21 controls. Brain. 2007;130(12):3297–307.
5. Shill HA, Adler CH, Beach TG. Pathology in essential tremor. Parkinsonism Relat Disord. 2012;18(Suppl 1):S135–7.
6. Tan EK, Teo YY, Prakash KM, et al. LINGO1 variant increases risk of familial essential tremor. Neurology. 2009;73(14):1161–2.
7. Deuschl G, Bain P, Brin M. Consensus statement of the movement disorder society on tremor. Ad hoc scientific committee. Mov Disord. 1998;13(Suppl 3):2–23.

8. Koller WC, Vetere-Overfield B. Acute and chronic effects of propranolol and primidone in essential tremor. Neurology. 1989;39(12):1587–7.
9. Zesiewicz TA, Elble RJ, Louis ED, et al. Evidence-based guideline update: treatment of essential tremor. Neurology. 2011;77(19):1752–5.
10. Raethjen J, Deuschl G. The oscillating central network of essential tremor. Clin Neurophysiol. 2012;123(1):61–4.
11. Shibasaki H. Cortical activities associated with voluntary movements and involuntary movements. Clin Neurophysiol. 2012;123(2):229–43.
12. Kane A, Hutchison WD, Hodaie M, Lozano AM, Dostrovsky JO. Enhanced synchronization of thalamic theta band local field potentials in patients with essential tremor. Exp Neurol. 2009;217(1):171–6.
13. Hellwig B, Haussler S, Schelter B, et al. Tremor-correlated cortical activity in essential tremor. Lancet. 2001;357(9255):519–23.
14. Schnitzler A, Munks C, Butz M, Timmermann L, Gross J. Synchronized brain network associated with essential tremor as revealed by magnetoencephalography. Mov Disord. 2009;24(11):1629–35.
15. Fekete R, Jankovic J. Revisiting the relationship between essential tremor and Parkinson's disease. Mov Disord. 2011;26(3):391–8.
16. Perlmutter JS, Eidelberg D. To scan or not to scan. Neurology. 2012;78(10):688–9.
17. Fukuhara T, Gotoh M, Asari S, Ohmoto T, Akioka T. Magnetic resonance imaging of patients with intention tremor. Comput Med Imaging Graph. 1994;18(1):45–51.
18. Martinelli P, Rizzo G, Manners D, et al. Diffusion-weighted imaging study of patients with essential tremor. Mov Disord. 2007;22(8):1182–5.
19. Lemaire JJ, Sakka L, Ouchchane L, Caire F, Gabrillargues J, Bonny JM. Anatomy of the human thalamus based on spontaneous contrast and microscopic voxels in high-field magnetic resonance imaging. Neurosurgery. 2010;66(3 Suppl Operative):161–72.
20. Lenglet C, Abosch A, Yacoub E, De Martino F, Sapiro G, Harel N. Comprehensive in vivo mapping of the human basal ganglia and thalamic connectome in individuals using 7 T MRI. PLoS One. 2012;7(1):e29153.
21. Quattrone A, Cerasa A, Messina D, et al. Essential head tremor is associated with cerebellar vermis atrophy: a volumetric and voxel-based morphometry MR imaging study. Am J Neuroradiol. 2008;29(9):1692–7.
22. Cerasa A, Messina D, Nicoletti G, et al. Cerebellar atrophy in essential tremor using an automated segmentation method. Am J Neuroradiol. 2009;30(6):1240–3.
23. Daniels C, Peller M, Wolff S, et al. Voxel-based morphometry shows no decreases in cerebellar gray matter volume in essential tremor. Neurology. 2006;67(8):1452–6.
24. Benito-León J, Alvarez-Linera J, Hernández-Tamames JA, Alonso-Navarro H, Jiménez-Jiménez FJ, Louis ED. Brain structural changes in essential tremor: voxel-based morphometry at 3-tesla. J Neurol Sci. 2009;287(1–2):138–42.
25. Bagepally BS, Bhatt MD, Chandran V, et al. Decrease in cerebral and cerebellar gray matter in essential tremor: a voxel-based morphometric analysis under 3 T MRI. J Neuroimaging. 2012;22(3):275–8.
26. Henley SMD, Ridgway GR, Scahill RI, et al. Pitfalls in the use of voxel-based morphometry as a biomarker: examples from huntington's disease. Am J Neuroradiol. 2010;31(4):711–9.
27. Klein JC, Lorenz B, Kang J, et al. Diffusion tensor imaging of white matter involvement in essential tremor. Hum Brain Mapp. 2011;32(6):896–904.
28. Nicoletti G, Manners D, Novellino F, et al. Diffusion tensor MRI changes in cerebellar structures of patients with familial essential tremor. Neurology. 2010;74(12):988–94.
29. Saini J, Bagepally BS, Bhatt MD, et al. Diffusion tensor imaging: tract based spatial statistics study in essential tremor. Parkinsonism Relat Disord. 2012;18(5):477–82.
30. Wiegell MR, Tuch DS, Larsson HB, Wedeen VJ. Automatic segmentation of thalamic nuclei from diffusion tensor magnetic resonance imaging. Neuroimage. 2003;19(2 Pt 1):391–401.
31. Behrens TE, Johansen-Berg H, Woolrich MW, et al. Non-invasive mapping of connections between human thalamus and cortex using diffusion imaging. Nat Neurosci. 2003;6(7):750–7.

32. Hyam JA, Owen SL, Kringelbach ML, et al. Contrasting connectivity of the ventralis intermedius and ventralis oralis posterior nuclei of the motor thalamus demonstrated by probabilistic tractography. Neurosurgery. 2012;70(1):162–9; discussion 169.
33. Hyam JA, Owen SL, Kringelbach ML, et al. Contrasting connectivity of the vim and vop nuclei of the motor thalamus demonstrated by probabilistic tractography. Neurosurgery. 2011;70(1):162–169.
34. Pouratian N, Zheng Z, Bari AA, Behnke E, Elias WJ, Desalles AA. Multi-institutional evaluation of deep brain stimulation targeting using probabilistic connectivity-based thalamic segmentation. J Neurosurg. 2011;115(5):995–1004.
35. Klein JC, Barbe MT, Seifried C, et al. The tremor network targeted by successful VIM deep brain stimulation in humans. Neurology. 2012;78(11):787–95.
36. Coenen VA, Allert N, Madler B. A role of diffusion tensor imaging fiber tracking in deep brain stimulation surgery: DBS of the dentato-rubro-thalamic tract (drt) for the treatment of therapy-refractory tremor. Acta Neurochir (Wien). 2011;153(8):1579–85; discussion 1585.
37. Allison JD, Meador KJ, Loring DW, Figueroa RE, Wright JC. Functional MRI cerebral activation and deactivation during finger movement. Neurology. 2000;54(1):135–42.
38. Bucher SF, Seelos KC, Dodel RC, Reiser M, Oertel WH. Activation mapping in essential tremor with functional magnetic resonance imaging. Ann Neurol. 1997;41(1):32–40.
39. Berg D, Preibisch C, Hofmann E, Naumann M. Cerebral activation pattern in primary writing tremor. J Neurol Neurosurg Psychiatry. 2000;69(6):780–6.
40. Miyagishima T, Takahashi A, Kikuchi S, et al. Effect of ventralis intermedius thalamotomy on the area in the sensorimotor cortex activated by passive hand movements: FMR imaging study. Stereotact Funct Neurosurg. 2007;85(5):225–34.
41. Passamonti L, Novellino F, Cerasa A, et al. Altered cortical-cerebellar circuits during verbal working memory in essential tremor. Brain. 2011;134(8):2274–86.
42. Cerasa A, Passamonti L, Novellino F, et al. Fronto-parietal overactivation in patients with essential tremor during stroop task. Neuroreport. 2010;21(2):148–51.
43. Anderson JS, Dhatt HS, Ferguson MA, et al. Functional connectivity targeting for deep brain stimulation in essential tremor. AJNR Am J Neuroradiol. 2011;32(10):1963–8.
44. Popa T, Russo M, Vidailhet M, et al. Cerebellar rTMS stimulation may induce prolonged clinical benefits in essential tremor, and subjacent changes in functional connectivity: an open label trial. Brain Stimul. 2013;6(2):175–9.
45. Hallett M, Dubinsky RM. Glucose metabolism in the brain of patients with essential tremor. J Neurol Sci. 1993;114(1):45–8.
46. Boecker H, Wills AJ, Ceballos-Baumann A, et al. The effect of ethanol on alcohol-responsive essential tremor: a positron emission tomography study. Ann Neurol. 1996;39(5):650–8.
47. Jenkins IH, Bain PG, Colebatch JG, et al. A positron emission tomography study of essential tremor: evidence for overactivity of cerebellar connections. Ann Neurol. 1993;34(1):82–90.
48. Wills AJ, Jenkins IH, Thompson PD, Findley LJ, Brooks DJ. Red nuclear and cerebellar but no olivary activation associated with essential tremor: a positron emission tomographic study. Ann Neurol. 1994;36(4):636–42.
49. Wills AJ, Jenkins IH, Thompson PD, Findley LJ, Brooks DJ. A positron emission tomography study of cerebral activation associated with essential and writing tremor. Arch Neurol. 1995;52(3):299–305.
50. Brooks DJ, Playford ED, Ibanez V, et al. Isolated tremor and disruption of the nigrostriatal dopaminergic system: an 18F-dopa PET study. Neurology. 1992;42(8):1554–60.
51. Ceballos–Baumann AO, Boecker H, Fogel W, et al. Thalamic stimulation for essential tremor activates motor and deactivates vestibular cortex. Neurology. 2001;56(10):1347–54.
52. Perlmutter JS, Mink JW, Bastian AJ, et al. Blood flow responses to deep brain stimulation of thalamus. Neurology. 2002;58(9):1388–94.
53. Molnar GF, Sailer A, Gunraj CA, Lang AE, Lozano AM, Chen R. Thalamic deep brain stimulation activates the cerebellothalamocortical pathway. Neurology. 2004;63(5):907–9.
54. Elble RJ, Deuschl G. An update on essential tremor. Curr Neurol Neurosci Rep. 2009;9(4):273–7.

55. Paris-Robidas S, Brochu E, Sintes M, et al. Defective dentate nucleus GABA receptors in essential tremor. Brain. 2012;135(1):105–16.
56. Boecker H, Weindl A, Brooks DJ, et al. GABAergic dysfunction in essential tremor: an 11C-flumazenil PET study. J Nucl Med. 2010;51(7):1030–5.
57. Asenbaum S, Pirker W, Angelberger P, Bencsits G, Pruckmayer M, Brucke T. [123I]beta-CIT and SPECT in essential tremor and Parkinson's disease. J Neural Transm. 1998;105(10–12):1213–28.
58. Isaias IU, Canesi M, Benti R, et al. Striatal dopamine transporter abnormalities in patients with essential tremor. Nucl Med Commun. 2008;29(4):349–53.
59. Isaias IU, Marotta G, Hirano S, et al. Imaging essential tremor. Mov Disord. 2010;25(6):679–86.
60. Louis ED, Shungu DC, Chan S, Mao X, Jurewicz EC, Watner D. Metabolic abnormality in the cerebellum in patients with essential tremor: a proton magnetic resonance spectroscopic imaging study. Neurosci Lett. 2002;333(1):17–20.
61. Pagan FL, Butman JA, Dambrosia JM, Hallett M. Evaluation of essential tremor with multivoxel magnetic resonance spectroscopy. Neurology. 2003;60(8):1344–7.
62. Muthuraman M, Heute U, Arning K, et al. Oscillating central motor networks in pathological tremors and voluntary movements. What makes the difference? Neuroimage. 2012;60(2):1331–9.
63. Raethjen J, Deuschl G. The oscillating central network of essential tremor. Clin Neurophysiol. 2012;123(1):61–4.
64. Stockner H, Wurster I. Transcranial sonography in essential tremor. Int Rev Neurobiol. 2010;90:189–97.
65. Berg D. Hyperechogenicity of the substantia nigra: pitfalls in assessment and specificity for Parkinson's disease. J Neural Transm. 2011;118(3):453–61.
66. Budisic M, Trkanjec Z, Bosnjak J, Lovrencic-Huzjan A, Vukovic V, Demarin V. Distinguishing Parkinson's disease and essential tremor with transcranial sonography. Acta Neurol Scand. 2009;119(1):17–21.
67. Doepp F, Plotkin M, Siegel L, et al. Brain parenchyma sonography and 123I-FP-CIT SPECT in Parkinson's disease and essential tremor. Mov Disord. 2008;23(3):405–10.

Chapter 13
Imaging in Huntington's Disease and Other Choreas

Andrew McGarry and Kevin M. Biglan

Introduction to Huntington's Disease

Huntington's disease (HD) is a progressive, fatal neurodegenerative disorder characterized by loss of neurons in the basal ganglia and cortex, resulting in abnormalities in movement, cognition, and behavior. The genetic defect in HD is a polyglutamine expansion in the IT15 gene on chromosome 4, resulting in a mutant huntingtin protein thought to have toxic effects on transcriptional processes and bioenergetics. Initial clinical manifestations are typically subtle, with mood alterations or insufficiencies of executive function that can develop well in advance of motor manifestations and ultimately lead to disability. While chorea is the cardinal movement disorder associated with HD, dystonia and parkinsonism are common as the disease progresses, eventuating in a hypokinetic, bradyphrenic state. There is currently no cure for HD. Treatments focus on behavioral stabilization, suppression of chorea, and supportive care, and optimization of safety.

Computed Tomography

Computer (assisted) tomography (CT) has been in widespread use to image the neuraxis for decades. In HD it shows progressive atrophy, particularly in the cortex and caudate nuclei [1]. Terrence et al. [1] compared the size of frontal horns and distance

A. McGarry (✉)
Department of Neurology, Movement Disorders Division,
Cooper University Hospital at Rowan University,
3 Cooper Plaza, Suite 320, Camden, NJ 08103, USA
e-mail: McGarry-Andrew@cooperhealth.edu

K. M. Biglan
Department of Neurology, University of Rochester,
1325 Mt. Hope Avenue, Suite 160, Rochester, NY 14620, USA
e-mail: kevin_biglan@urmc.rochester.edu

F. B. Nahab, N. Hattori (eds.), *Neuroimaging of Movement Disorders,*
Current Clinical Neurology 44, DOI 10.1007/978-1-62703-471-5_13,

between caudate nuclei in 12 HD patients, expressed as a frontal horn/bicaudate ratio. This value was significantly reduced compared with controls, reflecting caudate atrophy as a main anatomic feature of HD. Other anatomic parameters have been assessed on CT and compared with clinical performance, including the ratio of bicaudate diameter/external diameter of the skull across the narrowest point of the heads of the caudate nuclei and the bicaudate diameter/maximum internal diameter of the skull [2]. Using these measures, as well as a frontal horn/bicaudate ratio, the authors demonstrated a correlation to functional capacity [2]. Sharma et al. [3] also noted highly significant differences in caudate head volume for HD subjects compared with controls, with radiographic diagnosis using this measure and demonstrating 87.5 % sensitivity. In 11 HD subjects matched for disease duration (5 years) and age of onset (21–30 years), a significant correlation was noted between bicaudate measurement and CAG length [4].

CT has maintained a role in the diagnosis of HD by virtue of reliably demonstrating caudate atrophy in patients who otherwise command attention from a clinical standpoint. From a research perspective, it has been supplanted by higher resolution techniques and functional imaging that allow for the earlier detection of abnormalities and offer more insights into phenotypic relationships and progression.

Magnetic Resonance Imaging

The higher resolution views of cerebral structures possible with magnetic resonance imaging (MRI) precipitated interest in a more accurate characterization of early anatomic changes and disease progression in HD. Aylward et al. [5] performed the first longitudinal study of MRI in HD, in which they compared images taken at least 10 months apart in 23 HD patients at varying stages of disease. They demonstrated significant reduction in volume of the caudate, putamen, and basal ganglia overall, with a correlation to age of onset and CAG length. Neither symptom severity at the time of first imaging nor duration of symptoms correlated to magnitude of volume change. Similarly, Rosas et al. [6] showed that MRI volume of the striatum inversely correlated with CAG number in 27 HD subjects. Frontal volume as well as caudate and putamen volume correlated to cognitive scores (e.g., visuospatial tasks, episodic memory, verbal fluency, perceptual performance) in a study by Backman et al. [7], substantiating the notion of a relationship between frontal atrophy on MRI and cognitive capability. Additional studies by Aylward et al. further evaluated the frontal lobes; they measured gray and white matter volume in 20 mild to moderately affected HD patients as well as normal controls. Frontal lobe volumes were similar between controls and mildly affected subjects, whereas those moderately affected demonstrated 17 % and 28 % reduction in total frontal volume and white matter volume, respectively [8]. Frontal lobe volume, but not total brain volume, correlated with symptom severity and cognitive performance.

Voxel-based morphometry (VBM) is a technique used to spatially normalize MRI signal intensity based on three-dimensional data surrounding a given area, with

improved sensitivity to see more subtle differences in volume [9]. Kassubek et al. [10] looked at 44 symptomatic subjects with voxel-based morphometry (VBM) and observed striatal, hypothalamic, and opercular atrophy relative to age-matched controls. In addition, VBM demonstrated a dorsal-to-ventral gradient of atrophy corresponding to disease severity and histopathologic studies. They also showed global brain volume reduction compared with controls—a seemingly constitutive feature of HD that did not reflect clinical state particularly well. However, more regional atrophy correlated better to clinical deficits [11]. VBM has been shown in other studies of early symptomatic HD to reflect atrophy in the striatum, thalamus, globus pallidus, hypothalamus, amygdala, insular cortex, and premotor/sensorimotor cortices compared with controls [12]. In a longitudinal 12-month study, Ruocco et al. [13] used VBM to evaluate atrophy in relation to CAG length and Unified Huntington's Disease Rating Scale (UHDRS) scores for 49 HD subjects. Larger CAG values correlated to faster and more diffuse atrophy, particularly in the caudate, midbrain, thalamus, insula, and frontal lobes. Rosas et al. [14] used high-resolution surface-based VBM analysis to measure cortical thickness in 33 HD subjects of varying severity. Overall, progressive HD thinning was present in the sensorimotor cortex, superior parietal cortex, occipital cortex, partial superior temporal cortex, precuneus, parahippocampal gyrus, and posterior portions of the superior and middle frontal regions, with particularly early thinning in the sensorimotor and primary visual cortices. Subjects with more dystonia and bradykinesia had more thinning in the anterior frontal cortical regions, inclusive of the premotor and supplementary motor cortices, although striatal volume was no different compared with subjects with more chorea.

Fennema-Notestine et al. [15] observed cortical and striatal atrophy on morphometric analysis as seen in other studies, but also noted reduction in cerebellar gray and white matter volume in 15 HD subjects. In another study, thalamic atrophy was noted in the dorsomedial, centromedian, parafasicular, and ventrolateral nuclei consonant with abnormal clinical performance on verbal fluency tasks and Stroop/Digit Symbol testing [16]. Taken together, MRI allowed the identification of a wide range of anatomic changes in HD not previously appreciated with CT.

MRI in Premanifest Disease

Premanifest HD (pre-HD) has been extensively evaluated with MRI, in an effort to identify the earliest and most reliable predictors of disease onset, burden, and progression. Neuroimaging techniques hold promise as early markers of disease progression and sensitive outcome measures for therapeutic trials aimed at delaying or preventing the onset of disease.

Thieben et al. [17] used VBM in pre-HD subjects to demonstrate volumetric reduction in the left striatum, bilateral insula, dorsal midbrain, and bilateral intraparietal sulci relative to controls. There was also substantial white matter atrophy that was progressive with age in gene-positive subjects. Ciarmello et al. [18] analyzed

71 HD subjects ranging from pre-HD to severe with VBM and also observed significant white matter volume reduction in 24 pre-HD subjects, in addition to general reduction in gray and white matter volume reduction in all stages of disease. Jurgens et al. [19] compared 14 normal controls with 16 motorically asymptomatic HD gene carriers. Despite no notable clinical difference, caudate, putamen, and globus pallidus volumes were significantly reduced in HD compared with controls. Among HD gene-positive subjects, smaller globus pallidus volume correlated to poorer motor performance, whereas a smaller putamen volume correlated to worse scores on the Symbol Digit Modalities Task and Trail Making Test B. Henley et al. [20] looked at whole-brain atrophy in pre-HD cases, finding threefold higher rates of volume reduction (compared with controls) that were proportional to CAG length.

PREDICT-HD was a large, multicenter prospective study that broke ground with respect to intensive study of people at risk for developing HD. The PREDICT-HD investigators evaluated gray matter volume on MRI in premanifest gene carriers [21]. Carriers were divided into three groups on the basis of time to predicted onset (a calculation dependent on CAG length and age). Subjects with at least a 33 % chance of developing HD in 5 years were identified with MRI alone (no other clinical information) 69 % of the time, whereas the accuracy of specifying regions known to selectively change in HD increased to 83 %. The PREDICT group also looked at MRI images from 657 subjects again classified as near (less than 9 years), mid (9–15 years), or far (more than 15 years) from expected clinical onset based on CAG repeat length and age [22]. Total brain volume, cerebrospinal fluid (CSF) volume, striatum, thalamus, cortical gray matter, and white matter all differed significantly compared with controls, with the striatum showing the largest difference as expected; white matter changes were noted as predictive by themselves toward estimated clinical diagnosis, substantiating prior observations regarding the importance of white matter degeneration in HD imaging. In addition, the analysis of a very large cohort helped reify aforementioned data regarding degenerative patterns seen on MRI in numerous smaller studies, and further legitimized following striatal and white matter changes decades in advance of symptomatic disease in the hypothetical context of a therapeutic trial. In 220 pre-HD carriers without motor symptoms from the PREDICT cohort, VBM and cross-sectional analysis of MRI demonstrated gray matter changes in the hypothalamus that were able to distinguish carriers from controls [23]. These changes were seen in some subjects not expected to manifest motorically for a decade or more and are consonant with premotor changes in sleep hygiene, metabolism, and behavior that are well recognized as early elements of HD. The PREDICT cohort was further examined for regional cortical volume changes compared with controls [24]. In 523 pre-HD subjects, the mid-diagnosis and near-diagnosis groups demonstrated significant volume decrement and cortical thinning, most notably in the posterior and superior cerebral regions. In a 2-year longitudinal analysis, 211 premanifest PREDICT subjects of all three groups showed continued atrophy in the striatum, total brain, and white matter, although the cortex both in totality and regionally was not different [25]. Notably, when age-related atrophy was accounted for, white matter atrophy was more statistically significant than that seen in the striatum, further suggesting that white matter changes may be a useful

variable to follow disease progression. Biglan et al. [26] examined the PREDICT cohort for motor changes in premanifest disease utilizing data from 106 gene-negative and 733 gene-positive subjects (277 far, 252 mid, and 184 near diagnosis). Elevated total motor scores at baseline were associated with greater chance of disease diagnosis in the near future and striatal atrophy. Bradykinesia and chorea were most closely correlated with diagnostic immediacy, with multiple motor domains worsening with proximity to diagnosis. In particular, finger tapping, tandem gait, Luria manual sequencing task, and saccade initiation appeared to connote greater diagnostic probability.

Other premanifest studies have added insight to HD neuroanatomy. In a study of 21 pre-HD gene carriers and 21 matched controls, global brain volume and gray matter volumes were significantly decreased, with focal losses particularly notable in the left prefrontal cortex, cerebellum, and right posterior temporal cortex [27]. Visuomotor integration task performance correlated to prefrontal volume loss and CAG number. In a study of 39 pre-HD subjects and 25 controls, automated VBM and tractography using diffusion-weighted images showed not only focal gray matter loss in basal ganglionic and thalamocortical pathways but also diffuse white matter degeneration, suspected to be demyelination [28]. The extent of both gray and white matter changes correlated to estimated time of clinical onset. Faster rates of whole-brain atrophy on MRI over a 2-year period were observed in manifest HD subjects compared with controls, in addition to the suggestion of acceleration from the first to second year [29]. Significant atrophy and acceleration of change were not seen in the premanifest group—an average of nearly two decades from disease onset—nor in the control group. Rosas et al. [30] looked at three groups of HD subjects divided according to the age of onset and observed that earlier disease was associated with more rapid rates of atrophy over longitudinal analysis. Interestingly, cortical atrophy was regionally variable, with faster changes in frontal and parietal regions, whereas there was no difference in the rate of change for basal ganglia between the three groups. Furthermore, although previous studies have suggested a relationship between CAG repeat length and onset as well as rate of progression, many areas in this study did not demonstrate tight correlations to CAG repeats. Taken together, age and CAG length seemed to play only a partial role in rates of atrophy in some regions, suggesting that there may be a number of unidentified environmental or genetic variables that influence HD neurodegeneration. Overall, these studies highlight the substantial anatomic changes that precede clinical signs in HD.

The TRACK-HD prospective observational study aimed to identify biomarkers using 3-T MRI in 123 controls, 123 early symptomatic, and 120 premanifest subjects [31]. Cross-sectional analysis of baseline data demonstrated whole-brain volume and regional gray/white matter volume reduction in premanifest and early HD patients compared with controls. In a 12-month longitudinal examination of the TRACK-HD cohort, generalized and regional brain atrophy was again demonstrated in all premanifest and early HD subjects, with imaging significantly correlated to disease burden and total functional capacity [32]. Cognitive and motor deficits were demonstrable across pre-HD and early HD subgroups, lending credence to the notion of following

such measures as outcome measures for future clinical trials. The TRACK-HD cohort was further analyzed for regional subcortical atrophy, demonstrating continued caudate and putamen volume reduction more than a decade in advance of predicted clinical onset [33]. In addition, the nucleus accumbens and pallidum were atrophic in subjects within a decade of predicted onset. These structures, along with the putamen and hippocampus, had significant associations with motor and psychometric scores. After 24 months, continued atrophy in gray matter, white matter, regional, and whole-brain parameters were observed, with the largest effect sizes in the caudate and white matter [34]. Early HD demonstrated reduction in cognitive and motor outcomes, with the greatest effect size noted in the Symbol Digit Modality Test, in addition to decline of the Total Motor Score and Total Functional Capacity. However, the premanifest cohort demonstrated fewer functional changes despite volume loss, with deficits seen in the Total Motor Score, emotional recognition, and rapid finger taps. As such, premanifest subjects may require larger samples and more sensitive measures going forward in clinical trials, but functional measures such as the Total Motor Score may emerge as useful tools across varying stages of disease.

Other Magnetic Resonance Applications

Using magnetization transfer imaging (MTI), a modality that offers better resolution for white matter diseases, in particular, 16 pre-HD subjects were analyzed using whole-brain, gray matter, and white matter imaging to create histograms [35]. Lower peak heights of the carrier gray matter histogram were significantly associated with worse UHDRS motor performance, whereas lower peak heights for all parameters were associated with CAG length. MTI did not distinguish between carriers and noncarriers, and carriers without clinical changes were not identifiable with this technique. The utility of MTI as a biomarker of progression has not been clarified.

Perfusion MRI, a technique that highlights differences in cerebral blood flow, was evaluated by Wolf et al. [36]. Eighteen premanifest gene carriers demonstrated decreased regional cerebral blood flow (rCBF) in medial and lateral prefrontal regions compared with controls, with increased rCBF in the precuneus. In subjects closer to onset, diminished rCBF was also seen in the putamen, but increased in the hippocampus. Conventional MRI data did not show robust reductions of gray matter volume, raising the possibility of perfusion changes as a useful biomarker independent of volume change. MRI has been evaluated for feasibility of measuring caudate volume reduction in an experimental therapeutic setting during the CARE-HS study [37]. Caudate volume reduction was significant during the 30-month trial, and relatively low numbers of subjects would be required to power a trial for assessing change using this outcome. Bartzokis et al. [38] used field-dependent relaxation rate increase to assess basal ganglia iron content in 11 HD subjects, observing increases in iron in the caudate, putamen, and globus pallidus and decreases in the frontal lobes compared with controls.

Diffusion Tensor Imaging

Diffusion tensor imaging (DTI) is a variant of MRI that relies on the freedom or restriction of water molecule movement to reflect surrounding structural anatomy, with particular applications in assessing the structural integrity of white matter [39]. Bohanna et al. [40] evaluated 17 HD subjects and controls, finding abnormalities in the corpus callosum and external and extreme capsules. The genu of the corpus callosum was more abnormal in more severe cognitive dysfunction, whereas motor symptoms better correlated to body degeneration. In another study, 12 HD subjects and controls were examined for corticostriatal connectivity using DTI [41]. The most robust differences compared with controls were in connections from the primary motor and sensory cortex to the striatum. Motor features of HD correlated to increased mean diffusivity (an index of degeneration) in sensorimotor portions of the striatum. DTI in HD has also demonstrated degeneration in the fornix, external and extreme capsules, inferior frontal occipital fasiculus, and inferior longitudinal fasiculus [42]. Areas of atrophy bore close relationships to levels of motor and cognitive dysfunction.

In 17 premanifest HD gene carriers, Kipps et al. [43] used a tensor-based technique to assess regional gray and white matter volume changes. In a 2-year study, bilateral putaminal, left caudate, left ventral midbrain near the substantia nigra (SN), and bilateral globus pallidus externa atrophy was seen without notable progression clinically. These data further reify a growing sense that anatomic parameters may hold promise to track disease progression independently of clinical measures, with specific potential as a tool in therapeutic trials.

Functional MRI

Functional MRI (fMRI) relies on differences in the magnetic properties of oxygen-rich and oxygen-poor blood to measure changes in cerebral blood flow, with the contrast taken as an index of cellular activity [44]. fMRI has drawn significant attention as a means to assess differences in activity that may reflect pathological process or compensatory measures, given the relationship between neuronal functional demands and perfusion.

Clark et al. [45] reported reduced signal (lessened blood flow) in the occipital, parietal, and motor cortices as well as the caudate for three HD subjects during the Porteus Maze task, a test of visuospatial and executive function, with increased signal in the left postcentral and right middle frontal gyri compared with controls. Elsewhere, HD subjects with chorea were disinhibited in cognitive tasks requiring ignoring priming stimuli before quickly answering questions [45]. This is clinically consistent with impulsivity and correlated with concomitantly increased activity in the caudate and thalamus [46]. In a study of eight premanifest and early symptomatic HD subjects given a reaction time task, significant activation of the right caudate head, bilateral thalami, left middle temporal, right superior temporal, right middle/inferior frontal, and right postcentral gyri was noted, with a relative reduction in comparison

with controls for the right middle frontal, left middle occipital, left precuneus, and left middle frontal gyrus [47]. In a cohort of gene-positive individuals ranging from asymptomatic to severe phenotype, decreased flow was observed in the frontal and temporal cortices as well as the striatum for all subjects, in addition to an inverse relationship between white matter volume and estimated time to symptomatic onset on MRI [48]. Working memory tasks were assessed using fMRI and VBM in 16 presymptomatic HD subjects in comparison with controls [49]; of note, while performance did not differ appreciably, decreased left dorsolateral prefrontal cortical activation was seen in gene-positive subjects with intermediate and high complexity tasks, despite this region lacking cortical atrophy. Reduction of activation in this region also correlated with UHDRS cognitive scores in premanifest subjects. In participants closer to the expected onset of symptoms, the left inferior parietal lobule and right superior frontal gyrus were more active on fMRI. In a study of fMRI combined with T1- and diffusion-weighted MRI (DWI) in premanifest subjects, measurements of the caudate, white matter corticospinal tract, and insular cortex on fMRI correlated well to established methods to characterize disease progression (product of CAG length and age) [50]. Taken together, fMRI offers exciting prospects toward further understanding of dynamic changes in all stages of HD.

Magnetic Resonance Spectroscopy

Magnetic resonance spectroscopy (MRS) offers the ability to identify chemical profiles in areas of interest, which in turn can give an indication of metabolic changes or dysfunction. Substances often evaluated include N-acetyl-aspartate (NAA; a marker of cellular integrity), choline (Cho; an index of membrane synthesis/turnover), creatine (Cr; a measure of metabolism), glutamate/glutamine (Glx; a reflection of bioenergetics), and lactate, also reflecting metabolism [44]. An initial MRS study of five early HD patients demonstrated elevated Glu/Cr ratios in the striatum, with no changes in cortical regions compared with controls [51]. One subject also had this finding in the thalamus, whereas controls displayed no abnormalities. The thalami of 22 HD subjects demonstrated reductions of the NAA/Cr ratio, suggestive of neuronal loss, which did not correlate to motor performance but did correlate to length of illness [52].

Consonant with increasing interest in pre-HD for potential imaging biomarker applications in a variety of modalities, MRS has been evaluated for data it generates in this population as well as symptomatic HD. Eight of 17 clinically affected HD cases as well as four asymptomatic gene carriers all had lactate peaks in the frontal cortices not seen in controls, raising the possibility of evidence for energetic abnormalities in HD [53]. The NAA/Cho ratio, an index of cellular loss, was significantly reduced in symptomatic subjects and proportional to clinical severity. Another evaluation of 31 HD subjects corroborated the finding of elevated lactate in the occipital cortex, as well as in the striatum [54]. Curiously, the striatal changes were highly asymmetric, with more present on the dominant side. Decreases in NAA/Cr ratios as well as

increased Cho/Cr ratios (suggestive of degeneration) were noted and correlated to duration of symptoms as well as CAG repeat length. Three of eight asymptomatic carriers had elevated lactate in the striatum. In another study, decreases in basal ganglia NAA and Cr were seen in severe and premanifest gene carriers, with the latter group found to be motorically and cognitively normal [55]. Reynolds et al. [56] saw no hemispheric differences in the putamens of HD subjects for NAA, Glx, lactate, or Cr, and observed overall reductions in NAA, increased glutamate, elevations in lactate, and reduction of creatine that were heterogenous. Two premanifest subjects showed normal MRS spectra, in contrast to aforementioned findings from other studies. In a study of 17 pre-HD subjects, Cho concentration (an indicator of membrane integrity and turnover) was reduced in frontal cortex compared with controls, with a correlation between reduction and slowing of visuomotor tests [57]. Conversely, no differences were seen for Cho, Cr, and NAA in the putamen and thalamus for 19 pre-HD subjects compared with controls, although decreases in the putamen/thalamus ratio of NAA correlated weakly to the product of CAG length and age [58]. As part of the TRACK-HD study, 85 subjects with premanifest HD, early HD, or control status were assessed with MRS in the left putamen and clinical motor measures [59]. NAA was decreased in early HD as well as premanifest HD, whereas myoinositol (a glial marker) was elevated in early HD compared with premanifest status by 50 %, a change that correlated with motor performance. As such, there is suggestion that MRS may prove capable for identifying abnormalities in presymptomatic subjects as a biomarker, although this role needs to be clarified.

Other studies have investigated whether MRS can detect changes after use of agents thought to facilitate energy abnormalities in HD. Koroshetz et al. [60] also demonstrated increased lactate in the cortex of HD subjects, which decreased after administration of coenzyme Q10, a contributor to oxidative metabolism. This decrease abated after coenzyme Q10 was stopped. In a trial using creatine, a compound thought to boost energy metabolism, administration to 20 symptomatic HD subjects for 8–10 weeks resulted in no change in parietooccipital cortical Cr, Cho, glucose, or lactate [61]. However, Glx was reduced by 7.8 %, potentially suggestive of a reduction of glutaminergic excitotoxic potential. Tabrizi et al. [62] followed 13 HD subjects on creatine supplementation for 2 years and saw sustained presence of higher creatine levels in brain on MRS (as ascertained by NAA/Cr and phosphocreatine (PCr)/ATP ratios) but no overall clinical benefit. Of note, some subjects at similar points in disease trajectory seemed to have differing degrees of improvement in clinical outcome measures, suggesting certain patients may respond preferentially compared with others. This has yet to be substantiated.

Juvenile HD has demonstrated reductions in NAA, Cr, and PCr, consistent with cell loss and altered energetics [63]. Elevated myoinositol was also observed. Another study of seven HD subjects younger than 21 years showed low striatal Cr and diffusely elevated Glx [64].

MRS at 7 T has shown abnormalities in HD [65]. Reduced NAA and Cr were seen in the caudate and putamen of manifest HD subjects, with lower glutamate also seen in the putamen. Controls and pre-HD showed no significant difference, although values in premanifest HD were lower.

Positron Emission Tomography

Positron emission tomography (PET) technology involves the tagging of a biologically active molecule with a radiotracer that is then followed after injection to areas of interest, which in turn can reveal functional or biochemical changes [44]. PET can be coregistered to CT or MRI, thereby superimposing functional and anatomical data. PET holds promise to gain insight into the degenerative processes of HD.

Antonini et al. [66] demonstrated decreased [^{18}F] fluorodeoxyglucose (FDG) and [^{11}C] raclopride uptake (a measure of glucose metabolism and D_2 receptor binding, respectively) in the caudate and putamen of asymptomatic and untreated symptomatic subjects. Reduction in uptake correlated with volume reduction in the caudate over serial images 18 and 36 months later. They also examined the relationship between CAG length, age, and [^{11}C] raclopride D_2 receptor binding in ten asymptomatic and eight manifest HD subjects, finding a correlation between CAG length and reduction of striatal binding divided by age [67]. The slopes of these correlation lines differed significantly for presymptomatic versus symptomatic subjects, with seemingly greater changes in racloproide reduction per unit increase in CAG count for premanifest subjects compared with symptomatic ones, suggesting that striatal degeneration may not be uniform in its progression through the HD disease arc. In a 2-year prospective study of 18 preclinical gene carriers, rate of raclopride binding reduction per year (2.6 %) did not differ significantly from controls [68]. Curiously, in three subjects who developed early features of HD, no change in raclopride binding was observed through this transition.

A study of five HD subjects and five controls showed reduction in D_1 and D_2 postsynaptic receptor density correlating to duration of illness, with a particular reduction in D_1 receptor density in the temporal cortex [69]. Using [^{11}C] B-CIT to bind dopamine transporters (DAT), a 50 % reduction in the striatum was observed; together, these data suggested presynaptic terminal loss and reduction of dopamine transporter as part of degeneration, presumably from cell loss. D_1/D_2 density and DAT binding in the caudate and putamen correlated to cognitive performance for executive functions, visuospatial tasks, episodic memory, verbal fluency, and perception speed/reasoning [70]. H_2[^{15}O] PET was used to compare seven subjects with chorea with controls during rest and while performing paced movements of the dominant arm [71]. While moving, underactive contralateral primary motor, medial premotor, bilateral prefrontal, and bilateral parietal cortices were observed, in addition to increased insular activation bilaterally. This pattern is similar to that seen in Parkinson's disease and speculated to result from striatofrontal pathway degeneration with resultant bradykinesia, an often underappreciated feature of even early HD. H_2[^{15}O] PET was also used in eight HD subjects to assess somatosensory function [72]. Using vibratory stimulation applied to the index finger, decreased activation of the contralateral secondary sensory cortex, parietal Brodmann areas 39 and 40, lingual gyrus, bilateral prefrontal cortex, and contralateral basal ganglia was seen. Of note, ipsilateral primary, secondary, and insular cortex activity was increased; it is not known if this reflects dysfunction or compensatory changes in the setting of

dysfunction. PET using an [^{11}C] flumazenil ligand showed an inverse relationship between raclopride binding and [^{11}C] flumazenil in the putamen, thought to represent increased gamma-aminobutyric acid (GABA) receptor density [73].

In seven subjects who underwent intrastriatal fetal transplantation, PET data over 2 years showed widespread reduction in dopamine D_2 receptor binding and no change in already reduced D_1 receptor binding glucose uptake [74]. Whether this reflects poor graft performance or disease progression is not known, but PET detected no benefit of transplantation. Reuter et al. [75] followed two subjects who were also transplanted with fetal allografts, with one subject demonstrating no clinical or imaging improvement but the other with increased striatal D_2 binding and prolonged clinical improvement over 5 years. Further data are needed to ultimately determine the viability and efficacy of transplantation techniques in HD, with PET potentially serving as a valuable adjunctive means of assessing graft survival.

Pavese et al. [76] used [^{11}C]-PK11195 PET, a measure of microglial activation, as well as [^{11}C] raclopride to demonstrate increased microglial activity in the striatum that correlated to reductions in raclopride, UHDRS scores, and CAG length. As such, there has been speculation for activated microglia as a possible biomarker of disease activity in HD.

Using a novel ligand for type 1 cannabinoid (CB1) receptors, reduced binding was noted diffusely in the cerebrum, cerebellum, and brain stem in 20 symptomatic HD subjects compared with controls [77]. Prefrontal and premotor cortices demonstrated an inverse relationship between binding and CAG length. Mutant huntingtin protein is thought to repress CB1, itself thought to have an important regulatory role in neurotransmission, although a more direct role in HD pathogenesis remains unclear.

Role of PET in Preclinical HD

Similar to conventional MRI, PET has drawn attention as a potentially useful tool for characterizing premanifest HD. In initial studies, 27 preclinical HD gene carriers were examined for [^{18}F]-FDG PET uptake, with two-thirds being normal [78]. D_2 receptor binding measured with raclopride was decreased in 50 % and correlated to age and CAG repeat length. In a study of 18 premanifest HD subjects, 13 early HD subjects, and 8 controls, FDG PET revealed presymptomatic reductions in striatal metabolism as well as mediotemporal and occipital reductions for presymptomatic and early symptomatic participants (Fig. 13.1) [79]. Over the course of 3 years, progressive loss of striatal raclopride binding was also observed in the amygdala, temporal, and frontal cortices in 12 premanifest subjects [80]. UHDRS and cognitive performance tasks correlated poorly to reductions in binding, with the exception of planning tasks (one-touch Tower of London test). Feigin et al. [81] also used raclopride and FDG PET to assess premanifest carriers longitudinally over 44 months, showing progressive decline in striatal D_2 receptor binding. Thalamic metabolism was initially elevated but gradually declined as subjects

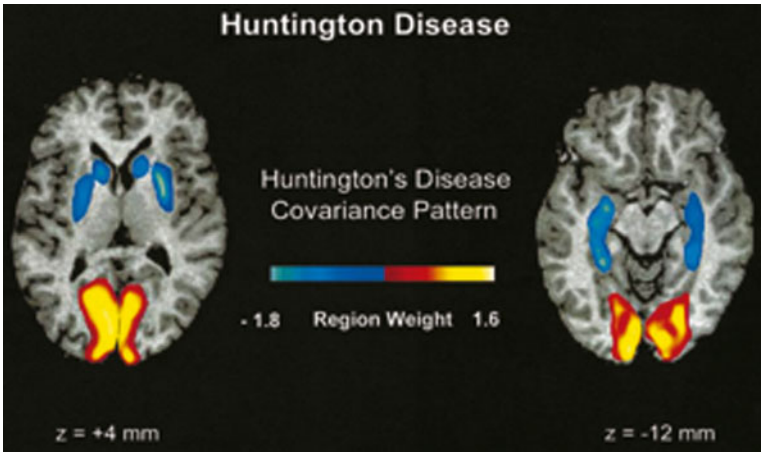

Fig. 13.1 Metabolic network abnormalities in early Huntington's disease, and [^{18}F]-FDG PET study [79]

became symptomatic, suggesting a potential compensatory role for the thalamus as HD evolves.

Using [^{11}C]-PK11195 and raclopride PET in ten premanifest and nine symptomatic HD gene carriers, decreased raclopride binding and increased PK binding was observed for both groups in the hypothalamus, implicating the hypothalamus in disorders of weight maintenance, circadian rhythms, and behavior seen in HD [82].

In a study using magnetic resonance (MR) and PET ([^{11}C]-PK11195 and raclopride), reduced D_2 and D_3 binding was observed in sensorimotor striatum, associative striatum, stria terminalis bed nucleus, amygdala, and hypothalamus in asymptomatic carriers, with further reductions in symptomatic subjects for the SN, globus pallidus, limbic striatum, cingulate, and insula [83]. Microglial activation was increased in areas of premanifest carriers in a similar distribution to reduced dopamine receptor binding, whereas symptomatic subjects also had activated microglia in the globus pallidus, limbic striatum, and anterior prefrontal cortex. Activated microglia in the striatum and regions associated with cognition correlated to sooner predicted onset, raising the possibility that microglia activation may be a biomarker of use in conjunction with early cognitive assessment.

Pavese et al. [84] used raclopride to demonstrate decreased cortical binding in 62.5 % of symptomatic HD subjects and 54.5 % of premanifest carriers, particularly in the temporal and frontal areas. Symptomatic HD subjects with reductions in binding fared worse on executive function and attention testing than those with normal cortical binding. Conversely, D_2 receptor binding as assayed by [^{11}C] FLB 457 was not significantly altered compared with controls in the thalamus and cortex of early-to-middle-stage HD subjects in a PET study by Esmaeilzadeh et al. [85], whereas the striatum was reduced as expected.

Single Photon Emission Computed Tomography

Single photon emission computed tomography (SPECT) allows the combination of a radiotracer and ligand to be localized to a region relevant to the chosen ligand [44]. The gamma-emitting tracer 99-technetium hexamethylpropylene amineoxime (99-Tc HMPAO) is absorbed by cerebral tissues in a perfusion-dependent fashion, allowing ascertainment of regional blood flow. SPECT demonstrated the greatest reduction in blood flow compared with controls in the caudate, which was affected in this regard more than the putamen despite greater volume loss in putaminal regions [86]. In 10 of 29 total subjects with symptomatic HD less than 6 years, SPECT revealed reduction of cortical perfusion without atrophy on MRI, with overall cortical perfusion correlating to functional abilities and disease duration [87]. For all subjects, prefrontal blood flow was closely related to cognitive performance and motor cortical areas likewise demonstrated a relationship to movement disability and functional activities of daily living scores. Perfusion to the basal ganglia was significantly reduced in all subjects. Leslie et al. [88] used [^{123}I] epidepride to examine 21 presymptomatic to severe subjects, noting that striatum/occiput and striatum/whole-brain uptake ratios suggested reduction of uptake in moderate and severe disease but not in asymptomatic or early HD. In seven HD subjects asked to solve mazes, blood flow was increased in all areas except the caudate, with reductions during activity compared with rest in the striatum and in the orbital cortex in particular [89]. Gamez et al. [90] used [^{123}I] FP-CIT, the ligand selective for the presynaptic dopamine transporter used in the DAT scan for Parkinson's disease, and observed semiquantitative reduction in 4 of 12 HD subjects, primarily in the putamen. More substantial reductions in ligand uptake correlated to worse UHDRS scores.

Ultrasonography

Ultrasonography involves the transmission of sound waves through a chosen area, which are then analyzed on the basis of their rate and intensity of return to indicate the relative density of structures in question. In a cohort of 45 HD patients, 18 had hyperechogenicity in at least one basal ganglia region, with 12 having changes in the SN, 6 in the caudate head, and 3 in the lentiform nucleus [91]. CAG length and clinical performance correlated with hyperechogenicity in the SN (SN+). Deckel and Cohen [92] used transcranial Doppler ultrasonography in nine gene-positive subjects to assess blood flow velocity during cognitive tasks, finding increased flow in the anterior cerebral artery distribution but not in the middle cerebral artery during out loud verbal fluency tests compared with controls. Blood flow in the anterior cerebral artery (ACA) distribution was able to predict control versus mild or moderate HD. It is not yet established if ultrasound will be a useful biomarker for therapeutic trials.

Imaging in Other Disorders with Prominent Chorea

Chorea-acanthocytosis

Chorea-acanthocytosis (ChAc), or neuroacanthocytosis, is one of several clinically related syndromes characterized by abnormal erythrocytes (acanthocytes) and multiple movement disorders, notably chorea [93]. Other clinical features include lip/tongue biting, tics, dysarthria and dysphagia, amyotrophy, neuropathy, and parkinsonism. As the second most common hereditary choreiform disorder, it is important for the differential diagnosis for the movement disorder clinician evaluating chorea. In a case report of a patient originally thought to have HD, CT scanning revealed caudate atrophy, underscoring the radiographic similarity between the two conditions [94]. Other authors also report misdiagnosis, with reference to caudate atrophy on MRI and chorea prompting diagnosis of HD [95]. Neuroacanthocytosis has been misdiagnosed as schizophrenia and Tourette's syndrome in a pair of monozygotic twins, who demonstrated caudate atrophy and reduced PET glucose uptake in the striatum, particularly on the right [96]. Striatal dopamine and hypothalamic serotonin binding on SPECT was similar to controls. In 13 subjects with ChAc, substantial reduction in MRI volume was observed in the putamen and particularly the caudate in a dorsal/ventral gradient [97]. These changes had no relationship to duration of illness, suggesting that they may precede expression of phenotype. In a PET/MRI evaluation of three ChAc patients, PET demonstrated reduced blood flow and oxygen metabolism in the putamen and caudate relative to controls, with mild reductions in blood flow also noted in the bilateral frontal, left temporal, left parietal, and bilateral thalamic regions [98]. The frontal and temporal lobes demonstrated reductions in oxygenation, whereas MR demonstrated increased signal intensity on T2 in the caudate and putamen with corresponding decreased signal on T1. Cortical atrophy on MRI in ChAc has been described, as has white matter signal increase on T2 images in cerebral periventricular areas, lentiform nuclei, thalamus, cerebral peduncles, and corpus callosum [99]. A report of two ChAc siblings detailed striatal changes as in other literature and cerebellar atrophy [100]. On susceptibility-weighted imaging, an MRI sequence that can highlight iron deposition, abnormal dark paramagnetic signal was observed in the bilateral striatum, with striped regions in the lateral pallidum that were not present on gradient-echo sequences [101]. The role of iron metabolism dysfunction in this setting is currently unclear.

Wilson's Disease

Wilson's disease (WD) is an autosomal-recessive disorder of copper metabolism due to a defect in the copper-transporting ATPase ATP7B, with resultant failure to excrete copper [93]. Copper accumulates in the blood and overwhelms excretion

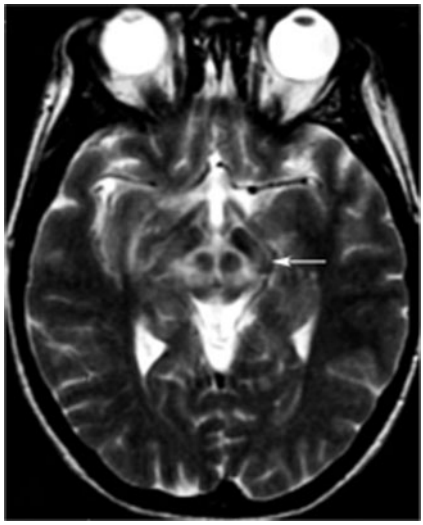

Fig. 13.2 The "double panda" sign in Wilson's disease [108]

capacity, eventually depositing in the liver, kidney, bones, and brain with progressive dysfunction. WD has been associated with a wide variety of abnormal movements, including chorea, dystonia, myoclonus, tremor, and parkinsonism [102, 103]. In a report on 45 WD cases, chorea was noted in 13.3 % of subjects [104].

Early reports using MRI showed T1/T2 hypointensity in the lentiform nuclei and T1 hypointensity in the thalamus with cerebral atrophy [105], as well as the "face of the panda" sign, characterized by high signal in the tegmentum save for the red nucleus (Fig. 13.2) [106–108]. In particular, the putamen appears to be frequently abnormal in WD, with numerous reports describing abnormalities [109, 110]. Prayer et al. [111] saw MRI findings in 22 of 38 subjects, reporting T2 hyperintensity in caudate, thalamic, and lenticular nuclei as well as brain stem regions and white matter, although little was seen on T1 imaging. Hydrocephalus ex vacuo was also noted, with no correlation between severity of MR abnormalities and clinical severity. In an evaluation of 25 WD patients, MR was abnormal in 22, with lesions most frequently in the putamen (86 %) [112]. Other affected gray matter areas included the thalamus (54 %), caudate (45 %), and pallidum (41 %), especially the outer rim of the putamen and ventral thalamic nuclei. Lesions were widespread in the brain stem and also seen in the tectum, tegmentum, SN, red nuclei, pons, and superior/middle cerebellar peduncles. Notably, atrophy was observed in a majority of patients (82 %), with substantial cortical white matter changes (59 %). Severity of signal intensity change correlated to total duration of disease and length of untreated disease. In a study of 100 WD patients, 93 of whom were symptomatic, atrophy in the cerebrum (70 %), cerebellum (52 %), and brain stem (66 %) was notable, with signal changes most commonly in the putamen followed by the caudate, thalamus, midbrain, pons, cerebral white matter, cortex, medulla, and cerebellum [113]. Observed also were pallidal

hypointensity (34 %), "face of the panda" sign (12 %), T1 hyperintensity (6 %), central pontine myelinosis (7 %), and claustral hyperintensity (4 %). Midbrain diameter in symptomatic WD is significantly reduced compared with controls and WD subjects without neurological symptoms [114]. White matter abnormalities have been described in numerous areas, notably in the corticospinal tracts, dentatorubrothalamic tracts, and pontocerebellar tracts have been described [115, 116]. Aikath et al. [117] reported a genetically confirmed WD subject with diffuse white matter disease and resistance to pharmacotherapy. A 12-year-old WD subject demonstrated significant improvement in white matter changes while treated and imaged over a 5-year period [118]. In a study of 81 patients, 42 % had white matter changes on FLAIR, with almost one-quarter with corpus callosal lesions in the splenium [119]. In an MRI analysis of 56 WD patients compared with 44 relatively young subjects with extrapyramidal disorders (including HD), the most typical findings were tectal plate and pontine hyperintensities (75 and 62.5 %), collective basal ganglia, thalamus, and brainstem signal change (55.3 %), and the "panda" sign (14.3 %) [120].

Of note, treatment appears to have some effect on imaging in WD. MR abnormalities before and after initiation of penicilliamine chelation therapy have been compared, with reduction in hyperintensities of the thalamus, brainstem, and basal ganglia over 5–24 months reported by Roh et al. [121]. Neurological symptoms also improved, although brain atrophy, when present, was unchanged by treatment over this interval. Penicillamine treatment also improves D_2 receptor binding on [^{11}C] raclopride PET and [^{123}I] iodobenzamide SPECT in the caudate and putamen, corresponding to T2 hyperintensity improvement on MR in these regions observed over an initial 4-month treatment period [122]. Others have reported clinical improvement in tremor after penicillamine treatment with corresponding reduction in lesion burden in thalamic and red nuclear regions [123]. A study of 18 neurological WD subjects comparing longitudinal MR changes for penicillamine and zinc treatment groups showed a tendency toward radiographic worsening over time in the zinc group without clinical correlate, with no clinical difference over time between the two groups [124]. Follow-up PET after treatment in three patients revealed improved glucose utilization in two and increased striatal D_2 receptor binding in three patients, correlating to clinical improvement. As such, there is evidence that WD has a dynamic phase in which functional and radiographic improvement can be identified after treatment. However, reports of clinical decompensation after initiation of penicillamine treatment also exist, given its ability to transiently increase exposure of tissues to copper. Huang and Chu [125] reported a 28-year-old subject who developed parkinsonism and dystonia after treatment for 2 weeks, with corresponding development of T2 hyperintensities in the thalamus, basal ganglia, pons, and midbrain. Slow clinical and radiographic improvement followed after change to zinc therapy. A 20-year-old patient demonstrated improvement on FGD PET measures in the striatum and cortex with accompanying clinical improvement over 14 months after initiation of chelation therapy [126]. Liver transplant, the definitive treatment for WD, elicited improvement in ataxia and tremor over several months, with T2 hyperintensities in the thalami and red nuclei regressing as well [127].

Other Imaging Modalities in WD

Severity of neurological disease correlated to striatal glucose consumption on PET as well as MR abnormalities in 18 WD subjects, although no relationship was found with D_2 receptor binding [128]. β-CIT SPECT has shown significant loss of dopamine transporter binding in the striatum, suggestive of presynaptic nigrostriatal damage [129]. MRS demonstrated no differences in NAA/Cho, NAA/Cr, and Cho/CR ratios in comparing WD with controls [130]. SPECT demonstrated perfusion reduction in superior frontal, prefrontal, parietal, and occipital cortices as well as the caudate and putamen for 19 of 25 WD subjects, 12 of whom had neurological symptoms; 10 of those with neurological symptoms had abnormal SPECT scans [131]. MRS in 12 heterozygous carriers, three of whom had low ceruloplasmin and one with low serum copper, showed higher Glx/Cr and Lip/Cr ratios in the pallidum and thalamus compared with controls, leading to speculation that heterozygotes may accumulate copper [132]. In a SPECT study of the globus pallidus, NAA/Cr ratios seen as low before treatment increased significantly after 1 year of treatment [133].

Diffusion-weighted MRI over 18 months demonstrated a change from restricted diffusion to elevated diffusion in the putamen and caudate, suggestive of a progression from cytotoxic edema to necrosis and demyelination [134]. A case involving sudden onset of right-sided hemichorea revealed hyperintense lesions in the striatum, thalamus, and midbrain bilaterally, with DWI-positive lesions in the subthalamic nuclei bilaterally, more so on the left, with slightly increased apparent diffusion coefficient (ADC) values [135]. After 2 years of treatment, elevated DWI signals largely disappeared. Decreases in diffusion signal in the putamen have been detected in WD subjects without T2 lesions or neurological symptoms, with substantial increases once symptoms emerge in the putamen, pallidum, and subcortical white matter corresponding to new lesions on T2 [136]. ADC signal was noted as high in the putamen, pallidum, white matter, and mesencephalon in symptomatic but not asymptomatic subjects, where some without neurological deficits in fact had decreased ADC signal. More substantial diffusion signal correlated to symptom severity. Similar to DWI, ADC values in the literature have been observed to be variable, suggesting the disease trajectory may involve multiple pathogenic mechanisms over time [137].

Transcranial sonography demonstrated lenticular hyperechogenicity in symptomatic and asymptomatic subjects, with the area of change correlating to clinical severity [138]. Thalamic hyperechogenicity, lateral ventrical width, and third ventricle width also correlated to intensity of symptoms. Hyperechogenicity of the SN noted in 10 of 21 WD subjects did not correlate to disease severity. Only 12 of 19 subjects with lenticular hyperechogenicity had corresponding lesions on MRI. Oder et al. [139] correlated MR findings and clinical features, observing associations between parkinsonism/cognitive impairment and dilation of the third ventricle, ataxia/tremor with thalamic lesions, and chorea/dyskinesia, dysarthria, and personality disturbances with lesions in the putamen and pallidum.

Conclusions and Future Directions

Recent advances in imaging have clarified regional changes in choreic disorders, notably symptomatic and presymptomatic HD, with promise to further demarcate stages of the disease and its evolution over time. For HD, anatomic changes as well as functional alterations have become clearer, though limitations in knowledge regarding specific molecular mechanisms of HD pathogenesis currently represent a major challenge for future advances. The ability to identify sensitive and specific molecular signatures for successive stages of HD, if in fact stages of progression involve variations in the function or quantity of certain biomolecules, would represent a major advance in tracking the disease. Moreover, knowledge and quantification/localization of such biomarkers would likely boost design and development of therapeutic agents tailored for different disease stages or specific molecular defects. Going forward, future clinical trials will likely draw on these increasingly sophisticated imaging modalities to measure efficacy of interventions, representing yet another dimension to the revolutionary role imaging has already started to play in our understanding of neurodegenerative disorders.

References

1. Terrence CF, Delaney JF, Alberts MC. Computed tomography for Huntington's disease. Neuroradiology. 1977;13(4):173–5.
2. Stober T, Wussow W, Schimrigk K. Bicaudate diameter—the most specific and simple CT parameter in the diagnosis of Huntington's disease. Neuroradiology. 1984;26(1):25–8.
3. Sharma P, Savy L, Britton J, Taylor R, Howick A, Patton M. Huntington's disease: a molecular genetic and CT comparison. J Neurol Neurosurg Psychiatry. 1996;60(2):206–8.
4. Culjkovic B, Stojkovic O, Vojvodic N, Svetel M, Rakic L, Romac S, Kostic V. Correlation between triplet repeat expansion and computed tomography measures of caudate nuclei atrophy in Huntington's disease. J Neurol. 1999;246(11):1090–3.
5. Aylward EH, LI Q, Stine OC, Ranan N, Sherr M, Barta PE, Bylsma FW, Pearlson GD, Ross CA. Longitudinal change in basal ganglia volume in patients with Huntington's disease. Neurology. 1997;48(2):394–9.
6. Rosas HD, Goodman J, Chen YI, Jenkins BG, Kennedy DN, Makris N, Patti M, Seidman LJ, Beal MF, Koroshetz WJ. Striatal volume loss in HD as measured by MRI and the influence of CAG repeat. Neurology. 2001;57(6):1025–8.
7. Backman L, Robins-Wahlin TB, Lundin A, Ginovart N, Farde L. Cognitive deficits in Huntington's disease are predicted by dopaminergic PET markers and brain volumes. Brain. 1997;120(Pt 12):2207–17.
8. Aylward EH, Anderson NB, Bylsma FW, Wagster MV, Barta PE, Sherr M, Feeney J, Davis A, Rosenblatt A, Pearlson GD, Ross CA. Frontal lobe volume in patients with Huntington's disease. Neurology. 1998;50(1):252–8.
9. Ashburner J, Friston KJ. Voxel-based morphometry—the methods. Neuroimage. 2000;11:805–21.
10. Kassubek J, Juengling FD, Kioschies T, Henkel K, Karitzky J, Kramer B, Ecker D, Andrich J, Saft C, Kraus P, Aschoff AJ, Ludolph AC, Landwehrmeyer GB. Topography of cerebral atrophy in early Huntington's disease: a voxel-based morphometric study. J Neurol Neurosurg Psychiatry. 2004;75(2):213–20.

11. Kassubek J, Landwehrmeyer GB, Ecker D, Juengling FD, Muche R, Schuller S, Weindl A, Peinemann A. Global cerebral atrophy in early stages of Huntington's disease; quantitative MRI study. Neuroreport. 2004;15(2):363–5.
12. Douaud G, Guara V, Ribiero MJ, Lethimonnier F, Maroy R, Verny C, Krystkowiak P, Damier P, Bachoud-Levi AC, Hantraye P, Remy P. Distribution of grey matter atrophy in Huntington's disease patients: a combined ROI-based and voxel-based morphometric based study. Neuroimage. 2006;32(4):1562–75.
13. Ruocco HH, Bonilha L, Li LM, Lopes-Cendes I, Cendes F. Longitudinal Analysis of regional grey matter loss in Huntington's disease: effects of the length of the expanded CAG repeat. J Neurol Neurosurg Psychiatry. 2008;79(2):130–5.
14. Rosas HD, Salat DH, Lee SY, Zaleta AK, Pappu V, Fischl B, Greve D, Hevelone N, Hersch SM. Cerebral cortex and the clinical expression of Huntington's disease; complexity and heterogeneity. Brain. 2008;131(Pt 4):1057–68.
15. Fennema-Notestine C, Archibald SL, Jacobson MW, Corey-Bloom J, Paulsen JS, Peavy GM, Gamst AC, Hamilton JM, Salmon DP, Jernigan TL. In vivo evidence of cerebellar atrophy and cerebral white matter loss in Huntington's disease. Neurology. 2004;63(6):989–95.
16. Kassubek J, Juengling FD, Ecker D, Landwehrmeyer GB. Thalamic atrophy in Huntington's disease co-varies with cognitive performance: a morphometric MRI analysis. Cereb Cortex. 2005;15(6):846–53.
17. Thieben MJ, Duggins AJ, Good CD, Gomes L, Mahant N, Richards F, McCusker E, Frackowiak RS. The distribution of structural neuropathology in preclinical Huntington's disease. Brain. 2002;125(Pt 8):1815–28.
18. Ciarmiello A, Cannella M, Lastoria S, Simonelli M, Frati L, Rubinsztein DC, Squiteri F. Brain white-matter volume loss and glucose hypometabolism precede the clinical symptoms of Huntington's disease. J Nucl Med. 2006;47(2):215–22.
19. Jurgens CK, van de Wiel L, van Es AC, Grimbergen YM, Witjes-Ane MN, van der Grond J, Middelkoop HA, Roos RA. Basal ganglia volume and clinical correlates in 'preclinical' Huntington's disease. Neurology. 2008;255(11):1785–91.
20. Henley SM, Wild EJ, Hobbs NZ, Frost C, MacManus DG, Barker RA, Fox NC, Tabrizi SJ. Whole-brain atrophy as a measure of progression in premanifest and early Huntington's disease. Mov Disord. 2009;24(6):932–6.
21. Kloppel S, Chu C, Tan GC, Draganski B, Johnson H, Paulsen JS, Kienzle W, Tabrizi SJ, Ashburner J, Frakowiak RS, PREDICT-HD investigators of the Huntington's Study Group. Automatic detection of preclinical neurodegeneration: presymptomatic Huntington's disease. Neurology. 2009;72(5):426–31.
22. Paulsen JS, Nopoulos PC, Aylward E, Ross CA, Johnson H, Magnotta VA, Juhl A, Pierson RK, Mills J, Langbehn D, Nance M, PREDICT-HD Investigators and Coordinators of the Huntington's Study Group. Striatal and white matter predictors of estimated diagnosis for Huntington's disease. Brain Res Bull. 2010;82(3–4):201–7.
23. Soneson C, Fontes M, Zhou Y, Denisov V, Paulsen JS, Kirik D, Petersen A, Huntington's Study Group PREDICT-HD Investigators. Early changes in the hypothalamic region in prodromal Huntington's disease revealed by MTI analysis. Neurobiol Dis. 2010;40(3):531–43.
24. Nopoulos PC, Aylward EH, Ross CA, Johnson HJ, Magnotta VA, Juhl AR, Pierson RK, Mills J, Langbehn DR, Paulsen JS. Cerebral cortex structurein prodromal Huntington's disease. Neurobiol Dis. 2010;40(3):544–54.
25. Aylward EH, Nopoulos PC, Ross CA, Langbehn DR, Pierson RK, Mills JA, Johnson HJ, Magnotta VA, Juhl AR, Paulsen JS, PREDICT HD Investigators and Coordinators of the Huntington's Study Group. Longitudinal change in regional brain volumes in prodromal Huntington's disease. J Neurol Neurosurg Psychiatry. 2011;82(4):405–10.
26. Biglan KM, Ross CA, Langbehn DR, Aylward EH, Stout JC, Queller S, Carlozzi NE, Duff K, Beglinger LJ, Paulsen JS. Motor abnormalities in premanifest persons with Huntington's disease: the PREDICT-HD study. Mov Disord. 2009;24(12):1763–72.
27. Gomez-Anson B, Alegret M, Munoz E, Monte GC, Alayrach E, Sanchez A, Boada M, Tolosa E. Prefrontal cortex volume reduction on MRI in preclinical Huntington's disease relates to visuomotor performance and CAG number. Parkinsonism Relat Disord. 2009;15(3):213–9.

28. Stoffers D, Sheldon S, Kuperman JM, Goldstein J, Corey-Bloom J, Aron AR. Contrasting grey and white matter changes in preclinical Huntington's disease: an MRI study. Neurology. 2010;74(15):1208–16.
29. Wild EJ, Henley SM, Hobbs NZ, Frost C, MacManus DG, Barker RA, Fox NC, Tabrizi SJ. Rate and acceleration of whole-brain atrophy in premanifest and early Huntington's disease. Mov Disord. 2010;25(7):888–95.
30. Rosas HD, Reuter M, Doros G, Lee SY, Triggs T, Malarick K, Fischl B, Salat DH, Hersch SM. A tale of two factors: what determines the rate of progression in Huntington's disease? A longitudinal MRI study. Mov Disord. 2011;26(9):1691–7.
31. Tabrizi SJ, Langbehn DR, Leavitt BR, Roos RA, Durr A, Craufurd D. Kennard C, Hicks SL, Fox NC, Scahill RI, Borowsky B, Tobin AJ, Rosas HD, Johnson H, Reilmann R, Frost C, Langbehn DR, Reilmann R, Landwehrmeyer GB, Stout JC, TRACK-HD Investigators. Biological and clinical manifestations of Huntington's disease in the longitudinal TRACK-HD study: cross-sectional analysis of baseline data. Lancet Neurol. 2009;8(9):791–801.
32. Tabrizi SJ, Scahill RI, Durr A, Roos RA, Leavitt BR, Jones R, Landwehrmeyer GB, Fox NC, Johnson H, Hicks SL, Kennard C, Craufurd D, Frost C, Langbehn DR, Reilmann R, Stout JC, TRACK-HD Investigators. Biological and clinical changes in premanifest and early stage Huntington's disease in the TRACK-HD study: the 12-month longitudinal analysis. Lancet Neurol. 2011;10(1):31–42.
33. Van den Bogaard SJ, Dumas EM, Acharya TP, Johnson H, Langbehn DR, Scahill RI, Tabrizi SJ, van Buchem MA, van der Grond J, Roos RA, TRACK-HD Investigator Group. Early atrophy of pallidum and accumbens nucleus in Huntington's disease. J Neurol. 2011;258(3):412–20.
34. Tabrizi SJ, Reilmann R, Roos RA, Durr A, Leavitt B, Owen G, Jones R, Johnson H, Craufurd D, Hicks SL, Kennard C, Landwehrmeyer B, Stout JC, Borowsky B, Scahill RI, Frost C, Langbehn DR, TRACK-HD Investigators. Potential endpoints for clinical trials in premanifest and early Huntington's disease in the TRACK-HD study: analysis of 24-month observational data. Lancet Neurol. 2012;11(1):42–53.
35. Jurgens CK, Bos R, Luyendijk J, Witjes-Ane MN, van der Grond J, Middelkoop HA, Roos RA. Magnetization transfer imaging in 'premanifest' Huntington's disease. J Neurol. 2010;257(3):426–32.
36. Wolf RC, Gron G, Sambataro F, Vasic N, Wolf ND, Thomann PA, Saft C, Landwehrmeyer GB, Orth M. Magnetic resonance perfusion imaging of resting-state cerebral blood flow in preclinical Huntington's disease. J Cereb Blood Flow Metab. 2011;31(9):1908–18.
37. Aylward EH, Rosenblatt A, Field K, Yallapragada V, Kieburtz K, McDermott M, Raymond LA, Almqvist EW, Hayden M, Ross CA. Caudate volume as an outcome measure in clinical trials for Huntington's disease: a pilot study. Brain Res Bull. 2003;62(2):137–41.
38. Bartzokis G, Tishler TA. MRI evaluation of basal ganglia ferritin iron and neurotoxicity in Alzheimer's and Huntington's disease. Cell Mol Biol. 2000;46(4):821–33.
39. Le Bhan D, Mangin JF, Poupon C, Clark C, Pappata S, Molko M, Chabriat H. Diffusion tensor imaging: concepts and applications. J Magn Reson Imaging. 2001;13:534–46.
40. Bohanna I, Georgiou-Karistianis N, Sritharan A, Asadi H, Johnston L, Churchyard A, Egan G. Diffusion tensor imaging in Huntington's disease reveals distinct patterns of white matter degeneration associated with motor and cognitive deficits. Brain Imaging Behav. 2011;5(3):171–80.
41. Bohanna I, Georgiou-Karistianis N, Egan F. Connectivity-based segmentation of the striatum in Huntington's disease: vulnerability of motor pathways. Neurobiol Dis. 2011;42(3):475–81.
42. Della Nave R, Ginestroni A, Tessa C, Giannelli M, Piacentini S, Filippi M, Mascalchi M. Regional distribution and clinical correlates of white matter structural damage in Huntington's disease; a tract-based spatial statistics study. Am J Neuroradiol. 2010;31(9):1675–81.
43. Kipps CM, Duggins AJ, Mahant N, Gomes L, Ashburner J, McCusker EA. Progression of structural neuropathology in preclinical Huntington's disease: a tensor based morphometry study. J Neurol Neurosurg Psychiatry. 2005;76(5):650–5.
44. Grossman R, Yousem D. Neuroradiology: the requisites. 2nd ed. Philadelphia: Mosby; 2003.

45. Clark VP, Lai S, Deckel AW. Altered functional MRI responses in Huntington's disease. Neuroreport. 2002;13(5):703–6.
46. Aron AR, Schlaghecken F, Fletcher PC, Bullmore ET, Eimer M, Barker R, Sahakian BJ, Robbins TW. Inhibition of subliminally primed responses is mediated by the caudate and thalamus: evidence from functional MRI and Huntington's disease. Brain. 2003;126(Pt 3):713–23.
47. Kim JS, Reading SA, Brashers-Krug T, Calhoun VD, Ross CA, Pearlson GD. Functional MRI study of a serial reaction time task in Huntington's disease. Psychiatry Res. 2004;131(1): 23–30.
48. Ciarmiello A, Cannella M, Lastoria S, Simonelli M, Frati L, Rubinsztein DC, Squitieri F. Brain white-matter volume loss and glucose hypometabolism precede the clinical symptoms of Huntington's disease. J Nucl Med. 2006;47(2):215–22.
49. Wolf RC, Vasic N, Schonfelt-Lecuona C, Landwehrmeyer GB, Ecker D. Dorsolateral prefrontal cortex dysfunction in presymptomatic Huntington's disease: evidence from event-related fMRI. Brain. 2007;130(Pt 11):2845–57.
50. RIzk-Jackson A, Stoffers D, Sheldon S, Kuperman J, Dale A, Goldstein J, Corey-Bloom J, Poldrack RA, Aron AR. Evaluating imaging biomarkers for neurodegeneration in pre-symptomatic Huntington's disease using machine learning techniques. Neuroimage. 2011;56(2):788–96.
51. Taylor-Robinson SD, Weeks RA, Bryant DJ, Sargentoni J, Marcus CD, Harding AE, Brooks DJ. Proton magnetic resonance spectroscopy in Huntington's disease: evidence in favor of the glutamate excitotoxic theory. Mov Disord. 1996;11(2)167–73.
52. Ruocco HH, Lopes-Cendes I, LI M, Cendes F. Evidence of thalamic dysfunction in Huntington's disease by proton magnetic resonance spectroscopy. Mov Disord. 2007;22(14):2052–6.
53. Harms L, Meierkord H, Timm G, Pfeiffer L, Ludolph AC. Decreased N-acetylaspartate/choline ration and increased lactate in the frontal lobe of patients with Huntington's disease: a proton magnetic resonance spectroscopy study. J Neurol Neurosurg Psychiatry. 1997;62(1):27–30.
54. Jenkins BG, Rosas HD, Chen YC, Makabe T, Myers R, MacDOnald M, Rosen BR, Beal F, Koroshetz WJ. 1H NMR spectroscopy studies of Huntington's disease: correlations with CAG repeat numbers. Neurology. 1998;50(5):1357–65.
55. Sanchez-Pernaute R, Garcia-Segura JM, del Barrio Alba A, Viano J, de Yebenes JG. Clinical correlation of striatal 1H MRS changes in Huntington's disease. Neurology. 1999;53(4): 806–12.
56. Reynolds NC Jr, Prost RW, Mark LP. Heterogeneity in 1H-MRS profiles of presymptomatic and early manifest Huntington's disease. Brain Res. 2005;1031:(1):82–9.
57. Gomez-Anson B, Alegret M, Munoz E, Sainz A, Monte GC, Tolosa E. Decreased frontal choline and neuropsychological performance in preclinical Huntington's disease. Neurology. 2007;68(12):906–10.
58. Van Oostrom JC, Sijens PE, Roos RA, Leenders KL. 1H magnetic resonance spectroscopoy in preclinical Huntington's disease. Brain Res. 2007;1168:67–71.
59. Sturrock A, Laule C, Decolongon J, Dar Santos R, Coleman AJ, Creighton S, Bechtel N, Reilmann R, Hayden MR, Tabrizi SJ, Mackay AL, Leavitt BR. Magnetic resonance spectroscopy biomarkers in premanifest and early Huntington's disease. Neurology. 2010;75(19):1702–10.
60. Koroshetz WJ, Jenkins BG, Rosen BR, Beal MF. Energy metabolism defects in Huntington's disease and effects of coenzyme Q10. Ann Neurol. 1997;41(2):160–5.
61. Bender A, Auer DP, Merl T, Reilmann R, Saemann P, Yassouridis A, Bender J, Weindl A, Dose M, Gasser T, Klopstock T. Creatine supplementation lowers brain glutamate levels in Huntington's disease. J Neurol. 2005;252(1):36–41.
62. Tabrizi SJ, Blamire AM, Manners DN, Rajagopalan B, Styles P, Schapira AH, Warner TT. High-dose creatine therapy for Huntington's disease: a two-year clinical and MRS study. Neurology. 2005;64(9):1655–6.
63. Schapiro M, Cecil KM, Doescher J, Kiefer AM, Jones BV. MR imaging and spectroscopy in juvenile Huntington's disease. Pediatr Radiol. 2004;34(8):640–3.
64. Reynolds NC, Prost RW, Mark LP, Joseph SA. MR-spectroscopic findings in juvenile-onset Huntington's disease. Mov Disord. 2008;23(13):1931–5.

65. Van den Bogaard SJ, Dumas EM, Teeuwisse WM, Kan HE, Webb A, Roos RA, van der Grond J. Exploratory 7-Tesla magnetic resonance spectroscopy in Huntington's disease provides in vivo evidence for impaired energy metabolism. J Neurol. 2011;258(12):2230–9.
66. Antonini A, Leenders KL, Spiegel R, Meier D, Vontobel P, Weigell-Weber M, Sanchez-Pernaute R, de Yebenez JG, Boesiger P, Weindl A, Maguire RP. Striatal glucose metabolism and dopamine D2 receptor binding in asymptomatic gene carriers and patients with Huntington's disease. Brain. 1996;119(Pt 6):2085–95.
67. Antonini A, Leenders KL, Eidelberg D. [11C] raclopride-PET studies of the Huntington's disease rate of progression: relevance of the trinucleotide repeat length. Ann Neurol. 1998;43(2):253–5.
68. Van Oostrom JC, Dekker M, Willemsen AT, de Jong BM, Roos RA, Leenders KL. Changes in striatal dopamine D2 receptor binding in pre-clinical Huntington's Disease. Eur J Neurol. 2009;16(2):226–31.
69. Ginovart N, Lundin A, Farde L, Hallidin C, Backman L, Swahn CG, Pauli S, Sedvall G. PET study of the pre- and post-synaptic dopaminergic markers for the neurodegenerative process in Huntington's disease. Brain. 1997;120(Pt 3):503–14.
70. Backman L, Robins-Wahlin TB, Lundin A, Ginovart N, Farde L. Cognitive deficits in Huntington's disease are predicted by dopaminergic PET markers and brain volumes. Brain. 1997;(Pt 12):2207–17.
71. Weeks RA, Ceballos-Baumann A, Piccini P, Boecker H, Harding AE, Brooks DJ. Cortical control of movement in Huntington's disease. A PET activation study. Brain. 1997;120(Pt 9):1569–78.
72. Boecker H, Ceballos-Baumann A, Bartenstein P, Weindl A, Siebner HR, Fassbender T, Munz F, Schwaiger M, Conrad B. Sensory processing in Parkinson's and Huntington's disease: investigations with 3D H(2)(15)O-PET. Brain. 1999;(Pt 9):1651–65.
73. Kunig G, Leenders KL, Sanchez-Pernaute R, Antonini A, Vontobel P, Verhagen A, Gunther I. Benzodiazepine receptor binding in Huntington's disease: [11C]flumazenil uptake measured using positron emission tomography. Ann Neurol. 2000;47(5):644–8.
74. Furtado S, Sossi V, Hauser RA, Samii A, Schulzer M, Murphy CB, Freeman TB, Stoessl AJ. Positron emission tomography after fetal transplantation in Huntington's disease. Ann Neurol. 2005;58(2):331–7.
75. Reuter I, Tai YF, Pavese N, Chaudhuri KR, Mason S, Polkey CE, Clough C, Brooks DJ, Barker RA, Piccini P. Long term clinical and positron emission tomography outcome of fetal striatal transplantation in Huntington's disease. J Neurol Neurosurg Psychiatry. 2008;79(8):948–51.
76. Pavese N, Gerhard A, Tai YF, Ho AK, Turkheimer F, Barker RA, Brooks DJ, Piccini P. Microglial activation correlates with severity in Huntington's disease: a clinical and PET study. Neurolgoy. 2006;66(11):1638–43.
77. Van Laere K, Casteels C, Dhollander I, Goffin K, Grachev I, Bormans G, Vandenberghe W. Widespread decrease of type 1 cannabinoid receptor availability in Huntington's disease in vivo. J Nucl Med. 2010;51(9):1413–7.
78. Van Oostrom JC, Maguire RP, Verschuuren-Bemelmans CC, Veenma-vander Duin L, Pruim J, Roos RA, Leenders KL. Striatal dopamine D2 receptors, metabolism, and volume in preclinical Huntington's disease. Neurology. 2005;65(6):941–3.
79. Feigin A, Leenders KL, Moeller JR, Missimer J, Kuenig G, Spetsieris P, Antonini A, Eidelberg D. Metabolic network abnormalities in early Huntington's disease: an [(18)F] FDG PET study. J Nucl Med. 2001;42(11):1591–5.
80. Pavese N, Andrews TC, Brooks DJ, Ho AK, Rosser AE, Barker RA, Robbins TW, Sahakian BJ, Dunnett SB, Piccini P. Progressive striatal and cortical dopamine receptor dysfunction in Huntington's disease: a PET study. Brain. 2003;126(Pt 5):1127–35.
81. Feigin A, Tang C, Ma Y, Mattis P, Zgaljardic D, Guttman M, Paulsen JS, Dhawan V, Eidelberg D. Thalamic metabolism and symptom onset in preclinical Huntington's disease. Brain. 2007;130 (Pt 11):2858–67.
82. Politis M, Pavese N, Tai YF, Tabrizi SJ, Barker RA, Piccini P. Hypothalamic involvement in Huntington's disease: an in vivo PET study. Brain. 2008;131(Pt 11):2860–9.

83. Politis M, Pavese N, Tai YF, Kiferle L, Mason SL, Brooks DJ, Tabrizi SJ, Barker RA, Piccini P. Microglial activation in regions related to cognitive dysfunction predicts disease onset in Huntington's disease: a multimodal imaging study. Hum Brain Mapp. 2011;32(2)258–70.
84. Pavese N, Politis M, Tai YF, Barker RA, Tabrizi SJ, Mason SL, Brooks DJ, Piccini P. Cortical dopamine dysfunction in symptomatic and premanifest Huntington's disease carriers. Neurobiol Dis. 2010;37(2):356–61.
85. Esmaeilzadeh M, Farde L, Karlsson P, Varrone A, Halldin C, Waters S, Tedroff J. Extrastriatal dopamine D2 receptor binding in Huntington's disease. Hum Brain Mapp. 2011;32(10): 1626–36.
86. Harris GJ, Aylward EH, Peyser CE, Pearlson GD, Brandt J, Roberts-Twille JV, Barta PE, Folstein SE. Single photon emission computed tomographic blood flow and magnetic resonance volume imaging of basal ganglia in Huntington's disease. Arch Neurol. 1996;53(4):316–24.
87. Sax DS, Powsner R, Kim A, Tilak S, Bhatia R, Cupples LA, Myers RH. Evidence of cortical metabolic dysfunction in early Huntington's disease by single-photon-emission computed tomography. Mov Disord. 1996;11(6):671–7.
88. Leslie WD, Greenberg CR, Abrams DN, Hobson D. Clinical deficits in Huntington's disease correlate with reduced striatal uptake on iodine-123 epidepride single-photon emission tomography. Eur J Nucl Med. 1999;26(11):1458–64.
89. Deckel AW, Weiner R, Szigeti D, Clark V, Vento J. Altered patterns of regional cerebral blood flow in patients with Huntington's disease: a SPECT study during rest and cognitive or motor activation. J Nucl Med. 2000;41(5):773–80.
90. Gamez J, Lorenzo-Bosquet C, Cuberas-Borros G, Carmona F, Hernandez-Vara J, Castillo J, Castell-Conesa J. Does reduced [123(I)]-FP-CIT binding in Huntington's disease suggest presynaptic dopaminergic involvement? Clin Neurol Neurosurg. 2010;112(10):870–5.
91. Postert T, Lack B, Kuhn W, Jergas M, Andrich J, Braun B, Przuntek H, Sprengelmeyer R, Agelink M, Buttner T. Basal ganglia alterations and brain atrophy in Huntington's disease depicted by transcranial real time sonography. J Neurol Neurosurg Psychiatry. 1999;67(4):457–62.
92. Deckel AW, Cohen D. Increased CBF velocity during word fluency in Huntington's disease patients. Prog Neuropsychopharmacol Biol Psychiatry. 2010;24(2):193–206.
93. Fahn S, Jankovic J. Principles and practice of movement disorders. Philadelphia: Elsevier; 2007.
94. Kutcher JS, Khan MJ, Andersson HC, Foundas AL. Neuroacanthocytosis masquerading as Huntington's disease: CT/MRI findings. J Neuroimaging. 1999;9(3):187–9.
95. Meenakshi-Sundaram S, Arun Kumar MJ, Sridhar R, Rani U, Sundar B. Neuroacanthocytosis misdiagnosed as Huntington's disease: a case report. J Neurol Sci. 2004;219(1–2):163–6.
96. Muller-Vahl KR, Berding G, Emrich HM, Peschel T. Chorea-acanthocytosis in monozygotic twins: clinical findings and neuropathological changes as detected by diffusion tensor imaging, FDG-PET and (123)I-beta-CIT-SPECT. J Neurol. 2007;254(8):1081–8.
97. Walterfang M, Looi JC, Styner M, Walker RH, Danek A, Niethammer M, Evans A, Kotschet K, Rodrigues GR, Hughes A, Velakoulis D. Shape alterations in the striatum in chorea-acanthocytosis. Psychiatry Res. 2011;192(1):29–36.
98. Marson AM, Bucciantini E, Gentile E, Geda C. Neuroacanthocytosis: clinical, radiological, and neurophysiological findings in an Italian family. Neurol Sci. 2003;24(3):188–9.
99. Nicholl DJ, Sutton I, Dotti MT, Supple SG, Danek A, Lawden M. White matter abnormalities on MRI in neuroacanthocytosis. J Neurol Neurosurg Psychiatry. 2004;75(8):1200–1.
100. Katsube T, Shimono T, Ashikaga R, Hosono M, Kitagaki H, Murakami T. Demonstration of cerebellar atrophy in neuroacanthocytosis of 2 siblings. Am J Neuroradiol. 2009;30(2):386–8.
101. Lee JH, Lee SM, Baik SK. Demonstration of striatopallidal iron deposition in chorea-acanthocytosis by susceptibility-weighted imaging. J Neurol. 2011;258(2):321–2.
102. Barbosa ER, Silveira-Moriyama L, Machado AC, Bachesci LA, Rosemberg S, Scaff M. Wilson's disease with myoclonus and white matter lesions. Parkinsonism Relat Disord. 2007;13(3):185–8.

103. Sudmeyer M, Saleh, A, Wojtecki L, Cohnen M, Gross J, Ploner M, Hefter H, Timmerman L, Schnitzler A. Wilson's disease tremor is associated with magnetic resonance imaging lesions in basal ganglia structures. Mov Disord. 2006;21(12):2134–9.
104. Oder W, Grimm G, Kollegger H, Ferenci P, Schneider B, Deecke L. Neurological and neuropsychiatric spectrum of Wilson's disease: a prospective study of 45 cases. J Neurol. 1991;238(5):281–7.
105. De Haan J, Grossman RI, Civitello L, Hackney DB, Goldberg HI, Bilaniuk LT, Zimmerman RA. High-field magnetic resonance imaging of Wilson's disease. J Comput Tomogr. 1987;11(2):132–5.
106. Hitoshi S, Iwata M, Yoshikawa K. Midbrain pathology of Wilson's disease: MRI analysis of three cases. J Neurol Neurosurg Psychiatry. 1991;54(7):624–6.
107. Liebeskind DS, Wong S, Hamilton RH. Faces of the giant panda had her cub: MRI correlates in Wilson's disease. J Neurol Neurosurg Psychiatry. 2003;74(5):682.
108. Jacobs DA, Markowitz CE, Liebeskind DS, Galetta SL. The "double panda" sign in Wilson's Disease. Neurology. 2003;61(7):969.
109. Magalhaes AC, Caramelli P, Menezes JR, Lo LS, Bacheschi LA, Barbosa ER, Rosemberg LA, Magalhaes A. Wilson disease: MRI with clinical correlation. Neuroradiology. 1994;36(2):97–100.
110. Saatci I, Topcu M, Baltaoglu FF, Kose G, Yalaz K, Renda Y, Besim A. Cranial MR findings in Wilson's disease. Acta Radiol. 1997;38(2):250–8.
111. Prayer L, Wimberger D, Kramer J, Grimm G, Oder W, Imhof H. Cranial MRI in Wilson's disease. Neuroradiology. 1990;32(3):211–4.
112. King AD, Walshe JM, Kendall BE, Chinn RJ, Paley MN, Wilkinson ID, Halligan S, Hall-Craggs MA. Cranial MR imaging in Wilson's disease. Am J Roentgenol. 1996;167(6): 1579–84.
113. Sinha S, Tally AB, Ravishankar S, Prashanth LK, Venugopal KS, Arunodaya GR, Vasudev MK, Swamy HS. Wilson's disease: cranial MRI observations and clinical correlation. Neuroradiology. 2006;48(9):613–21.
114. Strecker K, Schneider JP, Barthel H, Hermann W, Wegner F, Wagner A, Schwartz J, Sabri O, Zimmer C. Profound midbrain atrophy in patients with Wilson's disease and neurological symptoms? J Neuroradiol. 2006;253(8):1024–9.
115. Hedera P, Brewer GJ, Fink JK. White matter changes in Wilson disease. Arch Neurol. 2002;59(5):866–7.
116. van Wassenaer-van Hall HN, van den Heuvel AG, Jansen GH, Hoogenraad TU, Mali WP. Cranial MR in Wilson disease: abnormal white matter in extrapyramidal and pyramidal tracts. Am J Neuroradiol. 1995;16(10):2021–7.
117. Aikath D, Gupta A, Chattopadhyay I, Hashmi MA, Gangopadhyay PK, Das SK, Ray K. Subcortical white matter abnormalities related to drug resistance in Wilson disease. Neurology. 2006;67(5):878–80.
118. Laranout A, Ammar N, Mourad Z, Naji S, Hentati F. Wilson's disease: appreciable improvement of sub-cortical white matter abnormalities after copper chelating treatment: five years follow-up. Neuropediatrics. 2008;39(3):176–8.
119. Trocello JM, Guichard JP, Leyendecker A, Pernon M, Chaine P, El Balkhi S, Poupon J, Chappuis P, Woimant F. Corpus callosum abnormalities in Wilson's disease. J Neurol Neurosurg Psychiatry. 2011;82(10):1119–21.
120. Prashanth LK, Sinha S, Taly AB, Vasudev MK. Do MRI features distinguish Wilson's disease from other early onset extrapyramidal disorders? An analysis of 100 cases. Mov Disord. 2010;25(6):672–8.
121. Roh JK, Lee TG, WIe BA, Lee SB, Park SH, Chang KH. Initial and follow-upbrain MRI findings and correlation with the clinical course in Wilson's disease. Neurology. 1994;44(6):1064–8.
122. Schwarz J, Antonini A, Kraft E, Tatsch K, Vogl T, Kirsch CM, Leenders KL, Oertel WH. Treatment with D-penicillamine improves dopamine D2-receptor binding and T2-signal intensity de novo in Wilson's disease. Neurology. 1994;44(6):1079–82.

123. Takahashi W, Yoshii F, Shinohara Y. Reversible magnetic resonance imaging lesions in Wilson's disease: clinical-anatomical correlation. J Neuroimaging. 1996;6(4):246–8.
124. Da Costa Mdo D, Spitz M, Bacheschi LA, Leite CC, Lucato LT, Barbosa ER. Wilson's disease: two treatment modalities. Correlations to pretreatment and posttreatment brain MRI. Neuroradiology. 2009;51(10):627–33.
125. Huang CC, Chu NS. Wilson diseae: resolution of MRI lesions following long term oral zinc therapy. Acta Neurol Scand. 1996;93(2–3):215–8.
126. Cordato DJ, Fulham MJ, Yiannikas C. Pretreatment and posttreatment positron emission tomographic scan imaging in a 20-year old patient with Wilson's disease. Mov Disord. 1998;13(1):162–6.
127. Wu JC, Huang CC, Jeng LB, Chu NS. Correlation of neurological manifestations and MR images in a patient with Wilson's disease after liver transplantation. Acta Neurol Scand. 2000;102(2):135–9.
128. Schlaug G, Hefter H, Engelbrecht V, Kuwert T, Arnold S, Stocklin G, Seitz RJ. Neurological impairment and recovery in Wilson's diseaes: evidence from PET and MRI. J Neurol Sci. 1996;136(1–2):129–39.
129. Jeon B, Kim JM, Jeong JM, Kim KM, Chang YS, Lee DS, Lee MC. Dopamine transporter imaging with [123I]-beta-CIT demonstrates presynaptic nigrostriatal dopaminergic damage in Wilson's disease. J Neurol Neurosurg Psychiatry. 1998;65(1):60–4.
130. Alanen A, Komu M, Penttinen M, Leino R. Magnetic resonance imaging and proton MR spectroscopy in Wilson's disease. Br J Radiol. 1999;72(860):749–56.
131. Piga M, Murru A, Serra A, Sias A, Loi G, Marrosu F, Demelia L. Brain MRI and SPECT in the diagnosis of early neurological involvement in Wilson's disease. Eur J Nucl Med Mol Imaging. 2008;35(4):716–24.
132. Tarnacka B, Szeszkowski W, Buettner J, Golebiowski M, Gromadzka G, Czlonkowska A. Heterozygous carriers for Wilson disease—magnetic spectroscopy changes in the brain. Metab Brain Dis. 2009;24(3):463–8.
133. Tarnacka B, Szeszkowski W, Golbiowski M, Czlonkowska A. MR spectroscopy in monitoring the treatment of Wilson's disease patients. Mov Disord. 2008;23(11):1560–6.
134. Sener RN. Diffusion MR imaging changes associated with Wilson disease. Am J Neuroradiol. 2003;24(5):965–7.
135. Kawamura N, Ohyagi Y, Kawajiri M, Yoshiura T, Mihara F, Furuya H, Kira J. Serial diffusion-weighted MRI in a case of Wilson's disease with acute onset hemichorea. J Neurol. 2004;251(11):1413–4.
136. Favrole P, Chabriat H, Guichard JP, Woimant F. Clinical correlates of cerebral water diffusion in Wilson's disease. Neurology. 2006;66(3):384–9.
137. Sener RN. Diffusion MRI findings in Wilson's disease. Comput Med Imaging Graph. 2003;27(1):17–21.
138. Walter U, Krolikowski K, Tarnacka B, Benecke R, Czlonkowska A, Dressler D. Sonographic detection of basal ganglia lesions in asymptomatic and symptomatic Wilson disease. Neurology. 2005;64(10):1726–32.
139. Oder W, Prayer L, Grimm G, Spatt J, Ferenci P, Kollegger H, Schneider B, Gangl A, Deecke L. Wilson's disease: evidence of subgroups derived from clinical findings and brain lesions. Neurology. 1993;43(1):120–4.

Chapter 14
Neuroimaging of Ataxias

Anelyssa D'Abreu and Fernando Cendes

Introduction

Ataxia is a common neurological symptom characterized by incoordination of movement and loss of balance. Ataxias can be divided into three major etiologic groups: acquired ataxias, hereditary ataxias, and nonhereditary degenerative ataxias [1]. Acquired or symptomatic ataxias encompass a rather heterogeneous group that includes cerebrovascular disease, exogenous intoxication, alcoholic cerebellar degeneration, vitamin deficiency, inflammatory and demyelinating disorders, infection, paraneoplastic cerebellar degeneration, and hypothyroidism [1, 2]. The hereditary ataxias are usually divided by their mode of inheritance, and their final diagnosis relies on molecular testing [3]. The nonhereditary or sporadic degenerative ataxias are a group of ataxias in which a specific etiology, either acquired or genetic could not be determined. The main examples in this group are multiple system atrophy (MSA) and the sporadic adult-onset ataxia of unknown etiology [1].

The value of imaging studies is different for each one of those etiological groups. Magnetic resonance imaging (MRI) is considered mandatory in the evaluation of any patient presenting with ataxia in order to exclude symptomatic ataxias [4, 5]. MRI is usually not helpful in the differential diagnosis of hereditary ataxias, as it frequently demonstrates nonspecific findings such as cerebellar and vermian atrophy. However, even in this group some signs may guide future investigation or point to the diagnosis; for example, white matter (WM) changes in mitochondrial disorders (Fig. 14.1) and middle cerebellar peduncle (MCP) hyperintensity in fragile-X-associated tremor/ataxia syndrome (FXTAS; Fig. 14.2) [4, 5]. Similarly,

A. D'Abreu (✉) · F. Cendes
Department of Neurology, State University of Campinas-UNICAMP, Rua Vital Brasil, 251, Cidade Universitária Zeferino Vaz, Campinas, São Paulo 13083-888, Brazil
e-mail: anelyssa@gmail.com

F. Cendes
e-mail: fcendes@unicamp.br

F. B. Nahab, N. Hattori (eds.), *Neuroimaging of Movement Disorders,* Current Clinical Neurology 44, DOI 10.1007/978-1-62703-471-5_14,

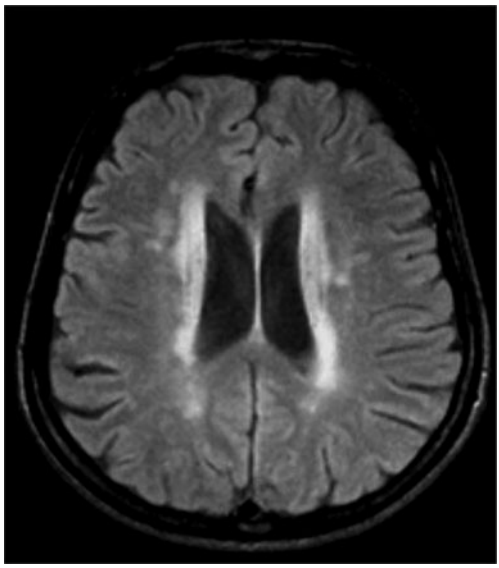

Fig. 14.1 Axial Fluid Attenuated Inversion Recovery (FLAIR) MRI in a patient with Myoclonic Epilepsy with Ragged Red Fibers (MERRF)

the presence of the "hot cross bun sign" may suggest the diagnosis of MSA in the appropriate clinical scenario (Fig. 14.3) [6].

Multiple recent studies in progressive ataxias have used different neuroimaging techniques to uncover their pathophysiology and to search for possible surrogate markers of disease onset and progression. This chapter will focus on the most common progressive degenerative ataxias, hereditary and sporadic. We will describe general findings of visual MRI analysis that might assist in the diagnosis of specific ataxic syndromes. Second, we will address recent neuroimaging findings and their contribution in the understanding of progressive ataxias.

Spinocerebellar Ataxias (SCAs)

The spinocerebellar ataxias comprise a large and heterogeneous group of autosomal dominant ataxias. There are at least 28 subtypes identified. They lead to degeneration of the cerebellum and its tracts, but also of the brainstem, basal ganglia, cortex, and peripheral nervous system [7]. Although multiple studies have described various MRI findings in SCAs, no specific pattern of atrophy or sign is pathognomonic of a particular sporadic ataxia [8–10]. MRI findings correlate poorly with disease severity, with some asymptomatic carriers showing mild atrophy while mildly symptomatic patients may have normal imaging results [9]. Image processing methods have, however, produced interesting results that increased our understanding of the progression of some of the SCAs and their clinical correlations.

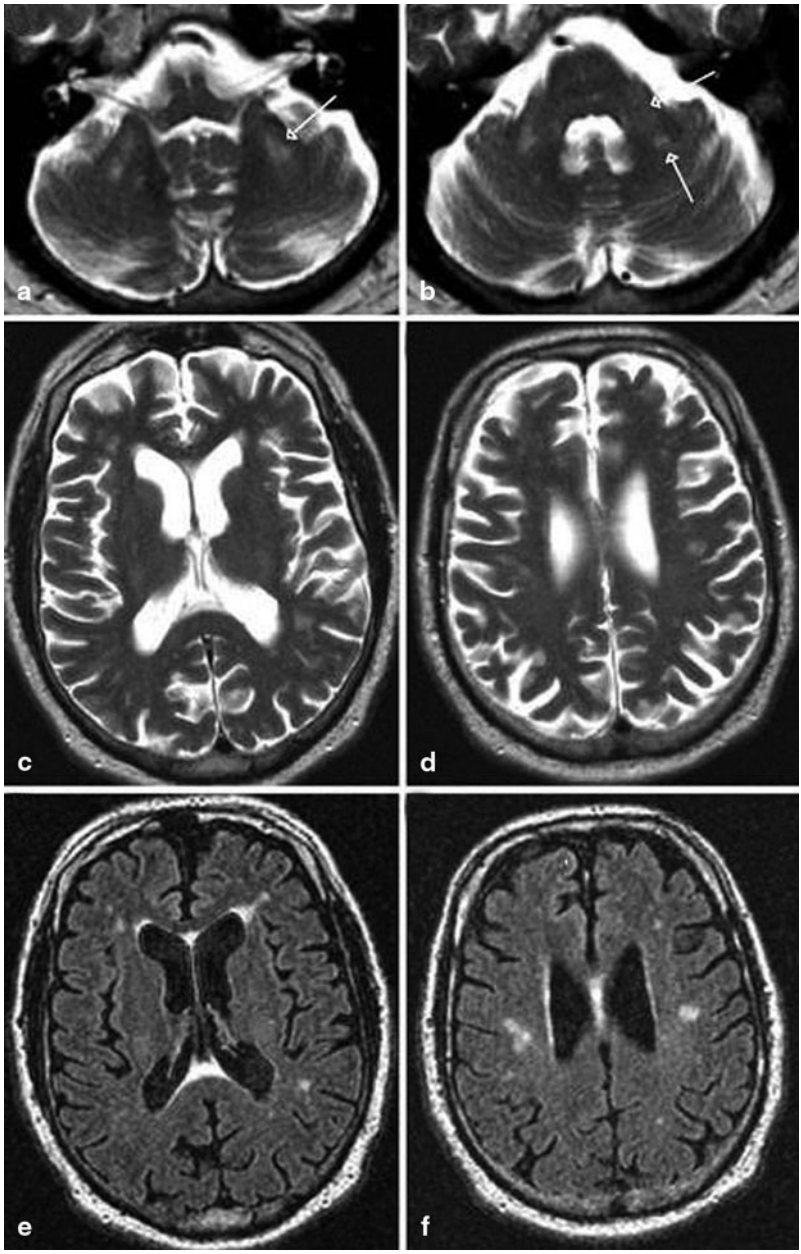

Fig. 14.2 MRI findings associated with FXTAS. **a**–**d** T2-weighted MRI; **e**, **f** FLAIR MRI. **a** Hyperintense sign in the deep white matter surrounding the dentate nucleus. **b** Hyperintense sign in the MCP that is both mild (*anterior arrow* in **b**) and moderate (*posterior arrow* in **b**) in severity. **c**–**f** Moderate cortical volume loss and mild increase of the lateral ventricles; nonspecific increased signal intensity in frontal and parietal white matter, most conspicuous on matching FLAIR images (**e**, **f**). (With kind permission from John Wiley and Sons: Movement Disorders (2007) 22: 2018–2030; Berry-Kravis E et al.; Fig. 1)

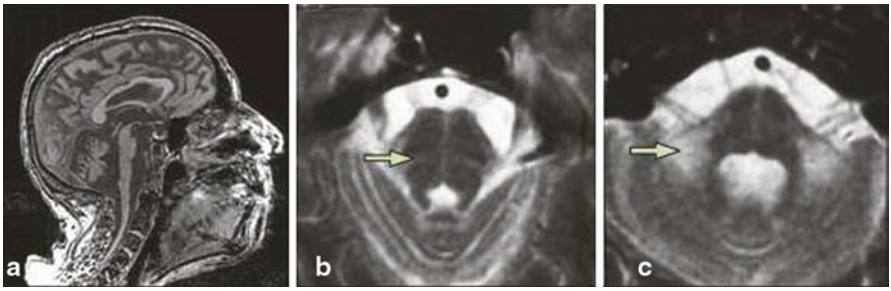

Fig. 14.3 MSA-C. **a** Severe atrophy of the cerebellum and brainstem, with characteristic flattening of the pons. **b**, **c** Hyperintense signal changes in the pons, and in the MCP on T2-weighted images. (Reprinted from The Lancet Neurology, Vol 9, Thomas Klockgether, Sporadic ataxia with adult onset: classification and diagnostic criteria, Pages 94–104, Copyright (2010), with permission from Elsevier)

Studying Brain Morphometry

Manual volumetry demonstrated a differential pattern of atrophy when comparing SCA1, SCA3, and SCA6. Cerebellar atrophy was more pronounced in SCA6 and SCA1 than SCA3, while pontine atrophy was more severe in SCA1 and SCA3. Duration of disease correlated with ventral pontine atrophy in SCA3, and with cerebellar atrophy in SCA3 and SCA6 [11]. In addition to the cerebellum and brainstem, Murata et al. evaluated the dentate nucleus, red nucleus, and globus pallidus in SCA6 [12] and SCA3 [13]. They used a graded semiquantitative approach to evaluate cortical atrophy. In SCA6, they observed atrophy of the cerebellum, vermis, pons, MCP, and red nucleus [12]. In SCA3, they showed a more widespread compromise with atrophy of the brainstem, cerebellum, frontal, temporal and occipital lobes, superior cerebellar peduncle (SCP), MCP, and globus pallidus. Pontine and midbrain atrophy in SCA3 were age-dependent while decreased globus pallidus diameter and the degree of temporal and occipital lobe atrophy correlated with duration of illness. Fourteen SCA3 patients (45.2 %) had high signal intensity in the transverse pontine fibers [13]. In SCA1, ataxia correlated with brainstem atrophy, while in SCA3 it correlated with brainstem and cerebellar atrophy [14].

CAG repeat size and age play an important role in disease progression in SCA3 [15, 16]; moreover, the progression of the cerebral involvement is not uniform. While the atrophy of the pontine base and the cerebellum significantly correlated with age, midbrain and pontine tegmentum atrophy did not show progression in a longitudinal study [17]. Pontine tegmentum atrophy seems to occur much earlier than in the pontine base, which remained in the control range long after symptom onset [18]. In addition, SCA3 patients with dystonia had smaller thalamic volumes than those without [19].

Fig. 14.4 T1-weighted sagittal MRI in SCA7: observe brainstem and pontine atrophy

A morphometric study in SCA2 used a semiquantitative score system to grade atrophy in infratentorial and supratentorial structures [20]. All patients presented a typical olivopontocerebellar atrophy pattern and frontal lobe atrophy. The parietal, temporal, and occipital lobes were also involved in a small percentage of patients. Interestingly, while there was no correlation between the infratentorial atrophy and clinical measures, supratentorial atrophy correlated with disease duration [21]. In a more recent study, the manually demarcated raw volumes of the cerebellum and pons in SCA2 correlated with the functional staging and disease duration, but not with CAG repeat size [21].

The primary brain target of neurodegeneration in SCA7 appears to be the brainstem, not the cerebellum. The pontine volume in SCA7 is significantly smaller than in SCA3 and SCA6, and pontine atrophy is present regardless of the degree of cerebellar atrophy, clinical severity, and duration of disease (Fig. 14.4) [22]. Spinal cord atrophy has only been evaluated in SCA3 and SCA6, and it is present only in the former [23].

While previously cited studies were based on preselected regions of interest (ROIs), voxel-based morphometry (VBM) allows for an unbiased evaluation of the entire brain and establishing important clinical correlations. For instance, SCA1 showed a symmetric loss of the gray matter (GM) in the rostral cerebellar vermis and the paramedian portion of the cerebellar lobes when compared to healthy controls. White matter was decreased in the peridentate region and MCPs. The cerebellar

and brainstem GM and WM volume loss correlated with disease duration, the International Cooperative Ataxia Rating Scale and the Inherited Ataxia Clinical Scale scores [24]. In SCA2, VBM demonstrated a significant atrophy in several cerebellar and brainstem areas, as well as the left inferior parietal lobule, the corticospinal tracts and the thalamus. Performance on the peg-board version of the Tower of London (coordination) correlated with the anterior cerebellum, while the computerized version (working memory and executive function) correlated with the posterior cerebellum. Authors concluded that neuropsychological tests requiring motor coordination may not be adequate to evaluate patients with SCAs [25].

A comprehensive study performed in SCA3 showed significant GM atrophy in the cortex, subcortex, cerebellum, and brainstem [26]. WM atrophy was restricted to the cerebellum. Age, CAG-repeat length, and disease duration predicted GM density in several ROIs, with age and repeat length being the most important. Interestingly, a longitudinal evaluation, after a 12-month interval, did not reveal significant progression, possibly due to a ceiling effect. In SCA7, VBM showed widespread decrease in GM involving the cerebellar cortex, insula, precentral and postcentral gyri, superior, inferior, and medial frontal gyri, inferior parietal lobule, parahippocampal gyrus, middle occipital gyrus, cuneus, precuneus, and lingual gyrus [27]. SCA17 patients had GM volume reduction in the posterior lobe of the cerebellum bilaterally that correlated with the length of expanded CAG repeats [28]. Atrophy was also observed in the caudate nucleus, postcentral gyrus, and cingulate gyrus. In a longitudinal analysis with an 18-month interval between MRIs, progression of GM atrophy in SCA17 was detected in the cerebellum, globus pallidus, middle temporal gyrus, inferior frontal gyrus, parahippocampus, cingulate gyrus, and precuneus. The progression of the motor symptoms correlated with the progression of the cerebellar atrophy, while the progression of the neuropsychiatric symptoms correlated with GM reduction in cortical areas [29].

Several VBM studies have compared different SCAs in an attempt to establish disease biomarkers and to differentiate patterns of atrophy among them. The findings showed that SCA1 and SCA2 share a similar pattern of atrophy [30, 31]. In SCA1, the volume of the brainstem inversely correlated with the Inherited Ataxia Clinical Scale score; the cerebellar volume correlated with disease duration in both SCA1 and SCA2 [31]. When compared to SCA3, SCA1 presented GM atrophy in clusters within the cerebellar hemispheres and left inferior frontal gyrus; SCA2 revealed clusters of atrophy in several hemispheric cerebellar areas and vermis [30]. WM atrophy was more pronounced in SCA1 and SCA2 than SCA3 (Fig. 14.5). Only SCA1 showed a correlation between the International Cooperative Ataxia Rating Scale score and atrophy in the cerebellum. Importantly, all SCAs demonstrated atrophy in supratentorial regions [30]. When compared to controls, SCA6 yielded GM loss restricted to the cerebellum and vermis, while SCA1 and SCA3 showed GM atrophy in the cerebellum, vermis, brainstem, caudate nucleus, putamen, and temporal lobes [32]. WM loss was present in the brainstem, pons, MCPs, cerebellar hemispheres, and midbrain in SCA1 and SCA3, but no WM changes were evident in SCA6 [33].

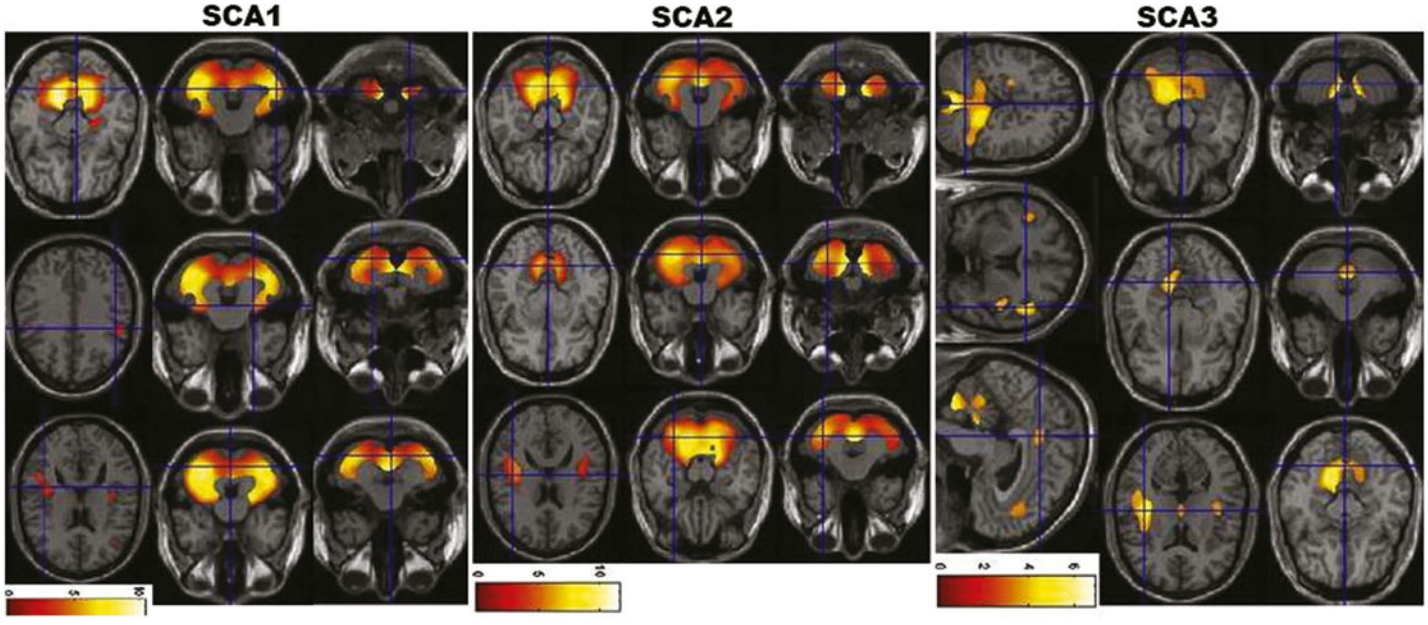

Fig. 14.5 Voxel-based morphometry findings in SCA1, SCA2, and SCA3. Observe the similarities between the pattern of atrophy between SCA1 and SCA2, and the differential atrophy in SCA3. (Reprinted from Parkinsonism & Related Disorders, Vol 17, Gaurav Goel et al, Gray matter volume deficits in spinocerebellar ataxia: An optimized voxel-based morphometric study, pages 521–527, Copyright (2011), with permission from Elsevier)

Diffusion Tensor Imaging (DTI)

There are few studies using DTI in the SCAs. DTI analysis was not able to differentiate SCA1 from SCA2, however it still demonstrated important clinical-imaging correlations [34]. In SCA1 and SCA2, fractional anisotropy (FA) was reduced in the corticospinal tract, transverse pontine fibers, SCP, MCP, and cerebellar WM; increased mean diffusivity (MD) was described in the same areas in SCA2, but only in the MCP and cerebellar WM in SCA1. Different ROIs correlated to either MD or FA in each SCA, however, only the MCP correlated with FA and MD in both diseases. In general, changes were more pronounced in SCA2. Another study confirmed the above results in SCA1 and SCA2, but also uncovered differences in MD and FA in the inferior cerebellar peduncles, medial and lateral lemnisci, spinothalamic tracts, and corpus callosum [35]. Group analysis of DTI data using tract-based spatial statistics (TBSS) showed correlation with disease severity in SCA1 and SCA2. Solodkin et al. [36] demonstrated that mean FA levels in the SCP in six SCA1 patients increased with disease duration and inversely correlated with scores on the Scale for the Assessment and Rating of Ataxia (SARA), possibly establishing FA as a marker of disease progression in SCA1. In SCA7 a widespread WM compromise is present, and some symptom evolution may correlate with WM integrity, since there was a significant negative correlation between disease duration and FA values in the callosal body, optic radiations, and corticospinal tract [27].

Magnetic Resonance Spectroscopy (MRS)

Proton MRS is also a valid tool in the evaluation of neurodegenerative ataxias, but due to the different methodologies applied in each study, the small number of patients included and the multiple ROIs chosen, it is difficult to compare and interpret results. A detailed metabolic assessment in SCA1 showed that the strongest biomarkers in separating patients from controls were total N-acetylaspartate (NAA), myoinositol (mI), glutamate/glutamine (Glx), and total creatine (Cr) in the cerebellar hemispheres and NAA, mI and Glx in the pons. The NAA/mI ratio in both regions presented 100 % specificity and sensitivity [37]. NAA, Cr, mI, and NAA/mI ratio were the best MRS predictors to distinguish between SCA1, SCA2, SCA6, and MSA-cerebellar variant (MSA-C) with at least 90 % accuracy [38]. Both of these studies demonstrate the utility of using metabolites as surrogate end-points in clinical studies.

Contrasting SCA2 to SCA6, NAA/Cr and Cho/Cr were lower in SCA2 than SCA6 using short echo time (TE); and using long TE, NAA/Cr was lower and Cho/Cr higher in SCA2. Lactate peaks were also present in SCA2, but not SCA6. These findings suggest a distinct pattern of cellular degeneration in both SCAs [39]. Another study compared SCA2 with MSA-C and it also demonstrated lactate peaks in SCA2, but not MSA-C [40]. SCA1 and SCA2 patients presented decreased absolute NAA values in the brainstem and cerebellum [31], while another study failed to show statistical difference in NAA/Cr in SCA6 compared to controls [41]. In SCA3, MRS in the deep

cerebral WM showed decreased levels of NAA/Cr, suggestive of a more widespread neurodegeneration [42]. Yabe et al. [43] performed [^{31}P]-MRS in the calf muscle of eight male patients with SCA3 and 11 healthy males before, during, and after a 4-minute plantar flexion exercise and demonstrated a reduction in maximum rate of mitochondrial ATP production over the course of 2 years.

Nuclear Imaging

The use of nuclear imaging in ataxia has provided both confirmatory findings to those of MRI in addition to the identification of altered metabolic patterns in presymptomatic individuals and differential metabolic patterns within the SCAs [44–48].

Dopamine transporter imaging using [^{11}C]d-threo-methylphenidate ([^{11}C]dMP) in SCA1, SCA2, SCA3, and SCA6 has revealed reduced striatal [^{11}C]dMP binding potential in SCA2 and SCA3, but not in SCA1 and SCA6. The decrease were similar to those observed in idiopathic Parkinson disease (iPD). Interestingly, features of parkinsonism have been described in SCA2 and SCA3, even though none of the patients studied presented parkinsonian signs on their neurologic exam [44]. Similar findings were observed in SCA2 subjects, without clear parkinsonism but with dystonia using single photon emission computed tomography (SPECT) to assess the presynaptic dopamine reuptake site with 12β-carboxymethyl-3β-(4-iodophenyl)-tropane (β-CIT) and the postsynaptic dopamine D2 receptors with ^{123}I-iodobenzamide (IBZM) [49]. Both were abnormal in SCA2 demonstrating impaired striatal dopaminergic transmission. In SCA3, impairment of presynaptic dopamine function occurs at an early stage, prior to symptom onset. (99m)Tc-TRODAT-1 brain SPECT used to assess uptake values in bilateral striatal areas in asymptomatic SCA3 gene carriers showed decreased uptake values when compared to the control group [50].

An ^{18}F-deoxyglucose positron emission tomography (FDG) study comparing seven asymptomatic SCA3 patients and controls showed subclinical changes of FDG uptake in the cerebellar hemispheres, brainstem, and occipital, parietal, and temporal cortices in SCA3, suggesting preclinical disease activity [51]. Discriminant function analysis found that cerebellar FDG uptake ratios were able to correctly identify controls and symptomatic SCA3 with a sensitivity and specificity of 100 % and differentiate asymptomatic from symptomatic patients in 14 out of 15 subjects [51].

While considered by most to be clinically a predominant cerebellar syndrome, a study using (99m)Tc-TRODAT-1 SPECT in SCA6 showed a variable degree of striatal dopaminergic impairment. It should be noted, however, that some of the patients included had mild parkinsonism [52]. FDG in SCA6 also showed decreased cerebral glucose utilization in cortical areas and basal ganglia [53].

Friedreich's Ataxia (FRDA)

Friedreich's ataxia is the most common autosomal recessive ataxia and is characterized by ataxia, head titubation, distal amyotrophy, and areflexia, Babinski sign, decreased joint position sense and vibratory sensation, cardiac involvement, and diabetes [54]. In most cases it is caused by a homozygous GAA intronic expansion at the frataxin gene (9q13) [54]. Prior to genetic testing becoming widely available, MRI findings provided initial clues to the clinical diagnosis of FRDA due to the major atrophy observed in the cervical spinal cord and a relatively normal cerebellum [55]. However, especially in patients with late-onset FRDA, cerebellar atrophy is not uncommon (Fig. 14.6) [56, 57]. A volumetric study measuring the cross-sectional area of the SCP found a 60 % reduction in the area in FRDA compared to controls. More importantly, SCP cross-sectional area inversely correlated with the Friedreich's Ataxia Rating Scale scores and disease duration, and directly correlated with the age of onset [58].

Although GM atrophy has been concordant in most studies using different neuroimaging techniques (dorsal medulla, cerebellar hemispheres, the rostral vermis, dentate nucleus), WM involvement is discrepant [59–61]. França et al. [59] studied cerebral involvement by means of VBM and reported WM loss in the posterior cingulate gyrus, middle frontal gyrus and paracentral lobule, as well as inferomedial portions of cerebellar hemispheres and rostral vermis, while in another VBM study the WM loss was restricted to the posterior fossa [60]. França et al. corroborated their findings of WM changes with single voxel MRS acquired over the superior–posterior region of the right hemisphere at the level of the corpus callosum. They found a significant reduction of NAA/Cr in FRDA compared to controls. Two studies utilizing DTI confirmed the involvement of the WM in FRDA in areas outside the cerebellum and brainstem, though the particular regions identified were different among the studies [62, 63].

Ataxia Telangiectasia (AT)

Ataxia Telangiectasia is the second most common autosomal recessive ataxia [64]. The onset is usually before age 5, and is characterized by progressive cerebellar ataxia, oculomotor apraxia, teleangiectasia, choreoathetosis, high risk of malignancy, recurrent sinopulmonary infections due to immunoglobulin deficiencies and enhanced sensitivity to ionizing radioactivity [64, 65]. At symptom onset, the MRI may be normal but as disease progresses there is considerable cerebellar atrophy (see Fig. 14.6) [66–68]. Cerebral capillary telangiectasias are best seen on postcontrast T1-weighted images or T2*-weighted gradient-echo images and cases with multiple brain telangiectasias in the brain and brainstem have been identified [69, 70]. There are few neuroimaging studies in AT. In a study using DWI and apparent diffusion coefficient (ADC) maps, authors calculate trace ADC values in 16 ROIs. ADC values of the cerebellar WM and cortex differentiated patients from controls with 100 %

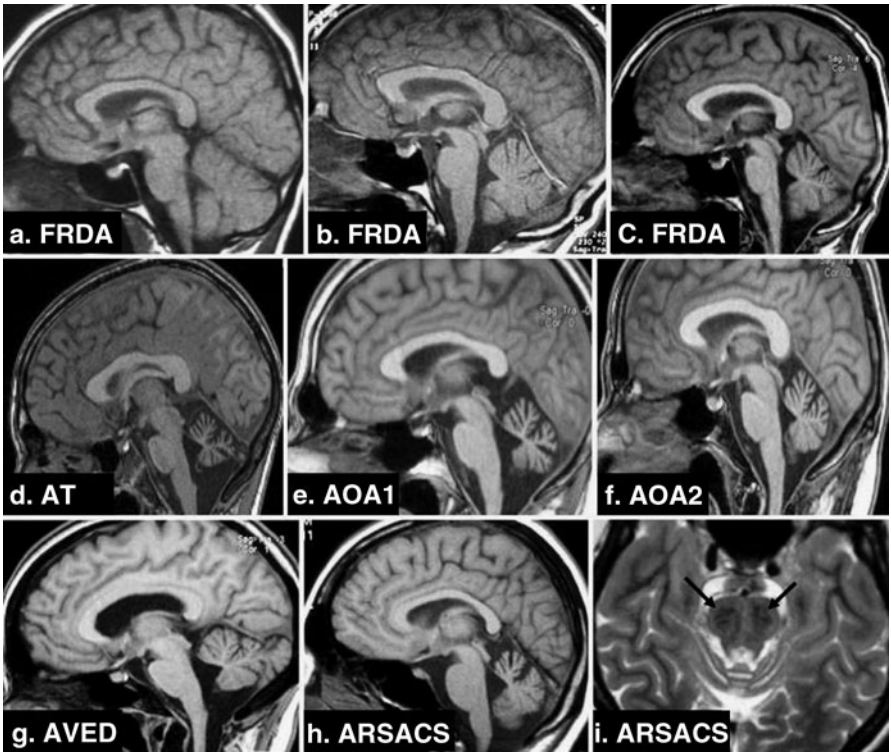

Fig. 14.6 **a**–**h** Sagittal T1-weighted imaging; **i** Axial T2-weighted imaging. **a** Early-onset FRDA 1-year disease duration. **b** Early-onset FRDA, 10-year disease duration. **c** Early-onset FRDA, 20-year disease duration. Note a pattern of progressive atrophy of the cerebellum and spinal cord. **d** AT: evident cerebellar atrophy. **e** AOA1: striking cerebellar atrophy. **f** AOA2: clear cerebellar atrophy. **g** AVED: moderate cerebellar atrophy. **h** ARSACS: noticeable cerebellar atrophy. **i** ARSACS: linear bilateral hypointensities in the pons. (With kind permission from Springer Science + Business Media: Neurogenetics (2010) 11:1–12; Anheim M et al.; Fig. 2.)

certainty. The cut-off ADC value of 0.699 mm^2/s in the middle cerebellar cortex yielded 100 % sensitivity and specificity [71]. Contrary to other cerebellar ataxias that usually show reduced NAA levels on MRS, cases with AT show an increase in cerebellar Cho levels, suggesting an ongoing process of cellular degeneration and membrane breakdown [70].

Fragile-X-Associated Tremor/Ataxia Syndrome (FXTAS)

Fragile-X-associated tremor/ataxia syndrome is caused by a CGG expansion (55–200 repeats; premutation range) of the fragile X mental retardation 1 (*FMR1*) gene. FXTAS is clinically characterized by action tremor, cerebellar ataxia, cognitive and

psychiatric symptoms. The primary MRI findings consist of atrophy of the cerebral hemispheres, brainstem, and cerebellum, along with increased T2 signal intensity in the WM of the MCP and the WM surrounding the dentate nuclei (see Fig. 14.2) [72]. Other findings include increased T2 or FLAIR signal in periventricular and deep WM regions of the cerebral hemispheres and corpus callosum [72]. A VBM study compared three groups: symptomatic premutation carriers (PFX+), asymptomatic premutation carriers (PFX−) and controls [73]. When compared to healthy controls, PFX+ had significant GM reduction in mostly the frontal lobes, but also temporal, parietal, and occipital lobes, cerebellum, and thalamus. The bilateral posterior superior/middle temporal gyri also showed increased GM in the PFX+ group. A comparison of PFX+ and PFX− showed GM reductions in the cerebellum, dorsomedial prefrontal cortex, and precuneus in the PFX+ group. Other findings included significant neuroimaging and clinical correlations such as: GM loss in the left amygdala and increased levels of obsessive–compulsiveness and depression; decreased GM in the left inferior frontal cortex and anterior cingulate cortex and poor working memory performance; clinical severity and a reduction of vermal GM [73]. Female patients with FXTAS present a similar pattern of cerebral and cerebellar involvement, though to a lesser degree [74]. Significant WM compromise is also present in FXTAS. Patients with FXTAS showed decreased FA in several WM tracts, mostly the MCP, SCP, cerebral peduncle, fornix, and stria terminalis. Axial and radial diffusivities were increased in the MCP of asymptomatic premutation carriers [75].

Prefrontal cortex impairment seems to be responsible for the cognitive dysfunction in FXTAS. Functional MRI (fMRI) performed during a verbal working memory task in symptomatic and asymptomatic carriers exhibited reduced activation in the right ventral inferior frontal cortex and left premotor/dorsal inferior frontal cortex when compared to controls. Symptomatic carriers showed decreased activation of the right premotor/dorsal inferior frontal cortex. There was also a negative correlation between the right ventral inferior frontal cortex activity and the levels of *FMR1* mRNA after excluding the effect of disease severity [76].

Autosomal Recessive Spastic Ataxia of Charlevoix–Saguenay (ARSACS)

Autosomal Recessive Spastic Ataxia of Charlevoix–Saguenay is a neurodegenerative disease that encompasses early onset spasticity, cerebellar ataxia, distal amyotrophy, peripheral neuropathy, skeletal deformities, and retinal hypermyelination [65]. It is caused by mutations in the *SACS* gene. MRI shows early atrophy of the superior vermis and progressive atrophy of the cerebellar hemispheres and the spinal cord (see Fig. 14.6) [66]. A linear hypointensity on T2-weighted images and FLAIR may be present in the pons [66, 77]. This area has been shown to be the pontocerebellar fibers, using diffusion tensor color encoded MRI maps, whereas the pyramidal tracts were thin and not in their usual location [78]. Recently, hypointense lesions in the MCP were described in T2-weighted and FLAIR images [79].

Other Autosomal Recessive Ataxias

In ataxia with oculomotor apraxia (AOA)-1 and AOA-2, cerebellar atrophy occurs early in the course of the disease and is present in the vast majority of patients [66, 80]. There are very few reports of MRI in ataxia with isolated vitamin E deficiency (AVED) [66] (see Fig. 14.6).

Multiple Systems Atrophy

Multisystem Atrophy is a neurodegenerative disease clinically characterized by a variable combination of autonomic, cerebellar, parkinsonian, and pyramidal signs [81]. The distinctive neuropathological feature is glial cytoplasmic inclusions in oligodendroglial cells [1]. Clinically, MSA is usually divided in two subtypes: one with a predominant parkinsonism (MSA-P) and another with predominant cerebellar findings (MSA-C). Routine MRI is the most important diagnostic test in MSA and the introduction of different sequences and imaging analyses have improved the diagnosis and may lead to potential surrogate biomarkers [81]. Most imaging studies of MSA typically focus on differentiating the various atypical parkinsonisms from idiopathic PD [82–88]. Since this is beyond the scope of this chapter, we will concentrate on MSA-C.

The most common MRI findings are a hyperintense rim at the lateral edge of the dorsolateral putamen and the "hot cross bun" sign (see Fig. 14.3) [1, 89]. However, the latter has been described in other ataxias, including SCA2, SCA3, SCA7, and SCA8 [90, 91]. Significant infratentorial atrophy is also noted.

Studies comparing MSA-P to MSA-C have demonstrated a similar pattern of cerebral compromise, however, with a differential degree of atrophy within the involved areas [92–95]. A VBM and voxel-based relaxometry study comparing MSA-C and MSA-P showed differences only in the infratentorial ROIs, which were more severe in MSA-C than in MSA-P [92]. Conversely, comparing to controls, Wang et al. [94] found an increase in ADC values in the MCP and cerebellum; a reduction in FA in the pyramidal tract, MCP, and WM of the cerebellum in both MSA-C and MSA-P. This confirmed a previous study that found increased ADC values at the MCP and pons in MSA-C [96]. In addition, isotropic diffusion-weighted image (DWI) values were decreased in the cerebellar cortex and deep cerebellar nuclei in MSA-C and increased in the basal ganglia in MSA-P [94]. Pellecchia et al. [93] used DWI images and measured the diffusion Trace(D) brain maps. They demonstrated that in MSA-P Trace(D) values were significantly increased in the putamen, while in MSA-C Trace(D) values were significantly higher in the cerebellar WM and MCP.

VBM has also revealed supratentorial volume loss and pyramidal tract involvement in MSA-C [97–99]. A longitudinal evaluation using quantitative 3D volumetry (approximately 2-year-interval between MRIs) established that the total cerebellum volume of MSA-C patients showed a reduction of 7.3 ml/year compared to a rate of 0.3 ml/year in controls [98]. Microstructural widespread WM involvement in

MSA-C, determined by DTI images, is also present in infratentorial and supratentorial areas, and correlates with several clinical markers [100, 101]. FA correlated significantly with Barthel index score in the cerebellar WM, MCP, basis pontis, periaqueductal area, genu and posterior limb of internal capsule, and temporal WM; while MD correlated with the Barthel index score in the cerebellar WM, periaqueductal area, and lateral midbrain. SARA score correlated with FA in the cerebellar WM, MCP, and posterior limb of internal capsules; and with MD in the cerebellar WM. Interestingly, the MD of pontine tegmentum correlated significantly with severity of orthostatic hypotension. Disease duration correlated with FA in the cerebellar WM, MCP, basis pontis, periaqueductal area, posterior limb of internal capsules, and periventricular area; and with MD in the MCP, periaqueductal area, and lateral midbrain [100].

MRS evaluated metabolites concentration at the pons and medulla. Myo-Inositol was higher in MSA-C than controls in the pons and medulla, and NAA and Cho were lower in both. Cr concentration was higher in the pons in MSA-C, whereas mean Glx/Cr was lower. A direct correlation was observed between myo-Inositol/Cr and total UMSARS score; myo-Inositol/Cr ratio in the medulla and disease duration [102]. These results suggested the presence of neuronal loss and gliosis, and identified the myo-Inositol/Cr as a possible biomarker of disease severity of MSA-C.

Conclusions and Future Perspectives

Till date, the neuroimaging findings on the ataxias provide a wealth of knowledge regarding the regions of involvement and potential characteristics by which to differentiate particular ataxias from another. Most of the cited studies were performed using 1.5 T and 2 T MRI scanners, however, imaging studies employing 3 T and 4 T scanners are increasing in number, and their availability may allow more detailed results. Advancements in hardware and image analysis methods will continue to enhance our understanding of the progressive ataxias, and eventually lead to the discovery of a reliable biomarker of disease onset and progression in these disorders.

There is also a great need for longitudinal studies in progressive ataxias. Whereas multiple cross-sectional studies have demonstrated correlations between imaging findings and clinical markers, such as disease duration and motor scale scores, it is necessary to replicate these results in longitudinal studies in order to validate these methods for use in future clinical trials.

References

1. Klockgether T. Sporadic ataxia with adult onset: classification and diagnostic criteria. Lancet Neurol. 2010;9:94–104.
2. Abele M, Burk K, Schols L, et al. The aetiology of sporadic adult-onset ataxia. Brain. 2002;125:961–8.

3. Whaley NR, Fujioka S, Wszolek ZK. Autosomal dominant cerebellar ataxia type I: a review of the phenotypic and genotypic characteristics. Orphanet J Rare Dis. 2011;6:33.
4. Degardin A, Dobbelaere D, Vuillaume I, et al. Spinocerebellar ataxia: a rational approach to aetiological diagnosis. Cerebellum. 2012;11(1):289–99.
5. Brusse E, Maat-Kievit JA, Van Swieten JC. Diagnosis and management of early- and late-onset cerebellar ataxia. Clin Genet. 2007;71:12–24.
6. Köllensperger M, Wenning GK. Assessing disease progression with MRI in atypical parkinsonian disorders. Mov Disord. 2009;24:S699–702.
7. Paulson HL. The spinocerebellar ataxias. J Neuroophthalmol. 2009;29:227–37.
8. Viau M, Boulanger Y. Characterization of ataxias with magnetic resonance imaging and spectroscopy. Parkinsonism Relat Disord. 2004;10:335–51.
9. Döhlinger S, Hauser T-K, Borkert J, Luft A, Schulz J. Magnetic resonance imaging in spinocerebellar ataxias. Cerebellum. 2008;7:204–14.
10. Ormerod IE, Harding AE, Miller DH, et al. Magnetic resonance imaging in degenerative ataxic disorders. J Neurol Neurosurg Psychiatry. 1994;57:51–7.
11. Nagaoka U, Suzuki Y, Kawanami T, et al. Regional differences in genetic subgroup frequency in hereditary cerebellar ataxia, and a morphometrical study of brain MR images in SCA1, MJD and SCA6. J Neurol Sci. 1999;164:187–94.
12. Murata Y, Kawakami H, Yamaguchi S, et al. Characteristic magnetic resonance imaging findings in spinocerebellar ataxia 6. Arch Neurol. 1998;55:1348–52.
13. Murata Y, Yamaguchi S, Kawakami H, et al. Characteristic magnetic resonance imaging findings in Machado-Joseph disease. Arch Neurol. 1998;55:33–7.
14. Jacobi H, Hauser T-K, Giunti P, et al. Spinocerebellar ataxia types 1, 2, 3 and 6: the clinical spectrum of ataxia and morphometric brainstem and cerebellar findings. Cerebellum. 2012;11:1–12.
15. Onodera O, Idezuka J, Igarashi S, et al. Progressive atrophy of cerebellum and brainstem as a function of age and the size of the expanded CAG repeats in the MJD1 gene in Machado-Joseph disease. Ann Neurol. 1998;43:288–96.
16. Abe Y, Tanaka F, Matsumoto M, et al. CAG repeat number correlates with the rate of brainstem and cerebellar atrophy in Machado-Joseph disease. Neurology. 1998;51:882–4.
17. Horimoto Y, Matsumoto M, Yuasa H, et al. Brainstem in Machado-Joseph disease: atrophy or small size? Eur J Neurol. 2008;15:102–5.
18. Yoshizawa T, Watanabe M, Frusho K, Shoji S. Magnetic resonance imaging demonstrates differential atrophy of pontine base and tegmentum in Machado-Joseph disease. J Neurol Sci. 2003;215:45–50.
19. D'Abreu A, Franca MC, Yasuda CL, Souza MSA, Lopes-Cendes I, Cendes F. Thalamic volume and dystonia in Machado-Joseph disease. J Neuroimaging. 2011;21:e91–3.
20. Giuffrida S, Saponara R, Restivo DA, et al. Supratentorial atrophy in spinocerebellar ataxia type 2: MRI study of 20 patients. J Neurol. 1999;246:383–8.
21. Ying SHM, Choi SIB, Perlman SLM, Baloh RWM, Zee DSM, Toga AWP. Pontine and cerebellar atrophy correlate with clinical disability in SCA2. Neurology. 2006;66:424–6.
22. Bang OY, Lee PH, Kim SY, Kim HJ, Huh K. Pontine atrophy precedes cerebellar degeneration in spinocerebellar ataxia 7: MRI-based volumetric analysis. J Neurol Neurosurg Psychiatry. 2004;75:1452–6.
23. Lukas C, Hahn H, Bellenberg B, et al. Spinal cord atrophy in spinocerebellar ataxia type 3 and 6. J Neurol. 2008;255:1244–9.
24. Ginestroni A, Della Nave R, Tessa C, et al. Brain structural damage in spinocerebellar ataxia type 1. J Neurol. 2008;255:1153–8.
25. D'Agata F, Caroppo P, Boghi A, et al. Linking coordinative and executive dysfunctions to atrophy in spinocerebellar ataxia 2 patients. Brain Struct Funct. 2011;216:275–88.
26. D'Abreu A, França MC Jr, Yasuda CL, Campos BAG, Lopes-Cendes I, Cendes F. Neocortical atrophy in Machado-Joseph disease: a longitudinal neuroimaging study. J Neuroimaging. 2011. doi:101111/j1552-6569201100614 × 2011.

27. Alcauter S, Barrios FA, Diaz R, Fernandez-Ruiz J. Gray and white matter alterations in spinocerebellar ataxia type 7: an in vivo DTI and VBM study. Neuroimage. 2011;55:1–7.
28. Reetz K, Kleiman A, Klein C, et al. CAG repeats determine brain atrophy in spinocerebellar ataxia 17: a VBM study. PLoS One. 2011;6:e15125.
29. Reetz K, Lencer R, Hagenah J, et al. Structural changes associated with progression of motor deficits in spinocerebellar ataxia 17. Cerebellum. 2010;9:210–7.
30. Goel G, Pal PK, Ravishankar S, et al. Gray matter volume deficits in spinocerebellar ataxia: an optimized voxel based morphometric study. Parkinsonism Relat Disord. 2011;17:521–7.
31. Guerrini L, Lolli F, Ginestroni A, et al. Brainstem neurodegeneration correlates with clinical dysfunction in SCA1 but not in SCA2. A quantitative volumetric, diffusion and proton spectroscopy MR study. Brain. 2004;127:1785–95.
32. Schulz JB, Borkert J, Wolf S, et al. Visualization, quantification and correlation of brain atrophy with clinical symptoms in spinocerebellar ataxia types 1, 3 and 6. Neuroimage. 2010;49:158–68.
33. Lukas C, Schöls L, Bellenberg B, et al. Dissociation of grey and white matter reduction in spinocerebellar ataxia type 3 and 6: a voxel-based morphometry study. Neurosci Lett. 2006;408:230–5.
34. Mandelli ML, De Simone T, Minati L, et al. Diffusion tensor imaging of spinocerebellar ataxias types 1 and 2. Am J Neuroradiol. 2007;28:1996–2000.
35. Della Nave R, Ginestroni A, Tessa C, et al. *Brain white matter damage in SCA1 and SCA2. An in vivo study using voxel-based morphometry, histogram analysis of mean diffusivity and tract-based spatial statistics. Neuroimage.* 2008;43:10–19.
36. Solodkin A, Peri E, Chen E, Ben-Jacob E, Gomez C. Loss of intrinsic organization of cerebellar networks in spinocerebellar ataxia type 1: correlates with disease severity and duration. Cerebellum. 2011;10:218–32.
37. Öz G, Hutter D, Tkác I, et al. Neurochemical alterations in spinocerebellar ataxia type 1 and their correlations with clinical status. Mov Disord. 2010;25:1253–61.
38. Öz G, Iltis I, Hutter D, Thomas W, Bushara K, Gomez C. Distinct neurochemical profiles of spinocerebellar ataxias 1, 2, 6, and cerebellar multiple system atrophy. Cerebellum. 2011;10:208–17.
39. Boesch SM, Schocke M, Bürk K, et al. Proton magnetic resonance spectroscopic imaging reveals differences in spinocerebellar ataxia types 2 and 6. J Magn Reson Imaging. 2001;13:553–9.
40. Boesch SM, Wolf C, Seppi K, Felber S, Wenning GK, Schocke M. Differentiation of SCA2 from MSA-C using proton magnetic resonance spectroscopic imaging. J Magn Reson Imaging. 2007;25:564–9.
41. Hadjivassiliou M, Wallis LI, Hoggard N, Grünewald RA, Griffiths PD, Wilkinson ID. MR spectroscopy and atrophy in Gluten, Friedreich's and SCA6 ataxias. Acta Neurol Scand. 2011. doi:10.1111/j.1600-0404.2011.01620.x.
42. D'Abreu A, Franca M, Appenzeller S, Lopes-Cendes I, Cendes F. Axonal dysfunction in the deep white matter in Machado-Joseph disease. J Neuroimaging. 2009;19:9–12.
43. Yabe I, Tha KK, Yokota T, et al. Estimation of skeletal muscle energy metabolism in Machado-Joseph disease using P-31-MR spectroscopy. Mov Disord. 2011;26:165–8.
44. Wullner U, Reimold M, Abele M, et al. Dopamine transporter positron emission tomography in spinocerebellar ataxias type 1, 2, 3, and 6. Arch Neurol. 2005;62:1280–5.
45. Honjo K, Ohshita T, Kawakami H, et al. Quantitative assessment of cerebral blood flow in genetically confirmed spinocerebellar ataxia type 6. Arch Neurol. 2004;61:933–7.
46. Etchebehere EC, Cendes F, Lopes-Cendes I, Pereira JA, Lima MC, Sansana CR, Silva CA, Camargo MF, Santos AO, Ramos CD, Camargo EE. Brain single-photon emission computed tomography and magnetic resonance imaging in Machado-Joseph disease. Arch Neurol. 2001;58:1257–63.
47. Taniwaki T ST, Kobayashi T, Kuwabara Y, Otsuka M, Ichiya Y, Masuda K, Goto I. Positron emission tomography (PET) in Machado-Joseph disease. J Neurol Sci. 1997;145:63–7.

48. Wang PS, Liu RS, Yang BH, Soong BW. Regional patterns of cerebral glucose metabolism in spinocerebellar ataxia type 2, 3 and 6—a voxel-based FDG-positron emission tomography analysis. J Neurol. 2007;254:838–45.
49. Boesch SM, Donnemiller E, Müller J, et al. Abnormalities of dopaminergic neurotransmission in SCA2: a combined 123I-βCIT and 123I-IBZM SPECT study. Mov Disord. 2004;19: 1320–5.
50. Yen TC, Tzen KY, Chen MC, et al. Dopamine transporter concentration is reduced in asymptomatic Machado-Joseph disease gene carriers. J Nucl Med. 2002;43:153–9.
51. Soong BW, Liu RS. Positron emission tomography in asymptomatic gene carriers of Machado–Joseph disease. J Neurol Neurosurg Psychiatry. 1998;64:499–504.
52. Kim J-M, Lee J-Y, Kim HJ, et al. The wide clinical spectrum and nigrostriatal dopaminergic damage in spinocerebellar ataxia type 6. J Neurol Neurosurg Psychiatry. 2010;81:529–32.
53. Soong B, Liu R, Wu L, Lu Y, Lee H. Metabolic characterization of spinocerebellar ataxia type 6. Arch Neurol. 2001;58:300–4.
54. Koeppen AH. Friedreich's ataxia: pathology, pathogenesis, and molecular genetics. J Neurol Sci. 2011;303:1–12.
55. Koeppen A, Morral J, McComb R, Feustel P. The neuropathology of late-onset Friedreich's ataxia. Cerebellum. 2011;10:96–103.
56. De Michele G, Di Salle F, Filla A, et al. Magnetic resonance imaging in "typical" and "late onset" Friedreich's disease and early onset cerebellar ataxia with retained tendon reflexes. Ital J Neurol Sci. 1995;16:303–8.
57. Bhidayasiri R, Perlman SL, Pulst SM, Geschwind DH. Late-onset Friedreich ataxia: phenotypic analysis, magnetic resonance imaging findings, and review of the literature. Arch Neurol. 2005;62:1865–9.
58. Akhlaghi H, Corben L, Georgiou-Karistianis N, et al. Superior cerebellar peduncle atrophy in Friedreich's ataxia correlates with disease symptoms. Cerebellum. 2011;10:81–7.
59. França M, D'Abreu A, Yasuda C, et al. A combined voxel-based morphometry and 1H-MRS study in patients with Friedreich's ataxia. J Neurol. 2009;256:1114–20.
60. Della Nave R, Ginestroni A, Giannelli M, et al. Brain structural damage in Friedreich's ataxia. J Neurol Neurosurg Psychiatry. 2008;79:82–5.
61. Iltis I, Hutter D, Bushara KO, et al. 1H MR spectroscopy in Friedreich's ataxia and ataxia with oculomotor apraxia type 2. Brain Res. 2010;1358:200–10.
62. Della Nave R, Ginestroni A, Tessa C, et al. Brain white matter tracts degeneration in Friedreich ataxia. An in vivo MRI study using tract-based spatial statistics and voxel-based morphometry. Neuroimage. 2008;40:19–25.
63. Rizzo G, Tonon C, Valentino ML, et al. Brain diffusion-weighted imaging in Friedreich's ataxia. Mov Disord. 2011;26:705–12.
64. Anheim M, Tranchant C, Koenig M. The autosomal recessive cerebellar ataxias. N Engl J Med. 2012;366:636–46.
65. Palau F, Espinos C. Autosomal recessive cerebellar ataxias. Orphanet J Rare Dis. 2006;1:47.
66. Anheim M, Fleury M, Monga B, et al. Epidemiological, clinical, paraclinical and molecular study of a cohort of 102 patients affected with autosomal recessive progressive cerebellar ataxia from Alsace, Eastern France: implications for clinical management. Neurogenetics. 2010;11:1–12.
67. Chun HH, Gatti RA. Ataxia-telangiectasia, an evolving phenotype. DNA Repair. 2004;3:1187–96.
68. Tavani F, Zimmerman RA, Berry GT, Sullivan K, Gatti R, Bingham P. Ataxia-telangiectasia: the pattern of cerebellar atrophy on MRI. Neuroradiology. 2003;45:315–9.
69. Ciemins JJ, Horowitz AL. Abnormal white matter signal in ataxia telangiectasia. Am J Neuroradiol. 2000;21:1483–5.
70. Wallis LI, Griffiths PD, Ritchie SJ, Romanowski CAJ, Darwent G, Wilkinson ID. Proton spectroscopy and imaging at 3 T in ataxia-telangiectasia. Am J Neuroradiol. 2007;28:79–83.
71. Firat AK, Muammer KH, Firat Y, Yakinci C. Quantitative evaluation of brain involvement in ataxia telangiectasia by diffusion weighted MR imaging. Eur J Radiol. 2005;56:192–6.

72. Berry-Kravis E, Abrams L, Coffey SM, et al. Fragile X-associated tremor/ataxia syndrome: clinical features, genetics, and testing guidelines. Mov Disord. 2007;22:2018–30.
73. Hashimoto R, Javan AK, Tassone F, Hagerman RJ, Rivera SM. A voxel-based morphometry study of grey matter loss in fragile X-associated tremor/ataxia syndrome. Brain. 2011;134:863–78.
74. Adams JS, Adams PE, Nguyen D, et al. Volumetric brain changes in females with fragile X-associated tremor/ataxia syndrome (FXTAS). Neurology. 2007;69:851–9.
75. Hashimoto R-i, Srivastava S, Tassone F, Hagerman RJ, Rivera SM. Diffusion tensor imaging in male premutation carriers of the fragile X mental retardation gene. Mov Disord. 2011;26:1329–36.
76. Hashimoto R, Backer KC, Tassone F, Hagerman RJ, Rivera SM. An fMRI study of the prefrontal activity during the performance of a working memory task in premutation carriers of the fragile X mental retardation 1 gene with and without fragile X-associated tremor/ataxia syndrome (FXTAS). J Psychiatr Res. 2011;45:36–43.
77. Martin M-H, Bouchard J-P, Sylvain M, St-Onge O, Truchon S. Autosomal recessive spastic ataxia of Charlevoix-Saguenay: a report of MR imaging in 5 Patients. Am J Neuroradiol. 2007;28:1606–8.
78. Gazulla J, Vela AC, Marín MA, et al. Is the ataxia of Charlevoix-Saguenay a developmental disease? Med Hypotheses. 2011;77:347–52.
79. Shimazaki H, Takiyama Y, Honda J, et al. Middle cerebellar peduncles and pontine T2 hypointensities in ARSACS. J Neuroimaging. 2013;23(1):82–5.
80. Anheim M, Monga B, Fleury M, et al. Ataxia with oculomotor apraxia type 2: clinical, biological and genotype/phenotype correlation study of a cohort of 90 patients. Brain. 2009;132:2688–98.
81. Wenning GK, Litvan I, Tolosa E. Milestones in atypical and secondary Parkinsonisms. Mov Disord. 2011;26:1083–95.
82. Juh R, Pae C-U, Lee C-U, et al. Voxel based comparison of glucose metabolism in the differential diagnosis of the multiple system atrophy using statistical parametric mapping. Neurosci Res. 2005;52:211–9.
83. Paviour DC, Price SL, Jahanshahi M, Lees AJ, Fox NC. Regional brain volumes distinguish PSP, MSA-P, and PD: MRI-based clinico-radiological correlations. Mov Disord. 2006;21:989–96.
84. Nicoletti G, Fera F, Condino F, et al. MR Imaging of middle cerebellar peduncle width: differentiation of multiple system atrophy from Parkinson disease 1. Radiology. 2006;239:825–30.
85. Lee J-Y, Yun J, Shin C-W, Kim H-J, Jeon B. Putaminal abnormality on 3-T magnetic resonance imaging in early parkinsonism-predominant multiple system atrophy. J Neurol. 2010;257:2065–70.
86. Kwon K-Y, Choi CG, Kim JS, Lee MC, Chung SJ. Comparison of brain MRI and 18F-FDG PET in the differential diagnosis of multiple system atrophy from Parkinson's disease. Mov Disord. 2007;22:2352–8.
87. Kwon KY, Choi CG, Kim JS, Lee MC, Chung SJ. Diagnostic value of brain MRI and 18F-FDG PET in the differentiation of parkinsonian type multiple system atrophy from Parkinson's disease. Eur J Neurol. 2008;15:1043–9.
88. Blain CRVM, Barker GJP, Jarosz JMM, et al. Measuring brain stem and cerebellar damage in parkinsonian syndromes using diffusion tensor MRI. Neurology. 2006;67:2199–205.
89. Watanabe H, Saito Y, Terao S, et al. Progression and prognosis in multiple system atrophy. Brain. 2002;125:1070–83.
90. Marrannes J, Mulleners E. Hot cross bun sign in a patient with SCA-2. JBR-BTR 2009;92:263.
91. Lee YC, Liu CS, Wu HM, Wang PS, Chang MH, Soong BW. The 'hot cross bun' sign in the patients with spinocerebellar ataxia. Eur J Neurol. 2009;16:513–6.
92. Minnerop M, Specht K, Ruhlmann J, et al. Voxel-based morphometry and voxel-based relaxometry in multiple system atrophy—a comparison between clinical subtypes and correlations with clinical parameters. Neuroimage. 2007;36:1086–95.

93. Pellecchia MT, Barone P, Mollica C, et al. Diffusion-weighted imaging in multiple system atrophy: a comparison between clinical subtypes. Mov Disord. 2009;24:689–96.
94. Wang P-S, Wu H-M, Lin C-P, Soong B-W. Use of diffusion tensor imaging to identify similarities and differences between cerebellar and Parkinsonism forms of multiple system atrophy. Neuroradiology. 2011;53:471–81.
95. Bhattacharya K, Saadia D, Eisenkraft B, et al. Brain magnetic resonance imaging in multiple-system atrophy and Parkinson disease: a diagnostic algorithm. Arch Neurol. 2002;59:835–42.
96. Kanazawa M, Shimohata T, Terajima K, et al. Quantitative evaluation of brainstem involvement in multiple system atrophy by diffusion-weighted MR imaging. J Neurol. 2004;251:1121–4.
97. Brenneis C, Boesch SM, Egger KE, et al. Cortical atrophy in the cerebellar variant of multiple system atrophy: a voxel-based morphometry study. Mov Disord. 2006;21:159–65.
98. Hauser T-K, Luft A, Skalej M, et al. Visualization and quantification of disease progression in multiple system atrophy. Mov Disord. 2006;21:1674–81.
99. Specht K, Minnerop M, Abele M, Reul J, Wullner U, Klockgether T. In vivo voxel-based morphometry in multiple system atrophy of the cerebellar type. Arch Neurol. 2003;60:1431–5.
100. Tha KK, Terae S, Yabe I, et al. Microstructural white matter abnormalities of multiple system atrophy: in vivo topographic illustration by using diffusion-tensor MR imaging. Radiology. 2010;255:563–9.
101. Shiga K, Yamada K, Yoshikawa K, Mizuno T, Nishimura T, Nakagawa M. Local tissue anisotropy decreases in cerebellopetal fibers and pyramidal tract in multiple system atrophy. J Neurol. 2005;252:589–96.
102. Takado Y, Igarashi H, Terajima K, et al. Brainstem metabolites in multiple system atrophy of cerebellar type: 3.0-T magnetic resonance spectroscopy study. Mov Disord. 2011;26: 1297–302.

Chapter 15
Other Gait Disorders

Joseph C. Masdeu

Introduction

Neural Structures Controlling Posture and Gait

At the simplest level of analysis, the act of standing and walking requires sensory information reaching specific brain centers and a motor output from those centers [1–3]. Sensory information includes proprioception, vision, and vestibular input. Some brain centers important for posture are the vestibular nuclei, the medullary and pontine reticular formation, the pedunculopontine nucleus, at the junction between the pons and midbrain, and the substantia nigra, in the midbrain. The cerebellum, basal ganglia, and thalamus play a major role in the central control of gait. In man, the medial frontal cortex, particularly the supplementary motor area and the paracentral lobule, also contribute to the control of gait. On the motor side, the corticospinal, vestibulospinal, and reticulospinal tracts, among others, convey to the spinal cord output from higher centers. In their turn, the anterior horn cells through their axons stimulate muscles that turn that output into specific movements. Imaging of the relevant structures in brain and spinal cord, but not peripheral nerve or muscle imaging, will be covered in this chapter.

Classification of Gait Disorders

Several classifications have attempted to organize the complex semiology and anatomy of gait disorders into a rational system [4–7]. Some gait disorders are

J. C. Masdeu (✉)
Section on Integrative Neuroimaging
National Institutes of Health (NIH/NIMH-CBDB), Intramural Research Program
9000 Rockville Pike Building 10, Room 3C111 Bethesda, MD 20892-1365
e-mail: masdeu@nih.gov

New York Medical College, Valhalla, NY, USA
e-mail: masdeu@nymc.edu

2301 Wyoming Avenue NW, Washington, DC 20008, USA

F. B. Nahab, N. Hattori (eds.), *Neuroimaging of Movement Disorders,*
Current Clinical Neurology 44, DOI 10.1007/978-1-62703-471-5_15,

easily classifiable, because they are stereotyped and always related to lesions in the same structures: witness the very characteristic spastic gait resulting from lesions of the corticospinal tract. Others are much more difficult to classify. In some instances, like freezing of gait, because their anatomical underpinnings are still unclear; in others, such as disequilibrium, because they can be caused by lesions in a variety of structures, preventing a neat correspondence of gait pattern to anatomy. We will follow a functional classification that tries to facilitate the correlation between the clinical examination of the gait pattern and the neuroimaging findings.

Simpler Gait Disorders

The application of neuroimaging to the study of some of these disorders is straightforward. For this reason, they will not be discussed in this chapter.

Sensory and Lower Motor Gait Disorders

Lesions in the peripheral nervous system or sensory or motor nuclei in the spinal cord or brain stem result in sensory and lower motor gait disorders, such as the waddling gait of proximal muscle disease, the steppage gait of peripheral neuropathies and the visual, vestibular, or proprioceptive ataxias resulting from damage of the corresponding pathways. Here and in the next type of gait disorders, imaging findings are straightforward or are discussed in other chapters of this book.

Simpler Gait Disorders of Central Origin

These disorders follow lesions located more centrally than the ones causing sensory and lower motor gait disorders. Disorders of pyramidal (spastic gait), cerebellar (ataxic gait), or nigral motor systems (parkinsonian, choreic, and dystonic gait) cause distortion of appropriate postural and locomotor synergies [5]. In general, the correct postural and locomotor responses are selected, but their execution is faulty. Parkinson disease and ataxia are discussed in previous chapters.

Complex Gait Disorders of Central Origin

These disorders, on which this chapter is centered, are less well characterized than the ones previously described. Nonetheless, they are probably more common, particularly in the elderly population [7–9]. Their clinical appearance was masterfully described by Critchley [10] in 1948:

> There exists a large group of cases where the gait in old people becomes considerably disordered, although the motor power of the legs is comparatively well preserved. A paradoxical state of affairs is the result: testing of the individual movements of the legs while the patient

> reclines upon the couch shows little, if any, reduction in the strength. The tonus may not be grossly altered and the reflexes may betray only minor deviations. Sensory tests show no unusual features. But when the patient is instructed to get out of bed and to walk, remarkable defects may be witnessed. The patient, first of all, appears most reluctant to make the attempt. His stance is bowed and uncertain. He props himself against the end of the bed and seeks the aid of the bystanders. Encouraged to take a few steps, he advances warily and hesitatingly. Clutching the arms of two supporters, he takes short, shuffling steps. The legs tend to crumble by giving way suddenly at the knee joints. Progression, as far as it is possible, is slow and tottery. The patient veers to one side or the other. Frequently the legs cross, so that one foot gets in the way of the other.

The clinical picture described by Critchley is a stereotype and one of an advanced gait disorder. Different patients have different disorders, depending on the main anatomic location of the lesion. Earlier stages present only with impaired balance and a propensity to tripping and falling. At this point, the patients or, more often, their families, may consult a physician. The responsible lesion could be at a number of places in the neuraxis. Often, several lesions combine to produce the gait disorder [11]. In some cases, they are caused by compression of the cervical cord or lesions of brain stem nuclei. Some others are due to damage of the control loop that begins in the paracentral and premotor cortex and projects to the putamen. Through direct and indirect pathways, modified by input from the substantia nigra and subthalamic nucleus, the putamen projects to the medial globus pallidus, which inhibits the activity of thalamic neurons in the ventrolateral and ventral anterior nuclei. These thalamic nuclei project back to the frontal cortex. This loop probably plays an important role in mediating overlearned, unconscious motor activity that runs in the background, such as gait and postural reflexes. Patients with lesions here can improve their gait markedly by paying attention to it. They have a faulty "automatic pilot" for postural reflexes. Finally, other gait disorders result from direct dysfunction of the cortex in the posterior portion of the medial frontal region.

Spinal Cord or Brain Stem Disequilibrium

To a lesser or greater degree, these patients have poor equilibrium. Some may feel unsteady, whereas there is little evidenced by the neurological examination. Poor equilibrium without overt sensory or pyramidal findings in an older person is not infrequently the manifestation of spinal cord compression by cervical spondylosis, an entity that will be discussed in the Etiology section.

In patients with atherosclerosis, isolated *pontine* hyperintense lesions on magnetic resonance imaging (MRI) correlated with disequilibrium [12]. The lesions were located in the basis pontis, possibly involving the corticopontine or corticospinal fibers, the pontocerebellar fibers, and the pontine nuclei. The rest of the brain appeared normal on MRI. Pyramidal signs were equally distributed among patients and controls [12].

The laterodorsal region of the *midbrain* contains the mesencephalic locomotor region, which plays an important role in locomotion, as documented in both experimental animals and humans [13]. This area contains the nucleus cuneiformis and

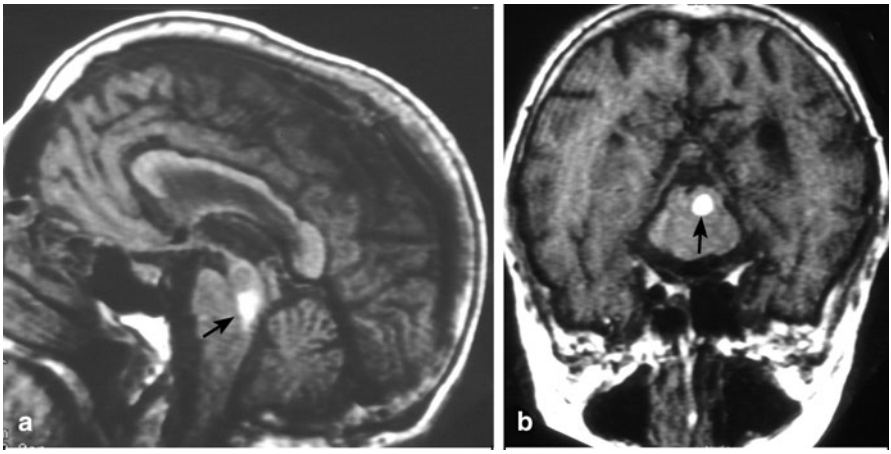

Fig. 15.1 Mesencephalic gait failure. MRI of an 83-year-old woman with gait failure after a hemorrhage in the locomotor mesencephalic region. Lesion is shown in the sagittal (**a**) and coronal (**b**) planes, *arrow*. (Reprinted with permission from Masdeu et al. [15])

the cholinergic pedunculopontine nucleus. Stimulation of the pedunculopontine nucleus has been reported to improve gait freezing in Parkinson's disease [14]. Discrete vascular damage in this region (Fig. 15.1) can give rise to severe disequilibrium and a loss of the rhythmic, alternating feet movement that characterize normal walking [15]. It is conceivable that other brain stem nuclei, still poorly identified, may also play an important role in postural mechanisms.

Disequilibrium with "Automatic Pilot" Disorder

The disorders described next are characterized not only by disequilibrium, but also by a striking difference between the patient's poor performance when they walk spontaneously and a better performance when they think about walking, for instance, by stepping over an obstacle or trying to take long strides. All of these lesions affect the corticobasal ganglionic–thalamo–cortical loop, described at the beginning of this section. The basal ganglia are part of an important loop that controls proximal movements participating in postural synergies.

1. *Basal ganglia lesions.* Rarely, acute lesions of the basal ganglia may be associated with a syndrome of unsteadiness without the loss of isometric power, where a patient without an apparent weakness cannot, however, stand normally [16]. Disequilibrium and akinesia are also characteristic of advanced stages of disorders affecting the striatum, such as in the subcortical form of Creutzfeldt–Jakob disease (Fig. 15.2).
2. *Thalamic lesions.* Chronic lesions of the basal ganglia are better known to cause axial motor impairment than acute ones, whereas the opposite is true for thalamic lesions. A syndrome of impaired axial postural movements has been described

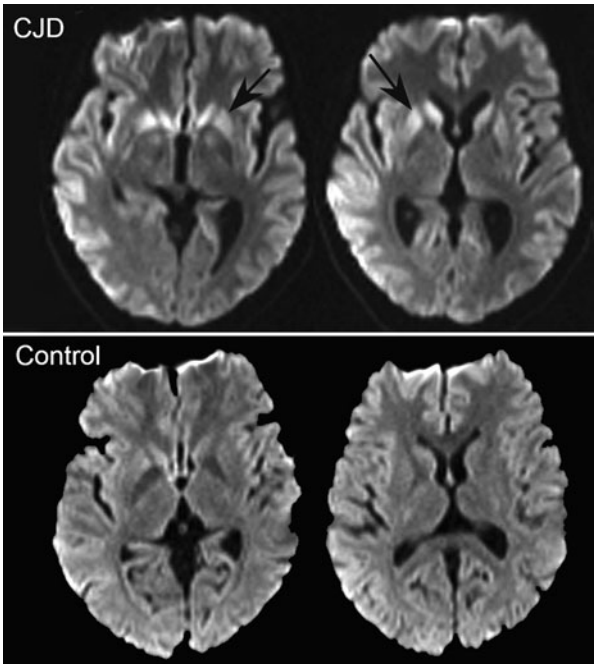

Fig. 15.2 Creutzfeldt—Jakob disease. Images shown (FLAIR MRI) are from a 39-year-old woman who developed chorea, followed by anxiety, progressive cognitive and motor impairment, leading to inability to walk and marked dysarthria and dementia by the time this imaging study was obtained, 5 months after symptom onset. Note the high intensity of the caudate and of the anterior portion of the lenticular nuclei (*arrows*). For comparison purposes, the *lower* image row was obtained with a similar technique, but from a control individual

with acute infarction or hemorrhage in the centromedian or ventrolateral nucleus of the thalamus or suprathalamic white matter (Fig. 15.3) [17–19]. Alert, with normal or near normal strength on isometric muscle testing and a variable degree of sensory loss or cerebellar ataxia, these patients cannot stand or even sit up unassisted for several days after an ischemic or hemorrhagic stroke. They fall backward or toward the side contralateral to the lesion. These patients seem to have a deficit of overlearned motor activity of an axial and postural nature. The syndrome has been called "thalamic astasia" and grouped by some among the central disequilibrium syndromes [6, 18].

3. *Hemispheric paracentral periventricular white matter lesions.* The output of the thalamus critical for gait is directed to the areas of the cortex involved in lower extremity movements. This area of the cortex is the medial frontal region, specifically, the paracentral lobule and the supplementary motor cortex. The fibers reaching this area from the thalamus course through the periventricular white matter. Thus, it is not surprising that lesions here may result in impaired gait. Ischemic disease of the white matter is common in the elderly. Beginning with a report in 1989, many studies have confirmed that white matter abnormalities on computed tomography (CT) and MRI correlate with impaired gait unbalance in older people [20–22]. The kind of gait impairment seen most often in these

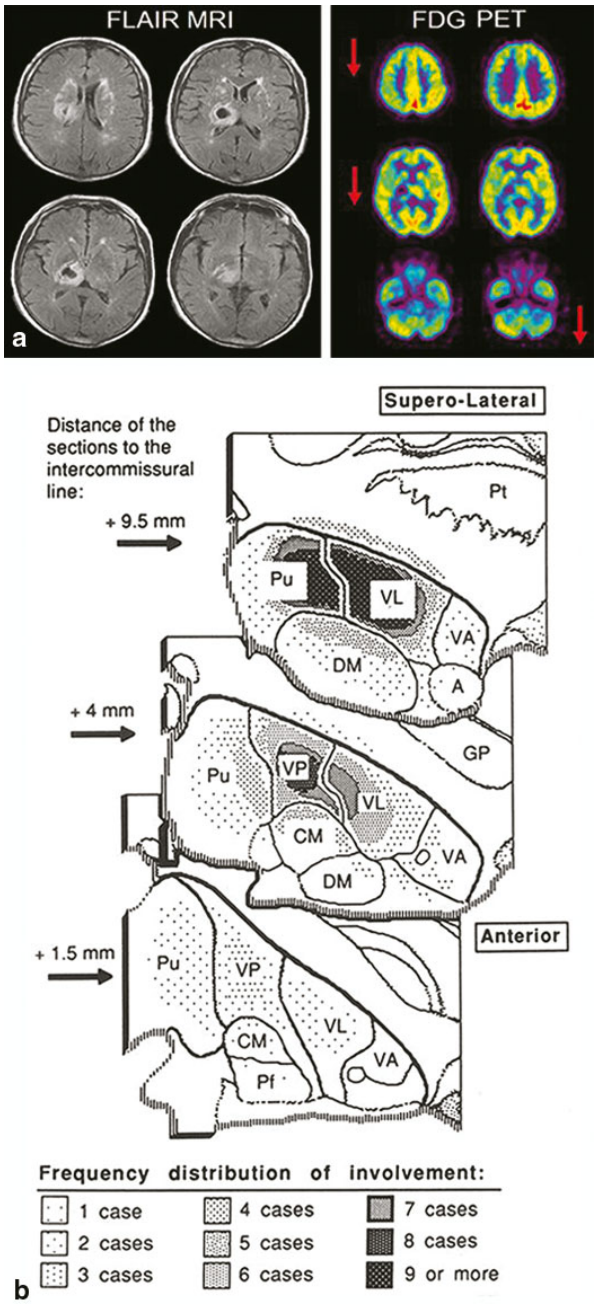

Fig. 15.3 Thalamic astasia. **a** Axial FLAIR MRI images showing a thalamic hematoma centered in the ventrolateral nucleus, from a 62-year-old man initially unable to walk, who at the time of this scan had marked gait unsteadiness, which improved when the patient concentrated on his gait. The ^{18}F fluoro-deoxy-glucose (FDG) positron emission tomography (PET) study showed not only the deeply reduced metabolism at the site of the thalamic hematoma, but also reduced metabolism in ipsilateral frontoparietal cortex and contralateral cerebellum, including the vermian region. **b** Anatomic location of the lesion in 15 cases of thalamic astasia [18]. On successive axial sections of the thalamus, the frequency of involvement is indicated by the density of shading. Both right and left-sided lesions were plotted on the left thalamus. *A* anterior nuclear group, *CM* centromedian nucleus, *DM* dorsomedial nucleus, *GP* globus pallidus, *Pf* parafascicular nucleus, *Pt* putamen, *Pu* pulvinar, *VA* ventral anterior nucleus, *VL* ventrolateral nucleus, *VP* ventral posterior nucleus

patients corresponds to what has been termed the "cautious gait." [23]. As they have poor balance, their steps are shorter, possibly to lessen the single-foot stance portion of the gait cycle. Like patients with thalamic lesions, these individuals may seem to walk rather normally so long as they pay attention to their gait. However, when they engage the "automatic pilot," and the motor control system for involuntary movements begins to be relied upon, they tend to fall. Sudden buckling of the knees may precipitate them to the floor.

Disequilibrium may also be prominent in patients with hydrocephalus and with lesions in the medial aspect of the frontal lobe. However, those patients tend to have the gait disorder described further in this chapter as "magnetic gait." Central disequilibrium is probably the commonest cause of the so-called "drop attacks," sudden falls without warning or loss of consciousness in older individuals. Drop attacks were originally attributed to disease of the vertebrobasilar system, but this etiology of drop attacks in the elderly is probably not as common as subcortical hemispheric disease [24].

Freezing of Gait

With preserved balance, these patients experience gait hesitation and may freeze in the course of locomotion, particularly on a turn [5, 6]. Once the patient begins to walk, steps are short and shuffling, but become larger and the foot clearance increases as the patient continues to walk. The base of support is normal. Postural responses are preserved. Eye closure does not induce abnormal swaying. Maneuvers that bring about a "cortical strategy," such as trying to kick an imaginary ball, step over a cane, or counting the steps help the patient initiate and maintain gait. Minus the disequilibrium, this disorder mimics the "automatic pilot disorder" described in the previous section. The anatomical localization of this disorder is still undefined, but involvement of frontobasal ganglionic mechanisms is suspected, because it shares features of the parkinsonian gait and the magnetic gait described next. It is likely that freezing is caused by lesions in a number of regions involved in gait [25]. The so-called "pure freezing of gait" is associated with a variety of progressive supranuclear palsy (PSP), a disorder where neuronal loss in the pedunculopontine nucleus has been documented [26–28]. Stimulation of the caudal pedunculopontine region improves freezing of gait in idiopathic Parkinson disease (iPD), without necessarily improving or affecting other aspects of gait [14, 29, 30]. ^{18}F-deoxy-glucose (FDG) PET has shown decreased midbrain metabolism in pure freezing of gait, whereas in PSP, there was additional involvement of the frontal cortex [31]. The involvement of the mesencephalic locomotor region has been supported by a study using blood-oxygen-level-dependent (BOLD) signal with functional MRI (fMRI) and volumetric measurements in patients with Parkinson disease without freezing and patients with freezing of gait [32]. Patients with freezing had atrophy and gait-related hyperactivity of the mesencephalic locomotor region; the hyperactivity correlated with the severity

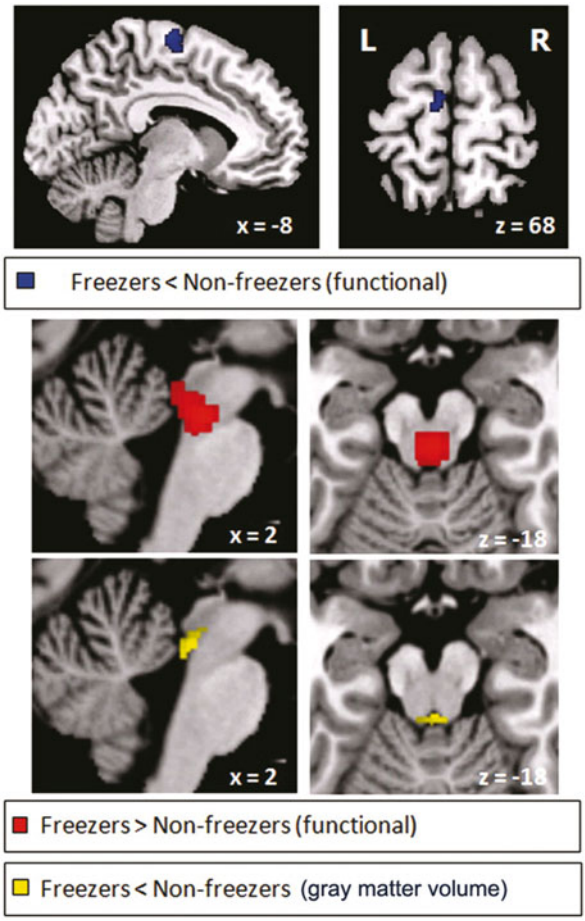

Fig. 15.4 Freezing of gait: brain correlates. Brain areas in which the relative increase in activity for motor imagery versus visual imagery differed between patients with freezing of gait (freezers) and patients without freezing of gait (nonfreezers). Freezers had decreased activity in the supplementary motor cortex (region of interest analysis, $P = 0.06$ corrected for multiple comparisons using family-wise inference on voxel level) and increased activity in the mesencephalic locomotor region (whole brain search, $P < 0.05$ similarly corrected for multiple comparisons); the corresponding statistical parametric maps are shown superimposed on standard brain sections (*top*: supplementary motor cortex, *middle*: mesencephalic locomotor region). The *bottom* brain sections show in *yellow* the small cluster with significantly smaller gray matter volume in patients with freezing of gait in the mesencephalic locomotor region. (From Snijders et al. [32])

and duration of gait freezing (Fig. 15.4). However, changes were also detected in the medial frontoparietal region, in this [32] and other neuroimaging studies [33, 34], and a similar gait pattern has been described with lesions or atrophy in the medial frontoparietal region [35–37].

Fig. 15.5 Subdural hematomas. Axial FLAIR MRI image showing bilateral convexity subdural hematomas in an 82-year-old man with gait freezing and an attentional disorder

Magnetic Gait

This disorder corresponds to what Nutt et al. [6] call "frontal gait disorder" and others have described as "*marche à petit pas*" or "arteriosclerotic parkinsonism." Meyer and Barron called it "apraxia of gait," because despite the severe gait disorder the patients can move their legs at will, lacking any sensory loss or weakness on isometric strength testing [38]. Although able to stand, these patients have such an inability to lift their feet and walk that their feet may seem to be glued to the floor. Some patients have great difficulty initiating walking and, when pushed forward, the heels are lifted but the toes seem to grab the floor. There may be a dissociation between gait and distal volitional movements, in that the patient may be quite able to draw figures with her feet, or to do normally the heel-shin maneuver. For this reason, some authors argue that calling this disorder "apraxia" is inappropriate, because in apraxia complex motor sequences, such as to draw a figure, are maximally affected [39, 40]. Milder forms of the same disorder resemble the parkinsonian gait, with short, shuffling steps and truncal rigidity. Arm swing during walking may be preserved or even exaggerated and if so, helps differentiate this disorder from iPD [37]. The turns are very slow and broken down into many steps. Turning may bring up the tendency for the feet (or for one foot more than the other when the problem is asymmetrical) to become glued to the floor. Freezing may become evident, as the steps halt and the patient remains motionless or develops tremor-like movements of the lower legs. Falls are common, particularly in patients who have disequilibrium. This disorder may be caused by bilateral lesions of the medial frontal cortex (Fig. 15.5) [36, 37], severe hydrocephalus, or bilateral ischemic lesions of the white matter. Hydrocephalus and ischemic lesions will be discussed in the next section on Etiology.

Etiology of Complex Gait Disorders

Having discussed the phenomenological classification and some of the neuroimaging findings in gait disorder, the next section includes a description of the neuroimaging findings in the three most common causes of gait disorders in adults, namely, cervical spondylosis, vascular brain disease, and hydrocephalus.

Cervical Myelopathy from Cervical Spondylosis

Cervical myelopathy from cervical spondylosis has been reported as the second most common cause of gait impairment in the older adult [41, 42]. As it is potentially treatable, cervical myelopathy should be considered in any older adult presenting with gait impairment [43]. Some patients present with the characteristic clinical picture of cervical radicular pain and spastic paraparesis, but most do not have radicular pain. Initially, at the time when surgery is most likely to be successful and prevent further deterioration, the gait impairment may be very subtle, noticeable to the patient but yielding minimal findings on neurological examination [44]. The paucity of findings may delay the diagnosis. In the Yale series, the investigators felt that the diagnosis had been delayed in the average by 6.3 years [44]. The earliest consistent symptom in all of their 22 patients was a gait abnormality. Early diagnosis is important, because the myelopathy of cervical spondylosis is often progressive if untreated [44].

MRI of the cervical spine is helpful in the diagnosis of cervical myelopathy from cervical spondylosis, but, in the absence of the clinical findings, the presence of spondylitic changes by themselves does not make the diagnosis. Rather severe changes can be seen in asymptomatic older adults [45–47]. Baseline plain x-rays are useful when surgery is being considered for comparison with postoperative x-rays or when the patient cannot undergo MRI, for instance, in the case of someone bearing a pacemaker. However, MRI is the screening test of choice in most instances [44]. Boney osteophytes can be seen as black ridges compressing the canal and, if the compression is severe, causing high-intensity changes in the spinal cord on T2-weighted images (Fig. 15.6).

In addition to the narrowing of the spinal canal by spondylitic hypertrophy of bones and ligaments, two changes are frequently observed in the cord itself: decreased diameter and a hyperintense signal on T2-weighted images. How often a hyperintense area is observed depends on the stage of progression, with gliosis and microcavitation of the gray matter, and other poorly understood factors. In some series, as many as 40 % of the patients have this finding [48]. Some have found the presence of this finding and its irreversibility after surgery to predict a poor outcome, while others have not [48, 49]. MRI may show other changes within the spinal cord itself due to chronic compression such as syrinx formation. MRI is also of great value in the differential diagnosis of myelopathy, because conditions such as tumor and infection can be easily ruled out.

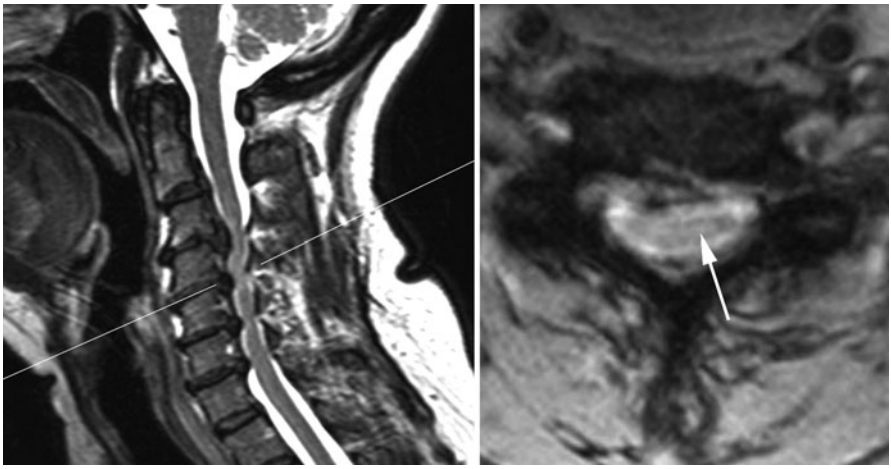

Fig. 15.6 Cervical myelopathy from spondylosis. Sagittal (*left*) and axial (*right*) MRI images from a 61-year-old man with an ataxic-spastic gait, showing spinal cord compression by osteophytes at the C3-C6 levels. At those levels, the spinal cord is abnormally hyperintense in these T2-weighted images (detail on the *right* image, *arrow*). The level of the axial image, at the C4-C5 disc level, is indicated by a *thin line* on the sagittal image

Although MRI is not as good as CT in showing osteophytes or ossification of the posterior longitudinal ligament [50, 51], it has replaced CT almost completely in the evaluation of cervical spondylosis [52]. Very rarely, thin-slice CT of the cervical spine after intrathecal introduction of a nonionic water soluble contrast material may be of help (Fig. 15.7).

Vascular Brain Disease

Vascular disease of the brain ranks among the three top causes of gait impairment in the older adult [41, 42]. These are patients referred for progressive gait impairment; here we are not discussing patients with a stroke that leaves them with hemiparesis and gait difficulty. Ischemic brain disease tends to follow one of three patterns, discernible by clinical evaluation and with the help of neuroimaging procedures: (1) cortical infarcts, most often related to embolic disease; (2) subcortical disease, often in the form of widespread lacunes and white matter changes, most often related to arteriolar disease; and (3) a mixture of the two patterns, often related to atheromatous disease of the major vessels [24]. Subcortical infarcts strategically located may impair equilibrium and gait with little or no limb weakness on isometric testing [24]. Although acute stroke tends to be associated with overt neurological findings, gait impairment may be neglected as a neurological finding and yet be the result of small, "silent" lacunar strokes [53]. Vascular disease causing this syndrome most often

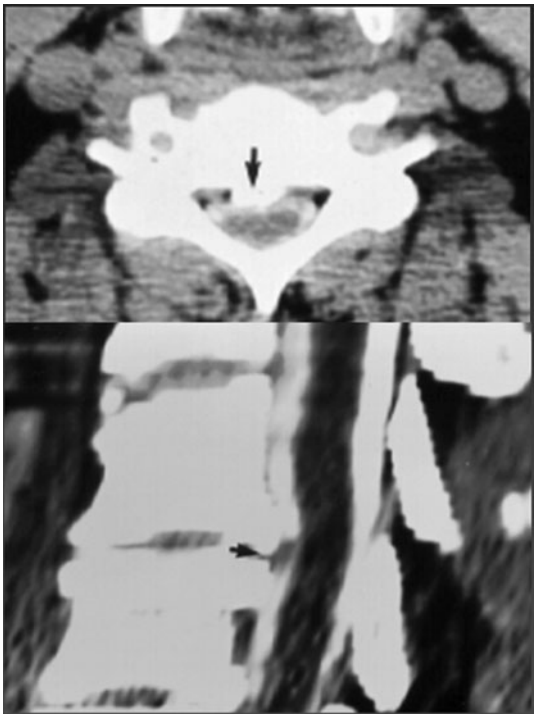

Fig. 15.7 Posterior longitudinal ligament calcification. Axial (*top*) and sagittal (*bottom*) CT images of the cervical spine, obtained after the infusion of metrizamide in the subarachnoid space through a lumbar puncture. Note that the bony details are better visualized with CT than with MRI (see Fig. 15.6). But changes in the spinal cord itself are better seen with MRI (see Fig. 15.6)

affects the supratentorial compartment in the form of lacunar disease or ischemic disease of the white matter. Less often, it affects the posterior circulation, involving vestibular or cerebellar structures, and very rarely, other brainstem structures important for gait, such as the mesencephalic locomotor center (see Fig. 15.1).

1. *Lacunar disease of gait-critical structures.* CT and MRI are the diagnostic tests most useful for the study of these syndromes. Hemorrhagic lesions can be readily detected by either modality, whereas acute lacunar lesions may pass unnoticed unless MR diffusion imaging is used (Fig. 15.8). Very small older lacunes may also be missed, because the infarcted tissue retracts and healthy tissue takes up its place. The resulting atrophy can be quantified using region of interest (ROI) methods or voxel-based morphometry [54, 55]. Larger lacunes can be easily appreciated on MRI as elongated lesions, following the trajectory of the arteriolar perforators, bright on T2-weighted images, including fluid-attenuated inversion recovery (FLAIR) images, and dark on T1-weighted images (Fig. 15.9). Although in the supratentorial compartment small lacunes are easier to spot on FLAIR images, conventional T2-weighted images are superior for lesions in the brainstem [56]. Supratentorial lacunes most likely to cause gait and balance problems affect the ventrolateral nucleus of the thalamus, suprathalamic white matter, basal ganglia, and the paracentral white matter. In order to cause persistent impairment, the lesions have to be bilateral and reach a volume threshold. The correlation of the

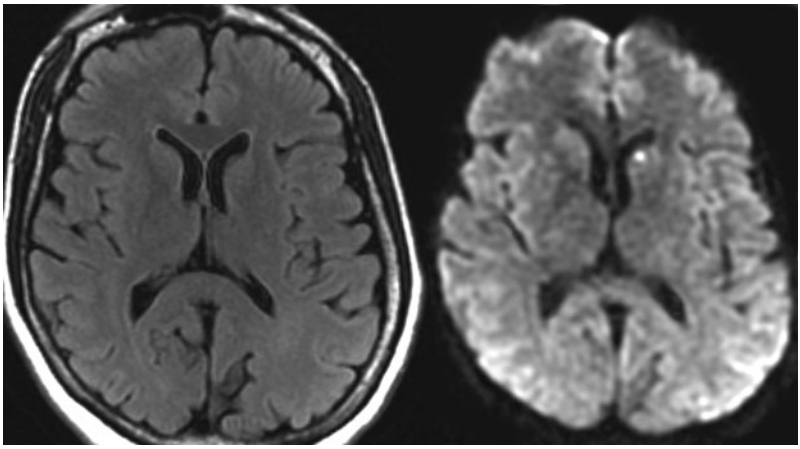

Fig. 15.8 Acute lacunar stroke. MRI from a 60-year-old man with a left caudate nucleus infarct, visible on the diffusion-weighted image (*right*), but not on the acute FLAIR image (*left*)

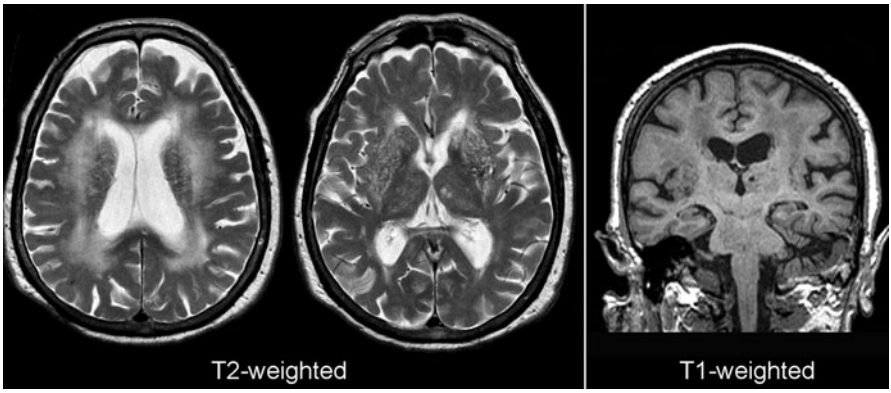

Fig. 15.9 Microvascular white matter disease. Shown are axial T2-weighted and coronal T1-weighted images from an 80-year-old woman with impairment of cognition and gait. Note the thalamic infarctions and the large areas of altered signal (increased on T2 and decreased on T1) in the centrum semiovale. The thalamic lacunes are bright on T2 and dark on T1-weighted images

imaging data with the clinical findings is often difficult because the gait impairment caused by these lesions affects the unconscious control of gait and posture (the "automatic pilot") [18, 57]. Often, patients with a shuffling, unsteady gait at home perform normally at a physician's office: they are successfully engaging the cortical mechanisms of gait to compensate for the impaired subcortical mechanisms. Here, the history, coupled with the neuroimaging findings, can be most helpful [58].

2. *White matter disease.* White matter changes on CT or MRI are very frequent in older people (see Fig. 15.9). On MRI, some degree of white matter change is

present in about 95 % of subjects over the age of 60 and increases with age [59, 60]. Areas in the hemispheric white matter are hypodense on CT and markedly hyperintense on T2-weighted images and FLAIR, and hypointense on T1-weighted images (see Fig. 15.9). However, high-intensity areas on T2-weighted MRI are often undetected on CT. On T2-weighted MR images, it may be difficult to differentiate tissue damage from increased water content due to dilation of perivascular spaces with normal aging because both have increased intensity values [61]. For this reason, in older persons it seems preferable to quantify lesions visible on T1-weighted images or CT as indicators of true white matter damage. However, there are little data available in this age group exploring the functional significance of white matter changes visible only on T2-weighted images versus those visible on both T2 and T1-weighted images. In multiple sclerosis, and therefore in a younger age group, it is known that T1 lesion volume correlates better than T2 volume with hemispheric dysfunction [62]. T1-mapping, which determines tissue-specific T1-relaxation times, has been used recently to correlate postmortem changes [63, 64]. It may reflect pathological processes related to intraparenchymal changes in water content such as edema, widening of the extracellular space, subtle blood–brain barrier leakage, or glial proliferation [63, 64].

Quantification of White Matter Disease

A number of techniques are available to evaluate the extent of white matter involvement based on intensity changes. Initial methods were semiquantitative, and involved the visual inspection of images. Changes could be compared among individuals, on a cross-sectional basis, or longitudinally in the same individual. Cross-sectional comparisons have been made by simply grouping the scans of patients and controls from 1 (least amount of white matter changes) to 8 (greatest amount) [22]. Most often used are scales describing the amount of white matter changes. The Fazekas Scale [65] has a range of 1–6. In the periventricular regions scores 0–3 can be given, and in the subcortical region scores 1–3 can be given for mild, moderate, or severe lesions, respectively. The age-related white matter changes (ARWMC) scale [66] has a range from 0 to 30, where scores 0–3 can be given in 5 regions, left and right each. The Scheltens Rating Scale [67] ranges from 0 to 84 (scores 0–6 can be given in 13 subcortical regions and scores 0–2 for three periventricular regions). An example of longitudinal scale is the Rotterdam Progression Scale [68] (range − 7 to 7), which measures decrease, no change, or increase (− 1, 0, 1, respectively) of white matter changes for three periventricular regions and four subcortical regions. These visual methods are giving way to semiautomatic [69] or even completely automatic methods, which use the matrix output from the scanner to select voxels likely to correspond to abnormal white matter [70]. Ideally, images to be processed automatically should be obtained with good magnetic field homogeneity or with an additional sequence for inhomogeneity correction, small voxel size (1–2 mm^3), and with 3D acquisitions, where the entire brain is imaged with voxels having the same size in all

three planes. In good quality scans, automatic or semiautomatic segmentation methods can measure the extent of white matter changes accurately and with a minimum of operator effort [71]. Not only does the global amount of white matter changes, but their location can also be assessed automatically [72].

Diffusion tensor imaging (DTI) has been extensively applied to the study of white matter changes in older people [73–78]. DTI measurements indicating white matter damage, particularly decreased functional anisotropy and increased radial diffusivity, have been found at autopsy to correlate with white matter ischemic lesions, free-radical injury, and aberrant oligodendrocytes [79]. Not surprisingly, there is a better correlation between DTI measurements and intensity on FLAIR in those areas likely to be mildly to moderately affected, such as those located farther from the ventricles [80]. The correlation is lost in the periventricular region, with very high FLAIR values. DTI measurements of the corpus callosum have been used in the study of gait [81]. The corpus callosum affords an easy and appropriate target for DTI studies, because most fibers run parallel to each other and there is very little fiber crossing. In regions where major pathways cross perpendicularly, such as the superior longitudinal fasciculus and the corticospinal tract, axonal loss in one of the pathways may actually result in an increased anisotropy, as more of the remaining fibers are parallel to each other [82]. As regards gait, genu DTI abnormalities may simply reflect the involvement of frontal pathways by the disease process and the callosal fibers may have little or nothing to do with gait. DTI findings in participants with a range of microvascular brain disease must be interpreted with caution, because hemodynamic changes, regardless of the integrity of white matter, can affect fractional anisotropy and other DTI parameters [83].

As the histology underlying white matter changes in older people remains elusive in many cases, Hachinski [84] coined the descriptive term "leuko-araiosis" for the CT findings and this term was later on applied to the MRI findings as well. Many authors use other purely descriptive terms, such as white matter hyperintensities [58]. Several authors have reported normal histology, but ischemic changes similar to the findings in subcortical arteriosclerotic encephalopathy (SAE), have been present in cases with pronounced changes on T1-weighted MRI or CT [85, 86], or even T2 changes [87]. Microglial proliferation, arteriolar thickening, and biochemical indicators of tissue hypoxia are present within regions with abnormal MRI signal [87, 88]. Attempts at remyelination have been detected in periventricular but not subcortical lesions [88]. Cerebrovascular disease and hypertension are frequent correlates of SAE [89, 90]. Amyloid angiopathy can also cause white matter disease [91, 92]. In addition to white matter changes, amyloid angiopathy results in subcortical hemorrhages (Fig. 15.10).

Disorders of gait and equilibrium are the most prominent correlate of white matter CT or MRI changes in older people [24, 53, 57]. In controlled studies of elderly prone to falling, impaired gait and balance correlated with the presence of white matter disease on CT or MRI [22, 58]. Studies relating gait to DTI changes are scarce. In a study of 173 community-dwelling elderly, DTI measurements in the genu of the corpus callosum correlated with gait function measured by the Tinetti gait and balance scores [81].

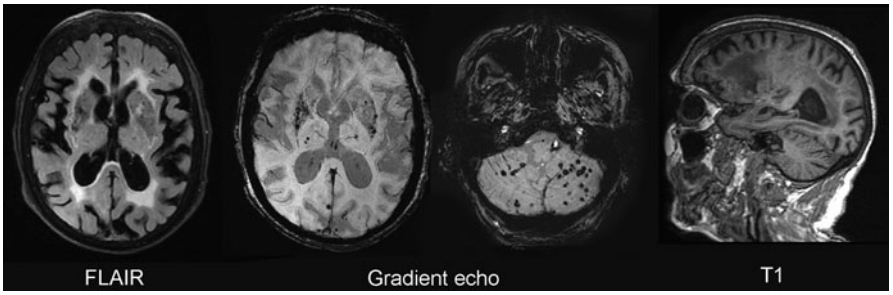

Fig. 15.10 Cerebral amyloid angiopathy (CAA). Shown are MR images from a 72-year-old woman with dementia and CAA. The white matter contains many abnormal areas, which appear hyperintense on the transverse FLAIR image and hypointense on the sagittal T1-weighted image. Multiple lacunar infarcts are present in the lenticular nuclei and few in the thalami. Microbleeds, best seen on the gradient echo images, dot the lenticular nuclei, thalami, and the cerebellum. Scattered microbleeds can also be seen in the cortex or subcortical white matter

Hydrocephalus

This section will refer to chronic hydrocephalus in the adult, and not to pediatric hydrocephalus, or to hydrocephalus secondary to head trauma or aneurysmal subarachnoid hemorrhage. Although at an annual incidence of 1.8 cases/100,000 inhabitants [93], symptomatic hydrocephalus is not a frequent cause of gait disorder, it presents initially with a gait disorder and should be recognized because it is potentially treatable [94, 95]. Patients with hydrocephalus have a variety of gait disorders, but slowing of gait, short steps, and balance disturbances have been recorded most often [96–98]. Start hesitation and freezing of gait are occasionally observed [99]. In severe cases, a magnetic gait may be present. In some series, instability was associated with a poor response after shunting [100]. Balance has been recorded to improve after shunting or cerebrospinal fluid (CSF) drainage in some series [99, 101], but not in others [98]. It has been postulated that the best predictor of shunting success is the response to CSF withdrawal: if gait is observed to improve after CSF removal, a good response is likely [95]. However, as gait improves when cortical strategies, rather than the "automatic pilot" are used, patients often do walk better after CSF has been removed and they are "expected" to walk better. This placebo effect has been documented in individual cases [102]. For this reason, more objective structural neuroimaging findings are very helpful.

Enlarged ventricles are frequently present in patients with gait disorders [103] and are associated with gait impairment [104]. From these data, some authors concluded that symptomatic hydrocephalus was common and shunting procedures multiplied in the last three decades. However, even in series with carefully selected patients, some failed to improve after shunting or only had a short-lived improvement, suggesting that hydrocephalus was not the cause of their gait disorder [100, 105]. For this reason, it is important to apply more sensitive diagnostic criteria in the work up of these patients [94]. In the opposite end of the spectrum, patients with gait or balance

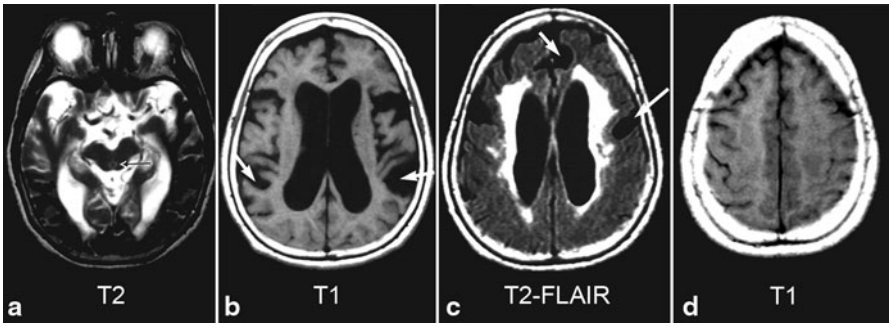

Fig. 15.11 Hydrocephalus. **a–d** are axial sections of the MRI from a 71-year-old woman with progressive gait and cognitive impairment, as well as urinary incontinence. She recovered after shunting. Although the basal cisterns (**a**) and the interhemispheric and sylvian fissures (**b**, **c**) are dilated, the sulci in the high convexity (**d**) are compressed. Transependymal reabsorption of CSF, suggested by the homogeneous high signal in the periventricular white matter (**c**), need not occur in all cases of symptomatic hydrocephalus. Note rounding (ballooning) of the depth of some of the most dilated sulci (*white arrows*)

impairment caused by symptomatic hydrocephalus may not be shunted because the MRI shows large sulci, giving the impression of hydrocephalus *ex vacuo* (Fig. 15.11).

It is commonly thought that in chronic hydrocephalus, unlike in hydrocephalus *ex vacuo*, the ventricles are enlarged out of proportion with sulcal enlargement [104]. However, measurements of the ventricular volume and sulcal volume, normalized by total intracranial volume, as well as a ratio of ventricular to sulcal volume did not predict success after shunting [106]. Often, the cortical sulci are compressed. However, in many patients sulci may be enlarged, sometimes greatly so (see Fig. 15.11) [107, 108]. In these cases, sulcal enlargement involves particularly the basal cisterns, sylvian fissures, and other major sulci on the convexity of the hemispheres. In cases with large sulci, two findings on MRI or CT help to make the diagnosis:

1. *Disproportionate sulcal dilation.* While some sulci are dilated, others appear normal or even compressed for the patient's age. Typically, the larger primary sulci, such as the Sylvian fissure are dilated, while the sulci in the high parietal convexity and medial aspect of the parietal lobe are compressed (see Fig. 15.11). Disproportionate sulcal dilation is also found in cortical neurodegenerative disorders and particularly in the lobar atrophies characteristic of frontotemporal dementia (Fig. 15.12). These patients, however, seldom present with gait impairment. Here, the correlation with the clinical picture is paramount. For instance, a patient with Alzheimer disease and a Balint syndrome had a marked dilation of the intraparietal sulci, corresponding to her clinical presentation (Fig. 15.13).
2. *Ballooned sulci.* Another finding that helps distinguish sulcal dilation due to hydrocephalus is that the sulci are ballooned out, with the depth of the sulcus in the shape of a U (see Fig. 15.11) [108]. By contrast, sulci dilated from atrophy have the shape of a V (Compare Figs. 15.11 and 15.13a).

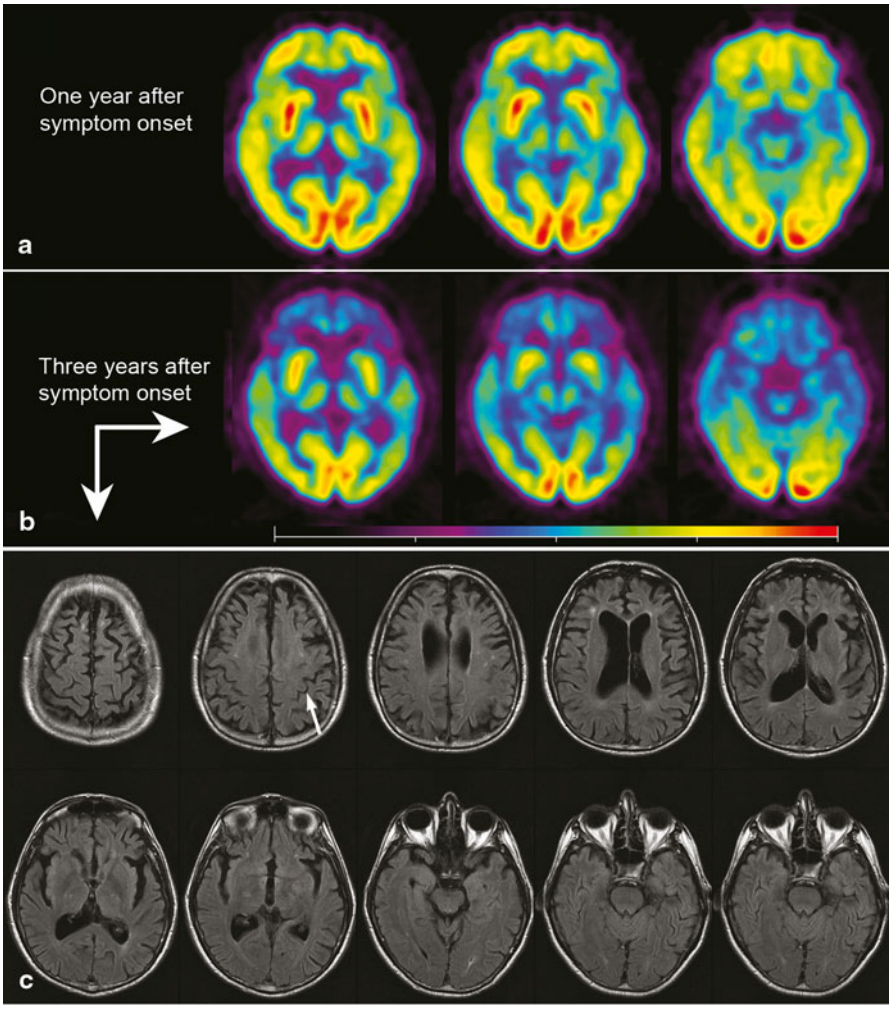

Fig. 15.12 Sulcal dilation in frontotemporal dementia. Shown are FDG-PET (**a**, **b**) and FLAIR MRI (**c**) studies from a 51-year-old man with progressive speech apraxia and impaired planning, to the point of mutism and complete dependency for activities of daily living when studies **b** and **c** were obtained, on the same day. Metabolism was already decreased on the initial PET study, particularly on the frontal opercula and temporal tips, but it is much more obvious on the follow-up study, showing extensive frontotemporal hypometabolism. Note that despite the lobar atrophy predominating in the frontal region, the sulci of the pariental convexity are visible (*arrow*). Compare with the similar region in hydrocephalus (see Fig. 15.11d)

These structural findings are extremely helpful to make the diagnosis of hydrocephalus even in patients with mild, but definite impairment of gait or balance.

An increased aqueductal CSF flow void on proton density-weighted, non-flow-compensated, conventional spin-echo images has been described as characteristic of normal-pressure hydrocephalus [109]. This effect is not present in fast spin-echo

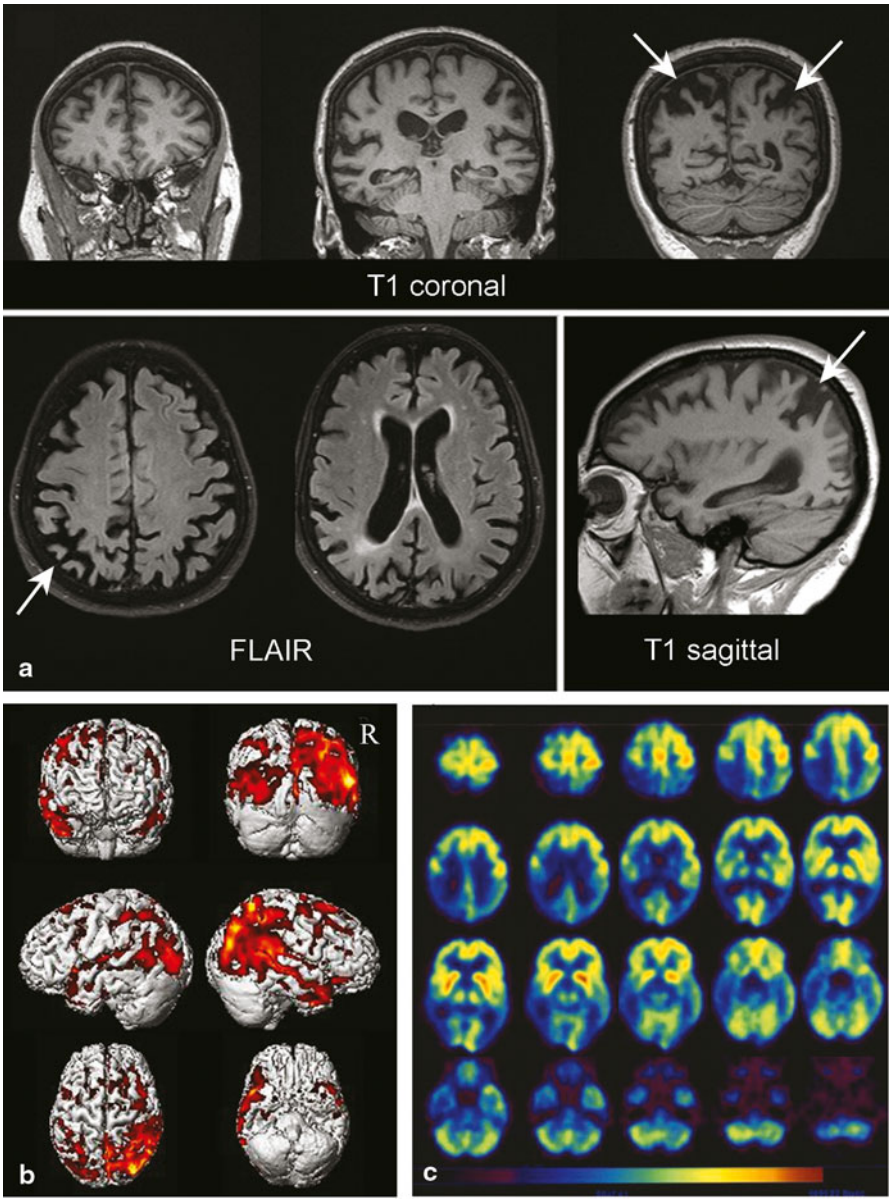

Fig. 15.13 Sulcal dilation in Alzheimer disease. Shown are the MRI and PET studies from a 61-year-old woman with a 3-year history of progressive reading difficulties, agraphia, and dressing apraxia. On examination, she had a Balint's syndrome, with simultanagnosia, apraxia of eye movements, optic ataxia, and "tunnel vision." Note the marked atrophy in the lateral parietal lobe, with dilation of the intraparietal sulcus (*arrows*). Dilated sulci do not have the ballooned appearance present in hydrocephalus (see Fig. 15.11b and 15.11c, *arrows*)

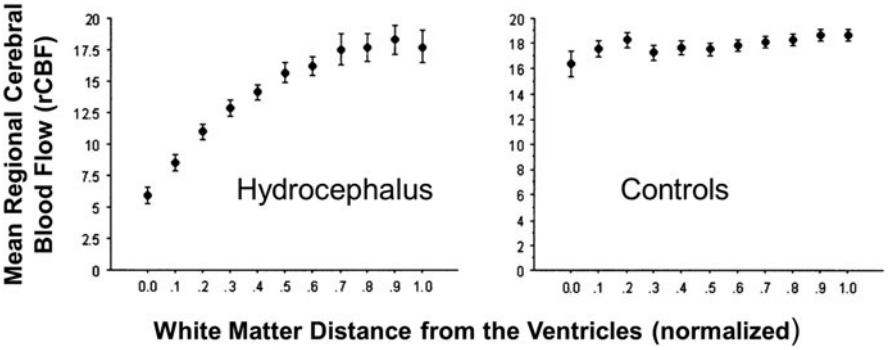

Fig. 15.14 Periventricular hypoperfusion in chronic hydrocephalus. Relationship between the distance from the lateral ventricles and the mean regional white matter cerebral blood flow (CBF) at that distance in patients (Kruskal ± Wallis, $P < 0.0001$) and absence of relationship in controls ($P = 0.0748$). Mean and standard error of the mean (*error bars*). (From Momjian et al. [114])

images and only in some cases studied with flow-compensation. The flow void corresponds to the volume of CSF pulsating back and forth through the aqueduct during systole or diastole, known as the "aqueductal CSF stroke volume." This volume can be measured using phase-contrast cine MR imaging; an increased volume has been correlated with a good outcome after shunting [110]. However, several studies have failed to find a correlation between an aqueductal flow void scores and outcome after shunting [110–112].

The mechanisms causing idiopathic hydrocephalus and gait improvement after shunting have been debated. There is little doubt that hydrocephalus causes not only compression of the periventricular white matter, housing projections from the thalamus to the medial frontoparietal regions, but also ischemia and myelin loss. Reduced fractional anisotropy of the periventricular white matter has been documented by means of DTI [113]. Reduced blood flow in the periventricular white matter has been documented by $H_2^{15}O$ PET to recover after shunting (Fig. 15.14) [114]. However, it has been postulated that the periventricular ependymal and white matter changes are not the result of hydrocephalus in the older adult, but its cause [115]. In arrested hydrocephalus, characterized by an increased intracranial volume, the periependymal region plays an important role in CSF resorption [116, 117]. Thus, ischemic changes impairing resorption in this region may lead to an increased ventricular pressure and ventricular dilation [118]. Another view holds that the main problem in idiopathic hydrocephalus is reduced venous outflow [119]. A well-documented reduction in the blood flow returning via the sagittal sinus is compatible with both theories [119]. The same can be said of the recent finding that changes in MR apparent diffusion coefficient over the cardiac cycle were more pronounced in patients with idiopathic hydrocephalus than in either healthy control subjects or patients with *ex vacuo* ventricular dilatation [120]. During systole, brain expansion is induced by dilation of the intracranial arteries. In healthy brains, this expansion is dampened by venous and CSF outflow, as well as by displacement of the intracranial spinal

cord from the cranium. In hydrocephalus, diminished intracranial compliance would lead to a tighter mechanical coupling between blood flow and CSF pulsation in the cardiac cycle [120]. Cerebrovascular reactivity, measured with the acetazolamide SPECT perfusion technique, has been found to be decreased in hydrocephalus and to improve after shunting [121].

As regards the target of the thalamocortical periventricular fibers, in the medial frontal regions, medial frontal perfusion defects correlated with the degree of gait impairment and improved after shunting [122]. Some have postulated an impaired function of the mesencephalic locomotor center, because deformation of the midbrain, documented by CT, was corrected by shunting [123]. However, other researchers have not been able to document this effect [124].

Cerebrovascular disease, in the form of lacunar strokes or abnormal white matter on CT or MRI, is more frequent in patients with hydrocephalus than in controls [125] and is an important confounder in the diagnosis of treatable hydrocephalus [126]. Vascular changes in the brain have predicted a poor outcome after shunting in some large studies [127], but not in smaller ones [128], and it is present in about 50 % of patients being shunted [93]. When the clinical or CT-MR diagnosis is dubious, a pattern of decreased perfusion or metabolism in the association cortex of the parietal lobes on SPECT or PET may predict a poor outcome [105]. This pattern is usually seen in Alzheimer's disease and Parkinson's with dementia.

Summary and Future Perspectives

In summary, neuroimaging is a powerful tool for the study of the alterations in neural structures that are correlated with abnormal gait and posture. Many of the structures mediating gait and posture were known from the neuropathological correlation of clinical findings, but neuroimaging has provided a more thorough understanding of their role. In some cases, for instance, the acute deficit in "automatic pilot" performance with laterodorsal thalamic lesions, the transient nature of the deficit rendered it unknown until it was studied with CT or MRI in patients with acute lesions. In this and other gait disorders, recovery involves a series of readjustments in neural networks globally known as plasticity but very poorly understood in their specific details. For instance, how does the brain adapt so that a patient with a thalamic hematoma that occupies exactly the same space on MRI acutely, when the patient cannot even stand by herself, and 2 weeks later, when she walks almost normally, may experience such remarkable recovery? Thanks to metabolic studies with PET, we know that with the motor recovery there is an associated recovery of frontal and cerebellar metabolism, despite the persistence of a thalamic metabolic gaping hole. Studies using resting state fMRI and PET, including studies of metabolism and receptor plasticity, may eventually unlock the processes the brain employs to repair defective networks related to gait and posture. A better understanding of these processes may lead to more effective tools in treating patients with disorders leading to impaired gait or posture. An example from the related field of neurophysiology is the discovery of transcallosal inhibition of the affected hemisphere by the healthy one after a unilateral stroke [129]. This finding led to the application of transcranial

magnetic stimulation to dampen the healthy hemisphere. There is some evidence that this approach may improve the recovery of upper extremity function [129, 130]. The clarification of plasticity mechanisms for gait in humans, through the use of neuroimaging and other tools is also likely to yield novel treatment approaches for gait disorders.

References

1. Nutt JG, Horak FB, Bloem BR. Milestones in gait, balance, and falling. Mov Disord. 2011;26:1166–74.
2. Mori S. Neurophysiology of locomotion: recent advances in the study of locomotion. In: Masdeu J, Sudarsky L, Wolfson L, editors. Gait disorders of aging. Falls and therapeutic strategies. Philadelphia: Lippincott & Raven; 1997. p. 55–78.
3. Nashner L. Physiology of balance, with special reference to the healthy elderly. In: Masdeu J, Sudarsky L, Wolfson L, editors. Gait disorders of aging. Falls and therapeutic strategies. Philadelphia: Lippincott & Raven; 1997. p. 37–53.
4. Liston R, Mickelborough J, Bene J, Tallis R. A new classification of higher level gait disorders in patients with cerebral multi-infarct states. Age Ageing. 2003;32:252–8.
5. Marsden C, Thompson P. Toward a nosology of gait disorders: descriptive classification. In: Masdeu J, Sudarsky L, Wolfson L, editors. Gait disorders of aging. Falls and therapeutic strategies. Philadelphia: Lippincott & Raven; 1997. p. 135–46.
6. Nutt J, Marsden C, Thompson P. Human walking and higher-level gait disorders, particularly in the elderly. Neurology. 1993;43:268–79.
7. Snijders AH, van de Warrenburg BP, Giladi N, Bloem BR. Neurological gait disorders in elderly people: clinical approach and classification. Lancet Neurol. 2007;6:63–74.
8. Verghese J, Ambrose AF, Lipton RB, Wang C. Neurological gait abnormalities and risk of falls in older adults. J Neurol. 2010;257:392–8.
9. Newman G, Dovenmuehle R, Busse E. Alterations in neurologic status with age. J Am Geriatr Soc. 1960;8:915–7.
10. Critchley M. On senile disorders of gait, including the so-called "senile paraplegia". Geriatrics. 1948;3:364–70.
11. Rubenstein L, Josephson K. Interventions to reduce the multifactorial risks for falling. In: Masdeu J, Sudarsky L, Wolfson L, editors. Gait disorders of aging. Falls and therapeutic strategies. Philadelphia: Lippincott & Raven; 1997. p. 309–26.
12. Kwa VI, Zaal LH, Verbeeten B Jr, Stam J. Disequilibrium in patients with atherosclerosis: relevance of pontine ischemic rarefaction. Amsterdam Vascular Medicine Group. Neurology. 1998;51:570–3.
13. Thevathasan W, Pogosyan A, Hyam JA, et al. Alpha oscillations in the pedunculopontine nucleus correlate with gait performance in parkinsonism. Brain. 2012;135:148–60.
14. Thevathasan W, Cole MH, Graepel CL, et al. A spatiotemporal analysis of gait freezing and the impact of pedunculopontine nucleus stimulation. Brain. 2012;135:1446–54.
15. Masdeu J, Alampur U, Cavaliere R, Tavoulareas G. Astasia and gait failure with damage of the pontomesencephalic locomotor region. Ann Neurol. 1994;35:619–21.
16. Labadie E, Awerbuch G, Hamilton R, Rapcsak S. Falling and postural deficits due to acute unilateral basal ganglia lesions. Arch Neurol. 1989;261:492–6.
17. Elwischger K, Rommer P, Prayer D, Mueller C, Auff E, Wiest G. Thalamic astasia from isolated centromedian thalamic infarction. Neurology. 2012;78:146–7.
18. Masdeu J, Gorelick P. Thalamic astasia: inability to stand after unilateral thalamic lesions. Ann Neurol. 1988;23:596–603.
19. Karnath HO, Johannsen L, Broetz D, Kuker W. Posterior thalamic hemorrhage induces "pusher syndrome". Neurology. 2005;64:1014–9.

20. Baloh RW, Spain S, Socotch TM, Jacobson KM, Bell T. Posturography and balance problems in older people. J Am Geriatr Soc. 1995;43:638–44.
21. Camicioli R, Moore MM, Sexton G, Howieson DB, Kaye JA. Age-related brain changes associated with motor function in healthy older people. J Am Geriatr Soc. 1999;47:330–4.
22. Masdeu JC, Wolfson L, Lantos G, et al. Brain white-matter changes in the elderly prone to falling. Arch Neurol. 1989;46:1292–6.
23. Sudarsky L, Tideiksaar R. The cautious gait, fear of falling, and psychogenic gait disorders. In: Masdeu J, Sudarsky L, Wolfson L, editors. Gait disorders of aging. Falls and therapeutic strategies. Philadelphia: Lippincott & Raven; 1997. p. 283–95.
24. Masdeu J. Cerebrovascular disease and hydrocephalus. In: Bronstein A, Brandt T, Woollacott M, Nutt J, editors. Clinical disorders of balance, posture and gait. London: Arnold; 2004. p. 222–44.
25. Nutt JG, Bloem BR, Giladi N, Hallett M, Horak FB, Nieuwboer A. Freezing of gait: moving forward on a mysterious clinical phenomenon. Lancet Neurol. 2011;10:734–44.
26. Zweig R, Whitehouse P, Casanova M, Walker L, Jankel W, Price D. Pedunculopontine cholinergic neurons in progressive supranuclear palsy. Ann Neurol. 1987;22:18–25.
27. Factor SA, Higgins DS, Qian J. Primary progressive freezing gait: a syndrome with many causes. Neurology. 2006;66:411–4.
28. Compta Y, Valldeoriola F, Tolosa E, Rey MJ, Marti MJ, Valls-Sole J. Long lasting pure freezing of gait preceding progressive supranuclear palsy: a clinicopathological study. Mov Disord. 2007;22:1954–8.
29. Ferraye MU, Debu B, Fraix V, et al. Effects of pedunculopontine nucleus area stimulation on gait disorders in Parkinson's disease. Brain. 2010;133:205–14.
30. Wilcox RA, Cole MH, Wong D, Coyne T, Silburn P, Kerr G. Pedunculopontine nucleus deep brain stimulation produces sustained improvement in primary progressive freezing of gait. J Neurol Neurosurg Psychiatry. 2011;82:1256–9.
31. Park HK, Kim JS, Im KC, et al. Functional brain imaging in pure akinesia with gait freezing: [18F] FDG PET and [18F] FP-CIT PET analyses. Mov Disord. 2009;24:237–45.
32. Snijders AH, Leunissen I, Bakker M, et al. Gait-related cerebral alterations in patients with Parkinson's disease with freezing of gait. Brain. 2011;134:59–72.
33. Bartels AL, Leenders KL. Brain imaging in patients with freezing of gait. Mov Disord. 2008;23 Suppl 2:S461–7.
34. Youn J, Cho JW, Lee WY, Kim GM, Kim ST, Kim HT. Diffusion tensor imaging of freezing of gait in patients with white matter changes. Mov Disord. 2012;27:760–4.
35. Kostic VS, Agosta F, Pievani M, et al. Pattern of brain tissue loss associated with freezing of gait in Parkinson disease. Neurology. 2012;78:409–16.
36. Nadeau SE. Gait apraxia: further clues to localization. Eur Neurol. 2007;58:142–5.
37. Thompson PD. Gait disorders accompanying diseases of the frontal lobes. In: Ruzicka E, Hallett M, Jankovic J, editors. Advances in neurology. Vol. 87. Gait disorders. Philadelphia: Lippincott Williams and Wilkins; 2001. p. 235–41.
38. Meyer JS, Barron DW. Apraxia of gait: a clinico-physiological study. Brain. 1960;83:261–84.
39. Nutt JG. Classification of gait and balance disorders. In: Ruzicka E, Hallett M, Jankovic J, editors. Advances in neurology. Vol. 87. Gait disorders. Philadelphia: Lippincott Williams and Wilkins; 2001. p. 135–41.
40. Zadikoff C, Lang AE. Apraxia in movement disorders. Brain. 2005;128:1480–97.
41. Sudarsky L. Clinical approach to gait disorders of aging: an overview. In: Masdeu J, Sudarsky L, Wolfson L, editors. Gait disorders of aging. Falls and therapeutic strategies. Philadelphia: Lippincott & Raven; 1997. p. 147–57.
42. Fuh JL, Lin KN, Wang SJ, Ju TH, Chang R, Liu HC. Neurologic diseases presenting with gait impairment in the elderly. J Geriatr Psychiatry Neurol. 1994;7:89–92.
43. Holly LT, Moftakhar P, Khoo LT, Shamie AN, Wang JC. Surgical outcomes of elderly patients with cervical spondylotic myelopathy. Surg Neurol. 2008;69:233–40.
44. Sadasivan KK, Reddy RP, Albright JA. The natural history of cervical spondylotic myelopathy. Yale J Biol Med. 1993;66:235–42.

45. Healy JF, Healy BB, Wong WH, Olson EM. Cervical and lumbar MRI in asymptomatic older male lifelong athletes: frequency of degenerative findings. J Comput Assist Tomogr. 1996;20:107–12.
46. Reul J, Gievers B, Weis J, Thron A. Assessment of the narrow cervical spinal canal: a prospective comparison of MRI, myelography and CT-myelography. Neuroradiology. 1995;37:187–91.
47. Weis E Jr. Abnormal magnetic-resonance scans of the cervical spine in asymptomatic subjects. J Bone Joint Surg Am. 1991;73:1113.
48. Yone K, Sakou T, Yanase M, Ijiri K. Preoperative and postoperative magnetic resonance image evaluations of the spinal cord in cervical myelopathy. Spine. 1992;17:S388–92.
49. Matsuda Y, Miyazaki K, Tada K, et al. Increased MR signal intensity due to cervical myelopathy. Analysis of 29 surgical cases. J Neurosurg. 1991;74:887–92.
50. Matsunaga S, Nakamura K, Seichi A, et al. Radiographic predictors for the development of myelopathy in patients with ossification of the posterior longitudinal ligament: a multicenter cohort study. Spine. 2008;33:2648–50.
51. Rao RD, Currier BL, Albert TJ, et al. Degenerative cervical spondylosis: clinical syndromes, pathogenesis, and management. J Bone Joint Surg Am. 2007;89:1360–78.
52. Houten JK, Cooper PR. Laminectomy and posterior cervical plating for multilevel cervical spondylotic myelopathy and ossification of the posterior longitudinal ligament: effects on cervical alignment, spinal cord compression, and neurological outcome. Neurosurgery. 2003;52:1081–7; discussion 1087–8.
53. Franch O, Calandre L, Alvarez-Linera J, Louis ED, Bermejo-Pareja F, Benito-Leon J. Gait disorders of unknown cause in the elderly: clinical and MRI findings. J Neurol Sci. 2009;280:84–6.
54. Ashburner J. A fast diffeomorphic image registration algorithm. Neuroimage. 2007;38:95–113.
55. Ashburner J, Friston KJ. Voxel-based morphometry–the methods. Neuroimage. 2000;11:805–21.
56. Brant-Zawadzki M, Atkinson D, Detrick M, Bradley WG, Scidmore G. Fluid-attenuated inversion recovery (FLAIR) for assessment of cerebral infarction. Initial clinical experience in 50 patients. Stroke. 1996;27:1187–91.
57. Masdeu JC. Dysequilibrium syndromes. In: Ruzicka E, Hallett M, Jankovic J, editors. Advances in neurology. Vol. 87. Gait disorders. Philadelphia: Lippincott Williams and Wilkins; 2001.
58. Srikanth V, Beare R, Blizzard L, et al. Cerebral white matter lesions, gait, and the risk of incident falls: a prospective population-based study. Stroke. 2009;40:175–80.
59. de Leeuw FE, de Groot JC, Achten E, et al. Prevalence of cerebral white matter lesions in elderly people: a population based magnetic resonance imaging study. The Rotterdam Scan Study. J Neurol Neurosurg Psychiatry. 2001;70:9–14.
60. Qiu C, Cotch MF, Sigurdsson S, et al. Microvascular lesions in the brain and retina: the age, gene/environment susceptibility-Reykjavik study. Ann Neurol. 2009;65:569–76.
61. Kirkpatrick J, Hayman L. White-matter lesions on MR imaging of clinically healthy brains of elderly subjects: possible pathologic basis. Radiology. 1987;162:509–11.
62. Comi G, Rovaris M, Leocani L, Martinelli V, Filippi M. Assessment of the damage of the cerebral hemispheres in MS using neuroimaging techniques. J Neurol Sci. 2000;172:S63–6.
63. Gouw AA, Seewann A, Vrenken H, et al. Heterogeneity of white matter hyperintensities in Alzheimer's disease: post-mortem quantitative MRI and neuropathology. Brain. 2008;131:3286–98.
64. Vrenken H, Geurts JJ, Knol DL, et al. Normal-appearing white matter changes vary with distance to lesions in multiple sclerosis. AJNR Am J Neuradiol. 2006;27:2005–11.
65. Fazekas F, Chawluk JB, Alavi A, Hurtig HI, Zimmerman RA. MR signal abnormalities at 1.5 T in Alzheimer's dementia and normal aging. AJR Am J Roentgenol. 1987;149:351–6.
66. Wahlund LO, Barkhof F, Fazekas F, et al. A new rating scale for age-related white matter changes applicable to MRI and CT. Stroke. 2001;32:1318–22.

67. Scheltens P, Barkhof F, Leys D, et al. A semiquantative rating scale for the assessment of signal hyperintensities on magnetic resonance imaging. J Neurol Sci. 1993;114:7–12.
68. Prins ND, van Straaten EC, van Dijk EJ, et al. Measuring progression of cerebral white matter lesions on MRI: visual rating and volumetrics. Neurology. 2004;62:1533–9.
69. Gouw AA, van der Flier WM, van Straaten EC, et al. Reliability and sensitivity of visual scales versus volumetry for evaluating white matter hyperintensity progression. Cerebrovasc Dis. 2008;25:247–53.
70. Tiehuis AM, Vincken KL, Mali WP, et al. Automated and visual scoring methods of cerebral white matter hyperintensities: relation with age and cognitive function. Cerebrovasc Dis. 2008;25:59–66.
71. de Boer R, Vrooman HA, van der Lijn F, et al. White matter lesion extension to automatic brain tissue segmentation on MRI. Neuroimage. 2009;45:1151–61.
72. van der Lijn F, Verhaaren BF, Ikram MA, et al. Automated measurement of local white matter lesion volume. Neuroimage. 2012;59:3901–08.
73. Jones DK, Lythgoe D, Horsfield MA, Simmons A, Williams SC, Markus HS. Characterization of white matter damage in ischemic leukoaraiosis with diffusion tensor MRI. Stroke. 1999;30:393–7.
74. Fu JL, Zhang T, Chang C, Zhang YZ, Li WB. The value of diffusion tensor imaging in the differential diagnosis of subcortical ischemic vascular dementia and Alzheimer's disease in patients with only mild white matter alterations on T2-weighted images. Acta Radiol. 2012;53:312–7.
75. Kim SH, Park JS, Ahn HJ, et al. Voxel-based analysis of diffusion tensor imaging in patients with subcortical vascular cognitive impairment: correlates with cognitive and motor deficits. J Neuroimaging. 2011;21:317–24.
76. Burzynska AZ, Preuschhof C, Backman L, et al. Age-related differences in white matter microstructure: region-specific patterns of diffusivity. Neuroimage. 2010;49:2104–12.
77. Barrick TR, Charlton RA, Clark CA, Markus HS. White matter structural decline in normal ageing: a prospective longitudinal study using tract-based spatial statistics. Neuroimage. 2010;51:565–77.
78. Vernooij MW, de Groot M, van der Lugt A, et al. White matter atrophy and lesion formation explain the loss of structural integrity of white matter in aging. Neuroimage. 2008;43:470–7.
79. Back SA, Kroenke CD, Sherman LS, et al. White matter lesions defined by diffusion tensor imaging in older adults. Ann Neurol. 2011;70:465–76.
80. Zhan W, Zhang Y, Mueller SG, et al. Characterization of white matter degeneration in elderly subjects by magnetic resonance diffusion and FLAIR imaging correlation. Neuroimage. 2009;47 Suppl 2:T58–65.
81. Bhadelia RA, Price LL, Tedesco KL, et al. Diffusion tensor imaging, white matter lesions, the corpus callosum, and gait in the elderly. Stroke. 2009;40:3816–20.
82. Douaud G, Jbabdi S, Behrens TE, et al. DTI measures in crossing-fiber areas: increased diffusion anisotropy reveals early white matter alteration in MCI and mild Alzheimer's disease. Neuroimage. 2011;55:880–90.
83. Rudrapatna US, van der Toorn A, van Meer MP, Dijkhuizen RM. Impact of hemodynamic effects on diffusion-weighted fMRI signals. Neuroimage. 2012;61:106–14.
84. Hachinski V, Potter P, Merskey H. Leuko-araiosis. Arch Neurol. 1987;44:21–3.
85. Yamanouchi H. Loss of white matter oligodendrocytes and astrocytes in progressive subcortical vascular encephalopathy of Binswanger type. Acta Neurol Scand. 1991;83:301–5.
86. Gold G. Defining the neuropathological background of vascular and mixed dementia and comparison with magnetic resonance imaging findings. Front Neurol Neurosci. 2009;24:86–94.
87. Fernando MS, Simpson JE, Matthews F, et al. White matter lesions in an unselected cohort of the elderly: molecular pathology suggests origin from chronic hypoperfusion injury. Stroke. 2006;37:1391–8.
88. Simpson JE, Fernando MS, Clark L, et al. White matter lesions in an unselected cohort of the elderly: astrocytic, microglial and oligodendrocyte precursor cell responses. Neuropathol Appl Neurobiol. 2007;33:410–9.

89. van Swieten JC, Geyskes GG, Derix MM, et al. Hypertension in the elderly is associated with white matter lesions and cognitive decline. Ann Neurol. 1991;30:825–30.
90. de Leeuw FE, de Groot JC, Oudkerk M, et al. Hypertension and cerebral white matter lesions in a prospective cohort study. Brain. 2002;125:765–72.
91. Gray F, Dubas F, Roullet E, Escourolle R. Leukoencephalopathy in diffuse hemorrhagic cerebral amyloid angiopathy. Ann Neurol. 1985;18:54–9.
92. Mead S, James-Galton M, Revesz T, et al. Familial British dementia with amyloid angiopathy: early clinical, neuropsychological and imaging findings. Brain. 2000;123(Pt 5):975–91.
93. Krauss JK, Halve B. Normal pressure hydrocephalus: survey on contemporary diagnostic algorithms and therapeutic decision-making in clinical practice. Acta Neurochir (Wien). 2004;146:379–88.
94. Graff-Radford NR. Normal pressure hydrocephalus. Neurol Clin. 2007;25:809–32, vii-viii.
95. Marmarou A, Young HF, Aygok GA, et al. Diagnosis and management of idiopathic normal-pressure hydrocephalus: a prospective study in 151 patients. J Neurosurg. 2005;102:987–97.
96. Blomsterwall E, Bilting M, Stephensen H, Wikkelso C. Gait abnormality is not the only motor disturbance in normal pressure hydrocephalus. Scand J Rehabil Med. 1995;27:205–9.
97. Krauss JK, Faist M, Schubert M, Borremans JJ, Lucking CH, Berger W. Evaluation of gait in normal pressure hydrocephalus before and after shunting. In: Ruzicka E, Hallett M, Jankovic J, editors. Advances in neurology. Vol. 87. Gait disorders. Philadelphia: Lippincott Williams and Wilkins; 2001. p. 301–10.
98. Stolze H, Kuhtz-Buschbeck JP, Drucke H, et al. Gait analysis in idiopathic normal pressure hydrocephalus—which parameters respond to the CSF tap test? Clin Neurophysiol. 2000;111:1678–86.
99. Bugalho P, Guimaraes J. Gait disturbance in normal pressure hydrocephalus: a clinical study. Parkinsonism Relat Disord. 2007;13:434–7.
100. Klassen BT, Ahlskog JE. Normal pressure hydrocephalus: how often does the diagnosis hold water? Neurology. 2011;77:1119–25.
101. Blomsterwall E, Svantesson U, Carlsson U, Tullberg M, Wikkelso C. Postural disturbance in patients with normal pressure hydrocephalus. Acta Neurol Scand. 2000;102:284–91.
102. Gupta A, Lang AE. Potential placebo effect in assessing idiopathic normal pressure hydrocephalus. J Neurosurg. 2011;114:1428–31.
103. Fisher C. Hydrocephalus as a cause of disturbances of gait in the elderly. Neurology. 1982;32:1358–63.
104. Palm WM, Saczynski JS, van der Grond J, et al. Ventricular dilation: association with gait and cognition. Ann Neurol. 2009;66:485–93.
105. Graff-Radford N, Godersky J, Jones M. Variables predicting outcome in symptomatic hydrocephalus in the elderly. Neurology. 1989;39:1601–4.
106. Palm WM, Walchenbach R, Bruinsma B, et al. Intracranial compartment volumes in normal pressure hydrocephalus: volumetric assessment versus outcome. AJNR Am J Neuroradiol. 2006;27:76–9.
107. Holodny AI, George AE, de Leon MJ, Golomb J, Kalnin AJ, Cooper PR. Focal dilation and paradoxical collapse of cortical fissures and sulci in patients with normal-pressure hydrocephalus. J Neurosurg. 1998;89:742–7.
108. Kitagaki H, Mori E, Ishii K, Yamaji S, Hirono N, Imamura T. CSF spaces in idiopathic normal pressure hydrocephalus: morphology and volumetry. AJNR Am J Neuroradiol. 1998;19:1277–84.
109. Bradley WG. Normal pressure hydrocephalus: new concepts on etiology and diagnosis. Am J Neuroradiol. 2000;21:1586–90.
110. Bradley W Jr, Scalzo D, Queralt J, Nitz WN, Atkinson DJ, Wong P. Normal-pressure hydrocephalus: evaluation with cerebrospinal fluid flow measurements at MR imaging. Radiology. 1996;198:523–9.
111. Algin O, Hakyemez B, Taskapilioglu O, Ocakoglu G, Bekar A, Parlak M. Morphologic features and flow void phenomenon in normal pressure hydrocephalus and other dementias: are they really significant? Acad Radiol. 2009;16:1373–80.

112. Krauss JK, Regel JP, Vach W, Jungling FD, Droste DW, Wakhloo AK. Flow void of cerebrospinal fluid in idiopathic normal pressure hydrocephalus of the elderly: can it predict outcome after shunting? Neurosurgery. 1997;40:67–73; discussion 73–4.
113. Kanno S, Abe N, Saito M, et al. White matter involvement in idiopathic normal pressure hydrocephalus: a voxel-based diffusion tensor imaging study. J Neurol. 2011;258:1949–57.
114. Momjian S, Owler BK, Czosnyka Z, Czosnyka M, Pena A, Pickard JD. Pattern of white matter regional cerebral blood flow and autoregulation in normal pressure hydrocephalus. Brain. 2004;127:965–72.
115. Bradley WG. Idiopathic normal pressure hydrocephalus: new findings and thoughts on etiology. AJNR Am J Neuroradiol. 2008;29:1–3.
116. Bradley WG, Safar FG, Hurtado C, Ord J, Alksne JF. Increased intracranial volume: a clue to the etiology of idiopathic normal-pressure hydrocephalus? AJNR Am J Neuroradiol. 2004;25:1479–84.
117. Masdeu JC, Pascual B, Bressi F, et al. Ventricular wall granulations and draining of cerebrospinal fluid in chronic giant hydrocephalus. Arch Neurol. 2009;66:262–7.
118. Bradley WG, Bahl G, Alksne JF. Idiopathic normal pressure hydrocephalus may be a "Two hit" disease: benign external hydrocephalus in infancy followed by deep white matter ischemia in late adulthood. J Magn Reson Imaging. 2006;24:747–55.
119. Bateman GA. The pathophysiology of idiopathic normal pressure hydrocephalus: cerebral ischemia or altered venous hemodynamics? AJNR Am J Neuroradiol. 2008;29:198–203.
120. Ohno N, Miyati T, Mase M, et al. Idiopathic normal-pressure hydrocephalus: temporal changes in ADC during cardiac cycle. Radiology. 2011;261:560–5.
121. Chang CC, Kuwana N, Ito S, Ikegami T. Impairment of cerebrovascular reactivity to acetazolamide in patients with normal pressure hydrocephalus. Nucl Med Commun. 2000;21:139–41.
122. Klinge PM, Brooks DJ, Samii A, et al. Correlates of local cerebral blood flow (CBF) in normal pressure hydrocephalus patients before and after shunting—a retrospective analysis of [(15)O]H(2)O PET-CBF studies in 65 patients. Clin Neurol Neurosurg. 2008;110:369–75.
123. Mocco J, Tomey MI, Komotar RJ, et al. Ventriculoperitoneal shunting of idiopathic normal pressure hydrocephalus increases midbrain size: a potential mechanism for gait improvement. Neurosurgery. 2006;59:847–50.
124. Hiraoka K, Yamasaki H, Takagi M, et al. Is the midbrain involved in the manifestation of gait disturbance in idiopathic normal-pressure hydrocephalus? J Neurol. 2011;258:820–5.
125. Krauss JK, Regel JP, Vach W, et al. White matter lesions in patients with idiopathic normal pressure hydrocephalus and in an age-matched control group: a comparative study. Neurosurgery. 1997;40:491–5; discussion 495–6.
126. Caplan LR. White-matter hyperintensities and subcortical infarcts as predictors of shunt surgery outcome. AJNR Am J Neuroradiol. 2002;23:894; author reply 894–5.
127. Boon AJ, Tans JT, Delwel EJ, et al. Dutch Normal-Pressure Hydrocephalus Study: the role of cerebrovascular disease. J Neurosurg. 1999;90:221–6.
128. Tullberg M, Jensen C, Ekholm S, Wikkelso C. Normal pressure hydrocephalus: vascular white matter changes on MR images must not exclude patients from shunt surgery. AJNR Am J Neuroradiol. 2001;22:1665–73.
129. Kirton A, Chen R, Friefeld S, Gunraj C, Pontigon AM, Deveber G. Contralesional repetitive transcranial magnetic stimulation for chronic hemiparesis in subcortical paediatric stroke: a randomized trial. Lancet Neurol. 2008;7:507–13.
130. Conforto AB, Anjos SM, Saposnik G, et al. Transcranial magnetic stimulation in mild to severe hemiparesis early after stroke: a proof of principle and novel approach to improve motor function. J Neurol. 2012;259:1399–405.

Chapter 16
Neuroimaging of Basal Ganglia Calcifications

Norbert Brüggemann and Johann Hagenah

Introduction and Terminology

In the 1970s, the implementation of cranial computerized tomography (CT) in routine clinical practice revealed a surprisingly high number of symptomatic and asymptomatic individuals with intracerebral calcifications. In radiological studies of unselected cases, frequencies of 0.3–1.5 % have been reported [1–9]. The degree of mineral deposition may range from minimal faint punctuated spots in the pallidum in elderly persons to coarse bilateral symmetric conglomerates in multiple brain regions. The calcifications often have no clinical significance and remain asymptomatic throughout the entire life [10]. The basal ganglia are frequently involved, and symmetrical intracerebral basal ganglia calcifications are often referred to as Fahr's disease.

The terms Fahr's disease, Fahr's syndrome, or Morbus Fahr are misnomers and should, in principle, no longer be used. In 1930, the German neuropathologist Karl Theodor Fahr reported *postmortem* findings of a patient with diffuse calcifications of the brain vessels predominantly in the white matter and only sparsely in the basal ganglia [11, 12]. Retrospectively, this patient may rather have suffered from hypoparathyroidism, the most common reason for secondary intracerebral calcifications. Fahr was not the first one to describe intracerebral calcifications in humans, since Delacour first characterized this peculiar condition in 1850 [13]. The existence of more than 30 alternative names demonstrates the heterogeneity and huge uncertainty associated with this disorder [14]. To date, the descriptive terms "idiopathic basal ganglia calcification (IBGC)" and "bilateral striato-pallido-dentate calcinosis (BSPDC)" are often used in the scientific literature, highlighting the brain regions

N. Brüggemann (✉)
Department of Neurology, University of Lübeck,
Ratzeburger Allee 160, 23552 Lübeck, Germany
e-mail: norbert.brueggemann@neuro.uni-luebeck.de

J. Hagenah
Department of Neurology, Westküstenklinikum Heide,
Esmarchstraße 50, 25746 Heide, Germany
e-mail: jhagenah@wkk-hei.de

F. B. Nahab, N. Hattori (eds.), *Neuroimaging of Movement Disorders,*
Current Clinical Neurology 44, DOI 10.1007/978-1-62703-471-5_16,

that are most commonly involved [14]. In order to avoid confusion, the abbreviation BSPDC is used in this chapter, as calcifications are usually not restricted to the basal ganglia.

Etiology

Familial forms of BSPDC are common and follow most frequently an autosomal dominant pattern of inheritance. More than 30 families have been reported so far. Linkage analysis has revealed several chromosomal loci referred to as IBGC1 (chromosome 14q) [15], IBGC2 (chromosom2q37) [16], and IBGC3 (chromosome 8p21.1-q11.23) [17]. The *SLC20A2* gene has recently been identified as the causative gene for IBGC3 in six families from different ethnic backgrounds [18]. *SLC20A2* mutations were functionally associated with an impairment of a phosphate transporter linking BSPDC with phosphate homeostasis. In other families, linkage to the mentioned loci has been excluded pointing toward an even broader genetic heterogeneity of this disorder [19–21]. It is worth mentioning that two classes of penetrance have to be distinguished, the clinical penetrance (manifestation of clinically overt symptoms) and the histopathological penetrance (formation of mineral deposits). Approximately 45 % of subjects with intracerebral calcifications remain clinically unaffected regardless of whether they have an inherited or a sporadic form of BSPDC [22, 23]. Nonetheless, it may be assumed that the disorder is rare even though accurate prevalence estimates are not available.

Nonarteriosclerotic depositions of minerals are typically found within the vascular walls of smaller arteries and veins, capillaries, and perivascular spaces [24, 25]. Extracerebral calcification is not evident in the idiopathic form. The main components of the deposits are calcium spheroids, but phosphorus, zinc, glycosaminoglycans, iron, aluminum, magnesium, and potassium have also been detected [24, 25].

Classification

The diagnostic criteria for BSPDC include (1) symmetric calcifications of basal ganglia and either the dentate nucleus, thalamus, white matter structures, or a combined involvement of these regions, (2) normal growth and development during childhood, (3) progressive neurological dysfunction, (4) normal biochemical and endocrinological tests, and (5) absence of an infectious, toxic, or traumatic cause [14, 23, 26].

By far the most frequent causes of secondary intracerebral calcifications are abnormalities of calcium/phosphate homeostasis, e.g., primary or secondary hypoparathyroidism, pseudohypoparathyroidism, pseudopseudohypoparathyroidism, or hyperparathyroidism. Other rare causes include carbon monoxide poisoning, lead intoxication, vascular malformations, cerebral hemorrhage, phacomatoses, hypothyroidism, birth anoxia, systemic lupus erythematodes, mitochondrial disorders, tumors, radiotherapeutic treatment, encephalitis, and cerebral parasitoses [4, 14, 27].

Secondary causes of intracerebral calcifications are often accompanied by extracerebral manifestations.

Clinical Manifestations

The first symptoms typically develop between the ages of 30 and 60 years, although a couple of cases have been described with an age at onset as early as the first decade. The mineral deposition precedes the clinical manifestation often by decades, a stage where the affected subjects remain clinically asymptomatic [28]. In familial BSPDC, an anticipatory effect with onset of symptoms more than two decades earlier in later generations has been observed in a few pedigrees, a finding that requires further confirmation [15, 21]. Male gender seems to be more frequently associated with symptomatic BSPDC with a gender ratio of approximately 2:1 (male:female) [22, 23, 29], and the volume of mineral deposits may also be higher in men [29].

Clinically, BSPDC is characterized by a combination of various ataxic and nonataxic movement disorders, neuropsychiatric symptoms, and dysarthria. The age at clinical manifestation, phenotype, and distribution of calcifications vary within and between affected families [25, 29]. Movement disorders are the most common feature, and by far the most frequent movement disorder in BSPDC is parkinsonism, often presenting with symmetrical onset [29, 30]. Single case reports suggest that the response to dopaminergic drugs is variable [30–32]. In levodopa-responsive patients, idiopathic Parkinson's disease may coexist [30]. Apart from parkinsonism, patients may exhibit severe gait impairment with freezing of gait, paroxysmal and nonparoxysmal dyskinesia, chorea, athetosis, dystonia, tremor, and cerebellar ataxia [21, 26, 29, 33–36]. Nonmotor signs include cognitive and psychiatric features (e.g., executive dysfunction, depression, schizophrenia-like psychosis, and suicidal behavior) as well as sensory changes and chronic headache. It is hypothesized that cognitive and psychiatric symptoms are associated with an involvement of frontostriatal cortico-subcortical neuronal circuits [37]. Frequently, BSPDC presents with a combination of parkinsonism, cerebellar signs, and dementia. This triad should prompt clinicians to obtain a cerebral CT scan, which is still the imaging diagnostic gold standard. It is important to mention that neither of the available neuroimaging techniques is capable of discriminating between idiopathic and secondary calcifications because the distribution patterns overlap or match each other. Once calcifications have been identified, an investigation for secondary causes needs to be performed.

Neuroimaging of Basal Ganglia Calcifications

Computerized Tomography

Nonenhanced CT is a very sensitive technique to detect even minimal intracerebral calcifications. On CT, intracerebral calcifications generate a marked and bone-like

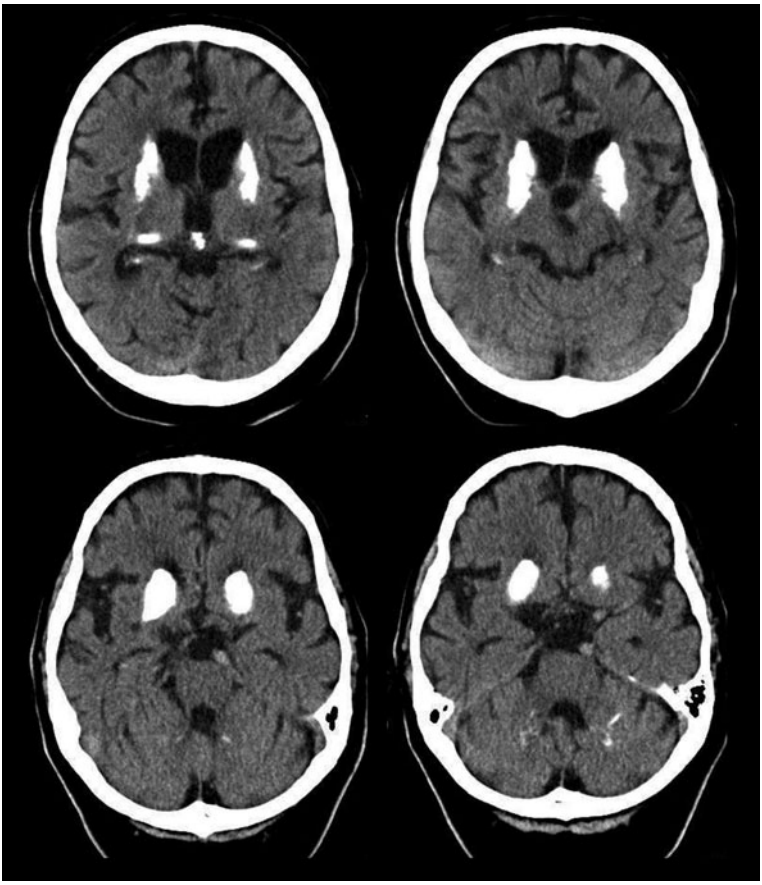

Fig. 16.1 Nonenhanced CT scan of a patient with BSPDC demonstrating bilateral, nearly symmetric calcifications of the basal ganglia and posterior thalamus. Less intense (and more punctuated) calcifications are seen in the dentate nucleus. An additional finding includes a left-sided posterior cerebral artery stroke, which is unrelated to BSPDC

signal (Fig. 16.1). Prior to the implementation of CT in clinical routine, skull radiography was the only method to visualize calcifications in vivo. Compared with CT, the sensitivity was low, as only 4–10 % of CT-positive calcifications could be detected [2, 5, 38, 39].

In BSPDC, the calcifications on CT show a fairly symmetric distribution [29]. The pallidum is most frequently affected [38]. A combination of calcium deposits in the striatum, dentate nucleus, thalamus, and white matter is common, whereas cortical calcifications appear to be less frequent [29, 40]. There are conflicting findings as to whether the extent and the localization of calcifications correlate with the neurological impairment [5, 25, 29, 41, 42]. In a study including CT scans of 31 BSPDC patients, the mean amount of calcifications in the basal ganglia was not

different between symptomatic and asymptomatic subjects, whereas the total amount of intracerebral deposits were higher in the group of subjects with symptoms [29]. In one patient, subsequent CT scans revealed an increasing volume of calcifications corresponding to the progression of neurological impairment [29]. At a later point in time, the degree of calcifications decreased, presumably because of the onset of secondary brain atrophy. Circumscribed temporal and frontal cortical atrophy is common at a later disease stage [43]. Taxer et al. [41] found that the symptomatology may be independent of the localization of intracerebral calcifications, whereas the amount of calcium deposits corresponds to the severity of symptoms particularly with respect to extrapyramidal symptoms and dementia. In another study, patients with a parkinsonian phenotype and calcifications in the basal ganglia were clinically indistinguishable from Parkinson's disease patients without calcifications [42]. In this study, however, also patients with unilateral or asymmetric calcifications were included, and thus, it remains questionable whether they really represent classical BSPDC.

Magnetic Resonance Imaging

Magnetic resonance imaging (MRI) has a lower sensitivity and lower specificity than CT in diagnosing intracerebral calcifications [44–48]. In T1-weighted images, the signal contrast caused by calcifications is often inconsistent. In general, calcium deposits reduce the T1 relaxation time by a surface relaxation mechanism [49]. With an increasing amount of deposits, T1 intensity is supposed to increase initially and to then decrease subsequently [49]. In the majority of cases, the T1 signal is hyperintense, but isointense or hypointense signal behavior can also be observed within the same subject or between different subjects [45, 50, 51]. The changes in T1 signal may be related to the disease stage, differences in calcium metabolism, and the volume of deposits [52]. In contrast, T2 signal changes and calcified brain regions upon CT show a varying distribution. Confluent hyperintense T2 lesions of the white matter in the centrum semiovale are common, and they do not correspond to the localization of calcifications [23, 45, 53]. It is speculated that the T2 hyperintensities represent slowly progressive metabolic and inflammatory processes that result in and correlate with progressive neurological deficits [45].

Transcranial Sonography

Transcranial sonography (TCS) has become a useful diagnostic tool in the differential diagnosis of movement disorders. TCS may also be helpful in establishing an early diagnosis of Parkinson's disease [54]. Advantages of TCS are its widespread availability, cost effectiveness, noninvasiveness, and the avoidance of exposure to x-rays. The method allows unlimited repeated measures and is even applicable in agitated patients. An experienced investigator is able to perform a TCS scan within 5–10 min.

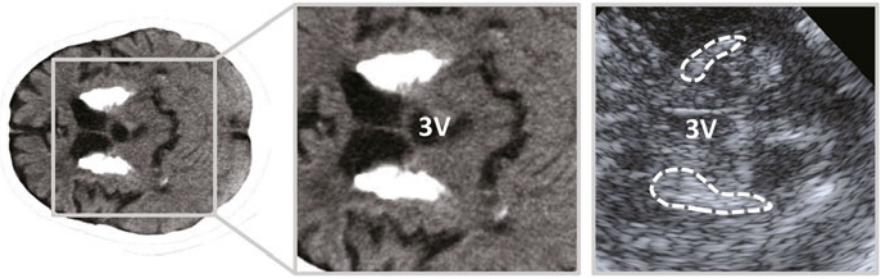

Fig. 16.2 Striatal calcifications (*left* image, magnified on the *middle* image) on a CT scan and on an anatomically corresponding TCS image (*right* image). Hyperechogenic striatal areas are highlighted in the TCS image. *3V* third ventricle

A striking finding in Parkinson's disease is an enlarged area of hyperechogenicity projecting to the anatomical site of the midbrain substantia nigra [55]. Abnormal hyperechogenic areas within the caudate and lenticular nucleus have been reported in atypical parkinsonian syndromes [56], Huntington's disease [57], multiple sclerosis [58], primary dystonia [59, 60], spinocerebellar ataxia type 3 [61], and Wilson's disease [62, 63]. Several factors have been discussed as the possible underlying pathoanatomical correlate of basal ganglia hyperechogenicity: increased local iron [58, 64] and copper concentration [62], gliosis [58], and enlarged perivascular spaces or simply artifacts (see Chap. 6 for a more in-depth discussion). Moreover, diffuse hyperechogenicity of the basal ganglia and thalami is a frequent and nonpathologic finding in premature infants that is no longer detectable 1 month after delivery [65]. The most intense and striking hyperechogenicity in adulthood seems to derive from the accumulation of calcium compounds. Thus, BSPDC provides the unique opportunity to study basal ganglia alterations with a defined histopathology. Using TCS, small intracranial calcifications may occasionally be detected even prior to CT imaging [55, 62]. So far, striking basal ganglia hyperechogenicity in BSPDC has been reported in seven patients from different sites [21, 31, 66]. The hyperechogenic areas upon TCS correspond excellently to the symmetric distribution pattern as shown with either CT [21, 31] or MRI [66] and show almost the same level of intensity as the contralateral skull bone and the frequently calcified pineal gland (Fig. 16.2). Hyperechogenicity in extended calcified lesions as in BSPDC can be distinguished from the pattern observed in the context of a mixture of gliosis and iron and/or copper accumulation, which may be less striking. Apart from the high signal-to-noise ratio of the hyperechogenic signal, the highly symmetric distribution and the large conglomerates may be specific TCS features of BSPDC.

Functional Radioligand Imaging Techniques

Functional radioligand imaging techniques, including single photon emission tomography (SPECT) and positron emission tomography (PET), complement anatomical

brain imaging methods such as CT and MRI. They are useful to study local brain perfusion, brain metabolism, and the nigrostriatal function in vivo.

In symptomatic BSPDC subjects, Tc-99^{m} hexamethylpropylene amine oxime (HMPAO) SPECT revealed hypoperfusion in widespread subcortical and cortical regions, including the basal ganglia, thalamus, cerebellum as well as frontal, parietal, temporal, and insular cortical areas [21, 34, 51, 67, 68]. In two further case reports, hypoperfusion was restricted to the right-sided basal ganglia [69] and the thalami bilaterally [70] despite the fact that the calcifications were widely dispersed in these patients. In the latter study, Tc-99^{m} ethylcysteinate was used instead of HMPAO to visualize the local cerebral blood flow. Using this agent, the reduction of cerebral perfusion was not per se associated with the amount of mineral deposits [70]. The clinical phenotype corresponds well to hypoperfused brain regions in BSPDC. Ones et al. [69], for example, reported a case of unilateral striatal hypoperfusion and contralateral parkinsonism. In one clinically asymptomatic subject, the regional brain perfusion was unremarkable [34].

In conformity with hypoperfusion in calcified regions and interconnected areas, ^{18}F-fludeoxyglucose (FDG) PET revealed reductions of glucose metabolism in similar regions, including frontotemporal and cingulate cortices as well as the basal ganglia in symptomatic BSPDC, whereas asymptomatic subjects show a normal glucose brain metabolism [34, 71–73]. The hypometabolism corresponds to the clinical deficits and may result from a deafferentiation of striatal and cortical regions due to basal ganglia pathology. The multifaceted symptomatology may thus be explained by a disruption of motor, limbic, and associative cortico-subcortical neuronal circuits.

Using FP-CIT SPECT and ^{18}F-DOPA PET, the dopaminergic nigrostriatal neurotransmission was shown to be impaired in several BSPDC patients presenting with parkinsonism. The reduced striatal tracer uptake was either asymmetric, and thus resembling idiopathic Parkinson disease [21], or symmetric [25, 68]. One patient with generalized chorea and neuropsychiatric symptoms but without features of Parkinson's disease had a normal FP-CIT scan [21]. Normal presynaptic ^{18}F-DOPA uptake has been observed in one asymptomatic patient and one patient with dementia and bradykinesia [44]. In two symptomatic subjects, PET displayed reduced striatal dopamine D_1 and D_2 receptor binding [25]. Thus, postsynaptic striatal dysfunction may be postulated in some affected individuals due to an interference of calcium deposits with postsynaptic dopamine receptors.

Conclusions and Future Directions

A combination of parkinsonism, cognitive deterioration, and cerebellar signs is a typical finding in BSPDC and should prompt clinicians to perform a cerebral CT scan, which remains the most effective screening tool. MRI is useful in detecting white matter pathology in uncalcified brain areas but its effectiveness in verifying intracerebral calcifications is limited. Preliminary data suggest that intracerebral calcifications show a distinct pattern of hyperechogenic areas upon TCS. In the hand

of an experienced investigator, it may be justified to use TCS as a first screening tool. To date, however, a CT scan is still needed in order to verify or exclude intracerebral calcifications. Future developments in various neuroimaging modalities will provide the ability to detect changes early while improving our understanding of symptom-related changes in brain function.

References

1. Kiroglu Y, Calli C, Karabulut N, Oncel C. Intracranial calcifications on CT. Diagn Interv Radiol. 2010;16(4):263–9.
2. Murphy MJ. Clinical correlations of CT scan-detected calcifications of the basal ganglia. Ann Neurol. 1979;6(6):507–11.
3. Vles JS, Lodder J, van der Lugt PJ. Clinical significance of basal ganglia calcifications detected by CT (a retrospective study of 33 cases). Clin Neurol Neurosurg. 1981;83(4):253–6.
4. Harrington MG, Macpherson P, McIntosh WB, Allam BF, Bone I. The significance of the incidental finding of basal ganglia calcification on computed tomography. J Neurol Neurosurg Psychiatry. 1981;44(12):1168–70.
5. Kazis AD. Contribution of CT scan to the diagnosis of Fahr's syndrome. Acta Neurol Scand. 1985;71(3):206–11.
6. Stellamor K, Stellamor V. Roentgen diagnosis of Fahr's disease. Rontgenblatter. 1983;36(6):194–6.
7. Konig P. Psychopathological alterations in cases of symmetrical basal ganglia sclerosis. Biol Psychiatry. 1989;25(4):459–68.
8. Cohen CR, Duchesneau PM, Weinstein MA. Calcification of the basal ganglia as visualized by computed tomography. Radiology. 1980;134(1):97–9.
9. Tedrus GM, Fonseca LC, Nogueira E Jr. Basal ganglia calcification on computed tomography: clinical characteristics in 25 patients. Arq Neuropsiquiatr. 2006;64(1):104–7.
10. Forstl H, Krumm B, Eden S, Kohlmeyer K. Neurological disorders in 166 patients with basal ganglia calcification: a statistical evaluation. J Neurol. 1992;239(1):36–8.
11. Fahr T. Idiopathische Verkalkung der Hirngefäße. Zentralbl Allg Pathol. 1930;50:129–33.
12. Klein C, Vieregge P. Fahr's disease—far from a disease. Mov Disord. 1998;13(3):620–1.
13. Delacour A. Ossification des capilaires du cerveau. Ann Med Psychol. 1850;2:458–61.
14. Manyam BV. What is and what is not 'Fahr's disease'. Parkinsonism Relat Disord. 2005;11(2):73–80.
15. Geschwind DH, Loginov M, Stern JM. Identification of a locus on chromosome 14q for idiopathic basal ganglia calcification (Fahr disease). Am J Hum Genet. 1999;65(3):764–72.
16. Volpato CB, De Grandi A, Buffone E, et al. 2q37 as a susceptibility locus for idiopathic basal ganglia calcification (IBGC) in a large South Tyrolean family. J Mol Neurosci. 2009;39(3): 346–53.
17. Dai X, Gao Y, Xu Z, et al. Identification of a novel genetic locus on chromosome 8p21.1-q11.23 for idiopathic basal ganglia calcification. Am J Med Genet B Neuropsychiatr Genet. 2010;153B(7):1305–10.
18. Wang C, Li Y, Shi L, et al. Mutations in SLC20A2 link familial idiopathic basal ganglia calcification with phosphate homeostasis. Nat Genet. 2012;44(3):254–6.
19. Brodaty H, Mitchell P, Luscombe G, et al. Familial idiopathic basal ganglia calcification (Fahr's disease) without neurological, cognitive and psychiatric symptoms is not linked to the IBGC1 locus on chromosome 14q. Hum Genet. 2002;110(1):8–14.
20. Oliveira JR, Spiteri E, Sobrido MJ, et al. Genetic heterogeneity in familial idiopathic basal ganglia calcification (Fahr disease). Neurology. 2004;63(11):2165–7.

21. Kostic VS, Lukic-Jecmenica M, Novakovic I, et al. Exclusion of linkage to chromosomes 14q, 2q37 and 8p21.1-q11.23 in a Serbian family with idiopathic basal ganglia calcification. J Neurol. 2011;258(9):1637–42.
22. Kobari M, Nogawa S, Sugimoto Y, Fukuuchi Y. Familial idiopathic brain calcification with autosomal dominant inheritance. Neurology. 1997;48(3):645–9.
23. Ellie E, Julien J, Ferrer X. Familial idiopathic striopallidodentate calcifications. Neurology. 1989;39(3):381–5.
24. Miklossy J, Mackenzie IR, Dorovini-Zis K, et al. Severe vascular disturbance in a case of familial brain calcinosis. Acta Neuropathol. 2005;109(6):643–53.
25. Wszolek ZK, Baba Y, Mackenzie IR, et al. Autosomal dominant dystonia-plus with cerebral calcifications. Neurology. 2006;67(4):620–5.
26. Sobrido MJ, Hopfer S, Geschwind DH. Familial idiopathic basal ganglia calcification. In: Pagon RA, Bird TD, Dolan CR, Stephens K, Adam MP, editors. GeneReviews. Seattle (WA); 1993.
27. Bonazza S, La Morgia C, Martinelli P, Capellari S. Strio-pallido-dentate calcinosis: a diagnostic approach in adult patients. Neurol Sci. 2011;32(4):537–45.
28. Manyam BV, Bhatt MH, Moore WD, Devleschoward AB, Anderson DR, Calne DB. Bilateral striopallidodentate calcinosis: cerebrospinal fluid, imaging, and electrophysiological studies. Ann Neurol. 1992;31(4):379–84.
29. Manyam BV, Walters AS, Narla KR. Bilateral striopallidodentate calcinosis: clinical characteristics of patients seen in a registry. Mov Disord. 2001;16(2):258–64.
30. Manyam BV, Walters AS, Keller IA, Ghobrial M. Parkinsonism associated with autosomal dominant bilateral striopallidodentate calcinosis. Parkinsonism Relat Disord. 2001;7(4): 289–95.
31. Bruggemann N, Schneider SA, Sander T, Klein C, Hagenah J. Distinct basal ganglia hyperechogenicity in idiopathic basal ganglia calcification. Mov Disord. 2010;25(15):2661–4.
32. Hui JS, Lew MF. Calcification of the basal ganglia. Handb Clin Neurol. 2007;84:479–86.
33. Diaz GE, Wirrell EC, Matsumoto JY, Krecke KN. Bilateral striopallidodentate calcinosis with paroxysmal kinesigenic dyskinesia. Pediatr Neurol. 2010;43(1):46–8.
34. Saiki M, Saiki S, Sakai K, et al. Neurological deficits are associated with increased brain calcinosis, hypoperfusion, and hypometabolism in idiopathic basal ganglia calcification. Mov Disord. 2007;22(7):1027–30.
35. Klein C, Vieregge P, Kompf D. Paroxysmal choreoathetosis in a patient with idiopathic basal ganglia calcification, chorea, and dystonia. Mov Disord. 1997;12(2):254–5.
36. Micheli F, Fernandez Pardal MM, Casas Parera I, Giannaula R. Sporadic paroxysmal dystonic choreoathetosis associated with basal ganglia calcifications. Ann Neurol. 1986;20(6):750.
37. Cummings JL, Gosenfeld LF, Houlihan JP, McCaffrey T. Neuropsychiatric disturbances associated with idiopathic calcification of the basal ganglia. Biol Psychiatry. 1983;18(5):591–601.
38. Koller WC, Cochran JW, Klawans HL. Calcification of the basal ganglia: computerized tomography and clinical correlation. Neurology. 1979;29(3):328–33.
39. Sachs C, Ericson K, Erasmie U, Bergstrom M. Incidence of basal ganglia calcifications on computed tomography. J Comput Assist Tomogr. 1979;3(3):339–44.
40. Koller WC, Klawans HL. Cerebellar calcification on computerized tomography. Ann Neurol. 1980;7(2):193–4.
41. Taxer F, Haller R, Konig P. Clinical early symptoms and CT findings in Fahr syndrome. Nervenarzt. 1986;57(10):583–8.
42. Vermersch P, Leys D, Pruvo JP, Clarisse J, Petit H. Parkinson's disease and basal ganglia calcifications: prevalence and clinico-radiological correlations. Clin Neurol Neurosurg. 1992;94(3):213–7.
43. Shibayama H, Kobayashi H, Nakagawa M, et al. Non-Alzheimer non-Pick dementia with Fahr's syndrome. Clin Neuropathol. 1992;11(5):237–50.
44. Manyam BV, Bhatt MH, Moore WD, Devleschoward AB, Anderson DR, Calne DB. Bilateral striopallidodentate calcinosis: cerebrospinal fluid, imaging, and electrophysiological studies. Ann Neurol. 1992;31(4):379–84.

45. Avrahami E, Cohn DF, Feibel M, Tadmor R. MRI demonstration and CT correlation of the brain in patients with idiopathic intracerebral calcification. J Neurol. 1994;241(6):381–4.
46. Holland BA, Kucharczyk W, Brant-Zawadzki M, Norman D, Haas DK, Harper PS. MR imaging of calcified intracranial lesions. Radiology. 1985;157(2):353–6.
47. Oot RF, New PF, Pile-Spellman J, Rosen BR, Shoukimas GM, Davis KR. The detection of intracranial calcifications by MR. AJNR Am J Neuroradiol. 1986;7(5):801–9.
48. Kozic D, Todorovic-Djilas L, Semnic R, Miucin-Vukadinovic I, Lucic M. MR imaging—an unreliable and potentially misleading diagnostic modality in patients with intracerebral calcium depositions. Case report. Neuro Endocrinol Lett. 2009;30(5):553–7.
49. Henkelman RM, Watts JF, Kucharczyk W. High signal intensity in MR images of calcified brain tissue. Radiology. 1991;179(1):199–206.
50. Bottcher J, Sauner D, Jentsch A, et al. Visualization of symmetric striopallidodentate calcinosis by using high-resolution susceptibility-weighted MR imaging. An account of the impact of different diagnostic methods of M. Fahr. Nervenarzt. 2004;75(4):355–61.
51. Smith FW, Gemmell HG, Sharp PF, Besson JA. Technetium-99m HMPAO imaging in patients with basal ganglia disease. Br J Radiol. 1988;61(730):914–20.
52. Scotti G, Scialfa G, Tampieri D, Landoni L. MR imaging in Fahr disease. J Comput Assist Tomogr. 1985;9(4):790–2.
53. Yoshikawa H, Abe T. Transient parkinsonism in bilateral striopallidodentate calcinosis. Pediatr Neurol. 2003;29(1):75–7.
54. Vlaar AM, Bouwmans A, Mess WH, Tromp SC, Weber WE. Transcranial duplex in the differential diagnosis of parkinsonian syndromes: a systematic review. J Neurol. 2009;256(4):530–8.
55. Berg D, Godau J, Walter U. Transcranial sonography in movement disorders. Lancet Neurol. 2008;7(11):1044–55.
56. Walter U, Dressler D, Probst T, et al. Transcranial brain sonography findings in discriminating between parkinsonism and idiopathic Parkinson disease. Arch Neurol. 2007;64(11):1635–40.
57. Postert T, Lack B, Kuhn W, et al. Basal ganglia alterations and brain atrophy in Huntington's disease depicted by transcranial real time sonography. J Neurol Neurosurg Psychiatry. 1999;67(4):457–62.
58. Walter U, Wagner S, Horowski S, Benecke R, Zettl UK. Transcranial brain sonography findings predict disease progression in multiple sclerosis. Neurology. 2009;73(13):1010–7.
59. Naumann M, Becker G, Toyka KV, Supprian T, Reiners K. Lenticular nucleus lesion in idiopathic dystonia detected by transcranial sonography. Neurology. 1996;47(5):1284–90.
60. Walter U, Buttkus F, Benecke R, Grossmann A, Dressler D, Altenmuller E. Sonographic alteration of lenticular nucleus in focal task-specific dystonia of musicians. Neurodegener Dis. 2012;9(2):99–103.
61. Postert T, Eyding J, Berg D, et al. Transcranial sonography in spinocerebellar ataxia type 3. J Neural Transm Suppl. 2004;68:123–33.
62. Walter U, Krolikowski K, Tarnacka B, Benecke R, Czlonkowska A, Dressler D. Sonographic detection of basal ganglia lesions in asymptomatic and symptomatic Wilson disease. Neurology. 2005;64(10):1726–32.
63. Svetel M, Mijajlovic M, Tomic A, Kresojevic N, Pekmezovic T, Kostic VS. Transcranial sonography in Wilson's disease. Parkinsonism Relat Disord. 2012;18(3):234–8.
64. Zecca L, Berg D, Arzberger T, et al. In vivo detection of iron and neuromelanin by transcranial sonography: a new approach for early detection of substantia nigra damage. Mov Disord. 2005;20(10):1278–85.
65. van Wezel-Meijler G, Leijser LM, Wiggers-de Bruine FT, Steggerda SJ, van der Grond J, Walther FJ. Diffuse hyperechogenicity of basal ganglia and thalami in preterm neonates: a physiologic finding? Radiology. 2011;258(3):944–50.
66. Toscano M, Canevelli M, Giacomelli E, et al. Transcranial sonography of basal ganglia calcifications in Fahr disease. J Ultrasound Med. 2011;30(7):1032–33.
67. Uygur GA, Liu Y, Hellman RS, Tikofsky RS, Collier BD. Evaluation of regional cerebral blood flow in massive intracerebral calcifications. J Nucl Med. 1995;36(4):610–2.

68. Paschali A, Lakiotis V, Messinis L, et al. Dopamine transporter SPECT/CT and perfusion brain SPECT imaging in idiopathic basal ganglia calcinosis. Clin Nucl Med. 2009;34(7):421–3.
69. Ones T, Dede F, Gunal D, et al. The clinical utility of 99mTc-HMPAO SPECT in Fahr's disease. Ann Nucl Med. 2008;22(5):425–8.
70. Ogi S, Fukumitsu N, Tsuchida D, Uchiyama M, Mori Y, Matsui K. Imaging of bilateral striopallidodentate calcinosis. Clin Nucl Med. 2002;27(10):721–4.
71. Hempel A, Henze M, Berghoff C, Garcia N, Ody R, Schroder J. PET findings and neuropsychological deficits in a case of Fahr's disease. Psychiatry Res. 2001;108(2):133–40.
72. Benke T, Karner E, Seppi K, Delazer M, Marksteiner J, Donnemiller E. Subacute dementia and imaging correlates in a case of Fahr's disease. J Neurol Neurosurg Psychiatry. 2004;75(8): 1163–5.
73. Le Ber I, Marie RM, Lalevee C, Chabot B, Allouche S, Defer GL. Familial idiopathic striato-pallido-dentate calcifications: clinical and brain imaging study in a family. Rev Neurol (Paris). 2003;159(1):43–9.

Index

F. B. Nahab, N. Hattori (eds.), *Neuroimaging of Movement Disorders,* Current Clinical Neurology 44, DOI 10.1007/978-1-62703-471-5,